

Государственное образовательное учреждение  
высшего профессионального образования  
**«Томский государственный университет  
систем управления и радиоэлектроники»**

## **ТЕМАТИЧЕСКИЙ РЕФЕРАТИВНЫЙ СБОРНИК № 49-2/2**

**“НЕМТ”**

**(«Транзисторы с высокой подвижностью электронов»)**

Публикации в трудах конференций

Источник: *Digital Library IEEEExplore*

Язык: *английский*

Глубина поиска: *2001 – 2006 гг.*

Дата формирования: *март 2011 г.*

Составитель: *В.И. Карнышев*

**Томск – 2011**

## ТЕМАТИЧЕСКИЙ РЕФЕРАТИВНЫЙ СБОРНИК № 49-2/2

### "HEMT"

#### («Транзисторы с высокой подвижностью электронов»)

Публикации в трудах конференций

#### "High Performance 94 GHz Resistive Mixer Using GaAs Metamorphic HEMT Technology"

We present the high performance 94 GHz resistive mixer including IF amplifier using 0.1  $\mu\text{m}$  metamorphic HEMT. For 94 GHz resistive mixer, the metamorphic HEMT of excellent characteristics was developed. The circuit performance of resistive mixer with IF amplifier shows conversion gain of 1.3 dB at LO power of 7 dBm. In this work, we fabricated the resistive mixer which has high performance using metamorphic HEMT. The fabricated resistive mixer shows the superior conversion gain than that of previous reported results [C1158]

#### "Wideband and High Gain Cascode Amplifier using Metamorphic HEMT for Millimeter-wave Applications"

In this paper, millimeter-wave coplanar high gain and wideband cascode amplifiers based on metamorphic high electron mobility transistor (MHEMT) were designed and fabricated. The fabricated 100 nm gate length MHEMT devices exhibit DC characteristics with a drain current density of 471 mA/mm and an extrinsic transconductance of 845 mS/mm. The current gain cutoff frequency ( $f_T$ ) and the maximum oscillation frequency ( $f_{\text{max}}$ ) are 193 GHz and 325 GHz, respectively. The matching circuit of cascode amplifier was designed for wideband characteristics using CPW (coplanar waveguide) transmission line. The one-stage amplifier showed a very wide 3 dB bandwidth of 37 GHz from 31.3 GHz to 68.3 GHz. The average  $S_{21}$  gain was 9.7 dB in band, with the maximum gain of 11.3 dB at 40 GHz. The two-stage amplifier had a 3 dB bandwidth of 29.5 GHz from 32.5 GHz to 62.0 GHz. The two-stage amplifier showed an excellent gain characteristic with average  $S_{21}$  gain of 20.4 dB in band and the maximum gain of 22.3 dB at 36.5 GHz. To our knowledge, these results have higher gain-per-stage with wider bandwidth than some other millimeter-wave amplifiers [C1159]

#### "Charge Effects and Transient Simulation of p-HEMT Meander Gate Switches"

This paper presents a simulation of the transient behavior of a filtronic SP6T switch. By employing a non-linear switch model a representation of the switching dynamics is presented. The simulations predict that the changing control voltages has quickly attenuate the fundamental power, however harmonic performance is dependant on the total bias applied to the switch and hence relaxes to its steady state condition 0.15 $\mu\text{s}$  after the control voltages have settled. Within this paper we demonstrate the importance of understanding the behavior of the switch during transitions between equilibrium conditions with respect to the radiated spectral content [C1160]

#### "A Ka-band MMIC Oscillator Using a Miniaturized CPW 1-D PBG Structure"

A Ka-band monolithic microwave integrated circuit (MMIC) oscillator was implemented by using a coplanar waveguide photonic bandgap (PBG) resonator and a 0.1 $\mu\text{m}$  GaAs pseudomorphic high electron mobility transistor (p-HEMT). A coplanar labyrinthine one-dimensional PBG resonator was used for reduction in MMIC size. The fabricated MMIC oscillator had an output power of 6.5 dBm at 30.3 GHz and a free-running phase noise of -80 dBc/Hz at 100 kHz offset [C1161]

#### "A W-band MMIC One-Chip Set for Automotive Radar Sensor by using a 0.15 $\mu\text{m}$ mHEMT Process"

A monolithic microwave integrated circuit (MMIC) one-chip set consisting of a transmitter and an 8-stage low noise amplifier has been developed for automotive radar sensors at 77 GHz. The chip set was fabricated using a 0.15  $\mu\text{m}$  gate-length InGaAs/InAlAs/GaAs metamorphic high electron mobility transistor (mHEMT) process based on a 4-inch substrate. The transmitter achieved an output power of 11 dBm at 76.5 GHz with a conversion gain of 6 dB for an input power of 5 dBm and a 38.25 GHz input frequency. The chip size is 5.1 mm times 2.2 mm. The 8-stage low noise amplifier exhibited a gain of 35 dB over a 76 to 77 GHz band with a noise figure of 6 dB. The chip size is 4.1 mm times 2.2 mm. This MMIC one-chip set is suitable for the 77 GHz automotive radar sensors and related applications in a W-band [C1162]

### "Study of Field Plate AlGaIn/GaN HEMTs by Means of a 2D-Hydrodynamic Model for Power Applications"

Field plate AlGaIn/GaN HEMT (high electron mobility transistor) structures, are very promising to improve the microwave power performance. This device permits to improve the breakdown voltage but the field plate (FP) electrode involves an increase of the parasitic capacitances and consequently a drop of the current gain transition frequency. So a compromise must be found depending on the operating frequency. In this paper, a theoretical 2D-hydrodynamic model is developed to study the impact of the FP on the device performance [C1163]

### "Studies of InGaAs layers growth by metalorganic chemical vapor deposition for InP-HEMTs; Effects of trimethylindium and triethylindium"

We studied an InGaAs epitaxial layers growth by metalorganic chemical vapor deposition (MOCVD) for InP-based high electron mobility transistors (HEMTs). The InGaAs channel layer of HEMTs was grown by a new material combination of triethylindium (TEI), triethylgallium (TEG) and arsine (AsH<sub>3</sub>). An electron mobility of the HEMTs structure sample was 20% higher than the one grown by trimethylindium (TMI), TEG and AsH<sub>3</sub>. And the DC characteristics of the HEMTs, the drain current and transconductance, were increased compared with the one. It is confirmed that this growth method is quite effective for the improvement of a characteristics of InP-based HEMTs [C1164]

### "Microwave Class-F and Inverse Class-F Power Amplifiers Designs using GaN Technology and GaAs pHEMT"

This paper presents the designs and results of two high-efficiency harmonics-tuned microwave power amplifiers (PA): the first one is a 2 GHz class-F PA in monolithic integrated circuit (MMIC) by using GaN HEMT technology, and the other one is a 2.45-GHz inverse class-F PA using packaged GaAs pHEMT devices with PCB technology. In the class-F MMIC PA, field-plated GaN HEMT device is used for high-power performance. The 2.0-GHz class-F MMIC PA achieves a PAE of 50%, 38 dBm output power, and 6.2 W/mm power density. The inverse class-F PA at 2.45 GHz achieves 22.6 dBm output power and 73% PAE at 3 dB compression, and has very low cost [C1165]

### "GaN HEMT Performance-Measurements and Simulations of a 3.6 mm Device from Cree"

The premise of GaN HEMT devices to offer superior power amplification performance in microwave frequencies lead to an extensive research in this field, and to numerous publications emphasizing individual performance records such as, current & power densities, linearity and break down voltage. The performance of these, primarily experimental devices, is often reported in the terms of their intended applications, offering either the saturated output power, or 3dB compressed output power, or OFDM and CDMA waveform-specific output power, making the comparison among the devices, and a comparison with other technologies such as LDMOS & GaAs rather difficult. The authors are engaged in the design of a wideband (10:1 BW) 50W @ 1dB compression point linear power amplifier operating up to 2GHz. As a step in this process we determine the performance of an actual, 3.6 mm periphery, pre-production GaN HEMT from CREE. The device performance is simulated using CREE model, and it is compared with the measurements we have taken, both reported in this paper. The results obtained exhibit good convergence with the model, and are presented using the more common performance parameters such as power and efficiency at 1dB compression point, and the linearity in terms of IP<sub>3</sub> [C1166]

### "Compact K-band Watt-level GaAs PHEMT Power Amplifier MMIC with integrated ESD protection"

The performance of a compact K-band power amplifier MMIC fabricated in standard 6-inch 0.15-μm GaAs power PHEMT technology is reported. The circuit features on-chip ESD protection including input short-circuit stub, dual capacitors at RF ports and high-current diode arrays on each gate pad. Occupying less than 3 mm<sup>2</sup>, this 3-stage power amplifier achieves a linear gain of more than 20-dB over the 17 to 24 GHz frequency range with 6-dB noise figure. It also delivers a CW output power of more than 29-and 30-dBm, in the 17-20 GHz band, at 5- and 6-V respectively. Preliminary ESD characterization shows the circuit withstands 180-V in human body model test (tester limit), and 100-V machine model (equivalent to at least 500-V HBM), without DC or RF performance degradation. Finally, performance in standard 24-lead plastic QFN package (4times4 mm<sup>2</sup>) is presented: the device exhibits more than 17.5-dB linear gain over 17-24 GHz, with P<sub>1dB</sub> greater than 28-dBm in the 17.7-19.7 GHz radio range [C1167]

### "44-GHz High Power and Driver Microstrip Amplifier MMICs using 6-inch 0.15-μm PHEMTs"

A family of robust and cost effective 44-GHz microstrip MMIC power amplifiers has been developed based on a standard 6-inch, 0.15- $\mu\text{m}$  GaAs power pHEMT production process on 100- $\mu\text{m}$  substrate thickness. These amplifiers provide high output powers at 44-GHz with a MTTF exceeding two million hours at 75 °C backplate temperature. The single-ended, 3-stage amplifier MMIC has more than 15 dB small signal gain at 44 GHz and 28 dBm output power for a chip area of 5.6 mm<sup>2</sup>. For the same frequency band, a balanced 1.25-W power amplifier and a doubly-balanced 2.25-W amplifier achieved linear gain of more than 18 dBm and better than -20 dB S11 and S22, with chip areas of 10.8 and 21.5 mm<sup>2</sup> respectively. To our knowledge, in terms of power and power density per chip area, these results are among the highest output power levels reported to date at this frequency for single chip MMICs on 100- $\mu\text{m}$  substrate with acceptable lifetime [C1168]

#### "A Non-Quasi-Static, Relaxation-Time Small-Signal HEMT Model Compatible with Large-Signal Modeling"

A non-quasi-static, relaxation-time small-signal HEMT model is proposed that is fully compatible with large-signal modeling. The small-signal model is derived by linearization from a large-signal, charge-conserving model that uses a relaxation-time approximation. The model's topology is fully symmetrical with respect to the gate, and makes use of a comprehensive extrinsic network [C1169]

#### "GaAs Power pHEMT Characterization for Extracting Nonlinear Parameters of Drain Current by Harmonic Measurement"

This paper presents a simple method to extract nonlinear parameters of GaAs pseudomorphic high electron mobility transistor (pHEMT) for Volterra-Series analysis. With measuring the harmonic powers and phase polarities at various attenuations, the nonlinear parameters could be solved in least-square sense to reduce the measured uncertainties. The extracted data are validated by the two-tone measurements for a wide-range bias sweep [C1170]

#### "Frequency domain-based approach for nonlinear quasi-static FET model extraction from large-signal waveform measurements"

A novel approach to extract the state functions of microwave FET-type quasi-static models from large-signal waveform measurements is described. The approach employs a one-port quasi-static nonlinear state functions frequency domain-based extraction method together with a procedure to transform, by proper loading at the control terminals, the two-port extraction problem into multiple one-port extraction problems. The main advantage of this approach is that it provides directly the charge-voltage state functions, without the need to perform the integration of the incremental capacitance-voltage characteristics as required by time domain-based approaches. The performance of the resulting approach is assessed by extracting the nonlinear state functions of a HEMT quasi-static model from large-signal microwave measurements [C1171]

#### "Generic robust LVCMOS-compatible control logic for GaAs HEMT switches"

Robust digital control logic for an X-band five-bit digital attenuator and six-bit phase shifter has been developed and tested. The circuit uses an innovative combination of feedback and feed forward. The devices have been developed in the 6-inch 0.5  $\mu\text{m}$  power pHEMT process (PP50-10) of WIN Semiconductors. The use of this process results in cost effective devices with a high power capability [C1172]

#### "77GHz Low Noise Sub Block MMICs with 120 nm In<sub>0.4</sub>AlAs/In<sub>0.35</sub>GaAs Metamorphic HEMTs"

77 GHz CPW low noise sub block (LNB) MMICs, which are consisted of a 3 stage LNA and a resistive mixer, have been successfully developed by using 120nm In<sub>0.4</sub>AlAs/In<sub>0.35</sub>GaAs metamorphic high electron mobility transistors (MHEMTs). The devices show an extrinsic transconductance  $g_{m0}$  of 760 mS/mm, a maximum drain current of 750 mA/mm, and a gate drain breakdown voltage of -8.5 V. A cut-off frequency ( $f_T$ ) of 172 GHz and a maximum oscillation frequency ( $f_{max}$ ) of over 300 GHz are achieved. The LNA exhibited small signal gain of 19.2 dB and conversion gain of the LNB is measured to be 11 dB at 500 kHz IF [C1173]

#### "4-8 GHz Low Noise Amplifiers using metamorphic HEMT Technology"

This paper describes two metamorphic high electron mobility transistor (mHEMT) amplifiers with low noise in the frequency band 4-8 GHz. One amplifier contains the complete circuitry on a monolithic microwave integrated circuit (MMIC) chip and the other is configured with the input network on a low loss duroid substrate together with an MMIC. The measurements at room temperature for the MMIC gave a gain of 28 dB and a typical noise temperature of 56 K. The measurements at room temperature for the hybrid-MMIC gave a gain of 29 dB and a minimum noise temperature of 41 K. When cooled to 20 K the hybrid-MMIC obtained a

minimum noise temperature of 6 K. The hybrid-MMIC is compared to InP based hybrid LNAs at cryogenic temperature [C1174]

#### "A 100W Class-E GaN HEMT with 75% Drain Efficiency at 2GHz"

A 100W class-E GaN HEMT device has been developed for high power and high efficiency amplifier. The authors achieved superior measurement results; drain efficiency of 75%, CW output power of 100W and associated power gain of 12dB at 2.14GHz and 50V drain bias operation with acceptable frequency band characteristics in simple class-E circuit topology [C1175]

#### "Very High Performance GaN HEMT devices by Optimized Buffer and Field Plate Technology"

One of the main expected benefits of AlGaIn HEMT technology for microwave applications is related to the higher operating bias voltage achievable with these devices. However, various technological issues, concerning material properties and device technology must be properly tailored to fully exploit the potential of that kind of devices. In this work we report on the realization of HEMT device showing improved performance in terms of breakdown voltage, device isolation and reverse current leakage achieved by improved epilayer buffer properties and optimized field plate gate geometry. In particular the low defect density and the high resistivity obtained by using an HT-AlN crystallization layer for the growth of the GaN layer has lead to an effective 2DEG carrier concentration of 8 times  $10^{12}\text{cm}^{-2}$  with related mobility of  $1700\text{cm}^2/\text{Vs}$  and corresponding devices with a very high voltage breakdown ( $V_B > 200\text{V}$ ), excellent active device isolation and limited reverse current leakage [C1176]

#### "Control of Short-Channel Effects in GaN/AlGaIn HFETs"

GaN/AlGaIn HEMTs can suffer from short channel effects as a result of insufficient buffer doping. The paper show that controlled iron doping of the GaN buffer during MOVPE growth can suppress all short-channel effects in  $0.25\mu\text{m}$  gate length devices. The authors show that optimised iron doping has no effect on the RF output power or on the knee walkout (current-slump), but significantly improves the power added efficiency [C1177]

#### "Enhanced Schottky Gate and Pulsed IV Characteristics of AlGaIn-GaN HEMT on Si with Gate-annealing and SiNx Passivation"

Using the post-gate-annealing, the SiNx passivation and the post-passivation-annealing, the gate characteristics of  $0.4\mu\text{m}$  Al  $0.26\text{GaIn}$ -GaN HEMT on Si were successfully improved. With SiNx passivation using remote-plasma enhanced chemical vapor deposition, the current collapse was effectively suppressed. And it was found that annealing after passivation can improve the gate characteristics without serious change of the pulsed IV characteristics of the devices. As a result, maximum extrinsic transconductance,  $I_{\text{DSS}}$  and pulsed drain-source current are increased by 12 %, 32 % and 31 %, respectively. And the gate-drain breakdown voltage was increased from 23 V to 80 V [C1178]

#### "New drain current model for MESFET/HEMT devices based on pulsed measurements"

In this work, a new  $I_{\text{ds}}$  current equation and FET model are proposed based on DC and pulsed I/V measurements. Its implementation is based on the identification of a new function that characterizes the differences between dynamic and static conditions. The performance of the model was evaluated with scattering, DC and pulsed measurements on different kinds of devices. The results show good agreement for low-high power transistors [C1179]

#### "A Large-Signal Model of GaN HEMTs for Linear High Power Amplifier Design"

A nonlinear large-signal table-based model of AlGaIn/GaN HEMTs that able to predict output nonlinearities including intermodulation distortions (IMD) is described. The equivalent circuit model elements of the dispersive model are derived from S-parameter and pulsed DC I(V) measurements. With proper data processing and implementation, the speed and accuracy of simulations under multi-tone excitations are improved. Particularly, making the data available for larger grid voltage has minimized unrealistic extrapolation by circuit simulator. Similarly, data interpolation for denser voltage grid before implementation in the circuit simulator reduced interpolation problems. Using a continuously differentiable analytical model for the main nonlinear parameter (the drain current) can further enhance the IMD prediction capability at lower power levels [C1180]

#### "Monte Carlo Comparison Between InP-Based Double-Gate and Standard HEMTs"

The intrinsic static and dynamic performance of InAlAs/InGaAs double-gate high electron mobility transistors



(DG-HEMTs) is studied by means of an ensemble 2D Monte Carlo simulator. Our model allows going deeply into the physical behavior of this novel device in comparison with similar standard HEMTs. Different gate lengths are analyzed in order to check the attenuation of short-channel effects expected in the DG-structures. The intrinsic cut-off frequency  $f_{\text{cof}}$  of the DG-HEMTs is found to be similar to that of HEMTs, but the higher values of the figures of merit  $g_m/g_{\text{dand}}$  and  $C_{gs}/C_{\text{gdlead}}$  lead to an improvement of  $f_{\text{max}}$  [C1181]

### "An 8ГfB—8 Switch Matrix MMIC Integrating Eight InP-HEMT SP8T Switches for 10-Gbit/s Systems"

An 8times8 switch matrix MMIC using cold-FET SP8T switches is presented. InP HEMTs with a low  $R_{\text{on}} \cdot C_{\text{off}}$  product enable us to construct a dc-to-over-10-GHz SP8T switch in a series configuration. The multilayer interconnection with top-metal- and dielectric-layer thickness of 5  $\mu\text{m}$  allows us to configure interconnection transmission lines quite compactly, which is essential for wideband operation. The switch matrix IC using these technologies with a novel size-reduction technique is as small as 0.4  $\text{mm}^2$  (core area) and achieves low insertion loss ( $<3.9$  dB) and high isolation ( $>26.5$  dB) below 10 GHz. We confirmed error-free operation up to 12.5 Gbit/s with good eye openings even when eight data signals are simultaneously input to the switch IC [C1182]

### "Advanced High Power Amplifier Chain for X-Band T/R-Modules based on GaN MMICs"

Power amplifiers for a next generation of T/R-modules in future active array antennas are realized as monolithically integrated circuits on the bases of novel AlGaIn/GaN HEMT structures. Both, driver and high power amplifiers are designed for X-band frequencies. The monolithically integrated circuits (MMICs) are designed, simulated and fabricated using a novel via-hole microstrip technology. Output power levels of 1.6 W (32 dBm) for the driver amplifier (DA) and 20 W (43 dBm) for the high power amplifier (HPA) are measured. An amplifier chain circuitry, with mounted GaN DA and HPA MMICs, is designed based on a multi-layer LTCC technology [C1183]

### "Advanced Neural Network Techniques for GaN-HEMT Dynamic Behavior Characterization"

This paper presents a new approach to build RF dynamic behavioral models, based on time-delay neural networks (TDNNs), suitable for FET devices, and capable to identify the working class and to characterize both short- and long-term device memory, through a time-domain training procedure, for a wide range of input power levels. The presented model has been effectively applied to GaN-based devices, working in class A, AB and B [C1184]

### "A novel high purity, highly efficient, broadband MMIC frequency multiplier implemented in metamorphic HEMT technology"

A new principle of a high efficiency active frequency multiplier is presented. High efficiency is achieved by operating the transistor in deep Class C by using a source RC-bias-network, forcing the conduction angle to be substantially less than 180deg. The principle can also be extended to balanced frequency multipliers for higher rejection of the fundamental frequency. The 'proof of concept' is demonstrated in a practical MMIC design. This design achieves, to our knowledge, the highest reported efficiency for a balanced frequency doubler, with high bandwidth [C1185]

### "Constant Linearity Variable Gain Traveling Wave Amplifier MMIC for 1 to 26.5 GHz Applications"

This paper describes the design and test results of a constant linearity variable gain traveling wave amplifier (VGTWA) suitable for 1 to 26.5GHz applications. The constant linearity VGTWA consists of variable feedback cascode stages, input artificial transmission line, output artificial transmission line, and a drain DC biasing network. The VGTWA was fabricated by the Avago's 0.25 $\mu\text{m}$  enhancement mode PHEMT process thus requires only a positive supply for bias and control. The constant linearity VGTWA exhibits 9 +/- 2 dB of maximum small signal gain between 1 and 26.5GHz frequencies with 15dB gain control. The TGTWA exhibits 14dBm minimum output 3rdorder intercept point over the gain controlling range. The VGTWA also exhibits constant input/output return losses over the gain controlling conditions [C1186]

### "Load Pull Characterization of GaN/AlGaIn HEMTs"

This work presents a large signal characterization of a high power GaN/AlGaIn HEMT transistor utilizing a harmonic load pull setup. Two different methods for passive automated tuners have been compared to synthesize the load impedances [C1187]

### "Conversion Matrix Analysis of GaAs HEMT Active Gilbert Cell Mixers"

In this paper, the nonlinear model of the GaAs HEMT active Gilbert cell mixer is investigated. Based on the model, the conversion gain expression of active Gilbert cell mixers is derived theoretically by using conversion matrix analysis method. The expression is verified by harmonic balance simulation with Angelov HEMT model in Agilent Advanced Design System (ADS) and by chip measurement results [C1188]

### "Design Method and New Architecture of Sub-Harmonic Balanced Cold FET Mixer for MVDS Applications"

This paper reports a novel MMIC balanced sub-harmonic cold FET mixer for MVDS applications using 0.15  $\mu\text{m}$  GaAs pHEMT. The mixer, which includes a LO buffer amplifier, was optimized for highly linear up-conversion performance in the 40.5-43.5 GHz RF band, 19.5-20.5 GHz LO band and 2.45-3.45 GHz IF band. A dedicated simulation method has been developed to optimize conversion loss and determine optimum matching. To achieve better (2LO-to-RF) isolation a specific balanced architecture for sub-harmonic mixing has been elaborated. This leads to simulation results of 13 plusmn 0.5dB conversion losses associated to high IF input power at 1dB compression of 17dBm, and (2LO-to-RF) isolation of 40dB [C1189]

### "Multiphysics Simulation of Electromagnetic Shielding and Thermal Stressing within Ceramic and Silicon Multilayer Packages for RF Applications"

A multiphysics finite element method (FEM) based software, COMSOLtrade has been used to simulate coupled electromagnetic shielding and thermal stress issues for system-in-package (SiP) modules. The ceramic and silicon carriers under study have embedded shielding ground planes. Power HEMT RF devices in GaAs technologies are embedded on and within the carrier causing local thermal hotspots. Thermal cooling is performed using thermal vias. The electromagnetic interaction of thermal vias with the embedded ground plane is studied for hole clearance and via size [C1190]

### "Constant Linearity Variable Gain Traveling Wave Amplifier MMIC for 1 to 26.5 GHz Applications"

This paper describes the design and test results of a constant linearity variable gain traveling wave amplifier (VGTWA) suitable for 1 to 26.5GHz applications. The constant linearity VGTWA consists of variable feedback cascode stages, input artificial transmission line, output artificial transmission line, and a drain DC biasing network. The VGTWA was fabricated by the Avago's 0.25 $\mu\text{m}$  enhancement mode PHEMT process thus requires only a positive supply for bias and control. The constant linearity VGTWA exhibits 9+/-2 dB of maximum small signal gain between 1 and 26.5GHz frequencies with 15dB gain control. The TGTWA exhibits 14dBm minimum output 3rd order intercept point over the gain controlling range. The VGTWA also exhibits constant input/output return losses over the gain controlling conditions [C1191]

### "Sub-10 ps Pulse Generator with Biphas Modulation Function in 0.13- $\mu\text{m}$ InP HEMT"

A next-generation ultra-wideband (UWB) pulse generator with a biphas function is reported. To obtain ultrashort duration pulses, a novel speeding-up and circuit and biphas modulator circuit were developed. The IC was fabricated in a 0.13- $\mu\text{m}$ -gate InP-HEMT technology, which has gmof 1520 mS/mm and a fTof 195 GHz. A pulse with a full width at half maximum of 9 ps and a 15-ps biphas modulated pulse were obtained. The power consumption of the ICs were 620 mW and 640 mW, respectively. [C1192]

### "Sub-10 ps Pulse Generator with Biphas Modulation Function in 0.13- $\mu\text{m}$ InP HEMT"

A next-generation ultra-wideband (UWB) pulse generator with a biphas function is reported. To obtain ultrashort duration pulses, a novel speeding-up AND circuit and biphas modulator circuit were developed. The IC was fabricated in a 0.13- $\mu\text{m}$ -gate InP-HEMT technology, which has a gmof 1520 mS/mm and a fTof 195 GHz. A pulse with a full width at half maximum of 9 ps and a 15-ps biphas modulated pulse were obtained. The power consumption of the ICs were 620 mW and 640 mW, respectively. [C1193]

### "RF Dynamic Behavioral Model Suitable for GaN-HEMT Devices"

This paper presents a new RF dynamic behavioral model based on a neural network (NN) approach suitable for FET devices in a wide range of working classes, and capable to identify the device response, through the training procedure, for a wide range of input power levels. The presented model has been effectively applied to GaN-based devices at 1 GHz, working in class A and B [C1194]

### "Taking Advantage of PHEMT Nonlinear Behavior for RFID Applications"

This paper presents two frequency converting PHEMT-based active antennas to be used in RFID applications. A proper characterization of the transistor nonlinear behavior revealed the existence of two biasing regions where the response signal, the second harmonic or the IF component, can be generated with maximum conversion gain and phase opposition. This attractive issue has been taken advantage of, to BPSK modulate the response in two approaches: in a frequency doubling active antenna and in a phase conjugating circuit for retrodirective arrays. Aperture coupled patch radiators were designed, to integrate these modulators in low cost, compact and high performance transponders [C1195]

### "Class F design criteria validation through non linear load pull simulation"

In this paper an approach for class F power amplifier design criteria validation is presented. The aim is to validate class F PA design theory, which is provided by theoretical limits used for calculus simplification. The method is based on full nonlinear simulations carried on a nonlinear PHEMT device model. In particular the difference between theoretical and real optima, and the cases in which this occurs, were evidenced. For such validation a dedicated software tool using a linearization technique, were discussed [C1196]

### "Measurements of Envelope Frequency Dependent Nonlinearity in GaN HEMT Power Device"

This paper proposes a measurement setup for analyzing and measuring the nonlinearity and memory effects in active power device as well as power amplifier (PA). In order to reduce the memory effect in the measurement data, new dynamic measurement setup with combination of two bias tees is developed for realizing short termination at envelope frequencies. Furthermore, for full automatic control of the measurement setup, controlling software using Agilent VEE programming software is developed. Moreover, measurement of envelope frequency dependent nonlinearity in GaN HEMT power device is presented [C1197]

### "Bias Selection for Conversion and Linearity Optimization in a GaN HEMT Resistive Mixer"

In this paper, an experimental GaN HEMT grown on sapphire substrate is employed for designing and testing a resistive mixer. Based on an appropriate characterization of the transistor output conductance and its higher order derivatives, the gate-to-source bias voltage may be selected for optimizing the conversion loss, while the use of a small drain-to-source bias value helps improving its linearity. Simulation and measurement results are provided, demonstrating a significant reduction of third order intermodulation distortion, about 14 dBs less than the true cold FET operation case, maintaining the same information signal level at the output [C1198]

### "GaN HEMT Technology Development Assessment through Nonlinear Characterization"

HEMT devices based on AlGaIn/GaN heterostructures exhibit constantly improving power performances. Nonlinear characterization is needed at each new device generation, both to assess the maximum power capabilities and to guide the next technological step, by highlighting open problems related to the device layout or material defects. This paper demonstrates the capabilities of the Politecnico di Torino dedicated test-set to nonlinear characterization of SELEX-SI GaN HEMTs, including the investigation of the device scaling properties and the maximum output power in different classes of operation and with several loading condition. The set-up overcomes measurements problems related to high power dissipation and device heating, high output reflection coefficients required for optimum load conditions, and the risk of device damage as a consequence of high voltage operation. The acquisition of the time-domain gate and drain waveforms together with a real-time active load-pull characterization is shown to lead to better insight into the device power performances [C1199]

### "Phase Characterization of Intermodulation Products Including Electrothermal Memory Effects"

This communication presents a model for an equivalent hypothetical load impedance which improves the correspondence between simulations and experimental measurements in microwave HEMT amplifiers with memory effects that are not explained using purely electrical models and may thus be attributed to thermal effects. The proposed load impedance has been obtained from measurements of magnitude and phase for third-order intermodulation (IM) products accomplished by a simple but effective experimental method based on a two-tone test. Closed-form theoretical expressions for the IM products are derived employing a Simplified Newton (SN) approach, concluding that IM products's variation with frequency separations is related to the load impedance seen by the drain node of the amplifier. An equivalent load impedance and its circuit model are presented, and a good agreement between measurements and simulations is achieved when they are inserted [C1200]

### "Power Amplifier Design Strategy to null IMD asymmetry"



In this contribution the minimisation of the asymmetry between lower and upper sideband intermodulation products is discussed, using a Volterra series approach. From the inferred relationships new conditions to minimise IMD asymmetry are obtained and verified through the design of a C-band 2nd harmonic tuned hybrid power amplifier using a GaN PHEMT device. The proposed approach, without linearization schemes, achieves the minimisation of AM-PM conversion and asymmetry up to 400 MHz tone spacing, with a minimum 32.5 dBm output power and over 60 % drain efficiency @ 5.5 GHz [C1201]

#### **"A High-Performance 14.4 to 19.7 GHz Power Detector Fabricated with Flip-Chip Technology"**

A rugged flip-chip technology with potential for low cost at high manufacturing volume was employed to fabricate a power detector using mixed device technologies. The circuit consists of one discrete GaAs pHEMT chip and one GaAs dual-Schottky-diode chip flip-attached to a 3.5 mm by 2.1 mm substrate containing only passive circuitry. The power detector offers two different modes of operation to enable compensation for drift of the detector diode response over temperature [C1202]

#### **"30-Watt Power Amplifier for 3.5GHz WiMAX Base station Application"**

This paper describes the design of a 30W GaAs pHEMT PA (power amplifier) for WiMAX applications. The PA is realized on a CuW carrier with various ceramic matching components. The PA attained 10dB small signal gain and 30W CW output power with a drain efficiency of around 60% at a supply voltage of 12V. Under WiMAX 802.16-2004 OFDM modulation (3.5MHz BW, 64QAM sub carrier modulation and peak to average ratio of 10dB) the PA achieves better than 2% EVM (error vector magnitude), -45dBc ACPR (adjacent channel power ratio) at 34dBm (2.5W)  $P_{avg}$  (average output power) with 16% average drain efficiency in a frequency band of 3.3-3.7GHz [C1203]

#### **"Novel Instability-Probing Simulation for Power Amplifiers"**

A novel instability-probing simulation for power amplifiers is presented. Instabilities of power amplifiers with use of very-high performance pHEMT should be observed from a single-gate pHEMT among the multi-gate configuration of the pHEMT, where the power amplifiers are not yet symmetric. A conventional orthogonal (even- and odd-) mode analysis, based on the symmetric power combining, is not complete to predict various instabilities in the power amplifiers. This paper demonstrates a novel instability-probing simulation method that incorporates an ideal transformer. The proposed method successfully predicted microwave and millimeter-wave spurious oscillations observed for a Ku-band MMIC power amplifier [C1204]

#### **"Comparative investigation between a single ended and a balanced IF VGA"**

Variable gain IF amplifier (VGA) based on single ended and Gilbert Cell topology have been designed and characterized. A comparative investigation has been carried out between the two topologies. The source feedback topology has been used for the single ended VGA and for the Gilbert Cell VGA, the gain is controlled by steering the drain current. Overall dynamic gain variation range is 13 dB with a maximum gain of 13 dB for the single ended VGA whereas for the Gilbert cell VGA, it is 16 dB and 10 dB, respectively. The -3 dB bandwidth is 4 GHz and the maximum value of 1 dB output compression is -6.2 dBm for the single ended VGA. The measured IP3 is 8.2 dBm referred to the output. DC power consumption is 75 mW. For the Gilbert Cell VGA, the -3 dB bandwidth is 2.25 GHz and maximum dissipated DC power is 100 mW. Maximum value of 1 dB compression point and IP3, both referred to the output, are 2 dBm and 9.87 dBm, respectively. Both the circuits were implemented on 0.15μm GaAs pHEMT technology. The active circuit area of Gilbert Cell VGA is 1.7 mm times 1.6 mm and the single ended VGA is 1.3 mm times 1.3 mm [C1205]

#### **"A Switch-Type Power Amplifier and Its Application to a CDMA Cellphone"**

To address the demand for miniaturization and low cost in a cellphone, we aimed to eliminate the isolator and DC-DC converter. We propose a novel switch-type power amplifier (PA) using a strong junction PHEMT (JPHEMT) PA instead of HBT from the point of view of the performance under load-impedance variation. In high output power mode, the performance of this PA is the same as that of the conventional PA. In low output power mode, it operates as a single-stage PA and satisfies distortion characteristics without causing deterioration of efficiency [C1206]

#### **"A G-Band 160 GHz T/R Module Concept for Planetary Landing Radar"**

In this work, the concept of a G-band transmit/receive (T/R) module centered at 160 GHz was discussed. The design makes use of state-of-the-art G-band MMIC low noise amplifiers and power amplifiers, and a high speed SPDT InGaAs PIN diode switch. The paper reports on the designs, chip results, and the integration concept for a

160 GHz T/R module. The G-band T/R module has applications toward precision altimetry and velocimetry measurements in landing radar, such as in future planetary landers on the surface of Mars [C1207]

#### "Microwave Class-F and Inverse Class-F Power Amplifiers Designs using GaN Technology and GaAs pHEMT"

This paper presents the designs and results of two high-efficiency harmonics-tuned microwave power amplifiers (PA): the first one is a 2 GHz class-F PA in monolithic integrated circuit (MMIC) by using GaN HEMT technology, and the other one is a 2.45-GHz inverse class-F PA using packaged GaAs pHEMT devices with PCB technology. In the class-F MMIC PA, field-plated GaN HEMT device is used for high-power performance. The 2.0-GHz class-F MMIC PA achieves a PAE of 50%, 38 dBm output power, and 6.2 W/mm power density. The inverse class-F PA at 2.45 GHz achieves 22.6 dBm output power and 73% PAE at 3 dB compression, and has very low cost [C1208]

#### "Proton Tolerance of InAs Based HEMT and DHBT Devices"

The paper presents measurements of proton induced degradation in emerging low power high performance InAs based devices, including InAs/AlSb high electron mobility transistors (HEMT) and In<sub>0.86</sub>Ga<sub>0.14</sub>As base 6.0 År lattice constant double heterojunction bipolar transistor (DHBT) devices [C1209]

#### "Compact K-band Watt-level GaAs PHEMT Power Amplifier MMIC with integrated ESD protection"

The performance of a compact K-band power amplifier MMIC fabricated in standard 6-inch 0.15-μm GaAs power PHEMT technology is reported. The circuit features on-chip ESD protection including input short-circuit stub, dual capacitors at RF ports and high-current diode arrays on each gate pad. Occupying less than 3 mm<sup>2</sup>, this 3-stage power amplifier achieves a linear gain of more than 20 dB over the 17- to 24 GHz frequency range with 6-dB noise figure. It also delivers a CW output power of more than 29- and 30 dBm, in the 17-20 GHz band, at 5- and 6 V respectively. Preliminary ESD characterization shows the circuit withstands 180-V in human body model test (tester limit), and 100-V machine model (equivalent to at least 500-V HBM), without DC or RF performance degradation. Finally, performance in standard 24-lead plastic QFN package (4 times 4 mm<sup>2</sup>) is presented: the device exhibits more than 17.5-dB linear gain over 17-24 GHz, with P-1dB greater than 28-dBm in the 17.7-19.7 GHz radio range [C1210]

#### "Advances in GaN-based discrete power devices for L- and X-band applications"

Progress in fabrication of packaged discrete L- and X-band power AlGaIn/GaN HFETs is presented. By exploiting typical GaN HFET related features such as improved linearity, power density, gain and broad band capability the devices allow for novel architectures for base stations in mobile communications and for space applications. Highlights to be presented are L-band power bar devices designed for continuous wave (cw) operation delivering an cw output power of 30 W and 100 W with 20 dB and 14 dB linear gain respectively. The architecture of these devices is based on novel gate "feed plate" structures. Furthermore discrete, hermetically packaged X-band devices for space based SSPAs in the power range of 10 W (continuous wave) at 8 GHz are presented [C1211]

#### "44-GHz High Power and Driver Microstrip Amplifier MMICs using 6-inch 0.15-μm PHEMTs"

A family of robust and cost effective 44-GHz microstrip MMIC power amplifiers has been developed based on a standard 6-inch, 0.15-μm GaAs power pHEMT production process on 100-μm substrate thickness. These amplifiers provide high output powers at 44-GHz with a MTTF exceeding two million hours at 75degC backplate temperature. The single-ended, 3-stage amplifier MMIC has more than 15 dB small signal gain at 44 GHz and 28 dBm output power for a chip area of 5.6 mm<sup>2</sup>. For the same frequency band, a balanced 1.25-W power amplifier and a doubly-balanced 2.25-W amplifier achieved linear gain of more than 18 dBm and better than -20 dB S<sub>11</sub> and S<sub>22</sub>, with chip areas of 10.8 and 21.5 mm<sup>2</sup> respectively. To our knowledge, in terms of power and power density per chip area, these results are among the highest output power levels reported to date at this frequency for single chip MMICs on 100-μm substrate with acceptable lifetime [C1212]

#### "An Efficient and Accurate Approach for Characterizing Non-Linear Capacitance in MESFET/HEMT Devices"

This paper presents an accurate and efficient approach of characterizing the non-linear capacitance in MESFET/HEMT devices. This approach utilizes a feed-forward neural network program using the back-propagation method with the Levenberg-Marquardt (LM) algorithm implemented. Using the LM algorithm provides accurate modeling of the non-linear capacitance with minimal training time. This approach is truly

independent of device process and technology, and can therefore be applicable to FET devices from SiC, GaN, MOSFETs to GaAs and InP HEMTs. Excellent agreement is also observed between the novel approach and measured results. [C1213]

#### "GaN HEMT Performance-Measurements and Simulations of a 3.6 mm Device from Cree"

The premise of GaN HEMT devices to offer superior power amplification performance in microwave frequencies lead to an extensive research in this field, and to numerous publications emphasizing individual performance records such as, current and power densities, linearity and break down voltage. The performance of these, primarily experimental devices, is often reported in the terms of their intended applications, offering either the saturated output power, or 3dB compressed output power, or OFDM and CDMA waveform-specific output power, making the comparison among the devices, and a comparison with other technologies such as LDMOS and GaAs rather difficult. The authors are engaged in the design of a wideband (10:1 BW) 50W at 1dB compression point linear power amplifier operating up to 2GHz. As a step in this process the performance of an actual, 3.6 mm periphery, pre-production GaN HEMT from CREE was determined. The device performance is simulated using CREE model, and it is compared with the measurements that were taken, both reported in this paper. The results obtained exhibit good convergence with the model, and are presented using the more common performance parameters such as power and efficiency at 1dB compression point, and the linearity in terms of IP3 [C1214]

#### "Temperature analysis of AlGaIn/GaN High-Electron-Mobility Transistors using micro-Raman scattering spectroscopy and Transient Interferometric Mapping"

The paper reports on the measurement of the temperature, i.e. self-heating effects, in active AlGaIn/GaN HEMTs grown on sapphire substrate. Micro-Raman spectroscopy is used to measure temperature with 1  $\mu\text{m}$  spatial resolution and 10degC temperature accuracy under the DC conditions. Transient interferometric method combined with a thermal simulation is used for analysis in the transient state. The results match well the results obtained by an electrical method performed both in DC and transient mode. The thermal resistance of 210 K/W (280 K/W) has been determined for 8 (2) finger device [C1215]

#### "A Low Phase Noise Microwave Oscillator with a Miniaturized LTCC Resonator for SIP Design"

This paper presents an oscillator employing miniature, high-Q, low temperature cofired ceramic (LTCC) resonator in conjunction with a novel implementation technique for achieving low phase noise. The reduced-size LTCC resonator is realized with a dielectric material having  $\epsilon_{\text{r}} = 68$ , the first ever reported. As well, the oscillator circuitry design exploits the seldom used device-line technique for obtaining the lowest possible phase noise with any chosen component. A free-running, 6 GHz oscillator using GaAs p-HEMT active device is built in a planar hybrid format suitable for system-in-package (SIP) designs. The measured phase noise is -125 dBc/Hz at 1 MHz offset, with over 8 dBm of output power, which compares favorably with the best C-band oscillators. The technique herein demonstrates the feasibility of miniaturized, low-cost, SIP products [C1216]

#### "A V-band MMIC Self Oscillating Mixer Active Integrated Antenna Using a Push-Pull Patch Antenna"

In this paper, a V-band MMIC self oscillating mixer active integrated antenna using a push-pull patch antenna is presented. The SOM AIA is based on the coupled active parallel feedback oscillator. By using a push-pull patch antenna, the isolation between balanced RF input and in-phase local oscillation is established. Furthermore, since the push-pull patch antenna has very low radiation efficiency for the in phase signal injection, the LO radiation was efficiently suppressed. The circuit is fabricated using the 0.15 $\mu\text{m}$  pHEMT process on 100 $\mu\text{m}$  thick GaAs substrate. The local oscillation frequency is 58.46GHz. The LO radiation level is measured to be lower than -50dBm at distance of 1cm. The circuit shows about -18.9dB effective isotropic conversion gain at 1.54GHz IF [C1217]

#### "AlGaIn/GaN HFETs on Si Substrates for WiMAX Applications"

AlGaIn/GaN HFETs on Si substrates are tested under OFDM modulations and show excellent performance from 3.3GHz to 3.8GHz. Performance on an 8mm device (NPT35010) in power small outline package (PSOP2) shows 1.5W output power, 11.2dB gain, 28.6% drain efficiency and 2% EVM at 3.5GHz. Large periphery 36mm devices were mounted in ceramic packages (NPT35050) and showed greater than 7W output power, > 11dB gain, 27.2% drain efficiency and 2% EVM at 3.5 GHz. Additionally data was taken across process from 23 devices and 5 process lots to demonstrate repeatability. Finally the same RF data was collected over flange temperature from -40degC to +85degC and demonstrated stable performance over temperature. These results demonstrate

the potential for GaN-on-Si HEMTs for use in WiMAX applications [C1218]

#### "Single function drain current model for MESFET/HEMT devices including pulsed dynamic behavior"

A new approach to modeling the dynamic behavior of microwave devices based on pulsed measurements is presented. DC and pulsed I/V characteristics of these devices are modeled using a single function derived from an existing and well-established MESFET/HEMT nonlinear static current model. The robust methodology in this work can be applied to other current models and subsequently implemented into a new large-signal circuit as a single current source, capable of accurately predicting both static and small-signal performance of FET devices [C1219]

#### "A Compact W-Band Dual-Channel Receiver Module"

A very compact W-band dual-channel receiver module has been developed for use in active and passive high-resolution imaging systems. The WR-10 waveguide module contains two fully integrated heterodyne receiver MMICs which have been realized using a 0.1  $\mu\text{m}$  InAlAs/InGaAs based depletion type metamorphic high electron mobility transistor (MHEMT) technology in combination with conductor-backed coplanar circuit topology (CBCPW) and cascode transistors, thus leading to a very low noise figure and high conversion gain at millimeter-wave frequencies. The MMICs consist of a two-stage low noise amplifier, a balanced resistive HEMT mixer, and a single-stage local oscillator (LO) buffer amplifier. To divide the LO-signal a magic-T was embedded in the WR-10 waveguide module. The assembled dual-channel front end achieved a conversion gain of 7 dB and a noise figure of 4 dB over the frequency range from 75 to 100 GHz with an LO-power of only -5 dBm [C1220]

#### "An RF Chipset for Impulse Radio UWB Using 0.13 $\mu\text{m}$ InP-HEMT Technology"

A novel ultra wideband impulse radio architecture for 24 GHz-band short-range radar was developed using 0.13  $\mu\text{m}$  InP-HEMT technology. The transmitter part generates an extremely wide band impulse from a pulse generator and then filters it by using a band pass filter (BPF). The obtained impulse shows a bandwidth of over 40 GHz and achieves flatness in the target band. The power amplifier (PA) for the transmitter has a gain of 15 plusmn 0.05 dB, and the low noise amplifier (LNA) for the receiver has a gain of 40 plusmn 1 dB. The achieved flatness of the integration gain including the PA, LNA, and RF-switch is less than plusmn 1.1 dB. These RF circuits with gain flatness make possible a simple matched filter configuration without the use of a conventional correlator composed of a local oscillator [C1221]

#### "Ultra-High-Speed Low-Noise InP-HEMT Technology"

InP-based high electron mobility transistors (InP-HEMTs) with an ultra-high current gain cutoff frequency ( $f_T$ ) of over 550 GHz and a maximum oscillation frequency ( $f_{\text{max}}$ ) of 500 GHz are realized. The excellent performance is achieved through lateral and/or vertical device scaling in combination with a reduction of parasitic resistances and capacitances. Key device technologies for ultra-high-speed, low-noise performance are described [C1222]

#### "4-Watt Ka-Band AlGaIn/GaN Power Amplifier MMIC"

A broadband Ka-band AlGaIn/GaN on SiC HEMT power amplifier MMIC was developed for millimeter-wave antenna applications. The output stage is composed of a 1.2-mm-wide device with 0.18  $\mu\text{m}$  gate length. The two-stage 50-ohm matched MMIC produces 13plusmn1 dB of gain from 26 GHz to 36 GHz. At 35 GHz, the measured CW saturated output power was 4 W, indicating a power density of 3.3 W/mm. The power added efficiency was 23%. Across the band, the measured CW output power was > 2 W. While individual (or partially matched single stage) devices have been demonstrated with good output power, to the best of our knowledge, this is the first report of a 10 GHz-bandwidth Ka-band GaN MMIC with high output power, gain, and return loss [C1223]

#### "W-Band Oscillator on Metamorphic HEMT"

We present for the first time an un-buffered W-band oscillator on a metamorphic HEMT GaAs substrate. The oscillator has an output power of +1.5 dBm and a phase noise of -101 dBc/Hz at a 1 MHz offset. This oscillator will be part of an integrated monolithic front end [C1224]

#### "Design of a X-band GaN oscillator: from the low frequency noise device characterization and large signal modeling to circuit design"

Although GaN technologies were initially developed for solid state source amplifiers, it was recently



demonstrated that AlGaIn/GaN HEMT transistors were also suitable for low noise applications such as LNA (Tartarin et al., 2005). The frequency synthesis is not yet widely explored for these technologies. In this paper the design of a low phase noise X-band oscillator is proposed. The low frequency noise performance and the residual phase noise, as well as dynamic S-parameters were carried out on AlGaIn/GaN HEMT grown on SiC. A large-signal modeling technique is also presented. The reduced complexity and the good accuracy of our large signal model permits an efficient circuit design, without intensive knowledge of the technological device parameters. These characterization and modeling tools are used for the design of an 1-stage oscillator working at 10 GHz delivering 20dBm [C1225]

#### "20W GaN HPAs for Next Generation X-Band T/R-Modules"

High power amplifiers for a next generation of T/R-modules for future X-band active array antennas are realized on the bases of novel AlGaIn/GaN HEMT structures, which are epitaxially grown on SiC wafer substrates. Both, hybrid and monolithically integrated circuits are designed and realized as key elements for transmit chains. Based on hybrid designs excellent peak power levels of 23 W (43.6 dBm) with an associated power added efficiency (PAE) of 29% are realized. Over a bandwidth of 2 GHz (X-band) the output power levels are above 20 W. In a more sophisticated approach first monolithically integrated circuits (MMICs) are designed, simulated and fabricated using a novel via-hole microstrip technology. Output power levels of 20 W (43 dBm) with an associated PAE of 30% are measured on small size 12 mm<sup>2</sup> chips. Highest ever reported maximum power added efficiency values of up to 36.5% are achieved [C1226]

#### "Performance and RF Reliability of GaN-on-SiC HEMT's using Dual-Gate Architectures"

AlGaIn/GaN HEMTs on SiC have been fabricated with dual and single gate device geometries. Subthreshold characteristics and drain bias dependence of large signal parameters were compared to identify differences in electric field. Degradation under RF stress reveals the relative impact of temperature and electric field. The results illustrate the beneficial effects of the dual gate geometry for performance and reliability [C1227]

#### "A 45% Drain Efficiency, -50dBc ACLR GaN HEMT Class-E Amplifier with DPD for W-CDMA Base Station"

A 10W GaN HEMT class-E amplifier for W-CDMA base station is demonstrated in this paper. We first demonstrate that a low pass type class-E circuit has quite similar performance to widely used series L-C resonance class-E circuit by simulating voltage and current waveforms with 50V operation GaN HEMT at 2.1GHz. We achieved measurement results; drain efficiency of 82%, CW output power of 11W and linear gain of 19.5dB at 2.1GHz and 50V drain bias operation with a simple low pass class-E circuit. And ACLR of -50dBc was obtained with 45% drain efficiency under 2-carrier W-CDMA, 7.8dB PAR (0.01%) signals, by using digital pre-distortion (DPD) operation [C1228]

#### "A 500W Push-Pull AlGaIn/GaN HEMT Amplifier for L-Band High Power Application"

We have successfully developed a 500W AlGaIn/GaN HEMT power amplifier with a frequency of 1.5GHz in L-Band, operating at 65V drain bias voltage. This amplifier consists of 4-chips of HEMT die developed for L-band frequency operation with push-pull configuration. The developed amplifier has an output power of 500W and a high linear gain of 17.8dB at the frequency of 1.5GHz under pulsed conditions at a duty of 10% with a pulse width of 100msec. To the best of our knowledge, this is the highest power ever reported for L-band GaN-related amplifier [C1229]

#### "Accurate Large-Signal Modeling of AlGaIn-GaN HEMT Including Trapping and Self-Heating Induced Dispersion"

An accurate large-signal model for AlGaIn-GaN HEMT is presented. This model is derived from a distributed small-signal model that efficiently describes the physics of the device. An improved drain current model accounts for trapping and self-heating effects is implemented. The model shows very good results for simulating the high-power operation of a 8times125μm gate width AlGaIn-GaN HEMT even beyond the 1-dB gain compression point [C1230]

#### "Evaluation of GaN HEMT Technology Development Through Nonlinear Characterization"

This paper presents a comprehensive evaluation of GaN HEMT technology development on SiC substrates, relying on an electro-thermal model validated against DC, pulsed DC and S-parameter measurements. The measured devices are backside mounted, but the layout is also conceived for flip-chip mounting. Based on accurate estimation of the device thermal resistance, the model enables to explore and assess the device



performances in both backside and flip-chip configurations; results are shown both for conventional ceramic AlN flip-chip mountings, and for advanced (diamond) heat sinks [C1231]

### "Low Specific On-Resistance AlGaIn/GaN HEMT on Sapphire Substrate"

On-resistance of AlGaIn/GaN HEMTs with MIS and MES gate structures has been investigated. In the case of the MES gate structure, the HEMT with specific on-resistance lower than  $0.1 \text{ m}\Omega\text{cm}^2$  was obtained by shortening the drain-source length to  $2.2 \text{ }\mu\text{m}$ . The maximum transconductance  $g_{m,\text{max}}$  and the off-state breakdown voltage were  $220 \text{ mS/mm}$  and  $35 \text{ V}$ , respectively. Tradeoff characteristic of the specific on-resistance and the breakdown voltage of the AlGaIn/GaN MES-gate HEMT exceeded theoretical limit of Si-based devices. In the case of the MIS-gate HEMTs, by shortening the source-drain length to  $1.8 \text{ }\mu\text{m}$ , the specific on-resistance lower than  $0.17 \text{ m}\Omega\text{cm}^2$  and the maximum drain current of  $920 \text{ mA/mm}$  were obtained [C1232]

### "Power amplifier linearization using a diode"

The emphasis on higher data rates and spectral efficiency has driven the industry towards linear modulation techniques such as QPSK, 64 QAM, or multi-carrier configurations. The result is a signal with a fluctuating envelope which generates intermodulation distortion (IMD) from the power amplifiers. Since most of the IM power appears as interference in adjacent channels, it is important to use a highly linear power amplifier. This paper describes the novel approach of using a diode as an active linearizer in view of minimizing non linear distortion introduced by the power amplifiers in wireless communication circuits. In case of pHEMTs, this technique reduces the effect of nonlinear terms generated by the voltage variable input capacitance of the active device. A two stage power amplifier using  $0.5 \text{ }\mu\text{m}$  gate length GaAs pHEMT process shows that the power amplifier is linear up to  $5 \text{ dBm}$  of input power after linearization, where as it becomes nonlinear at  $-4 \text{ dBm}$  of input power before linearization [C1233]

### "Feasibility Study of AlGaIn/GaN HEMT for Multi-megahertz DC/DC Converter Applications"

The DC and AC characteristics of a  $30 \text{ V}$  AlGaIn/GaN HEMT was investigated by numerical simulations. By properly model the 2DEG in the AlGaIn/GaN interface, we obtain a maximum transconductance of  $221 \text{ mS/mm}$ , a saturation current density of  $1.28 \text{ A/mm}$ , a specific  $R_{\text{dson}}$  of  $2.5 \text{ m}\Omega\text{-mm}^2$ , a specific  $Q_{\text{gd}}$  of  $0.62 \text{ nC/mm}^2$  and the value of FOM of  $1.6 \text{ m}\Omega\text{ganC}$ . The comparison with of the state-of-the-art Si-LDMOS and Si-Trench MOSFET were carried out and the results indicate that HEMTs could be a good candidate for very high frequency DC/DC converter applications [C1234]

### " $0.07 \text{ }\mu\text{m}$ InP HEMT MMIC Technology for G-band Power Amplifiers"

First Page of the Article [C1235]

### "Efficient ANN based noise modeling of microwave FETs against temperature"

An improved noise modeling technique for microwave MESFET/HEMT versus temperature is presented. It is based on an artificial neural network (ANN) that produces noise parameters as its outputs for device temperature, S parameters and frequency at its inputs. Once trained, the proposed model can be used for efficient prediction of transistor noise parameters over a wide temperature range. Since the model is based on ANN, all noise-generating mechanisms are included and therefore it is more accurate than empirical transistor models, as it is shown on a numerical example [C1236]

### "Ultra-Low-Power Wideband High Gain InAs/AlSb HEMT Low-Noise Amplifiers"

Two antimonide-based compound semiconductor (ABCS) microstrip MMICs, single-stage and three-stage ultra-low-power wideband  $0.01\text{-}11 \text{ GHz}$  low-noise amplifiers using  $0.1\text{-}\mu\text{m}$  gate length InAs/AlSb metamorphic HEMTs, have been fabricated and characterized on a GaAs substrate. From  $0.3\text{-}11 \text{ GHz}$ , the single-stage wideband LNA demonstrated a typical associated gain of  $16 \text{ dB}$  with less than  $1.7 \text{ dB}$  noise figure ( $2\text{-}11 \text{ GHz}$ ) at  $5 \text{ mW}$  DC power dissipation, and the three-stage wideband LNA demonstrated a typical associated gain of  $30 \text{ dB}$  with less than  $2.6 \text{ dB}$  noise figure ( $2\text{-}11 \text{ GHz}$ ) at  $7.5 \text{ mW}$  DC power dissipation. We believe these low noise amplifier MMICs demonstrate the lowest DC power consumption with the highest gain-bandwidth product of any MMIC to date. These results demonstrate the outstanding potential of ABCS HEMT technology for ultra-low-power wideband applications [C1237]

### "Very Compact High-gain Broadband Low-noise Amplifier in InP HEMT Technology"

We successfully developed an InP high electron mobility transistor (HEMT) low-noise amplifier (LNA) using

multi-layer transmission lines. The fabricated five-stage LNA achieved a 43 dB gain with a noise figure (NF) of 1.9 dB at 23 GHz and a gain of more than 40 dB from 18 to 43 GHz. The maximum gain was 49.5 dB at 32 GHz and the chip size was only 1.8 times 0.9 mm<sup>2</sup>, resulting in a gain density of 30.5 dB/mm<sup>2</sup>. To the best of our knowledge, this gain density is the highest performance in any Ka-band LNA reported to date. In addition, the design accuracy of the LNA was also demonstrated [C1238]

#### "Full Ka-band High Performance InP MMIC LNA Module"

A 0.1-μm InP HEMT Ka-band LNA with high and flat gain, very low noise figure and low VSWR has been developed. Across the entire Ka-band, of 26 GHz to 40 GHz, the MMIC LNA demonstrated associated gain of 21.9 plusmn 0.9 dB and an average noise figure of 1.5 dB with a minimum of 1.3 dB at 34 GHz. The LNA chip was cryogenically cooled to 12 K where it exhibited an associated gain of 23.0 plusmn 1.1 dB and an average noise temperature of 15.5 K, i.e. 0.23-dB noise figure. Two LNA chips were cascaded and assembled into a module. At room temperature, the module achieved an associated gain of 37.6 dB plusmn 1.8 dB and an average noise figure of 1.3 dB. At 15 K, the average noise temperature was improved to 11.4 K with 41.0 plusmn 2.4 dB associated gain [C1239]

#### "An Introductory Course in Nanoelectronics at the Senior/Graduate Level"

This paper describes the rationale, organization and topic coverage for a course introducing seniors and first year graduate students in electrical engineering and related disciplines to the exciting and revolutionary developments occurring in the electronics realm at the nanoscale, i.e. nanoelectronics. Included is a survey and introduction to carbon nanotube based FETs, devices based on electron spin (spintronics), nanowires and nanotransistors, single electron transistors and molecular electronics. Also examined are recent advancements in silicon devices, such as nanoscale and strained MOSFETs, multigate MOSFETs (FinFETs) and compositional grading at the nanoscale in SiGe HBTs. The bandgap engineering of multilayer semiconductor structures at the nanoscale and its use in modern III-V HEMTs, HBTs and quantum structures is also surveyed. Finally, briefly introduced are a variety of new nanoscale fabrication technologies that are emerging, such as micro-contact and dip pen nanolithography, and recently developed nanoscale imaging techniques, such as atomic force microscopy. While the available time in a single quarter or semester course does not permit an in-depth discussion of these topics, the course is intended to acquaint the student with the most recent developments at the forefront of the electronics field, to excite their curiosity and imagination, and to provide the student with a basic understanding of the underlying concepts to enable subsequent study. [C1240]

#### "High Performance AlGaIn/GaN HEMT Switches Employing 500°C Oxidized Ni/Au Gate for Very Low Leakage Current and Improvement of Uniformity"

The electrical characteristics of HEMT such as leakage current and breakdown voltage were improved considerably by oxidation of Ni/Au Schottky gate of HEMT. Leakage current was decreased from 4.2μA to 3.3nA and uniform high breakdown voltage of ~480V was obtained with floating gate. On-resistance was also decreased from 4.32mΩ-cm<sup>2</sup> to 3.89mΩ-cm<sup>2</sup> when oxidation time was 5min due to the improvement of the 2DEG which was increased from 7.82times10<sup>12</sup>/cm<sup>2</sup> to 9.61times10<sup>12</sup>/cm<sup>2</sup>. Our experimental results show that oxidation of Ni/Au Schottky gate which is rather simple may be suitable for improvement of AlGaIn/GaN HEMT [C1241]

#### "GaN Switching Devices for High-Frequency, KW Power Conversion"

Large periphery GaN HEMT switches were designed and fabricated using field-plated gates on semi-insulating SiC substrates. The device layout was designed to handle both large currents and support the high bias conditions required for 100V switching. Blocking voltage of >200V was achieved on devices with saturation currents of 0.8A/mm. The switching characteristics of devices with gate periphery of 30-60mm were measured with both resistive and inductive loads, and showed rise- and fall-times of <25ns. Turn-on and turn-off switching losses of 11 μJ were measured at 100V/11A switching in resistive load. Maximum switching currents of 8 and 23A were measured with an inductive load at 60 and 40V, respectively. These results are the first demonstration of high-power (920W), high-speed (<25ns) switching of GaN devices for kW power conversion applications [C1242]

#### "The Perspective Structures for Microwave Heterotransistors for Communication Techniques"

This information contains the main elementary base of nanoheterostructural electronics, which combines high electron mobility transistors (HEMT), heterojunction bipolar transistors (HBT) and GaN transistors [C1243]

### "Single-Chip 60 GHz Transmitter and Receiver MMICs in a GaAs mHEMT Technology"

Single-chip 60 GHz transmitter (TX) and receiver (RX) MMICs have been designed and characterized in a 0.15  $\mu\text{m}$ ,  $\sim 120\text{ GHz fT/} > 200\text{ GHz fMAX}$  GaAs mHEMT MMIC process. This paper describes the second generation of single-chip TX and RX MMICs developed in our group. Compared to our first designs in a commercial pHEMT technology, the MMICs presented in this paper show the same high level of integration but occupy smaller chip area and have higher gain and output power at only half of the DC power consumption. The system operates with an LO signal in the range 7-8 GHz. This LO signal is multiplied in an integrated multiply-by-eight (times8) LO chain, resulting in an IF center frequency of 2.5 GHz. The single chip TX MMIC consists of a balanced resistive mixer with an integrated ultra wideband IF balun, a three-stage amplifier and the times8 LO chain. The times8 is a multifunction design by itself consisting of a quadrupler, a feed back amplifier, a doubler, and a buffer amplifier. The TX chip delivers 4.1 plusmn 1.5 dBm over an RF frequency range of 56.5 to 64.5 GHz. The peak output power is 5.6 dBm measured at 60 GHz and the overall TX chip consumes 420 mW of DC power. The single chip RX MMIC contains a three-stage low noise amplifier, an image reject mixer with an integrated ultra wideband IF hybrid and the same times8 as used in the TX chip. The RX chip has more than 10.7 dB gain between 54.5 and 64.5 GHz and more than 13 dB of image rejection ratio between 57.5 and 67.5 GHz with a peak image rejection ratio of 22.5 dB at 64 GHz. The input referred third order intercept point, IIP3 is measured to -10 dBm at 60 GHz and the overall RX chip consumes 450 mW of DC power [C1244]

### "A Low Power/Low Noise MMIC Amplifier for Phased-Array Applications using InAs/AlSb HEMT"

In this paper, we present a two-stage low-power/low-noise MMIC amplifier. At 10-GHz, the amplifier demonstrates high gain ( $\sim 18\text{-dB}$ ) and moderate noise figure ( $< 1.8\text{-dB}$ ) at a total DC power consumption of only 1.38-mW. The ultra-low power MMIC amplifier utilizes InAs/AlSb metamorphic HEMT technology, which enables a low-power/low-noise operating point of 0.15-V and 40-mA/mm for each gain stage, considerably lower than either InP or GaAs low-power bias points. The compact design ( $1.6\text{times}2.6\text{-mm}^2$ ) is realized in coplanar waveguide architecture (CPW), including CPW spiral inductors [C1245]

### "Impact of AlN Interlayer on Reliability of AlGaIn/GaN HEMTS"

RF stability measurements have been performed on over 300 MBE and MOCVD grown devices with and without a thin ( $\sim 10\text{ Å}$ ) AlN interlayer located between the AlGaIn barrier and GaN channel. 70 % of devices with the AlN interlayer showed an increase in gate leakage during RF stress, while only 28 % of the devices without the AlN interlayer showed an increase in gate leakage during RF stress. An increase in gate leakage is inconsistent with increased trapping as the degradation mechanism for decreased output power. The unusual increase of gate leakage in devices with AlN interlayers was further explored. The results suggest one mechanism for the increase of gate leakage seen during RF stability measurements in devices with an AlN interlayer is due to localized breakdown along the gate finger caused by the inability to control the AlN interlayer thickness to within a monolayer along the entire gate width. Devices without an AlN interlayer typically exhibit a decrease in gate leakage with stress time, consistent with increased trapping at the gate edge [C1246]

### "Molecular Beam Epitaxy of Heterostructures on the Basis of III-V Materials for UHF Transistors"

Described is MBE technology, whose essence is the growth of heterostructures for UHF transistors including nitride technology. We demonstrate that buffer layer optimization allows improving GaAs FETs parameters. Procedures of AlGaAs/InGaAs/GaAs heterostructures growth for PHEMT, as well as the heterostructures themselves, have been also optimized. Presented in this paper is the data on MBE technology development, especially as regards GaN/AlGaIn heterostructures with two-dimensional electronic gas for HEMT [C1247]

### "On-Wafer Vector Network Analyzer Measurements in the 220-325 GHz Frequency Band"

We report on a full two-port on-wafer vector network analyzer test set for the 220-325 GHz (WR3) frequency band. The test set utilizes Oleson Microwave Labs frequency extenders with the Agilent 8510C network analyzer. Two port on-wafer measurements are made with GGB Industries coplanar waveguide (CPW) probes. With this test set we have measured the WR3 band S-parameters of amplifiers on-wafer, and the characteristics of the CPW wafer probes. Results for a three stage InP HEMT amplifier show 10 dB gain at 235 GHz as presented in D. Dawson et al. (2005), and that of a single stage amplifier, 2.9 dB gain at 231 GHz. The approximate upper limit of loss per CPW probe range from 3.0 to 4.8 dB across the WR3 frequency band [C1248]

### "40 W Gallium-Nitride Microwave Doherty Power Amplifier"

This paper presents a 40 W gallium-nitride microwave Doherty power amplifier for WCDMA repeater

applications. The main and peaking amplifier are implemented using two 20 W PEP GaN HEMTs. Its performance is evaluated for broadband gain, power efficiency and adjacent-channel-power-ratio (ACPR). The experimental results of the GaN Doherty amplifier yielded a power gain over 11 dB from 1.8 GHz to 2.5 GHz, 65 % power added efficiency at 40 W peak power. Good linearity performance of -55 dBc ACPR is obtained after using a baseband digital pre-distortion technique [C1249]

### "Plastic Packaged High Linearity Low Noise Amplifier for 12-30GHz Multi-band Telecom Applications"

The packaged MMIC design and measured performance of from 12 to 30GHz are reported in this paper. A mature 0.25μm gate length low noise pseudomorphic HEMT technology has been used with a BCB-based protection allowing easy and high reliability chip integration into plastic packages. A standard plastic QFN SMD package has been successfully used: 25dB typical gain has been measured with less than 2.0 dB noise figure in all the frequency band from 12 to 30GHz and more than 26dBm output IP3 has been measured in the 18-26GHz frequency band [C1250]

### "65 nm RFCMOS technologies with bulk and HR SOI substrate for millimeter wave passives and circuits characterized up to 220 GHz"

Today, measurement of 65 nm CMOS technology demonstrates  $F_t$  around 200 GHz and  $F_{max}$  higher than 250 GHz as stated in G. Dambrine et al. (2005), which are clearly comparable to advanced commercially available 100 nm III-V HEMT or state-of-the-art SiGe HBT based in P. Chevalier et al. (2004). This increase allows new millimeter wave (MMW) applications on silicon. One of the success keys is then the passive integration. In this paper, on-chip microstrip and coplanar waveguide, which have been achieved in STMicroelectronics 65 nm RF CMOS bulk ( $p=20\text{ m}\Omega\text{cm}$ ) and HR SOI ( $p>1\text{ k}\Omega\text{cm}$ ) processes, were characterized up to 220 GHz. In addition, active device performances are reviewed. Then, circuit examples are given up to 220 GHz. Finally, a benchmarking with state of the art Si, III-V and HR SOI comparable transmission lines (TLs) structures is proposed [C1251]

### "Trends in Microwave/Millimeter-Wave Front-End Technology"

Unique, high-performance components are utilized between the air or fiber-optic media interface and baseband/digital signal processing functions. TriQuint and other suppliers have developed power amplifiers, filters, duplexers, switches, phase shifters, and frequency conversion components specifically for this niche in systems ranging from RF-frequency cellular handsets to millimeter-wave frequency point-to-point radio transceivers. Examples of the use of specialized front-end technologies are: combining surface acoustic wave devices with GaAs switches and power amplifiers in a handset modules, linear millimeter-wave power amplifiers for point-to-point radio links, millimeter wave switches using GaAs PIN diodes, and combining GaAs HBT, PHEMT, and VPIN technology in a 77-GHz Tx/Rx front-end for automotive radar. Finally, future GaN HEMT technology is showcased by discrete transistors setting new levels of power density [C1252]

### "InP-Based InAlAs/InGaAs Double-Gate Transistors Beyond Conventional HEMT's Limitations"

We report on the design, fabrication and characterization of 100nm T-gates  $\text{In}_{0.52}\text{Al}_{0.48}\text{As}/\text{In}_{0.53}\text{Ga}_{0.47}\text{As}$  double-gate HEMTs (DG-HEMT) on InP substrate. In comparison with single gate conventional HEMT, maximum oscillation frequency ( $f_{max}$ ) was increased by 30% when the DG-HEMT operate in simple gate command (DG-HEMT-SC) due to the reduction of short channel effects. On the other hand, in double-gate command operation mode (DG-HEMT-DC), control of the threshold voltage of DG-HEMT was achieved while keeping constant DC and RF performances. In this operation mode, these three-port devices were considered as being very effective for millimeter-wave mixing applications and were promising devices for the fabrication of velocity modulation transistor (VMT) (Sakaki, 1982) [C1253]

### "Millimeter-Wave Front-End Components in Metamorphic HEMT Technology"

We report on the latest results of millimeter-wave IC components realized using IAF's metamorphic HEMT technology, ranging from small-signal low-noise amplifiers to nonlinear applications such as power amplifiers and frequency converters. A G-band four-stage cascode amplifier MMIC achieves 21 dB gain at 220 GHz. At 155 GHz, a two-stage cascode design reaches 15 dB gain with a noise figure of 4 dB. Frequency conversion is demonstrated in a doubler, achieving more than 0 dBm output power over the frequency range from 180 to 220 GHz. The same doubler is combined with a resistive mixer to form a G-band down-converter with as low as 10 dB conversion loss. At 94 GHz, a two-stage power amplifier MMIC achieves 23.3 dBm [C1254]



### "Novel Encoder and Correlator for Optical Code Division Multiple Access Networks"

A novel structure that encodes and decodes very high speed optical code division multiple access (OCDMA) signals is proposed. This scheme is based on the analogy between the distributed amplifier and the transversal filter. By simple adjustments, the proposed device acts as a high-speed ( $>40$  GChip/s) encoder (transmitter) or correlator (receiver). Theoretical analysis and potential implementation using MMIC HEMT foundry process are presented [C1255]

### "X-Band Power AlGaIn/GaN HEMT"

In this paper, the results of design and manufacture of middle power X-band AlGaIn/GaN HEMT are presented. It has Gain=11 dB,  $P_{OUT} = 1.4$  W/mm at  $F=10$  GHz [C1256]

### "L-Band Low Noise AlGaIn/GaN HEMT"

This paper presents the results of design and manufacture of low noise AlGaIn/GaN HEMT for L-band. It has  $NF_{min} < 1.4$  dB gain  $> 15$  dB at  $F=1.5$  GHz. GaN HEMT has been designed and manufactured in SRI "Pulsar" [C1257]

### "Visual Design of 1.5-2.5 GHz MMIC Low-Noise Amplifier"

The design of 1.5-2.5 GHz MMIC amplifier is presented using a new interactive "visual" technique. In this paper, we demonstrate the design of MMIC low-noise amplifier (LNA) using a new interactive "visual" technique. The design technique allows the exact synthesis of compensation/feedback networks directly from simultaneous set of performance specifications, including the gain, gain flatness, noise figure, input/output matching, and stability. With these tools, we have designed a 1.5-2.5 GHz MMIC LNA for wireless systems based on the 0.2  $\mu$ m pHEMT GaAs technology (OMMIC, France) [C1258]

### "A Reliable Low Gate Bias Model Extraction Procedure for AlGaIn/GaN HEMTs"

A reliable low gate bias model extraction procedure for AlGaIn/GaN is discussed. This method does not bias the device at a untenable high gate voltage in order to extract the parasitic inductance and resistance. The modeling procedure is reliable and simple with high accuracy up to 40GHz. The influence of extracted parasitic components is discussed [C1259]

### "Identification of RF Power Amplifier Memory Effect Origins using Third-Order Intermodulation Distortion Amplitude and Phase Asymmetry"

This paper describes a technique to determine the physical origins of memory effects in RF power amplifiers using amplitude and phase asymmetries of two-tone third order intermodulation distortion (IMD) products measured over a range of power levels and frequency spacing. Determining the origins of the memory effects is done by extracting the portion of the IMD product in each sideband that contributes to the asymmetry, and comparing these on a statistical basis to the responses of simple equivalent circuit models that represent thermal self-heating, and bias voltage feedback. A 90W, singled-ended GaN pHEMT PA stage is compared to a 650W push-pull combined Si LDMOS PA at 2.14 GHz. It is shown that the GaN PA memory effects are dominated by bias feedback (which is later improved), and that the LDMOS PA memory effects are dominated by thermal self-heating. These results are further quantified by comparing memory ratios [C1260]

### "Linear broadband GaN MMICs for Ku-band Applications"

AlGaIn/GaN-based HEMT MMICs on s.i. SiC wafer substrates are designed and realized for linear broadband amplifiers. Electrical performance data and assembly technology issues are presented in this paper. The linear broadband amplifier MMIC operates in the frequency range from 9 GHz to 19 GHz and is fabricated in microstrip technology including via-holes. The measured small signal gain is about 13 dB and the output power at 1dB compression is in the range of 27dBm. Two-tone measurements show good linearity. Up to 26dBm output power the IM3 value is better than 30dBc. A reliable assembly process for the MMICs is necessary in order to achieve good thermal conductivity between the underlying SiC wafer substrate and the heatspreader beneath [C1261]

### "A 3-Watt Q-Band GaAs pHEMT Power Amplifier MMIC For High Temperature Operation"

A three-stage Q-band pHEMT power amplifier for 42-46GHz operation has been designed and built. The conservative stage peripheries of 2.64:5.28:7.68mm were chosen to ensure high temperature operation. Although designed for a nominal bias of 5.5V and 170mA/mm, the amplifier operates with biases of 2-6V and 65-190mA/mm. Record powers for this frequency range have been obtained. Biased at 6V and 170mA/mm the



amplifier provided 4W of power at 20% efficiency over 42.5-43GHz at 30degC, and an average of 3W with 17% efficiency over 43.5-45.5GHz at 90degC. At 5.5V and 128mA/mm an average power of 3W with 20% efficiency was obtained over 43.5-45.5GHz at room temperature [C1262]

#### **"A 20-mW G-band Monolithic Driver Amplifier Using 0.07- $\mu$ m InP HEMT"**

In this paper, a four-stage driver amplifier MMIC covering 160 GHz to 195 GHz is reported. The amplifier uses 0.07- $\mu$ m T-gate pseudomorphic InGaAs/InAlAs/InP HEMTs with 2-mil substrate thickness. With two MMICs cascaded in WR-5 housing, the assembly exhibits 25-40 dB linear gain from 160 GHz to 195 GHz. When biased at 1.2V, 10-mW saturated output power and 6.5% power-added-efficiency are achieved. 20-mW saturated output power is obtained when 2V drain voltage is applied. The performance of the reported driver amplifier represents state-of-the-art power performance achieved at G-band [C1263]

#### **"0.4 V, 5.6 mW InP HEMT V-band Low-Noise Amplifier MMIC"**

This paper demonstrates the low-power operation of an InP HEMT V-band low-noise amplifier (LNA) MMIC. The device used here is a commercial 0.1- $\mu$ m InP HEMT developed for high-speed digital ICs. The fabricated two-stage LNA MMIC, chip size of 0.9 mm<sup>2</sup>, employs two 50- $\mu$ m gate-width InP HEMTs and coplanar waveguides. Under 0.4 V supply voltage operation, the MMIC achieves a noise figure of 2.86 dB at 60 GHz with an associated gain of 12.3 dB. The power dissipation of the MMIC was only 5.6 mW. The input IP<sub>3</sub> was -9 dBm at 60 GHz. A 3-dB bandwidth of 44.6 GHz to 67.2 GHz was also achieved. These results indicate the InP HEMT technology has a great potential for the low-voltage and low-power ICs that are needed for future millimeter-wave high-speed wireless applications [C1264]

#### **"A Novel Non-Uniform Distributed Amplifier/Attenuator for Millimetre-wave Transmitter MMICs"**

A non-uniform distributed pHEMT amplifier/attenuator is presented. The topology ensures good intermodulation (OIP<sub>3</sub> > 24 dBm) and more than 16 dB of dynamic range. Rather than optimising the gate and drain transmission line lengths, this design varies transistor width, in both the amplifier and shunt-attenuator devices, to minimise width and maximise performance. These factors make the presented design useful for the construction of compact, high-performance millimetre-wave transmitter MMICs [C1265]

#### **"Single supply 1W Ku-band Power Amplifier Based on 0.25 $\mu$ m E-mode PHEMT"**

Development of enhancement mode PHEMT (E-PHEMT), single supply, 13 to 17GHz power amplifier MMIC is described. The amplifier was designed with highly integrated lumped-passive based design techniques utilizing a 0.25 $\mu$ m GaAs E-PHEMT production process. The designed power amplifier exhibit 30 dB of small signal gain, 31dBm 1dB gain compression output power with 31% PAE at 16 GHz. This MMIC was fabricated in Avago's advanced E-PHEMT process and have been demonstrated in fully production capability [C1266]

#### **"A 1/2 Watt High Linearity and Wide Bandwidth PHEMT Driver Amplifier MMIC for Millimeter-Wave Applications"**

This paper presents a high linearity and wide bandwidth driver/power amplifier MMIC, which covered entire Q-band. The MMIC amplifier was designed for 38GHz point-to-point radio application using TriQuint's 0.15  $\mu$ m power GaAs PHEMT technology. This balanced three-stage power amplifier, with chip size of 2.9 mm<sup>2</sup> on 100  $\mu$ m GaAs substrate, achieved 27 dBm P<sub>1dB</sub> output power with nominal 18 dB small signal gain over 33-40 GHz. The RF performance of this power amplifier can be further extended to cover frequencies of 33-48 GHz. Meanwhile, high output linearity was measured with lower than -34 dBc third order intermodulation (IM<sub>3</sub>) at 19 dBm per tone output power level. This state-of-the-art millimeter wave power amplifier sets the benchmark of linearity and bandwidth for a single MMIC chip reported to date among Q-band medium power amplifiers [C1267]

#### **"Optical mixing in InP-based high-electron mobility transistors by use of a focused laser beam"**

Optical mixing in InP-based ultra-fast high-electron mobility transistors (HEMTs) using a focused laser beam onto the surface was studied in detail. Position-dependent optical responses in the HEMT and optical signal detection at 10 GHz were demonstrated. [C1268]

#### **"A Ka Band, Low Power Dissipation, High Spectral Purity GaAs pHEMT MMIC X4 Multiplier."**

Frequency translation circuits are an integral part of transceiver systems. A novel wideband frequency quadrupler is implemented in 0.15 $\mu$ m pseudomorphic HEMT technology with an  $f_t$  = 85GHz. The multiplier is split into two bands, to cover 27-34GHz and 35-40GHz. The circuit provides times4 multiplication of the input LO with greater

than 30dBc suppression of undesired fundamental and all harmonics over a 24% bandwidth in the low band. The low conversion loss of 5dB is an added advantage coupled with the low power dissipation at 163mW which is an attractive feature of this multiplier. The low power consumption, low conversion loss and high spectral purity makes this chip integral to the requirements of multifunction MMIC transceivers. The novel MMIC quadrupler measures only 4.5times1.5mm [C1269]

#### "AlGaIn/GaN Dual-Gate HEMT Mixers for 24 GHz Pulse-Modulation"

We have fabricated dual-gate AlGaIn/GaN high-electron-mobility transistors (HEMTs) with a short gate on SiC substrates for use in high-power mixers and have measured their pulse modulation characteristics. A device with a T-shaped gate (0.15  $\mu\text{m}$  times 200  $\mu\text{m}$ ) modulates a 24-GHz local (LO) signal with 0.4-ns-wide pulses. The peak output power is as high as 8.9 dBm and the bandwidth is over 2 GHz. These results indicate that this high-power mixer can directly drive an antenna and is applicable for 24-GHz ultra-wideband (UWB) applications [C1270]

#### "X-Band High-Power Microstrip AlGaIn/GaN HEMT Amplifier MMICs"

This work describes AlGaIn/GaN power amplifier MMICs in microstrip line technology on s.i. SiC substrate for X-band frequencies with output power levels well beyond 15 W. A dual-stage design supplies 18 dB of gain at 10 GHz with a pulsed output power of 20 W at  $V_{DS} = 40$  V. Further, a single-stage MMIC with 6 mm gate width provides a P-1dBof 14.5 W and a maximum output power of 22.4 W, also at 10 GHz [C1271]

#### "MMIC and Module Design and Performance for Millimetric Transceiver Front-ends for Transport Applications"

Millimeter wave transceiver front-end modules have been made for use in high data rate telematics transceiver applications in the frequency band 63 to 64 GHz. The modules incorporate a highly integrated core-transceiver MMIC, fabricated using a commercially available production GaAs pHEMT technology, for up- and down-conversion, signal amplification and image rejection functions. Packaging technologies are identified to realise potential low cost production of the front-ends. Under the millimetric transceivers for transport applications (MILTRANS) project, a consortium of UK organisations, this hardware has been used in a system demonstrator based on modulation schemes compliant with the IEEE 802.11a standard and using a custom antenna designed for vehicle-to-roadside and vehicle-to-vehicle communications. Front-end performance characteristics are reported together with initial system performance for a network of nodes operated in static and mobile configurations [C1272]

#### "Comparing High Mobility InGaAs FETs with Si and GOI Devices"

We demonstrate a dislocation-free InAlAs/InGaAs/InAlAs-on-Insulator (IIIVOI) HEMT on a Si substrate, which has a high drain current and 8,100  $\text{cm}^2/\text{Vs}$  mobility. To reduce the Schottky gate leakage current in the device, a high- $\Gamma$ , Bi Al<sub>2</sub>O<sub>3</sub>/InGaAs gate stack was used. By using this structure the gate leakage current was lower than that for a SiO<sub>2</sub>/Si MOSFET at the same equivalent-oxide-thickness (EOT), and the measured 451  $\text{cm}^2/\text{Vs}$  effective mobility was 2.5X higher. [C1273]

#### "Gate Sinking Effect of 0.1 $\mu\text{m}$ InP HEMT MMICs Using Pt/Ti/Pt/Au"

Gate sinking effect of 0.1  $\mu\text{m}$  InAlAs/InGaAs/InP HEMT MMICs (with Pt/Ti/Pt/Au gate metals) subjected to elevated temperature lifetests has been investigated. The results show that Pt sinking is the dominant degradation mechanism caused by Pt diffusing into the In<sub>0.52</sub>Al<sub>0.48</sub>As Schottky barrier layer. Pt sinking explains the observed evolutions of Schottky diodes,  $I_{ds}$ -Gm transfer characteristics, and the S<sub>21</sub> increase. Scanning-transmission-electron-microscope micrographs substantiate the alleviation of Schottky junction degradation of InP HEMTs using Pt/Ti/Pt/Au gates. Moreover, 2-temperature lifetest shows that the activation energy is approximately 1.55 eV, based on a failure criterion of  $\Delta I_{DSS} = -20\%$ . The results from this study demonstrate that Pt sinking is the primary degradation mechanism of 0.1  $\mu\text{m}$  InP HEMT MMICs with Pt/Ti/Pt/Au gate metals [C1274]

#### "Sub-threshold characteristics of the 0.2 $\mu\text{m}$ capless InP/In/sub 0.52/Al/sub 0.48/As/In/sub 0.53/Ga/sub 0.47/As p-HEMTs having a self-aligned gate"

Sub-threshold characteristics of a 0.2  $\mu\text{m}$  self-aligned gate (SAG) capless InAlAs/InGaAs p-HEMT having a highly strained InAs sub-channel were investigated. The extracted ION/IOFF ratio and sub-threshold slope of the SAG capless HEMT (1.27times10<sup>4</sup> and 78 mV/dec) was better than those of the conventional recessed p-HEMT (5.1times10<sup>3</sup> and 120 mV/dec), respectively. The capless p-HEMT showed an ION/IOFF ratio twice larger than

that of the conventional recessed p-HEMT having a heavily doped InGaAs cap layer. Even without the heavily n-doped InGaAs cap layer, the 0.2  $\mu\text{m}$  SAG capless p-HEMT showed the maximum gm, fT, and v sat(saturation velocity) of 1.12 S/mm, 185 GHz, and 3.3times107cm/sec, respectively [C1275]

### "Ultra fast Gunn effect at THz frequencies in HEMTs"

When the drain-source bias is sufficiently high the emission spectra of HEMTs show peaks at THz frequencies. In this work, we will show the results of Monte Carlo simulations of 80-nm-gate InAlAs/InGaAs HEMTs where ultra-high frequency (in the THz range) Gunn-like oscillations in the gate-drain region of the devices have been observed. Such high frequency implies that the drift velocity of the high field travelling domain approaches 5times105m/s (a fivefold increase with respect to the steady-state saturation velocity of electrons). This unexpectedly high velocity comes from the presence of extremely fast ballistic electrons in that region, able to go through the high field domain without overcoming intervalley transfer [C1276]

### "Nanometer Scale InGaAs HEMT Technology for Ultra High Speed IC"

We have successfully fabricated various nanometer scale InGaAs HEMTs based on novel nano-patterning techniques, including sidewall-gate process and e-beam resist flowing method. The sidewall-gate process was developed to lessen the final line length, by means of the sequential procedure of dielectric re-deposition and etch-back. The e-beam resist flowing was effective to obtain fine line length, simply by applying thermal excitation to the semiconductor so that the achievable final line could be reduced by the dimension of the laterally migrated e-beam resist profile. Applying these methods to the device fabrication, we were able to succeed in making 30 nm InGaAs HEMTs with excellent fT exceeding 400 GHz. Based on nanometer scale InGaAs HEMT technology, several high performance integrated circuits have been successfully fabricated, such as 77 GHz MMIC chipsets for automotive car radar application and 40 Gb/s digital circuits [C1277]

### "The Impact of Side-Recess Spacing on the Logic Performance of 50 nm InGaAs HEMTs"

We are investigating InGaAs HEMTs as a future high-speed, low-power logic technology for beyond CMOS applications. In this work, we have experimentally studied the role of the side-recess spacing (L side) on the logic performance of 50 nm In0.7Ga 0.3As HEMTs. We have found that Lsidehas a large impact on electrostatic integrity (short channel effects), gate leakage current, gate-drain capacitance, and source and drain resistance. For our device design, an optimum value of Lsideof 150 nm is found. 50 nm In0.7Ga0.3As HEMTs with this value of Lsideexhibit ION/IOFFratios in excess of 104, subthreshold slopes smaller than 90 mV/dec, and logic gate delays of about 1.3 ps at a VCCof 0.5 V. In spite of the fact that these devices are not optimized for logic, these values are comparable to state-of-the-art MOSFETs of similar gate lengths. Our work shows that in the landscape of alternatives for beyond CMOS technologies, InAs-rich InGaAs HEMTs hold considerable promise [C1278]

### "50nm GaAs mHEMTs and MMICs for Ultra-Low Power Distributed Sensor Network Applications"

We report well-scaled 50 nm GaAs metamorphic HEMTs (mHEMTs) with DC power consumption in the range 1-150  $\mu\text{W}$ / $\mu\text{m}$  demonstrating fT of 30-400 GHz. These metrics enable the realisation of ultra-low power (<500  $\mu\text{W}$ ) radio transceivers for autonomous distributed sensor network applications [C1279]

### "Low-Frequency-Noise Characteristic of Quasi-Enhancement-Mode HEMT Using a Selectively Hydrogen-Pretreatment"

The DC, RF, and low-frequency noise characteristics were investigated for a quasi-enhancement-mode (QE) HEMT using a selective hydrogen pretreatment (SHP). The QE-HEMT with SHP showed a large shift in threshold voltage without severe degradation of RF performances including cut-off frequency and maximum oscillation frequency, compared with those of HEMT without SHP. Moreover, the QE HEMT exhibited a reduction of low-frequency noise bulges compared with those of depletion-mode HEMT without an SHP, leading to an one-order smaller input noise spectral density at 100Hz, and offered a potential for application to a low phase noise oscillator [C1280]

### "Accurate Noise Modeling of HEMT for Low-Noise Applications"

A novel physical device model was developed for designing a low-noise-application-oriented HEMT structure and modeling a high-frequency noise characteristic of HEMT. To calculate accurate noise figure as a figure-of-merit indicating the high-frequency noise characteristics, two factors were considered based on Ando's model: (1) The parasitic effects which are more dominant at higher frequency, including a gate-to-drain shunt feedback capacitance and a gate resistance, were taken into account. (2) The electron saturation velocity was assumed to

depend on the gate length. Through the above two modifications, we calculated sheet carrier density, DC, RF parameters and noise figure (NF) [C1281]

#### "Validation of a statistical non-linear model of GaAs HEMT MMIC's by hypothesis testing and principal components analysis"

A distance-dependent non-linear statistical model of the active part of a very short-length HEMT-based MMIC, expressed in terms of principal components, is presented. A statistical model has been extracted for 0.1  $\mu\text{m}$  GaAs HEMT devices and MMIC's. Validation of the model is presented, based on principal component analysis and statistical hypothesis testing [C1282]

#### "Effect of Schottky layer thickness on DC, RE and noise of 70-nm gate length InP HEMTs"

The Schottky layer thickness of 70-nm InP HEMTs has been studied with respect to DC, RF and noise performance. An optimum gate-to-channel distance between 13-14 nm was found. Biased at a drain-to-source voltage of 0.7 V, a 2times50  $\mu\text{m}$  device exhibited an extrinsic transconductance,  $g_m$ , of 1.1 mS/mm. The maximum frequency of oscillation,  $f_{\text{max}}$ , and the transit frequency,  $f_T$ , were extracted to 200 GHz and 170 GHz, respectively. A 50 Omega noise temperature of 140 K was measured at room temperature [C1283]

#### "Electrical models for detrimental effects in metamorphic HEMTs"

Metamorphic HEMT, MHEMT (InP based layers on GaAs substrate), which are devices still in development, show very promising performances for high bit rate optical links, but still present limitations. In this paper, we propose different new electrical models of detrimental effects affecting the Metamorphic HEMT (MHEMT) functioning. First, we measured devices, particularly in terms of DC characteristics, gate and drain lag effects and on-state and off-state breakdown voltages. Then, we put into evidence the impact ionization mechanism developed in the active layer, and particularly its consequence on the drain current, the gate current and the on-state breakdown voltage. We propose electrical models for the impact ionization, the kink effect, the gate current bell shape model representative of the impact ionization mechanism. Another one permits to take into account the increase of drain current due to the MHEMT burnout (specification of the safe operating area of the MHEMT). All these models have been developed in order to be inserted into a cascade amplifier simulated with ADS software [C1284]

#### "Metal-organic vapor-phase epitaxy growth of InP using triethylphosphine with phosphine as phosphorous source"

Metal-organic vapor-phase epitaxy (MOVPE) growth of InP was investigated by using both triethylphosphine (TEP) and phosphine (PH<sub>3</sub>) simultaneously as phosphorus sources. Excellent surface morphology was obtained at 630 and 660degC by using both TEP and phosphine simultaneously at an optimized balance even though the phosphine supply amount was drastically reduced. The regular monolayer-step array of the sample surface indicates the enhancement of step-flow growth attributed to the enhancement of phosphorus source supply. By using this method, we obtained the InP recess-etching stopper layers of InP-based high electron mobility transistors (HEMTs) with excellent etching selectivity. Low-temperature InP growth at 475degC and below was also examined for the growth of emitter in InP-based heterojunction bipolar transistors (HBTs). It is confirmed that this growth method is quite effective for the improvement of InP crystal quality of InP-based epiwafers and the cost reduction for epiwafer production [C1285]

#### "AlGaIn/GaN HEMT on Diamond Technology Demonstration"

This letter is a first report on the operation of AlGaIn/GaN high-electron mobility transistors (HEMTs) atomically attached to a CVD diamond substrate. This technology demonstration shows the feasibility of producing GaN based devices on polycrystalline CVD diamond substrates to maximize heat extraction from devices operating at high power by situating the diamond substrates in the immediate proximity of the transistor channel. Such an approach offers tremendous opportunity for efficient and effective heat management of high power devices. We demonstrate the ability to preserve the electrical properties of AlGaIn/GaN HEMTs throughout the GaN-on-diamond atomic attachment process and report on the fabricated DC and small-signal HEMT characteristics [C1286]

#### "2006 ROCS Workshop"

The following topics are dealt with: reliability in emerging GaN technologies; HEMT reliability; and HBT reliability [C1287]



### "Performance Characterization, Repeatability, and Consistency of X-Band GaN HEMTs Prior to High Temperature RF Reliability Testing"

This paper reports the measured performance results on over 50 discrete GaN HEMTs mounted in high temperature RF/DC test fixtures capable of testing at > 250degC. The RF and DC parameters presented are prior to burn-in and accelerated life testing. Typical device performance variation from room temperature to 250degC is shown. The discussion focuses on the repeatability and consistency of the test fixture concept as well as the performance achieved by state-of-the art GaN devices. The highlighted performance parameters includes: gate-bias level and consistency; measured RF power output at 1dB compression; measured RF saturated power; measured power added efficiency (PAE); and realized power density in W/mm. This work demonstrates a procedure to address a major issue surrounding the difficulty of implementing a high temperature RF lifetest program [C1288]

### "High-quality InAlN/GaN high electron mobility transistors on Si (111) by metalorganic chemical vapor deposition"

We successfully fabricated high-quality InAlN/GaN heterostructures for high electron mobility transistors (HEMTs) on Si (111) substrate by metalorganic chemical vapor deposition (MOCVD). X-ray diffraction measurements revealed that InAlN/GaN heterostructures grown under optimal conditions have a flat surface and an abrupt heterointerface. The surface roughness evaluated from atomic force microscopy (AFM) is improved, compared with previous reports. Electron mobility of about 1,200 and over 1,800 cm<sup>2</sup>/V-s are obtained for InAlN/GaN heterostructures without and with an AlN interlayer, respectively. These mobility values are the highest ones ever reported for InAlN/GaN heterostructures grown on Si substrates [C1289]

### "A Planar Integration Process for E/D-mode AlGaIn/GaN HEMT DCFL Integrated Circuits"

We demonstrate a new planar fabrication technology for integrating enhancement/depletion (E/D) mode AlGaIn/GaN HEMTs using fluoride-based plasma treatment techniques. The CF<sub>4</sub>plasma treatment is used in two separate steps to achieve two objectives: 1) active device isolation; and 2) threshold voltage control for the E-mode HEMT formation. By using the planar process, the E/D-mode HEMTs are integrated on the same chip, and a direct-coupled FET logic inverter and a 17-stage ring oscillator are fabricated. Compared with the devices formed by standard mesa etching, the HEMTs by planar process have comparable DC and RF characteristics, with no obvious difference in device isolation. At a supply voltage of 3.3 V, the E/D-mode inverter shows an output swing of 2.85 V, with the logic low and logic high noise margins at 0.34 and 1.47 V. The fabricated ring oscillator yields an oscillating frequency of 159 MHz at a supply voltage of 4.5 V. After a 44 hrs thermal stress at 350degC, the devices show negligible change in DC and RF characteristics, indicating excellent thermal stability of the planar process [C1290]

### "X-band AlGaIn/GaN HEMT with over 80W Output Power"

AlGaIn/GaN high electron mobility transistors (HEMTs) were developed for X-band applications. The operating voltage and temperature dependence of output power characteristics in CW operating conditions were investigated. The developed AlGaIn/GaN HEMT with combined two dies of 11.52 mm gate periphery exhibits output power of over 81.3W with a power added efficiency (PAE) of 34% under VDS=30V, CW operating condition at 9.5GHz, and a gain compression level of 3dB [C1291]

### "The Impact of Multiple-Gated Layout on the Drain-Source Current of pseudomorphic-HEMTs"

The measurement and analysis to search the impact of multiple-gated structure of a GaAs based p-HEMT device towards the drain-source current ( $I_{ds}$ ) is presented here. The experimental works had been carried out on the GaAs wafer that consists of 2times60, 4times75 and 6times150 p-HEMT device layouts for the I-V characteristic. The I-V measurement was performed using on-wafer probing technique which applied semi-auto probe station and Keithley parameter analyzer to extract I-V curve. From the I-V data, it was found that the p-HEMT layout that had higher number of gates exhibited a significant impact on the  $I_{ds}$  at the same  $V_{gs}$  bias value. The  $I_{ds}$  of six-gated layout was improved about 40% as compared to 4-gated layout and about 60% to 2-gated layout. The effect on the I-V performance due to the number of gates in the layout has also been discussed in detail for circuit design applications [C1292]

### "Interdigital-Gated HEMT Structure for High Frequency Devices"

Interdigital-gated AlGaAs/GaAs high electron mobility transistor (HEMT) structure was used to investigate the interaction between the drifting carrier plasma waves and electromagnetic (EM) waves. It was shown



theoretically that the interaction in the range from microwave to terahertz (THz) at room temperature should produce negative conductance characteristics when the carrier drift velocity slightly exceeds the phase velocity of EM waves. S-parameter reflection measurements were carried out at room temperature for a frequency range from 1 to 20 GHz and a drastic change in conductance was observed at 5GHz and 10GHz with the increase of drain-source voltage. Large conductance change over 1000 mS/mm was obtained and it showed a peak at a certain frequency. The peak position could be controlled by changing the pitch size of the interdigital gates. These characteristics can be used for high frequency applications such as high-speed switching devices although a feature size of our interdigital-gated HEMT device is much larger than conventional HEMT device [C1293]

### "Effect of Indium Content in the Channel on the Electrical Performance of Metamorphic High Electron Mobility Transistors"

Metamorphic InAlAs/InGaAs high electron mobility transistors (HEMT) has demonstrated several advantages over pseudomorphic-HEMT on GaAs and lattice matched-HEMT on InP substrate. The high Indium content of the channel (50%) lattice matched to the substrate is the key factor behind the superior metamorphic HEMT performance. Metamorphic HEMT allows a flexible range of InGaAs channel compositions from 30% to 80% (based on the applications) [1] on a compositionally graded buffer. Commercially available TCAD is used to simulate the metamorphic HEMT to study the effect of varying Indium % in the channel layer on the electrical characteristics of the device. [C1294]

### "Physical Investigation of High-Field Degradation Mechanisms in GaN/AlGaIn/GaN HEMTs"

High-electric-field degradation phenomena are investigated in GaN-capped AlGaIn-GaN HEMTs by comparing experimental data with numerical device simulations. Simulations indicate that the stress-induced amplification of gate-lag effects and the correlated gate-leakage-current reduction can be ascribed to the generation of acceptor traps at the gate-drain surface. The drop in DC drain current observed after stress should rather be attributed to trap accumulation within the GaN buffer region. Only the simultaneous generation of surface and buffer traps can account for all of the observed degradation modes [C1295]

### "The Effect of Gate Current on the Degradation of GaAs PHEMT MMICs"

Scanning transmission electron micrographs were used to investigate the gate metal sinking effect in 0.15  $\mu\text{m}$  GaAs PHEMT MMICs subjected to elevated temperature lifetesting. Gate metal sinking causes a decrease of the Schottky barrier height, therefore reducing the Schottky diode's forward turn-on voltage. The progressive gate metal sinking eventually leads to a drastic increase in the three-terminal forward gate current. Accordingly, a distinct degradation phenomenon in MMICs due to high forward gate current and gate resistors was observed. The degradation causes a decrease in transconductance and small signal gain, following the earlier gate sinking. In conclusion, a dependence of DC performance and small signal gain on the forward gate current was observed in GaAs PHEMT MMICs [C1296]

### "Modeling of a 10GHz Dielectric Resonator Oscillator in ADS"

Oscillators are basic microwave energy sources for all microwave communication systems. This paper will discuss the theory and the design of a low phase noise 10GHz parallel feedback GaAs PHEMT dielectric resonator oscillator. The coupling coefficient between the dielectric resonator and the parallel microstrip lines are represented in the form of double coil transformer, while the dielectric resonator is modeled as a parallel RLC component. The coupling gap can be adjusted to optimize the ratio of the loaded to the unloaded quality factor to give a better phase noise. An optimum low phase noise can be achieved when an insertion loss of 9.5dB is obtained. The dielectric resonator oscillator model design was simulated using Agilent ADS software, where at 10GHz exhibited an insertion loss of 8.562 dB with a phase noise of -105.283 dBc/Hz at 100 kHz frequency offset. The output power was exhibited at +15.551 dBm [C1297]

### "6C-5 Planar Integration of SAW Filter with HEMT on AlGaIn/GaN Heterostructure Using Fluoride-based Plasma Treatment"

We demonstrate a new planar fabrication technology for integrating surface acoustic wave (SAW) filters with high-electron mobility transistors (HEMTs) on AlGaIn/GaN heterostructures using fluoride-based ( $\text{CF}_4$ ) plasma treatment techniques. The  $\text{CF}_4$  plasma treatment has been shown capable of effectively depleting the two-dimensional electron gas (2DEG) without removing the top AlGaIn layer. It is not only able to achieve the same level of active device isolation, but also able to permit the acousto-electric transductions in the interdigital transducers (IDTs) of the SAW filters. The RF characteristics of the planar SAW filter was similar to those of

SAW filters directly fabricated on GaN layer exposed by using the mesa etching. Compared to the SAW device without HEMT, the integrated SAW/HEMT exhibited an insertion loss that was 5.129 dB lower because of the amplification by the output HEMT [C1298]

#### "Fabrication of 35-nm zigzag T-gate Al<sub>0.25</sub>Ga<sub>0.75</sub>As/In<sub>0.2</sub>Ga<sub>0.8</sub>As/GaAs pHEMTs"

In this paper, a novel process using two-step electron beam lithography and zigzag T-gate method is proposed to fabricate 35-nm T-gates and demonstrated by fabricating high performance Al<sub>0.25</sub>Ga<sub>0.75</sub>As/In<sub>0.2</sub>Ga<sub>0.8</sub>As/GaAs pHEMTs. Two-step lithography adopting a low temperature development method reduces electron forward scattering and the detrimental effect of the head exposure on foot definition. Thus, this method enables 35-nm T-gate patterning using a tri-layer (PMMA-MAA/PIVIGI/PIV1MA) resist structure under a low 20 keV electron beam acceleration condition. The zigzag style T-gate enhances mechanical support for the 35-nm T-gate to remain standing after metal lift-off process. It is shown here that 35-nm zigzag T-gate Al<sub>0.25</sub>Ga<sub>0.75</sub>As/In<sub>0.2</sub>Ga<sub>0.8</sub>As/GaAs pHEMTs with f<sub>ro</sub> 200 GHz can be realized using this process. [C1299]

#### "New Design Approach to minimise IMD Asymmetry and IM3 products in Microwave FETs"

The minimisation of asymmetry between the lower and upper side band intermodulation products is discussed in the first part of this contribution using a Volterra series analysis. From the inferred relationships, not only the base band but also the harmonic device terminations effects were analysed, establishing new conditions to minimise the IMD asymmetry. Under these conditions and following the Volterra approach, also the IM3 products were minimized through a suitable second harmonic load selection as verified by nonlinear simulations on a HEMT device model. This approach allows to avoid complex linearization schemes in the base band frequencies obtaining similar results and simpler design. [C1300]

#### "Theoretical Study of The Charge Control in AlGa<sub>N</sub>/Ga<sub>N</sub> HEMTs"

This paper presents a simplified numerical model for the charge control in AlGa<sub>N</sub>/Ga<sub>N</sub> high electron mobility transistor (HEMT). The model is based on solution of Poisson's equation in the AlGa<sub>N</sub> layer, including the effect of spontaneous and piezoelectric polarizations. A non-linear formulation of the strain-induced polarization fields has been considered. The model results indicate a close agreement with other complicated models. Theoretical study of the effects of structural and processing parameters on the charge control has been presented. The examined parameters are: the AlGa<sub>N</sub> barrier layer thickness and doping, the spacer layer thickness, and the Al mole fraction  $x$ . Completely different effects for some parameters have been detected and explained [C1301]

#### "Plasma Wave HEMTs for THz applications"

New THz chip solid-state detectors and sources are waited for many applications. The idea of new sources and detectors, based on the oscillations of bidimensional plasma, was theoretically and experimentally demonstrated. We present technological process of nanometric devices dedicated to THz emission. In this structure, a MIM gate-source capacitance is integrated to HEMT to achieve the boundary condition of plasma wave generation and to keep possible the gate biasing, necessary for frequency tuning. High electron mobility material like InAlAs/GaInAs heterostructure is used otherwise the plasma wave is dumped by electron scattering. Electrical and THz measurements are realized. [C1302]

#### "Current Collapse Simulation of Ga<sub>N</sub> HEMTs"

Using a two-dimensional simulator, current collapse effect is simulated in Ga<sub>N</sub> HEMTs. Dynamic picture of trapping of hot electron under gate pulse is discussed. The trapped charge may accumulate under punch-off gate voltage at gate edge drain side due to the large electric field strain. Self-heating effect is a consequence of the current collapse. [C1303]

#### "Electrical control of ballistic spin-dependent conductance through magneto-electric barriers in the 2D-electron gas of GaAs heterostructure"

In this article, the method of resonant tunneling through a double-pair potential barrier to induce spin-polarized current in the 2D-electron gas (2DEG) of a high-electron-mobility-transistor (HEMT) heterostructure is discussed. The effect of electrical barriers which can be conveniently established by applying electrical voltage to the ferromagnetic gates of the HEMT device. The electrical potential could be utilized here to control not only the spin current, but also the charge current. The pre-requisite is symmetrical magnetic potential ( $A_y$ ) must first be established along the 2DEG  $x$ -axis by magnetizing the ferromagnetic gates accordingly. Subsequent application of asymmetrical electric potential turns on spin current, while symmetrical potential turns off spin

current. However, charge current persists even in the absence of spin current. Increasing the strength of the symmetrical electric potential switches off both charge and spin current. [C1304]

### "Parasitic Effects on Harmonic Reflection in Active Microwave Frequency Triplers"

This paper presents an analysis of the nonlinear mechanisms in FET/HEMT devices leading to harmonic generation in microwave frequency triplers. Previous developments are extended to show the modifications, which occur due to the introduction of device parasitics. Major impacts are demonstrated. [C1305]

### "Modeling of Polyimide MIM Capacitors for Applications in Planar Monolithic Microwave Integrated Circuits"

Polyimide metal-insulator-metal (MIM) overlay capacitors for use in monolithic microwave integrated circuits (MMICs) based on high electron mobility transistors (HEMTs) on gallium arsenide substrates are presented. Modeling of the capacitors was performed using a 2-dimensional electromagnetic CAD simulator to obtain Scattering (S-) parameters for different capacitor dimensions for operating frequencies from 0.05 to 8 GHz. The behaviour of the capacitor as a function of operating frequencies is studied by means of Smith chart. The capacitor is finally represented by a proposed equivalent circuit model to describe its overall behavior for planar MMIC simulations. [C1306]

### "New I-V Model For AlGaIn/GaN HEMT At Large Gate Bias"

Most theoretical I-V models appeared in the literature for AlGaIn/GaN HEMTs fail to exactly fit the experimental data and a large deviation is reported, especially at large gate bias. Because the exact nature of the AlGaIn/GaN heterostructure is not fully described, we assume that there is a new phenomena in the device which causes this deviation. Here we compute this phenomena mathematically for doped and undoped devices using a new method. The model results will be useful in CAD programs to extract more accurate I-V characteristics for the AlGaIn/GaN heterostructure on sapphire substrate. [C1307]

### "Extraction of the Small-Signal Equivalent Circuit Elements in HEMTs"

The aim of this paper is to provide an accurate extraction method for the small-signal equivalent circuit elements in HEMT, which can be used to determine the electrical properties and the high frequency performance of the device. Initially, the bias dependent parameters are determined using a quasi-static approach based on analytical expressions developed by us elsewhere. The extrinsic resistances are found by fitting the calculated I-V characteristics to the measured data. The other bias independent elements are determined using available extraction technique based on fitting the calculated S or Y-parameters obtained from circuit analysis to those measured at certain bias levels. The validity of the model is checked through the consistency of the transconductance and cutoff frequency values obtained from DC analysis to those obtained from RF analysis [C1308]

### "High-Performance In<sub>0.52</sub>Al<sub>0.48</sub>As/In<sub>0.6</sub>Ga<sub>0.4</sub>As Power Metamorphic HEMT for Ka-Band Applications"

A 70-nm In<sub>0.52</sub>Al<sub>0.48</sub>As/In<sub>0.6</sub>Ga<sub>0.4</sub>As power MHEMT with double delta-doping was fabricated and evaluated. The device has a high transconductance of 827 mS/mm. The saturated drain-source current of the device is 890 nA/mm. A current gain cutoff frequency (f<sub>T</sub>) of 200 GHz and a maximum oscillation frequency (f<sub>max</sub>) of 300 GHz were achieved due to the nanometer gate length and the high Indium content in the channel. When measured at 32 GHz, the 4 times 40 μm device demonstrates a maximum output power of 14.5 dBm with P<sub>1dB</sub> of 11.1 dBm and the power gain is 9.5 dB. The excellent DC and RF performance of the 70-nm MHEMT shows a great potential for Ka-band power applications. [C1309]

### "Device Characteristics of HEMT Structures based on Backgate Contact Method"

This paper presents a novel technique to obtain device characteristics of high electron mobility transistors (HEMT) structures based on the backgate contact method, thus avoiding the need for complete gate formation. The gate contact was prepared on the back side of the substrate. Measurements performed on various HEMT structures shows typical transistor characteristics. Significant changes in drain-source current as a function of backgate voltage bias was observed for different HEMT structures. Increasing the channel thickness from 8 to 26 nm shows an increase in the threshold voltage of the transistor and a noticeable variation in drain-source current. This result leads to an effective and novel technique for the determination of sample quality prior to the further fabrication process to obtain the complete device. [C1310]

### "GaN HFET for W-band Power Applications"

In this paper we report high frequency GaN power device and measured power performance of the first W-band (75 GHz-110 GHz) MMIC fabricated in GaN material system. The first W-band GaN MMIC with 150  $\mu\text{m}$  of output gate periphery produces 316 mW of continuous wave output power (power density = 2.1 W/m) at a frequency of 80.5 GHz and has associated power gain of 17.5 dB. By comparison the reported state of the art for other solid state technologies in W-band is 427 mW measured in a pulsed mode on an InP HEMT MMIC with 1600  $\mu\text{m}$  of output periphery (power density = 0.26 W/mm). The reported result demonstrates tremendous superiority of GaN device technology for power applications at frequencies greater than 75 GHz [C1311]

### "Monolithic integration of thermally stable enhancement-mode and depletion-mode InAlAs/InGaAs/InP HEMTs utilizing Ir-gate and Ag-ohmic contact technologies"

This paper reports a newly developed fabrication process for monolithic integration of thermally stable InAlAs/InGaAs/InP E/D-HEMTs based on Ir-gate and Ag-ohmic contact technologies. The Ir-gate and Ag-ohmic contacts were annealed simultaneously after passivation using a SiNx layer. Both integrated E/D-HEMTs with gate-length of 0.2  $\mu\text{m}$  demonstrated excellent DC and RF characteristics [C1312]

### "Scaling Behavior of In<sub>0.7</sub>Ga<sub>0.3</sub>As HEMTs for Logic"

We have experimentally investigated the impact of lateral and vertical scaling of In<sub>0.7</sub>Ga<sub>0.3</sub>As HEMTs on their logic performance. Reducing the In<sub>0.52</sub>Al<sub>0.48</sub>As insulator thickness results in much better electrostatic integrity and improved short-channel effects down to a gate length of 60 nm. Our nearly enhancement-mode 60 nm HEMTs feature  $V_T = -0.02$  V, DIBL = 93 mV/V and  $S = 88$  mV/V. For a given value of  $I_{ON}/I_{OFF} = 103$ , we obtain  $CV/I = 0.85$  ps at  $V_{cc} = 0.5$  V. For the same leakage current, these devices exhibit 2.5 times more current drive than state-of-the-art low-power 65 nm CMOS [C1313]

### "Processes and Device Technologies for AlGaIn/GaN High Electron Mobility Transistors"

The AlInGaIn-based high electron mobility transistor (HEMT) has proven to be the leading candidate for simultaneously realizing ultra-high frequency and ultra-high power amplifiers. The potential for these devices extends into operation in the mm-wave regime. Processes and device technologies that have resulted in these tremendous improvements are addressed [C1314]

### "An Internally-matched GaN HEMT Amplifier with 550-watt Peak Power at 3.5 GHz"

A high-power amplifier using two 28.8-mm-periphery GaN HEMTs was demonstrated with all matching components inside the package. When biased at 55 V, a power bandwidth of 3.3-3.6 GHz was obtained, with 550-W<sub>peak</sub> output, 12.5-dB associated gain and 66% drain efficiency at 3.45 GHz [C1315]

### "High PAE 1mm AlGaIn/GaN HEMTs for 20 W and 43% PAE X-band MMIC Amplifiers"

This work represents state-of-the-art performances of both large gateperiphery discrete GaN HEMTs devices and its application toward GaN MMICs amplifiers with state-of-the-art performances in simultaneous output power, PAE, and MMIC power density [C1316]

### "Intermodulation Behaviour of a Transient Trapping Model"

Trapping in microwave devices affects the time domain and frequency domain behaviour. In the time domain, surface traps result in the well known gate lag effect. A model, developed to predict these effects in HEMT devices, is used to simulate frequency domain behaviour of trapping in HEMT device. Trapping is known to cause distortion in intermodulation behaviour of the device, that is, a null in the third order intermodulation. The model can predict this intermodulation distortion frequency and its dependence on drain bias [C1317]

### "The Optimum Design of A Broad Band Low Noise Amplifier"

An optimum design of a low noise amplifier (LNA) in S microwave band working at 2-4 GHz is described in this paper. Choosing FHC40LG HEMT (high electronic mobility transistor), the noise factor of the designed amplifier simulated by Microwave Office is no more than 1.5 dB, meanwhile the gain is no less than 20 dB in the given bandwidth. The simulated results agree with the performance of the transistor itself well considering its own minimum noise factor (0.3 dB) and associated gain (15.5 dB). Simultaneously, the stability factor of the designed amplifier is no less than 1 in the given bandwidth. [C1318]



### "Wave guide type photo receiver module with 20 dB amplifier at 60 GHz millimeter wave frequency band"

60 GHz Millimeter wave band photo receiver modules with wave guide type photo detector and InP HEMT preamplifier were developed. The photo-RF conversion gains of photo receiver modules in 60 GHz band were measured as about 20 dB. [C1319]

### "A Normally-off AlGaIn/GaN Transistor with $R_{on-A}=2.6\text{m}\Omega\text{cm}^2$ and $BV_{ds}=640\text{V}$ Using Conductivity Modulation"

We report a normally-off GaN-based transistor using conductivity modulation, which we call GIT (gate injection transistor). This new device principle utilizes hole-injection from p-AlGaIn to AlGaIn/GaN heterojunction, which increases electron density in the depleted channel resulting in dramatic increase of the drain current owing to the conductivity modulation. The fabricated GIT exhibits the threshold voltage of 1.0V with high maximum drain current of 200mA/mm. The obtained on-state resistance ( $R_{on-A}$ ) and off-state breakdown voltage ( $BV_{ds}$ ) are  $2.6\text{m}\Omega\text{cm}^2$  and 640V, respectively. These values are the best ones ever reported for GaN-based normally-off transistors [C1320]

### "High-Breakdown Enhancement-Mode AlGaIn/GaN HEMTs with Integrated Slant Field-Plate"

Enhancement-mode (E-mode) AlGaIn/GaN high-electron mobility transistors (HEMTs) with integrated slant field-plates were developed for high breakdown voltage (VBD) and low on-resistance (RON). Combination of the self-aligned slant field-plate technology for high VBD and self-aligned CF<sub>4</sub> plasma treatment for E-mode operation yielded high-performance device with a VBD of 1400V, which is one of the highest reported VBD value among GaN-based E-mode HEMTs. Using the active area of the device, the RON was calculated to be below  $3\text{m}\Omega\text{cm}^2$  [C1321]

### "Can InAlN/GaN be an alternative to high power / high temperature AlGaIn/GaN devices?"

The performance of novel InAlN/GaN HEMTs for high power / high temperature applications is discussed. With 0.25  $\mu\text{m}$  gate length the highest maximum output current density of more than 2 A/mm at room temperature and more than 3 A/mm at 77 K have been obtained even with sapphire substrates. Cut-off frequencies were  $f_T=50\text{ GHz}$  and  $f_{MAX}=60\text{ GHz}$  for 0.15  $\mu\text{m}$  gate length without T-gate. Pulsed measurements reveal a less unstable surface than in the case of AlGaIn/GaN structures. Although limited by buffer layer leakage, with field plates a maximum drain bias of 100 V has been reached with these devices. The high chemical stability of this unstrained heterostructure and its surface has been demonstrated with successful operation at 1000 degC in vacuum [C1322]

### "High Voltage and High Switching Frequency Power-Supplies using a GaN-HEMT"

This paper reports 13.56 MHz and 27.1 MHz class-E amplifiers with a high voltage GaN-HEMT as the main switching device showing the possibility of GaN-HEMTs in high frequency switching power applications such as RF power-supply applications. The 380 V/1.9 A GaN power-HEMT was designed and fabricated for high-voltage power electronics applications. The demonstrated 13.56 MHz circuit achieved the output power of 13.4 W and the power efficiency of 91 % under a drain-peak voltage as high as 330 V. For a 27.1 MHz circuit, the output power was 13.8 W with the efficiency of 89.6 %. These results show that high voltage GaN-devices are suitable for high frequency switching applications under high DC input voltages of over 100 V [C1323]

### "MMIC Class-F Power Amplifiers using Field-Plated AlGaIn/GaN HEMTs"

Two simple class-F MMIC power amplifiers are described using 0.7 $\mu\text{m}$  field-plated GaN HEMT devices. One circuit was designed for operation at 2.0 GHz and achieved a power-added-efficiency of 50%, 38 dBm output power, and 6.2 W/mm power density. A second circuit was designed at 2.8 GHz and achieved a PAE of 46% with 37 dBm output power and 7.0 W/mm power density [C1324]

### "A 3-34 GHz GaAs PHEMT Distributed Mixer with Low DC Power Consumption"

A low DC power consumption broadband coplanar waveguide (CPW) distributed mixer using 0.15- $\mu\text{m}$  GaAs PHEMT technology has been described in this paper. This MMIC mixer composed of four identical sections with a single-gate PHEMT. From 3 to 34 GHz, the measured results show a conversion loss of better than 6.7 dB, and a DC power consumption of only 6 mW with a DC power supply voltage of 1 V. To the authors' best knowledge, this work is the lowest DC power consumption among all the reported GaAs-based HEMT distributed mixers. The measured LO-to-IF and LO-to-RF isolations are all better than 13 dB, and the measured input IP<sub>3</sub>



is better than 12 dBm for overall operating frequency band. The compact chip size of this distributed mixer utilizing CPW lines is only 1.8 mm times 1.0 mm [C1325]

### "Wideband Dual-Gate GaN HEMT Low Noise Amplifier for Front-End Receiver Electronics"

A highly survivable wideband low noise amplifier (LNA) for front-end receiver electronics is presented utilizing 0.2  $\mu\text{m}$  AlGaIn/GaN HEMT process on SiC substrate. This novel amplifier utilizes dual-gate devices with current feedback and drain bias network to attain wideband performance in terms of lower noise and higher gain. Nominal operation at 125 mA/mm at a drain voltage of 10 volts provided 12.5 to 18 dB gain and 1.3 to 2.5 dB noise figure. Due to high breakdown voltage, the amplifier is capable of better than 25 dBm of output power and can withstand an input power level approaching 38 dBm. This paper will also document performance comparison with a similar circuit using 0.15  $\mu\text{m}$  pseudomorphic InGaAs/AlGaAs/GaAs HEMT low noise amplifier to demonstrate the outstanding survivability of AlGaIn/GaN low noise amplifiers [C1326]

### "GaN Wide Band Power Integrated Circuits"

Gallium nitride (GaN) amplifiers have demonstrated very high power density as well as wide bandwidth in previous research. This paper examines their use in supplying flat gain, power, and linearity across a large bandwidth. It demonstrates two types of power amplifiers: a Ft Doubler (FT2) amplifier and a Cascode amplifier, both of which require a simple PCB tune. Both amplifiers show 0.2 to 4GHz bandwidth with 30 dBm PldB output power. The 3GPP WCDMA output power is 20 dBm at -45 dBc ACLR. Also, a WiMAX design is presented for the 3.2-3.8 GHz band to show the feasibility of a GaN HEMT amplifier in a relatively broad band, high linearity commercial application, with 27 dBm output at 2% EVM [C1327]

### "Demonstration of a Sub-Millimeter Wave Integrated Circuit (S-MMIC) using InP HEMT with a 35-nm Gate"

In this paper, we present two single stage MMIC amplifiers with the first demonstrating a measured S21gain of 3-dB at 280-GHz and the second demonstrating 2.5-dB gain at 300-GHz, which is the threshold of the sub-millimeter wave regime. The high-frequency operation is enabled by a high-speed InP HEMT with a 35-nm gate. This is the first demonstrated S21gain at sub-millimeter wave frequencies in a MMIC [C1328]

### "Coplanar 94 GHz Metamorphic HEMT Low Noise Amplifiers"

We report four low noise amplifiers for a 94 GHz cloud profiling radar. The LNAs are designed using coplanar waveguides and they were manufactured with a 100-nm metamorphic high electron mobility transistor technology. The chip sizes are 2.00 times 1.00 mm<sup>2</sup> and 2.25 times 1.00 mm<sup>2</sup>. The gate width of the transistor is 4times15  $\mu\text{m}$ . The scattering parameters and the noise figures of the amplifiers were measured at W-band and the results are presented. The measured gain at 94 GHz was 17-23 dB and the measured noise figure 3.0-3.3 dB using a 0.8 V drain-to-source voltage and a drain current of 8-16 mA per stage [C1329]

### "A Ka-band High Power Frequency Doubler in SMT Package"

This paper describes the development of a packaged Ka-band high power frequency doubler. The frequency doubler MMIC is developed using 0.15 $\mu\text{m}$  GaAs p-HEMT technology and packaged into a low cost QFN package for SMT application. This packaged frequency doubler delivers above +22dBm saturated output power of the 2nd harmonic signal with greater than 60dBc rejection of the fundamental and 3rd harmonic signal across the 28 to 30GHz band [C1330]

### "High Mobility III-V Mosfet Technology"

In recent years, fundamental interface issues have been overcome and GaAs MOS technology has advanced to the level of device fabrication. This development has been enabled by a molecular beam epitaxy (MBE) deposited Ga<sub>2</sub>O<sub>3</sub> template with the unique property of unpinning the Fermi level on GaAs, and a GdGaO dielectric layer which provides required band offsets while neither disrupting the template nor creating a secondary interface. MOSFET wafers with an InGaAs channel layer are grown by MBE on III-V substrates including the high-k dielectric GdGaO/Ga<sub>2</sub>O<sub>3</sub> stack (k  $\approx$  20). Electron mobilities exceeding 12,000 and 6,000 cm<sup>2</sup>/Vs for sheet carrier concentration  $n_{\text{sof}}$  of about 2.5 times 10<sup>12</sup> cm<sup>-2</sup> have been measured on InP and GaAs based MOSFET structures, respectively. Our enhancement-mode MOSFETs employ a new, implant-free device concept, which allows one to take advantage of high mobility in MOSFET channel layers. N-channel enhancement-mode GaAs MOSFETs have been fabricated with important DC figures of merit such as maximum drain current and transconductance approaching predicted performance [C1331]

### "A high-efficiency, broadband and high output power PHEMT balanced K-band doubler with integrated balun"

A high-efficiency and high output power K-band frequency doubler using InGaAs PHEMT power device is developed, which features high fundamental frequency rejection, high efficiency, good conversion gain over wide bandwidth, and high output power. A compact lumped rat-race hybrid and an output buffer amplifier are implemented on chip for a balanced design and high output power. The circuit exhibits measured conversions gain about 8 dB over the output frequencies from 12 to 22 GHz. The fundamental frequency suppression is better than 20 dB and the second harmonic saturation output power is higher than 12 dBm with a miniature chip size of 2 mm x 1 mm. [C1332]

### "Improved DC and RF performance of high power AlGaIn/GaN HEMTs with a novel inner field-plate"

An AlGaIn/GaN high electron mobility transistor (HEMT) device based on a novel inner field-plate (IFP) structure is proposed and fabricated. At an optimum bias condition of the inner field-plate (VIFP), the gate leakage current of the device has been reduced by more than 15%. In addition, the microwave performance has been found to be improved considerably with increased cut-off frequencies of  $f_T = 6.9$  GHz and  $f_{MAX} = 14.4$  GHz at a gate length of 1  $\mu\text{m}$ . The IFP-HEMT biased at the inner field-plate voltage of  $V_{IFP} = 8$  V and  $V_{DS} = 15$  V demonstrated an increased maximum output power of 16.4 dBm at 2 GHz compared to the maximum output power of 15.5 dBm for the reference case in which the inner plate is connected to the gate electrode ( $V_{IFP} = V_{GS}$ ). [C1333]

### "Ka-band flip-chip assembled power amplifier"

In this paper, we present a Ka-band two-stage power amplifier with flip-chip assembled 0.15  $\mu\text{m}$ -gate pHEMTs. With characterized 0.15  $\mu\text{m}$ -gate GaAs pHEMT and consideration of the Au-Sn pillar bump transition, the GaAs pHEMTs were flip-chip assembled on  $\text{Al}_2\text{O}_3$  substrate where the passive components and coplanar waveguide (CPW) connection were designed and fabricated. The measured maximum  $S_{21}$  at 38.56 GHz is 20.7 dB with bias conditions of  $V_D = 3$  V,  $V_{G1} = -0.2$  V,  $V_{G2} = -0.15$  V,  $I_{D1} = 52$  mA, and  $I_{D2} = 110$  mA. The output power at 38 GHz is larger than 15 dBm with linear gain of 15 dB. The load-pull measurement was also carried out on the amplifier to demonstrate the difference from 50  $\Omega$  load measurement. The difference shows the capability of pHEMT model used at Ka-band for delivering the maximum power. [C1334]

### "A high performance Ka-band push-push oscillator design using finite ground cpw structure"

A Ka-band push-push oscillator and a Ku-band fundamental oscillator designed using GaAs pHEMT 0.15  $\mu\text{m}$  technology are reported in this paper. The use of finite ground CPW structure that enhanced Q value of the passive element and improved the phase noise with the value of -113.2 dBc/Hz at 1 MHz offset of the push-push oscillator. The push-push oscillator achieves an oscillating frequency of 30.3 GHz while exhibiting a maximum output power of -1.5 dBm with the DC power consumption of 29 mW, together with a figure-of-merit (FOM) of -188.2 dBc/Hz at 1 MHz offset. [C1335]

### "The Physics of Reliability for High Voltage AlGaIn/GaN HFET's"

High voltage HFET's fabricated from nitride semiconductors utilizing the AlGaIn/GaN heterojunction demonstrate excellent RF performance with RF output power greater than an order of magnitude higher than available from GaAs and InP based devices. However, the nitride devices demonstrate a reliability problem where the dc current and RF output power continually decrease as a function of time. The reliability problem is related to the conduction characteristics of the gate electrode and an electron tunneling mechanism where electrons leak from the gate to the surface of the semiconductor. In this work the physics responsible for this behavior are investigated and described [C1336]

### "A GaN HEMT Class F Amplifier at 2 GHz with >80 % PAE"

A Class F amplifier has been designed, fabricated, and tested using a GaN HEMT transistor and a hybrid PCB. The amplifier has a peak PAE of 85 % with an output power of 16.5 W. An output power and drain efficiency tradeoff, dependant on the drain impedance at the fundamental frequency due to the on-state resistance, is explored. A comparison between Class F and inverse F, given particular operating conditions for this device, are made [C1337]

### "Recent progress of high power GaN-HEMT for wireless application"

In this paper, we describe the recent progress of high power GaN high electron mobility transistors (GaN HEMTs) for wireless base station application. First we introduce device technology and RF power performance of GaN HEMTs. Next, we discuss their reliability and cost issues which are great important for practical applications. As an example, GaN HEMTs on a low-cost conductive 3-inch SiC substrate are discussed. In addition, next generation wireless base station system will require extremely high efficiency power amplifiers when GaN HEMTs will be used at near saturation region. To suppress a forward gate leakage current at the saturation region, we developed a metal-insulator-semiconductor (MIS) gate GaN HEMT with an output power of over 100 W. [C1338]

#### "High linearity-wideband PHEMT Darlington amplifier with +40 dBm IP3"

This paper reports on a 0.1-3 GHz broadband matched Darlington feedback amplifier with over 40 dBm of OIP3 operating from a 5V supply. The Darlington performance is enabled by 0.5μm E- mode PHEMTs with  $f_T \sim 30$  GHz. The PHEMT Darlington achieves 13 dB of gain at 2 GHz and is monolithically matched to 50 ohms across a wide 0.1-3 GHz bandwidth. The IRL and ORL are better than 15 dB across the band. Noise figure of 3.3 dB and OIP3 of 41.4 dBm are achieved at 2 GHz with a PldB compression of 21.8 dBm. The monolithically matched amplifier achieves > 40 dBm IP3 across a wide 3 GHz band. The total current consumption is only 115 mA through a 5V supply and the LC-measured junction temperature is less than 125C @ 85C base-plate. These are believed to be the best IP3 results reported for a 5V wide band Darlington feedback amplifier at 2 GHz and above. [C1339]

#### "8-Watt internally matched GaAs power amplifier at 16-16.5GHz"

This paper describes a new 19.2mm GaAs PHEMT chip with high gain, high power and high power-added efficiency. Devices which are packaged by internal-matching use one such FET that has been developed at 16-16.5GHz. At 16.5GHz, the device has achieved power, gain, and power-added efficiency of 39.1dBm, 6.1dB and 26.1% respectively at the 1dB gain compression point. It is first reported that high gain, PAE and output power combination have achieved by a single FET power amplifier at such high frequency [C1340]

#### "Electrical properties of metamorphic In<sub>0.52</sub>Al<sub>0.48</sub>As/In<sub>0.65</sub>Ga<sub>0.35</sub>As HEMT's on GaAs substrate"

Variable magnetic field Hall measurements were performed to investigate the electrical properties in In<sub>0.52</sub>Al<sub>0.48</sub>As/In<sub>0.65</sub>Ga<sub>0.35</sub>As metamorphic high electron mobility transistors (MMHEMTs) on GaAs substrate at the temperature range from 4 to 100 K. The Shubnikov-de Hass (SdH) measurement shows the two-dimensional electronic behavior and two-subband electron occupation in MMHEMTs. The electron densities and mobilities of the two subbands are obtained by fast Fourier transform analysis. Both the SdH oscillations and conventional Hall analysis are in good agreement in the determination of total electron density, which is about 2.1 times 10<sup>12</sup>cm<sup>-2</sup> due to incomplete transfer of the electrons. The temperature dependence of the electron mobility indicates that at low temperature alloy scattering dominates, whereas at high temperature, the mobility is mainly limited by optical phonon scattering [C1341]

#### "MOCVD grown AlGaN/AlN/GaN HEMT structure with compositionally step-graded AlGaN barrier layer"

Unintentionally doped AlGaN/AlN/GaN high electron mobility transistor (HEMT) structures with compositionally step-graded AlGaN barrier layer were grown on sapphire substrates by metalorganic chemical vapor deposition (MOCVD). The HEMT structure exhibited typical two-dimensional electron gas (2DEG) mobility of 1600cm<sup>2</sup>/Vs at room temperature and 6412cm<sup>2</sup>/Vs at 79K with almost equal 2DEG concentration of 1.0times10<sup>13</sup>/cm<sup>2</sup>. The 50mm HEMT wafer exhibited an average sheet resistance of 318.0Ω/square, with a good resistance uniformity of 0.89%. Atomic force microscopy (AFM) measurements revealed a smooth AlGaN surface with root-mean-square roughness (RMS) of 0.199nm and 0.295nm for scan area of 2μmtimes2μm and 5μmtimes5μm, respectively. A combined using of compositionally step-graded AlGaN barrier structure and AlN interlayer results in the high electrical performance and smooth surface of this heterostructure [C1342]

#### "Effect of Passivation on Increasing of AlGaN/GaN HEMT Gate Reverse Leakage"

AlGaN/GaN HEMT gate leakage increasing induced by passivation was investigated by employing double gate surface leakage test structure, circle and rectangular Schottky contact structure and metal float gate structure. It was demonstrated that surface leakage is not a major contributor to increasing of gate leakage. Increase of gate leakage depends on augmenting of Schottky contact edge effect and inhibiting "visual gate" between gate and drain [C1343]

### "Liquid Phase Oxidation on GaAs-based Transistor Applications"

The GaAs-based MOS-HEMT with oxide as the gate dielectric and HBTs with surface passivation prepared by liquid phase oxidation has been successfully demonstrated. As compared to its counterpart HEMTs, the larger gate swing voltages, lower gate leakage currents, and higher breakdown voltages make the proposed technique suitable for power device applications. Moreover, the HBTs with oxide passivation possess the characteristics of lower surface recombination currents, higher breakdown voltage, and improved higher dc current gain [C1344]

### "50 nm AlGaIn/GaN HEMT Technology for mm-wave Applications"

First Page of the Article [C1345]

### "Effect of Source-Connected Field Plate on Electric Field Distribution and Breakdown Voltage in AlGaIn/GaN HEMTs"

Electric field distribution in the channel and breakdown characteristics of an AlGaIn/GaN HEMT with a source-connected field plate (SC-FP) were investigated using a two-dimensional device simulation. The analysis of electric field distribution and breakdown voltage varying with the changes of the insulator thickness  $t$  and the field plate length LFP revealed that to maximize the breakdown voltage,  $t$  has to be increased to make the peak electric field at drain side of gate edge approaching breakdown electric field and LFP be long enough to prevent the high-field region at gate edge and that nearby FP edge from overlapping. For the simulated device, optimum  $t$  is about 0.2  $\mu\text{m}$  and LFP around 2.2  $\mu\text{m}$ , from which a breakdown voltage 365V was obtained [C1346]

### "Study of Surface Passivation with Different a-SiN<sub>x</sub>:H Films Effect on AlGaIn/GaN HEMTs"

The effects of surface passivation with different a-SiN<sub>x</sub>:H films on AlGaIn/GaN high-electron-mobility transistors (HEMTs) have been investigated. The surface passivation layer of a-SiN<sub>x</sub>:H is deposited by plasma enhanced chemical vapor deposition (PECVD) using a 13.56 MHz direct plasma system and a SiH<sub>4</sub>/NH<sub>3</sub>/N<sub>2</sub> gas mixture. The current-voltage and gate-drain diode characteristics of AlGaIn/GaN HEMTs before and after passivation using different PECVD recipes are analyzed. The drain current increases and the threshold voltage shifts to negative values after passivation, because surface passivation reduces the surface state density and so increases the sheet carrier density. We have also analyzed the role of the [N]/[Si]-ratio  $x$  and H atom content of a-SiN<sub>x</sub>:H films on the passivation properties. Silicon-rich a-SiN<sub>x</sub>:H film with refractive index of 2.01 and large Si-H content contains less K<sup>+</sup> centers and has high-quality surface passivation. The possible mechanisms by which a surface passivant prevents current collapse are discussed [C1347]

### "Energy Efficient Wide Bandgap Devices"

As wide bandgap devices begin to become commercially available, it is becoming clear that electrical efficiency improvement is one of the key drivers for their adoption. For RF applications, GaN HEMTs allow the use of highly efficient class E circuit topologies demonstrating high powers of 63 Watts at 2 GHz with 75% power added efficiency. In broadband WiMax applications, GaN HEMTs offer very wide bandwidths while meeting the IEEE 802.16e standard with >25% drain efficiency. SiC Schottky diodes are allowing up to a 25% reduction in losses in power supplies for computers and servers when used in the power factor correction circuit. Even higher efficiencies can be obtained when the SiC Schottkys are combined with a SiC MOSFET as the switch, resulting in yet another 22% reduction in losses. For motor control, SiC Schottkys allow a >35% reduction in losses, as demonstrated for a 3 HP motor drive [C1348]

### "2006 IEEE CSIC Symposium"

The following topics are dealt with: W-band and beyond; oxide-semiconductor device and circuit technologies; millimeter wave frequency conversion; reconfigurable and tunable works; GaN MMICs; reliability and simulation; advanced III-V HEMTs; compound semiconductor MOSFETs; RF GaAs based amplifiers; III-V HBTs; automotive radar; high-speed digital circuits; WiMAX; and wide bandgap technology [C1349]

### "120-GHz Tx/Rx Waveguide Modules for 10-Gbit/s Wireless Link System"

This paper describes the development of waveguide modules for 120-GHz wireless applications. The MMIC in the modules were fabricated using 0.1- $\mu\text{m}$ -gate InP-HEMTs and coplanar waveguides. The transmitter (Tx) module contains a Tx MMIC and a multiplier MMIC for carrier generation. The Tx MMIC contains a frequency doubler, ASK modulator, and an amplifier. Output power of the Tx module is 0 dBm. The receiver (Rx) module contains a Rx MMIC with a low-noise amplifier and ASK demodulator. For high-power operation of transmitter, we developed a power amplifier (PA) waveguide module that attaches to the Tx module. This PA module



contains one-chip PA MMIC, and has 13-dBm output power with associated gain of 10.5 dB at 125 GHz. A back-to-back test of the Tx/Rx modules with and without the PA module have shown it to be fully functional at 10-Gbit/s data rate with BER =  $1e-10$  at -34.5-dBm and -36.1-dBm input powers for the receiver, respectively [C1350]

#### "From 100 GHz to Terahertz Electronics-Activities in Europe"

This paper presents an overview on selected results in the area of millimeter-wave and sub-millimeter-wave integrated circuits and devices in Europe for application in the frequency range between 100 GHz and 2THz. Advanced integrated circuits for millimeter-wave applications based on metamorphic InAlAs/InGaAs HEMTs on 4" GaAs substrates were developed and manufactured at the Fraunhofer Institute IAF. An extrinsic transit frequency of 410 GHz for 50 nm gate length devices is achieved. Two-stage low-noise amplifiers demonstrate a small signal gain of 20 dB and a noise figure of 2.4 dB at 94 GHz. An amplifier MMIC developed for G-band operation exhibits a gain of 21 dB at 220 GHz. These results are compatible with those achieved using state-of-the-art InP-based HEMT technologies. Recent results of HBVs (heterojunction barrier varactors), Schottky diodes and HEBs (hot-electron bolometers) for signal generation and detection up to terahertz frequencies obtained by various research groups in Europe are presented [C1351]

#### "Structure Optimization of Field-Plate AlGaIn/GaN HEMTs"

AlGaIn/GaN high electron mobility transistors (HEMTs) on 6H-SiC with varying field-plate length and gate-drain spacing were fabricated and analyzed. The classical small signal FET model and the well-known ColdFET method were used to extract the small signal parameters of the devices. Though the devices with field-plates exhibited lower better  $f_T$  characteristic, they did demonstrate better  $f_{max}$ , MSG and power density performances than the conventional devices without field-plate. Besides, no independence of DC characteristic on field-plate length was observed. With the increase of the field-plate length and the gate-drain spacing, the characteristic of  $f_T$  and  $f_{max}$  degraded due to the large parasitic effects. Loadpull method was used to measure the microwave power performance of the devices. Under the condition of continuous wave at 5.4GHz, an output power density of 4.69W/mm was obtained for device with field-plate length of 0.5μm and gate-drain length of 2μm [C1352]

#### "Investigation of Surface Charging Effects in AlGaIn/GaN HEMT by a New Measurement Method"

A new measurement method was confirmed that it was available to investigate the current collapse in AlGaIn/GaN HEMT due to the surface trapping process of electrons. A characteristic time constant of the trapping process  $\tau_{p0}$  was defined and obtained to be about 0.38s in a specially designed HEMT by this method. We observed an abnormal trapping time resulting from the transport of the trapped electrons and demonstrated that there was a dynamic equilibrium distribution of the charged surface states when the bias stress is applied longer than  $\tau_{p0}$  [C1353]

#### "Effects of an Fe-doped GaN Buffer in AlGaIn/GaN Power HEMTs on Si Substrate"

AlGaIn/GaN power high electron mobility transistors (HEMTs) with a Fe-doped GaN buffer on a Si substrate were presented for high power switching applications. In order to investigate the effects of an Fe-doped GaN buffer on device characteristics, HEMT devices with an Fe-doped GaN buffer on Si were fabricated alongside with the conventional devices utilizing an unintentionally doped (UID) GaN buffer on Si, and their device characteristics were compared. It was shown that the AlGaIn/GaN HEMT with a conventional structure was not suitable for realizing a high breakdown voltage (BV) due to the unstable off-state breakdown behavior. On the other hand, the AlGaIn/GaN HEMT with a Fe-doped GaN buffer on Si exhibited much more stable and higher BVs by successfully suppressing the premature failure caused by Si breakdown. As a result, a BV of 295 V and the specific on-resistance ( $AR_{DS(ON)}$ ) of 2.44 mΩcm<sup>2</sup> was achieved [C1354]

#### "Characteristics of InGaIn Channel HEMTs Grown by MOCVD"

The AlGaIn/InGaIn/GaN high electron-mobility transistors (HEMTs) structure was grown by metal organic chemical vapor deposition (MOCVD) on (0001) sapphire substrates. The electron transport properties were investigated by variable temperature Hall effect measurements. The fabricated devices with gate length of 0.8μm and gate width of 120 μm show a transconductance of 136mS/mm and maximum drain current of 435mA/mm. The small signal properties were also achieved with the current gain cut-off frequency ( $f_T$ ) of 5.8GHz and the maximum frequency of oscillation ( $f_{MAX}$ ) of 17GHz [C1355]

#### "A Novel E-mode PHEMT Linearized Darlington Cascode Amplifier"

This paper reports the first results of a new Darlington cascode topology implemented with 0.5μm E-mode

PHEMTs. The Darlington cascode employs active self-bias and a linearizing Darlington cascode (DCAS) circuit for achieving robust bias and enhanced gain and IP3-bandwidth performance. The Darlington cascode achieves 12.5 dB gain with a 16 GHz 3-dB BW-a 60% BW improvement over the conventional Darlington. The DCAS obtains an IP3 of 29 dBm with a 13 GHz BW-an 80% improvement in IP3-BW over the conventional Darlington approach. These improvements have been obtained without significantly compromising NF, stability, or bias robustness. The new DCAS amplifier design can be applied to other semiconductor technologies and offers an approach for compacting high microwave performance into a small area without the use of distributed techniques [C1356]

#### "High Performance Dual Recess 0.15- $\mu$ m pHEMT for Multi-Function MMIC Applications"

This paper describes a dual recess 0.15- $\mu$ m gate length pseudomorphic high electron mobility transistor (pHEMT) technology for multi-function MMIC applications at microwave and millimeter-wave frequencies. This 0.15- $\mu$ m power pHEMT not only produces high efficiency power amplification at Ka- and Q-band but also exhibits excellent noise and third-order-intercept (TOI) performance. At 35 GHz, output power density of 0.86 W/mm, power gain of 5.6 dB, and power-added efficiencies of 38 to 44 % were demonstrated. Low noise figure of 1.0 dB at 26 GHz was also measured. Additionally, we have demonstrated a gain of 11.7 dB and a TOI of 35 dBm at 18 GHz for a 300- $\mu$ m unit cell. This microwave device technology is suitable for producing high performance power amplifier, low noise receiver, high linearity, transmit/receive and multi-function MMICs. [C1357]

#### "Broadband Dual-Gate Balanced Low Noise Amplifiers"

In this paper, we present three MMIC low noise amplifiers using dual-gate GaAs HEMT devices in a balanced amplifier configuration. The designs target three different frequency bands including 5-9 GHz, 9-18 GHz and 20-40 GHz. These dual-gate balanced designs demonstrate the excellent qualities of balanced amplifiers in terms of bandwidth, matched characteristics and bandwidth, but demonstrate higher bandwidth than designs with a single-stage common-source device. Additionally, noise performance is excellent, with the 5-9 GHz LNA demonstrating <1.75-dB NF, the 9-18 GHz LNA <2.75-dB NF and the 20-40 GHz LNA <2.5 dB NF. Demonstrating high gain and excellent bandwidth, the dual-gate devices seem a logical choice for the balanced amplifier topology [C1358]

#### "A Fully Matched Ku-band 9W PHEMT MMIC High Power Amplifier"

A 9 watt AlGaAs/InGaAs/GaAs PHEMT MMIC power amplifier for Ku band applications is presented. This two-stage amplifier with chip size of 11.12 mm<sup>2</sup>(4.52 mm times 2.46 mm) is designed to fully match 50 ohm input and output impedance. With 8 volts and 900 mA DC bias condition, 12 dB small signal gain, 39.5 dBm (9 Watt) saturated output power with 30% power-added efficiency from 14 to 14.2 GHz can be achieved. This high power amplifier also achieved the best power densities (809 mW/ mm<sup>2</sup>) at Ku band reported to date [C1359]

#### "Indium Antimonide Based Technology for RF Applications"

Indium antimonide has the highest electron mobility and saturation velocity of any semiconductor, so gives the prospect of extremely high frequency operation with very low power dissipation. We report uncooled transistors with cut-off frequency of 340 GHz at a source-drain voltage of 0.5 V, leading towards this goal [C1360]

#### "A comparison of cryogenically cooled pseudomorphic and lattice matched InP HEMTs: Implementation in an ultra-low noise amplifier"

A comparison between lattice matched (Im) and pseudomorphic HEMTs (pHEMTs) aimed for cryogenically cooled low-noise amplifiers (LNAs) has been performed. The DC and RF performance of the HEMTs at room temperature (RT) has been investigated. The devices have been tested in a hybrid 4-8 GHz LNA. While the gain and noise were superior for the pHEMT compared with the Im HEMT at RT, the noise performance was slightly inferior for the pHEMT when cooled to 20 K. The gain was still higher for the pHEMT at 20 K. [C1361]

#### "Tunable coplanar filter for F-band wireless receivers"

A tunable-filter for a 120-GHz-band receiver MMIC, which is used for a 10-Gbit/s wireless link, was designed and fabricated. The filter can change both the center frequency and bandwidth simultaneously. The filter is a Bessel-type filter and composed of three dual coplanar open stubs and variable-reactance circuits. The filter was monotonically fabricated with InP HEMTs on a single-chip, which occupies only 400  $\mu$ m times 500  $\mu$ m. We measured the tuning range of the filter. The center frequency can be adjusted from 118 to 122 GHz with the bandwidth of 15 GHz, and the 3-dB bandwidth can be adjusted from 11 to 16.5 GHz at the center frequency of

120 GHz. [C1362]

### "Field-Plate Optimization of AlGaIn/GaN HEMTs"

An investigation on the field plate technique in AlGaIn/GaN power HEMTs is presented. The critical geometrical variables controlling the field distribution in the channel are determined and optimized for improved device reliability using two-dimensional numerical simulations. The results are implemented in the design of devices fabricated with 600 nm down to 150 nm gate lengths. Good agreement between experimental and simulation data is achieved [C1363]

### "Large-signal modelling and comparison of AlGaIn/GaN HEMTs and SiC MESFETs"

The Large Signal (LS) model for GaN and SiC FET devices was developed and evaluated with DC, S, and LS measurements. Special attention was paid to improve the management of harmonics and to provide a more physical treatment of the dispersion. The model was implemented in a commercial CAD tool and exhibits good overall accuracy. [C1364]

### "A high power performance 60 GHz push-push oscillator MMIC in metamorphic HEMT technology"

This paper reports a high power 60 GHz push-push oscillator fabricated using 0.12  $\mu\text{m}$  GaAs metamorphic high electron-mobility transistors (MHEMTs). The devices with a 0.12  $\mu\text{m}$  gate-length exhibited good DC and RF characteristics such as a maximum drain current of 700 mA/mm, a peak  $g_{\text{mof}}$  of 660 mS/mm, an  $f_{\text{Tof}}$  of 170 GHz, and an  $f_{\text{MAXof}}$  of more than 300 GHz. By combining two sub-oscillators having 6 x 50  $\mu\text{m}$  peripheries MHEMT, the push-push oscillator achieved 5.8 dBm of output power at 59.9 GHz with good fundamental suppression. This is the first monolithic push-push oscillator in 60 GHz band fabricated using MHEMT technology, and demonstrates a potential of MHEMT for cost effective millimeter wave commercial applications. [C1365]

### "Volterra series approach to behavioral modeling: Application to an FET amplifier"

In this paper nonlinearities due to FET amplifiers are described by using a novel behavioral modeling approach. While our proposed method requires the identification of delays and coefficients like in a standard diagonal memory polynomial model, the importance of out-of-diagonal terms is emphasized if the amplifier exhibits memory effects. Furthermore, the different terms, delays and coefficients are shown to be related to Volterra kernels. In order to validate this approach a HEMT amplifier has been constructed and characterized with W-CDMA signals at diverse symbol rates and input levels. The predictions obtained with the proposed model demonstrate a very good agreement with experimental results and have been compared with a diagonal memory polynomial model. [C1366]

### "High-efficiency GaN/AlGaIn HEMT oscillator operating at L-band"

This paper presents a new design method to implement the high efficiency oscillator based on the AlGaIn/GaN HEMT for the wireless power transmission (WPT) system. The oscillator has been developed with  $\text{Se}_2\text{O}_3$ -passivated AlGaIn/GaN HEMT and has achieved the maximum efficiency of 40.5% and the maximum output power of 23 dBm for WPT applications. With both the high output power of the circuit and inherent device material advantages, the phase noise performances of -97 dBc/Hz and -125 dBc/Hz at offsets of 100 kHz and 1 MHz, respectively, have been achieved. To our knowledge, the achieved efficiency is the highest ever reported for a GaN oscillator. [C1367]

### "Residual and oscillator phase noise in GaAs metamorphic HEMTs"

Residual phase noise measurements have been carried out on GaAs metamorphic high electron mobility transistors, mHEMT in order to explain phase noise results from mHEMT based VCOs. Noise is measured for several biases and input powers. The measurements show that the residual phase noise is increasing with increasing drain source voltages even in saturation, possibly due to the triggering of impact ionization mechanisms. This increase in noise will act deleterious on the phase noise performance of a VCO that have the drain bias increased in order to achieve higher power in the tank and thus reduce the phase noise. The reduction in phase noise due to higher power in the tank is shown to be counteracted by the increase in residual phase noise from the mHEMTs for higher drain source voltages. [C1368]

### "Numerical investigation on thermal characteristics of GaN HFETs for high power applications"

In this paper, numerical investigation on GaN HFETs is carried out using hybrid finite element method (FEM) which combines the FEM with the preconditioned conjugated gradient technique. The maximum temperatures of

the HFETs operating under continuous-waves (CW) and pulsed-waves (PW) are both captured accurately. The effects of temperature- dependent thermal conductivities of the materials on the temperature distribution are also studied and compared for different substrate materials, such as sapphire, silicon, and SiC. [C1369]

### "Low Noise Direct Detection Sensors for Millimeter Wave Imaging"

As millimeter wave electronic component technologies have matured, passive millimeter wave (mmW) imaging using direct detection is emerging as a cost effective approach to imaging through obscuring materials such as clothing for concealed weapons detection or sand for rotorcraft landing. This paper reviews the basic operation of W band direct detection receivers, and describes progress made at HRL in the development of mmW front end IC components. InP HEMT LNAs provide high gain and low noise, appropriate for high sensitivity front ends that require relatively short integration times. Sb-based MMIC detectors provide high sensitivity and low noise, relaxing the gain requirements of the LNA. Finally, promising results of the ongoing DARPA MIATA program demonstrate reasonable sensitivity of a purely passive imaging module, the first step toward imaging without the need for LNAs [C1370]

### "A 77 GHz Transceiver for Automotive Radar System Using a 120nm In<sub>0.4</sub>AlAs/In<sub>0.35</sub>GaAs Metamorphic HEMTs"

In this work, the authors demonstrate a compact 77GHz single-chip transceiver for an automotive radar system. The transceiver consists of a low noise amplifier, mixer, doubler and power amplifier. The MMIC chip set is fabricated using a 120nm-gate-length In<sub>0.4</sub>AlAs/In<sub>0.35</sub>GaAs mHEMT. The low noise amplifier demonstrated a small signal gain of 19dB at 77GHz. The resistive mixer achieved a -11dB conversion gain. The doubler achieved 0.4dBm output power, a -5.6dB conversion gain and a difference of 18.4dBc between the 77GHz output and the fundamental output. The power amplifier demonstrated a small signal gain of 21.4dB at 77GHz with 12.3dBm output power. The single-chip transceiver demonstrated 9.3dBm output power at the transmitter and a 5dB conversion gain at the receiver [C1371]

### "A 1V, 0.9dB noise-figure high linearity LNA MMIC for concurrent GPS handset application"

A highly linear low-noise amplifier (LNA) for concurrent GPS (S-GPS) application is described. In addition to the out-of-band sensitivity requirements of the non- concurrent GPS systems, the additional difficulties facing S-GPS operation is analyzed and simulation results presented. It is shown that in order for GPS reception to co-exist simultaneously with cellular band frequencies, there needs to be at least 42 dB of isolation between the power amplifier output and the GPS input and very linear GPS LNA performance. These results define the necessary specifications for the GPS LNA in the new S-GPS applications. The LNA was designed in an enhancement-mode pHEMT process for the best linearity- noise combination. The LNA operates down to 1V supply with input IIP3 better than +3 dBm gain achieved is 14 dB with 0.9 dB noise figure. Power consumption is less than 5 mW. The complete design is packaged in an ultra-thin 0.4 mm plastic package occupying 2 mm x 1.3 mm area. [C1372]

### "Ka-band MMIC high power amplifier (4W at 30GHz) with record compact size"

We report a compact and efficient Ka-band high power amplifier with output power of over 4W at 30GHz and record compact area of 8.63mm<sup>2</sup> in a Ka-band high power amplifier (HPA) class. The bias capacitors ( 80pF) are included inside the MMIC so that it reduces the assembly cost in the package or module. We employed a dual-recessed 0.15μm power pHEMT production process and 2mil-substrate technology to achieve high output power with high efficiency and compact design. The output power (CW measurement) is 36.2dBm, and, the gain, 22.5dB, at 30GHz. These results set the benchmark of CW output power per millimeter square area for the reported performance of Ka-band HPA MMICs. [C1373]

### "ESD protection for pHEMT MMIC amplifiers"

In this paper, we discuss ESD characterization data on typical circuit elements used in GaAs pHEMT MMIC amplifiers. At microwave and mm-wave frequencies, basic circuit performance considerations drive design decisions. Human body model (HBM) data for basic circuit elements can provide guidance for layout and topology trade-offs to improve ESD performance. Critical circuit elements include a) closely spaced conductors, b) FETs, and c) capacitors. Construction details and spacing affect ESD performance of passive conductors. Total FET gate width is the critical factor for FETs. Area and dielectric thickness are critical for capacitors. On-chip diode networks can provide practical protection for gate bias terminals, easily exceeding 2000 V HBM. [C1374]



### "Fabrication and characterization of N-face AlGaIn/GaN/AlGaIn HEMTs"

The paper reports on the characteristics of N-face AlGaIn/GaN/AlGaIn HEMTs. Ohmic contact optimization experiments based on the Ti/Al/Ni/Au metallization scheme commonly used for Ga-face AlGaIn/GaN HEMTs were carried out and a low contact resistance of 1.3 Ohm/mm was achieved. The devices were then characterized before and after SiN passivation. Before passivation, large current dispersion was observed in 80μs pulsed I-V measurements compare to the DC I-V curves. The adoption of a SiN passivation layer improved the I-V pulsed characteristics at 80μs but current dispersion was still severe when using shorter (200ns) pulse widths [C1375]

### "High-power stable field-plated AlGaIn-GaN MOSHFETs"

We describe novel AlGaIn-GaN metal-oxide-semiconductor heterostructure field-effect transistors (MOSHFETs) with record high power-voltage efficiencies (PVE = RF power/Drain bias), up to 0.43W/V-mm at 2 GHz. The RF powers of 15 W/mm at 35 V (PVE=0.43 W/V-mm) and 20 W/mm at 55 V (PVE= 0.36W/V-mm) were measured, which are approximately 50% higher than the previously reported values of PVE=0.25 W/V-mm (30 W/mm at 120 V). The MOSHFET devices exhibit an extremely stable operation for times in excess of 120 hours at power levels close to 20 W/mm. This is also the first demonstration of stability for a III-N microwave FET device at such a high power level. The key features of our new device design are (i) current collapse-free operation using trapped charge removing field-plates over leaky dielectric layers; (ii) selective area doping to achieve record low access resistances and (iii) an insulated gate design suppressing forward gate currents responsible for device degradation. In the paper we will present detailed experimental evidence to support our explanations for achieving the record RF-performance for the III-N FETs for the first time [C1376]

### "Design of a microwave channelized active filter for MMIC"

The emergence of new wireless communication systems is always increasing the need for smaller, lighter and cheaper components while technical issues are harder to address as higher frequencies are used. We present the design of a fully integrated microwave bandpass filter, using only lumped components and HEMTs, to fulfill the input requirements of a LMDS client. The channelized filter approach has been used, since it has been demonstrated that this approach can achieve high selectivity in high frequency bands. A three branches design is used. All branches must be optimized so that their individual responses are added in the bandpass while they interfere outside to result in a very selective behavior. Each branch comprises two identical amplifiers and a third order Butterworth filter properly optimized. Final design simulations show that the filter is very selective with a 400 MHz bandpass bandwidth centered at 28.1 GHz. The bandpass gain is slightly over 4 dB and the rejection over 80 dB. The resulting circuit would cover an area of about 10 mm<sup>2</sup>. Further study shows that the circuit is somewhat sensitive to component tolerances. However, the sensitivity is associated with the lumped filters components used in each branch and not with the amplifiers' characteristics. Consequently, manufacturing yield should not be substantially less than the yield of the HEMT process itself [C1377]

### "Planar tunneling-coupled field-effect transistor for low-power mixed-signal applications"

In this paper, we report a prototype demonstration of room-temperature resonant tunneling-coupled transistors in FET layout (TCT), in which tunneling characteristics such as negative differential resistance (NDR) and peak current are directly controlled by surface Schottky gate with high gain and transconductance. Functionality of the device can also be switched between FET mode and tunneling transistor mode. The fabrication process is fully compatible with conventional FET processes, offering a fully integrable and scalable tunneling transistor technology. Prototype planar TCTs were fabricated with resonantly-coupled dual-channel InAlAs/InGaAs/InP HEMT heterostructures by providing independent electrical contacts to each channel. The current-voltage characteristics are determined by an interwell and intersubband tunneling. The fabrication process was done using an I-line Cannon stepper on full 3-inch wafers with implanted back-gates defined prior to MBE growth of closely-coupled dual-channel HEMT layers. The highest mobility of the closely-coupled dual-channel HEMT layers observed so far is 9600 cm<sup>2</sup>/Vs at room temperature [C1378]

### "AlGaIn/GaN power HEMT for Ka-band"

Results of design and manufacturing of power AlGaIn/GaN HEMT for Ka-band are submitted. It has P<sub>out</sub> = 1, 4W/mm, efficiency 33% at F = 35 GHz. [C1379]

### "Computer-aided design of ultrawide-band MMIC amplifier"

The design of 2-10 GHz feedback MMIC amplifier is presented using a new interactive "visual" technique. The existing design procedures for microwave amplifiers with compensation/feedback networks are cumbersome and

time-consuming. In this paper, we demonstrate the design of single-stage ultrawide-band feedback MMIC amplifier using a new interactive "visual" technique. The technique allows the exact synthesis of compensation/feedback networks directly from a simultaneous set of performance specifications, including the gain, gain flatness, noise figure, input/output matching, and stability. The procedure is implemented in our "visual" CAD tools, AMP-CF and LOCUS, providing the fast and convenient amplifier design. With these tools, we have designed and fabricated a 2-10 GHz feedback MMIC amplifier that can be served as an amplifier block for different applications. Amplifier has been implemented in 0.2  $\mu\text{m}$  pHEMT GaAs technology (OMMIC, France), providing gain  $11.7 \pm 1.1$  dB, noise figure 2.2 dB, input and output return losses -9.6 dB and -11.7 dB, respectively [C1380]

#### "Millimeter wave HEMTs of R&PC &Istok&Gt;"

First results of heterostructure field effect transistors with 120, 300 and 600  $\mu\text{m}$  gate widths developed in R&PC &Istok&Gt; are presented. Pseudo-morphic high electron mobility epitaxial structure were grown by molecular beam epitaxy. Typical channel carrier concentration  $2.0 \cdot 10^{12} \text{cm}^{-2}$  with mobilities  $>6000 \text{ cm}^2/\text{V}\cdot\text{s}$  were obtained at 300 K. The transistors were fabricated with 0.15-0.25  $\mu\text{m}$  T-gate. The devices demonstrate minimum noise figure less than 2 dB, associated gain more than 5 dB at 40 GHz, and output power density about 900 mW/mm at centimeter wave-length band with power added efficiency more than 30%. [C1381]

#### "Enhancement-mode InAlAs/InGaAs/InP HEMTs with Ir-based gate metallization"

The reliability of high electron mobility transistors (HEMTs) significantly depends on the stability of the gate Schottky contact to the semiconductor. Gate sinking during the fabrication and device operation alters transconductance, gate capacitance, and threshold voltage, which are crucial device parameters for modeling HEMT devices and designing circuits. In particular for enhancement-mode InAlAs/InGaAs/InP HEMTs (eHEMTs) where thermally-treated Pt is utilized as the gate metallization, thermal stability has always constituted a problem due to the diffusion of Pt. Although aspects of this diffusion are utilized to enhance e-mode behavior, no quantitative measurements have been conducted to estimate the diffusion depth of Pt in InAlAs. Further, it would be preferable to develop a metallization scheme where the Schottky contact barrier height is similar to that of Pt but with a much lower diffusivity. To this end, we have developed a gate metal structure based on Ir for InAlAs/InGaAs/InP HEMTs and investigated its thermal stability in comparison to the conventional Pt-based contact. A 0.15  $\mu\text{m}$ -gate-length eHEMT utilizing Ir/Ti/Pt/Au gate was fabricated to demonstrate the potential of Ir-based gate technology [C1382]

#### "Vertically-scaled 100nm T-gate AlGaIn/GaN HEMTs with 125GHz $f_{\text{sub T}}$ and 174GHz $f_{\text{sub MAX}}$ "

In this work, we report on vertically scaled, 100nm gate-length Al<sub>0.31</sub>Ga<sub>0.69</sub>N/AlN/GaN HEMTs with a low sheet resistance of 260  $\Omega/\text{square}$ , an  $f_{\text{ToF}}$  of 125 GHz and an  $f_{\text{max}}(U_g)$  of 174 GHz. Careful device design and unique process features also resulted in a high peak  $G_m$ , ext of 498 mS/mm, an  $I_{\text{dssof}}$  of 1.2A/mm, and a gate-to-drain breakdown of 30V [C1383]

#### "AlGaIn/GaN HEMTs with an InGaN-based back-barrier"

In this work, we use an ultra-thin InGaN layer below the GaN channel to increase the confinement of the electrons. In this novel approach, the polarization induced electric field in the InGaN layer is used to raise the conduction band energy in the buffer layer with respect to the channel. With this technique, a double-heterojunction transistor can be formed without the need of a high bandgap or p-doped buffer. Poisson-Schrodinger simulations (Wu, et.al.) have confirmed the increased electron confinement at electron temperatures as high as 3000 K [C1384]

#### "Switching characteristics of high-breakdown voltage AlGaIn/GaN HEMTs"

In this report we present the switching measurements on large area AlGaIn/GaN HEMT devices with high breakdown voltage achieved with the help of multiple field plates. AlGaIn/GaN high electron mobility transistors have shown potential advantages over Si and SiC based transistors for high power switching. The very high electron mobility in the AlGaIn/GaN HEMT system combined with the high density of polarization induced 2D electron concentration yield a very low on-resistance and high switching frequency. Also the high band gap energy of AlGaIn/GaN system results in a high critical electric field. Hence it is possible to have high voltage power switches capable of operating at high frequencies ( $\sim 100\text{MHz}$ ). However there are some difficulties, which have prevented the achievement of very high breakdown voltages at high frequency operation [C1385]

### "260 GHz FT, 280 GHz fMAX AISb/InAs HEMT technology"

{no data available} [C1386]

### "New HEMT structures for THz applications"

THz radiations present a great interest for applications in different fields ranging from telecommunications to sensors for biology and medicine. This paper reviews two new field effect devices especially suited for THz applications: double-gate HEMTs (DG-HEMT) and plasma wave transistors [C1387]

### "A highly efficient Q-band MMIC 2.8 Watt output power amplifier based on 0.15µm InGaAs/GaAs pHEMT process technology"

A highly efficient and high power monolithic power amplifier operating at Q-band is presented utilizing 0.15µm pseudomorphic InGaAs/GaAs HEMT production process on 2-mil thick substrate. Over 42 to 46GHz frequency range, the amplifier demonstrated maximum power of 2.8 watts (34.5 dBm) and power-added-efficiency of 23 to 26% when operated at 5 volts and 250ma/mm. The amplifier attained maximum PAE of 24 to 29% and power of 33.6 to 34dBm when it is biased at 5 volts and 125ma/mm. At these power levels and power-added efficiencies, the amplifier exhibited power densities in excess of 430mW/mm. With device periphery ratio of 1:2.857, effective phase compensation of the input feed network, and low loss output combining network, the power amplifier has been able to attain state-of-the-art efficiency and power performance. [C1388]

### "Prediction of harmonic tuning performance in pHEMTs"

This paper focuses on the characterization and optimization of microwave power transistors using a commercial on-wafer harmonic load pull system. Specific attention is paid to the output tuning of the second harmonic impedance presented to the device. The ability to quantify the level of accuracy in a load pull system is explored by using various calibration validation methods. Experiments and simulation comparisons are described for a GaAs pHEMT and a GaAs HJFET. The measured harmonic load pull data pointed to different guidance on how one would match the 2ndharmonic for best performance. [C1389]

### "Noise behavior of buried channel SiGe HFETs for high speed circuit's applications"

Microwave and low frequency noise performance of buried channel SiGe HFETs fabricated on several strain relieved buffer (SRB) are presented. The impact of such SRB on microwave device noise performance is estimated by a proper noise de-embedding technique. The influence of device gate length on high microwave noise parameters is also discussed. High frequency noise properties measured in the 2.5-18 GHz frequency range are simulated means of the small signal equivalent circuit. Good agreement between measurement and modeling is obtained Furthermore, the low frequency noise properties for devices with different gate dimensions are discussed in order to predict further improvements on noise performance when shrinking the gate length below 100 nm. [C1390]

### "The future of compound semiconductors for aerospace and defense applications"

We present an overview of the current state of the art and discuss issues associated with competition and the future of compound semiconductor technology, especially for aerospace and defense applications. [C1391]

### "Metamorphic HEMT amplifier for K- and Ka-band applications"

This paper presents an integrated high gain two-stage amplifier covering frequency range from 18 GHz to 40 GHz. The chip was manufactured using a commercially available 0.15 µm GaAs based metamorphic HEMT technology and the chip size is 2.1 mm Ч 1.1 mm. Parallel resistive feedback is used for obtaining a broadband and flat gain response and for stabilizing the amplifier. We measured in on-wafer tests for the amplifier a small-signal gain of 22.5 ± 2.5 dB at K- and Ka-bands. The measured 1 dB output compression point is better than +13 dBm at K-band and better than +9.5 dBm at Ka-band using a low 2.5 volts supply. In addition, we measured 10 amplifier chips to verify the performance variation from chip to chip. The measurements showed a maximum of 2 dB deviation in small-signal gain. [C1392]

### "A 150-215 GHz InP HEMT low noise amplifier with 12 dB gain"

We present a 150-215 GHz InP HEMT MMIC with greater than 12dB gain across this band. The MMIC is a 3-stage, single-ended microstrip design implemented using 0.07 mum T-gate InP HEMT MMIC technology with 50 mum substrate [C1393]

#### "A low power AlSb/InAs HEMT X-band low noise amplifier"

We present design and characterization of a low power single stage X-band low noise amplifier in an AlSb/InAs HEMT integrated circuit technology. Gain, noise, linearity, and phase noise characterization are presented [C1394]

#### "Artificial neural network-based procedure for cryogenic microwave noise characterization of HEMT's"

{no data available} [C1395]

#### "A novel 50-Gbit/s NRZ-RZ converter with retiming function using InP HEMT technology"

We developed a novel electrical non-return-to-zero (NRZ) to return-to-zero (RZ) converter circuit based on a master-slave D-type flip-flop (D-FF). Its decision and re-timing function makes the converter without any delay or phase control circuitry, which are usually employed to adjust the phase alignment of data and clock. The circuit achieved 50-Gbit/s operation by using 0.13  $\mu\text{m}$  gate-length InP HEMT technology. The supply voltage was -5.2 V and the power consumption was 1.1W. A module with the circuit mounted realized 44-Gbit/s operation. [C1396]

#### "Field-plated GaN HEMTs and amplifiers"

Field-plates remarkably enhanced large-signal performance of GaN HEMTs by reducing trapping effect and increasing breakdown voltages. Power densities exceeding 30W/mm at 4GHz were demonstrated with gate-connected field plates. Further development of source-connected field plates boosted large-signal gain by 5-7dB, while maintaining the benefit of the field plates. Short-channel GaN HEMTs with field plates also showed promise at millimeter-wave bands. Amplifiers with 1.08-mm-wide device periphery generated 5W at 35GHz. [C1397]

#### "MMIC-oscillator designs for ultra low phase noise"

Various balanced VCO-topologies like cross-connected (negative gm), coupled cross-connected, coupled Colpitt and Clapp oscillators, all with a fully integrated tank are reported. In this study, different MMIC/RFIC technologies such as SiGe HBT, InGaP-GaAs-HBT, PHEMT, MHEMT, and CMOS are represented and parameters such as phase-noise, output power, dc-power consumption, and tuning range are compared. All oscillators are designed for low phase noise. Low phase noise can be achieved by CMOS, PHEMT and MHEMT technologies although SiGe and InGaP-GaAs HBT based oscillators have demonstrated the lowest phase noise. Both fundamental and second harmonic VCOs are represented in the evaluation. [C1398]

#### "A family of 1, 2 and 4-watt power amplifier MMICs for cost effective VSAT ground terminals"

A complete family of cost effective power amplifier MMICs for Ka-band VSAT ground terminals has been developed. Taking advantage of a 6-inch, 0.15 $\mu\text{m}$  pHEMT process on 100- $\mu\text{m}$  thick substrate, the amplifiers exhibit high performance at the lower processing cost: the single-ended, 3-stage amplifier MMIC has more than 27-dB gain at 30GHz and 1-watt saturated output power within a chip size of less than 3.9mm<sup>2</sup>. Two versions of 2-watt power amplifiers, differing in bandwidth, have small signal gain of 24 and 21dB between 28 and 32GHz with excellent additional characteristics (36% PAE and 41-dBm OIP3); their chip sizes are 9.5 and 7.4mm<sup>2</sup>. Finally, a balanced power amplifier achieves 4watts from 28 to 30GHz, with a power added efficiency of more than 31% and 43-dBm OIP3, in a chip area of 14mm<sup>2</sup>. In term of power and gain density per chip area, these results are among the best reported for GaAs pHEMT on 100- $\mu\text{m}$  substrates. [C1399]

#### "High-efficiency class-E power amplifier using field-plated GaN HEMTs"

This paper presents class-E microwave monolithic integrated circuit (MMIC) power amplifiers at 2.0 GHz, which is based on field-plated GaN HEMT technology. The 2-stage power amplifier consists of a class-F driver stage and a class-E power stage. The circuit schematic, layout and fabrication are described. The amplifier achieves an output power of 37.5dBm into a 50H load, a power added efficiency (PAE) of 50%, and a gain of 18.2dB. A power density of 5.6W/mm is achieved. [C1400]

#### "Highly uniform AlGaIn/GaN power HEMT on a 3-inch conductive N-SiC substrate for wireless base station application"

Highly uniform AlGaIn/GaN high electron mobility transistors (HEMTs) were fabricated on a low-cost 3-inch



conductive n-SiC substrate for the first time. Average values of threshold voltage ( $V_{th}$ ) and transconductance ( $g_m$ ) of AlGaIn/GaN HEMT were -1.55V and 194 mS/mm. Standard variations of those values were only 0.15V and 3.9mS/mm across an entire 3-inch conductive substrate. The 1-mm-gate-periphery GaN HEMT chip, which was operated at 60V, achieved high CW output power density of 7.0W/mm, with a high linear gain of 22.2dB and power added efficiency (PAE) of 70% at 2.14GHz. Standard variations of power density, linear gain and PAE at 50V were only 0.42W/mm, 0.2dB and 3.0 point, respectively. This low-cost highly uniform high-gain chip technology is sufficient for mass production of wireless base station application using GaN-HEMTs. [C1401]

#### "Improved efficiency, IP3-bandwidth and robustness of a microwave Darlington amplifier using 0.5 $\mu$ m ED PHEMT and a new circuit topology"

This paper reports on the first results of a self-biased e-mode PHEMT Darlington amplifier. The e-mode PHEMTs enable a FET Darlington implementation while a new Darlington active bias topology reduces bias variation over temperature and supply, and improves overall efficiency by reducing supply operation. A 3.3V-75mA amplifier achieves a BW of 0.1-14GHz, 12.3dB gain, NF of 3.5dB, IP3 and P1dB of 33.1dBm and 16dBm @ 2GHz, respectively. A 5V-75mA amplifier achieves a 0.1-10 GHz BW, 20.2 dB gain, NF of 2.9 dB, IP3 and P1dB of 34.2dBm and 21.8dBm @ 2 GHz, respectively. The new PHEMT Darlington amplifier design enables a factor of 2 better IP3-bandwidth product and lower voltage operation capability compared to InGaP-based Darlington amplifiers. [C1402]

#### "Temperature behavior of AlGaIn/GaN on SiC HEMTs"

This study presents extensive characterization and comparison of current GaN/SiC devices (from 5 US manufacturers) across temperature (-25-125°C). The changes with temperature for: saturated current ( $I_{dss}$ ), transconductance ( $g_m$ ), and maximum stable gain (MSG) are measured and statistics are studied. The typical temperature-coefficients (TC) are established for  $I_{dss}$ ,  $g_m$ , and MSG in GaN technology. This information is useful for MMIC designs. The minimum temperature coefficients compare well with theoretical expectations. Finally, a correlation is observed between the temperature behavior of RF and DC parameters. [C1403]

#### "The magnetic controlled autogenerator superhigh frequencies"

Investigations of superhigh-frequency oscillator are presented on the basis of transistor structure consisting of bipolar and HEMT of transistors. The possibility of both magnetic and electric frequency control of generation is shown [C1404]

#### "A 60 GHz MMIC pHEMT image reject mixer with integrated ultra wideband IF hybrid and 30 dB of image rejection ratio"

A 60 GHz image reject mixer (IRM) with an integrated ultra wideband IF hybrid has been designed, fabricated and characterized in a commercial pHEMT MMIC process. A measured conversion loss ( $L_c$ ) of 10.2 to 11.4 dB over the frequency range 55 to 65 GHz is obtained with a state-of-the-art image rejection ratio (IRR) of 30 dB at the 60 GHz center frequency. For an IF frequency between 2 and 3 GHz, the variation in  $L_{cis}$  is less than 1 dB, and the IRR is better than 24 dB which is the best reported figures for an IRM operating at mm-wave frequencies with integrated IF hybrid. LO power as low as 1 dBm is sufficient to obtain the reported  $L_{cand}$  IRR. The mixer consumes virtually zero DC power since resistive mixers are used for the actual down conversion. To further minimize the overall power consumed by the system in which the IRM will be used, the combination of the two 90° out of phase IF signals are performed on-chip in an ultra wideband lumped element hybrid. This allows the system to use only one instead of two power-consuming analog to digital converters (ADCs) which thereby significantly reduces the power consumption for the overall system. [C1405]

#### "An novel L-shape active leaky-wave antenna with power combining and scanning capability"

In this paper, an active-integrated leaky-wave antenna with power combining scanning capability is presented. This leaky-wave antenna with the novel perpendicular L-shape topology is integrated with a varactor-tuned high-electron mobility transistor (HEMT) voltage controlled oscillator (VCO) on the same plane. Changing the VCO frequency, we can control not only the dual-beam scanning angle but also derive the power combining effect with the sum ( $\Sigma$ ) or difference ( $\Delta$ ) radiation patterns. The power combining effect of difference mode, which is the dual-beam pattern and the sum mode pattern, which is a 3-beam pattern, with the 3rd beam located along the middle direction (45°, 135°) of the X and Y axes. The measured scanning angle is steered over a range of 24-46° for the right beam and 127-148° for the left beam. Compared with single microstrip leaky-wave antenna, the L-shape LWAs configuration has the advantages of switchable radiation patterns as the VCO varied from 10GHz to 10.6GHz. [C1406]

### "Temperature dependence of DC and microwave characteristics of InGaAs/InP composite channel HEMTs"

Submicron high electron mobility transistors (HEMTs) lattice-matched to InP with InGaAs/InP composite channel were fabricated. Temperature dependence of DC and RF characteristics of the HEMTs were studied in the temperature range from 20 to 100 °C. It has been found that the DC and microwave characteristics of the composite channel HEMTs are insensitive to the temperature. In particular, an increase in the maximum frequency of oscillation ( $f_{max}$ ) was observed at elevated temperature. The InP HEMTs with an InGaAs/InP composite channel shown good thermal stability. The device may have great potential to be operated with a wide temperature range for microwave applications. [C1407]

### "Measurements of Complex Permittivity and Loss Tangent of Silicon Carbide at Millimeter Wavelengths"

High purity semi-insulating 4H-SiC is highly desirable for SiC MESFET and GaN HEMT based power microwave devices. With the presented measurement techniques, namely cavity-length variation technique of open resonator operating at 60GHz, together with dispersive Fourier transform spectroscopy (DFTS), we successfully carried out the precise dielectric measurements of a pair of high purity semi-insulating 4H-SiC wafer specimens. Excellent agreement was obtained between two experimental systems. Therefore, it proves the versatility and accuracy of our established measurement techniques [C1408]

### "Broadband 7 GHz VCO in mHEMT technology"

The design and characterization of a broadband VCO in a 0.15  $\mu\text{m}$  mHEMT technology is presented. The VCO have an output power of 0 dBm and a broad output frequency from 6.5 to 7.4 GHz using a wide multi fingered mHEMT as varactor. Phase noise is -87 dBc/Hz at 100 kHz offset exhibiting a 30 dB/decade slope due to large flicker noise sources. A comparison both to a similar pHEMT VCO and other pHEMT VCOs in the literature is included. [C1409]

### "Analysis of Temperature Model on Device Characteristics for AlGaIn/GaN MODFET for High Power Electronics"

An investigation of the temperature model of a 1  $\mu\text{m}$  gate AlGaIn/GaN n-type modulation-doped field effect transistor (MODFET) is presented. The investigated temperature range is from 100 degK-600 degK. The critical parameters for dc characteristics are the maximum drain current ( $I_{Dmax}$ ), the threshold voltage ( $V_{th}$ ), and the peak dc transconductance ( $g_m$ ). The small signal microwave parameters have been evaluated to determine the unity current gain cut-off frequency ( $f_T$ ). High  $f_T$ (10-70 GHz) values and high current levels ( ~450 mA/mm) are achieved for a 1  $\mu\text{m}$  AlGaIn/GaN MODFET [C1410]

### "0.25 $\mu\text{m}$ In<sub>0.52</sub>Al<sub>0.48</sub>As/In<sub>0.53</sub>Ga<sub>0.47</sub>As/InAs<sub>0.3</sub>P<sub>0.7</sub> composite channel HEMTs with an $f_T$ of 115GHz"

In this paper we report growth, fabrication and characterization of In<sub>0.52</sub>Al<sub>0.48</sub>As/In<sub>0.53</sub>Ga<sub>0.47</sub>As/InAs<sub>0.3</sub>P<sub>0.7</sub> composite channel HEMTs with a gate length of 0.25  $\mu\text{m}$ . In comparison with InAlAs/InGaAs/InP composite channel HEMTs, these devices have better band structure for transferring electrons to the composite channel under high electric field, thus exhibit excellent DC and microwave performance with a peak extrinsic transconductance of 888.3 mS/mm, an  $f_{To}$  of 115 GHz, and an  $f_{max}$  of 137 GHz. To our knowledge, this is the first report of InAlAs/InGaAs/InAsP composite channel HEMTs. The  $f_T$  is the highest ever reported for any composite channel HEMTs with the same gate length. [C1411]

### "A 1.8-2.3GHz wideband and compact power amplifier module using AlGaIn/GaN HEMTs"

We have developed a wideband and compact power amplifier module (PA-module) for a driver stage amplifier of a base station transmitter system using AlGaIn/GaN high electron mobility transistors (HEMTs), a nonhermetic package, clip leads, and a printed circuit board (PCB). Linear gain of 30dB, gain flatness of less than 0.5dBp-p, and saturation output power of more than 40dBm were achieved from 1.8GHz to 2.3GHz, operating at drain bias voltage ( $V_{ds}$ ) of 50V and gate bias voltage ( $V_{gs}$ ) of -3V. We demonstrated an adjacent channel leakage power ratio (ACLR) of -50dBc at average output power of 19dBm in practical 2-carrier W-CDMA signals, dissipating 13W. This PA-module covered wide frequency band and its package volume was only 2cm<sup>3</sup>. It could be compactly incorporated into various base station transmitter systems without difficulty. [C1412]

### "Analytical Modeling and Simulation of $V_{th}$ and $V_{tl}$ of the Delta-Doped MOS-Gate

### **Si/SiGe HEMT"**

The delta-doped HEMT, a subcategory of HEMT, uses a thin layer of doping in the supply layer. There are quite a few advantages of the delta-doped HEMT over the regular-doped HEMT that include increase in mobility and cutoff frequency. The model for the threshold voltage of the delta-doped MOS-gate HEMT proposed by Gokhale et al. (1993) is valid only when the delta-doped layer is very thin and the distance of the layer from the SiO<sub>2</sub>/Si interface is much larger than the thickness of the layer. Although, delta-doped HEMTs normally use a highly doped thin layer, varying the width of the layer, the threshold voltage, minimum gate voltage, transconductance, cut-off frequency etc. can be changed. In this paper, a model for the threshold voltage ( $V_{th}$ ) and the minimum gate voltage ( $V_{tl}$ ) of the p-channel delta-doped MOS-gate Si/SiGe HEMT is proposed which is valid for any thickness of the delta-doped layer. Also, the effect of the width of the delta-doped layer on the threshold voltage and the minimum gate voltage has been investigated using the analytical model. All results have been compared with Medcittrade simulation [C1413]

### **"Basic Study of Plasma Wave Interactions in GaAs Interdigital- Gated HEMT Devices from Microwave up to THz Frequencies"**

The purpose of this paper is to investigate theoretically and experimentally possible interactions between the surface plasma wave in drifting carriers in 2D electron gas (2DEG) and electromagnetic space harmonics in a GaAs interdigital-gated HEMT device from microwave to THz frequencies [C1414]

### **"AlGaIn/GaN HEMTs: Experiment and Simulation of DC Characteristics"**

This paper presents simulated DC characteristics of an AlGaIn/GaN HEMT along with corroborating experimental measurements for validation. GaN-based HFETs are vigorously pursued for possible applications in high power presented in I. Daumiller et al. (1998), high temperature presented in Y.-F. Wu et al. (2004), and high frequency devices and circuits. Theoretical experimentation is required for device optimization to realize higher power and operation at frequencies through W-band [C1415]

### **"High Breakdown Voltage AlGaIn/GaN MIS-HEMT with SiN and TiO<sub>2</sub> Gate Insulator"**

{no data available} [C1416]

### **"Advanced mm-wave ICs and applications"**

High performance integrated circuits and modules for millimeter-wave applications based on metamorphic InAlAs/InGaAs HEMTs on 4" GaAs substrates are presented. An extrinsic transit frequency of 410 GHz for 50 nm gate length devices is achieved. The IC process features high yield on both transistor and circuit levels. Two-stage low-noise amplifiers demonstrate a small signal gain of 20 dB and a noise figure of 2.4 dB at 94 GHz. An amplifier MMIC developed for G-band operation exhibits a gain of 21 dB at 220 GHz. High-gain modules featuring low-noise performance are discussed which enable novel applications, such as millimeter-wave imaging up to 220 GHz. [C1417]

### **"Microwave noise characteristics of AlGaIn/GaN HEMTs on high-resistivity silicon substrate"**

AlGaIn/GaN high-electron-mobility-transistors (HEMTs) with 0.8- $\mu$ m- and 0.3  $\mu$ m-gate-length were successfully fabricated on high-resistivity (HR) silicon substrate. The cutoff frequency  $f_T$  values of 7 GHz, 22 GHz and maximum oscillation frequency  $f_{max}$  values of 23 GHz, 40 GHz were achieved for 0.8- $\mu$ m- and 0.3- $\mu$ m-gate-length device, respectively. A minimum noise figure ( $NF_{min}$ ) of 2.0 dB and an associate gain ( $G_{ass}$ ) of 10.3 dB were achieved at 10 GHz in 0.3- $\mu$ m-gate-length device. This shows the promising potential of AlGaIn/GaN HEMTs on high-resistivity Si for cost effective low noise amplifiers. [C1418]

### **"Development of GaN-based micro chemical sensor nodes"**

Sensors based on III-N technology are gaining significant interest due to their potential for monolithic integration of RF transceivers and light sources and the capability of high temperature operations. We are developing a GaN-based micro chemical sensor node for remote detection of chemical toxins, and present electrical responses of AlGaIn/GaN HEMT (high electron mobility transistor) sensors to chemical toxins as well as other common gases. Upon exposure to a chemical toxin, the sensor showed immediate increase in source-drain current ( $I_{ds}$ ). The electrical response of the sensor was clear, reproducible and characteristic of the concentration of the analyte. This is the first time that electrical responses of chemical toxins are measured with a GaN-based microsensor. Detailed analysis on response time, sensitivity and temperature dependence will be discussed [C1419]

### "SAW chemical sensors based on AlGa<sub>N</sub>/Ga<sub>N</sub> piezoelectric material system: acoustic design and packaging considerations"

In this paper, we present the modeling of the mechanical part of a MEMS (microelectromechanical systems)-based sensor for identifying environmental contaminants and chemical or biological agents in large applications scale. The mechanical part involves the structure for the generation and reception of the surface acoustic wave likewise the packaging and housing structure of the sensor. Sensor detection mechanism is based on the changes of the surface acoustic wave (SAW) propagation along the substrate. By using various coatings on the surface of the SAW device, various cells, chemicals, gases and bio materials can be detected due to changes of the velocity or phase of a propagating acoustic wave induced by the outer environment. The AlGa<sub>N</sub>/Ga<sub>N</sub> material system preferentially grown on both silicon and sapphire (Al<sub>2</sub>O<sub>3</sub>) substrates by metal organic vapor phase epitaxy (MOCVD) or by molecular beam epitaxy (MBE) is a promising platform for fabrication of a new generation of wireless SAW sensor devices. This implicate the development of high electron mobility transistor (HEMT) structure integrated in a single chip with the SAW sensor and thus creating a unique acoustic velocity tuning device with low acoustic loss and high frequency. [C1420]

### "Bias dependent scalable noise models of MESFETs/HEMTs based on neural networks"

A bias-dependent scalable microwave MESFET/HEMT noise model is proposed in this paper. It is based on a multilayer perceptron neural network that produces noise parameters at its outputs for device gate width, biases and frequency presented at its inputs. In that way determination of the noise parameters is enabled for various values of gate width and for all operating points over a wide frequency range. Once the network is trained its structure remains unchanged. After the network training, the noise parameters determination is done without additional optimizations and without need for the measured data that are required for the network training only. [C1421]

### "Microwave circuit models using the structured genetic algorithm"

This paper describes an application of the structured genetic algorithm to the construction of microwave circuit neural network models. The algorithm is used to create a neural network model of a high electron mobility transistor (HEMT) power amplifier. Results are compared to other neural network training algorithms such as back-propagation and the Levenberg-Marquardt algorithm. Models of one and two-stage amplifiers created with the ADS circuit simulator give good predictions of measurement results. [C1422]

### "Stability of preamplifier in 84-116 GHz receiver"

The stability of InP HEMTs preamplifiers has been investigated in time and frequency domains at various cryogenic temperatures. It achieved a gain fluctuation of  $5 \times 10^{-6} \sqrt{\text{Hz}}$  and an Allan time of 9 seconds at 4 GHz bandwidth. The stability of a sideband separating (2SB) mixer receiver is tested with the IF (4-8 GHz) preamplifier at 4 K. [C1423]

### "Comparison of Hetero and Mono FET and BT Structures Hrvoje Ocvetic, Tomislav Svedek"

The properties of hetero and mono FET and BT devices are reviewed and discussed in the context of their suitability for high frequency and noise. GaAs based devices have a defined place in commercial and many more applications. The heterojunction bipolar transistor (HBT) basically is a modified bipolar transistor. The emitter and base layers are formed with different bandgap material. The emitter having the wider band gap, thus the emitter delivers a barrier against the hole injection into the base. HBT technology has become a major player in wireless communication, power amplifier, mixer, and frequency synthesizer applications. HBTs extend the advantages of silicon bipolar transistors to significantly higher frequencies. The HEMT delivers the lowest noise figure with a high gain performance. This high gain in some cases is a disadvantage for problem free volume applications in low frequency range [C1424]

### "Selective wet etching process for AlGaAs/InGaAs pHEMT fabrication"

The designed selective wet etching process for AlGaAs/InGaAs pHEMT is discussed. Proposed technology provides precise control of channel etching and demonstrates high uniformity of device characteristics [C1425]

### "New avalanche breakdown model for nonuniform electric fields"

It is shown that correct avalanche breakdown voltages for submicron MESFETs and especially for HEMTs can be obtained only if we substitute the phenomenological avalanche coefficients dependencies on electric field magnitude with the similar dependencies of these coefficients on the mean energies of electron and hole gases.



The same substitution for other kinetic coefficients is usual in so called temperature models used for simulation systems with nonuniform electric fields. Application of new model for MESFET simulation leads to noticeable improvement of measured and simulated breakdown voltages coincidence and in HEMT simulation one can obtain sensible results for current-voltage characteristics only with the help of the new model. The new model success is based on more physically meaningful operation with the great contact electric fields which are common in submicron gate MESFETs and HEMTs [C1426]

#### "Thermally self-consistent Monte Carlo simulation of InGaAs/AlGaAs HEMTs"

This paper presents results from the application of a thermally self-consistent Monte Carlo (MC) simulator to In<sub>0.15</sub>Ga<sub>0.85</sub>As/Al<sub>0.28</sub>Ga<sub>0.72</sub>As HEMTs. The simulator employs an iterative procedure which couples a MC electronic trajectory simulation with a fast Fourier series solution of the heat diffusion equation (HDE). Monte Carlo is one of the most accurate methods for simulating sub-micron semiconductor devices, as it is free from low-field, near-equilibrium approximations. In addition, the microscopic description of electron-phonon scattering in this method provides an inherent prediction of the spatial distribution of heat generation within a device. The thermal power distribution calculated from the net rate of phonon emission is fed to an HDE solver. The resulting temperature distribution is incorporated into the subsequent MC iteration. Electronic transport is simulated using three-valley spherical non-parabolic energy bandstructures. The simulations consider both the effect of optical and acoustic phonons mediating intravalley and intervalley electronic transitions. Ionised impurity, alloy disorder and electron-electron scattering processes are also included. The expected thermal droop is observed from the I-V characteristics of the simulated devices. Temperature distributions associated with different thermal power distributions are shown to be non-uniform with maximum values dependent upon the bias and the semiconductor die dimensions. [C1427]

#### "The Tenth High Frequency Postgraduate Student Colloquium (IEEE Cat. No. 05TH8848)"

{no data available} [C1428]

#### "Verification of a generalized nonlinear FET/HEMT modeling through a class A power amplifier design"

A pHEMT transistor is modeled via a generalized nonlinear FET/HEMT modeling approach. The model shows an accurate response over all three variables (power level, bias, and frequency) compared to measurements. Modeling also includes the nonlinear response at the gate. The pHEMT transistor model is utilized in this paper to design a 3 GHz class A power amplifier to verify its validity. The predicted output power, gain, and drain efficiency at 1 dB gain compression are 14.2 dBm, 14.7 dB, and 32.1%. The measured are 12 dBm, 13.5 dB, and 27.4%, which shows good agreement with the simulation [C1429]

#### "Self-aligned AlGaIn/GaN MODFET with liquid phase deposited oxide gate for microwave power applications"

As promising candidates for future microwave power devices, GaN-based high-electron mobility transistors (HEMTs) have attracted much research interest. An investigation of the operation of AlGaIn/GaN n type self-aligned MOSFET with modulation doped GaN channels is presented. Liquid phase deposited (LPD) SiO<sub>2</sub> is used as the insulating material. An analytical model based on modified charge control equations is developed. The investigated critical parameters of the proposed device are the maximum drain current (I<sub>Dmax</sub>), the threshold voltage (V<sub>th</sub>), the peak DC trans-conductance (g<sub>m</sub>), break down voltage (V<sub>br</sub>) and unity current gain cut-off frequency (f<sub>T</sub>). The typical DC characteristics for a gate length of 1 μm with 100 μm gate width are following: I<sub>max</sub> = 800 mA/mm, V<sub>break-down</sub> = 50 V, g<sub>m,extrinsic</sub> = 200 mS/mm, V<sub>pinchoff</sub> = -10 V. The analysis and simulation results on the transport characteristics of the MOS gate MODFET structure is compared with the previously measured experimental data. The calculated values of f<sub>T</sub>(20-130 GHz) suggest that the operation of the proposed device effectively, has sufficiently high current gain cutoff frequencies over a wide range of drain voltage, which is essential for high-power performance at microwave frequencies. The proposed device offers lower on-state resistance. The results so obtained are in close agreement with the experimental data [C1430]

#### "Ultra-low-power HEMT and HBT devices and circuit demonstrations"

During the past four years, the Defense Advanced Research Project Agency (DARPA) through its antimonide-based compound semiconductor (ABCS) program has sponsored development of high-electron-mobility transistor (HEMT) and heterojunction bipolar transistor (HBT) devices and circuits based on narrow-band-gap materials such as InAs or In<sub>x</sub>Ga<sub>1-x</sub>As with high In composition (x). These development efforts have sought to exploit the very high electron mobility and peak electron velocity of InAs for high speed circuit applications

requiring very low power dissipation. At Northrop Grumman Space Technology (NGST), InAs/AlSb HEMT and In<sub>0.86</sub>Ga<sub>0.14</sub>As/In<sub>0.86</sub>Al<sub>0.14</sub> As HBT devices have successfully been developed, and ultra-low-power circuits have successfully been demonstrated for both of these device technologies [C1431]

#### **"A Fully 2-dimensional Poisson-Schrodinger modeling of the HEMT: Effects of short gate lengths"**

{no data available} [C1432]

#### **"Researches and applications of monolithic millimeter-wave integrated circuits at National Taiwan University"**

The recent research efforts of monolithic millimeter-wave integrated circuits at National Taiwan University are presented in this paper. The scope of our researches includes III-V compound based HEMT and HBT MMICs, as well as the silicon-based (CMOS and SiGe BiCMOS) RF/MMICs. State-of-the-art results have been achieved and some of the applications are also addressed. [C1433]

#### **"The Band 3 receiver (84-116 GHz) for ALMA"**

Test results are presented of the Band 3 module integrated into the Atacama large millimeter array (ALMA) front end receiver. The 84 to 116 GHz collected signal by the Band 3 receiver is split into two orthogonal polarisations using an orthomode transducer and then down-converted to 6 GHz over 4 GHz bandwidth using sideband separating mixers with better than 10 dB of image rejection. The single sideband system's low noise of 35 to 45 K is achieved by cascading superconductor-insulator-superconductor (SIS) mixers and low noise cryogenic amplifiers that consist of three stage high mobility transistors (HEMT) operating at 4 K. [C1434]

#### **"Terahertz Photomixing in Heterostructure Device Based on Integration of High-Electron Mobility Transistor and Quantum-Well Infrared Photodetector"**

We propose and evaluate the excitation of terahertz (THz) oscillations in a heterostructure photomixing device based on the integration of a high-electron-mobility transistor (HEMT) and quantum-well infrared photodetector (QWIP) caused by middle or far infrared signals. The transient infrared radiation results in the ac current across the QWIP active region. This ac current excites THz plasma oscillations in the HEMT channel and, consequently, oscillating charges in contacts and an antenna that leads to THz emission. We develop a device model for HEMT-QWIP photomixer which combines both analytical description of electron processes and their ensemble Monte Carlo particle modeling. [C1435]

#### **"High-power GaN-HEMT devices operating at MM-wave frequencies"**

This paper summarizes the unique performance capabilities of high-power GaN high electron mobility transistor (HEMT) devices for possible integration in high power solid-state amplifiers capable of operating under severe thermal and mechanical environments. Optimum device parameters, higher bias levels, and higher cutoff frequencies are needed to achieve higher power densities at MM-wave frequencies. High power GaN-HEMTs have potential applications in third-generation mobile communications systems, auto-collision radars, and high power T/R modules used in long range missile defense radars. [C1436]

#### **"One single traveling-wave MMIC for highly linear broadband mixers and variable gain amplifiers"**

A traveling-wave circuit concept allowing device application both as ultra-broadband mixer and variable gain distributed amplifier is presented and demonstrated. The compact layout MMIC is realized in a 0.15μm GaAs pHEMT technology. Cascode amplifier cells with current-voltage feedback are used in eight-stage distributed configuration. In VGA mode, the gain may be controlled between 5-12dB with a near-constant bandwidth of up to 43GHz and excellent power matching properties. The amplifier is capable of delivering 20dBm to a 50Ω load. Being operated as traveling-wave mixer, the device exhibits 2dB conversion loss in a bandwidth exceeding 50GHz, while requiring the comparatively low LO power of 5dBm. Mixer operation is demonstrated both for downconversion to fixed IF- and for broadband conversion using fixed LO frequencies. In mixer mode, exceptionally high input-related linearity of 6dBm is reached. [C1437]

#### **"Low-voltage and broadband V-band InP HEMT frequency doubler MMIC"**

A broadband single-ended V-band InP HEMT frequency doubler MMIC is demonstrated. The fabricated frequency doubler MMIC was operated at 1 V drain supply voltage. The doubler consists of a fundamental input matching circuit and a (proposed herein) fundamental signal rejection filter that also operates as an output matching circuit. The fundamental signal rejection bandwidth of the proposed filtering circuit is more than four

times wider than that of a conventional open stub circuit. The doubler MMIC realizes around 0 dB conversion gain and more than 22 dB isolation between the fundamental signal and 2nd harmonic signal over the output frequencies from 54 GHz to 70 GHz. The bandwidth over which both the 3-dB bandwidth and the isolation of 20 dB are satisfied is more than 26%. The maximum conversion gain is 1.8 dB with 30.4 dB fundamental signal suppression at 60 GHz output frequency. The MMIC occupies just 0.89 mm<sup>2</sup> and consumes only 8mW. [C1438]

### "Design of power FETs based on coupled electro-thermal-electromagnetic modeling"

A comprehensive modeling approach is applied to the study of pHEMT transistors for microwave power amplifier applications. This approach combines physical, electromagnetic and thermal simulations to model large power transistors used in these applications, allowing both the individual finger contribution and the global performance to be investigated in an efficient manner, which can be used with commercial CAD tools. In this way, the design of the transistor structure contributes to the optimization of the RF performances of the complete amplifier. Discrete transistor and MMIC designs are investigated using this work with validation based on infrared and microwave measurements. [C1439]

### "Hot carrier effect on power performance in GaAs PHEMT MMIC power amplifiers"

This paper describes hot electron effects on power performance of GaAs PHEMT MMIC power amplifiers (PAs). Hot electrons are generated in PAs under RF-drive at room temperature. A long term life test of PAs under high hot electron stress was performed to investigate the effect of hot carrier induced degradation (HCID) on power performance. Accordingly, an empirical model was developed to predict the power performance of V-band PA modules by the end of life (EOL). This information is crucial for system engineers in order to budget sufficient output power so that system can still maintain performance capability by the EOL. [C1440]

### "Current performance of high speed transistors"

This work presents a comparison of high speed performance parameters between the main devices used nowadays in high speed demanding applications: SiGe HBT, InP HBT and InP HEMT. First of all, a description of the material properties and the structure characteristics is presented. Secondly, the merit figures that define the performance in this application field are discussed, and then the evolution of the transition frequency in the last twenty years is shown. [C1441]

### "Numerical 2D simulation of surface states effects in AlGaIn/GaN HEMT and GaN MESFET devices"

The consequences of surface states in field-effect devices based on GaN are analyzed in this work. DC and transient effects on drain current response are evaluated under several conditions of trap distributions at the ungated surface. Initially, a basic analysis with static surface charges is presented, revealing important consequences in the device characteristics and the type of traps. A detailed study focused on dynamic surface traps is also performed. Both, static and transient simulations provide a good understanding of the current collapse, gate-lag and related effects, showing a good agreement to experimental data. The study has been carried out in MESFET and HEMT devices using a numerical 2D simulation tool that includes polarization charges, trap ionization and hole accumulation at the surface in the electrostatic and transport equations. This model allows us to deduce the role of other device parameters such as contact resistance and leakage currents on the trap-related collapse and transient effects. [C1442]

### "S-band low noise amplifier for TT&C receiver in LEO satellites"

This paper describes the design, simulation and measurements of a 2025 to 2120 MHz single stage Pseudomorphic High Electron Mobility Transistor (pHEMT) Low Noise Amplifier (LNA), intended for use in a TT&C receiver in low Earth orbit (LEO) satellite. The LNA has been simulated with software and the results show that it provides a gain of more than 10 dB, a noise figure below 0.58 dB and VSWR less than 1:1.35. The circuit is designed on Roger's Duroid 5880 microwave laminate. The power consumption is 27 mW at VDD=12 V. [C1443]

### "Influence of kink effect on the dynamic and noise performance of short-channel InAlAs/InGaAs HEMTs"

We perform a microscopic analysis of the degradation originated by the kink effect in the dynamic and noise performance of short-channel InAlAs/InGaAs lattice matched HEMTs by using a 2D ensemble Monte Carlo simulator. The onset of kink effect leads to a significant increase of the drain conductance, whose frequency dependence reflects the influence of the processes at the origin of the kink effect. Concerning the noise

performance, the kink effect provokes an enhancement in the drain- and gate-current noise at low frequency, with a characteristic cutoff frequency related to the impact ionization rate and hole recombination time. [C1444]

#### "High temperature operation of AlGaIn/GaN HEMT"

We investigated high temperature operation of AlGaIn/GaN HEMTs. At channel temperature of 269 degC, a linear gain of 12.3 dB and a power added efficiency of 53.6% were achieved at 2.14 GHz, less than 50 V operations. These are sufficient performance to practical application. At channel temperature of 368 degC, the linear gain was 10.4 dB and a power added efficiency of 43.9% was achieved. We also investigated the temperature dependence of equivalent circuit values, and found that the temperature dependence of saturated output power and the linear gain is originated from the temperature dependence of electron velocity in the channel. [C1445]

#### "A C-band AlGaIn/GaN HEMT with Cat-CVD SiN passivation developed for an over 100 W operation"

We applied a Cat-CVD (catalytic chemical vapor deposition) passivation film to AlGaIn/GaN HEMTs, to resolve the trade-off between their drain current transient time and gate-drain break down voltage. We did not employ any field plate because it degrades high frequency operation over C-band. The SiN passivation film, deposited after a NH<sub>3</sub>treatment, resulted in less transient time and less gate leakage current than conventional PE-CVD passivation. A T-shaped gate HEMT fabricated by this technique, with L<sub>g</sub> = 0.4 μm and W<sub>g</sub> = 50.4 μm, delivered an output power over 140 W (2.79 W/mm), which was a record power at C-band. [C1446]

#### "W-band metamorphic HEMT with 267 mW output power"

This paper reports the highest W-band power output of metamorphic HEMT (MHEMT) technology to date. 267 mW single stage performances at 90 GHz are achieved on a 0.15 micron GaAs-based production line with improved manufacturability over InP HEMT. The single stage circuits presented here are building blocks for future MHEMT power amplifier development. [C1447]

#### "A high power density TaN/Au T-gate pHEMT with high humidity resistance for Ka-Band applications"

A 0.8 W/mm high power pHEMT with high humidity resistance is reported. By using tantalum nitride as the refractory gate metal and a silicon nitride layer prepared by a catalytic chemical vapor deposition technique for passivation of this transistor, tough moisture resistance was obtained showing no Id degradation even after 500 hours at 130 degrees centigrade and 85% humidity. Moreover, the Schottky breakdown voltage of the TaN gate is higher than that of a WSiN gate. A one-stage prematched amplifier with the new pHEMT has achieved 0.83 W/mm output power at V<sub>ds</sub> = 8 V, with 8.5 dB gain and 40% power added efficiency in the Ka-band. These are some of the highest power figures ever reported. [C1448]

#### "Nonlinear HEMT modeling using artificial neural network technique"

An improved nonlinear modeling technique for high electron mobility transistors (HEMT) based on the combination of the conventional equivalent circuit and artificial neural network (ANN) modeling techniques is presented. Effective initial values of the artificial neural network for each nonlinear element in HEMT model are evaluated from a semi-analytical parameter extraction technique. A multi-goal DC, S-parameter, and harmonic (DC/S/HB) training process has been formulated. Good agreement is obtained between the model and data of the DC, S-parameter, and harmonic performance for a 200μm gate width 0.25μm PHEMT (FHX04LG) over a wide range of bias points. [C1449]

#### "Improvement of PHEMT intermodulation prediction through the accurate modelling of low-frequency dispersion effects"

Large-signal dynamic modelling of III-V FETs cannot be simply based on dc i/v characteristics, when accurate performance prediction is needed. In fact, dispersive phenomena due to self-heating and/or traps (surface state densities and deep level traps) must be taken into account since they cause important deviations in the dynamic drain current. In this paper, a recently proposed large-signal i/v measurement setup is exploited to extract an empirical model for low-frequency dispersive phenomena in microwave electron devices. This i/v model is then embedded into a microwave large-signal PHEMT model. Eventually, a Ka-band highly linear power amplifier, designed by Ericsson using the triquint GaAs 0.25μm PHEMT process, is used for model validation. Excellent intermodulation distortion predictions are obtained with different loads despite the extremely low power level of IMD products involved. This entitles the proposed model to be also used in the PA design process instead of



conventional load-pull techniques whenever the high-linearity specifications play a major role. [C1450]

### "High power, high efficiency, AlGaIn/GaN HEMT technology for wireless base station applications"

We report AlGaIn/GaN high-electron-mobility-transistors (HEMT) on SiC substrates with field modulation plates (FP) of various dimensions and different gate widths. As a measure of the status of GaN technology achieved in this work, small periphery 150  $\mu\text{m}$  HEMT demonstrated a continuous wave (CW) output power density of 22.7 W/mm at 2.14 GHz with power added efficiency (PAE) of 54% when biased at a drain-source voltage (VDS) of 80 V. As a demonstration of the scalability of this technology, a 20-mm-wide device exhibited 100 W CW output power and a simultaneous peak PAE of 55.3% at 2.14 GHz when biased at class AB and VDS=48V. WCDMA measurements on the 20mm part demonstrated ACP of -35 dBc at 42.5 dBm output power and 30% PAE under the same bias condition. Analysis of FP related performance tradeoffs are also presented in this work. [C1451]

### "150 W GaN-on-Si RF power transistor"

A large periphery high power AlGaIn/GaN HFET grown on a silicon substrate has demonstrated over 150 W of CW RF output power along with excellent drain efficiency of 65%. When operated under WCDMA modulation and 28 Vdc drain supply voltage, these devices produced 20 W of RF output power with a corresponding drain efficiency of 27% while achieving an adjacent channel power ratio (ACPR) of -39 dBc. A 36 mm device was tested in a DPD linearizer under multi-carrier WCDMA modulation and achieved 20 dB of linearity improvement with 35% drain efficiency. Lastly, device reliability data is presented and shows extrapolated 20 year drift estimates of less than 1 dB for Psat. [C1452]

### "Sub-50 nm T-gate pseudomorphic HEMTs using low temperature development method"

This paper demonstrates the use of a low temperature development method as a second development stage in the sub-50 nm T-gate process for  $\text{Al}_{0.25}\text{Ga}_{0.75}\text{As}/\text{In}_{0.2}\text{Ga}_{0.8}\text{As}/\text{GaAs}$  pseudomorphic HEMTs. As the development temperature goes down, clearing doses for PMMA and PMMA-MAA are increased. This reduction of sensitivity in low temperature development reduces the detrimental effect on the second stage by the first exposure in the tri-layer (PMMA/PMMA-MAA/PMMA) T-gate process for HEMTs. Thus, both resolution and vertical profile are enhanced in this process. A 25 nm T-shaped resist profile was patterned and a 40 nm T-gate was fabricated after metal lift-off using low temperature development under a low 20 kV E-beam acceleration voltage condition. This method was used to successfully fabricate 40 nm T-gate pHEMTs with 580 mS/mm. [C1453]

### "High power density InGaP PHEMTs for 26 V operation"

This paper presents a high power density and high efficiency InGaP barrier PHEMT technology for 26 V operation. This device was evaluated for 3G infrastructure applications at 2.14 GHz and WiMAX applications at 3.5 GHz. At 2.14 GHz, under a two carrier WCDMA signal, a 32.4 mm packaged device delivered 10 W average power with 11.4 dB gain and 31.4% drain efficiency at -37 dBc IM3. At 3.5 GHz, under CW stimulus, a 14.4 mm device generated an output power of 22 W with associated drain efficiency of 56% and gain of 10.2 dB. [C1454]

### "A novel RF high-Q metal-semiconductor-metal planar inter-digitated varactor based on double-channel AlGaIn/GaN HEMT structure"

A novel GaN-based double-channel metal-semiconductor-metal configuration planar inter-digitated varactor, fabricated with a HEMT compatible process, is presented. Our varactors achieved high Q-factor, wide tuning range, and high minimum Q-factor ( $Q_{\text{min}}$ ). The double-channel heterostructure extends the useful high Q-factor capacitance tuning range of the varactors. The operation of the varactor is explained by a physical equivalent circuit, in which the whole changing trend of extracted Q-factors over bias voltage and extracted resistance can be explained. The measurement results of the novel double-channel varactors are compared with varactors fabricated on a single channel heterostructure in order to show their superior performance. [C1455]

### "High current operation of GaN power HEMT"

{no data available} [C1456]

### "A 5 GHz pHEMT transformer-coupled VCO"

A transformer-coupled technique is shown to be an area-efficient method for reducing oscillator phase noise. Higher signal amplitude and inductor Q can be achieved without breakdown. A pHEMT process was used to fabricate the 5 GHz VCO. The measured phase noise at 3 MHz offset frequency is -129 dBc/Hz. The VCO

dissipates 9 mW. [C1457]

#### "Hot-electron-stress degradation in unpassivated GaN/AlGaIn/GaN HEMTs on SiC"

{no data available} [C1458]

#### "Hot carrier reliability in GaAs PHEMT MMIC power amplifiers"

{no data available} [C1459]

#### "An ultra-low distortion 3P2T antenna switch MMIC for dual-band W-CDMA applications"

We propose an ultra-low distortion 3P2T antenna switch MMIC for dual-band W-CDMA systems. The switch MMIC consists of a GaAs MMIC with 0.4  $\mu\text{m}$ -gate p-HEMT and Si CMOS IC with a decoder and charge pump circuit. Ultra-low distortion and low insertion loss were achieved by controlling 2-stacked FETs with a voltage of 7 V up-converted from a supply voltage of 2.4 V. The switch MMIC provides IMD2 and IMD3 levels less than -110 dBm, which well satisfies the out-of-band blocking specification for W-CDMA systems. The MMIC shows insertion loss of 0.27 dB for 800 MHz and 0.38 dB for 2 GHz bands. [C1460]

#### "An antenna switch MMIC for GSM/UMTS handsets using E/D-mode JPHEMT technology"

An antenna switch MMIC for quad band GSM/UMTS handsets using enhancement mode and depletion mode junction gate pHEMT (E/D-mode JPHEMT) technology has been developed. An SP7T configuration was adopted to minimize the insertion loss. The high gate turn-on voltage ( $V_f$ ) in the JPHEMT enables a logic circuit to be integrated with an antenna switch without degradation in the RF performance. A novel ESD protection device using E-mode JPHEMT (P-EFET) has been deployed. The maximum survival voltage under a human body model (HBM) test is as high as 2000 V. A low insertion loss of 0.39 dB at 1.95 GHz and a high isolation value of 27.5 dB at 2.14 GHz in the UMTS TRx path are achieved. The 2nd and the 3rd harmonics in GSM 850/900 Tx mode are at sufficiently low levels of -57.5 dBm and -35.5 dBm, respectively. [C1461]

#### "Low cost X-band power amplifier MMIC fabricated on a 0.25 $\mu\text{m}$ GaAs pHEMT process"

A family of X-Band MMIC power amplifiers using a low cost GaAs pHEMT process is reported. The stepper based volume 0.5 micron and 0.25 micron GaAs pHEMT processes utilize 4 inter-level metallisation and four dielectric layers for high frequency performance whilst maintaining the economies of scale of 150 mm (6") diameter substrates. The fabricated GaAs X-Band PA MMICs exhibit 5 W to 10 W RF output power under pulsed conditions; 16 dB of power gain and power added efficiencies approaching 40%. Excellent repeatability and high yields over a number of wafers have been demonstrated. The design and GaAs process approach taken here with DUV stepper and 150 mm wafer diameter will lead to a significant cost reduction for high performance power amplifier MMICs up to 30 GHz. [C1462]

#### "Single spin-FET for programmable logic gates"

A magnetic device that enables the realization of various logic functions in a single transistor is proposed. The device consists of a current-conducting 2DEG layer, and a set of four ferromagnetic (FM) gates and two non-magnetic (NM) gates deposited on top of a HEMT heterostructure. FM gates are magnetized perpendicular-to-plane so that magnetic fields ( $B$ ) extend vertically through the 2DEG plane. Electrical voltages are applied to the NM gates so that a periodic series of magneto-electric barriers is established across the 2DEG conduction path. This device selects the functions of AND, OR, NAND, NOR, XOR, NOT, YES, according to the magnetizations of FM1, FM3, and the electrical potentials ( $U$ ) of NM1, NM2. FM2 and FM4 function as the two inputs to the logic gate depending on the selection. Electron motion is described by the minimal coupling Hamiltonian with the Zeeman perturbation term at the  $\delta B$  field region. [C1463]

#### "A design of 10-GHz delta-sigma modulator using a 4-level differential resonant-tunneling quantizer"

An ultrahigh-speed continuous-time delta-sigma modulator using a 4-level resonant-tunneling quantizer has been investigated. The quantizer consists of four resonant-tunneling diodes (RTDs) and a source-coupled high-electron-mobility transistor (HEMT) pair, and operates in the fully-differential mode. Circuit simulation shows that the present first-order delta-sigma modulator has a signal-to-noise ratio (SNR) of 49.4 dB at a sampling frequency of 10 GHz and an input bandwidth of 100 MHz. An improvement in the SNR by 5.6 dB is obtained by increasing the number of quantization level from two to four. [C1464]

### "On the design and performance of a balanced-cascade LNA for FDD-WCDMA direct-conversion node-B RF receiver"

In this paper, the design requirements, design procedure, and performance of a low noise amplifier (LNA) used in wideband code division multiple access (WCDMA) base station receiver, is illustrated. The amplifier design is aimed for a direct-conversion architecture. It simultaneously achieves good input-match, ultra-low noise figure and high linearity in terms of low third order intermodulation (IMD3). The LNA achieves an overall gain of 55 dB, noise figure (NF) better than 0.7 dB, and IMD3 less than -67 dBc. Devices used are E-pHEMT type with gate widths of 800  $\mu\text{m}$  and 6400  $\mu\text{m}$ . A distributed type quadrature-hybrid is used for balanced configuration with good amplitude and phase balance. [C1465]

### "A concurrent multi-band LNA for multi-standard radios"

A source-degenerated cascade LNA, which works at 2.4 GHz and 5.8 GHz simultaneously, is designed for Bluetooth and IEEE wireless LAN 802.11 a/b/g receivers. In this design, 0.15  $\mu\text{m}$  GaAs PHEMT technology and embedded passives in an MCM-D substrate are implemented. At 2.4 GHz and 5.8 GHz, this LNA provides 12.2 dB and 15.3 dB gain, respectively. Noise figures of the LNA are 0.53 dB and 1.43 dB, respectively. Good input matching and output matching are also achieved-S11 and S22 at both frequencies are less than -10 dB. [C1466]

### "Active frequency selective surfaces for antenna applications electronically to control phase distribution and reflective/transmissive amplification"

A planar dipole grid antenna is described deposited on an active frequency selective (FSS) or polarization sensitive surface (PSS) electronically tuneable to control the spatial phase distribution and reflective/transmissive amplification. Such dipole grids can be used, for example, in reflector antenna systems composed of multiple reflective and/or transmissive subsystems to achieve and serve highly cost-effective multi-purpose applications. It is discussed how the resonant frequency or/and the type of polarization can be tuned just by varying the steering voltage or current of electronically tunable components such as varactor diodes or YIG films, respectively, implemented and integrated with each of the radiating dipole elements. The theoretical analysis for this paper is based upon a specific Floquet theory approach for single/double/triple periodic antenna structures. The resulting system of coupled vector integral equations for the unknown electric and magnetic current distribution is numerically solved by applying the method of moments supported by Galerkin's process of weighting. The experimental investigations were performed by developing a waveguide simulation technique in the frequency range of 7 to 16 GHz. Results of selected measurements are presented for quantities such as: the spatially dependent reflection/transmission coefficients (magnitude, phase) as a function of signal frequency; the intrinsic input impedance/matching of the various dipole elements involved, etc.; and-in addition to that-the resulting electronically achievable phase advance/delay and amplification of the active antenna system as well. A one/two-dimensional enlarged planar dipole grid of about 40 mm  $\times$  25 mm in aperture size was deposited inside an adequately tapered waveguide to reduce tolerance problems and to suppress higher order modes. Typical results are presented and discussed to demonstrate, e.g., that the resonant frequency -10 GHz can electronically be tuned around 9.85 GHz by a bandwidth of 7 % and around 10.1 GHz by 14 % in case of capacitive or inductive tuning, respectively. Investigations show that electronic tunability is achieved preferably by using high-Ohmic voltage controlled components instead of low-Ohmic current-controlled components, for instance, supporting low-loss and low-noise performance. Using properly selected HEMT-type integrated transistors the achievable amplification measured turned out be about 5.4 dB at 10.3 GHz for an active one-element strip dipole grid (reflection-type amplifier) and about 3 dB at 9.3 GHz for an active one-element slot dipole grid (transmission-type amplifier), respectively. A concluding discussion indicates how such kind of planar/conformal dipole grids may set up an integrated system of multiple reflective/transmissive subreflectors of a powerful low-weight multi-purpose microwave antenna system of frequency multiplex and dual polarization capability to serve various technical applications at the same time and at a high degree of flexibility and cost-effectiveness as well. [C1467]

### "A novel oscillation circuit using a resonant-tunneling diode"

A novel oscillation circuit using a resonant-tunneling diode (RTD) is proposed. The circuit has a simple configuration consisting of an RTD, a high-electron-mobility transistor (HEMT), and an inductor. A large oscillation swing that substantially exceeds the RTD negative differential resistance region can be obtained, since the oscillation is based on the RTD switching between the peak and valley states. To analyze the large-signal behavior, circuit simulation has been carried out. It was found that the oscillation frequency increases by increasing the RTD peak current density  $j_{\text{p0}}$  or by decreasing the inductance  $L$ . A frequency as high as 180 GHz has been predicted when  $j_{\text{p0}}=14105\text{A/cm}^2$  and  $L=0.1\text{ nH}$ . [C1468]

### "Optimized design of source coupled logic gates in GaAs HEMT technology"

A simple model for the propagation delay of source coupled logic gates composed of a differential pair and a common drain output buffer in III-V HEMT technology is proposed. The propagation delay model has been used to develop a design strategy that permits pencil-and-paper design of the gates, accounting for power-delay trade-off. The methodology has been applied to a charge-control high-frequency model of the HEMT, but is general-purpose and applicable also to different models. In the present case, percentage errors lower than 15 % have been found in propagation delay evaluation. [C1469]

### "Extremely low noise characteristics of 0.1 $\mu$ m $\Gamma$ -gate power metamorphic HEMT on GaAs substrate"

The 0.1  $\mu$ m  $\Gamma$ -gate power metamorphic high electron mobility transistors (MHEMTs) has been fabricated and the DC, microwave, and noise performance of the device were characterized. The MHEMT device shows the DC output characteristics having an extrinsic transconductance of 830 mS/mm and a threshold voltage of  $\approx$ 0.62 V. The  $f_{Tand}$  and  $f_{max}$  obtained for the 0.1  $\mu$ m  $\times$  100  $\mu$ m MHEMT device are 165 GHz and 275 GHz, respectively. The MHEMTs exhibit the minimum noise figure,  $NF_{min}$ , of 0.64 dB and associated gain of 12.4 dB at 26 GHz. The  $NF_{min}$  measured at 40 GHz is 1.1 dB with associated gain of 9.7 dB. This noise data is the lowest value ever reported for  $\Gamma$ -gate power MHEMT devices with InGaAs channel of 53% In. [C1470]

### "Metamorphic 50 nm InAs-channel HEMT"

A 50 nm gate length metamorphic HEMT with InAs-channel and InAlAs-barriers for high frequency low power applications has been developed. Using a composite channel layout with backside doping an on-state breakdown voltage of 1.2 V and a  $g_{mmax}/g_{ratio}$  of four at  $V_{DS}$ =1.0 V was achieved. A low  $g_m$  dispersion of only 5 % was measured. The realized three-stage 70 GHz LNA shows a power dissipation as low as 1.9 mW with an associated small signal gain of 6 dB. [C1471]

### "Low noise high performance 50nm T-gate metamorphic HEMT with cut-off frequency $f_T$ of 440 GHz for millimeterwave imaging receivers applications"

The 50 nm m-HEMT exhibits extremely high  $f_T$ , of 440GHz, low  $F_{min}$  of 0.7 dB, associated gain of 13 dB at 26 GHz with an exceptionally high  $I_d$  of 200 mA/mm and  $g_m$  of 950 ms/mm at low noise biased point. [C1472]

### "Power potentiality at 94 GHz of InP HEMTs with large band gap channels"

We have investigated InP HEMT structures with large band gap channels for power amplification at 94 GHz. We show that structures containing InP and InAsP channels are very promising for power amplification at 94 GHz. [C1473]

### "A 77GHz automotive radar MMIC chip set fabricated by a 0.15 $\mu$ m MHEMT technology"

A MMIC chip set consisting of a power amplifier, a driver amplifier, low noise amplifier, and a frequency doubler has been developed for automotive radar systems at 77GHz. The chip set was fabricated using 0.15  $\mu$ m gate-length InGaAs/InAlAs/GaAs mHEMT process based on 4-inch substrate. The power amplifier demonstrated a measured small signal gain of over 20 dB from 76-77GHz with 15.5 dBm output power. The chip size is 2mm  $\times$  2mm. The driver amplifier exhibited a gain of 23dB over a 76-77 GHz band with an output power of 13dBm. The chip size is 2.1mm  $\times$  2mm. The low noise amplifier achieved a gain of 20 dB in a band between 76-77GHz with an output power of 10 dBm. The chip size is 2.2mm  $\times$  2mm. The frequency doubler achieved an output power of -6 dBm at 76.5 GHz with a conversion gain of -16dB for an input power of 10 dBm and a 38.25 GHz input frequency. The chip size is 1.2 mm  $\times$  1.2mm. This MMIC chip set is suitable for the 77 GHz automotive radar systems and related applications in W-band. [C1474]

### "A miniature dual-band low-noise amplifier module for IEEE 802.11 b/g/a WLAN applications"

This paper describes the design and implementation of a low-noise amplifier module in a single package that is capable of operating in both the 2.4 GHz band and the (4.9-6) GHz band. The module utilizes a MMIC fabricated using Agilent's proprietary low-noise enhancement-mode pHEMT process. A cascode configuration is used to obtain high gain and low currents for the 2.4 GHz band amplifier whilst a two-stage amplifier is used in the 5 GHz band. In the 2.45 GHz band, gain is 17 dB at 14 mA current with 0.9 dB of noise figure. In the 5 GHz band, gain is (22-24)dB at 22 mA and 1.5 dB average noise figure. Input  $P_{1dB}$  is -5.5 dBm for the 2.4GHz LNA and typically -14 dBm for the 5 GHz LNA.  $IIP_3$  is +5.5 dBm for the 2.4 GHz LNA and typically -2dBm for the 5GHz band. The complete design uses only one RF input matching component external to the MMIC inside the



module. The complete LNA is housed in a 3mm Ч 3mm molded chip-on-board package and requires only two external bypass capacitors in actual operation. [C1475]

#### **"InGaAs-InAlAs-InP HEMT technology for ultra-high frequency and ultra-low noise performance"**

InGaAs-InAlAs-InP HEMT is facing competition from the emerging MHEMT technology. Nonetheless, for top-performing applications requiring high gain and low noise, InP HEMT is still the preferred choice. We here present results from InP HEMT development for sub-100 nm gate length designs yielding  $f_{max}$  above 400 GHz and ultra-low noise hybrid amplifiers with a minimum noise temperature of 1.1 K when operated under cryogenic conditions. [C1476]

#### **"A metamorphic GaAs HEMT distributed amplifier with 50 GHz bandwidth and low noise for 40 Gbits/s"**

An eight stage distributed amplifier with  $12.5 \text{ dB} \pm 0.45 \text{ dB}$  gain and 50 GHz bandwidth has been demonstrated in a commercially available  $0.1 \text{ }\mu\text{m}$  metamorphic GaAs HEMT (MHEMT) technology. The amplifier has a minimum noise figure lower than 2.5 dB in the bandwidth. The group delay variation from 9 to 40 GHz is  $\pm 7.5 \text{ ps}$  and circuit consumption is 0.4 W. Such amplifier has been packaged with a high responsivity photodiode into a fiber pig-tailed module. Eye diagrams measurements demonstrate the successful high-speed operation of the photoreceiver. [C1477]

#### **"Low noise W-band MMIC amplifier using 50nm InP technology for millimeterwave receivers applications"**

We report on W-band LNA (MMICs) based around a 50nm InP-HEMTs with an  $f_{To}$  of 0.550 THz. The LNA noise figure is 2.5 dB and associated gain of 7.3 dB at 90 GHz with a bandwidth of 24 GHz [C1478]

#### **"Microwave noise characteristics of InP-based high electron mobility transistors with InGaAs channel and InGaAs/InP composite channel: a comparative study"**

A comparative study of the microwave noise performance between InP high electron mobility transistors (HEMTs) with InGaAs channel and InGaAs/InP composite channel is performed. Detailed microwave noise characteristics of InP-based HEMT with single channel and composite channel are presented. A model is carried out to extract the noise parameters and study the thermal noise performance of InP-based HEMT. Characterization of noise performance of InGaAs/InP composite channel HEMTs reveals a different bias dependence of  $NF_{min}$  compared to conventional single InGaAs channel devices. The composite channel HEMT shows a lower  $NF_{min}$  at high  $V_d$  with a relatively weak  $V_d$  dependence. This could be explained under the framework of suppression channel thermal noise due to the electron transfer from InGaAs channel to InP subchannel at high  $V_d$  [C1479]

#### **"Compound semiconductor IC's"**

This paper presents an overview of compound semiconductor electron devices. GaAs-based MESFET, HEMT, and HBT have deeply penetrated into the markets of communications fields. On the other hands, InP-based HEMT and HBT just are becoming ready for practical use in the ultra-high speed and low power electronics owing to the excellent transport properties. Finally, it will be shown that the wide bandgap material, GaN, has the great potentiality for high power and high frequency electronics [C1480]

#### **"Production InP MMICs for low cost, high performance applications"**

We report the progress of production InP MMICs for low cost, high performance applications at Northrop Grumman Space Technology (NGST). Both InP HEMT and HBT technologies are being developed on 100 mm diameter InP substrates and this development is leading to lower costs that will rival both GaAs-based MMICs including GaAs-based metamorphic technologies with superior performance. Two specific InP niche product areas will be discussed-high linearity InP HBT power amplifiers and high frequency W-band low noise amplifiers [C1481]

#### **"Kink effect in InAlAs/InGaAs short-channel HEMTs: influence on the dynamic and noise performance"**

The degradation introduced by the kink effect in the dynamic and noise performance of an InAlAs/InGaAs 100 nm gate high electron mobility transistor is analyzed by using Monte Carlo simulations. [C1482]

### "0.1 $\mu\text{m}$ InGaAs/InAlAs/InP HEMT low noise amplifiers with compact stacked cascode design and its de-bias effect induced failure (DBIF)"

Compact Q-band low noise amplifier modules using 0.1  $\mu\text{m}$  InGaAs/InAlAs/InP HEMT MMICs have been demonstrated with high performance and high manufacturability over a frequency band from 43.5 to 45.5 GHz at Northrop Grumman Space Technology (NGST). The compact InP HEMT LNAs and modules are essential for phased-array applications. The LNA modules demonstrate noise figure less than 2.5 dB over the frequency band of 43.5 to 45.5 GHz. The RF performance results achieved here, in conjunction with previously reported high reliability results, further demonstrate the readiness of NGST's 0.1  $\mu\text{m}$  InP HEMT MMIC technology for advanced phased-array applications. In addition, Ig de-bias effect induced failure (DBIF) was observed on InP HEMT MMICs with stacked cascode configuration subjected to elevated temperature lifetest. Accordingly, an acceptable lifetest temperature window was found to alleviate DBIF while performing lifetest on InP HEMT MMICs with stacked cascode configuration. [C1483]

### "Degradation mechanism and reliability improvement of InGaAs/InAlAs/InP HEMTs using new gate metal electrode technology"

The degradation mechanism of 0.1  $\mu\text{m}$  InGaAs/InAlAs/InP HEMTs subjected to elevated temperature lifetest has been resolved with the techniques of scanning transmission microscope (STEM) and high-resolution energy-dispersive X-ray analysis (EDX). The results show that Schottky junction degradation is the dominant degradation mechanism, consisting of Ti inter-diffusion and In<sub>0.52</sub>Al<sub>0.48</sub>As Schottky barrier layer degradation. The degradation of the In<sub>0.52</sub>Al<sub>0.48</sub>As Schottky barrier exhibits the formation of TiAs<sub>x</sub> and indium-rich In<sub>0.52+x</sub>Al<sub>0.48</sub>As and/or indium depleted In<sub>0.52-x</sub>Al<sub>0.48</sub>As under elevated temperature lifetest. The Schottky junction degradation mechanism can be alleviated by using a new gate metal electrode technology (NGMET), which exhibits superior reliability performance to that of the Ti/Pt/Au gate metal electrode. Moreover, InP HEMT MMICs using NGMET exhibit comparable RF performance to that of InP HEMT MMICs with Ti/Pt/Au gate metal. The results achieved here demonstrate the further enhancement of 0.1  $\mu\text{m}$  InP HEMT MMIC technology at Northrop Grumman Space Technology (NGST) using NGMET for military/space applications with high reliability performance requirement. [C1484]

### "Vertical scaling of gate-to-channel distance for a 70 nm InP pseudomorphic HEMT technology"

DC and HF performance for a 70 nm InP PHEMT technology have been studied as a function of gate-to-channel distance. The optimized PHEMT exhibited a maximum transconductance of 1.5 S/mm and  $f_{\text{max}}$  of 400 GHz. [C1485]

### "A miniaturized wideband 4x4 switch matrix IC using four InP-HEMT SP4T switches"

A new 4x4 switch matrix requires about 1/10 the area, a low number of interconnection transmission lines (ITLs) with greatly reduced length, and half the number of overlaps between ITLs compared to a conventional one consisting of 8 SP4T switches and 16 ITLs. InP HEMTs with a low  $R_{\text{on-Coff}}$  product enable us to configure a dc-to-over-10-GHz SP4T switch with a series-FET configuration, which requires half the control lines of a series-shunt configuration. The switch matrix IC has an extremely small core size of 409  $\times$  368  $\mu\text{m}^2$  and achieves lower insertion loss with less deviation ( [C1486]

### "A 20 GHz MOD-made BST thin film tunable phase shifter for phase adjustment of digital 360-degree PHEMT phase shifter"

We have newly designed and fabricated both Ba<sub>x</sub>Sr<sub>1-x</sub>TiO<sub>3</sub>(BST) ferroelectric thin film tunable phase shifter and pseudomorphic HEMT MMIC digital 360-degree phase shifter. A low loss BST thin film was obtained on MgO substrate by preparation of initial layer by pulsed laser deposition (PLD) and following metal-organic-decomposition (MOD) method. For the interdigital capacitors with finger spacing of 10  $\mu\text{m}$ , dielectric loss was found to be as low as 0.002 to 0.004 when applied surface electric field was from  $\pm 40$  kV/cm at measuring frequency of 1 MHz, where tunability was about 12%. Moreover, it increases up to about 40% in a Pt/BST/Pt stacked capacitor structure when the applied electric field was from  $\pm 170$  kV/cm at the same frequency. When applying dc bias voltage of 0 to 60 V to the electrodes of the CPW pattern (width: 60  $\mu\text{m}$ , gap: 10  $\mu\text{m}$ , length: 2.5 mm), a differential phase shift of 18 degree was obtained at 20 GHz with insertion loss of about -2 dB for Au/Cr interconnection. A 3-stage LC-ladder-type phase shifter with variable capacitors of BST film was designed to have a differential phase shift of about 40 degrees at 20 GHz. A fabricated phase shifter shows successfully the shift of 40 degree at 20GHz with bias of 60 V. The HEMT MMIC also shows a digital 360-degree phase shift with 11.25 degree interval, thus the BST phase shifter can be usable for phase adjustment of the MMIC. Finally it is found that the new BST film process is very promising for realizing a micro

and millimeter-wave tunable device. [C1487]

#### "A general procedure for extraction of bias dependent dynamic self heating model parameters"

A general method for characterizing electrothermal interaction due to self heating is proposed. The characterization is performed using only electrical measurements and is directly applicable to a wide range of device technologies. A rigorous small-signal analysis of the electrothermal problem forms the basis for the characterization and model parameter extraction technique. The proposed technique allows for extraction of both the thermal impedance and the thermal coefficient. The small-signal analysis is valid for any N-port subject to self-heating from a single heat source. The method is demonstrated on a 200  $\mu\text{m}$  pHEMT device. The main advantage with the proposed method is that the extraction is made at a single independent bias condition. This allows for the extraction of a bias dependent electrothermal model. This is a significant improvement compared to other electrothermal extraction techniques. [C1488]

#### "A V-band eight-way combined solid-state power amplifier with 12.8 Watt output power"

This paper describes the design and development of a V-band 12.8 Watt solid-state power amplifier (SSPA) unit that has been successfully demonstrated over a wide frequency band from 59 to 63 GHz. To achieve such power, high output power MMICs were designed with close to 1 Watt output power using the space qualified GaAs HEMT process at Northrop Grumman Space Technology. The power amplifier unit also implemented a unique waveguide combining method to efficiently combine half-height SSPA waveguide modules into full-height waveguide SSPA modules. The 8-way splitter/combiner is a Militech state-of-the-art hybrid ring "rat-race" waveguide design with extremely low loss at V-band frequencies. To the author's knowledge, these are the best reported results in V-band combiners to date. [C1489]

#### "High power GaN oscillators using field-plated HEMT structure"

5 GHz MMIC GaN oscillators based on AlGaIn/GaN HEMTs are presented. The use of field-plated HEMT structures in these oscillators resulted in increased output power and dc-to-RF efficiency. An oscillator using an AlGaIn/GaN HEMT with 0.5 mm gate width and 1.1  $\mu\text{m}$  field-plate extension, biased at  $V_{ds} = 40\text{ V}$  and  $V_{gs} = -4.5\text{ V}$ , delivers 1.9 W of output power with a dc-to-RF efficiency of 21.5%. Phase noise was measured to be -132 dBc/Hz at a 1 MHz offset frequency. The oscillator output power density was found to be 3.8 W/mm and is the highest yet reported. Studies of the output power, dc-to-RF efficiency, and phase noise with different field-plate extensions are also presented. [C1490]

#### "An ultra-low power InAs/AlSb HEMT W-band low-noise amplifier"

An antimonide-based compound semiconductor (ABCS) microstrip MMIC, a W-band low-noise amplifier using 0.2- $\mu\text{m}$  gate length InAs/AlSb metamorphic HEMTs, has been fabricated and characterized on a 50  $\mu\text{m}$  GaAs substrate. The compact 1.2 mm<sup>2</sup> five-stage W-band LNA demonstrated a 3.9 dB noise-figure at 94 GHz with an associated gain of 20.5 dB. The measured dc power dissipation of the ABCS LNA was an ultra-low 1.2 mW per stage, or 6.0 mW total which is less than one-tenth the dc power dissipation of a typical equivalent InGaAs/AlGaAs/GaAs HEMT LNA. Operation with degraded gain and noise figure at 3.5 mW total dc power dissipation is also verified. These results demonstrate the outstanding potential of ABCS HEMT technology for mobile and space-based millimeter-wave applications. [C1491]

#### "The flip-chip mounted MMIC technology using the modified MCM-D substrate for compact and low-cost W-band transceiver"

We present novel multi-chip module (MCM)-D technology to improve the mechanical and thermal properties of a MCM-D substrate for a motherboard of the flip-chip structure. Advantages of the flip-chip mounted MMIC technology using the modified MCM-D substrate were investigated. Based on this investigation, the W-band CPW MMIC amplifier using the 0.1- $\mu\text{m}$  GaAs pHEMT was successfully mounted on the modified MCM-D substrate by means of the flip-chip technology. Moreover, the W-band down-converter module with internal local oscillator (LO) source was realized with this technology. [C1492]

#### "Large-signal PHEMT switch model, which accurately predicts harmonics and two-tone inter-modulation distortion"

In this paper, we present a comprehensive large-signal PHEMT switch model and address critical switch modeling issues. Reciprocity, dispersion, leakages, and sub-pinchoff, and charge conservation all play important role in generating a realistic large-signal switch model. Device nonlinearities covering linear, saturation, sub-pinchoff and deep pinchoff regions are taken into account in the model. The model has been verified by

comparing simulated dc characteristics, S-parameters and power harmonics performance of switch devices with measured results. The model also successfully predicts harmonics, two-tone IP3 and cross-modulation in various switch circuits. [C1493]

#### **"A lattice matched InP chip set for a Ka band radiometer"**

An extremely sensitive Ka band radiometer, operating at a temperature of approximately 15 Kelvin, is being developed for the EC funded FARADAY radio astronomy project. To maximize the sensitivity of the radiometer lattice-matched indium phosphide HEMT technology has been used: all of the active components of the radiometer, with the exception of the detectors, have been manufactured on a single wafer process. The radiometer, which uses the band 26 to 36 GHz, will be used to make radio maps of the sky from a 32 metre diameter radio telescope. Several new MMICs have been designed, including a 10 GHz bandwidth low noise amplifier with average noise temperature less than 20 K, and a 180° phase switch using low noise HEMTs as the switching elements. Design principles are described, together with a comparison of modelled and measured results. [C1494]

#### **"A 60 GHz MMIC dual-quadrature mixer in pHEMT technology for ultra wideband IF signals and high LO to RF isolation"**

A 60 GHz MMIC dual-quadrature mixer (DQM) has been designed, fabricated in a commercial pHEMT MMIC process and characterized with probed measurements. A measured down conversion loss (LC) of  $8.5 \pm 1$  dB over the frequency range 47 to 67 GHz is obtained with an LO to RF isolation better than 20 dB and 8 dBm of LO power. Measurements verify that the IF bandwidth is truly ultra wideband with a total IF bandwidth of 11.5 GHz. Thus, with a fixed LO signal of 58 GHz, the RF band between 53 and 64.5 GHz can be down converted directly to the base band while maintaining a high LO to RF isolation. Single resistive mixers are used for the actual down conversion which results in a high IIP3 figure of 20 dBm and virtually no DC power consumption. Furthermore, the DQM exhibit very low reflection coefficients at the RF and LO ports due to the dual-quadrature topology. [C1495]

#### **"Medium power amplifiers covering 90-130 GHz for the ALMA telescope local oscillators"**

This paper describes a set of power amplifier (PA) modules containing InP high electron mobility transistor (HEMT) monolithic millimeter-wave integrated circuit (MMIC) chips. The chips were designed and optimized for local oscillator sources in the 90-130 GHz band for the Atacama large millimeter array telescope. The modules feature 20-45 mW of output power, to date the highest power from solid state HEMT MMIC modules above 110 GHz. [C1496]

#### **"MMIC HEMT switch for switch matrix of satellite communication system"**

A MMIC (monolithic microwave integrated circuit) switch chip using InGaAs/GaAs p-HEMT process has been developed for switch matrix of satellite communication system. This absorptive type MMIC switch has good reflection coefficients performances of input and output ports at both on and off-states. A quarter wavelength impedance transformer is realized with lumped elements of MIM capacitor and spiral inductor for 3GHz band to reduce the chip size. The MMIC switch covers the range of 3.2–3.6GHz. According to the on-wafer measurement, the fabricated MMIC switch with miniature size of 1.6mm $\times$ 1.3mm demonstrates insertion loss below 2dB, isolation above 56.8dB, respectively, and the performance coincides with simulation results. [C1497]

#### **"Double-balanced, hybrid mixer with multi-decade bandwidth"**

An ultra-broadband mixer design that uses a hybrid technology is described. The design incorporates a low-barrier diode mixer, thin film interconnect, and a pHEMT LO-drive amplifier. The mixer gives better than -35 dB conversion efficiency at RF frequencies from less than 10 MHz to greater than 110 GHz for at least 10,000:1 bandwidth. Simulations show that the mixer, with some improvements, can operate from 10 MHz to 150 GHz. Multiple mixers can be integrated into a single hybrid module. An integrated dual-mixer module with pHEMT RF-buffer amplifiers is also described. This mixer module is limited by the bandwidth of the buffer amplifiers, but still gives better than -35 dB conversion efficiency from less than 10 MHz to 100 GHz. [C1498]

#### **"Phase characterization of two-tone intermodulation distortion"**

An automated setup for the characterization of phase asymmetries in nonlinear microwave circuits under two-tone excitation is presented. The method includes a novel approach to generate two synchronized tones with the same amplitude and phase using an arbitrary-waveform signal generator. Special attention is devoted to the evaluation of two-tone IMD impairments as a consequence of memory effects and assesses its dependence on



their separation in frequency. Experimental results over a HEMT amplifier exhibiting phase asymmetries are compared with standard two-tone measurements and show that the accuracy of this procedure is good, with negligible non-systematic errors. [C1499]

#### "A new small signal model parameter extraction method applied to GaN devices"

A new parasitic elements extraction method applied to GaN devices is presented. First, using cold S-parameter measurements, high quality starting values for the extrinsic parameters are generated that would place the extraction close to the global minimum of the objective function for the distributed equivalent circuit model. In a second step, the optimal model parameter values are searched through optimization using the starting values already obtained. The validity of the developed method and the proposed small-signal model is verified by comparing the simulated wide-band small-signal S-parameter, over a wide bias range, with measured data of a 0.5  $\mu\text{m}$  GaN HEMT with 2 Ч 50  $\mu\text{m}$  gate width. [C1500]

#### "Metamorphic 94 GHz power amplifier MMICs"

In this paper, we present the development of two 94 GHz power amplifier MMICs for use in high-resolution synthetic aperture radar (SAR) systems. The amplifier circuits have been realized using a 0.1  $\mu\text{m}$  InAlAs/InGaAs based depletion type metamorphic high electron mobility transistor (MHEMT) technology in combination with coplanar circuit topology and dual-gate transistors, thus leading to an excellent power and gain performance at millimeter-wave frequencies. The realized two-stage driver amplifier (MPA) MMIC exhibited a small-signal gain of 16 dB and a saturated output power of 20.5 dBm at 94 GHz with a total gate width of 0.72 mm in the output stage. The two-stage high power amplifier (HPA) circuit achieved a linear gain of 10 dB and a saturated output power of 23.3 dBm with a total output periphery of 1.44 mm. [C1501]

#### "A 44-GHz high-linearity MMIC medium power amplifier with a low-loss built-in linearizer"

This paper presents a 44-GHz MMIC medium power amplifier with a low-loss built-in linearizer using a 0.15- $\mu\text{m}$  GaAs HEMT process. The proposed cold-mode HEMT linearizer can enhance the linearity of the power amplifier with a low insertion loss, a compact die-size, and zero dc consumption. These advantages make the linearizer more suitable for millimeter-wave applications. The experimental results show that the medium power amplifier output spectrum re-growth can be suppressed by 7-9 dB at 44 GHz. In addition, the EVM of the QPSK and 16-QAM modulated signal can be reduced from 4.5% to 3.7% and 10.8% to 7.4% respectively. To the best of our knowledge, this is the first attempt of using pre-distortion linearization techniques in millimeter-wave bands. [C1502]

#### "The design of a Ka-band two-stage monolithic low noise amplifier"

A Ka-band two-stage monolithic low noise amplifier has been designed using a commercial 0.18- $\mu\text{m}$  pseudomorphic high electron-mobility transistor (pHEMT) process. The gate widths of FETs and source inductors are adjusted to achieve best tradeoff among gain, noise figure and return loss. The simulated results of the low noise amplifier chip show a gain of more than 11 dB, a noise figure of less than 2 dB, an input return loss of greater than 15 dB, and an output return loss of greater than 9.7 dB in the frequency range of 27 to 33 GHz. The chip size is 1.4Ч0.9 mm<sup>2</sup>. [C1503]

#### "Low noise and high linearity LNA based on InGaP/GaAs HBT for 5.3 GHz WLAN"

This paper presents a low noise and high linearity LNA based on InGaP/GaAs HBT for 5.3 GHz WLAN. Previous LNAs based on FET series such as HEMT show excellent noise characteristics, but poor linearity. The InGaP/GaAs HBT LNA shows excellent linearity and noise characteristics because of its high base doping concentration. The proposed LNA is fully integrated in area of 0.9 /spl times/ 0.9 mm/sup 2/ single chip with high Q spiral inductors and MIM capacitors and biased at current point for optimum noise figure and gain characteristics, furthermore, excellent linearity is achieved. Measured result of the proposed LNA shows 13 dB gain, 2.1 dB noise figure, and excellent linearity in terms of IIP3 of 5.5 dBm. The figure of merit (FOM) defined as a function of the linearity and noise figure is 20.1 dB, which is the best result among previous LNAs. [C1504]

#### "A metamorphic GaAs HEMT distributed amplifier with 50 GHz bandwidth and low noise for 40 Gbits/s optical receivers"

An eight stage distributed amplifier with 12.5 dB /spl plusmn/ 0.45 dB gain and 50 GHz bandwidth has been demonstrated in a commercially available 0.1 /spl mu/m metamorphic GaAs HEMT (MHEMT) technology. The amplifier has a minimum noise figure lower than 2.5 dB in the bandwidth. The group delay variation from 9 to 40 GHz is /spl plusmn/ 7.5 ps and circuit consumption is 0.4 W. Such amplifier has been packaged with a high

responsivity photodiode into a fiber pig-tailed module. Eye diagrams measurements demonstrate the successful high-speed operation of the photoreceiver. [C1505]

#### "High efficiency 10 Gb/s optical modulator driver amplifier using a power pHEMT technology"

This paper presents the design and performance of a high efficiency GaAs MMIC distributed amplifier for 10 Gb/s optical driver applications. The power consumption is only 550 mW, approximately 40% lower than typical reported results for this application. It is shown that while the commonly-used cascode topology gives higher gain-BW performance, the ordinary common-source design gives better efficiency and stability performance. This makes it a better choice for 10 Gb/s applications when a suitable high power pHEMT process is used. [C1506]

#### "High gain 110-GHz low noise amplifier MMICs using 120-nm metamorphic HEMTs and coplanar waveguides"

This paper presents the design and performance of 110-GHz low noise amplifier MMICs, based on coplanar technology, and utilizing 120-nm gate-length metamorphic HEMTs. Thanks to a cascode device, a single-stage amplifier achieves 8-dB small signal gain, with less than 4-dB noise figure at 105 GHz, within a chip size of only 0.725 mm/sup 2/. The 2- and 3-stage LNAs exhibit small signal gains of more than 15- and 22-dB, respectively over the 100-115 GHz frequency range, with associated measured noise figures of 4.5 dB at 105 GHz; the chip area for these circuits are less than 2- and 3 mm/sup 2/. To the author's knowledge, these results are amongst the lowest noise figures reported to date for uniplanar amplifier MMICs operating at these frequencies. [C1507]

#### "A cost-effective 10 Watt X-band high power amplifier and 1 Watt driver amplifier chip-set"

An X-band power amplifier chip-set for communication and radar applications has been developed and tested. The chip set consists of a two- and three-stage high-power amplifier, which has an output power of 10 Watt over the 8.5-10.5 GHz frequency band and a driver amplifier with an output power of more than 1 Watt over the 8.5-11.5 GHz frequency band. The amplifiers have been developed in the 6-inch 0.5 /spl mu/m power pHEMT process (PP50-10) of WIN Semiconductors. The use of this process in combination with the used innovative design approach results in a cost effective chip set, which is competitive in both performance and price with any available solution. [C1508]

#### "Compact and broadband microstrip power amplifier MMIC with 400-mW output power using 0.15-/spl mu/m GaAs PHEMTs"

The performance of a compact power amplifier MMIC for 35 to 45 GHz applications is reported. Using a standard 6-inch, 0.15-/spl mu/m GaAs power PHEMT technology on 100-/spl mu/m substrate thickness, in combination with appropriate compact circuit topologies, this microstrip power amplifier achieved a linear gain of more than 24 dB over the 36 to 45 GHz frequency range. At 5 V and 500 mA bias, an output power at 1-dB compression of 26 dBm ( $P_{\text{sub}} - 1 \text{ dB} = 400 \text{ mW}$ ) was measured in the 37/spl sim/40 GHz band, with a saturated output power up to 0.5 Watt ( $P_{\text{sub sat}} = 27 \text{ dBm}$ ). The total chip size is only 3.6 mm/sup 2/ (2.4 /spl times/ 1.5 mm/sup 2/); compared to conventional power amplifier MMICs operating at these frequencies, the combined output power and gain densities per chip area are a factor two higher. [C1509]

#### "Investigation of IMD asymmetry in microwave FETs via Volterra series"

IMD asymmetry generation and its asymmetrical behaviour are discussed and clarified in this contribution using a Volterra series approach. The approach has been applied to a power PHEMT device for X-band application. The effects of harmonic terminations have been clarified, stressing the relevance of baseband terminations and in particular of the output susceptance. Simplified expressions are inferred to clarify the effects of output terminations. Finally, the opportunity to choose a suitable fundamental and second harmonic output termination to reduce intermodulation asymmetry is discussed. [C1510]

#### "A W-band MMIC amplifier using 70-nm gate length InP HEMT technology"

InP HEMT transistors using 70-nm gate length have been fabricated and modeled. Two different epitaxial structures have been tested based on either single- or composite InGaAs channel. The composite-channel HEMT exhibited significantly higher maximum transconductance, 1370 mS/mm, compared to 860 mS/mm for the single-channel HEMT whereas  $f_{\text{sub } 1/} / (f_{\text{sub max}})$  was approximately the same, 190 [260] GHz, and 200 (320) GHz, respectively. A W-band microstrip MMIC amplifier using 70-nm gate length InP HEMT technology has been designed and fabricated for the single-channel structure. The one-stage amplifier exhibited a gain of 8 dB at 94 GHz. [C1511]

### "S and C band over 100 W GaN HEMT 1-chip high power amplifiers with cell division configuration"

In this paper, GaN HEMT 1-chip high power amplifiers at S and C bands are presented, which are featured by the cell division configuration. Spurious oscillations, which often occur for large gate periphery microwave transistors, were suppressed by dividing 8 transistor cells in a single chip into 4 blocks each consisting of 2 cells and placing isolation resistors on matching circuits. 120 W and 140 W output powers were successfully extracted from single chip GaN HEMT transistors with 3.8 W/mm and 2.8 W/mm power densities at S and C bands, respectively. These are top-level output powers from single chip GaN HEMT transistors over 3 GHz. [C1512]

### "A high purity 60 GHz-band single chip /spl times/8 multiplier with low phase noise"

A single chip multiplier by eight (/spl times/8) MMIC for 52-62 GHz output frequency is presented. The multiplier consists of quadrupler stage followed by a high pass filter, an inter-stage amplifier and a doubler stage. The required output power is achieved by a two stage buffer amplifier on the output. An output power exceeding 7 dBm is achieved from 52 to 61 GHz. The rejection of the unwanted harmonics is better than 28 dB and the detected degradation of phase noise due to the circuit is less than 1 dB at 100 kHz offset from the carrier, compared to a theoretical value of 18.06 dB for a multiplier by eight. The bias configuration is optimized to reduce the number of the required bias voltages to three. The total power dissipation is 450 mW. The MMIC is designed and manufactured in a commercial 0.15 /spl mu/m PHEMT process from WIN foundry. To our knowledge this is the first reported MMIC multiplier by eight based on PHEMT technology. [C1513]

### "A low-noise X-band microstrip VCO with 2.5 GHz tuning range using a GaN-on-SiC p-HEMT"

A low-noise X-band microstrip hybrid VCO has been designed and realised using a 2 /spl times/ 50 /spl mu/m GaN-on-SiC pseudo-morphic HEMT as the active device. The transistor has been manufactured by TIGER and features a gate-length of 0.15 /spl mu/m, an  $f_{\text{sub T}}$  of 22 GHz, a break-down voltage of 42 Volts and an  $I_{\text{dss}}$  close to 1 A/mm. The VCO has been assembled with standard SMD reflow and chip-on-board technology on Rogers 4003 substrate material. The circuit is biased at +15 Volts and 38 mA and has a measured tuning range from 8.1 to 10.6 GHz, an output power level of +19 dBm and an average phase-noise level of -114 dBc/Hz @ 1 MHz offset. [C1514]

### "Ka-band AlGaIn/GaN HEMT high power and driver amplifier MMICs"

In this paper the MMIC technology, design and characterization of a high power amplifier and driver amplifier MMIC at 30 GHz in AlGaIn/GaN HEMT technology are presented. The MMICs are designed using CPW technology on a 390 /spl mu/m thick SiC substrate. The measured small-signal gain of the driver is 14 dB at 28.5 GHz and the measured output power is 28.6 dBm at 28 GHz. The power amplifier shows a measured small-signal gain of 10.7 dB at 25.5 GHz and output power of 34.1 dBm at 27 GHz. Both MMICs have a very good yield and performance for a first iteration design. [C1515]

### "A wideband balanced AlGaIn/GaN HEMT MMIC low noise amplifier for transceiver front-ends"

A 3-16 GHz wideband AlGaIn/GaN high electron mobility transistor (HEMT) low noise amplifier (LNA), using balanced configuration with a coplanar waveguide (CPW) Lange coupler, is designed and fabricated. The LNA shows a minimum noise figure of 4 dB with associated gain of 20 dB and gain flatness of +/- 3 dB across the 3-16 GHz frequency range. This balanced GaN LNA is suitable for transceiver front-ends due to the low input/output VSWR, high stability and redundancy, as well as, high power handling capability of GaN HEMTs. The design, fabrication and characterization results of the GaN HEMT balanced amplifier are described together with the details of design and characteristics of the individual LNAs and the CPW coupler. [C1516]

### "Noise assessment of AlGaIn/GaN HEMTs on Si or SiC substrates: application to X-band low noise amplifiers"

This study regards the low noise properties of X-band GaN-based LNAs as well as its associated robustness. Devices are processed on epilayers grown on SiC or Si substrates. The HEMTs present very low noise properties with  $NF_{\text{sub min}}$  and  $G_{\text{sub ass}}$  close to 1 dB and 13 dB at 12 GHz. The robustness tests show that the component withstands power level up to 34 dBm. A two-stages X-band LNA is fabricated showing a noise figure of 1.7 dB with a gain of 20 dB at 10 GHz. [C1517]

### "A microstrip X-band AlGaIn/GaN power amplifier MMIC on s.i. SiC substrate"

A two-stage high-power amplifier MMIC was realized with a chip size of 4.5 mm /spl times/ 3 mm operating

between 8 GHz and 10 GHz based on a fully integrated microstrip AlGaIn/GaN HEMT technology on s.i. SiC substrate. The MMIC device delivers a maximum pulsed output power of 8.9 W (39.5 dBm) at 8.5 GHz at  $V_{DS} = 31$  V, 10 % duty cycle, and more than 6 dB gain compression level, and features a linear gain in excess of 20 dB. [C1518]

#### "A 45 dB variable gain low noise MMIC amplifier"

A variable gain amplifier operating at 2.5 GHz based on single ended topology has been designed and characterized. Three such stages were cascaded preceded by a single stage LNA. A source follower is used at the output as an active load matching. Overall dynamic gain variation is 45 dB with a maximum gain of 47 dB. The -3 dB bandwidth is 0.800 GHz. A minimum noise figure of 0.81 dB is obtained in the highest gain mode. Maximum value of 1 dB compression at the output is -7.2 dBm and the corresponding third order intercept point is +5.3 dBm. Consumed DC power 285 mW and is immune to gain variation. The circuit is implemented with GaAs pHEMT technology. The combined area occupied by the multistage low noise VGA and the single ended VGA is 3.5 mm  $\times$  3 mm. [C1519]

#### "A C-band high efficiency second harmonic tuned hybrid power amplifier in GaN technology"

In this contribution, a C-band 2nd harmonic tuned hybrid power amplifier utilizing a PHEMT GaN device is presented, together with technological aspects, nonlinear device model and adopted design criteria. The amplifier has been realised in hybrid form, exhibiting a bandwidth larger than 20% around 5.5GHz, with a minimum output power of 33 dBm, and a drain efficiency of 60% at the centre frequency. [C1520]

#### "A Ku band monolithic power amplifier for TT&C applications"

The paper describes the design of a 38 dBm monolithic power amplifier at Ku band. The amplifier has to be used as the final stage of the downlink transmitter of a TT&C system. A commercial power p-HEMT process capable of handling a power density higher than 1 W/mm of active area has been selected for the amplifier design. The power capability of this process makes it possible to integrate in a monolithic chip the functionality up today supplied by hybrid modules. Since the circuit is a space product, the attention is focused on reliability issues; therefore performances have to be matched imposing the devices to work at de-rated conditions respect to the process maximum ratings. In this perspective, the device channel temperature becomes a very tight design objective and has to be carefully controlled by means of a thermal simulator. The paper describes the three dimensional thermal model built to predict the devices thermal behavior in the environment of a finite difference thermal simulator. The design of the circuit is also described from the specifications to the final layout. [C1521]

#### "Modeling of a 4-18GHz 6W flip-chip integrated power amplifier based on GaN HEMTs technology"

This paper reports on the design of a cascode GaN HEMT distributed power amplifier demonstrating significant improvement of the best power performances reported to date. The active device is 8  $\times$  50  $\mu$ m AlGaIn/GaN HEMT grown on SiSiC. The distributed power amplifier integrates 4 cascode cells capacitively coupled to the gate line for power optimization. The active part made of the 4 cascode cells is implanted on a GaN-based wafer while the distributed passive part made of the interconnection lines is implanted on an AlN substrate. Finally, the GaN-based wafer integrating the active part is flip-chipped onto the AlN substrate via electrical and mechanical bumps. The flip-chip integrated circuit demonstrates a mean gain of 10dB and input/output matching lower than -10dB over the 4-18GHz bandwidth. At an input power of 29dBm (1 dB comp.), power simulations exhibit a mean output power of 37.6dBm with a standard deviation of 0.3dB, a power gain of 8.6dB and 16% of PAE over the band. At an input power of 31dBm (2dB comp.), the distributed amplifier achieves a mean output power of 38.6dBm, a power gain of 7.6dB and 18% of PAE. [C1522]

#### "Wideband monolithic microwave integrated circuit frequency converters with GaAs mHEMT technology"

We present monolithic microwave integrated circuit (MMIC) frequency converter, which can be used for up and down conversion, due to the large RF and IF port bandwidth. The MMIC converters are based on commercially available GaAs mHEMT technology and are comprised of a Gilbert mixer cell core, baluns and combiners. Single ended and balanced configurations DC and AC coupled have been investigated. The instantaneous 3 dB bandwidth at both the RF and the IF port of the frequency converters is 20 GHz with excellent amplitude and phase linearity. The predicted conversion gain is around 10 dB. Simulated results are supported by experimental characterization. Good agreement is found between simulations and experiment is found after adjustment of technology parameters. [C1523]



### "Multistage broadband amplifiers based on GaN HEMT technology for 3G/4G base station applications with extremely high bandwidth"

GaN HFETs have been proposed for high power high linearity and high bandwidth applications and reached tremendous output power levels (Kikkawa et al., 2004). However, there are relatively few circuit examples especially for wideband power amplifiers fulfilling the requirements of future multiband/multistandard capable 3G/4G base stations. This work presents first promising results of realised GaN based wideband power amplifier demonstrators for the mentioned field of application. Two different amplifier concepts for the final stage of a power amplifier module for medium range multiband base station applications in the L- and S-Band have been implemented as first amplifier demonstrators. The amplifiers have been characterized by using single carrier W-CDMA signals and showed a promising high bandwidth for output power levels up to >10 W while meeting the 3GPP ACLR specification in a wide frequency range. [C1524]

### "Influence of envelope impedance termination on RF behaviour of GaN HEMT power devices"

The influence of envelope source and load terminations on the RF performance of high power GaN amplifiers is investigated. An error-corrected two-tone measurement system has been developed enabling load- and source pull measurements in the envelope frequency bandwidth. Measured results on a 0.5µm-HEMT with a gate width of 84125 µ show a variation of 1 dB output power and 8% PAE. [C1525]

### "CMP service for prototyping and low volume production"

CMP aims at providing universities, research laboratories and industries with the possibility to have their integrated circuits projects fabricated for prototyping and low volume production. Presently, users are serviced for CMOS double layer poly/double layer metal (DLP/DLM) 0.8, DLM/TLM 0.6µm, DLP/4LM 0.35µm, SLP/6LM 0.18µm, SLP/6LM 0.13µm, SLP/7LM 90nm, BiCMOS DLP/DLM 0.8µm, SiGe 0.35µm SLP/5LM, SiGe:C 0.25µm SLP/5LM and GaAs HEMT 0.2µm. About 40 multi-project runs are offered per year. Micro electro mechanical systems (MEMS) are also provided in standard CMP runs in CMOS DLP/DLM 0.8µm 0.6µm, BiCMOS DLP/DLM 0.8µm and HEMT GaAs 0.2µm, using compatible front-side bulk micro-machining. MUMPS processes are offered as surface micro-machining allowing integrating MEMS only microstructures [C1526]

### "Title page"

The following topics were dealt with: gallium arsenide semiconductors; compound semiconductors; field effect transistors; pseudomorphic high electron-mobility transistor; heterojunction bipolar transistors; PHEMT and HBT power amplifiers; microwave integrated mixers; low noise and broadband amplifiers; nanodevices for RF applications; photonic devices and circuits; 3D MCM modules for space applications; microwave and millimeter-wave circuits and sources; device reliability; monolithic millimeter-wave integrated circuits; cellular and WLAN (wireless local area network) applications; microwave device and circuit packaging; millimeter-wave frequency converters; and RF-MEMS technology [C1527]

### "Are we there yet?-a metamorphic HEMT and HBT perspective"

Metamorphic epitaxy technique offers the possibility of combining the advantages of low-cost and manufacturability of GaAs substrates and the high performance of InP-based devices. This paper presents the recent development of metamorphic HEMTs and HBTs and discusses their readiness for commercialization. [C1528]

### "Status of AlGaIn/GaN HEMT technology-a UCSB perspective"

The following major technological advances (i) the ability to grow high quality materials on sapphire and SiC, (ii) the advent of SiN passivation to eliminate current slump or dispersion, (iii) advanced processing, and (iv) implementation of field plates have taken AlGaIn/GaN HEMTs to commercialization in the relatively short time of approximately a decade. In this paper, we present the highlights of this research. [C1529]

### "Numerical Simulation of Al<sub>1-x</sub>Ga<sub>x</sub>N/GaN HEMT"

In this paper, a novel AlGaIn/GaN HEMT is simulated by self-consistently solving the Poisson-Schrödinger-Hydrodynamics equations. Compared with conventional AlGaIn/GaN HEMT, the numerical results show that the insertion of a very thin AlN interfacial layer has favorable influence on the device performance because of the increased effective  $\Delta E_c$ , which brings improved sheet electron density and DC output current. In addition, the AlN interfacial layer can impede the flow of electrons from the channel to the surface-states and defects of AlGaIn barrier layer, therefore the drain current collapse effect can be eliminated. [C1530]

### "Sub-Terahertz Wireless Communications Technologies"

This paper presents a 10-Gb/s wireless link system that uses a 120-GHz-band sub-terahertz electro-magnetic waves. In the transmitter, photonic techniques are used for generation, modulation, and emission of the sub-THz signals, while the receiver is composed of all-electronic devices using InP-HEMTs [C1531]

### "Investigation of the Transmission Line Loss on the Performance of the HBT\_HEMT Matrix Amplifier"

In this paper, an analytical approach is proposed to study the performance of HBT\_HEMT matrix amplifiers. A closed form relation for the central line attenuation function of the matrix amplifier is obtained which is very useful in the consideration of the influence of several parameters on the device performance. It is shown that this structure may have lower attenuation respect to the traditional HEMT\_HEMT and HEMT\_HBT matrix amplifiers. The proposed technique is applicable in improving the performance of microwave and mm-wave ICs [C1532]

### "A metamorphic GaAs HEMT-distributed amplifier with 50 GHz bandwidth and low noise for 40 Gbits/s photoreceiver"

An eight stage distributed amplifier with 12.5 dB plusmn 0.45 dB gain and 50 GHz bandwidth has been demonstrated in a commercially available 0.1 mum metamorphic GaAs HEMT (MHEMT) technology. The amplifier has a minimum noise figure lower than 2.5 dB in the bandwidth. The group delay variation, from 9 to 40 GHz is plusmn 7.5 ps and circuit consumption is 0.4 W. Such amplifier has been packaged with a high responsivity photodiode into a fiber pig-tailed module. Eye diagrams measurements demonstrate the successful high-speed operation of the photoreceiver [C1533]

### "A dual band (10/16 GHz) p-HEMT VCO"

We report a 0.15 /spl mu/m p-HEMT dual frequency VCO. The dual frequencies are achieved using a switched-resonator topology. Large devices can be used for switching, as their parasitic capacitance is absorbed into the resonator. The phase noise at 1 MHz offset was -101 dBc and -92 dBc at 10.6 and 16.3 GHz respectively. [C1534]

### "A 100 W high-efficiency GaN HEMT amplifier for S-band wireless system"

We have successfully developed a 100 W AlGaIn/GaN power amplifier with a bandwidth of 300 MHz in S-band, operating at 50 V drain bias voltage. This amplifier consists of one HEMT die developed for L/S-band frequency operation and a single-ended package. The developed amplifier has an output power of 100 W and a high linear gain of more than 13.5 dB in the frequency range of 2.6 GHz to 2.9 GHz under CW or pulsed conditions [200 usec (pulse width) and 2 msec (period)]. High drain efficiency of 58% was also achieved at an output power of 100 W and frequency of 2.8 GHz. To the best of our knowledge this is the first report of 100 W AlGaIn/GaN HEMT amplifier developed for S-band high power application. [C1535]

### "A low cost SMT integrated frequency doubler and power amplifier for 30 GHz DBS uplink applications"

A SMT (surface mount technology) MMIC (monolithic microwave integrated circuit) frequency multiplier (x2) and power amplifier has been designed for DBS (direct broadcast satellite) and other commercial applications. Using PHEMT technology this MMIC takes a 15 GHz input signal and passes it through a harmonic frequency doubler and then through three stages of power amplification at 30 GHz. This MMIC provides an output power of 21 dBm, fundamental suppression of 45 dBc and is stable across all voltages and temperatures. This single MMIC SMT solution frequency multiplier and power amplifier is unique compared to any known or published data. [C1536]

### "A 150 to 220 GHz balanced doubler MMIC using a 50 nm metamorphic HEMT technology"

A coplanar millimeter wave doubler MMIC covering the entire G-band was developed. Based on a 50 nm metamorphic HEMT technology, the circuit demonstrates an output power of more than -12 dBm between 150- and 220 GHz for an input power of 0 dBm. By increasing the input power to 12 dBm an output power exceeding 0 dBm was obtained in the frequency range between 180- and 220 GHz. Good fundamental rejection was ensured by using a Marchand balun for balancing the design. The doubler was also used to provide the LO signal for a 170 to 200 GHz resistive FET mixer, yielding a conversion loss of 10 dB. [C1537]

### "60 GHz GaAs MMIC mixers with integrated LO buffer"

Using the 0.15  $\mu\text{m}$  GaAs mHEMT process from WIN semiconductors, two 60 GHz down-conversion mixers have been designed, processed and measured. Both designs include a LO buffer amplifier to allow for a reduced external LO power level. With an LO power of +10 dBm, the measured RF input match is better than -15 dB at 60 GHz and the conversion loss is below 8 dB at 2 GHz intermediate frequency. [C1538]

### "A V band singly balanced diode mixer for space application"

The paper describes the design of a V band single balanced mixer to be employed in the front end of an on-board receiver for space applications. The V band receiver is a demonstrator for the use of different monolithic processes and interconnection/assembly technologies in space applications at such high frequencies. The receiver front-end consists of a multi-stage LNA amplification followed by an image reject filter, the mixer and a frequency doubler for the local oscillator. All the chips are mounted over an LTTC substrate using bumps/hot vias technology. Chip to chip interconnection is provided by coplanar waveguide on LTTC. The mixer employs a rat race 180° hybrid to balance the local oscillator and a couple of Schottky diodes as mixing elements. The technology employed is a 0.15  $\mu\text{m}$  pHEMT process that offers diodes with a cut off frequency higher than 300 GHz. The choices made for the mixer type and topology starting from the system specifications are covered in the paper along with the actual description of the circuit design. [C1539]

### "Frequency domain-based extraction method of one-port device's non-linear state functions from large-signal measurements"

A novel frequency domain-based method for the extraction of one-port device's non-linear constitutive relations directly from vector large-signal measurements is presented. A distinctive characteristic of the method is that it provides directly the charge-voltage state-function, without the need to perform the integration of the capacitance-voltage function as required by its time domain-based counterpart. The capabilities of the method are demonstrated by extracting the non-linear state-functions of a microwave diode from large-signal data generated by harmonic balance analysis, and the non-linear gate-source state-functions of a HEMT device under 'cold-FET' bias conditions from measured data. [C1540]

### "A realistic large-signal microwave PHEMT transistors model for SPICE"

A comprehensive large-signal HEMT model that provides a realistic description of measured characteristics over all operating regions for different PHEMTs is presented. The model was previously tested in harmonic-balance based simulators and for the first time it has been implemented inside the time domain SPICE simulator. In order to do that, a new set of routines and libraries has been developed. The procedure introduced here can be extended to properly simulate other kind of devices described in terms of equivalent circuits. DC and scattering simulation results show very good agreement with the experimental measurements. [C1541]

### "A novel wideband MMIC voltage controlled attenuator with a bandpass filter topology"

The design and analysis of a novel wideband, monolithic, bandpass,  $\pi$ -network, voltage controlled attenuator (VCA) is presented. A 24 to 32 GHz VCA was developed using 0.15  $\mu\text{m}$  GaAs pHEMT technology. This is the first reported VCA to use a bandpass filter topology to achieve the required operating frequency band and eliminate the effects of parasitic capacitances of the pHEMTs. The bandpass filter absorbs the parasitic capacitances and thereby eliminates their detrimental effects. The measured attenuation dynamic range is 12 dB  $\pm$  0.5 dB with minimum insertion loss of 2-3 dB. The input power handling capability is up to 0 dBm. The VCA is well matched and may be placed in a 50  $\Omega$  system (S.M. Halabi, 2004). [C1542]

### "Modelling of a 4-18 GHz 6 W flip-chip integrated power amplifier based on GaN HEMTs technology"

This paper reports on the design of a cascode GaN HEMT distributed power amplifier demonstrating significant improvement of the best power performances reported to date. The active device is a 8 $\times$ 50  $\mu\text{m}$  AlGaN/GaN HEMT grown on SiC. The distributed power amplifier integrates 4 cascode cells capacitively coupled to the gate line for power optimization. The active part made of the 4 cascode cells is implanted on a GaN-based wafer while the distributed passive part made of the interconnection lines is implanted on an AlN substrate. Finally, the GaN-based wafer integrating the active part is flip-chipped onto the AlN substrate via electrical and mechanical bumps. The flip-chip integrated circuit demonstrates a mean gain of 10 dB and input/output matching lower than -10 dB over the 4-18 GHz bandwidth. At an input power of 29 dBm (1 dB

comp.), power simulations exhibit a mean output power of 37.6 dBm with a standard deviation of 0.3 dB, a power gain of 8.6 dB and 16% of PAE over the band. At an input power of 31 dBm (2 dB comp.), the distributed amplifier achieves a mean output power of 38.6 dBm, a power gain of 7.6 dB and 18% of PAE. [C1543]

#### "A 45 dB variable gain low noise MMIC amplifier"

A variable gain amplifier operating at 2.5 GHz based on single ended topology has been designed and characterized. Three such stages were cascaded preceded by a single stage LNA. A source follower is used at the output as an active load matching. Overall dynamic gain variation is 45 dB with a maximum gain of 47 dB. The -3 dB bandwidth is 0.800 GHz. A minimum noise figure of 0.81 dB is obtained in the highest gain mode. Maximum value of 1 dB compression at the output is -7.2 dBm and the corresponding third order intercept point is +5.3 dBm. Consumed DC power 285 mW and is immune to gain variation. The circuit is implemented with GaAs pHEMT technology. The combined area occupied by the multistage low noise VGA and the single ended VGA is 3.5 mm /spl times/ 3 mm. [C1544]

#### "A Ku band monolithic power amplifier for TT&C applications"

The paper describes the design of a 38 dBm monolithic power amplifier at Ku band. The amplifier has to be used as the final stage of the downlink transmitter of a TT&C system. A commercial power p-HEMT process capable of handling a power density higher than 1 W/mm of active area has been selected for the amplifier design. The power capability of this process makes it possible to integrate in a monolithic chip the functionality up today supplied by hybrid modules. Since the circuit is a space product, the attention is focused on reliability issues; therefore performances have to be matched imposing the devices to work at de-rated conditions respect to the process maximum ratings. In this perspective, the device channel temperature becomes a very tight design objective and has to be carefully controlled by means of a thermal simulator. The paper describes the three dimensional thermal model built to predict the devices thermal behavior in the environment of a finite difference thermal simulator. The design of the circuit is also described from the specifications to the final layout. [C1545]

#### "Influence of envelope impedance termination on RF behaviour of GaN HEMT power devices"

The influence of envelope source and load terminations on the RF performance of high power GaN amplifiers is investigated. An error-corrected two-tone measurement system has been developed enabling load- and source pull measurements in the envelope frequency bandwidth. Measured results on a 0.5 /spl mu/m-HEMT with a gate width of 8/spl times/125 /spl mu/m show a variation of 1 dB output power and 8 % PAE. [C1546]

#### "GaAs MMICs for use in upconverter module for Ka-band OBS satellite transponders"

GaAs MMICs has been developed for use in the upconverter module for on-board switching Ka-band satellite transponders. There are four kinds of MMICs: an S-band medium power amplifier, a K-band medium power amplifier, an S to K-band mixer, and X to Ku-band frequency doubler. The four chips have been fabricated on a wafer using 0.15 /spl mu/m GaAs p-HEMT technologies. A upconverter module using the MMICs with a function of the frequency conversion from 3 GHz to 20 GHz has been developed and showed the RF performance of the 17.1/spl plusmn/0.2 dB conversion gain, the 0.2 nsp-p group delay, the 46.67 dBc C/IM/sub 3/, and 1.15:1 in/out VSWR. [C1547]

#### "Wideband monolithic microwave integrated circuit frequency converters with GaAs mHEMT technology"

We present monolithic microwave integrated circuit (MMIC) frequency converter, which can be used for up and down conversion, due to the large RF and IF port bandwidth. The MMIC converters are based on commercially available GaAs mHEMT technology and are comprised of a Gilbert mixer cell core, baluns and combiners. Single ended and balanced configurations DC and AC coupled have been investigated. The instantaneous 3 dB bandwidth at both the RF and the IF port of the frequency converters is /spl sim/ 20 GHz with excellent amplitude and phase linearity. The predicted conversion gain is around 10 dB. Simulated results are supported by experimental characterization. Good agreement is found between simulations and experiment is found after adjustment of technology parameters. [C1548]

#### "Multistage broadband amplifiers based on GaN HEMT technology for 3G/4G base station applications with extremely high bandwidth"

GaN HFETs have been proposed for high power high linearity and high bandwidth applications and reached tremendous output power levels (T. Kikkawa et al., 2004). However, there are relatively few circuit examples



especially for wideband power amplifiers fulfilling the requirements of future multiband/multistandard capable 3G/4G base stations. This work presents first promising results of realised GaN based wideband power amplifier demonstrators for the mentioned field of application. Two different amplifier concepts for the final stage of a power amplifier module for medium range multiband base station applications in the L- and S-band have been implemented as first amplifier demonstrators. The amplifiers have been characterized by using single carrier W-CDMA signals and showed a promising high bandwidth for output power levels up to >10 W while meeting the 3GPP ACLR specification in a wide frequency range. [C1549]

#### "A GaAs distributed amplifier with an output voltage of 8.5 V/sub PP/ for 40 Gb/s modulators"

In this paper, we report on a distributed amplifier (DA) with positive gain slope and 8.5 V/sub PP/ output voltage swing at 20 GHz. This makes the amplifier suitable for driving LiNbO<sub>3</sub> modulators. The amplifier consists of six cascode cells and is fabricated in a commercially available 150 nm GaAs power pHEMT technology. Gain equals to 9.8 dB at low frequencies and rises up to 12.8 dB at 38 GHz. This amplifier is then cascaded with a preamplifier. Losses at high frequencies due to cascading are compensated by the positive gain slope of the amplifier described here. The cascaded amplifiers exhibit a gain of 19.5 dB and a bandwidth of 38 GHz with a flat frequency response of  $\pm 0.6$  dB up to 28 GHz. [C1550]

#### "A millimeter-wave ultra-compact broadband diode mixer using modified Marchand balun"

In this paper, a broadband mixer has been developed using 0.15- $\mu$ m pHEMT technology. This singly balanced mixer was realized by using Schottky diodes. A modified Marchand balun was employed at the LO port and matched to the diodes directly to achieve wideband performance and compact size. This diode mixer achieves conversion loss of better than 10 dB from 46 to 78 GHz with LO power of 12.5 dBm, and the chip size is only 0.57 mm  $\times$  0.52 mm. Compared with previously reported MMIC mixers in millimeter-wave frequencies, this circuit has the smallest chip size with competitive performance and wide bandwidth. [C1551]

#### "A comparative study of active and passive GaAs microwave couplers"

This paper compares the design and performance of two types of wide band multi-octave MMIC couplers. An active coupler is based on pHEMT devices and fabricated in a GaAs foundry and a passive coupler uses coplanar waveguide (CPW) multilayer techniques. The multilayer couplers are fabricated on GaAs semi-insulating substrate and are reciprocal and directional. The active coupler design is adapted from the distributed amplifier circuit and is non-reciprocal. On-wafer RF measurements were carried out on the fabricated multilayer directional couplers and pHEMT based couplers. A multilayer quadrature directional coupler with coupling factor of 5 dB and isolation of 10 dB is realized over 10 to 35 GHz. A 180° coupler using pHEMT devices realized a coupling factor of 5 dB and isolation of 26.5 dB over 2 to 20 GHz. For the first time the relative merits of the performance and implementation of these couplers are compared in view of their respective applications. [C1552]

#### "Advanced meander gate p-HEMT model for accurate harmonic modeling of switch MMIC designs"

This paper presents a non-linear model of a meander gate p-HEMT for switch design. The model combines a modified Parker-Skellern IV form with a custom charge model to accurately predict large signal performance of meander-gate based switches. Comparison between modeled and measured results of a 0.5 mm gate length SPDT switch shows an accurate prediction of the 2<sup>nd</sup> and 3<sup>rd</sup> harmonic generation at the output. [C1553]

#### "AlGaIn/GaN high electron mobility transistor (HEMT) reliability"

The reliability characteristics of AlGaIn/GaN HEMTs are reviewed. Basic effects such as the discrepancy between DC predicted and RF measured power are addressed together with effects such as drain current and power degradation observed following RF stress. Technologies based on sapphire, SiC and Si substrates are considered. The impact of process such as passivation, as well as design i.e. barrier layer are considered. DC and microwave properties are considered in the study. Low frequency noise is also discussed in conjunction with degradation following stress. [C1554]

#### "Low frequency and linear high frequency noise performances of AlGaIn/GaN grown on SiC substrate"

Newly developed GaN technology offers great potential for military and space, as well as some high volume applications. The devices are grown on different substrates (sapphire, silicon and silicon carbide), involving differences on the performances, price, and technological complexity. The design of a fully integrated transceiver

in such a technology necessitates great noise performances for the linear (low noise amplifiers, LNA) and non-linear (voltage controlled oscillator, VCO) applications. The low noise figure already published on this technology up to X-band, associated to the capability to handle high power levels avoid the integration of a limiter stage that deteriorates the overall noise figure in conventional architectures. The low frequency noise performances are useful both for the technology assessment (maturity's indicator) and for the non-linear circuit design (conversion to phase noise around the carrier). This paper presents the noise performances of AlGaIn/GaN HEMT grown on SiC substrate. Low frequency noise contributors in the ohmic and saturated regime are discussed. Residual phase noise characterization at 10 GHz correlates the results about the noise sources involved, and linear high frequency noise figure measurements are also presented, targeting respectively VCO and LNA applications

[C1555]

#### "On the large-signal modelling of AlGaIn/GaN HEMTs and SiC MESFETs"

A general purpose LS model for GaN and SiC FET devices was developed and evaluated with DC, S, and large signal measurements (LS). The FET model is generalized and extended with new feature in order to improve the management of harmonics, provide a more physical treatment of the dispersion as well as delay and model other specific effects in these devices. The model was implemented in a commercial CAD tool and exhibit good overall accuracy. [C1556]

#### "Compact W-band SPQT MMIC switch using traveling wave concept"

A high performance W-band single-pole-quadruple-throw (SPQT) switch with a compact chip size using GaAs HEMT is demonstrated. This SPQT switch has a measured insertion loss of 3.9-5.5 dB and isolation higher than 30 dB from 70 to 102 GHz. A minimum insertion loss of 3.9 dB with isolation higher than 30 dB was measured at 90 GHz. [C1557]

#### "Advanced manufacturing techniques for next generation power FET Technology"

The development and incorporation of an evaporated airbridge technology into an established power pHEMT device is described. Advantages of this technology over a conventional plated technology are discussed. Use of this technology has resulted in improvements to the process flow in terms of reduced complexity and cycle time. Improvements in uniformity and reduced feature size have enabled the use of an automated visual inspection capability to reliably differentiate good and bad die. [C1558]

#### "A comprehensive class A to B power and load-pull characterization of GaN HEMTs on SiC and sapphire substrates"

An extensive power characterization of devices fabricated on GaN grown on SiC and sapphire substrates has been carried out, including power sweep and load-pull measurements in different bias conditions from class A to class B. An active load-pull bench optimized for high voltage and high power measurements allows to extend the load-pull characterization to the whole Smith chart, and to localize the optimum load conditions even for devices with almost reactive optimum terminations. The characterization procedure allows to verify scaling rules and the effects of defects and thermal degradation on the device power performances. The results of the SiC and sapphire-based devices show that, on one side, SiC-based devices exhibit state-of-the-art performances in Class A, and, on the other side, low-cost sapphire-based devices, when biased in high efficiency classes, can be viable candidates for medium power applications, despite the higher thermal resistivity of sapphire compared with the one of SiC [C1559]

#### "A 38-48-GHz miniature MMIC subharmonic mixer"

A 38-48-GHz miniature sub-harmonically pumped mixer has been developed using GaAs 0.15- $\mu\text{m}$  pHEMT technology. An anti-parallel diodes pair is used for frequency conversion with a low LO input power. Quasi-lumped matching topology is employed to minimize the chip size and cost. The mixer is fabricated in chip size 0.85  $\times$  0.85 mm<sup>2</sup>, and exhibit 12-15-dB up-conversion loss and 11-16-dB down-conversion loss with 10 dBm LO power. [C1560]

#### "Verification of a frequency dispersion model in the performance of a GaAs pHEMT travelling-wave MMIC"

The impact of frequency dispersive effects on typical figures of merit is investigated in a distributed MMIC realized in 0.15  $\mu\text{m}$  GaAs pHEMT technology. A novel compact dispersion model, allowing for accurate simulation of both static and dynamic multiple time constant IV characteristics, is employed. In a comparison of measurement and simulation, the model is both validated and used to quantify and interpret the error introduced

when neglecting frequency dispersion in the design of MMICs. Device operation is investigated with respect to gain, linearity and power-added efficiency, all of them affected by dispersion effects. The model is shown to significantly improve simulation accuracy by increasing the validity range in terms of the frequency- and voltage regimes. [C1561]

#### **"KORRIGAN-a comprehensive initiative for GaN HEMT technology in Europe"**

KORRIGAN is a large-scale joint multinational initiative of leading system houses and research laboratories in Europe aiming at the development of an independent and state-of-the-art capability in GaN HEMT technology. The main objective of KORRIGAN is to establish a stand alone European supply chain and foundry service. Several key research areas such as materials, processing, reliability evaluation, thermal management and packaging, are addressed and are involve in European industrial and university partners. The benefits of GaN technology are finally evaluated at system level for critical defence applications up to 20 GHz with the fabrication and test of circuit, MMIC and module demonstrators. [C1562]

#### **"Progress in microwave GaN HEMT grown by MBE on silicon and Smart Cut/spl trade/ engineered substrates for high power applications"**

SiCOI (SiC on insulator) composite substrates obtained by the Smart-Cuttrade process are alternative possible substrates for epitaxial growth of wide band gap (WBG) materials such as GaN and GaN alloys. Similar to bonded SOI structure, the SiCOI structures basically comprises a thin film of single SiC crystal bonded onto a substrate such as, for instance, silicon substrate. Additionally to the well known insulation properties, SiCOI substrates have been proven to be adapted to the growth of high quality GaN layer. This first study has proven compatibility of SiCOI structure for single layer GaN MBE growth. We present here last results of AlGaIn/GaN HEMT structure grown by MBE with NH<sub>3</sub> as nitrogen precursor onto SiCOI (on silicon) structure realised by Smart Cuttrade. First of all, complete SiCOI structure realisation will be described and typical physical characterization results will be presented for this kind of substrate. Then, will be detailed MBE epitaxy set-up and growth parameters for HEMT structure, including specific buffer layer stack description. Finally, physical and electrical characterisation results for epi-layers and HEMT structure will be presented. Those results show strong compatibility of SiCOI structure for MBE epitaxy of GaN based HEMT structure and demonstrate the interest of Smart Cuttrade approach to build composite substrates, like SiCOI, for hetero-epitaxy application [C1563]

#### **"High power/high bandwidth GaN MMICs and hybrid amplifiers: design and characterization"**

Broadband microstrip and coplanar MMIC amplifiers featuring beyond 10 W for X-band radar applications are realized in a AlGaIn/GaN HEMT technology on 2" s.i. SiC substrate. Single-stage and dual-stage demonstrators with flat gain from 1 GHz to 2.7 GHz and up to 40 W peak power in hybrid microstrip technology for basestation applications are presented. The performance illustrates the potential of this technology with very high bandwidth and superior power density in comparison to GaAs. [C1564]

#### **"GaAs MMICs for use in upconverter module for Ka-band OBS satellite transponders"**

GaAs MMICs has been developed for use in the Upconverter module for On-Board Switching Ka-band Satellite Transponders. There are four kinds of MMICs: an S-band Medium power amplifier, a K-band Medium power amplifier, an S to K-band Mixer, and X to Ku-band frequency doubler. The four chips have been fabricated on a wafer using 0.15µm GaAs p-HEMT technologies. A Upconverter module using the MMICs with a function of the frequency conversion from 3GHz to 20GHz has been developed and showed the RF performance of the 17.1±0.2dB conversion gain, the 0.2nsp-p group delay, the 46.67dBc C/IM3, and 1.15:1 In/Out VSWR. [C1565]

#### **"THz active devices and applications: a survey of recent researches"**

THz waves have recently attracted considerable interest mainly because of their various applications. Efficient and compact CW sources are currently under development using either electronic or optical components. On the electronic side, an important innovation of last years has been to excite THz plasma oscillations in short gate length HEMT. On the optoelectronic side, high speed photodetectors and photodiodes are currently under development with aim of a most efficient coupling with already existing 1.55 µm semiconductor laser technology. Besides active device review, studies devoted to controllable THz photonic crystals and specific antennas for the THz domain will also be discussed. [C1566]

#### **"GaAs distributed amplifiers with up to 350 GHz gain-bandwidth product for 40 Gb/s LiNbO<sub>3</sub> modulator drivers"**

In this paper, we report on two Distributed Amplifier (DA) concepts for 40 Gb/s modulator drivers. Both amplifiers

are fabricated in a commercially available 150 nm GaAs power pHEMT technology. The first DA is a six stages design with capacitive division on the gate line. Gain and bandwidth of this amplifier equal to 13.2 dB and 41 GHz, respectively. The other DA consists of nine cascode stages, achieving 20.1 dB gain and a bandwidth of 34.5 GHz. Output power of the two amplifiers is higher than 21 dBm or 7 Vpp up to 20 GHz, which makes them suitable for driving lithium-niobate (LiNbO<sub>3</sub>) modulators. [C1567]

#### "Efficient HFET power amplifier"

The design and performance of a high efficiency power amplifier operating in class-AB/F at X-band is presented. The single-ended 9.6-mm gate width HFET amplifier comprised of four state-of-the-art 2.4-mm unit-cell HFETs. The design was simulated using accurate small-and large-signal models of the 2.4-mm unit-cell HFET. Conventional microwave integrated circuit (MIC) technology was used to fabricate the amplifier. The correlation between the simulated and measured results is excellent. The amplifier exhibited power-added efficiency (PAE) of 42%, with an output power of 9 Watts at 1 dB gain compression-point, and a small-signal gain of 7 dB. [C1568]

#### "Microwave class-F power amplifier design including input harmonic terminations"

In this paper, we present the design of a high-efficiency class-F power amplifier in pHEMT technology using a novel load-pull/source-pull simulation-based approach. The 2nd harmonic input termination is shown to have a critical influence on PA performances, which is justified by the shape of the simulated waveforms. Experimental validation is carried out on a 2 GHz practical circuit using a medium-power packaged device. Two cases are compared both theoretically and experimentally: for the best and worst case 2nd harmonic input terminations, 76% and 42% saturated PAE are measured, respectively. The worst case termination degrades the saturated C/I<sub>3</sub> by 7.5 dB. [C1569]

#### "A compact Ka-band power amplifier using finite-ground coplanar waveguide design"

A compact 0.15μm InGaAs pHEMT power amplifier using finite-ground coplanar waveguide (FGCPW) design for Ka-band applications is presented. An optimum ratio between signal and ground width is demonstrated in this design. The proposed two stages FGCPW power amplifier delivers a 14.5dB linear power gain at 31GHz with 19.3% maximum power-added efficiency (Max PAE). Furthermore, the chip size is very compact less than 2 mm<sup>2</sup>. Compared to previously reported Ka-band amplifiers, the results are superior to those using the microstrip technique on MMIC power amplifier designs. [C1570]

#### "Intrinsic dependence of intermodulation distortion in HEMTs"

This paper analyses the intrinsic (the Taylor series coefficients) dependence of intermodulation distortion in HEMT (high electron mobility transistors) amplifiers. This analysis is very helpful for understanding the bias dependence of IM distortion since it critically depends on the bias dependence of Taylor series coefficients. [C1571]

#### "Advanced high performance MMICs for satellite transponder"

This paper presents the design and measured results of a high performance multifunction GaAs MMIC chipset for C and extended-C band receiver and channel amplifier for communication satellite onboard systems. All MMICs, i.e., low noise amplifier (LNA), double balanced mixer (DBM), variable gain amplifier (VGA) and amplifier with 4-bit digital attenuator are realized using 0.2μm GaAs PHEMT process. The goal is to reduce chip count and off chip components while achieving best system performance. Key features of these circuits are low noise, excellent gain and gain flatness, LO harmonic rejection and good linearity with gain control. In design, special attention was given to unconditional stability and good matching. This makes all MMICs cascadable, which eliminates isolators in system design. These MMICs provide a simple, ultra miniature (90gm), three-chip all MMIC solution to satellite on board receiver design with better RF performance (60dB gain with 1.2dB noise figure in full 5.6GHz-7.1GHz band). As the designs use same MMIC process, in next step, these MMICs can be combined to form a single chip receiver with same performance. MMIC chips are designed for two standard packages with chip size 2.6mm Ч 1.6mm and 2.6mm Ч 2.0mm. [C1572]

#### "High gain active microstrip antenna for 60 GHz WLAN"

A 60 GHz design comprising a three-stage pHEMT amplifier integrated with a high gain antenna on an alumina substrate is presented. The amplifier has 18 dB gain, and the antenna a directivity of 14 dBi. The amplifier is ribbon bonded to the substrate on which the antenna is etched. The antenna is a microstrip array antenna with a simple etched pattern for producibility at high frequencies. Mechanical simplicity is achieved with this design, and



unnecessary transitions are avoided. [C1573]

### "An over 100 W n-GaN/n-AlGaIn/GaN MIS-HEMT power amplifier for wireless base station applications"

Novel n-GaN/n-AlGaIn/GaN metal-insulator-semiconductor high electron mobility transistors (MIS-HEMTs) with Si<sub>3</sub>N<sub>4</sub> film were fabricated on a semi-insulating (S.I.) SiC substrate. An n-GaN/n-AlGaIn/GaN MIS-HEMT with a breakdown voltage of 400 V was obtained by using SiN/n-GaN cap structure. The single-chip GaN MIS-HEMT amplifier operated at 60 V achieves a high output power of 110 W with a linear gain of 13 dB at 2.14 GHz. This is the first report of an AlGaIn/GaN MIS-HEMT with an over 100 W output power. The MIS-HEMT amplifier, combined with a digital pre-distortion (DPD) system, also demonstrates an adjacent channel leakage power ratio (ACLR) of less than -50 dBc for 4-carrier W-CDMA signals [C1574]

### "High power, high AlGaIn/GaN-HEMTs with novel powerbar design"

Gallium nitride transistors for high power microwave application are often limited by power loss due to extended transistor finger size. A new design for the gate supply is presented which allows for higher power gain compared to conventional transistor designs. Using this technique a linear gain of 20 dB is measured for a packaged power device delivering 28 Watt at 2GHz [C1575]

### "8-watt GaN HEMTs at millimeter-wave frequencies"

Field-plated short-gate-length GaN HEMTs were developed for superior large-signal performance at millimeter-wave frequencies. 100- $\mu$ m-wide devices achieved 8.6 W/mm power density at 40 GHz. Scaled-up, pre-matched 1.05-mm-wide devices generated 5.4 & 5.2 W output power with associated PAE of 36 & 31 % at 30 and 35 GHz, respectively. A 1.5-mm-wide device produced 8 W at 30 GHz with 31 % PAE, representing the state-of-the-art for GaN HEMTs at millimeter-wave frequencies [C1576]

### "An AlGaIn/GaN push-pull HEMT amplifier with 400 MHz bandwidth and 100 W peak output power"

This work describes the operation of AlGaIn/GaN HEMTs on s.i. SiC substrate in a broadband AlGaIn/GaN push-pull amplifier for 3G/4G infrastructure applications between between 1.8 GHz and 2.2 GHz. The device yields linear gain of 12.9 dB, a 3 dB bandwidth of 400 MHz between 1.8 GHz and 2.2 GHz, and a maximum output power of 102 W at 1.95 GHz under single carrier 16 channel W-CDMA conditions. Linearity evaluation further yields a peak output power of 45 dBm for an ACLR of -45 dBc at 5 MHz offset at 1.95 GHz [C1577]

### "Thermal and source bumps utilizing carbon nanotubes for flip-chip high power amplifiers"

Carbon nanotubes (CNTs) have been successfully developed as thermal and source bumps for flip-chip high power amplifiers (HPAs). The newly developed 15  $\mu$ m long CNT bumps exhibit thermal conductivity of 1400 W/m-K. A flip-chip AlGaIn/GaN HEMT HPA with a gate width of 2.4 mm utilizing CNT bumps, operating voltage of 40 V, exhibits an output power of 39 dBm at a frequency of 2.1 GHz without any degradation due to heat-up. To our knowledge, this is the first report about, a practical application of CNTs using their high thermal conductivity [C1578]

### "GaN on patterned silicon (GPS) technique for GaN-based integrated microsensors"

We demonstrated a viable technology for GaN-based integrated microsensors using the suspended GaN microstructures fabricated with GaN on patterned silicon technique. Fundamental characteristics of the GPS technique are investigated. Active devices (HEMT) were fabricated on the AlGaIn/GaN cantilevers and qualitatively tested. The experiment shows that the HEMTs on cantilevers can effectively sense the change in the stress induced by deflections applied to the cantilevers [C1579]

### "AlGaIn/GaN devices for future power switching systems"

GaN/AlGaIn device technologies are presented aiming at the applications to power switching systems. In order to reduce on-resistance ( $R_{on}$ ), we developed SL (super lattice) capping and QA (quaternary alloy) over-layer techniques for GaN/AlGaIn HFET. Further, we achieved almost the same mobility keeping the same 2DEG density for GaN/AlGaIn hetero structure grown on Si (111) substrates, which will make the cost comparable to conventional Si one. The experimentally obtained  $R_{onA}$  of the FET is 1.9 m $\Omega$ cm<sup>2</sup>, which is 14 times lower than that of Si ones. Additionally, a novel approach to realize enhancement-mode operation of GaN/AlGaIn FET is examined over R-plane sapphire, where non-polar AlGaIn/GaN heterostructure, free from polarization charge, can be grown [C1580]

### "Monolithic integrated C-band low noise amplifier using AlGaIn/graded-AlGaIn/GaN HEMTs"

Monolithic integrated C-band low noise amplifier using 1  $\mu\text{m}$ -gate AlGaIn/graded-AlGaIn/GaN HEMT device was designed, fabricated and characterized. The LNA demonstrated a noise figure of 2.7 dB, an associated gain of 10.8 dB, an input return loss of -5.5 dB at 6 GHz, and an output return loss of -18 dB at 7 GHz. The IIP3 of the LNA is 12 dBm at 6 GHz. The LNA with 1  $\mu\text{m}$   $\times$  100  $\mu\text{m}$  device shows very high-dynamic range with decent gain and noise figure. [C1581]

### "A 2 GHz high isolation DPDT switch MMIC"

A double-pole double-throw (DPDT) switch monolithic microwave integrated circuit (MMIC) has been designed to operate from dc to 2 GHz using a commercial 0.18- $\mu\text{m}$  GaAs pseudomorphic high electron-mobility transistor (pHEMT) process. The DPDT switch employs four shunt FET blocks to achieve high isolation. The ON gate bias is set to 0.6 V to reduce the insertion loss. The simulated results of the DPDT switch chip show an insertion loss of less than 0.61 dB and isolation of more than 50 dB up to 2 GHz. [C1582]

### "A 100-120 GHz quadruple-LO pumped harmonic diode mixer using standard GaAs based 0.15- $\mu\text{m}$ PHEMT process"

A 100-120 GHz 4 $\times$  sub-harmonically pumped diode mixer using standard 0.15- $\mu\text{m}$  PHEMT process on 4-mil GaAs substrate is presented. Fourth order mixing was performed using an anti-parallel diode pair. Filters and harmonic stubs are implemented using grounded coplanar waveguide structure. The average conversion loss is 27 dB from 100 to 120 GHz, in a compact chip size of 1.0  $\times$  1.0 mm<sup>2</sup>. [C1583]

### "Low-noise pHEMT amplifier operating at extra-low supply voltage and power"

In this paper, a low-noise pHEMT amplifier with an extra-low supply (0.25 V, 2 mA) is presented. The two-stage amplifier, based on low-cost commercially available components, has a noise figure of about 1 dB and gain of 20  $\pm$  1 dB over the 1.5 to 2.5 GHz. The input/output return loss do not exceed -5/- 8 dB, thermal gain variation is of 0.05 dB/ $^{\circ}\text{C}$ . Via comparison with state-of-the-art low-power low-noise amplifiers, it is confirmed that pHEMT has a grate potential as active element for extra-low DC-power-consumption microwave amplifiers. [C1584]

### "Enhancement- and depletion-mode InGaP/InGaAs pHEMTs on 6-inch GaAs substrate"

The cost effective enhancement-mode (E-mode) and depletion-mode (D-mode) InGaP/InGaAs pseudomorphic high electron mobility transistors (pHEMTs) on 6-inch GaAs substrate have been developed. The 0.5  $\mu\text{m}$  gate fingers of E-mode and D-mode pHEMTs are deposited simultaneously in this process simplification. This InGaP/InGaAs E-mode pHEMT exhibits a maximum drain-to-source current ( $I_{\text{ds}}$ ) of 460 mA/mm, and a maximum transconductance ( $g_m$ ) of 430 mS/mm. Under 5.2 GHz operation, 216 mW/mm power density, 40% power added efficiency (PAE) and 0.81 dB minimum noise figure (NF<sub>min</sub>) are also achieved for E-mode device. In this study, D-mode pHEMTs are applied for switch monolithic microwave integrated circuit (MMIC) which provides an insertion loss of -1.8 dB and an isolation of -9.2 dB under the 28 dBm input power ( $P_{\text{in}}$ ) and 5.5 GHz operation. From these measured results, this cost effective E/D-mode InGaP/InGaAs pHEMT technology exhibits a highly potential for WLAN applications. [C1585]

### "Microwave class-E GaN power amplifiers"

Two MMIC class-E power amplifiers (PA) in GaN HEMT technology are reported. The single stage class-E MMIC PA operates at 1.9 GHz. At 30V drain bias, a power-added-efficiency (PAE) of 57% and a maximum output power of over 37 dBm are achieved. At 40V drain bias, an output power of 38.7 dBm is achieved at 50% PAE corresponding to a power density of 7.4 W/mm. The dual-stage class-E MMIC PA operating at 2.0 GHz is also reported. It achieves an output power of 37.5 dBm, a PAE of 50%, and a gain of 18.2 dB. [C1586]

### "High linearity SPDT switch for dual band wireless LAN applications"

This paper presents a high linear and power-handling single-pole double-throw (SPDT) switch for WLAN 802.11 a/b/g applications. The switch circuit has asymmetric and stacked topology to have high power-handling and linearity for the Tx path. This SPDT switch has been implemented with 0.25  $\mu\text{m}$  GaAs pHEMT process by ETRI. The designed SPDT switch has the measured insertion loss of better than 1dB and isolation of better than 40dB for the Tx path and 25dB for the Rx path and the high power handling capability with P1dBof about 23dBm with control voltage of -3/0 V. The fabricated SPDT switch chip size is 1.8 mm  $\times$  1.8 mm. [C1587]

### "V-band CPW balanced medium power amplifier for 60 GHz wireless LAN application"

In this work, balanced medium power amplifiers for 60 GHz wireless LAN application were designed and fabricated. The single-ended and the balanced medium power amplifier on MIMIC technology were designed using 0.1  $\mu\text{m}$   $\Gamma$ -gate GaAs PHEMT and CPW library. We compared the single-ended medium power amplifier on the balanced medium power amplifier of S-parameter and 1 dB gain compression point (P1dB). From measurement, the single-ended and the balanced medium power amplifiers show S21 gains of 13.14 dB and 12.8 dB, respectively, at 60 GHz. Also, we obtain P1dB of 5.9 dBm and 7.5 dBm at 60 GHz, respectively. The balanced medium power amplifier has better return losses and P1dB than those of the single-ended medium power amplifier within V-band region. [C1588]

### "Broadband high efficiency circularly polarized active integrated antenna"

This paper presents a broadband high efficiency circularly polarized active antenna integrated with class-E power amplifier (PA) at 2GHz. A single circular microstrip patch fed by a cross slot is employed as not only a broadband circularly polarized radiator but also as a harmonics-termination load network, which is directly connected with the class-E power amplifier output. A low cost PCB technology is employed in the circuit fabrication and a low voltage PHEMT transistor is used. A peak drain efficiency of 71.1% for the class-E amplifier is measured at 2.05GHz, together with a maximum radiated power of 28.2 dBm from the active integrated antenna (AIA). Power added efficiency (PAE) over 50% within a 17% bandwidth from 1.92GHz to 2.28GHz is achieved. Axial ratio below 3 dB is obtained over a 9% bandwidth from 1.99 GHz to 2.18 GHz. [C1589]

### "Dynamic AM-AM and AM-PM behavior in microwave PA circuits"

This paper explains the nonlinear dynamic memory effects observed on both AM-AM and AM-PM conversions of nonlinear microwave power amplifier, PA, circuits. The study is introduced via an analytic Volterra series analysis which is then illustrated with envelope simulations gathered from a GaN HEMT based microwave PA. This way, a theoretically supported explanation of the small- and large-signal dynamic asymptotic behavior, observed in the amplitude and phase conversions of microwave/RF PA's, could be achieved. [C1590]

### "An Novel L-shape Active Leaky-Wave Antenna with power combining and scanning capability"

In this paper, an active-integrated leaky-wave antenna with power combining scanning capability is presented. This leaky-wave antenna with the novel perpendicular L-shape topology is integrated with a varactor-tuned high-electron mobility transistor (HEMT) voltage controlled oscillator (VCO) on the same plane. Changing the VCO frequency, we can control not only the dual-beam scanning angle but also derive the power combining effect with the sum (L) or difference (A) radiation patterns. The power combining effect of difference mode, which is the dual-beam pattern and the sum mode pattern, which is a 3-beam pattern, with the 3rd beam located along the middle direction (450, 1350) of the X and Y axes. The measured scanning angle is steered over a range of 24-460 for the right beam and 127-1480 for the left beam. Compared with single microstrip leaky-wave antenna, the L-shape LWAs configuration has the advantages of switchable radiation patterns as the VCO varied from 10GHz to 10.6GHz. [C1591]

### "High-efficiency and wide-band single-ended 200W GaN HEMT power amplifier for 2.1 GHz W-CDMA base station application"

In this paper, we present high drain efficiency of 34% and wide-band characteristics of single-ended 200W GaN HEMT power amplifier for 2.1 GHz W-CDMA application. We also confirmed that GaN HEMT power amplifier has low memory effect and adjacent channel leakage power ratio (A.C.L.R.) is sufficiently reduced for the application by utilizing digital predistortion (D.P.D.) system. [C1592]

### "Effect of temperature on current voltage characteristics of lattice mismatched Al<sub>m</sub>Ga<sub>1-m</sub>N/GaN HEMTs"

In this paper we present an analytical model of temperature dependence of an AlGa<sub>m</sub>N/GaN HEMTs. The results of the theoretical study concerning the temperature dependence of electron mobility in two dimensional electron gas (2DEG) confined at the AlGa<sub>m</sub>N/GaN interface is reported. The increase in temperature results in decrease in the saturation carrier velocity in HEMTs, which in turn reduces the drain current. The effect of temperature on transconductance of device has also been studied. The results are in good agreement with the existing experimental data. [C1593]

### "Microwave noise in InP/InGaAs composite channel high electron mobility transistors (HEMTs)"

In this work, the study of the microwave noise performance for InGaAs/InP composite channel HEMT compared to InGaAs channel is performed. Detailed microwave noise characteristics of InP-based HEMT are presented. An interesting observation is that the minimum noise figure (NF<sub>min</sub>) in composite channel devices is insensitive to drain bias, which is different from the conventional single channel devices in which the minimum noise figure increases with the increase of the bias. An analytical model was provided to study the channel noise for both devices and verify the influence of the different channel structure on the noise performance. [C1594]

#### **"Design of a wideband active-buffered mixer in enhancement-mode GaAs pHEMT technology"**

A high linearity single balanced resistive FET mixer with conversion gain has been developed using 0.5  $\mu\text{m}$  enhancement-mode pHEMT technology. The mixer consists of an integrated LO buffer amplifier which acts as an active balun, a resistive pHEMT mixer, and a differential cascode IF amplifier at the output. The IF amplifier output is matched to an output balanced impedance using a sum terminating diplexer. The mixer achieves an input IP<sub>3</sub> of +23.5dBm with 9.5dB of conversion gain while consuming 110mA from a 5V supply. Useable RF frequency range is (450-2700 MHz). [C1595]

#### **"380V/1.9A GaN power-HEMT: current collapse phenomena under high applied voltage and demonstration of 27.1 MHz class-E amplifier"**

The current collapse phenomena in 380V/1.9A GaN power-HEMTs designed for high-voltage power electronics application is reported. The influence of these phenomena to the power-electronics circuit performance under high applied voltage is discussed using a 27.1 MHz class-E amplifier, which can be one of an industrial application candidate. It has been found that the optimized field plate structure minimizes the increase of conduction loss caused by the current collapse phenomena and thus improves the power efficiency of the circuit. The minimized device achieved the output power of 13.8 W and the power efficiency of 89.6 % for the demonstrated circuit even with the applied drain voltage of 330 V and the switching frequency of 27.1 MHz. These results show the nature possibility of a new GaN-device application with both high voltage and high frequency condition [C1596]

#### **"Design of 2-10 GHz feedback MMIC LNA using >technique"**

The design of broadband feedback MMIC LNA using a new interactive "visual" technique is presented. The technique allows the fast and convenient design of amplifiers with compensation/feedback two-terminal networks taking into account a simultaneous set of performances, including the gain, gain flatness, noise figure, input and output return losses, and stability. With "visual" CAD tools, AMP-CF and LOCUS, a 2-10 GHz single-stage MMIC LNA has been designed and implemented in 0.2  $\mu\text{m}$  HEMT GaAs technology, providing gain  $11.7 \pm 1.1$  dB, noise figure 2.2 dB, input and output return losses -9.6 dB and -11.7 dB, respectively. [C1597]

#### **"Optical ports: next generation of MMIC control devices?"**

The results of our research on the electro-optical control of MMICs are shown in this paper. Two different devices have been investigated: a GaAs chip monolithic amplifier at S band, and an AlGaAs chip MMIC voltage controlled oscillator at Ku. The possibilities of optical control of the amplifier are evidenced as follows: if the amplifier operates with the same biasing, the gain can be optically controlled from a condition of almost isolation, up to an active condition, which gives a range of optical control of about 15 dB and provides an improvement of the input and output matching in a range of 12dB and 6dB, respectively. The possibilities of optical control of the VCO by illumination of the PHEMT transistor are demonstrated through measurements of the oscillation output power and frequency. An optical control range of 8dB of oscillation output power and up to 400MHz of oscillation frequency has been obtained. This optical control suggests an interesting control of gain and matching for other microwave FET based active devices. [C1598]

#### **"Ultra broadband DC to 40 GHz 5-bit pHEMT MMIC digital attenuator"**

A broadband, DC to 40 GHz 5-bit MMIC digital attenuator has been developed. The attenuator has been fabricated with 0.15  $\mu\text{m}$  GaAs pHEMT process. This attenuator has 1 dB resolution and 23 dB dynamic range. High attenuation accuracy has been achieved over all attenuation range and full 40 GHz bandwidth with the reference state insertion loss of less than 6 dB at 20 GHz. The input and output return losses of the attenuator are better than 14 dB over all attenuation states and frequencies. [C1599]

#### **"Low noise high linearity ultra broadband monolithic amplifier using travelling-wave gain stages"**

A 2-20 GHz two-cascaded dual stage MMIC distributed amplifier (2-CDSA) is presented in this paper. It



consists of two cascaded dual-stage distributed amplifiers in order to achieve flat gain, good terminal match, low noise figure and high output power level. The topology of this amplifier joins the best features of the conventional distributed amplifiers and the cascaded distributed amplifiers. The measured small signal gain was  $17 \pm 0.57$  dB from 2 to 20 GHz. A minimum noise figure of 3 dB was achieved while a 14.9 dBm of output power was measured at the 1-dB compression point. The amplifier has been fabricated using the D01PH process provided by OMMIC. The chip size is  $2 \times 1.5$  mm<sup>2</sup>. [C1600]

#### "A 100W high-efficiency GaN HEMT amplifier for S-Band wireless system"

We have successfully developed a 100W AlGaIn/GaN power amplifier with a bandwidth of 300MHz in S-band, operating at 50V drain bias voltage. This amplifier consists of one HEMT die developed for L/S-band frequency operation and a single-ended package. The developed amplifier has an output power of 100W and a high linear gain of more than 13.5dB in the frequency range of 2.6GHz to 2.9GHz under CW or pulsed conditions [200usec (pulse width) and 2msec(period)]. High drain efficiency of 58% was also achieved at an output power of 100W and frequency of 2.8GHz. To the best of our knowledge this is the first report of 100W AlGaIn/GaN HEMT amplifier developed for S-band high power application. [C1601]

#### "A 150 to 220 GHz balanced doubler MMIC using a 50 nm metamorphic HEMT technology"

A coplanar millimeter wave doubler MMIC covering the entire G-band was developed. Based on a 50 nm metamorphic HEMT technology, the circuit demonstrates an output power of more than -12 dBm between 150 and 220 GHz for an input power of 0 dBm. By increasing the input power to 12 dBm an output power exceeding 0 dBm was obtained in the frequency range between 180 and 220 GHz. Good fundamental rejection was ensured by using a Marchand balun for balancing the design. The doubler was also used to provide the LO signal for a 170 to 200 GHz resistive FET mixer, yielding a conversion loss of 10 dB. [C1602]

#### "A novel technique for obtaining LO and RF (LSB) rejection in 25-40 GHz microwave up conversion mixers based on the concepts of distributed and double balanced mixing"

In this paper a new configuration of up converter is presented. In this circuit, the LO and RF (LSB) frequencies are rejected thanks to a distributed and balanced circuit. Eight GaAs PHEMTs with a gate-length of 0.25  $\mu$ m are used. A conversion gain of -6 dB and a rejection over 6 dB on LO and RF (LSB) are obtained. [C1603]

#### "A low cost SMT integrated frequency doubler and power amplifier for 30GHz DBS uplink applications"

A SMT (surface mount technology) MMIC (monolithic microwave integrated circuit) frequency multiplier ( $\times 2$ ) and power amplifier has been designed for DBS (direct broadcast satellite) and other commercial applications. Using PHEMT technology this MMIC takes a 15GHz input signal and passes it through a harmonic frequency doubler and then through three stages of power amplification at 30GHz. This MMIC provides an output power of 21dBm, fundamental suppression of 45dBc and is stable across all voltages and temperatures. This single MMIC SMT solution frequency multiplier and power amplifier is unique compared to any known or published data. [C1604]

#### "A novel wideband MMIC voltage controlled attenuator with a bandpass filter topology"

The design and analysis of a novel wideband, monolithic, bandpass,  $\pi$ -network, voltage controlled attenuator (VCA) is presented. A 24 to 32 GHz VCA was developed using 0.15 $\mu$ m GaAs pHEMT technology. This is the first reported VCA to use a bandpass filter topology to achieve the required operating frequency band and eliminate the effects of parasitic capacitances of the pHEMTs. The bandpass filter absorbs the parasitic capacitances and thereby eliminates their detrimental effects. The measured attenuation dynamic range is 12dB  $\pm$  0.5dB with minimum insertion loss of 2-3dB. The input power handling capability is up to 0dBm. The VCA is well matched and may be placed in a 50 $\Omega$  system (Halabi, 2004). [C1605]

#### "Laterally scaled down tiered-edge ohmic structure of InP-based HEMTs for 2-S/mm<sup>2</sup>/sub m/ and 500-GHz f<sub>sub T</sub>/"

DC and RF characteristics of InP-based HEMTs were improved by employing a laterally scaled down ohmic structure and an InGaAs/InAs composite channel. Through the combination of our process technology for fabricating this structure and that for scaling down a gate length, we successfully fabricated a 50-nm-gate HEMT exhibiting extrinsic transconductance of 2.0 S/mm and extrinsic current gain cutoff frequency ( $f_T$ ) of 496 GHz simultaneously. This is the first report of a transistor exhibiting 500-GHz  $f_T$  with large current-drivability [C1606]

### "Non-uniform degradation behavior across device width in RF power GaAs PHEMTs"

We have studied the electrical degradation of RF power PHEMTs by means of light-emission measurements performed during bias-stress experiments. We show that electrical degradation can proceed in a highly non-uniform manner across the width of the device. We identify the origin of this as a small systematic non-uniformity in the recess geometry that impacts the electric field and the impact ionization rate on the drain of the device. Our research suggests that a close examination of the width distribution of electric field in RF power PHEMTs (and FETs in general) is essential to enhance their long-term reliability [C1607]

### "Monolithic integration of enhancement-and depletion-mode AlGaIn/GaN HEMTs for GaN digital integrated circuits"

We demonstrate a novel technique for monolithic integration of enhancement and depletion-mode AlGaIn/GaN HEMTs using CF<sub>4</sub>plasma treatment. Direct-coupled FET logic circuits such as an E/D HEMT inverter and a 17-stage ring oscillator are demonstrated in GaN system for the first time. At a supply voltage (VDD) of 1.5V, the fabricated E/D inverter shows an output logic swing of 1.25V, logic-low noise margin of 0.21V and logic-high noise margin of 0.51V. The fabricated ring oscillator shows a minimum delay of 130 ps/stage at V<sub>DD</sub>= 3.5 V, and a minimum power-delay product of 0.113 pJ/stage at VDD= 1 V [C1608]

### "Performance evaluation of 50 nm In<sub>0.7</sub>Ga<sub>0.3</sub>As HEMTs for beyond-CMOS logic applications"

We have studied the suitability of nanometer-scale In<sub>0.7</sub>Ga<sub>0.3</sub>As HEMTs as a high-speed, low-power logic technology for beyond-CMOS applications. To this end, we have fabricated 50-150 nm gate length In<sub>0.7</sub>Ga<sub>0.3</sub>As HEMTs with different gate stack designs. The 50 nm HEMTs exhibit ION/IOFF ratios in excess of 105 and DIBL less than 90 mV/dec. Compared with state-of-the-art Si MOSFETs, the non-optimized 50 nm In<sub>0.7</sub>Ga<sub>0.3</sub>As HEMTs provide equivalent highspeed performance with 15 times lower DC power dissipation and at least 2.7 times higher f<sub>T</sub> at equivalent power dissipation level. In the landscape of alternatives for beyond CMOS technologies, InAs-rich InGaAs HEMTs hold considerable promise [C1609]

### "Evidence of traps creation in GaN/AlGaIn/GaN HEMTs after a 3000 hour on-state and off-state hot-electron stress"

A long-term 3000-hour test under on-state conditions (V<sub>DS</sub> = 25V, 6W/mm constant dissipated power) and off-state conditions (V<sub>DS</sub> = 46V, V<sub>GS</sub> = -6V) on GaN/AlGaIn/GaN HEMTs is presented. Trapping presence and hot-electrons effect are characterized by means of low-frequency techniques (low-frequency noise measurements, transconductance frequency dispersion, gate-lag). The on-state stress shows the most important degradation. Since our measurements point out to the creation of traps in the gate-to-drain surface region during the stress, this degradation is ascribed to the effect of hot-electrons [C1610]

### "Ge-spacer technology in AlGaIn/GaN HEMTs for mm-wave applications"

GaN-based high electron mobility transistors (HEMTs) are the most promising option for power amplification at frequencies above 30 GHz. However, the difficult technology of nitride devices has hindered the aggressive scaling of these transistors needed for high frequency applications. Also, the need of a relatively thick passivation layer to avoid current collapse in these transistors has significantly limited the high frequency performance of the devices. In this paper, we introduce an advanced technology which uses a Ge sacrificial layer to fabricate passivated AlGaIn/GaN HEMTs with gate lengths down to 90 nm, while maintaining a high breakdown voltage and minimum parasitic capacitances. Using these devices, we demonstrate record high frequency performance at both small and large signal levels [C1611]

### "A 4.5 GHz 3-4 dual-modulus frequency divider IC in GaAs technology"

This paper presents a divide-by-3/divide-by-4 dual-modulus frequency divider fabricated in a commercially available GaAs pHEMT technology. The highspeed architecture presented overcomes the inherent frequency limitations of the classical Johnson structure and allows the same speed of the simple divider-by-4 circuit from which it derives. Even if the circuit was designed specifically for its use in frequency generation modules of satellite transponder, it can be conveniently used as the first stage of high frequency dual-modulus prescalers. The fabricated circuit operates up to 4.5GHz with a total power consumption of 75mA from a 3.5V supply. [C1612]

### "A 1.5 to 37 GHz ultra-broadband MMIC Mouw's star mixer"

A MMIC ultra-broadband star mixer using Mouw's hybrid junction is presented in this paper. The MMIC chip uses 0.15  $\mu\text{m}$  HEMT process. The chip is measured in three mounting environments, namely, absorber backed, 15mil  $\text{Al}_2\text{O}_3$  substrate plus absorber, and conductor backed and all of them show ultra-broadband performances. The measured results show that the bandwidth is from 1.5 to 37GHz except a resonant dip near 23 GHz occurs in conductor backed case. The IF 3dB bandwidth is from DC to 2.5GHz. The chip can be used as either up- or down-converter. Because the spiral layout of the Mouw's hybrid junction shrinks the area significantly, no off chip baluns are required. The chip size is 2mm by 2mm. [C1613]

#### "Ion implantation for unalloyed ohmic contacts to AlGaIn/GaN HEMTs"

We report on the use of Si ion implantation for the fabrication of AlGaIn/GaN HEMTs with an as-deposited ohmic contact resistance of 0.4  $\Omega\text{mm}$ . Currently ohmic contact technology requires a high temperature (  $870^\circ\text{C}$ ) alloying step. The resulting contacts have an irregular shape and surface that can create difficulties in device reproducibility, reliability and yield, particularly for large periphery devices. The use of ion implantation to enable unalloyed ohmic contacts has the potential to reduce these obstacles to the manufacturability of AlGaIn/GaN HEMTs. Using ion implantation also has the potential to reduce access resistance by reducing ohmic contact resistance and gate-source spacing, to eliminate the need for etched device isolation, and to enable sophisticated device designs that take advantage of lateral dopant engineering. [C1614]

#### "Linearity performance of GaN HEMTs with field plates"

Recently, electric field modification with GaN-based high-electron-mobility-transistors (HEMTs) using field plates (FP) has resulted in dramatically enhanced power performance. Power densities up to 32 W/mm at 4 GHz have been demonstrated with power-added-efficiency (PAE) of 55%. When scaled to a large periphery, a total output power of 149 W was obtained at 2 GHz. Modern communication applications also require high linearity for power devices. Here we present the linearity performance of GaN-channel HEMTs with various FP lengths at biases up to 108V. [C1615]

#### "275 GHz fMAX, 220 GHz fT AlSb/InAs HEMT technology"

In this paper, we report record AlSb/InAs HEMT high frequency gain performance up to 275 GHz fMAX. The 0.1- $\mu\text{m}$  gate length and 80- $\mu\text{m}$  total gate periphery devices exhibited a small-signal available gain of 10 dB at 100 GHz, and extrapolated fT and fMAX performance of 220 and 275 GHz, respectively, at a drain voltage of 0.5 V and drain current of 27 mA. To the best of our knowledge, this is the highest reported fMAX and high-frequency available gain reported for InAs-channel HEMTs. Furthermore, it is first AlSb/InAs HEMT result that has achieved fMAX greater than fT, which clearly demonstrates that this approach is not intrinsically limited in regards to achieving high frequency and high-gain characteristics. [C1616]

#### "Device linearity enhancement of InGaP/InGaAs/GaAs camel-gate p-channel pseudomorphic high electron mobility transistor"

A high-performance InGaP/InGaAs/GaAs p-channel pseudomorphic modulation-doped field effect transistor based on p+-GaAs/n+-InGaP/p-InGaP camel-like gate structure is demonstrated. Due to the p-n depletion of the camel-like gate and the presence of relatively large  $\Delta E_v$  at InGaP/InGaAs heterostructure, an extremely large gate turn-on voltage than 2 V is measured. For a 14100  $\mu\text{m}^2$  device, the experimental results show a maximum saturation current density of -345 mA/mm and a widely broad gate voltage swing than 4 V with 80 % maximum transconductance. Furthermore, the fT and fmax values are 3.1 and 4.8 GHz, respectively. [C1617]

#### "Improved high power thick-GaN-capped AlGaIn/GaN HEMTs without surface passivation"

A record high power density on sapphire without passivation was achieved using an epitaxial approach to dispersion reduction. SiN passivation has been employed to reduce DC-to-RF dispersion of GaN-based HEMTs, but is sensitive to surface and deposition conditions. A proposed epitaxial solution is to grow a thick GaN cap on top of the conventional HEMT to increase the distance between surface and channel, reducing the effect of surface potential fluctuations on device performance. Initial results from a gate-recessed device structure showed that dispersion was reduced greatly without surface passivation. Nevertheless, high gate leakage and low breakdown limited the output power. We investigate the cause of these leakage and breakdown issues, propose solutions, and discuss the results. As a consequence, 8.5 W/mm with a PAE of 57% was achieved at 50 V at 4 GHz from unpassivated HEMTs on sapphire, the highest power density reported. [C1618]

#### "Use of multichannel heterostructures to improve the access resistance and fT linearity in GaN-based HEMTs"

The typical access resistance of GaN-based transistors is almost an order of magnitude higher than in other semiconductor materials like Si or GaAs. This very high access resistance represents a major difficulty for the fabrication of high-speed devices where parasitic delays currently dominate. In this paper, the use of high conductivity modulation doped multiple channel heterostructures in AlGaIn/GaN HEMTs is demonstrated. This has allowed the engineering of the differential resistance of the access regions in these transistors, allowing a significant improvement of their DC and RF characteristics. In the future, the combination of multiple channels separated by different barrier heights will increase even more the linearity of the AlGaIn/GaN HEMTs. [C1619]

#### "Will the velocity of GaN HEMTs ever overshoot? [Cmm-wave frequencies]"

Summary form only given. Traditionally, the electron velocity of III-V FETs overshoots as the gate length reduces to sub-micron scale, which overcomes the higher percentage of parasitic charging times as the intrinsic input capacitance reduces. This overshoot is not yet seen in GaN HEMTs. What is worse, the  $f_{\text{tof}}$  of these devices peaks at only 25-30% of the full-channel current and deteriorates severely at higher current levels. These problems are responsible for the measly 2-5 W/mm and 15-40% efficiency produced by GaN HEMTs at >30 GHz. This paper discusses the issues limiting the speed of GaN HEMTs at mm-wave frequencies, focusing on electron velocity overshoot effects. [C1620]

#### "An economic method for fabrication sub-quarter- $\mu\text{m}$ gate doped-channel FET's by photolithography"

This paper reports a new sub-0.5- $\mu\text{m}$  gate-length FET processing technique by using conventional i-line optical lithography. The key methodology is to thermally re-flow the patterned photo-resist upon two-step spin-coated SOG. According to this new process, the deposited gate metal has its final length and thickness be separately determined by taped resist profile and SOG thickness. The implemented gate length is as short as 0.41  $\mu\text{m}$ . Then it was successfully applied to fabrication of a newly designed hetero-doped-channel field-effect transistor with digital-graded In<sub>x</sub>Ga<sub>1-x</sub>As multi-layer forming a HEMT-like channel. This digital-graded In<sub>x</sub>Ga<sub>1-x</sub>As channel by changing x values from 0.1 to 0.2 has most electrons be closer to gate metal. The measured sheet carrier density and mobility are 4.3  $\times 10^{12}\text{cm}^{-2}$  and 3560  $\text{cm}^2\text{V}^{-1}\text{s}^{-1}$  while the peak carrier concentration is larger than 1  $\times 10^{19}\text{cm}^{-3}$ . A fabricated 0.41  $\times 100\text{ }\mu\text{m}^2$  HD-CFET exhibits the maximum transconductance of 370 mS/mm with an output current larger than 535 mA/mm and  $f_t$  ( $f_{\text{max}}$ ) of 26 (32) GHz. [C1621]

#### "Low-voltage, high-performance InAs/AlSb HEMTs with power gain above 100 GHz at 100 mV drain bias"

Ultra-low power circuits require transistors with usable RF gain at low bias voltages and currents. In the present paper, we report 100 nm gate-length InAs/AlSb HEMTs with  $f_{\text{rand}}$  and  $f_{\text{max}}$  both exceeding 100 GHz at a mere 100 mV of drain bias. The devices also show excellent peak value for  $f_{\text{rof}}$  235 GHz and, to the best of our knowledge, a record  $f_{\text{max}}$  of 235 GHz at a higher drain bias of 300 mV. [C1622]

#### "Comparative analysis of hot-phonon effects in nitride and arsenide channels for HEMTs"

Summary form only given. The cutoff frequency of a transistor is determined mainly by gate length and electron drift velocity. In general, the velocity reaches high values in a two-dimensional electron gas channel (2DEG). Thus, a high electron mobility transistor (HEMT) with a 2DEG channel can operate at frequencies corresponding to short millimeter waves. Though the highest values of drift velocity are similar for electrons in nitride and arsenide 2DEG channels, the frequency performance of an arsenide HEMT is superior, as compared with nitride HEMTs. However, it is not straightforward to see why hot phonons do not limit drift velocity in arsenide 2DEG channels and, in this paper, a comparative analysis of hot-phonon effects in AlInAs/GaInAs/AlInAs/InP, AlGaIn/GaN and AlGaIn/AlN/GaN channels is carried out. [C1623]

#### "Influence of the heterostructure design on noise figure of AlGaIn/GaN HEMTs"

In this work, we cover four topics. Three studies are presented on the effect of different epilayer structures on the noise figure of AlGaIn/GaN HEMTs in the 4-12 GHz frequency range. The material studies include varying aluminum composition in the barrier, sapphire vs. SiC substrates, and, for the first time, the influence of a thin AlN layer on the noise parameters; all three against frequency and drain current. In addition is a comparison of two equivalent circuit models at 5 GHz. [C1624]

#### "A new two-step recess technology using SiNx passivation and Pt-buried gate process and its application to 0.15 $\mu\text{m}$ Al<sub>0.6</sub>InAs/In<sub>0.65</sub>GaAs HEMTs"

A new two-step recess (TSR) technology was successfully demonstrated using SiNx passivation and Pt-buried



gate process. Applying the developed two-step recess (TSR) process to the fabrication of 0.15  $\mu\text{m}$  Al<sub>0.6</sub>InAs/In<sub>0.65</sub>GaAs HEMTs, remarkable improvements could be obtained such as the suppression of the kink effect, and the increase of  $G_{m,\text{max}}$ ,  $f_T$  and  $f_{\text{max}}$ . Since the side-recessed region was fully passivated by SiN<sub>x</sub> dielectric layer, this TSR technology is also to offer additional advantage of good reliability. [C1625]

#### "Influence of the access resistance in the rf performance of mm-wave AlGaIn/GaN HEMTs"

After demonstrating impressive performance in the X-band frequencies, one of the next goals for GaN-based power transistors is to increase the frequency of operation to the mm-wave range. Monte Carlo simulations predict that the saturation electron velocity in AlGaIn/GaN high electron mobility transistors (HEMTs) should be around 2.54 $\times 10^7$  cm/s (M. Singh and J. Singh, J. Appl. Phys. vol. 94, p. 2498, 2003). The study of  $f_T$  vs  $I_{\text{DS}}$  from pinch-off to saturation is a very useful tool to understand the maximum frequency performance of mm-wave HEMTs. In this work, we have studied the effect of parasitic resistances in the shape of the  $f_T$  vs  $I_{\text{DS}}$  curve.  $R_s$  increases with the current density in the channel. The extraction of the effect of the differential access resistance out of  $f_T$  greatly changes the shape of the curve. The access resistances play an important role in the rf behavior of AlGaIn/GaN transistors. Not only the absolute values, but also their increase with current must be controlled in order to get the maximum performance out of the GaN-based HEMTs. [C1626]

#### "The influence of HEMT nonlinear distributed modeling on transient performance of microwave circuits"

This paper presents the impact of electromagnetic wave propagation on HEMT device electrodes in transient response. The proposed model is used in analysis and simulation of a MMIC compatible, Ka band power amplifier. Final results are the comparison between the simulation results in semi-distributed and lumped models, respectively. [C1627]

#### "NASA ultra low noise X-band microwave feeds for deep space communication"

This work describes the configuration, detail design, and final performance of a new ultra low noise diplexed X-band microwave feed system, called X/X diplexing feed, for the deep space network (DSN) 70-m antennas. In this microwave feed, the transmitter signal is combined with the receive signal in a diplexing junction placed near the input of a wide-band feedhorn. This configuration allows the majority of the components in the receive path to be placed in a cryogenically cooled container resulting in a major reduction in the noise temperature of the feed. Combined with a low noise HEMT amplifier this feed provides the lowest noise diplexed feed in the DSN. The total noise temperature of the 70-m antennas at zenith with this feed is approximately 14.6 K. [C1628]

#### "Design of low cost broadband class-E power amplifier using low voltage supply"

The design of a broadband high efficiency class-E power amplifier for use in wireless communication systems is presented. A low cost PHEMT device is employed to enhance both efficiency and bandwidth performance. The design has been investigated theoretically and experimentally and simulated using the harmonic balance method in an advance design system (ADS). A peak PAE of 72.1% is achieved at 1.95 GHz with transducer power gain of 10.8 dB in the improved design, together with a resulting bandwidth of 35% (1.52 GHz to 2.16 GHz). Simulation and practical results confirm the validity of these approaches. [C1629]

#### "On-chip versus off-chip passives in multi-band radio design"

This paper presents on-chip versus off-chip passives in multi-band radio design. The analysis is demonstrated through several multi-band low noise amplifiers designs in SiGe BiCMOS and GaAs PHEMT. Cost-performance trade-off analysis shows that when on-chip passives are moved off chip, performance of RF circuits is always improved. However, simple RF circuits do not show obvious cost-benefits, whereas complex RF circuits such as multi-band radio can have significant cost savings by using off-chip passives. [C1630]

#### "Ultra low DC power consumption In-P HITFET based differential oscillator"

The monolithic integration of tunneling diodes (TDs) with other conventional semiconductor devices gives the opportunity to design ultra-low DC power consumption circuits by taking advantage of the intrinsic negative differential resistance (NDR) of TDs. In this paper, we present the design of a differential oscillator based on InP-HEMT/TD technology. The circuit is based on a couple of phase-locked 5.8 GHz VCOs. Each VCO draws a current of 1.1 mA at 500 mV and generates an output power of -9.0 dBm on a 50  $\Omega$  load. [C1631]

#### "A physics-based analytical model of a GaN/AlGaIn HEMT incorporating spontaneous and

### piezoelectric polarization"

A physics-based charge control model of an AlGaIn/GaN high electron mobility transistor (HEMT) has been used to predict large- and small-signal characteristics. The 2DEG concentration in the channel is calculated using the Schrodinger equation in conjunction with the triangular quantum well approximation. Spontaneous and piezoelectric polarizations at the heterointerface and finite effective width of the 2DEG have been incorporated in the analysis. The calculated results are compared with experimental data from an Al<sub>0.15</sub>Ga<sub>0.85</sub>N/GaN HEMT structure to show the agreement. The model predicted a maximum drain current of 523 mA/mm and transconductance of 138 mS/mm for a device of length 1  $\mu$ m and width 75  $\mu$ m. The calculated data is compared against experimental values. [C1632]

### "Microwave characterization and modeling of packaged HEMTs by a direct extraction procedure at cryogenic temperatures"

In the present work we employ a direct extraction procedure to determine small signal equivalent circuit of microwave GaAs FETs by means of scattering (S-) parameter measurements down to cryogenic temperatures. The direct extraction procedure was tested on packaged AlGaAs/InGaAs HEMTs and good agreement between the simulated and measured S-parameters was obtained at different bias and temperature conditions. We employed a properly designed cryogenic set-up operating in our laboratory that allows to perform DC and RF characterization down to 30 K. [C1633]

### "Device Research Conference (IEEE Cat. No.04TH8724)"

{no data available} [C1634]

### "Gallium nitride electronics: Watt is the limit? [Csummary of GaN semiconductor devices]"

Summary form only given. This work presents a summary of the use of gallium nitride and its alloys in the development of semiconductor devices. It begins with a description of the HEMT and its use in microwave and power switching applications. Then follows a brief examination of MOSHFETs, MISHFETs and MISFETs. HBTs are discussed, along with the problems of poor electronic properties of p-type GaN and leakage through p-n junctions and etched surfaces. The paper concludes by referring to the POLFET which is based on modulating a 3D electron slab created by grading the polarization in the system, resulting in a MESFET with no doping. [C1635]

### "Effect of gate recessing on linearity characteristics of AlGaIn/GaN HEMTs"

GaN-based HEMTs are the most promising device in order to meet the requirements of new generation communication systems. In this work, devices with planar (unrecessed) and gate recessed structures have been fabricated on the same wafer, and characterized by means of RF two-tone measurements at 10 GHz. For GaAs-based devices, increasing device transconductance by means of gate recessing proved to be very effective, resulting in an overall improvement of both large and small signal performance, especially their linearity characteristics. Further optimization of gate recessing may result in higher efficiency operation while maintaining low distortion level. [C1636]

### "Pre-amplifier-integrated uni-traveling-carrier photodiode module with a rectangular waveguide-output port for operation in the 120-GHz band"

This paper presents a compact waveguide-output UTC-PD module that integrates a UTC-PD and a HEMT pre-amplifier (PD-amp module), which is suitable for practical applications. A transmission experiment of 10 Gbit/s signal is also shown to demonstrate the feasibility of the fabricated module. [C1637]

### "High efficiency class-F power amplifier design"

In this paper, a high efficiency, low voltage, class-F power amplifier (PA) is described. The effect of different output harmonic terminations on the power-added efficiency (PAE) of the PA has also been analysed. A medium power PHEMT PA, operating at 900 MHz, is designed and measured. A peak PAE of 71.4% with 22 dBm output power (P<sub>out</sub>) and 14 dB power gain (G<sub>p</sub>) is achieved at a very low drain voltage (V<sub>ds</sub>) of 3 V. A PAE above 60% has been achieved over a bandwidth of 13%. [C1638]

### "Implementing RF signal limiter with heterojunction devices"

Microwave limiters are used to prevent burnout and permanent damage in power sensitive components such as receivers and mixers. State-of-the-art limiters are implemented employing PIN diodes, in which limiting is

provided by varying the RF resistance of the diode. The PIN diode is a cheap and easy-to-use devices but its bandwidth and power rating is limited. Furthermore, PIN diodes cannot readily be fabricated. in MMIC technology. Here, an investigation is presented on the feasibility of employing heterojunction devices in limiters. This paper presents a T-switch attenuator formed by HEMTs simulated at X-band. [C1639]

#### "Millimeter-wave optoelectronic mixers based on InP HEMT"

We investigate characteristics of InP HEMT optoelectronic mixers in 60 GHz band. They provide mixing function with high internal conversion gain over the wide LO frequency range. Utilizing them, 622 Mbps transmission is demonstrated in a fiber-supported 60 GHz wireless system. [C1640]

#### "A 76 GHz high performance subharmonic mixer MMIC using low 1/f noise diodes for automotive radars"

This paper describes a low-noise subharmonic mixer MMIC for 76-GHz automotive radar systems. To improve a noise figure in a 100-kHz low IF band, a low 1/f-noise Schottky barrier diode (SBD) has been developed for the mixer. This SBD can offer 20 dB better 1/f-noise levels than a conventional HEMT type SBD can under the same operating current density condition. The fabricated mixer delivers a measured conversion gain of better than -9 dB and a measured noise figure of 12 dB under the condition of a 3-dBm low LO power and a 100-kHz low IF band. This noise figure is 26 dB lower than that of an HEMT type SBD subharmonic mixer with the same circuit topology. To our knowledge, the noise figure at the low IF band is the best performance of 76-GHz mixers ever reported. [C1641]

#### "Integrated LNA-sub-harmonic mixer for 77 GHz automotive radar applications using GaAs pHEMT technology"

An integrated low-noise amplifier (LNA) and sub-harmonic mixer (SHM) for automotive radar applications has been designed using 0.15 $\mu$ m GaAs pHEMT technology. This MMIC operates at RF frequencies of 76 to 77 GHz, IF frequencies up to 3 GHz, and LO frequencies of 36 to 38.5 GHz. A typical conversion loss of 3dB has been measured for a 10 dBm LO input power with no observed compression up to -6 dBm RF input signal level. The resulting 2.5 mm<sup>2</sup>circuit area helps address the low-cost and small size needs of automotive radar components. [C1642]

#### "Hot-via interconnects: a step toward surface mount chip scale packaged MMICs up to 110 GHz"

Two new techniques based on the RF hot-via concept have been developed for use in chip-scale packaged (CSP) MMICs. The first one utilizes backside bumps for die attach onto a substrate carrier; excellent RF performance has been achieved on both active-, and passive MMIC devices up to 110 GHz. The second technique is based on direct soldering of the MMIC backside interconnects onto low cost substrate carrier (RO4003), making it ideal for a wire-bond free full surface mount approach. To the author's knowledge this is the first demonstration of such die attach-, and packaging techniques for MMICs. As application examples, experimental performance results obtained with both techniques, are presented for transmission lines, and broadband 30-GHz GaAs PHEMT amplifier MMICs. [C1643]

#### "Recent progress and future prospects of GaN HEMTs for base-station applications"

This paper describes the recent progress and future prospects of GaN high electron mobility transistors (HEMTs) for 3G-wireless base station applications. It introduces a summary of most important activities at several organizations all over the world. As the Fujitsu progress, a state-of-the-art 250-W AlGaIn/GaN-HEMTs push-pull transmitter amplifier operated at a drain bias voltage of 50 V is addressed. The amplifier, combined with a digital pre-distortion (DPD) system, also achieved an adjacent channel leakage power ratio (ACLR) of less than -50 dBc for 4-carrier W-CDMA signals with a drain supply voltage of 50 V. This paper also demonstrates a stable operation under RF stress testing for 1000 h at a drain bias voltage of 60 V. After comparing LDMOS, GaAs and GaN, future prospects of GaN-HEMT is discussed to verify that an AlGaIn/GaN HEMTs amplifier is suitable for 3G W-CDMA systems. [C1644]

#### "Device modeling for III-V semiconductors-an overview"

This work presents an overview of several key technical considerations required for state-of-the-art nonlinear circuit simulation models of III-V HBT and FET devices. A unified large-signal modeling framework that incorporates the voltage and current dependence of nonlinear transit time and depletion capacitances in III-V HBTs, as well as the multiple voltage dependence of nonlinear capacitances in FETs is presented. Considerations for modeling thermal and electro-thermal interactions in III-V HBTs and FETs are reviewed and

contrasted. Trends in advanced characterization techniques and their benefits for modeling are highlighted. Finally, selected recent advances in mathematical CAD techniques are reviewed with particular relevance for advanced circuit modeling of III-V devices. [C1645]

#### "Microwave mixers based on a novel zero bias diode"

A Ku-band mixer based on a zero bias diode (ZBD) and its application is described. The diode can easily be implemented in an MMIC technology if enhancement FET or HEMT devices are available in the MMIC-process. It was experimentally verified that a star mixer realized with zero bias diodes instead of ordinary gate-Schottky diodes requires less LO-power and result in lower conversion loss. The specific application described is intended for space use and the reliability of the mixer is expected to be improved due to a smaller gate current. [C1646]

#### "Monolithic GaAs PHEMT MMICs integrated with RF MEMS switches"

Low-loss RF MEMS switches have been integrated with HEMT MMIC circuits on GaAs substrates to allow the fabrication of a new class of high-performance microwave and millimeter-wave circuits. The integration process allows the co-integration of MEMS microrelays and GaAs PHEMT devices with no sacrifice in performance or yield to either device. Examples of circuits fabricated include multi-band low-noise amplifiers, transmit and receive (T/R) circuits, and a switched dual-width power amplifier at X-band. The power amplifier uses two MEMS switches at the input to guide the RF signal between two paths. Each path provides single-stage amplification using different size HEMT devices to optimize efficiency over a wide range of output power levels. [C1647]

#### "A 90-GHz InP-HEMT lossy match amplifier with a 20-dB gain using a broadband matching technique"

We demonstrated a 90-GHz InP-HEMT lossy match amplifier (LMA) with a 20-dB gain for the first time. We obtained this performance with the power consumption of 220 mW, which is the smallest one ever reported for an over 80-GHz broadband amplifier. The amplifier acts as a C-R coupled amplifier in the low to medium frequency range and as an L-C match amplifier at the high frequencies. Therefore, this configuration provides both high gain and wide bandwidth. The key to achieve a 90-GHz bandwidth is broadband matching in the L-C match amplifier. In this paper, we propose a broadband matching technique with a low Q network and describe the design guideline for the excellent performance. [C1648]

#### "120-GHz Tx/Rx chipset for 10-Gbit/s wireless applications using 0.1 $\mu$ m-gate InP HEMTs"

This paper describes the development of a InP-HEMT MMIC chipset for 120-GHz wireless applications. The transmitter chip includes a frequency doubler for carriers, an ASK modulator, an RF band-pass filter, and a power amplifier. The receiver chip includes a low-noise amplifier and an ASK demodulator. A back-to-back test of the chipset has shown it to be fully functional at 10-Gbit/s data rate with BER=e-12 at -45.7-dBm input power of the receiver chip. To our knowledge, this is the first report of the development of highly integrated MMIC chipset operating at 120 GHz for wireless data communication. [C1649]

#### "A high reliability GaN HEMT with SiN passivation by Cat-CVD"

This is the first report of catalytic vapor deposition (Cat-CVD) passivated AlGaIn/GaN HEMT. We have found out that the Cat-CVD passivation film with NH<sub>3</sub> treatment greatly enhances the reliability of the AlGaIn/GaN HEMT. It is rationalized, through the low frequency capacitance-voltage measurement, that the NH<sub>3</sub> treatment in the Cat-CVD reactor before the SiN film deposition minimizes the damage at the SiN/AlGaIn interface, leading to reducing the surface trap density. The AlGaIn/GaN HEMT passivated by the Cat-CVD SiN film suppresses the degradation of an output power to less than 0.4 dB under the RF operation of V<sub>d</sub> = 30 V, f = 5 GHz after 200 h. [C1650]

#### "Design and InP HEMT Technology for ultra-high speed digital ICs with beyond 80-Gbit/s operation"

There is great interest in increasing the operating speed of digital circuits. Using 0.10- $\mu$ m gate-length InP HEMT technology, to date we have developed a 144-Gbit/s multiplexer (MUX), a 80-Gbit/s demultiplexer (DEMUX), a 80-Gbit/s D-type flip-flop (D-FF), and a 90-GHz T-type flip-flop (T-FF). Key aspects of the fabrication, circuit design, and measurement are described in this paper. [C1651]

#### "Temperature-dependence of a GaN-based HEMT monolithic X- band low noise amplifier"

The temperature-dependent performance of a fully monolithic AlGaIn/GaN HEMT-based X-band low noise



amplifier is reported. The circuit demonstrated a noise figure of 3.5 dB, gain of 7.5 dB, input return loss of -7.5 dB, and output return loss of -15 dB at 8.5 GHz at room temperature. The noise figure at 9.5 GHz increased from 2.5 dB at -43°C to 5.0 dB at 150degC. [C1652]

#### "A fast low-power 4Ч4 switch IC using InP HEMTs for 10-Gbit/s systems"

A 4Ч4 switch IC using cold-FETs connected in series can be used as a single-ended 4Ч4 switch, an add drop multiplexer, or a differential 2Ч2 switch. An InP HEMT with a low  $R_{on}$ -Coff product enables us to configure a dc-to-over-10-GHz switch without using a shunt FET, which offers a logic-level-independent interface. A packaged IC achieves error-free operation up to 12.5 Gbit/s with either negative ( $V_H = 0$  V,  $V_L = -0.9$  V) or positive ( $V_H = +13$  V,  $V_L = +0.7$  V) logic-level input for all 16 possible states. The power consumption is less than 5 mW. The add drop multiplexing operation with an ultra-fast switching of 160 ps is also successfully demonstrated. [C1653]

#### "A 220 GHz metamorphic HEMT amplifier MMIC"

We present the development of two 220 GHz low-noise amplifier (LNA) MMIC's for use in high-resolution active and passive millimeter-wave imaging systems. The amplifier circuits have been realized using a 0.1  $\mu$ m InAlAs/InGaAs based depletion-type metamorphic high electron mobility transistor (MHEMT) technology in combination with coplanar circuit topology and cascode transistors, thus leading to a compact chip-size and excellent gain performance. The realized single-stage cascode LNA exhibited a small-signal gain of 5 dB at 220 GHz and a maximum gain of 7 dB at 215 GHz with an over-all chip-size of 1 Ч 1 mm<sup>2</sup>. The four-stage amplifier circuit achieved a linear gain of 20 dB at the frequency of operation and more than 10 dB over the bandwidth from 180 to 225 GHz while covering a chip-area of 1 Ч 2.5 mm<sup>2</sup>. [C1654]

#### "Low noise hybrid-monolithic amplifier with PHEMT transistors"

The paper presents the results of the development and manufacture of an X-band super miniature low noise amplifier. The amplifier design and manufacturing technology are considered. Measured microwave parameters are shown. [C1655]

#### "Optically controlled active generator for superhigh frequencies"

Investigations are presented of an SHF active generator based on HEMT type transistors, which have shown the possibility of both optical and electric control of the oscillation frequency. [C1656]

#### "The temperature model limits for high electron mobility transistors"

Comparison of temperature and hydrodynamic models for high electron mobility transistors has been carried out. It is shown that the real space transfer in the transistor heterostructures and the strongly energy dependent relaxation times are mostly responsible for the spectacular difference in calculations for HEMT with gate length sufficiently greater than momentum relaxation length. The temperature model may lead to more than 20% error in current and transconductance, beginning from length as long as 0.5 $\mu$ m, which markedly exceeds the gate length characteristic to modern HEMT. The different models produce a big difference in the drift velocity distribution in the transistor channel, especially when the channel is open and the real space transfer is considerable. The reasons for this effect are as follows: the lateral size of the quantum well is much less than electron momentum relaxation length and electron current flowing transverse to the heterostructure border is really high, even in comparatively low fields. The electron density in the quantum well strongly depends on transverse electron current, which is different for the temperature and hydrodynamic models. For example, in In<sub>0.52</sub>Al<sub>0.48</sub>As-In<sub>0.53</sub>Ga<sub>0.47</sub>As HEMT with 1  $\mu$ m gate length, the drift velocity under the gate is 30% more in the temperature model than in the hydrodynamic model. [C1657]

#### "The temperature dependency of a GaAs pHEMT wideband IQ modulator IC"

The author developed a GaAs wideband IQ modulator IC, which is utilized in Agilent RF signal source instruments. The layout is fully symmetric to obtain a temperature-stable operation. However, the actual temperature drift performance is poorer in some frequency ranges than the first generation of IC which has the same architecture. This paper presents the temperature drift of SSB performance and clarifies that the temperature dependency of equivalent series impedance dominates the quadrature phase shift. [C1658]

#### "Novel control architecture for JPHEMT power amplifiers achieving high efficiency EDGE application"

A saturated PA architecture for achieving best-in-class EDGE performance whilst maintaining dual-mode compatibility with GSM is presented. This technique has been developed to utilise the specific advantages the E-Mode J-PHEMT process provides for these applications. This represents a credible solution to the demand of a highly efficient integrated dual-mode (EDGE/GSM) PA control architecture. [C1659]

#### "Self-consistent numerical model and optimization of two-dimensional electron gases for AlGaIn/GaN HEMT"

AlGaIn/GaN HEMTs, also referred to as MODFETs, have been a subject of intense recent investigation and have emerged as attractive candidates for high voltage, high-power operation at microwave frequencies for its high peak electron velocity, saturation velocity, thermal stability and breakdown fields properties. In this paper, we take account of spontaneous and piezoelectric polarization effect at the hetero-interface in AlGaIn/GaN HEMT device and one-dimensional Poisson-Schrodinger equations using nonuniform mesh are solved self-consistently, from which the AlGaIn/GaN heterostructure conduction band and the 2DEG density are investigated. The dependences of 2DEG characteristics on the Al mole fraction, the thickness of each layer, the donor concentration and the gate voltage are investigated through simulation, respectively. The influence of spacer layer width on the 2DEG density is calculated for the first time. [C1660]

#### "High electron mobility transistor small signal model"

The small signal model of the ATF-36077 high electron mobility transistor is presented for both packaged and unpackaged cases. The model parameter extraction procedure is presented. It is shown that using the transistor without its package gives the possibility to expand the amplifier frequency range more than twice. [C1661]

#### "An experimental extraction of low noise field effect transistor's linear equivalent circuit and noise model"

An experimental extraction of a low noise field effect transistor's linear equivalent circuit and noise model is presented. The linear equivalent circuits and noise models are extracted for two types of FET (3P374A-5 manufactured by joint-stock company "Planet-GaAs", "Sozvezdiye-P" manufactured by FSUC RPC "Istok") and two types PHEMT manufactured by FSUC RPC "Istok" (molecular beam epitaxy structure and metalorganic vapor phase epitaxy structure). [C1662]

#### "Very high performance 50 nm T-gate III-V HEMTs enabled by robust nanofabrication technologies"

In this paper, we review a range of nanofabrication techniques which enable the realization of uniform, high yield, high performance 50 nm T-gate III-V high electron mobility transistors (HEMTs). These technologies have been applied in the fabrication of a range of lattice matched and pseudomorphic InP HEMTs and GaAs metamorphic HEMTs with functional yields in excess of 95%, threshold voltage uniformity of 5 mV, DC transconductance of up to 1600 mS/mm and fTof up to 480 GHz. These technologies and device demonstrators are key to enabling a wide range of millimeter-wave imaging and sensing applications beyond 100 GHz, particularly where array-based multi-channel solutions are required. [C1663]

#### "A 110-GHz AlSb/InAs MMIC amplifier"

We describe the first demonstration of a W-band amplifier using antimonide based compound semiconductor (ABCS) device technology. The three stage CPW MMIC uses two finger 0.1- $\mu$ m AlSb/InAs HEMT with a total periphery of 40 micron per device. Biased at a total MMIC dissipation of 3.7-m W the amplifier demonstrates  $11 \pm 1$  dB gain over a 80-110 GHz bandwidth. When biased at total MMIC dissipation of 9.0 mW, the amplifier demonstrates  $15 \pm 1$  dB gain over 80-100 GHz bandwidth. [C1664]

#### "Quantum corrected full-band cellular Monte Carlo simulation of AlGaIn/GaN HEMTs"

A full-band cellular Monte Carlo (CMC) approach (Saraniti and Goodnick, 2000) is applied to simulation of electron transport in AlGaIn/GaN HEMTs with quantum corrections included via the effective potential method. The full-band CMC transport model is based on a detailed model of the electron-phonon interactions in the wurtzite crystal structure using the rigid pseudo-ion model, where the anisotropic deformation potentials are derived from the electronic band structure, the atomic pseudopotential, and the phonon dispersion. Realistic polar-optical phonon, impurity, piezoelectric and dislocation scatterings are also included in the full-band CMC simulator, which shows good agreement with measured velocity-field data from pulsed I-V measurements at Arizona State University (Barker, 2002). [C1665]

### "High-gain direct-coupled matrix distributed amplifier using active feedback topology"

A high-gain matrix distributed amplifier (DA) was developed using a commercial GaAs PHMET foundry for 40-Gb/s baseband applications. Two tiers of matrix DA are directly coupled using a lumped DC level-shift circuit. The DC bias level of the second tier can be tuned using the level-shift circuit for optimum gain. The gain of the matrix DA has been optimized using an active feedback cascode topology, which allows the gain-bandwidth product (GBWP) to be maximized while avoiding instability problems. In order to improve the gain, the second tier is shifted to the output load. The fabricated single-chip matrix DA with a size of 2.4 mm Ч 1.4 mm showed a high gain of 19 dB, and an average noise figure of 5.7 dB with a 48-GHz bandwidth. The GBWP is 428 GHz, which corresponds to the highest performance using GaAs technology for matrix DAs. [C1666]

### "Broadband low-noise amplifiers for K- and Q-bands using 0.2 $\mu$ m InP HEMT MMIC technology"

Design, manufacturing, and performance of two MMIC low-noise amplifiers are presented in this paper. The circuits cover wide frequency ranges of 16-26 GHz and 25-49 GHz. The amplifiers are implemented using our in-house 0.2  $\mu$ m InP HEMT process. The measurements at room temperature show a gain higher than 14.5 dB and 11 dB and a corresponding mean noise temperature of 208 K and 235 K within the K- and Q-bands, respectively. Operated at the temperature of 10 K, the amplifiers exhibit a gain of higher than 13.5 dB and 10 dB within the frequency bands of 16-26 GHz and 23-44 GHz, respectively. [C1667]

### "Session TU1C: Advances in Low Noise HEMT Technology"

{no data available} [C1668]

### "A 10 GHz dielectric resonator oscillator using GaN technology"

A 10 GHz AlGaIn/GaN HEMT-based dielectric resonator oscillator (DRO) is presented. This device exhibits -118dBc/Hz phase noise at 100KHz offset frequency range and is the lowest yet reported. This phase noise and power capabilities of GaN HEMT oscillators are compared to those of two mature technologies, an Infineon SiGe HBT (BFP620) and Transcom GaAs pHEMT (TC1401). The oscillator output power density using a GaN HEMT was found to be 14 times greater than using an equivalent GaAs pHEMT. Phase noise improvements between two different GaN devices, resulting from developments in GaN technology, are also presented. [C1669]

### "Low phase-noise 5 GHz AlGaIn/GaN HEMT oscillator integrated with BaxSr1-xTiO3 thin films"

A C-band MMIC oscillator in GaN HEMT technology with BaxSr1-xTiO3(BST) film capacitors integrated as DC block capacitors has been designed, fabricated and characterized. The lumped LC resonator works with the common gate HEMT to generate negative resistance. The oscillator, based on AlGaIn/GaN HEMT with 0.7 $\mu$ m gate length and 200 $\mu$ m gate width, delivers 20.5 dBm output power when bias at Vds= 15 V and Vgs= -3 V, with dc-to-RF efficiency of 12.5%. Phase noise was measured to be -105 dBc/Hz at 100 KHz offset from 5.3 GHz carrier. The results show that AlGaIn/GaN HEMTs are attractive to both high power and low noise microwave source application. [C1670]

### "High performance and high reliability InP HEMT low noise amplifiers for phased-array applications"

This paper describes the development of a Q-band low noise amplifier unit using a 0.1  $\mu$ m InP HEMT MMICs that has been demonstrated with high RF performance and high reliability over a frequency band from 43.5 to 45.5 GHz at Northrop Grumman Space Technology (NGST). The InP HEMT LNAs with high RF performance and high reliability are crucial for the advanced phased-array applications. The module demonstrates superior performance with gain greater than 30.1 dB and noise figure less than 3.2 dB over the frequency band of 43.5 to 45.5 GHz. The InP HEMT technology has an activation energy of 1.9 eV and mean-time-to-failure of 108hours at Tjunctionof 125°C and these MMICs further demonstrate the readiness of NGST's 0.1  $\mu$ m InP HEMT MMICs technology for the advanced phased-array applications. [C1671]

### "Wideband AlGaIn/GaN HEMT MMIC low noise amplifier"

A 3-18 GHz AlGaIn/GaN high electron mobility transistor low noise amplifier on silicon carbide is reported. The measured gain (S21) is 20 dB +/- 2.5 dB between 3-18 GHz. The minimum measured noise figure is 2.4 dB. To the authors knowledge, this is the highest gain reported over multiple octaves up to 18 GHz using GaN technology. [C1672]

### "X-band GaAs mHEMT LNAs with 0.5 dB noise figure"

Two X-band LNA ICs have been demonstrated using a 0.15  $\mu\text{m}$  metamorphic GaAs HEMT technology. The amplifiers have an average noise figure of 0.5 dB and power gain greater than 31 dB from 7-10 GHz. A current-shared version had gain flatness better than 1 dB, return losses greater than 11 dB, and power consumption of 42 mW. A high linearity version has an output third-order intercept point greater than 20.5 dBm from 6-12 GHz. [C1673]

### "Coplanar AlGaIn/GaN HEMT power amplifier MMIC at X-band"

A power amplifier MMIC based on AlGaIn/GaN HEMTs was fabricated and measured. The coplanar balanced amplifier consists of two 8 $\times$ 100 $\mu\text{m}$  transistors. Wilkinson splitters were used to divide and combine the power. By biasing the amplifier at  $V_{\text{DS}}=30\text{V}$  a maximum CW output power of 39dBm corresponding to 5W/mm with a maximum power added efficiency (PAE) of 33.8% was achieved at 10GHz. Biasing the amplifier at  $V_{\text{DS}}=20\text{V}$  resulted in 36.7% PAE with 37.2dBm CW output power at 10GHz. To the author's knowledge these results represent the highest output power density so far achieved for GaN-based MMICs at X-band in CW mode. [C1674]

### "Low insertion loss and high linearity PHEMT SPDT and SP3T switch ICs for WLAN 802.11 a/b/g applications"

GaAs SPDT and SP3T antenna switch ICs for IEEE 802.11 a/b/g applications are developed. By using advanced Skyworks PHEMT technologies, it is possible to achieve an insertion loss as low as 0.55 dB for SPDT switch, 0.5 dB lower than any previously reported DC-6 GHz band switch, and high linearity with 55 dBm input IP3 and a high isolation over 20 dB at 3 V; the SP3T switch also exhibits excellent performance with an insertion loss of 0.9 dB, input IP3 of 47 dBm and isolation over 25 dB throughout DC-6 GHz band. The high performance comes from the following technologies: series and shunt topology with dual-gate FETs, AlGaAs/InGaAs/AlGaAs 0.5  $\mu\text{m}$  EPI-based process with a fully selective dual recess etch, and the relatively shallow pinch off voltage of -0.5 V (Y. Tkachenko et al., Euro. Microwave Conf. Dig., pp. 1041-1045, 1997). [C1675]

### "A GaAs-based 3-40 GHz distributed mixer with cascode FET cells"

A broadband MMIC distributed mixer with cascode FET cells was developed using commercial GaAs PHEMT foundry. The fabricated distributed mixer with a size of 1.8 mm $\times$ 1.0 mm showed a high conversion gain of 3.6 dB $\pm$ 0.5 dB over 3 to 40 GHz RF frequency ranges at the low LO power level of 5 dBm with a fixed IF frequency of 1 GHz. An average single-sideband noise figure was 11.7 dB without IF post amplification. The LO-to-IF and LO-to-RF isolations were better than 19 dB over the entire operating frequency band. To our knowledge, this corresponds to the highest gain-bandwidth product (85 GHz) achieved from the wideband mixers. [C1676]

### "A 10 Gbit/s switch matrix MMIC using InP HEMTs with a logic-level-independent interface"

An InP HEMT with a low on-resistance  $\times$  off-capacitance ( $R_{\text{on}} \times C_{\text{off}}$ ) product enables us to configure a dc-to-over-10 GHz switch without using a shunt FET. The series FET configuration makes possible control-voltage-polarity independence, and offers a logic-level-independent interface. A 2 $\times$ 2 switch matrix MMIC yields an insertion loss of less than 1.16 dB and an isolation of more than 21.2 dB below 10 GHz. The MMIC also achieves error-free switch matrix operation up to 12.5 Gbit/s, using either a source coupled FET logic SCFL (1 Vp-p, dc offset: -0.5 V) or low voltage differential signalling LVDS (0.3 Vp-p, dc offset: +1.2 V) level. [C1677]

### "L-simulator: a magPEEC-based new CAD tool for simulating magnetic-enhanced IC inductors of 3D arbitrary geometry"

This work presents a new PEEC-based inductor simulation tool, entitled L-simulator, which employs a magPEEC modeling algorithm and an existing FastCap modeling algorithm to address both magnetic and electrical coupling effects respectively, hence being capable to simulate 3D magnetic-enhanced RF IC inductors of arbitrary geometries. Applications on micromachined inductors in 0.2 $\mu\text{m}$  GaAs HEMT process and magnetic-cored micro inductors in 0.18 $\mu\text{m}$  CMOS technology are discussed. [C1678]

### "A novel DP4T antenna switch for dual-band WLAN applications"

In this paper, we present a novel DP4T antenna switch with very simple control logic and high power handling capabilities for dual-band WLAN applications. The suggested DP4T switch architecture requires only two control lines. The developed DP4T switch exhibits 1.2 to 1.7 dB of insertion loss, and 27/53 dB to 23/37 dB of isolation at 2.4 GHz and 5.25 GHz, respectively. It also demonstrates 31 dBm of input P0.1dB, 35 dBm of input P1dB in



3/0 V operation, as well as better than -62 dBc of 2nd harmonics and -73 dBc of 3rd harmonics response, respectively. The MMICs are developed in a commercial 0.25- $\mu$ m GaAs pHEMT process. This switch architecture is preferable for Si-based processes because substrate vias are not required due to its generic topology. To the best of our knowledge, this is the first report on a DP4T RF switch architecture with very simple control logic for dual-band WLAN applications. [C1679]

#### "A Ka/Q-band 2 Watt MMIC power amplifier using dual recess 0.15 $\mu$ m PHEMT process"

A compact, high power amplifier MMIC operating at Ka/Q-band was designed and developed using TriQuint's 3M1 dual-recess 0.15  $\mu$ m gate length GaAs PHEMT technology. This single-ended three-stage power amplifier, with chip size of 7.44 mm<sup>2</sup> (3.145 mm  $\times$  2.367 mm), on 100  $\mu$ m GaAs substrate achieved 33 dBm (2 Watt) P1dBCW output power and up to 2.5 Watts saturated output power with small signal gain of 21 dB over 33-36 GHz. The RF response of this amplifier can be further extended to cover frequencies of 32-38 GHz. For 37-38 GHz, this power amplifier demonstrated 32 dBm (1.6 Watt) saturated output power and 31 dBm P1dB with 18 dB small signal gain. This state-of-the-art power amplifier MMIC is a smallest chip size and highest output power density from a single MMIC reported to date at Ka/Q-band. [C1680]

#### "Cryogenic 2-4 GHz ultra low noise amplifier"

This paper describes two-stage InP-based cryogenic broadband amplifier with very low noise for the frequency band 1.5-4.5 GHz. For a band of 2-4 GHz at 15 K the measured gain is 30.0 $\pm$ 2 dB and a noise temperature below 5 K. The total DC power consumption of the amplifier is 6.8 mW. [C1681]

#### "2004 IEEE MTT-S International Microwave Symposium Digest (IEEE Cat. No.04CH37535)"

{no data available} [C1682]

#### "Characteristics of InP HEMT harmonic optoelectronic mixers and their application to 60 GHz radio-on-fiber systems"

We present device characteristics on InP HEMT as a harmonic optoelectronic mixer. A single InP HEMT device performs photodetection of optically transmitted data, and frequency up-conversion of them into 60 GHz band. Several mixer performance characteristics are investigated and 622 Mbps data transmission in 60 GHz radio-on-fiber system is successfully demonstrated using InP HEMT harmonic optoelectronic mixer. [C1683]

#### "Design and analysis of a miniature W-band MMIC subharmonically pumped resistive mixer"

A W-band monolithic sub-harmonically pumped (SHP) resistive mixer was designed and fabricated using a standard 0.15 $\mu$ m PHEMT process. A nonlinear model featuring modified drain-current characteristics was developed and used in circuit simulation. A small chip size of 1.5  $\times$  1.0 mm<sup>2</sup> was achieved by using a transformer as a LO balun. Measured results of this circuit showed 14-18 dB conversion losses from 75 to 88 GHz, and agree well with simulation. Analysis on circuit imbalance shows that the phase imbalance of the balun is the dominant factor on LO isolation, and the conversion loss is quite robust to all circuit imbalances. [C1684]

#### "A 26 volts, 45 Watts GaAs pHEMT for 2 GHz WCDMA applications"

An unmatched power AlGaAs/InGaAs pHEMT transistor in a ceramic package has been developed for 3G infrastructure applications. Operating at 2.14 GHz, under two carrier WCDMA a typical device delivers more than 9.2 Watts of average envelope power at -37 dBc IMD with drain efficiencies as high as 32% in class AB mode. Our paper presents the device technology, and the DC and RF performance under CW, WCDMA, and 2 carrier WCDMA signals. [C1685]

#### "50 watt MMIC power amplifier design for 2 GHz applications"

In this paper the design and the measurement of a 2 GHz 50 Watt (CW) MMIC power amplifier (PA) are discussed. The authors believe that this is the most powerful MMIC implementation that has been reported. The amplifier utilizes a class-F combining structure and realized using the company internal 0.5  $\mu$ m GaAs pHEMT power process. The MMIC measure 10 $\times$ 10 mm<sup>2</sup> and delivers 50 Watts of CW power at an efficiency greater than 45% over more than 10% bandwidth at a nominal 12 V supply voltage. The amplifier gain is 21 dB throughout the operational band. [C1686]

#### "An over 200-W output power GaN HEMT push-pull amplifier with high reliability"

We describe a state-of-the-art 250-W output power AlGaN/GaN HEMT push-pull transmitter amplifier operated at a drain bias voltage of 50 V. We also demonstrated stable operation under RF stress testing for 1000 h at a drain bias voltage of 60 V, for the first time. The amplifier, combined with a digital pre-distortion (DPD) system, also achieved an adjacent channel leakage power ratio (ACLR) of less than -50 dBc for 1-carrier W-CDMA signals with a drain supply voltage of 50 V. We show, for the first time, that an AlGaN/GaN HEMTs push-pull amplifier can fulfill the requirements of W-CDMA systems. [C1687]

#### "Design and analysis of a W-band multiplier chipset"

The design and analysis of a multiplier chipset with an output at W-band is presented. The MMIC designs have been fabricated on a 0.13  $\mu\text{m}$  AlGaAs/InGaAs/GaAs pHEMT process. Particular emphasis has been placed on EM analysis of key components and the optimization of models suitable for use in circuit simulators based on the EM simulations. The results show a first iteration design with an on-wafer saturated output power of 20.2 dBm at 92 GHz and greater than 18 dBm over a 9% bandwidth from 87.5-95.5 GHz. [C1688]

#### "Millimeter-wave photonic integrated circuit technologies for high-speed wireless communications applications"

This paper describes an IC technology for high-speed wireless-link systems, using photonic techniques, which provides 10 Gb/s at 120 GHz. Optical signals are converted to electrical signals and radiated into freespace using Si-based circuitry. Both the preamp and PA utilize 0.1  $\mu\text{m}$  gate InAlAs/InGaAs HEMTs with gains of 6-10 dB and 8.5 dB, respectively. [C1689]

#### "Reconfigurable RF circuits based on integrated MEMS switches"

MEMS phase shifters, based on switchable passive components, are used to achieve a variety of circuits with low insertion loss, wide bandwidth and compact die size. Integration of MEMS switches with active GaAs pHEMT MMICs achieves reconfigurable LNA and PA devices. A 4 b true time-delay phase-shifter achieves  $\leq 1.2$  dB insertion loss on a 7 mm<sup>2</sup> die. [C1690]

#### "Under 0.5W 50Gb/s full-rate 4:1MUX and 1:4 DEMUX in 0.13 $\mu\text{m}$ InP HEMT technology"

50Gb/s full-rate 4:1 MUX and 1:4 DEMUX ICs are fabricated in an InP HEMT technology. The MUX has an rms jitter of 283fs and a peak-to-peak jitter of 1.78ps. The DEMUX has a phase margin of 250° and a sensitivity of 80mV at 40Gb/s. The MUX and DEMUX consume 450mW and 490mW from a -1.5V supply, respectively. [C1691]

#### "A Q-band miniaturized uniplanar MMIC HEMT mixer"

A miniaturized uniplanar GaAs MMIC HEMT mixer is proposed based on a compact multifunction transition structure. By the independence nature of the coplanar-waveguide (CPW) mode and the coplanar-stripline (CPS) mode, a compact transition which converts the CPW mode into the CPS mode is realized. This transition structure also has the functions of 180° hybrid, RF and LO diplexer, and bandpass filter. Thus the size of the proposed mixer may be drastically reduced, and the LO-to-IF and LO-to-RF isolations and RF conversion gain are excellent. This mixer is designed to operate with RF frequency from 35 to 40 GHz, IF frequency from 0.5 to 6 GHz, and LO frequency at 35 GHz. The lower sideband conversion gain is about 5 dB, the single-sideband (SSB) noise figure is 6.5 dB, the isolations are all better than 30 dB, and the size of the mixer is much compact than those of the conventional mixers. [C1692]

#### "144-Gbit/s selector and 100-Gbit/s 4:1 multiplexer using InP HEMTs"

144-Gbit/s operation of a selector circuit and 100-Gbit/s operation of a 4:1 multiplexer (MUX) using a 0.10 $\mu\text{m}$  InP HEMT technology were achieved. To increase the timing margin while reducing power consumption, two-phase lock architecture was used for the MUX. In addition, to align the timing between data and clock, a critical issue at a high bit-rate, a Gilbert-cell-type delay buffer was applied to the clock tree to precisely compensate for gate delay in data blocks. We also tested the maximum speed of the core of the MUX, the selector circuit, achieving 144-Gbit/s operation. As far as we know, this is the highest operational speed reported to date for a digital circuit. [C1693]

#### "New nonlinear device model for microwave power GaN HEMTs"

This paper presents a new nonlinear device model, for microwave power GaN HEMTs, amenable for integration into a commercial harmonic balance simulator. All the steps taken to extract it are explained, starting with the

extrinsic elements' determination and ending with the intrinsic ones. This model was validated by comparing measured and simulated output power and intermodulation distortion data of a GaN HEMT. Very good agreement was obtained from small- to large-signal excitation regimes. [C1694]

#### "Numerical noise model for the AlGaN/GaN HEMT"

A numerical approach to simulate the intrinsic noise sources within transistors is described. Using a 2D numerical device solver, spectral densities for the gate and drain noise current sources and their correlation are evaluated using a Green's function approach, an equivalent of Shockley's impedance field method. Case studies with AlGaN/GaN HEMTs compare the numerical simulation results to those from measurements, showing good agreement. [C1695]

#### "Advanced non-linear model for accurate prediction of harmonically terminated power amplifier performance"

This paper presents recent advances in the state-of-the-art of neural network modeling of microwave FET devices. Enhanced accuracy of the adaptive knowledge-based neural network (AKBNN) model is shown by comparing predicted load-pull performance of the device to measurements in an automated harmonic load-pull system. Test devices are a 1.2 mm HFET measured at 2.2 GHz, and a 4.8 mm pHEMT at 8.4 GHz. Modeled versus measured comparisons include power-added efficiency and output power under fundamental frequency and second and third harmonic frequency tuning. The effectiveness of this modeling approach for the design of high-efficiency power amplifiers operating in Class-E or Class-F modes is discussed. [C1696]

#### "Novel T/R switch architectures for MIMO applications"

In this paper, we present new architectures for three kinds of RF switches (DPDT, DP4T, 4P4T) with very simple control logics and high power handling capabilities. Implementation of DPDT, DP4T, and 4P4T switch matrix for multi-input-multi-output (MIMO) applications is demonstrated with measurements. The suggested DPDT, DP4T, and 4P4T switch architectures require only one, two and three control lines, respectively, regardless of semiconductor technology. The developed DPDT switch demonstrates 1.0 dB of insertion loss, 19 dB of isolation, and 31 dBm of input P0.1 dB, 34.5 dBm of input P1 dB in 3/0 V operation at 5.8 GHz. The DP4T, 4P4T switches exhibit 1.8 dB, 2.8 dB of insertion loss, and 23/37 dB, 20/35/55 dB of isolation, respectively, and 31 dBm of input P0.1 dB, 35 dBm of input P1 dB in 3/0 V operation at 5.8 GHz. The MMICs are developed in a commercial 0.25- $\mu$ m GaAs pHEMT process. These switch architectures are preferable for the Si-based processes because the substrate vias are not required due to their generic topologies. To the best of our knowledge, this is the first report on the simple architectures for RF switch matrix for MIMO applications. [C1697]

#### "A high power density 26 V GaAs pHEMT technology"

This report presents a GaAs pHEMT technology optimized for 26 V drain bias. At this bias, a 2.14 GHz gate width scaling study demonstrates output power densities of 1.8-2.1 W/mm of output power at 1 dB gain compression (P1dB) for device sizes ranging from 14.4 mm down to 3.6 mm respectively. Power added efficiency (PAE) remains nearly constant at 59-61% for these device sizes. Devices with 14.4 mm gate widths produced a Pias of 26 W (1.8 W/mm) with an associated power-added efficiency (PAE) of 61%. Thermal imaging shows a thermal resistance of approximately 4.2°C/W at a 36°C case temperature for 14.4 mm (26 W) devices. A high temperature step stress reliability study shows a median time to failure (MTTF) of 1.64107hours for a 150°C channel temperature with a thermal activation energy of 1.8 eV. These results represent the best combination of power density, PAE, and reliability reported for any GaAs-based FET technology. [C1698]

#### "Wideband AlGaIn/GaN HEMT low noise amplifier for highly survivable receiver electronics"

Gallium Nitride has emerged as the technology of choice for the next generation high power electronics. However, its ability to handling high power also makes it the perfect technology candidate for highly survivable receiver components. This has obvious cost benefit for the footprint of the LNA will be smaller since no extra front-end protection circuitry is required. In this paper, a wideband Gallium Nitride HEMT low noise amplifier MMIC, using novel dual gate topology, has been design and manufactured to demonstrate Gallium Nitride low noise capability. [C1699]

#### "High efficiency power amplifier input/output circuit topologies for base station and WLAN applications"

The design and measured results of Class-F output and input circuits for high efficiency operation of power amplifiers is presented. With the circuits presented in this paper, drain efficiencies of 85% can be obtained if the

2nd and 3rd harmonics are controlled. Efficiencies rise to 95% if the 4th and 5th harmonics are also controlled. A Class-F input circuit proposed to overcome the negative effects on PAE and efficiency caused by input capacitance variation. By shaping the input waveform the Class-F circuit creates a 50% duty cycle which prevents excessive power dissipation on the gate resistance, hence preventing gain and PAE degradation. A 15 W power amplifier designed at 1.8 GHz was fabricated to validate the presented techniques. The amplifier was designed utilising a FCSL (Filtronic Compound Semiconductors Ltd.) pHEMT device with a total gate periphery of 24 mm. With an unmodulated carrier, 16 watts of output power at 76% drain efficiency and 16 dB small-signal gain was obtained. The amplifier delivered 5.2 watts with a PAE of 48% under EDGE modulation. [C1700]

### "Signal generation, control and frequency conversion AlGaIn/GaN HEMT MMICs"

In this summary we review the design and experimental results of three new AlGaIn/GaN HEMT MMICs: a voltage controlled oscillator, a single pole-double throw (SPDT) switch and a resistive FET mixer. The VCO exhibits frequency range between 8.5 and 9.5 GHz with maximum output power of 35 dBm (at  $V_{ds}=30$  V) across a 50 ohm load. The L/S band SPDT switch at 0.9, 1.8 and 2.1 GHz was measured to have 0.87, 0.96, 1 dB insertion loss and 46, 42 and 41 dB isolation respectively. The switch also shows linear performance for the power levels up to 1 Watt in the insertion mode. A singly-ended X-band resistive mixer have exhibited very low intermodulation, less than -60 dBc for the 2IF and 3IF at the RF power level of 10 dBm, and high power handling, P1dB is estimated to be at least 1 Watt, with the conversion loss of 17 dB. [C1701]

### "Microwave resistive and dielectric planar antennas with conical radiation patterns"

The theoretical and experimental results illustrating the basic characteristics of microwave metal and dielectric circular patch antennas with axisymmetric excitation have been presented. Required relations between electromagnetic and geometrical parameters of the experimental antenna prototypes have been selected from the theoretical considerations. Employment of HEMT technology allowed us to obtain both the antenna gain not worse than 12dB and its uniform radiation in the measured bandwidth of 12%. The level of cross-component is less than -25dB over the entire working frequency band. Radiation patterns of ceramic patch antennas are of interest for designing the multi-beam antenna systems and beam forming patch array antennas. [C1702]

### "Ultra-low-noise cooled microwave PHEMT amplifiers for radio astronomy applications"

The main aim of this work was to design octave-band amplifiers on commercially available transistors over the frequency range from 0.5 to 4 GHz with emphasis on noise and stability performances at cryogenic temperatures. The major area of application for such devices is microwave and mm-wave high-sensitive receivers, where these ones are usable either as input or IF amplifiers. Performance obtained is the best among devices on commercially available transistors. When incorporated in radioastronomy superheterodyne receivers as IF-amplifiers, they have largely determined implementation of record characteristics of high-sensitive mm-wave receiving systems. [C1703]

### "Using modified GaAs FET model function for the accurate representation of PHEMTs and varactors"

In the recent PSpice programs, several GaAs FET models of various classes have been implemented. However, some of them are sophisticated and therefore very difficult to measure and identify afterwards, especially the realistic model of Parker and Skellern. In the paper, simple enhancement of one of the standard models is proposed. The resulting modification is usable for the accurate modelling of both GaAs FETs and PHEMTs. Moreover, its updated capacitance function can serve as a precise representation of microwave varactors, which is more important. [C1704]

### "A novel uniplanar 44 GHz MMIC subharmonic mixer using CPW series stubs"

The design of a subharmonically pumped (SHP), monolithic microwave integrated circuit (MMIC) mixer for Satcom applications is described. The mixer uses an anti-parallel diode pair to achieve frequency translation by mixing the IF signal with the second harmonic of the fundamental local oscillator (LO) pump. The circuit was fabricated using OMMIC's ED02AH foundry process and contains two pairs of 0.18  $\mu$ m PHEMT based diodes, each, having two 15- $\mu$ m cathode fingers. The measured conversion loss is 8 dB for an RF output signal of 44.51 GHz and the RF port return loss is better than 13 dB over the RF frequency range (43.5 to 45.5 GHz). The 2\*fLO suppression is better than 17 dB over the RF range of 43.5 to 45.5 GHz. [C1705]

### "Fully monolithic 8 watt Ku-band high power amplifier"

This paper presents the design and performance of a compact MMIC high power amplifier operating at Ku-band.



The amplifier was fabricated using TriQuint's 3MI 0.25  $\mu\text{m}$  pHEMT production process on 100  $\mu\text{m}$  substrate. This balanced three-stage power amplifier with chip size of 11.21 mm<sup>2</sup>(2.872 mm $\times$ 3.907 mm) demonstrated 39 dBm (8 Watt) saturated output power with 22% power added efficiency from 13.5 GHz to 15 GHz and greater than 22 dB small signal gain. This HPA delivered among the best output power densities (708.5 mW/mm<sup>2</sup>) from a single MMIC chip at Ku-band reported to date. [C1706]

#### "A novel dual band transmitter for WLAN 802.11 a/g applications"

This paper presents a novel dual band P-HEMT power amplifier/frequency doubler module for 2.4 GHz and 5.8 GHz wireless LAN applications. The module operates as a power amplifier for 2.4 GHz and frequency doubler for 5.8 GHz. The transmitter module has 4.5 dB amplification gain at 2.4 GHz and 3 dB multiplication gain at 5.8 GHz frequency multiplier. At 2.4 GHz band, the 2nd harmonic is about 30 dB lower than the fundamental signal, and at 5.8 GHz band the fundamental and 3rd harmonic are 22 dB lower than the signal. The 2.4 GHz amplifier satisfies the ACPR mask requirement, and the frequency doubler output needs 10 dB ACPR improvement at 11 MHz offset from center frequency by using predistortion linearization. Matlab simulation shows the possibility of digital predistortion to satisfy the ACPR requirement. [C1707]

#### "Charge trapping and intermodulation in HEMTs"

Charge trapping effects in high electron mobility transistors (HEMTs) are linked to anomalous intermodulation behavior, known as memory effects. This behavior can be observed clearly as changes in intermodulation levels with tone-spacing, and two-tone asymmetry. A Volterra-series analysis of an HEMT with trapping predicts the distortion accurately, and allows an understanding of the mechanisms involved. [C1708]

#### "Design of low-cost 4W & 6W MMIC high power amplifiers for Ka-band modules"

Two Ka-band power amplifier MMICs, 4W and 6W, with high power density and gain are presented. Each amplifier was designed using a 5-stage topology to demonstrate over 30dB of gain. The 4W design exhibited a peak saturated output power of 37.2dBm and a chip output power density of 532 mW/mm<sup>2</sup>. This is the highest recorded power density for a Ka-band power amplifier design to date. The high gain and power density make them ideal for low-cost Ka-band transmit systems. [C1709]

#### "High heat flux cooling solutions for thermal management of high power density gallium nitride HEMT"

A package (base plate) level thermal management of high power density GaN High-Electron-Mobility-Transistors (HEMTs) is carried out by liquid micro-jet impingement and its subsequent phase change. Implemented on a 64-gate (9.6 mm gate periphery) device, the cooling technique demonstrates a 43% improvement in power density compared to the traditional air-cooling. Performance improvement could be significantly higher in a Monolithic Microwave Integrated Circuit (MMIC) where the internal thermal resistance (junction to case) of the device is much lower. In parallel, a high fidelity computational model is developed to explore the thermal field within the device and the peak device junction temperature. Practical methods to reduce the device temperature, such as variation of substrate thickness, are established through numerical simulation. For example, a 24% reduction in junction temperature or a 33% gain in power density is shown by reducing the SiC substrate thickness from 400  $\mu\text{m}$  to 75  $\mu\text{m}$ . Temperature rise due to local micro-scale hot spots (gate), gate-to-gate thermal interaction, and their combined effect towards peak junction temperature are investigated at various power levels. [C1710]

#### "An ultra-low power integrated T/R module for space-based radar technology"

The choice of InP HEMT technology is discussed for a highly efficient integrated T/R module. The module includes a receive path comprising of a low noise amplifier, phase shifter and amplifier consuming only 5 mW of DC power at X-band. The transmit path combines phase shifters and amplifiers to provide 10 mW of power per module at an efficiency of 50%. This is achieved by increasing the cut-off frequency of InP HEMT devices and sacrificing their gain for lower DC power consumption. This provides both DC and RF performance criteria for the space based radar antenna design requirements. Future T/R module technologies are also discussed, based on the antimonide based material system, which have already shown a factor of 3-4 reduction in DC power consumption compared to InP HEMT technology. [C1711]

#### "An 80 Gbit/s 1:2 demultiplexer in InP-based HEMT technology"

An 80 Gbit/s 1:2 demultiplexer (DEMUX) is presented that was fabricated using 0.1- $\mu\text{m}$ -gate-length InP-based HEMT technology. A data input buffer with a common-gate amplifier in front is employed to achieve a low return loss over wide frequency range and to suppress signal distortion, which is mainly caused by multiple reflections

between a DEMUX chip and a signal source. A DEMUX core consisting of a D-type flip-flop (FF) and a tri-stage FF assures the edge alignment of two channels of de-serialized signals. The 1:2 DEMUX operated at up to 80 Gbit/s, which was limited by our measurement equipment. At that bit-rate, the input sensitivity and clock phase margin estimated from monitoring eye-openings were about 100 mVp-p and 160 degrees, respectively. The skew of the two output signals was only 2 ps. [C1712]

#### **"InP-based optical system ICs operating at 40 Gbit/s and beyond"**

InP-based 40-Gbit/s optical system ICs are steadily progressing for the start-up of 40-Gbit/s optical systems. Also, InP-based ICs operating beyond 40 Gbit/s are being investigated for future post-40-Gbit/s optical systems. This paper describes our recent progress on InP-based ICs operating at 40 Gbit/s and beyond, which include optoelectronic (OE) ICs. In testing ICs beyond 40 Gbit/s and toward 100 Gbit/s, the absence of signal sources is becoming a critical issue. 100Gbit/s pulse-pattern generators, which are indispensable for investigating a variety of 100-Gbit/s ICs, are also presented. [C1713]

#### **"Electrothermal models of transistors based on finite element analysis for radar applications"**

Electrothermal models of power devices are necessary for an accurate analysis of their performances. For this reason, this paper deals with the methodology to obtain an electrothermal model based for its thermal part on a reduced model of a three dimensional Finite Element (FE) thermal simulation and on electrical measurements for its electrical part. The reduced thermal model is based on a Ritz vectors approach and its equivalent SPICE subcircuit implementation. The complete model has been successfully implemented in the Advanced Design Simulator (ADS) for two kind of X band power amplifiers of 8 W class. One is based on TRIQUINT PHEMT transistors and the other on UMS HBT transistors. Coupled to a distributed electrical model, this electrothermal model has been used in order to investigate the behavior of these two High Power Amplifiers (HPAs) during radar pulses. [C1714]

#### **"A study of output power stability of GaN HEMTs on SiC substrates"**

Gallium Nitride (GaN) HEMTs are the focus of intense research and development due to their potential for the realization of power amplifiers (PAs) with high gain and record levels of power delivery. Much of the work in GaN HEMT development has been concentrated on performance improvement, and the demonstration of exceedingly higher power densities ( $>10\text{W/mm}$ ). To demonstrate this performance, the device is typically subjected to bias levels greater than 40V, which result in large electric field stresses in the vicinity of the gate. Additionally, junction temperatures greater than  $250^\circ\text{C}$  are predicted for the corresponding density of dissipated power. There is a lack of a comprehensive understanding of the effect of these large electrical and thermal stresses on the aging and degradation of GaN devices. There has only been a limited number of reports on the stability of GaN devices over time under RF drive. In the present paper, we investigate the stability of GaN/AlGaN HEMTs under RF and DC stress. We provide a first look at the behavior of the device output power, quiescent currents, and leakage currents as a function of time under variable RF and DC stress conditions. [C1715]

#### **"Affordable high performance InP X-band transceiver module for large aperture phased array applications"**

The objective of this paper is to provide an implementation to construct an affordable and high performance transceiver module which can meet the stringent performance specification required for a large aperture phased array. An InP based transceiver chip set consisting of a HBT power amplifier with  $>60\%$  PAE and a HEMT LNA consuming [C1716]

#### **"A nonuniform thermal de-embedding approach for cryogenic on-wafer high-frequency noise measurements"**

A methodology to perform accurate on-wafer high-frequency noise measurements at cryogenic temperatures (77K) is presented. In this work, the distribution of the temperature along probes and cables at low temperatures is carefully taken into account in the de-embedding process using a 3-D thermal modelling software (@ANSYS) and thermal measurements. Cables and probes are modelled in @ADS software using a distributed RLCG network associated to this temperature distribution. The validity of this model has been checked by measuring the noise power of a  $50\ \Omega$  on-wafer resistance placed at several low temperatures. Finally, we apply this technique to the noise characterization of sub-100 nm gate's length MM-HEMT at 77K and 173K. [C1717]

#### **"Channel temperature model for microwave AlGaN/GaN power HEMTs on SiC and sapphire"**

A key parameter in the design trade-offs made during AlGaN/GaN HEMTs development for microwave amplifiers

is the channel temperature. An accurate determination can generally only be found using detailed software; however, a quick estimate is always helpful, as it speeds up the design cycle. This paper gives a simple technique to estimate the channel temperature of a generic AlGaIn/GaN HEMT on SiC or sapphire, while incorporating the temperature dependence of the thermal conductivity. The procedure is validated by comparing its predictions with the experimentally measured temperatures in microwave devices presented in three recently published articles. The model predicts the temperature to within 5 to 10 percent of the true average channel temperature. [C1718]

#### "Degradation mechanism of GaAs PHEMT power amplifiers under elevated temperature lifetest with RF-overdrive"

The degradation mechanism of 0.15  $\mu\text{m}$  GaAs PHEMTs subjected to three-temperature elevated lifetest ( $T_1=185^\circ\text{C}$ ,  $T_2=200^\circ\text{C}$ , and  $T_3=215^\circ\text{C}$  ambient temperatures in  $\text{N}_2$  atmosphere and stressed at  $V_{ds}=5\text{V}/I_{ds}=250\text{ mA/mm}$ ) under RF-overdrive at 20 GHz was investigated. The results show that Pout degradation is due to  $I_{ds}$  degradation induced by Ti gate metal interdiffusion into the AlGaAs Schottky barrier layer. However,  $\Delta I_{max}$ ,  $\Delta G_{mp}$ , and Ti interdiffusion depth depend on the RF-drive levels. Accordingly, a distinct difference of reliability performance between DC (no RF-overdrive) and RF-overdrive lifetests was demonstrated. It has been found that both DC and RF-overdrive lifetests exhibit similar activation energy, which is approximately 1.65 eV. However, the mean-time-to-failure (MTTF) of RF-overdrive lifetest is inferior to that of DC lifetest. The difference is attributed to the higher electric field present in the RF-overdriven lifetest. [C1719]

#### "GaN electronics with high electron mobility transistors"

The III-nitrides AlN, GaN, and InN alloys are expected to be basis of a strong development of a novel family of semiconductor devices, for optoelectronics as well as for electronics, GaN-based high electron mobility transistors (HEMTs) have shown superior power handling and operating temperatures at frequency ranges that are beyond the limits of devices fabricated from Si and other III-V materials. This paper presents the state-of-the-art GaN HEMT technology and describes the potentials for the future. [C1720]

#### "Fully-integrated core chip for X-band phased array T/R modules"

This paper discusses the final result of development effort leading to a fully-integrated phased-array core chip. The MMIC is especially useful for active electronically-steered arrays, and integrates a full functionality including low-noise amplifier (LNA), a medium-power amplifier (MPA) matched to common high-power amplifiers (HPA) and all control functions. The design and measurement results will be discussed. The integration of an LNA and MPA makes this MMIC an ideal candidate for a two chip T/R module solution. The MMIC is realised in the 0.25 $\mu\text{m}$  PHEMT and process of UMS. [C1721]

#### "High $f_T$ 0.05 $\mu\text{m}$ In<sub>0.52</sub>AlAs/In<sub>0.53</sub>GaAs HEMT's with strained 5 nm InAs sub-channel on InP substrate"

An In<sub>0.52</sub>AlAs/In<sub>0.53</sub>GaAs HEMT with 5 nm InAs-inserted-channel into the In<sub>0.53</sub>GaAs channel was fabricated using 0.05  $\mu\text{m}$  conventional T-shaped gate technology. The measured maximum transconductance ( $G_{m,max}$ ) is above 1 S/mm even at a lower drain voltage of 0.7 V and current gain cutoff frequency ( $f_T$ ) is 409 GHz. This excellent performance is attributed to the combination of the suppression of short-channel effect and the superior transport in 5 nm InAs-inserted-channel design concept. Higher  $f_T$  above 500 GHz is to be expected using the InAs-inserted-channel scheme, if reducing  $L_{gdown}$  to sub-0.05 $\mu\text{m}$  range. [C1722]

#### "Photoluminescence and electrical properties of InGaAs/InP composite channel metamorphic HEMT structures subjected to rapid thermal annealing"

The optical and electrical stabilities of MHEMT with an InGaAs/InP composite channel subjected RTA in the temperature range of 350 to 650  $^\circ\text{C}$  were studied. Although a metamorphic strain-relief buffer is included in MHEMT structure, no evidence of enhanced detriment of PL and electrical properties after RTA was observed. In fact, for the given structures, less degradations in the MHEMT were observed as compared to the referenced LHEMTs, which may partially ease the concerns on the thermal stability of the MHEMT structures. [C1723]

#### "The de-bias effect of gate current in InP HEMT MMICs"

Increased gate current of InP HEMTs subjected to elevated temperature lifetest has been observed. The higher the temperature and the larger the gate periphery, the higher the gate current. On the other hand, gate resistors ( $R_g$ ) are often used in the MMIC design for stability. As a result, the high gate current in conjunction with  $R_g$  de-biases the transistors in InP HEMT MMICs under elevated temperature lifetest. Accordingly, the evolution of DC

parameters between discrete transistors and MMICs illustrates distinct difference. Furthermore, the de-bias effect of gate current in InP HEMT MMICs strongly depends on the lifetest temperature, gate periphery, and gate resistor. As a result, consideration of lifetest temperature, gate periphery, and gate resistors in InP HEMT MMICs is crucial in order to mitigate the de-bias effect induced by elevated temperature lifetest. In this paper, the de-bias effect of gate current in InP HEMT MMICs was illustrated for the first time. [C1724]

#### "A 50-nm gate length InP pseudomorphic HEMT implemented in an MMIC broadband feedback amplifier"

We report a 50-nm InP pseudomorphic InAlAs/InGaAs/InP HEMT, demonstrated in a one-stage MMIC broadband amplifier exhibiting over 8-dB gain between 0 and 42 GHz. The extrinsic transit frequency ( $f_T$ ) and the maximum frequency of oscillation ( $f_{max}$ ) of the 50 nm InP HEMT were 180 GHz and 260 GHz respectively. The two-finger, 100  $\mu\text{m}$  gate-width HEMT showed an extrinsic DC peak transconductance of 910 mS/mm. [C1725]

#### "Tradeoff of DC/RF performance versus reliability in 0.1 $\mu\text{m}$ InP HEMTs"

The tradeoff of DC/RF performance versus reliability has been explored on 0.1  $\mu\text{m}$  InP HEMTs. The tradeoff between performance and reliability shows the dependence on the process techniques. While higher performance could be achieved with certain process techniques, the reliability performance is adversely affected. Nevertheless, all the process variations explored here exhibit activation energy of approximately 1.9 eV. However, the time-to-failure (TTF) at lifetest temperatures of 230°C and 250°C and median-time-to-failure (MTTF) at junction temperature of 125°C depend on the process techniques. The results are beneficial for balancing performance versus reliability through the adjustment of the processing technique. [C1726]

#### "Study of breakdown dynamics in InAlAs/InGaAs/InP HEMTs with gate length scaling down to 80 nm"

In this paper we present the correlation between the impact ionization gate current with the  $S_{22}$  scattering parameter measured in the 50 MHz-6 GHz frequency range in InAlAs/InGaAs/InP HEMTs. Devices with shorter gate length presenting larger I.I. gate current have shown larger inductive component in the output admittance  $Y_{22}$  at low frequencies. [C1727]

#### "Nanogate InP-HEMT technology for ultrahigh-speed performance"

We succeeded in fabricating decananometer-gate InGaAs/InAlAs high electron mobility transistors (HEMTs) with extremely high current gain cutoff frequencies ( $f_T$ 's) of up to 562 GHz. The superior high-speed performance was obtained through laterally scaling the gate length ( $L_g$ ) and the gate-recess length, introducing a double recessed cap structure, and vertically scaling the gate-channel distance. We investigated the effect of these structures on the high-frequency performance, and clarified their advantages for the ultrahigh-speed operation from the view point of enhanced electron overshoot velocity, reduced parasitic source and drain resistances, and suppressed short channel effect. [C1728]

#### "Degradation analysis of 0.1 $\mu\text{m}$ InP HEMTs using low frequency noise characterization"

Low frequency noise technique was introduced to characterize the gate and drain noise spectra on 0.1  $\mu\text{m}$  InP HEMTs before and after degradation (subjected to elevated temperature lifetest at  $T_{\text{junction}}$  of 240 °C for 936 hours). It has been found that the gate current noise on the degraded devices increases significantly and exhibits a Lorentzian peak around 15 KHz. The low frequency noise results indicate that the Schottky junction is the primary degradation origin, which is consistent with the electrical results-showing the forward and reverse Schottky junction degradation. Gate current low frequency noise spectra suggest that there are possible interface states and bulk defects generated in the degraded Schottky junction-this was further substantiated with a scanning transmission electron microscope. The results from this study shows that low frequency noise characterization provides a sensitive means to identify the degradation origin and Schottky junction attributes of a degraded InP HEMT. [C1729]

#### "Millimeter-wave and mixed-signal integrated circuits based on advanced metamorphic HEMT technology"

Integrated circuits based on metamorphic HEMT (MHEMT) technologies on 4" GaAs substrates for both millimeter-wave and mixed-signal applications are discussed in this paper. Extrinsic cut-off frequencies of  $f_T$ = 293 GHz and  $f_{max}$ = 337 GHz were achieved for the 70 nm gate length depletion type MHEMT technology. The



MMIC process features high yield on transistor and circuit levels. Single-stage low-noise amplifiers demonstrate a small signal gain of 12 dB and a noise figure of 2.2 dB at 94 GHz. An amplifier MMIC developed for D-band operation exhibits a gain of 15 dB from 155 to 160 GHz. The achieved results are equivalent to state-of-the-art InP-based HEMT technologies. In order to realize 80 Gbit/s mixed-signal circuits, a 100 nm gate length enhancement type HEMT process with a transit frequency of 200 GHz is applied. Three metalization layers are available for interconnects. The parasitic capacitance of the interconnects is kept low by using BCB and plated air bridge technology. Based on this process, static and dynamic frequency dividers are realized which achieve a maximum toggle frequency of 70 GHz and 108 GHz, respectively. Furthermore, 2:1 multiplexer and 1:2 demultiplexer ICs were developed and successfully tested at 80 Gbit/s data rate. [C1730]

#### "Improvement in reliability of InP-based HEMTs by suppressing impact ionization"

We have improved the reliability of InP-based high electron mobility transistors (HEMTs) by using two structures that suppress impact ionization: a lattice-matched composite channel InGaAs/ InAlGaAs structure and a double-doped structure. In the composite channel structure, electrons transfer from InGaAs to InAlGaAs when the electric field is strong, thereby suppressing impact ionization under high drain bias. In the double-doped structure, the intrinsic built-in field of the channel is smaller than it is in the conventional structure. The total electric field under a given drain bias voltage is therefore weaker, and this weaker field causes less impact ionization. Aging tests confirmed that both structures improved device reliability at a  $V_{ds}$  of 2 V. [C1731]

#### "High performance of 0.15 $\mu$ m quasi enhancement-mode (E-mode) In<sub>0.4</sub> GaAs/In<sub>0.4</sub> AlAs metamorphic HEMTs on GaAs substrate using new triple-gate technology"

In this paper, a novel gate technology with triple shaped gate structure has been proposed and developed in order to minimize unwanted gate fringing capacitance. Because high gate stem height was difficult to fabricate by means of conventional direct electron beam (e-beam) lithography method, additional PMGI sacrificial layer was utilized in this new scheme. Increasing gate stem height as an amount of PMGI resist thickness and forming T-shaped gate structure on top of the PMGI layer, triple shaped gate structure could be finally obtained. Applying the developed technology to the fabrication of 0.15  $\mu$ m In<sub>0.4</sub>GaAs/In<sub>0.4</sub>AlAs metamorphic HEMTs (M-HEMTs), excellent device cutoff frequency ( $f_T$ ) performance of 164 GHz even with 0.15  $\mu$ m technology has been shown owing to the remarkable reduction of gate fringing capacitance. In addition, the usage of 40% indium content in barrier layer gave rise to the improvements in Schottky gate characteristics such as gate turn-on voltage ( $V_{on}$ ) of +1.03 V and reverse breakdown voltage ( $BV_{GD}$ ) of -7.8 V, which has important meanings in enhancement-mode operation devices. [C1732]

#### "Investigation of drain current transient in InP-based high electron mobility transistors (HEMTs)"

A simple technique based on the measurement of the transient drain current is demonstrated for quickly assessing the properties of the hot-carrier-induced traps. Two different kinds of interface traps with distinctive time constants have been measured in our present devices. [C1733]

#### "Metamorphic HEMT and its application"

First Page of the Article [C1734]

#### "Characteristics of In<sub>x</sub> Al<sub>1-x</sub> As/In<sub>x</sub> Ga<sub>1-x</sub> As (x=50%, 60%) metamorphic HEMTs on GaAs substrates"

We have developed the In<sub>x</sub>Al<sub>1-x</sub>As/In<sub>x</sub>Ga<sub>1-x</sub>As (x = 50%, 60%) metamorphic HEMTs (m-HEMTs) on GaAs substrates. The current gain cut-off frequency ( $f_T$ ), and the threshold voltage have been investigated versus the gate-length. The improved microwave performance in smaller gate-length devices is mainly associated with the reduction of the electron-transit time. After analyzing the extrinsic total delay time, the effective velocity of electrons can be estimated, and the velocities are  $2.3 \times 10^7$  and  $2.8 \times 10^7$  cm/s for the indium composition of 50% and 60% in the InGaAs channel, respectively. [C1735]

#### "Integration of a novel, high quality Si<sub>3</sub> N<sub>4</sub> metal insulator metal (MIM) capacitors deposited by (ICP-CVD) at room temperature with 50 nm T-gate InP-HEMTs to realise monolithic millimetre-wave integrated circuits (MMICs)"

In this paper we report an array-based design methodology for the realisation of monolithic millimetre-wave integrated circuits (MMICs). This work focuses on the realisation of a 94 GHz MMIC amplifier using an array-based approach by integrating high performance 50 nm T-gate InP-HEMTs with an  $f_{To}$  of 480 GHz and a

Si<sub>3</sub>N<sub>4</sub>metal insulator metal (MIM) capacitor technology formed using room temperature inductively coupled plasma chemical vapour deposition (ICP-CVD) nitride deposition together with a range of more conventional coplanar waveguide-based passive components. The device developed in this work exhibits the highest  $f_T$  recorded for a 50 nm gate length technology. The one stage amplifier is predicted to have a gain of 8 dB and return loss of better than -10 dB at 94 GHz. The use of a room temperature nitride deposition process allows all passive components to be realised after active device realisation, and enables a mm-wave "sea-of-gates" array-based design methodology. [C1736]

#### "Investigation of enhancement-mode metamorphic InAlAs/InGaAs HEMTs by Schottky metal diffusion"

In this report, we have developed the enhancement mode (E-mode) InAlAs/InGaAs metamorphic HEMT's (mHEMTs) on GaAs substrates by using the thermally annealed Schottky metal diffusion approach. The activation energy of platinum (Pt) Schottky metal was systematically carried out. Based on the extracted device small-signal model, the improved devices  $rf$  transconductance ( $g_m$ ) is more significantly than the increased gate-to-source capacitance ( $C_{gs}$ ) after the Schottky metal diffusion, due to the reduction of gate-to-channel separation. Moreover, it also exhibits a high voltage gain and capacitance ratio resulting in a higher maximum oscillation frequency. [C1737]

#### "Passivation study for In<sub>0.4</sub> AlAs/In<sub>0.65</sub> GaAs HEMTs by UHV RPECVD grown SiN<sub>x</sub> dielectrics and their impact on I-V kink and low-frequency dispersion phenomena"

The influence of silicon nitride (SiN<sub>x</sub>) passivation on the DC and low-frequency transconductance dispersion behaviours of In<sub>0.4</sub>AlAs/In<sub>0.65</sub>GaAs HEMTs has been investigated. Although the surface passivation using MBE grown thin InP etch-stop is effective to suppress I-V kink phenomena, it has critical drawbacks of large gate leakage current, low gate turn-on ( $V_{on}$ ) and breakdown voltage ( $BV_{gd}$ ) due to low Schottky barrier height (SBH) of InP layer. To resolve this problem, we have developed innovative SiN<sub>x</sub>passivation process to prevent I-V kink as well as to maintain low gate leakage current by UHV remote-PECVD system. Through the optimized SiN<sub>x</sub>passivation process, the DC I-V kink and the low-frequency transconductance dispersion could be significantly improved. [C1738]

#### "Low-frequency transconductance dispersion characteristics of 0.13 $\mu$ m In<sub>0.65</sub> GaAs p-HEMTs with side-recessed InAlAs and InP surface"

Effects of side recess on kink effect and transconductance ( $g_m$ ) frequency dispersion characteristics of 0.13  $\mu$ m InGaAs p-HEMTs having InAlAs and InP surface were investigated. The p-HEMT having a 300 nm recessed InP surface showed negligible kink effect and  $g_m$ dispersion due to the reduction in surface-state induced trap density in the InP etch-stop and impact-ionization induced hole current ( $I_{g,hole}$ ). [C1739]

#### "Strain relaxation and dislocation filtering in metamorphic HBT and HEMT structures grown on GaAs substrates by MBE"

The production of InP-based epiwafers on GaAs substrates by molecular beam epitaxy is achieved through the use of metamorphic buffers (M-buffers) consisting of graded InAlAs or bulk InP layers. Each M-buffer demonstrates a unique surface morphology and strain relaxation mechanism, as demonstrated by AFM, SEM, and TEM. HEMTs and HBTs were grown on GaAs substrates using the two M-buffers, and their transport properties and dc parameters were compared with baseline structures grown on InP substrates. The structures grown with the InAlAs M-buffer were much closer to the baseline than those grown using the InP M-buffer. Incomplete dislocation filtering in the InP M-buffer may be the source of this degradation. [C1740]

#### "High performance millimeter wave 0.1 $\mu$ m InP HEMT MMIC LNAs fabricated on 100 mm wafers"

Millimeter wave 0.1  $\mu$ m InP HEMT MMICs fabricated on 100 mm InP substrates have been demonstrated at NGST. Production capability in 100 mm MBE growth, frontside processing, and backside processing has been established and is presented. MMIC performance is described for Ka-band, Q-band, and W-band low noise amplifiers and for a 0.5 to 80 GHz distributed amplifier. [C1741]

#### "InAlAs/InGaAs double-gate HEMTs with high extrinsic transconductance"

This paper reports fabrication, DC and RF characterization of the In<sub>0.52</sub>Al<sub>0.48</sub>As/In<sub>0.53</sub>Ga<sub>0.47</sub>As double-gate HEMTs with sub-micron gate lengths. These devices have obtained a maximum extrinsic transconductance  $g_{mof}$  2650 mS/mm with a corresponding drain current  $I_{dequal}$  to 310 mA/mm. This extrinsic transconductance is the

highest value ever reported for any transistor. Due to this high extrinsic transconductance, the ratio  $g_m/I_{dis}$  8V-1 indicating the high charge control efficiency. Low output conductance  $g_{dis}$  obtained, denoting the reduction of short channel effects. The combined high transconductance and the low output conductance induce an extremely high intrinsic unloaded voltage gain ( $g_m/g_d$ ) of 87. [C1742]

#### "Control of plasma induced fluorine damage in P-HEMT using InSb barrier layer"

We investigated plasma induced fluorine damage in P-HEMT by C2F6/CHF3RIE and found that fluorine atoms penetrated to the channel layer. We also found these fluorine atoms were apt to stack on a strained interface, like Si-planar doped layer and hetero interfaces, by thermal annealing. Utilizing the properties of fluorine atoms, we improved a P-HEMT structure that had an ultra thin InSb strained barrier layer above the Si-planar doped layer. The InSb barrier layer effectively absorbed the intruded fluorine atoms in P-HEMT, and the degradation in the carrier density and mobility was suppressed much more than that of conventional P-HEMT structure. [C1743]

#### "AlGaN/AlN/GaN High Electron Mobility Transistors with Improved Carrier Transport"

Geo-magneto-resistance measurements have been made on AlGaN/GaN HEMT structures both with and without an AlN interlayer. The results show significantly higher carrier mobility at low temperatures for devices with the interlayer. Furthermore, the drop in mobility with increasing 2DEG density, commonly exhibited by AlGaN/GaN HEMTs, is dramatically reduced by introduction of the interlayer. These results provide insight into the role of alloy and interface roughness scattering on 2DEG properties [C1744]

#### "Studies of Hot-Electron Degradation in GaN HEMTs with Varying Gate Recess Depths"

Hot-electron injection experiments were performed on Al<sub>0.2</sub>GaN<sub>0.8</sub>/GaN HEMTs with different gate recess depths formed by reactive ion etching. Flicker noise measured from the devices indicate systematic increase in  $S_v(f)$  for devices with increasing recess depths. Furthermore, when the devices were subjected to high dc voltage stress across the conduction channel, the devices with large gate recess were found to exhibit much more significant increase in  $S_v(f)$  compared to the control device with no gate recess. Since  $S_v(f)$  is directly proportional to the trap density at the AlGaN/GaN heterointerface, the experimental data clearly show that the reactive ion etching process has led to significant degradation in the integrity of the device [C1745]

#### "2004 Conference on Optoelectronic and Microelectronic Materials and Devices-COMMAD 04 Proceedings"

The following topics were dealt with: semiconductor growth (MBE, PECVD, MOCVD, MOVPE) and characterizations; high-electron mobility transistors (HEMTs); microcavity organic light emitting diode (MOLED); semiconductor superlattices; photodiode arrays; MEMS structures; lithography; semiconductor lasers; semiconductor optical amplifiers; surface treatment and annealing [C1746]

#### "High linearity GaN HEMT power amplifier with pre-linearization gate diode"

A high linearity MMIC RF power amplifier is reported in the AlGaN/GaN HEMT technology. In order to obtain high linearity, a pre-linearization gate diode is added at the input to compensate for the nonlinear input capacitance  $C_{gs}$  of the GaN HEMT device. Another single-ended class B power amplifier without the gate diode is also designed for comparison. The circuit with the pre-linearization gate diode demonstrates at least 4dB improvement on 3rd order intermodulation distortion (IMD3) performance over the one without the diode over the useful power range in two-tone measurement. [C1747]

#### "GaN HEMTs: material, device, circuit technology and applications"

With the rapid progress and maturation over the last several years, wide bandgap GaN-based HEMTs are now regarded as the next generation technology leader for high frequency and high power device applications as stated in U. K. Mishra et al. (2002). The Al<sub>x</sub>Ga<sub>1-x</sub>N-GaN heterostructure system enables high voltage, high current operation, resulting in the demonstration of >10<sup>4</sup> power performance than GaAs and Si technologies. The high RF power density (W/mm) translates into high watts per unit capacitance (W/pF), resulting in high impedance and simpler matching, an enabler for wide-bandwidth applications. This paper reviews the recent progress in material, device and circuit performance of GaN HEMTs by the Cree team. [C1748]

#### "The etching of GaAs, AlGaAs and InGaAs in different chemicals in p-HEMT mesa layers"

The etching of mesa layer in the fabrication of p-HEMT devices was studied and analyzed. The chemical compositions were varied to study the etch rate effect on the various materials in the mesa layer. The etching

rates and selectivity of the  $\text{H}_3\text{PO}_4\text{:H}_2\text{O}_2\text{:H}_2\text{O}$ ,  $\text{NH}_4\text{OH:H}_2\text{O}_2\text{:H}_2\text{O}$  and  $\text{H}_2\text{SO}_4\text{:H}_2\text{O}_2\text{:H}_2\text{O}$  is compared among GaAs, AlGaAs and InGaAs materials. The results show that the chemical ratio of 1:1:500 and 1:1:250 are suitable in the mesa etching based on the selectivity between AlGaAs over GaAs and AlGaAs over InGaAs.

[C1749]

#### "Design of GaAs-based pseudomorphic HEMTs by 2D device simulations"

In this paper, AlGaAs/InGaAs/GaAs pseudomorphic high electron mobility transistors (PHEMT's) was optimized by means of 2D device simulation. The commercial 2D device simulator Taurus-MEDICI is used to study the effect of varying barrier or supply doping concentration, NDsupply on the gate characteristics and current-gain cutoff frequency (fT) of the PHEMT. We show that values of fT in excess of 100GHz can be obtained by optimizing the supply doping concentration. [C1750]

#### "Comparison study of uniformly-doped and delta-doped Al<sub>0.22</sub> Ga<sub>0.78</sub> As/In<sub>0.22</sub> Ga<sub>0.78</sub> As pseudomorphic HEMTs"

Device performance of uniformly-doped and delta-doped AlGaAs/InGaAs pseudomorphic high electron mobility transistors are investigated with 2D numerical simulator, ATLAS/Silvaco. Simulation results demonstrates superior performance for the delta-doped structure. The advantages shown by delta-doped structure include better electron confinement and reduced parasitic conduction which are manifested as higher transconductance and improved drain current. [C1751]

#### "2004 IEEE International Conference on Semiconductor Electronics (IEEE Cat. No.04EX917C)"

{no data available} [C1752]

#### "Electrical characteristics of Al<sub>0.22</sub> Ga<sub>0.78</sub> As/In<sub>0.22</sub> Ga<sub>0.78</sub> As PHEMT with gate length in nano regime"

We investigated the gate length (Lg) dependence of the electrical characteristics in AlGaAs/InGaAs PHEMT using Silvaco simulation tools. Two PHEMTs with different structure are studied, namely uniformly doped PHEMT (U-HEMT) and PHEMT with double delta-doped (D-HEMT) layers. For both PHEMT, short channel effects affect characteristics significantly especially in devices with gate lengths of sub-100 nm regime. From simulation, a maximum fT of 165 GHz is obtained for 70 nm gate-length U-HEMT while the 70 nm gate-length D-PHEMT displays fT of 135 GHz. [C1753]

#### "Noise characteristics of field-plated GaN HEMTs"

Investigation into field-plated GaN HEMTs has revealed that, although addition of the field plate reduces cutoff frequencies, noise figure actually improves. An analysis is presented to explain this phenomenon, which is related to the trade-off between gate-drain capacitance and gate conductance. [C1754]

#### "Growth and characteristics of InP/In<sub>x</sub> Ga<sub>1-x</sub> As/In<sub>0.53</sub> Ga<sub>0.47</sub> As HEMTs"

The materials with In<sub>x</sub>Ga<sub>1-x</sub>As/In<sub>0.53</sub>Ga<sub>0.47</sub>As composite channel of InP HEMT have been designed and grown by MBE in this paper. This channel has high 2DEG density and mobility, and has better channel conductivity when X=0.7. In virtue of InGaAs/InAs/InGaAs composite channel, the electron mobility of the material reaches 13600 cm<sup>2</sup>/v\*s and the 2DEG density is 2.341012cm<sup>2</sup>. [C1755]

#### "MBE-grown AlGaN/GaN HEMTs on SiC"

We report on the development of AlGaN/GaN high-electron mobility transistors (HEMTs) grown on SiC using plasma-assisted molecular beam epitaxy (MBE). In this work, we show that performance comparable to state-of-the-art AlGaN/GaN HEMTs can be achieved using MBE-grown material. Buffer leakage was an important limiting factor for these devices. The use of either carbon-doped buffers, or low Al/N ratio in the nucleation layer growth was effective in reducing buffer leakage. Studies varying the thickness and concentration of the carbon doping were carried out to determine the effect of different carbon doping profiles on the insulating and dispersive properties of buffers. On devices without field plates, at 4 GHz an output power density of 12 W/mm was obtained with a power-added efficiency (PAE) of 46% and gain of 14 dB. 15.6 W/mm with PAE of 56% was obtained from these devices after field-plating. Two-tone linearity measurements of these devices were also carried out. At a C/I3 level of 30 dBc, the devices measured had an output power of 1.9 W/mm with a PAE of 53%. The effect of the Al/N ratio in the AlN nucleation layer on buffer leakage was studied. N-rich conditions yielded highly insulating GaN buffers without carbon doping. At 4 GHz, devices without field plates delivered 4.8



W/mm with a PAE of 62%. At a higher drain bias (50 V), 8.1 W/mm with a PAE of 38% was achieved. [C1756]

### "Design and performance of a ultra-low-NF, high gain, linear LNA for 3GPP wireless node-B application"

In this paper, we discuss the design methodology of a linear low noise amplifier (LNA) for optimum noise performance under good input match and reasonable output matching condition. Linearity is achieved with the use of balanced configuration and with overall high bias current gain of the LNA is optimised to be used in wideband code division multiple access (WCDMA) base-station receiver front-end. The balanced-cascade amplifier chain uses two E-pHEMT GaAsFET devices having gate widths of 800  $\mu\text{m}$  and 6400  $\mu\text{m}$ . Simulation performance shows an overall gain of 43 dB, noise figure less than 0.5 dB and third order intermodulation level (IMD3) better than -82 dBc under outdoor high-end mobile data rate of 384 kbps. [C1757]

### "Simulation and design of 3D geometric RF IC inductors by novel modeling techniques with magPEEC plus FastCap"

This, paper presents a new peec (partial element equivalent circuit)-based inductor simulation tool, entitled L-Simulator, which employs a novel magPEEC modeling algorithm and an existing FastCap modeling algorithm to address both magnetic and electrical coupling effects, respectively, in 3D conductor+magnet+dielectric geometries, hence, being capable to simulate and design 3D magnetic-enhanced RF IC inductors. Applications on micromachined inductors in a 0.2  $\mu\text{m}$  GaAs HEMT process and magnetic-cored micro inductors in a 0.18  $\mu\text{m}$  CMOS technology are discussed. [C1758]

### "Numerical simulation of selected semiconductor devices"

We present a review of industrial heterostructure devices, based on SiGe/Si and III-V compound semiconductors, analyzed by means of numerical simulation. Critical modeling issues are addressed. Results from 2D hydrodynamic analyses of heterojunction bipolar transistors (HBTs) and field-effect transistors (FETs) are presented, and are in good agreement with measured data. [C1759]

### "GaN MOS-HEMT using atomic layer deposition Al<sub>2</sub>O<sub>3</sub> as gate dielectric and surface passivation"

We report on a GaN metal-oxide-semiconductor high electron mobility transistor (MOS-HEMT) using atomic layer deposition (ALD) Al<sub>2</sub>O<sub>3</sub>film as a gate dielectric and for surface passivation simultaneously. Compared to the conventional AlGaIn/GaN HEMT of the same design, six order of magnitude smaller gate leakage current and tripled drain current at forward gate bias demonstrate the effectiveness of ALD Al<sub>2</sub>O<sub>3</sub>as a gate dielectric. The high transconductance and high effective two-dimensional electron mobility verify the high-quality of Al<sub>2</sub>O<sub>3</sub>/AlGaIn interface with low interface trap density. The Al<sub>2</sub>O<sub>3</sub>passivation effect is also studied by sheet resistance measurement and short pulse drain characterization. [C1760]

### "A new field-plated GaN HEMT structure with improved power and noise performance"

Field-plated structures can dramatically improve power capacity of GaN HEMT devices. In this paper, two different field-plated GaN HEMT structures were demonstrated and compared to each other. The results show that a new GaN HEMT structure improves both power and noise performance without additional processing or costs. [C1761]

### "Unstrained InAlN/GaN HEMT structure"

InAlN has been investigated as barrier layer material for GaN-HEMT structures, potentially offering higher sheet charge densities (Kuzmik, 2002) and higher breakdown fields (Kuzmik, 2001). Lattice matched growth of the barrier layer can be achieved with 17% in content, avoiding piezo polarization. In this configuration the sheet charge density is only induced by spontaneous polarization. First experimental results of unpassivated undoped samples realized on 111-Si substrate exceed a DC output current density of 1.8 A/mm for a gate length of 0.5  $\mu\text{m}$ . Small signal measurements yield a  $f_t$ = 26 GHz and  $f_{\text{max}}$ = 14 GHz, still limited by the residual conductivity of the Si-substrate. A saturated output power at 2 GHz in class A bias point yielded a density of 4.1W/mm at  $V_{\text{DS}}$ = 24 V. [C1762]

### "Stable high power GaN-on-GaN HEMT"

High power AlGaIn/GaN HEMTs on free-standing GaN substrates with excellent stability have been demonstrated for the first time. When operated at a drain bias of 50V, devices without a field plate showed a record CW output power density of 10.0W/mm at 10GHz with an associated power-added efficiency of 45%. The

efficiency reaches a maximum of 58% with an output power density of 5.5W/mm under a drain bias of 25V at 10GHz. Long-term stability of device RF operation was also examined. Under ambient conditions, devices biased at 25V and driven at 3dB gain compression remained stable at least up to 1,000 hours, degrading only by 0.35dB in output power. Such results clearly demonstrate the feasibility of GaN-on-GaN HEMT as an alternative device technology to the GaN-on-SiC HEMT in supporting reliable, high performance microwave power applications. [C1763]

#### "Low frequency noise parameters in an AlGaIn/GaN heterostructure with 33% and 75% Al mole fraction"

Transport and low frequency noise properties of undoped AlGaIn/GaN high electron mobility transistor (HEMT) heterostructures with 33% and 75% Al mole fractions in the ohmic and nonlinear regimes of applied voltages are studied. In contrast to the low Al mole fraction, the noise properties of 75% content structures are not affected by passivation. At small voltages both kinds of structures demonstrate about the same level of 1/f excess noise. Deviations from conventional flicker noise were observed at high applied voltages. Additionally, differences in noise behaviour between the two structures were revealed. In the 75% content structures, a noise level suppression was registered in the non-linear regime, which is important for the development of low noise oscillator circuits. [C1764]

#### "4-12 GHz InP HEMT-based MMIC low-noise amplifier"

In this paper, we present a monolithically integrated 3-stage low-noise amplifier working in the 4-12 GHz band. The circuit was fabricated on our in-house 0.2  $\mu\text{m}$  InP HEMT process using coplanar waveguide technology. In the band of interest, the fabricated amplifier shows an average noise figure of 1.25 dB and an average gain of 28 dB with a gain ripple of  $\pm 2$  dB at room temperature. The total dc power consumption of the LNA is 41 mW. At a temperature of 10 K, an average gain of 27 dB and average noise temperature of 13 K was achieved, whereas the dc power consumption was reduced to 5.7 mW. [C1765]

#### "100nm InAlAs/InGaAs double-gate HEMT using transferred substrate"

100nm T-gates InP double-gate HEMTs (DG-HEMT) have been fabricated by use of transferred substrate technique. These devices are compared with standard single 100nm T-gate HEMT. The maximum extrinsic transconductance  $g_m$  of DG-HEMT is two times higher than the HEMT one, and the extrinsic output conductance  $g_d$  is significantly reduced with DG-HEMT. The combined high  $g_m$  and low  $g_d$  induced an extremely high intrinsic unloaded voltage gain  $g_m/g_d$  of 100. So, these results allowed an improvement of the maximum oscillation frequency ( $f_{\text{max}}$ ) of 30% compared with standard single 100nm T-gate HEMT. These results are attributed to reduction of short channel effects, related to higher charge control efficiency and suppression of buffer effect. [C1766]

#### "Suppression of kink phenomenon in ultra-high-speed strained InAs- inserted E-mode HEMTs with a new 0.1 $\mu\text{m}$ Y-shaped Pt-buried gate and their impacts on device performance"

Kink phenomenon has been carefully investigated in InP-based HEMTs with a highly strained InAs channel. Although this narrow band-gap ( $\Delta E_g$ ) InAs channel layer with high hall mobility was effective to improve device speed characteristics, it also degraded high frequency power-gain severely in a depletion-mode operation (D-mode), mainly owing to the increased interactions associated with the impact-ionization induced holes. By operating InAs-based HEMT in an enhancement-mode (E-mode), Kink effect in I-V curve could be remarkably suppressed because the applied positive gate potential prevented the impact-ionization-induced holes from reacting with surface states, which also led to the improvements on high frequency gain ( $f_{\text{max}}$ ), on-state breakdown voltage ( $BV_{\text{ds,on}}$ ) and low-frequency transconductance ( $G_m$ ) dispersion characteristics. Pt-buried gate technology was used to operate InAs-based HEMT in E-mode region, and a new Y-shaped gate structure with 0.1  $\mu\text{m}$  gate length ( $L_g$ ) was successfully developed to enhance device cutoff frequency ( $f_T$ ) to the utmost by etching middle PMGI layer in tri-layer e-beam resist stack (ZEP520/PMGI/ZEP520). [C1767]

#### "Thermal, electrical and environmental reliability of InP HEMTs and GaAs PHEMTs"

This paper reviews current understanding of reliability of InP HEMTs and GaAs PHEMTs. Operating temperature, bias point, and the environment are all known to affect the long-term stability of these devices. Identifying the dominant failure mechanism in a given situation is difficult because fundamental understanding is still insufficient, several mechanisms have a similar signature, and because often times, there are multiple mechanisms acting simultaneously. In spite of this, GaAs PHEMTs and InP HEMTs are already remarkably reliable and the prospect of further improvements are good. [C1768]

### "A 100-W high-gain AlGaIn/GaN HEMT power amplifier on a conductive n-SiC substrate for wireless base station applications"

AlGaIn/GaN high electron mobility transistors (HEMTs) were fabricated on a low-cost conductive n-SiC substrate. A single-chip GaN HEMT amplifier, operating at 60 V, achieved high CW output power of (101 W), a high linear gain (155 dB) and 50 % power-added efficiency at 2.14 GHz. This is the first report about the greater than 100 W power performance of the single-chip GaN HEMT that was grown on a conductive substrate. [C1769]

### "Al<sub>0.3</sub>Ga<sub>0.7</sub>N/Al<sub>0.05</sub>Ga<sub>0.95</sub>N/GaN composite-channel HEMTs with enhanced linearity"

We report an Al<sub>0.3</sub>Ga<sub>0.7</sub>N/Al<sub>0.05</sub>Ga<sub>0.95</sub>N/GaN composite-channel HEMT with enhanced linearity. Through channel engineering, i.e. inserting a 6-nm thick AlGaIn layer with 5% Al composition in the channel region, a composite-channel HEMT was demonstrated. Transconductance and cutoff frequencies of a 1 μm × 100 μm HEMT are kept near their peak values throughout the low- and high-current operating levels, a desirable feature for linear power amplifiers. Driven by W-CDMA signals with a center frequency of 2 GHz, an adjacent channel leakage ratio (ACLR) of less than -45 dBc was achieved with a power added efficiency (PAE) of 45% and a power density of 3.4 W/mm for composite-channel HEMTs (CC-HEMTs) grown on sapphire substrates, without using any linearization techniques. [C1770]

### "Growth and characterization of AlGaIn/AlN/GaN HEMTs on 100-mm-diameter epitaxial AlN/sapphire templates"

Al<sub>0.26</sub>Ga<sub>0.74</sub>N/AlN/GaN heterostructures with a 1-nm-thick AlN interfacial layer were grown on 100-mm-diameter epitaxial AlN/sapphire templates by metalorganic vapor phase epitaxy. They exhibited very high Hall mobilities of approximately 2100 cm<sup>2</sup>/Vs at room temperature and approximately 25000 cm<sup>2</sup>/Vs at 15 K with a sheet carrier density of approximately 1 × 10<sup>13</sup>/cm<sup>2</sup>. High-electron-mobility transistors were successfully fabricated on the epitaxial wafers. The device exhibited a high drain current density of 832 mA/mm and high extrinsic transconductance of 189 mS/mm. [C1771]

### "Construction of the Korean VLBI network (KVN)"

Korea's new VLBI project to construct the Korean VLBI network (KVN) started in 2001, as a 7-year project that is fully funded by our government. We plan to build 3 new high-precision radio telescopes of 21-m diameter in 3 places in Korea which will be exclusively used for VLBI observations. We will install the 2/8, 22 and 43 GHz HEMT receivers within 2007 as a first target, and later we will expand the receiving frequency up to 86 and 129 GHz for astronomical, geodetic, and Earth science VLBI research. The millimeter-wave VLBI will be the ultimate goal of KVN. For the front-ends we are going to install a multi-channel receiver system that employs low-pass filters within a quasi-optical beam transportation system. This receiver system will give reliable phase calibrations for millimeter-wave VLBI as well as enable simultaneous multi-frequency band observations. The new hard-disk type mark 5 will be used as the main recorder of KVN. We have completed the design of the KVN DAS system of 2 Gbps sampling rate, which will use 4 data streams to meet the multi-channel requirement. A VERA type DAS modified for the mark 5 recorder is also under consideration. A new correlator project for KVN was recently approved from our government, and will start in the second half of this year. [C1772]

### "Millimetre wave metamorphic HEMT amplifiers"

First Page of the Article [C1773]

### "A novel terahertz plasma-wave photomixer with resonant-cavity enhanced structure"

Two-dimensional (2D) plasmon in a submicron transistor channel can make resonant oscillation in the terahertz range. We propose a novel terahertz plasma-wave photomixer that can improve the conversion gain and terahertz radiation power. The photomixer is based on a high-electron mobility transistor (HEMT) and incorporates doubly interdigitated grating strips for the gate electrodes that periodically localize the 2D plasmons in sub 100-nm regions with a micron-order interval. A vertical cavity structure is formed in between the top metal grating and a terahertz mirror placed at the backside. FDTD simulation demonstrates that a newly-introduced vertical cavity structure effectively enhances the conversion gain and radiation power. [C1774]

### "High-gain microwave GaN HEMTs with source-terminated field-plates"

GaN HEMTs with field-plates connected to the source terminal have been developed for high-gain, high-voltage operation at microwave frequencies. Due to the reduced feedback capacitance compared to the gate-terminated field-plate structures, improvement in large-signal gain of 5-7 dB is obtained. Superior performance including 21-

dB associated gain, 20-W/mm output power and 60% power-added-efficiency at 4 GHz and 118V bias, is achieved simultaneously. This translates to an extremely high voltage-frequency-gain product approaching 10 kV-GHz. [C1775]

#### "Millimeter-wave circuits based on advanced metamorphic HEMT technology"

Integrated circuits based on metamorphic InAlAs/InGaAs HEMTs with 70 nm gate length on 4" GaAs substrates for millimeter-wave applications are discussed in this paper. Extrinsic cut-off frequencies of  $f_t=293$  GHz and  $f_{max}=337$  GHz were achieved. The IC process features high yield on transistor and circuit levels. Single-stage low-noise amplifiers demonstrate a small signal gain of 12 dB and a noise figure of 2.2 dB at 94 GHz. An amplifier MMIC developed for G-band operation exhibits a gain of 19 dB at 200 GHz. These results are equivalent to those achieved using state-of-the-art InP-based HEMT technologies. [C1776]

#### "Recent advances in III-V nitride electronic devices"

The latest developments made using III-V nitride technology for microwave and mm-wave applications are reviewed. Design, processing issues are addressed and device, circuit performance is reported. The devices discussed are AlGaIn/GaN-based HEMTs, MISFETs and HBTs. Circuit types reviewed include power and low-noise amplifiers. Nitride technology is also investigated for mixer and switch applications. [C1777]

#### "Advances in III-V transistors (HEMTs and HBTs) for mm-wave applications"

This paper reveals state-of-the-art performance capabilities and projections for the AlGaIn/GaN-HEMT and AlGaIn/GaN-HBT devices for mm-wave applications. Wide band gap, appropriate doping impurities, and strong atomic bonds make these III-V nitride materials most attractive for microwave devices. Research studies performed by the author indicate that the nitride-based GaN-HEMTs and -HBTs when fabricated on silicon carbide substrate are capable of providing highest power density and power-added efficiency (PAE) at mm-wave frequencies. Deployment of a group III-V material with wide gap band (3.49 eV) and silicon carbide (6H-SiC) substrate with high room-temperature thermal conductivity close to 4.5 W/cm.<sup>2</sup>C is necessary for the development of high-power, high-efficiency GaN-HEMT and -HBT devices operating at mm-wave frequencies. Device reliability under high operating temperatures is strictly dependent on the thermal conductivity of the GaN film and substrate used. Note the operating voltages of GaN devices are five to ten times of those for GaAs devices. [C1778]

#### "Switched-mode high-efficiency Ka-band MMIC power amplifier in GaAs pHEMT technology"

A highly efficient monolithically integrated class-E power amplifier for the 22-25 GHz range is presented. The circuit is fabricated with a 0.12  $\mu$ m GaAs pHEMT process using coplanar waveguide technology. Careful selection and design of the load network is crucial for obtaining high efficiency. Measurement results show a peak power added efficiency of more than 42% at 23 GHz from a 2.2 V supply. To the authors' knowledge, this is the highest power added efficiency for class-E amplifiers at Ka-band reported up to date. [C1779]

#### "Characteristics of low noise 800MHz amplifier at cryogenic temperature"

Low noise amplifiers (LNA) have been designed and developed with high performance at cryogenic temperature in CDMA superconducting receiver front end. The low noise amplifier has been characterized at liquid nitrogen temperatures. The frequency band is in the range from 780MHz to 880MHz using Agilent PHEMT which has low noise figure at cryogenic temperatures. The components were implemented with lumped elements, which can make the LNA for the miniaturization and reduce the load consumption of the cooler. In the frequency band of operation at 60K, the achieved noise figure (NF) is within 0.3 dB from the minimum NF of a single transistor, the power gain is about 17 dB, flat is within 1 dB, the maximum input VSWR<sub>in</sub> and output VSWR<sub>out</sub> are lower than 1.3 individually. [C1780]

#### "Design of 2 GHz quasi-lumped element oscillator"

This paper discusses the design of a quasi-lumped element PHEMT oscillator, operating at 2 GHz. The quasi-lumped element resonator, fabricated on an FR4 printed circuit board, which consists of an interdigital capacitor in parallel with a straight line inductor, was used as a stabilizing element in the feedback type oscillator configuration. The quasi-lumped element oscillator operated at 2.056 GHz and the output power was 9 dBm. The phase noise at 10 kHz offset frequency was measured as approximately -82 dBc/Hz. [C1781]

#### "Simulation of the temperature injection PHEMT"



A new microwave device model is brought out and simulated, which is called TI-PHEMT. The maximum extrinsic transconductance at high temperature increases significantly and therefore the microwave performance of HEMT at high temperature is increased. A new concept "temperature injection" is put forward to explain the reason.

[C1782]

#### "Analysis of microwave X-band HEMT limiters based on self-limiting effect"

In this paper the self-limiting effect in microwave limiters using transistors with Schottky junction was investigated. The mathematical analysis how the input power detection influences on output power characteristic was presented. The analysis was done on the basis of the transistor IV curves. The calculations and measurement results of a realized limiter circuit was also presented. [C1783]

#### "High linearity power amplifier for PHS base station using a 50 mm AlGaAs/InGaAs/GaAs PHEMT"

A high linearity, high efficiency 1.9 GHz power amplifier sub-system using a 50 mm AlGaAs/InGaAs/GaAs PHEMT for PHS 500 mW base station is demonstrated. Under 10 V and 3.8 A bias condition, the output stage amplifier has achieved 12.5 dB small-signal gain, 43.7 dBm P<sub>1dB</sub> with 43% PAE and 44 dBm saturated output power with 41% PAE. For the amplifier sub-system, the ACPR at 600 KHz and 900 KHz offset from 1.906 GHz when operating at 38.5 dBm output power with pi/4-DQPSK signal are better than 75 dBc and 79 dBc, respectively. [C1784]

#### "In<sub>0.425</sub>Al<sub>0.575</sub>As/In<sub>0.65</sub>Ga<sub>0.35</sub>As metamorphic HEMT on GaAs"

A  $\delta$ -doped In<sub>0.425</sub>Al<sub>0.575</sub>As/ InGaAs metamorphic high electron mobility transistor (MHEMT) has been fabricated successfully and demonstrated. The In<sub>0.425</sub>Al<sub>0.575</sub>As Schottky layer provides good breakdown voltage due to larger energy-gap than that of In<sub>0.52</sub>Al<sub>0.48</sub>As. Experimentally, a high extrinsic transconductance of 277 mS/mm with V<sub>DS</sub>= 2 V and a high drain-source saturation current density of 484 mA/mm with V<sub>GS</sub>=0 V are obtained for a 0.65 $\times$ 200  $\mu$ m<sup>2</sup> device at 300 K. Due to good carrier confinement in the channel layer, good pinch-off characteristic can be achieved. The measured  $f_T$  and  $f_{max}$  for a 0.65  $\mu$ m gate device are 60.5 and 108.5 GHz at V<sub>DS</sub>= 2 V and V<sub>GS</sub>= -1.5V. The NF<sub>min</sub> is 0.93 dB at 2.4 GHz, and the associated gain is 23.1 dB.

[C1785]

#### "A 3.5GHz 2W MMIC power amplifier using AlGaAs/InGaAs/GaAs PHEMTs"

A 3.3-3.8GHz 2W MMIC power amplifier using AlGaAs/InGaAs/GaAs PHEMT for wireless local-area network and multi-channel multipoint distribution service applications is demonstrated. This two-stage amplifier is designed to match fully a 50 $\Omega$  input and output impedance. With dual-bias configuration, the amplifier possesses a 30.4dB small-signal gain, and a 34dBm 1-dB gain compression power with 37.1% power-added efficiency. Moreover, high linearity with a 41.5dBm third-order intercept point at a frequency of 3.5GHz is obtained. [C1786]

#### "110GHz high-gain flip-chip InP HEMT amplifier with resin encapsulation on an organic substrate"

First Page of the Article [C1787]

#### "Broadband HEMT-based frequency tripler for use in active multi-harmonic load-pull system"

First Page of the Article [C1788]

#### "The temperature characteristics of AlGa<sub>N</sub>/Ga<sub>N</sub> double heterostructure HEMTs"

AlGa<sub>N</sub>/Ga<sub>N</sub> double heterostructure high electron mobility transistors (DH-HEMT's) with a 2.0  $\mu$ m gate length and a 4  $\mu$ m channel length, exhibiting good temperature characteristics, have been demonstrated. The maximum drain current  $I_{ds}$  and extrinsic transconductance  $G_m$  are 1300 mA/mm 235 mS/mm, 85.0 mA/mm 174 mS/mm, and 475 mA/mm, 95 mS/mm, respectively at T = -194°C, 20°C and 400°C. The temperature coefficient of  $I_{ds}$  and  $G_m$  are -1.4 mA/°C and 0.24 mS/°C respectively. [C1789]

#### "Investigation on the sources of 2DEG in Al<sub>x</sub>Ga<sub>1-x</sub>N/GaN HEMT"

The AlGa<sub>N</sub>/Ga<sub>N</sub> HEMTs have many advantages for high frequency and high power applications because of its unique material properties. In this paper, AlGa<sub>N</sub>/Ga<sub>N</sub> HEMT has been investigated through computer simulation including spontaneous and piezoelectric polarization charges. By self-consistently solving the Schrodinger-Poisson equations, the information of electron distribution, density of 2DEG and electric field are obtained. In addition, the electronic tunneling probability of wz-GaN induced by strong interface electric field is discussed.

The simulation result shows that the tunneling charge in GaN channel layer is an important source of 2DEG besides the unintentional donor impurity in GaN channel layer and the ionized donor in AlGaIn barrier layer. Moreover the ratio of tunneling charges to 2DEG increases with the improvement of Al composition. [C1790]

#### "Recent advances in CDMA power amplifier module developments"

In this paper, the recent advances of CDMA power amplifier module developments for wireless handset applications are reviewed. Technology choices among GaAs, SiGe and PHEMT for linear PA designs are compared. The trade-offs of circuit design and module approaches are discussed in detail. The measured performances of some representative state of the art power amplifier modules are presented. The high integration of more front-end components and functionalities into the power amplifier module and the increasing demand for high linear efficiency at lower output power has become a widely acceptable trend. [C1791]

#### "High yield, high uniformity, high performance 50 nm T-gate In<sub>0.52</sub>Al<sub>0.48</sub>As/In<sub>0.70</sub>Ga<sub>0.30</sub>As HEMT process"

50 nm T-gates InP high electron mobility transistors (HEMTs) with a 70% indium channel were fabricated using a very robust fabrication process based on a novel UVIII/LOR/PMMA resist stack e-beam lithograph technology and on a "digital" gate recess technology. A typical device exhibited a gm<sub>0f</sub> 1400 mS/mm and an f<sub>tof</sub> 420 GHz. A source and drain saturation current (IDSS) uniformity of 40 A/mm, a threshold voltage uniformity of 10 mV and a functional yield of 96% were also achieved. [C1792]

#### "Studies of high field transport in GaN/AlGaIn heterostructures"

Experimental studies have been performed on the velocity-field characteristic of AlGaIn/GaN heterostructures. A pulsed voltage input (with a 10 ns pulse width) in combination with a four-point measurement was used in a 50 Ω environment to determine the drift velocity of electrons in the two-dimensional electron gas as a function of the applied electric field. These measurements show an apparent saturation velocity near 3.1 × 10<sup>7</sup> cm/s, at a field of 140 kV/cm. A comparison of these studies shows that the experimental velocities are close to previously published simulations based upon Monte Carlo techniques. Local inhomogeneities in the electric field are discussed as possible mechanisms for the slightly lower value of the velocity as compared to the simulation. [C1793]

#### "Instability of the induced potential distribution in undoped AlGaIn/GaN HEMTs and SiC transistor structures"

In this work, we discuss the results of investigation of potential distribution instabilities in undoped AlGaIn/GaN HEMTs and SiC transistor (FET) structures due to charge changes on the structure surface. An analysis of the state effects influence in the top layer of a passivated silicon nitride film reveals the possibility of the "memory effect" appearance due to electrons tunneling from an active area to different states in the silicon nitride film and AlGaIn layer. All considerations are followed by device characterization. A technological process for silicon nitride film deposition and a precision method of hydrogen bond concentration measurement by FTIR were developed to carry out experiments with a high accuracy. [C1794]

#### "InP-based IC technologies for 100-Gbit/s and beyond"

The research and development of InP-based devices and integrated circuits (ICs) are driven by applications in millimeter-wave wireless and broadband optical fiber communications systems. This paper describes recent progress in our InP-based HEMT and HBT devices, IC and optoelectronic IC (OEIC) technologies, measurement instruments, and discusses technical issues for future 100-Gbit/s class optical communication IC technologies. [C1795]

#### "High-speed series-connected voltage-balancing pulse driver using InP HEMTs"

A series-connected voltage-balancing circuit configuration can output a voltage proportional to the number of series-connected transistors. This paper presents this type of driver employing direct-coupled current switch architecture with a high-driving-capability input buffer and 0.1-μm InP HEMTs. By connecting two HEMTs in series the driver can output 3.6-V<sub>pp</sub> voltage swing, which is 1.6-times as high as the voltage that can be output by a single HEMT. The rise and fall times of the driver decrease from 33 to 16 ps and from 37 to 16 ps, respectively, by employing the input buffer. These short rise and fall times enable the driver to output clear 10-Gbit/s eye opening. [C1796]

### "High performance of W-band MMICs using 60 nm InGaAs HEMT technology"

A W-band coplanar wave-guide MMIC (a mixer, an oscillator and an ultra broad-band distributed amplifier) has been successfully developed by 60 nm gate length InGaAs HEMT technology. 60 nm gate length was defined by Si<sub>3</sub>N<sub>4</sub>/SiO<sub>2</sub>sidewall process. The device exhibits good DC and microwave characteristics of V<sub>th</sub>= -0.65 V, breakdown voltage = -4.1 V, extrinsic G<sub>m,max</sub>= 1.15 S/mm, f<sub>T</sub>= 250 GHz and f<sub>max</sub> of 263 GHz. A mixer exhibits conversion loss of 7 dB with 94 GHz LO signal and 90 GHz RF signal. An oscillator exhibits output power of -4 dB at 96 GHz. A broadband distributed amplifier achieves small signal gain of 6.6 dB over 0.4 110 GHz.

[C1797]

### "MSM varactor diodes based on AlGaIn/GaN/SiC HEMT layer structures"

First Page of the Article [C1798]

### "2004 International Conference on Indium Phosphide and Related Materials. 16th IPRM (IEEE Cat. No.04CH37589)"

{no data available} [C1799]

### "0.15 μm gate length MHEMT technology for 77 GHz automotive radar applications"

The 0.15 μm gate-length power metamorphic HEMTs (MHEMT) with wide head T-shaped gate has been fabricated and the DC, and microwave performance of the device were characterized. The MHEMT device shows the DC output characteristics having an extrinsic transconductance of 740 mS/mm and a threshold voltage of -0.75 V. The f<sub>T</sub> and f<sub>max</sub> obtained for the 0.15 μm Ч 100 μm MHEMT device are 150 GHz and 240 GHz, respectively. A MMIC 77 GHz 3-stage amplifier is reported in this paper. This MMIC chip demonstrated a measured small signal gain of over 12 dB from 70 GHz to 79 GHz with 7 dBm output power at 1 dB compression. The maximum small signal gain is above 13.5 dB from 77 to 78 GHz. This chip is fabricated using 0.15 μm MHEMT process based on 4-inch substrate. This MMIC chip size is 1.7 mm Ч 2 mm. This MMIC amplifier chip is suitable for the 77 GHz automotive radar systems and related transmitter applications in W-band. [C1800]

### "Methodology to compare on-state breakdown loci of GaAs FET's"

On-state breakdown loci of three technologies (power PHEMT, PHEMT and MESFET) have been measured using gate-current extraction techniques. We present a precise understanding of the correlation between the on-state breakdown voltage (BV on-state) locus and the reverse I<sub>gs</sub>-V<sub>gs</sub> characteristics. From the comparison of I<sub>gs</sub>-V<sub>gs</sub> characteristics, this study has allowed establishing a methodology to compare BV-on state of the devices under test. We have found that for technologies with impact ionization occurring at pinch off, such as the PHEMT technology with a high leakage gate current, the on-state breakdown locus presents a pronounced "exponential" shape. On the contrary, a technology with high impact ionization component in the gate current, such as the PPHEMT technology, presents a shape of the on-state breakdown locus rather "hyperbolic". We assess that technologies with impact ionization occurring at pinch off such as the PHEMT and PPHEMT present a more "hyperbolic" shape of the on-state breakdown locus than technologies with impact ionization occurring in open channel regime such as the MESFET. [C1801]

### "Degradation mechanisms of GaAs PHEMTs in high humidity conditions"

We have studied the degradation mechanism of AlGaAs/InGaAs pseudomorphic HEMTs (PHEMTs) under high humidity conditions. The samples show a decrease in maximum drain current (I<sub>max</sub>) and positive shift in threshold voltage (V<sub>th</sub>). It was found that the V<sub>th</sub> shift depends on gate orientation, caused by a piezoelectric effect due to stress change near the gate. Cross-sectional TEM images from the deteriorated devices reveal the existence of a damaged recess surface region and a peeling of the passivation film (PF). At the interface between the PF and AlGaAs surface, diffusion of Ga, As and Al into the PF was observed by SIMS. From these results, degradation of the PHEMT has two main mechanisms: positive shift in V<sub>th</sub> due to stress change under the gate which might be caused by the peeling of the PF, and a decrease in I<sub>max</sub> due to surface degradation at AlGaAs recess regions caused by diffusion phenomena of Ga, As and Al. The pre-deposition treatment effectively suppresses the degradation of PHEMTs under high humidity without degradation of high frequency performance.

[C1802]

### "Current instabilities and deep level investigation on AlGaIn/GaN HEMT's on silicon and sapphire substrates"

In this paper, we present static measurements and defect analysis performed on AlGaIn/GaN/Si or Al<sub>2</sub>O<sub>3</sub>HEMTs. Id-V<sub>ds</sub>-T, Id-V<sub>gs</sub>-T and Ig-V<sub>gs</sub>-T characteristics show anomalies (leakage current, degradation in saturation current, Kink effect, distortions on Id-V<sub>d</sub> characteristics in saturation region,... etc). These anomalies on output characteristics changes when we vary measurement conditions (temperature, polarisation, stress...). Deep defects analysis performed by capacitance transient spectroscopy (C-DLTS), frequency dispersion of the output conductance (G<sub>ds</sub>(f)) and random telegraph signal (RTS) prove the presence of deep defects with activations energies ranging from 0.05 eV to 1.8 eV. The presence of G-R centers acting like traps at the interface GaN/AlGaIn is confirmed by Ig-V<sub>gs</sub> and RTS measurements. The localization and the identification of these defects are presented. Finally, the correlation between the anomalies observed on output characteristics and defects is discussed and a little comparison between Al<sub>2</sub>O<sub>3</sub> and Si HEMTs is presented. [C1803]

#### "0.15 μm PHEMT 80 Gb/s selector"

To avoid the drawbacks of conventional selectors, a newly designed one is presented. In this chip, lumped devices are replaced by distributed ones, for example transmission lines instead of inductors. The bottleneck in the realization of the high speed selector is broken through by designing a third order Butterworth filter. The problem in input matching is also solved by using the same type of filter. It is guaranteed that this chip, tapped out with 0.15 μm PHEMT (pseudomorphic high electron mobility transistor) technology, can work up to 80 Gb/s by analyzing the results obtained at 80, 90, and 100 Gb/s. [C1804]

#### "The effect of elevated temperature lifetest on low frequency noise performance in GaAs PHEMT dual gate MMICs [CLNA example]"

The dual gate layout configuration has become a versatile approach for compact and high performance MMIC design for commercial, and military/space applications. In this paper, we describe a method that was developed to lifetest compact (0.81 mm<sup>2</sup>) dual gate GaAs PHEMT low noise amplifiers (LNAs) operating from DC to 1 GHz. The objective of the lifetest is to evaluate the effect of elevated temperature on low frequency noise performance from 10-40 MHz. The results exhibit a decrease of noise figure (NF) at 10-40 MHz (approximately 0.25 to 0.5 dB) in a dual gate LNA subjected to lifetest at T<sub>amb</sub> of 200°C. This might be attributed to the gate leakage current reduction at either the interface of gate metal-AlGaAs or nitride-AlGaAs, thus possibly reducing the effect of generation-recombination (primary origin of low frequency noise). On the other hand, the change of noise figure at frequencies beyond 100 MHz is not noticeable. In summary, we have demonstrated a method to effectively lifetest a compact and high performance MMIC designed with a dual gate configuration. [C1805]

#### "Transient analysis of nonlinear microwave circuits using small-signal scattering parameters"

A transient analysis method for nonlinear microwave circuit analysis is described in this paper. S-parameter microwave circuit theory and measurement-based small-signal scattering parameters of nonlinear devices are used directly to construct the large signal response of the circuits. This consistent modeling and analysis approach retains all the frequency-dependence information of the measured small-signal parameters. The method is applied to predict the large signal performance of a discrete AlGaIn/GaN high electron mobility transistor (HEMT), biased in the common source amplifier mode. Reasonable agreement between the simulated and measured results is obtained. This method does not have limitations on the number of input carrier frequencies or the total number of frequencies. It is expected to be a useful and efficient tool in waveform engineering applications. [C1806]

#### "An antenna switch MMIC using E/D mode p-HEMT for GSM/DCS/PCS/WCDMA bands application"

A monolithic antenna switch IC using enhancement and depletion (E/D) -mode AlGaAs/InGaAs pseudomorphic high electron mobility transistors (p-HEMTs) has been developed for GSM/DCS/PCS/WCDMA band digital mobile communication systems. This antenna switch MMIC achieves a low insertion loss and small chip size using a single pole double throw (SPDT) switch for GSM and single pole 4 throw (SP4T) switch for other band configurations, as well as internal logic circuits with an E/D mode p-HEMTs process. This MMIC achieves an insertion loss of 0.21 dB at 915 MHz and 0.53 dB at 1785 MHz. The isolation to the RX ports is more than 30 dB, and the input power at 0.1 dB compression is over 36 dBm at +2.7 V operation. [C1807]

#### "Novel high gain and broadband GaAs MMIC distributed amplifiers with traveling-wave gain stages"

Using the concept of traveling-wave gain stages, novel GaAs MMIC distributed amplifiers are designed to achieve high-gain over several octaves of bandwidth. The cascaded single-stage distributed amplifiers (CSSDAs)



are used as traveling-wave gain stages to improve the gain performance of conventional distributed amplifier (CDA). By selecting the low pass filter (LPF) topology for the CDA and CSSDA and tuning the gain shape of CDA and CSSDA, a wide-band performance of the broadband amplifier, called CDA-CSSDA-2 is obtained. The CDA-CSSDA-2 achieves  $22 \pm 1.5$  dB small signal gain from 0.1 to 40 GHz with a chip size of  $1.5 \times 2$  mm<sup>2</sup>. This distributed amplifier produces gain-bandwidth product (GBW) of 503 which is the highest among all GaAs based distributed amplifiers. The flat group delay of the proposed distributed amplifier also proves the feasibility of this methodology for digital optical communications and broadband pulse applications. [C1808]

#### "61st Device Research Conference. Conference Digest (Cat. No.03TH8663)"

First Page of the Article [C1809]

#### "The effect of dispersion on the bandwidth of distributed amplifier"

This paper presents a new GaAs P-HEMT distributed amplifier that employs a coplanar waveguide (CPW) as a transmission line taking into account the effect of CPW dispersion on the performance of the amplifier. It is shown that a wide-band amplifier can be designed if the effect of CPW dispersion is kept as minimum as possible. The CPW is first modeled with a pi-section and the parameters (capacitance and inductance) of this model were obtained using its S-parameters with ADS software. From the capacitance and inductance per unit length of CPW line, the length of CPW is calculated to provide required characteristic impedance of artificial transmission line for distributed amplifier. The method of moment (MOM) is used to analysis the dispersion of CPW line. By removing the substrate between the signal and ground metal which makes CPW inductive and less dispersive, a 20% bandwidth enhancement and 17% size reduction were achieved which are of great important for MMIC applications. [C1810]

#### "Time-domain characterization of nonlinear operation of an AlGaIn/GaN HEMT"

First Page of the Article [C1811]

#### "Single-ended amplifier that substantially improves PAE and ultra-broadband performance"

A single-ended amplifier with a simple reactive matching is shown to provide stable operation with substantially improved amplifier power-added efficiency (PAE) (>30%) across an ultra-broadband frequency range (2-18 GHz). The amplifier employs a Double Pseudomorphic High Electron Mobility Transistor (DPHEMT) power device. [C1812]

#### "Ku-band low noise amplifier with using short-stub ESD protection"

A Ku-band ESD-protected low noise amplifier is designed using 0.15μm pHEMT process. The input ESD protection is implemented with short-circuited stub. Since a short-circuited stub is used as an ESD protection as well as a matching element, there are no additional components and parasitic components associated with ESD protection. This endures 4400V (ESD tester limit) HBM test signal. The LNA has the noise figure of 1.24 dB and 24.5 dB gain at the frequency of 11.7-12.75 GHz. [C1813]

#### "Characterization of high electron mobility transistor under different temperatures"

The characteristics of high electron mobility transistor (HEMT) under different temperatures are studied. The study includes the effect of temperature on the Fermi level potential, sheet carrier concentration, and electron mobility. Also, the I/V characteristic is studied at different temperatures. Numerical results show that the drain current increases with increase in temperature. [C1814]

#### "New results on MMIC six-port's used in Ka band direct conversion receivers"

New results obtained on two Ka band Monolithic Microwave Integrated Circuit (MMIC) six-port junction circuits realized in GaAs PHEMT technology at TriQuint Texas Foundry are presented in this paper. Comparative results of simulated and measured S parameters are shown for both designs. The proposed MMIC six-port circuit is used to realize the QPSK demodulator of a Ka band direct conversion receiver. [C1815]

#### "A multilayer active hybrid-ring using ground-slot coupling technique"

A ground-slot coupling technique is applied to design a novel multilayer active hybrid-ring power divider. The prototype consists of three ground slots to couple signal between circuit layers, and two single-stage HEMT amplifiers to boost the coupled signal. It is tested in C-band with 40% -3 dB bandwidth. At 5 GHz center

frequency, it has 8 dB small-signal gain and 10 dBm output P1 dB. [C1816]

### "Large area GaN HEMT power devices for power electronic applications: switching and temperature characteristics"

Large area AlGaIn/GaN high electron mobility transistors (HEMT) for power electronic applications have been fabricated. These power devices offer lower on-resistance and higher switching speed than SiC devices due to higher electron mobility and high channel charge density achieved by a heterojunction. The GaN epi-layers were grown on semiinsulating 4H-SiC substrate by metal organic chemical vapor deposition (MOCVD) technique. The device structure was grown on SiC substrates due to its high thermal conductivity. The devices have been optimised with respect to electron mobility, sheet concentration, voltage breakdown, on-resistance and dispersion. Voltage breakdown of 1300 V was achieved on small devices while breakdown in the range 600-900 V was achieved on packaged devices depending on the number of devices that have been paralleled. The power device figure of merit  $VBR_2/R_{on}=9.94 \times 10^8 [V^2 \cdot \Omega^{-1} cm^{-2}]$ , where  $VBR_2$  is the breakdown voltage and  $R_{on}$  is the on-resistance, is the highest among any reported switching devices. Switching losses of large area 600 V/2.5 A power devices were measured using resistive and inductive loading. Switching times of 2 ns. The static and dynamic characteristics of GaN HEMT devices were also measured as a function of temperature up to 200°C. Finally, the temperature distributions in the active device area were measured using Raman spectroscopy (pyrospectroscopy). This technique can be used to measure temperatures with a spatial resolution of 1-2  $\mu m$ . Device temperatures from both the active areas and SiC substrates have been measured. [C1817]

### "Design of a 20-to-40 GHz bandpass MMIC amplifier"

A millimeterwave bandpass MMIC amplifier, which integrates both features of gain amplifier and bandpass filter, is presented. A synthesis method for such amplifier is developed from the image-parameter filter theory. By employing the proposed bandpass amplifier in a receiver, the bulky of chip filter may not be required. An experimental chip fabricated by 0.1  $\mu m$  PHEMT shows 14.2dB gain from 20 to 40 GHz and 60-dB attenuation below 7 GHz and above 60 GHz. This confirms the proposed method and shows the feasibility of the function integration of gain amplifier with bandpass filter in the millimeterwave range. [C1818]

### "Millimeter-wave MMIC switches with pHEMT cells reduced parasitic inductance"

High isolation millimeter-wave switches have been successfully developed using a newly developed line unified shunt pHEMT structure, which is effective to reduce parasitic inductance of its short circuit. The developed V-band SPDT switch shows an isolation of greater than 40 dB and an insertion loss of 1.8 dB at 60 GHz, and the W-band SP3T switch shows an isolation of greater than 35 dB and an insertion loss of 2.5 dB at 77 GHz. Input and output return losses are better than 12 dB in ON-state. These performances of high isolation and low insertion loss are the best among V-band and W-band pHEMT MMIC switches. The switches consume no DC power, and require no complex off-chip bias circuitry. [C1819]

### "C-band linear resistive wide bandgap FET mixers"

In this paper the performance of two C-band resistive FET mixers are presented and compared. The first mixer uses a SiC-MESFET as a mixing element and the second uses an AlGaIn/GaN-HEMT. The mixers have a minimum conversion loss of 7.8 dB and 7.3 dB respectively. The maximum third-order input intercept points are 30 dBm and 36 dBm respectively; for LO drives of 23 dBm and 30 dBm. [C1820]

### "A 100-Gbit/s 2:1 multiplexer in InP HEMT technology"

In this paper, we describe a 100-Gbit/s 2:1 multiplexer (MUX). In order to suppress the degradation of signals and to increase the operation speed, we designed interconnections for the circuit using impedance matching techniques. We fabricated the MUX with 0.13- $\mu m$  InP HEMT technology, which has a cutoff frequency of 175 GHz. By using this design, we succeeded in 100-Gbit/s operation of the MUX and obtained clear eye waveforms. We also developed a V-conductor module for the circuit, and achieved 80-Gbit/s operation. [C1821]

### "1.4-W 50-Gbit/s InP HEMT 1:4 demultiplexer IC with a multi-phase clock architecture"

High-speed and low-power operation of a 1:4 demultiplexer IC with a multi-phase clock (MPC) architecture is reported. The architecture features four parallel latch lines and a toggle flip-flop (TFF) that generates a four-phase clock. The IC, which was fabricated using InP HEMTs, exhibited 50-Gbit/s error-free operation with a power consumption of 1.42 W. Compared to a conventional tree-type InP HEMT 1:4 demultiplexer IC, the IC with the MPC architecture operates at the same operating speed with only one-quarter the power consumption. [C1822]

### "Single ended to differential MHEMT transimpedance amplifier with 66 dB- $\Omega$ differential transimpedance and 50 GHz bandwidth"

In this paper, we demonstrate a single ended to differential transimpedance amplifier (TIA) with 66 dB $\Omega$  transimpedance gain, a 50 GHz 3-dB bandwidth and up to 700 mVp-p differential output voltage, fabricated in a 6-inch MHEMT process. The state-of-the-art gain-bandwidth product of this amplifier ( $>3$  THz), combined with its small chip size (1.9 $\times$ 1.1 mm<sup>2</sup>), high sensitivity and low power consumption ( [C1823]

### "A zero-bias single-device balanced E-PHEMT mixer with conversion gain for RFID applications"

A zero-bias single-device singly-balanced mixer, using an enhancement mode pseudomorphic HEMT (E-PHEMT) is proposed. The mixer takes advantage of the slightly positive pinch-off voltage in this kind of device, for providing gain conversion with an acceptable linearity and avoiding the use of DC bias. A lab model has been designed to be used in an RFID tag, where a low frequency local data signal is up-converted to the 900MHz frequency band, once the device is excited with an interrogating carrier. [C1824]

### "Compact high-gain lumped differential 40 Gb/s driver amplifiers in production 0.15 $\mu$ m PHEMT technology"

High-performance and very compact 40 Gb/s driver amplifiers were realized in mature 0.15  $\mu$ m depletion PHEMT technology. The 3-stage lumped differential drivers feature a large differential 40 Gb/s output swing of up to 7.5 Vpp, RMS jitter of less than 800 fs, rise and fall times of less than 10 ps and more than 27 dB gain. The small size (1.4 $\times$ 1.7 mm) and ability to have DC coupled in- and output, enable compact and cost-effective optical 40 Gb/s long-haul transmitters with system grade NRZ and RZ eye diagrams. [C1825]

### "High-power and high-efficiency AlGaIn/GaN HEMT operated at 50 V drain bias voltage"

We describe high power 70 W CW operation at 52 V drain bias voltage (Vds) using 24-mm gate-periphery AlGaIn/GaN HEMTs on SiC substrate. A 48 W output power with the drain efficiency of 60% was also obtained at Vds of 50 V under the efficiency-matched condition near class-B. At 40 V, the drain efficiency reached 68%. Vds dependence of third order-intermodulation (IM3) was also characterized at Vds up to 50 V. This is the first report about IM3 profile characterization for a large gate-periphery device at Vds of 50 V. We also investigated RF-stress life test at Vds up to 40 V. The AlGaIn/GaN HEMT in this study exhibited good reliability over 100 h. [C1826]

### "The high voltage/high power FET (HiVP)"

A new device configuration is presented: the High-Voltage/High-Power device (HiVP). This original configuration can dramatically improve the power and decrease the complexity of designing power amplifiers, leading to low cost and higher power. The HiVP uses a new concept, never achieved before, to simultaneously bias a semiconductor device at high voltage while maintaining an optimum output matching impedance close to 50 Ohms. The concept could be applied to many device technologies such as the GaAs MESFET, HEMT, and the Si MOSFET, to combine the power of several devices to achieve higher power output over broader bandwidth. [C1827]

### "A high performance V-band monolithic quadruple sub-harmonic mixer"

In this paper, we present a high performance V-band quadruple sub-harmonic mixer monolithic circuit which is designed and fabricated for the millimeter wave down converter applications. While the typical sub-harmonic mixers use a half of fundamental frequency, we adopt a quarter of the fundamental frequency. The proposed circuit is based on sub-harmonic mixer with APDP (anti parallel diode pair). Upon the typical mixer design, additional stubs are placed with the modification of original stub length. And the 0.1  $\mu$ m pseudomorphic high electron mobility transistors (PHEMTs) providing better gain are positioned to each port. Used lumped elements at IF port, it provides selectivity of IF frequency, and increases isolation. Maximum conversion gain of 0.8 dB at a LO frequency of 14.5 GHz and at a RF frequency of 60.4 GHz is measured. Both LO-to-RF and LO-to-IF isolations are higher than 40 dB. These conversion gain results and isolation characteristic are the best performances reported among the quadruple sub-harmonic mixers operating in the V-band millimeter wave frequency thus far. [C1828]

### "40 GHz MMIC driver of electro-absorption modulator for high-speed optical pulse generation"

For the next generation of high-speed optical communications (4 $\times$ 40Gbit/s OTDM), the availability of very short

pulse sources is crucial. This work deals with optical pulse sources using electro-absorption modulators (EAM). With the aim of matching a 100 $\mu$ m-long EAM, a 40GHz MMIC driver was designed and fabricated using a GaAs PHEMT 0.15 $\mu$ m process. To handle the actual electro-optical objectives of the Driver+EAM function (short pulse 5ps, high extinction ratio 30dB) we have developed a specific design method, which includes modeling techniques of EAM and CAD-oriented electro-optical design rules. Preliminary optical measurements of the first assembled optical modules (with & without driver) show that the driver leads to more than 10dB improvement for the electro-optical response of the EAM pulse source in the 39.7-42GHz band. [C1829]

#### "A millimeter-wave harmonic optoelectronic mixer based on InAlAs/InGaAs metamorphic HEMT"

We investigate the InAlAs/InGaAs metamorphic HEMT on GaAs substrate as a harmonic optoelectronic mixer. The fabricated metamorphic HEMT simultaneously performs photodetection of 1.55  $\mu$ m lightwaves and harmonic optoelectronic up-conversion into the millimeter-wave band. By changing the bias conditions of the HEMT, the harmonic optoelectronic mixing efficiency can be selectively enhanced while suppressing undesired mixing components. The metamorphic HEMT as a harmonic optoelectronic mixer is a promising candidate that can simplify the base station architecture in fiber-optic millimeter-wave transmission systems. [C1830]

#### "InP HEMTs: physics, applications, and future"

In this paper, we review our recent results obtained for InP-based HEMTs. We have developed several fabrication techniques, and obtained an ultrahigh fToF of 562 GHz for a 25 nm long gate pseudomorphic InAlAs/InGaAs HEMT. We also discuss possible applications of our HEMTs and the future of InP-based HEMTs. [C1831]

#### "On the investigation of gate metal interdiffusion in GaAs HEMTs"

Ti interdiffusion of Ti/Pt/Au gate metal stacks in 0.15  $\mu$ m GaAs HEMTs subjected to high-temperature lifetest has been physically identified using STEM technique. Further EDX analysis substantiates the intermetallic formation of Ti-AlGaAs and Ti sinking into the AlGaAs Schottky barrier layer. Ti interdiffusion reduces the separation of the gate metal and InGaAs channel, thus leading to the evolution of a slight Gm increase, positive shift of pinchoff voltage, and S21 increase during the initial stage of lifetest. The STEM was further used to correlate Ti-InGaAs-channel-separation and Ti-sinking depth with a device parameter, Vgs-an indicator of Ti-InGaAs-channel-separation. It has been discovered that Ti-sinking-depth is insensitive to Vgs. However, as Ti interdiffuses, the separation of, the gate metal and InGaAs channel is decreased, therefore affecting the Idss degradation rate. As a result, we observe the dependence of  $\Delta$ Idss on Vgs. The results provide insight into a critical parameter, Vgs, for optimizing reliability performance based on  $\Delta$ Idss. [C1832]

#### "A 0.5-3 GHz high linearity enhancement mode pHEMT mixer with square wave drive and sum terminating diplexer"

A 0.5-3 GHz high linearity single balanced mixer has been developed using 0.5  $\mu$ m enhancement mode pHEMT technology. Features of the design include an integral LO buffer amplifier-active balun with drive waveshaping and a sum terminating diplexer that work together to provide an input third order intercept point of +30 dBm from a drive level of only -3dBm. The ideal mixing device drive waveform provides very low conversion loss and excellent LO drive saturation characteristics. The mixer operates from a 3-5 V supply and consumes 21 mA. [C1833]

#### "Novel heterostructure MSM photodetectors for Gigabit Ethernet"

A key element in the field of sensors for short haul communications is the development of high performance photodetectors. Along this direction, we present here an accurate investigation of photodetectors based on AlGaAs/GaAs heterojunction structures. In these devices, the absorption region is in the GaAs layer where is formed, at the interface with AlGaAs, a two-dimensional electron gas (2-DEG). This HMSM (heterostructure metal-semiconductor-metal) photodetector contains an AlGaAs distributed Bragg reflector for detection at 850 nm. The beneficial effect of the 2-DEG in the GaAs absorption layer is evidenced by comparing samples with and without doping in the AlGaAs layer. We start from properties of the grown structure, and then we investigate the static and dynamic properties. Particularly, photocurrent spectra exhibit a 30 nm wide peak at 850 nm, while time response measurements give a bandwidth over 30 GHz. A combination of very low dark current and capacitance, fast response, wavelength selectivity, and compatibility with high electron mobility transistors makes this device especially suitable for Gigabit Ethernet applications. [C1834]

#### "The effect of the gate Schottky diode on pHEMT power amplifier performance"



This paper presents for the first time a practical systematic investigation into the effects of gate Schottky parameter values on large-signal amplifier performance. The use of a new Schottky diode model for a packaged pHEMT device shows significant improvements over the vendor supplied model when used in the non-linear characterisation of a class A power amplifier. Special emphasis is placed on the effect these values exhibit on the ability of the large-signal model to predict measured power amplifier characteristics including gain, output power, efficiency, linearity, ACPR and non-linear spectral regrowth. [C1835]

### "Development of 60 GHz front end circuits for high data rate communication systems in Sweden and Europe"

Recent results from a Swedish program for development of 60 GHz MMICs for high data rate communication links are presented as well as results from similar programs in Europe. A GaAs PHEMT technology has been used for the realization of front-end circuits such as mixers, amplifiers, frequency multipliers, IF-amplifiers with gain-control, and VCOs. The GaAs PHEMT technology proved to give excellent circuit results, with the exception of the VCOs. Different GaAs PHEMT based VCO-topologies such as common gate push-push Colpitt and balanced negative gm, optimized for low phase noise have therefore been studied extensively. The latest results proves that it is possible to design VCOs comparable with the best published HBT-based oscillators. The metamorphic HEMT technology can offer additional advantages such as lower power consumption and InP-HEMT performance at the cost of GaAs. Recent results on 60 GHz amplifiers and mixers based on this technology are presented. [C1836]

### "Degradation mechanism of PHEMT under large signal operation"

We have studied the degradation mechanism of AlGaAs/InGaAs pseudomorphic HEMTs (PHEMTs) under large signal operation. The output power of the PHEMT is degraded with increasing drain voltage ( $V_d$ ), temperature, and humidity. The deteriorated devices show a decrease of the maximum drain current ( $I_{max}$ ) around the knee voltage ( $V_k$ ) and an increase of the drain resistance ( $R_d$ ). Cross-sectional transmission electron microscopy (TEM) images from the deteriorated devices reveal the existence of a damaged recess surface region at the drain side of the device. In this damaged region, a significant amount of oxygen is detected by energy dispersive X-ray spectroscopy (EDX), analysis. The damaged recess region leads to a reduced carrier density that results in decreased  $I_{max}$  and increased  $R_d$ . We suggest that the damaged recess region is caused by an electrochemical reaction that correlates with electric field, temperature and humidity. We have developed a special surface treatment that is applied prior to the deposition of the passivation film on the recess surface. This treatment successfully suppresses output power degradation in these devices. We demonstrate highly reliable RF operation with less than 0.2 dB reduction in output power during 1000 hr at  $V_d=5$  V and  $T_{ch}=175^\circ\text{C}$ . [C1837]

### "A 2.3 V PHEMT power SP3T antenna switch IC for GSM handsets"

A high power GaAs pHEMT SP3T antenna-switch IC for GSM handsets has been developed With P1dB over 36 dBm, this switch IC features high harmonic rejection of 70 dBc at 900 MHz and 34 dBm, and at 1800 MHz and 32 dBm input power, both operating at 2.3 V and at +85C Insertion loss of 0.55 dB and 0.750, and isolation of greater than 25 dB at 900 MHz and 1800 MHz, respectively, are also achieved. The high performance attributes to the combination of pHEMT process and design techniques. [C1838]

### "Status, challenges, and future opportunities for compound semiconductor electronics"

Recent developments and future opportunities for compound semiconductor electronics for analog and mixed signal circuits for the Department of Defense (DoD) are reviewed. The realization of extremely high performance transistors, often uniquely enable by compound semiconductor materials, will be highlighted. [C1839]

### "Progress in GaAs metamorphic HEMT technology for microwave applications"

This paper reviews recent progress in the development of GaAs metamorphic HEMT (MHEMT) technology for microwave applications. Commercialization has begun, while efforts to further improve performance, manufacturability and reliability continue. We also report the first multi-watt MHEMT MMIC power amplifiers, demonstrating up to 3.2W output power and record power-added efficiency (PAE) at Ka-band. [C1840]

### "Circuit modeling of low-noise microwave transistors: its role in supporting a complete device characterization"

This paper discusses the role of microwave low-noise transistor modeling at a circuit level to reduce characterization requirements, as from the author's experience in the field. It is well known that a complete procedure involving measurements of small-signal and noise parameters vs. frequency, bias and temperature

conditions is a hard task. The appropriate use of a linear circuit model equipped with noise sources offers a viable alternative to complex and time-consuming experimental tests aimed at extracting a large amount of information on the device performance. This work reports the results regarding the complete characterization of high electron mobility transistors (HEMT) which offer outperforming values of noise figure and gain at microwave and millimeter-wave frequencies. [C1841]

#### "A robust approach for the direct extraction of HEMT circuit elements vs. bias and temperature"

The results of our most recent activity in the implementation of robust and easy-to-perform techniques for the extraction of reliable equivalent circuits for microwave transistors is presented. Our effort also led to the development of a compact software tool written in Agilent VEE language for totally automated measurement and direct model extraction. Its effectiveness has been tested at several bias and temperature points and the modeling results have been compared with those obtained by application of other procedures. This procedure can be adopted for both Schottky-gate devices (MESFET's, HEMT's) and insulated gate devices (RF MOSFET's, CMOS) since no direct polarization of the gate is requested. [C1842]

#### "10 Gb/s soliton generation for ULH transmission using a wideband GaAs pHEmt amplifier"

A novel technique of generating 10 Gb/s soliton data using a wideband GaAs pHEmt amplifier is demonstrated and applied in a 10G transmission experiment. Bit-error-rate better than FEC threshold is achieved over 4000km. [C1843]

#### "V-band fully-integrated TX/RX single-chip 3-D MMICs using commercial GaAs pHEMT technology for high-speed wireless applications"

This paper demonstrates fully-integrated V-band single-chip transmitter and receiver 3D MMICs for high-speed wireless applications. These 3D MMICs provide full RF functions, including an oscillator, even though they are very compact. The transmitter MMIC realizes more than 10 dBm output power at 57-60 GHz, while the receiver MMIC achieves 33 dB conversion gain and less than 6 dB noise figure at the same frequency range. The chip sizes of the transmitter and the receiver are 2.89 mm<sup>2</sup> and 5.04 mm<sup>2</sup>, respectively. The V-band fully-integrated MMICs promise much cheaper millimeter-wave RF equipment due to their high-integration level, compactness, and few interconnections for other components. [C1844]

#### "Temperature dependence of the current-voltage characteristics of AlGaIn/GaN HEMT"

In this paper, we report on the DC and gate-lag pulsed (200ns) I-V characteristics of GaN-based HEMTs with and without SiN passivation between 77 K and 300 K. [C1845]

#### "Generation of coherent GHz acoustic phonons in AlGaIn/GaN microwave field effect transistors"

In this paper, the presence of large amplitude GHz coherent phonons in GaN/AlGaIn microwave HEMTs, by detecting the phonons using a local reflective optical probe at near normal incidence to active device, tightly focused (1  $\mu$ m) and scanned in the vicinity of the source-gate-drain region. Estimates of the total spatially integrated vibrational energy released from the 2D gas suggests that a possibly significant fraction of the dissipative energy can be released from the HEMT into coherent phonons, providing a potential avenue for bypassing conventional thermal management schemes. [C1846]

#### "550 GHz- $\mu$ T pseudomorphic InP-HEMTs with reduced source-drain resistance"

In this paper, we adopted a pseudomorphic InGaAs channel to further boost the electron velocity and applied a new multi-layer cap structure to reduce source and drain parasitic resistances to realize even higher RF performance. [C1847]

#### "Self-heating effects in AlGaIn/GaN high-power HEMTs"

In this paper, self-heating effects are more pronounced in high-power AlGaIn/GaN HEMTs, which have demonstrated more than 10 times power densities. The elevated junction temperature caused by the self-heating effects degrade the available drain current and subsequently the output power due to reduced electron saturation velocity and low-field mobility. [C1848]

#### "Ka-band CW power performance by AlGaIn/GaN HEMTs on SiC"

In this paper, we report state of the art CW power results of 0.25- $\mu$ m gate length AlGaIn/GaN HEMTs at both 30

and 35 GHz. At a drain bias of 30V, the 200 $\mu$ m gate width devices showed a record power density of 4.13 W/mm with 23% of power added efficiency (PAE) and 5.5 dB of associated gain at 35 GHz, which represent the best power density and efficiency achieved by a solid-state devices at this frequency. [C1849]

#### "High power AlGaIn/GaN HEMTs grown by plasma-assisted MBE operating at 2 to 25 GHz"

In this paper, AlGaIn/GaN heterostructures grown by plasma-assisted MBE on semi-insulating 6H-SiC. Optimization of MBE growth conditions now allows for the routine production of heterostructures with a room temperature mobility of 1400cm<sup>2</sup>/Vs at a sheet density of 1.14 $\times$ 10<sup>13</sup>cm<sup>-2</sup>. We discuss heterostructure designs found to minimize RF dispersion. All power data reported is achieved without the use of a SiN surface passivation layer. [C1850]

#### "Effect of surface passivation on breakdown of AlGaIn/GaN HEMTs"

We have investigated the effect of surface passivation on breakdown by electrical characterization and electroluminescence (EL) measurements of AlGaIn/GaN HEMTs. [C1851]

#### "Self-heating effect on device characteristics of GaN/AlGaIn HEMTs: 2D Monte Carlo device simulation"

In this paper, the mechanism of the self-heating in the GaN/AlGaIn HEMT and its influence on the device performance theoretically by 2D Monte Carlo device simulation. Three different substrates (i.e., 6H-SiC, sapphire and Si) have been used and compared in this work. [C1852]

#### "High speed, low power electronics using Sb-based semiconductors"

In this paper the current status of the design, fabrication, and characterization of Sb-based HEMTs (6.05Am) and HBTs (6.2Am) in our group will be presented. [C1853]

#### "Frequency and breakdown properties of AlGaIn/GaN HEMTs"

AlGaIn/GaN heterostructure transistors show potential in high-frequency high-power applications because of their high breakdown voltages and high electron saturation velocities. The operating drain voltage, limiting the maximum RF output power, should be lower than breakdown voltage of the device. The frequency and breakdown properties of the AlGaIn/GaN heterostructure transistors have been studied. [C1854]

#### "AlGaIn-GaN HEMTs: material, device, circuit technology and applications"

In this paper recent progress in material, device and circuit technology of GaN based HEMT is discussed. We have also developed GaN HEMT hybrid amplifiers as well as MMICs, including air wedge and MIMC capacitors and resistors. [C1855]

#### "Scattering limitations on electron transit velocity in AlGaIn/GaN HEMTs"

The authors show that the high field electron transit velocity in normal AlGaIn/GaN HEMTs is only about a half of the highest value obtained under ideal conditions. The investigation of structures with AlN interbarrier, demonstrate new potentials for control and minimization of the effects caused by the electron deconfinement and the build-up of non-equilibrium longitudinal optical phonons and an increase in the drift velocity and in the response frequency. [C1856]

#### "Broad-band transimpedance amplifier for multigigabit-per-second (40 Gbps) optical communication systems in 0.135 $\mu$ m PHEMT technology"

This paper presents the design and characterization of a high-bandwidth transimpedance GaAs MMIC suitable for the 40 Gbps data transmission rate. The circuit was implemented on a well established MMIC PH15 process from United Monolithic Semiconductors (UMS) offering good yield, high performance and low cost per chip. The circuit presents a 49dB $\Omega$  gain, a low noise figure and wide bandwidth for input capacitances in excess of 100 fF. An analysis considering noise, stability and the influence of bondwire inductance on the overall circuit behaviour was performed. Input capacitance tolerance and output impedance matching conditions were also evaluated. On-wafer characterisation results are also presented and confronted with simulation data showing good agreement with simulated results. [C1857]

#### "Enhancement mode GaAs PHEMT LNA with linearity control (IP3) and phased matched mitigated

### bypass switch and differential active mixer"

A new front end IC has been designed using a single supply enhancement mode GaAs PHEMT 0.5  $\mu\text{m}$  process for WCDMA and other wireless applications. This front end has a single ended LNA, single ended in and differential out active balanced mixer with integrated LO, active balun, and buffer amplifier. The LNA also has CMOS logic controllable linearity (IP3) control and a phased matched mitigated bypass switch. The LNA draws 8.5 mA current when switched to high linearity mode and has 15 dB gain, 1 dB NF, -6 dBm IP1dB and 7.3 dBm IIP3. In low linearity mode, it draws 3.5 mA current and has 14 dB gain, 1.1 dB NF, -6 dBm IP1dB and 2 dBm IIP3. In LNA bypass mode, the total bypass loss is 10 dB I/O return loss. The mixer, with active balun and buffer amplifier, consumes 8 mA current and has 12 dB gain, 7 dB noise figure, 0 dBm IIP3 and provides a differential IF out with a differential impedance of about 1000 ohms. The above performance is measured at 2.14 GHz for WCDMA applications. [C1858]

### "A coplanar 94 GHz low-noise amplifier MMIC using 0.07 $\mu\text{m}$ metamorphic cascode HEMTs"

A 94 GHz low-noise amplifier MMIC (LNA) has been developed, based on a coplanar technology utilizing 0.07  $\mu\text{m}$  depletion type metamorphic HEMTs (MHEMTs). The realized single stage cascode LNA achieved a small-signal gain of more than 12 dB and an average noise figure of 23 dB over the bandwidth from 80 to 100 GHz. With an indium content of 80% in the channel, a 2430  $\mu\text{m}$  MHEMT device has shown a transit frequency ( $f_t$ ) of 290 GHz, an extrinsic transconductance of 1450 mS/mm and a maximum stable gain (MSG) of 11 dB at 94 GHz. Using two HEMTs connected in cascode configuration, the MSG could be increased to 22 dB. To stabilize the cascode device and to increase the bandwidth of the amplifier circuit, a resistive feedback was integrated into the HEMT in common-gate configuration. Coplanar topology in combination with cascode transistors resulted in a chip-size of only 141 mm<sup>2</sup>. [C1859]

### "Metamorphic HEMT technology for millimeter-wave and 40-Gb/s fiber-optics applications"

We have developed a 0.15- $\mu\text{m}$  T-gate metamorphic HEMT process with three-level metal interconnects on 100-mm GaAs substrates for low noise and fiber-optics applications. Hall mobilities of greater than 10,000 cm<sup>2</sup>/Vsec and sheet charge densities of  $3.6 \times 10^{12} \text{ cm}^{-2}$  at room temperature were routinely achieved for MHEMT epitaxial layers. Very low noise figure of 0.3 dB and high associated gain of 14.5 dB were measured at 10 GHz. Three 40-Gb/s fiber-optics circuits and a 77 GHz oscillator were successfully demonstrated using this single-recess MHEMT on GaAs technology. OC768 transimpedance amplifiers (TIAs) with differential output exhibited state-of-the-art performance of greater than 55 dB $\Omega$  transimpedance. [C1860]

### "Growth of AlInAs using low-oxygen-content metalorganic precursors and application to HEMT structures"

An AlInAs layer and high electron mobility transistor (HEMT) structures were grown using low-oxygen-content metalorganic precursors by metalorganic vapor phase epitaxy (MOVPE). The oxygen concentration in the AlInAs layer measured by secondary ion mass spectrometry (SIMS) was  $7 \times 10^{15} \text{ cm}^{-3}$ . Moreover, the mobility and sheet carrier concentrations of the AlInAs/InP HEMT structure in which a 2.5  $\mu\text{m}$ -thick AlInAs buffer layer was inserted to reduce the diffusion of impurities from the substrate surface, were 5,500 cm<sup>2</sup>/Vs and  $1.0 \times 10^{12} \text{ cm}^{-2}$  at 300 K, and 110,000 cm<sup>2</sup>/Vs and  $8.7 \times 10^{11} \text{ cm}^{-2}$  at 77 K, respectively. For the AlInAs/GaInAs HEMT structure with the same buffer layer, mobility and sheet carrier concentrations were 12,000 cm<sup>2</sup>/Vs and  $1.2 \times 10^{12} \text{ cm}^{-2}$  at 300 K, and 92,000 cm<sup>2</sup>/Vs and  $1.2 \times 10^{12} \text{ cm}^{-2}$  at 77 K, respectively. [C1861]

### "On the development of automatic assembly line for InP HEMT MMICs"

We have developed the process of automatic assembly line (AAL) on InP HEMT MMICs to enhance the assembly throughput owing to the large volume assembly of InP HEMT MMIC parts for phased-array applications. The DC and RF characteristics before and after AAL were evaluated to assure that InP HEMTs are robust enough to undertake the AAL process. Furthermore, the bond-pull test was incorporated into AAL process to evaluate the bond-pull strength, which is critical for large volume assembly. The bond-pull strength experiment led to improvement of the bonding process from a 3.5-sigma to a 5.2-sigma. As a result, it reduces the attrition rate significantly of InP HEMT MMICs subjected to the AAL process. The results substantiate that InP HEMT MMICs are robust enough to be subjected to large volume of AAL assembly. [C1862]

### "An Nth-harmonic oscillator using an N-push coupled oscillator array with voltage-clamping circuits"

The push-push oscillator is commonly used for implementing a second-harmonic oscillator. By combining two out-of-phase oscillators, their fundamental frequency components are canceled and the second-harmonic components are enhanced. This structure can be extended to triple-push, quadruple-push and hence N-push



harmonic oscillators. From the oscillator injection-locking phenomenon, the relative phase between coupled oscillators can be controlled by the oscillator free-running frequency. As the output phase-shifted version signals are properly shaped and combined, the desired harmonic components are constructively added and lower-order harmonic components are canceled. This structure can be viewed as the general case of push-push oscillators. Since the output power is combined in a passive circuit, it does not suffer from the power limit of the output device in the cascade structure. The desired harmonic component can be selected by tuning the relative phase of the coupled oscillators and the conductive angle of the voltage-clamping circuit. Second-harmonic, third-harmonic and fourth-harmonic oscillators are designed and verified experimentally. [C1863]

#### **"A 1 watt, 3.2 VDC, high efficiency distributed power PHEMT amplifier fabricated using LTCC technology"**

A 1 watt distributed PHEMT amplifier, that operates from 800 MHz to 2.1 GHz, with a 3.2 Volt DC supply has been developed using a novel new approach. The amplifier was designed to provide high efficiency operation, targeted for broadband wireless applications. Key to the amplifier's performance, is a novel broadband impedance matching transformer, fabricated using LTCC technology, as well as a low loss tapered drain network. The class B design has 50  $\Omega$  terminal impedances and built-in bias decoupling. [C1864]

#### **"A W-band ultra low noise amplifier MMIC using GaAs pHEMT"**

This paper presents a newly developed 76 GHz three-stage LNA for automotive radar systems. The LNA utilizes multi band rejection filter type stabilizing circuits to achieve good noise figure together with good stability. The operating bias condition was carefully chosen to obtain low temperature dependence of gain. As a result, the LNA delivers a noise figure of 3.5 dB typically, small temperature dependence of gain of -0.016 dB/deg.C and high return loss using a highly conventional 0.19  $\mu\text{m}$  T-shaped gate AlGaAs/InGaAs/GaAs pHEMT process. [C1865]

#### **"Cryogenic measurements of 183 GHz MMIC low noise amplifiers"**

We report the packaging and first measurement of Indium Phosphide (InP) monolithic microwave integrated circuit (MMIC) low noise amplifiers (LNAs) operating at cryogenic temperatures above 140 GHz. The amplifiers were measured from 160 to 188 GHz at 20 K and tested for noise temperature and gain, with noise temperatures of 160 K. The packaging method and test setup are described, as well as detailed results at room and cryogenic temperatures. [C1866]

#### **"A n-state time-domain measurement test-bench for characterization of intermodulation distortion on device level"**

A flexible nonlinear measurement system is presented for the investigation of intermodulation distortion (IMD) on device level at Ka-band frequencies. The setup is unique in the way that a passive load-pull tuner embedded inside a full two-port test-set is combined with a hybrid receiver to one fully automated test system. The calibration problem of the resulting n-state test-set is formulated with a generalized 4-port error model, for the first time. The hybrid receiver is composed of a virtual 4 channel time-domain sampling oscilloscope and a spectrum analyzer. As an application, we show various two-tone sweep-scenarios applied to our GaAs HEMTs targeting high power applications at Ka-band frequencies. [C1867]

#### **"A V-band GaAs HEMT uniplanar monolithic integrated antenna and receiver front end"**

A V-band monolithic integrated folded-slot balanced mixer with LO source on the same chip is presented for the first time. The circuit is designed based on the uniplanar structures such as coplanar waveguide (CPW) and slotline. The embedding impedance of the folded-slot antenna is calculated by finite-difference time-domain (FDTD) method and compared with the impedance of the Schottky-Barrier diode at 60 GHz to design the mixer. The V-band voltage control oscillator (VCO) is developed based on the 0.15  $\mu\text{m}$  GaAs HEMT technology. A reduced-size CPW-to-slotline transition is designed for the LO pumping network. The measured results of the VCO, transition, and mixer are included. [C1868]

#### **"Impact ionization in AlGaAsSb/InGaAs/GaAsSb metamorphic HEMTs"**

We report the measurement of impact ionization induced gate current in AlGaAsSb/InGaAs/ AlGaAsSb metamorphic HEMT. These HEMTs are designed for high gain and low noise figure at millimeterwave frequencies by implementing high performance channel material, InGaAs with 80% indium, on GaAs substrates using a quaternary AlGaAsSb buffer and barrier. This structure improves the performance of millimeterwave transistors while retaining the low cost of established GaAs fabrication technologies by using the flexibility of

metamorphic growth of III-V semiconductors. [C1869]

#### "Schottky barrier height enhancement for In<sub>0.52</sub>AlAs layer by using in-situ Ar plasma pre-treatment and its application to In<sub>0.52</sub>AlAs/In<sub>0.53</sub>GaAs/InP HEMT's"

To increase a Schottky barrier height (SBH) for In<sub>0.52</sub>AlAs layer, in-situ Ar plasma pre-treatment method was proposed. Through the pre-treatment of Ar plasma before Schottky metallization, a SBH of +1.05 eV for In<sub>0.52</sub>AlAs layer was obtained by C-V measurement for a vertical type Schottky diode. It was thought to be an effective removal of native oxide on InAlAs layer. More pre-treatment would result in a decrease of SBH due to a plasma induced damage effect. This process was applied to fabricate In<sub>0.52</sub>AlAs/In<sub>0.53</sub>GaAs/InP HEMT, which led to an improvement in sub-threshold leakage, sub-threshold swing and reverse breakdown voltage characteristics. [C1870]

#### "InP HEMT-based CPW amplifiers for 94 and 110 GHz"

94 GHz and 110 GHz single- and two-stages amplifiers have been fabricated with our in-house 0.1  $\mu$ m lattice-matched InP HEMT process. The single transistors show state-of-the-art performances for this gate length with extrinsic  $f_{Tand}$  and  $f_{max}$  of 185 and 300 GHz, respectively and a maximum available gain (MAG) of 8.3 dB at 110 GHz. The single-stage amplifiers designed and fabricated in our laboratory showed excellent peak gains of 7.6 dB and 6.5 dB at 94 and 110 GHz, respectively. Two-stages amplifiers showed gain in excess of 12 dB at these frequencies with a 3 dB bandwidth better than 10 GHz. To improve the prediction accuracy of the circuit simulator, all transmission lines and T-junctions were modeled with an electromagnetic simulator. [C1871]

#### "Current collapse induced in AlGaIn/GaN HEMTs by short-term DC bias stress"

GaN HEMTs grown by MOCVD and by MBE were subjected to short term bias-stress. Current collapse was found to be induced in most of the devices after stress, apparently caused by the generation or activation of trapping centers. [C1872]

#### "Bias acceleration model of drain resistance degradation in InP-based HEMTs"

We formulated a lifetime of InP-based HEMTs in drain resistance increase using a bias E dependence model. Several bias accelerated tests at several bias points clarified that both an electric field and current density are necessary for a resistance increase in the drain side of a device. The obtained results suggest the degradation mechanism is that hot electrons created by impact ionization ionize impurities and those impurities are extracted by gate-drain electric field. The ionized impurities result in carrier donor passivation in the n-type InAlAs region and drain resistance increase. We reduced contamination in the fabrication process and thereby achieved long-lifetime HEMTs. In-addition, in a reliability study of 40 Gbit/s InP-HEMT ICs, a low operating voltage design was adopted and lifetime of over 14106h at 100°C was obtained. [C1873]

#### "Damage-free SiO<sub>2</sub> /SiN<sub>x</sub> side-wall gate process and its application to 40 nm InGaAs/InAlAs HEMT's with 65% InGaAs channel"

Highly reproducible side-wall process for the fabrication of the fine gate length as small as 40nm was developed. This process was utilized to fabricate 40nm InGaAs HEMTs with the 65% strained channel. With the usage of the dual SiO<sub>2</sub> and SiN<sub>x</sub> dielectric layers and the proper selection of the etching gas, the final gate length ( $L_g$ ) was insensitive to the process conditions such as the dielectric over-etching time. From the microwave measurement up to 40 GHz, extrapolated  $f_{Tand}$  and  $f_{max}$  as high as 371 and 345 GHz were obtained, respectively. We believe that the developed side-wall process would be directly applicable to finer gate fabrication, if the initial line length is lessened below the 100 nm range. [C1874]

#### "Fabrication of 0.1 $\mu$ m-gate InP HEMTs using i-line lithography"

We developed a new process (PATRASH: PAttern TRAnSfer SHrink) for fabricating T-shaped 0.1 $\mu$ m-gate InP HEMTs using i-line lithography. Higher throughput lithography processes were achieved by applying i-line lithography instead of electron beam (EB) lithography. The process we developed has three important technical aspects: shrinking the photoresist pattern, dry etching the multi-layer resists, and shrinking the PMMA resist. The controllability of gate lengths was good enough to realize circuit operation. Using our process, we fabricated a T-shaped 0.1 $\mu$ m-gate InP HEMT that showed a transconductance of 880 mS/mm and a cut-off frequency of 202 GHz. This performance equaled that of a device produced using EB lithography. [C1875]

#### "Double-gate HEMTs on transferred substrate"

We report the fabrication and DC characterization of the first  $\text{In}_{0.52}\text{Al}_{0.48}\text{As}/\text{In}_{0.53}\text{Ga}_{0.47}\text{As}$  double-gate HEMTs with simple-command (DG-HEMT-SC) and double-command (DG-HEMT-DC). These devices have been obtained by photolithography and by transferred substrate technique. Although layer structure has not been optimized, a maximum extrinsic transconductance of 460 mS/mm with a drain current  $I_{\text{dsof}}$  160mA/mm is achieved for 1.5  $\mu\text{m}$  gate length DG-HEMT-SC. A large ratio  $G_m/I_{\text{dsof}}$  3V-1 is obtained, which indicates improvement of charge command efficiency. [C1876]

#### "70 nm low-noise metamorphic HEMT technology on 4 inch GaAs wafers"

A 70 nm gate length metamorphic HEMT technology will be presented. Extrinsic cut-off frequencies of  $f_t = 293$  GHz and  $f_{\text{max}} = 337$  GHz were achieved. The transistors have an on-state breakdown voltage of 1.7 V. A median time to failure of 14106h at 125°C and an activation energy of 1.3 eV was extrapolated based on a 10% gm,max degradation in air. This is significant less than the 1.8 eV activation energy of our 100 nm gate-length 65% In process which is probably due to hot electron effects. The MMIC-process obtains high yields on transistor and circuit level. Low-noise amplifiers demonstrate a small signal gain of 13 dB and a noise figure of 2.8 dB at 94 GHz. The achieved results are comparable to state-of-the-art InP-based HEMT technologies. [C1877]

#### "W-band power metamorphic HEMT technology on GaAs"

Our 0.15  $\mu\text{m}$  power MHEMT development at W-band includes comparison of single (53%) and split channel (53/43%) material. Preliminary single stage microstrip amplifier results yield 225 mW/mm and >10dB small signal gain at 95 GHz. [C1878]

#### "A high isolation enhancement mode GaAs PHEMT buffer amplifier"

The design and implementation of a high isolation buffer amplifier is described. The IC uses a 2-gain stage topology with variable maximum output power up to 22 dBm, this being determined by the use of an external bias resistor. It has better than 40 dB of input-output port isolation and operates from 0.5 GHz to 6 GHz. The IC is fabricated on Agilent Technologies' proprietary enhancement-mode GaAs PHEMTs (pseudomorphic high-electron-mobility transistors) process. The enhancement-mode characteristic enables operation with a single supply voltage with high linearity and low noise. With a single 5 V supply, typical gain is 21dB with 40 mA quiescent current consumption. Total die size is 500  $\mu\text{m}$   $\times$  700  $\mu\text{m}$ . The IC is packaged in an 8-lead low-profile 2 mm  $\times$  2 mm plastic package and features input and output matched ports to 50 ohms impedance. Input and output impedance matching can be further optimized for different frequency bands by the use of a single input inductor and a load inductor at the power supply. Typical uses of the part are for isolating VCO (voltage controlled oscillator) outputs and mixer local oscillator inputs as well as a buffer amplifier for driving passive mixers. [C1879]

#### "Comparison of bistable circuits based on resonant-tunneling diodes"

Using computer-aided circuit simulation, the speed of RTD-based bistable circuits has been evaluated in terms of device parameters, such as the transistor's  $f_t$  and  $f_{\text{max}}$ , and circuit parameters, such as sizing. Two topologies studied in this work are: 1) monostable-to-bistable transition logic element (MOBILE), and 2) quantum bistable logic circuit (QBL). The transistors studied in this paper are: 1) heterojunction bipolar transistors (HBTs), and 2) high electron mobility transistors (HEMTs). Results indicate that, among the four configurations, the MOBILE circuit using HEMTs is the fastest. This circuit, however, is also the most likely to suffer significant performance reduction due to parasitic loads and variation of device characteristics. [C1880]

#### "0.15 $\mu\text{m}$ gate length InAlAs/InGaAs power metamorphic HEMT on GaAs substrate with extremely low noise characteristics"

The 0.15  $\mu\text{m}$  gate-length power metamorphic HEMTs (MHEMT) with wide head T-shaped gate has been fabricated and the DC, microwave, and noise performance of the device were characterized. The MHEMT device shows the DC output characteristics having an extrinsic transconductance of 740 mS/mm and a threshold voltage of -0.75 V. The  $f_t$  and  $f_{\text{max}}$  obtained for the 0.15  $\mu\text{m}$   $\times$  100 pm MHEMT device are 150 GHz and 240 GHz, respectively. The MHEMTs exhibit the minimum noise figure,  $NF_{\text{min}}$ , of 0.79 dB and associated gain of 10.5 dB at 26 GHz. The  $NF_{\text{min}}$  measured at 40 GHz is 1.21 dB with associated gain of 6.41 dB. This noise data is the lowest value ever reported for power MHEMT devices with InGaAs channel of 53% In. The excellent noise characteristics might result from the low gate resistance due to the wide head T-shaped gate and the improved device performance. [C1881]

### "A 38/77 GHz MMIC transmitter chip set for automotive applications"

This paper describes the successful development of 38/77 GHz transmit MMICs for automotive applications. They consist of a 38 GHz amplifier, a frequency doubler, and a 77 GHz power amplifier. These amplifiers achieve output powers of 16 dBm at 38 GHz and 15 dBm at 76.5 GHz at 1 dB gain compression point. The output power of the 77 GHz amplifier is one of the highest delivered by a single chip MMIC at 76.5 GHz. The frequency doubler delivers an output power of 5.7 dBm at 76.5 GHz. These results are promising for automotive applications in the W-band. [C1882]

### "A 19 GHz low phase noise HFET VCO MMIC"

A 19 GHz extremely low phase noise voltage controlled oscillator (VCO) MMIC is presented. To reduce the phase noise of the VCO, a heterostructure field effect transistor (HFET) is used as the active device, because its low frequency noise properties are superior to that of high electron mobility transistors (HEMT). This VCO showed a typical phase noise of -120 dBc/Hz at 1 MHz offset from the carrier. This performance is better than other VCOs operating above 10 GHz. The measured tuning range is 400 MHz and output power is 2 dBm. The fabricated MMIC chip size is 2.7 mm<sup>2</sup> 1.4 mm. [C1883]

### "Extraction of conversion matrices for P-HEMTs based on vectorial large-signal measurements"

We introduce a new technique which allows us to measure the admittance conversion matrix of a two port device, using a large-signal vector network analyzer. This method is applied to extract the conversion matrix of a 0.25  $\mu$ m PHEMT, driven by a 4.8 GHz signal, at different power levels, using an intermediate frequency of 600 MHz. A discussion of the up- and down-conversion is provided. [C1884]

### "2 and 4 watt Ka-band GaAs PHEMT power amplifier MMICs"

The design and performance of power amplifiers for Ka-band applications is presented. A three-stage amplifier demonstrated 22 dB small signal gain from 26.5 GHz to 31.5 GHz and saturated output power of 4W with 28% power added efficiency from 28 GHz to 31 GHz. Record power density of 670 mW per mm of device output periphery was achieved. The amplifiers were fabricated on a selective double-recess 0.2  $\mu$ m GaAs power PHEMT process. [C1885]

### "A multilayer active hybrid-ring using ground-slot coupling technique"

A ground-slot coupling technique is applied to design a novel multilayer active hybrid-ring power divider. The prototype consists of three ground slots to couple the signal between circuit layers, and two single-stage HEMT amplifiers to boost the coupled signal. It is tested at C-band with 40% -3dB bandwidth. At 5 GHz center frequency, it has 8 dB small-signal gain and 10 dBm output P1 dB. [C1886]

### "Ku-band low noise amplifier with using short-stub ESD protection"

A Ku-band ESD-protected low noise amplifier is designed using 0.15 $\mu$ m pHEMT process. The input ESD protection is implemented with short-circuited stub. Since a short-circuited stub is used as an ESD protection as well as a matching element, there are no additional components and parasitic components associated with ESD protection. This endures 4400V (ESD tester limit) HBM test signal. The LNA has the noise figure of 1.24 dB and 24.5 dB gain at the frequency of 11.7-12.75 GHz. [C1887]

### "Single-ended amplifier that substantially improves PAE and ultra-broadband performance"

A single ended amplifier with a simple reactive matching is shown to provide stable operation with substantially improved amplifier power-added efficiency (PAE) (>30%) across an ultra-broadband frequency range (2-18 GHz). The amplifier employs a Double Pseudomorphic High Electron Mobility Transistor (DPHEMT) power device. [C1888]

### "An 18-71 GHz multi-band and high gain GaAs MMIC medium power amplifier for millimeter-wave applications"

This paper presents the design and measurement results of a broadband high gain MMIC medium power amplifier. The proposed 18-71 GHz multiband amplifier provides a single chip solution for all 28 GHz, 38 GHz, and 60 GHz millimeter-wave applications with a chip size of 2.5 mm<sup>2</sup> 1 mm. The high gain performance of more than 20 dB from 41-63 GHz has been attained. It provides at least 16 dBm of maximum output power from 19-57 GHz. This amplifier consists of one distributed stage for broadband design and cascaded single-ended stages for medium power output. This chip demonstrates the highest frequency application using this combined



topology compared with all previously published results. The circuit was fabricated with a 0.15- $\mu\text{m}$  gate-length GaAs-based HEMT MMIC technology. [C1889]

#### "High conversion gain V-band quadruple subharmonic mixer using cascode structure"

In this paper, we present V-band high conversion gain quadruple subharmonic mixers adopting the cascode structure. The subharmonic mixers were successfully integrated by using 0.1  $\mu\text{m}$  GaAs PHEMTs and the coplanar waveguide structures. We show that the highest conversion gain of 3.4 dB thus far at a LO power of 13 dBm from the fabricated mixers. The millimeter-wave subharmonic mixer also ensure a high degree of isolation showing -53.6 dB in the LO-to-IF and -46.2 dB in the LO-to-RF, respectively, at a frequency of 14.5 GHz. The high conversion gain achieved in this work is the first report among the millimeter-wave monolithic IC subharmonic mixers. [C1890]

#### "Integrated power amplifier for 60 GHz wireless applications"

This paper presents an integrated power amplifier for the 60 GHz frequency range. The amplifier was fabricated with a commercially available 0.15  $\mu\text{m}$  gate length pseudomorphic HEMT process. The output stage consists of two 6435  $\mu\text{m}$  PHEMTs, forming a total output periphery of 420  $\mu\text{m}$ . The MMIC amplifier was simulated, fabricated and measured both on-wafer and in a split block package. The amplifier was characterized using linear and nonlinear methods. The odd mode stability was carefully analyzed. Large-signal scattering parameters were measured with on-wafer probes. The measured gain was 13.4 dB and 1 dB output compression point was at +17 dBm power level using 3.0 V supply voltage. The AM/AM and AM/PM characteristics were extracted from the large-signal S-parameter results. Finally, the amplifier chip was mounted in a split block package, which has WR-15 wave guide input and output interface. The measured results show 12.5 dB small-signal gain and better than 8 dB return losses in input and output for the packaged amplifier chip. [C1891]

#### "A balanced 2 watt compact PHEMT power amplifier MMIC for Ka-band applications"

A balanced form, compact power amplifier MMIC operating at Ka-band was designed and developed using TriQuint's 3MI 0.25 $\mu\text{m}$  gate length pHEMT technology. This balanced three-stage power amplifier, with chip size of 6.16mm<sup>2</sup>(2.84x2.2mm), on 100 $\mu\text{m}$  GaAs substrate achieved 32.8dBm (1.9Watt) P1dB output power and saturated output power above 2 Watts with higher small signal gain than 18dB at 30GHz. This chip provides a high power and low cost benchmark solution for Ka-band radio market. [C1892]

#### "A high power density, 6W MMIC for Ku/K-Band applications"

A Ku/K-Band very small size MMIC high power amplifier (HPA) providing 6W of CW output power, 23dB of gain and 30% power added efficiency for application in the Ku/K-Band is presented. It is produced on a low cost, commercially available 0.25 $\mu\text{m}$  pHEMT process. This MMIC is composed of three stage pHEMT and chip size is 3.5 x 3.0 mm<sup>2</sup>. The HPA achieved 570 mW output power per 1 mm<sup>2</sup> die area. This value is the highest power density at Ku/K/Ka-Band reported to date. [C1893]

#### "E-PHEMT, single supply, power amplifier for Ku band applications"

The development of enhancement mode PHEMT (E-PHEMT), single supply, 10.5 to 18GHz wide band power amplifier MMICs is described. The amplifier was designed with prematching techniques utilizing a 0.5 $\mu\text{m}$  GaAs E-PHEMT production process. The designed power amplifier exhibit 13 dB of small signal gain, 26.5dBm 1dB gain compression output power at 16 GHz. This MMIC was fabricated in Agilent's advanced E-PHEMT process and have been demonstrated in fully production capability. [C1894]

#### "New results on MMIC six-port's used in Ka band direct conversion receivers"

New results obtained on two Ka Band Monolithic Microwave Integrated Circuit (MMIC) six-port junction circuits realized in GaAs PHEMT technology at TriQuint Texas Foundry are presented in this paper. Comparative results of simulated and measured S parameters are shown for both designs. The proposed MMIC six-port circuit is used to realize the QPSK demodulator of a Ka band direct conversion receiver. [C1895]

#### "95 GHz metamorphic HEMT power amplifiers on GaAs"

This paper reports on the first 95 GHz metamorphic HEMT power amplifier demonstration including power as a function of temperature. Two power MHEMT materials with 53% and 53%/43% indium channels are investigated showing a slight advantage to the split channel material. At 95 GHz, Gmax values ranging 8.25-10.8 dB are shown for both materials. Single stage 0.15 mm periphery amplifiers using single 4437.5  $\mu\text{m}$  FETs show >10 dB

small signal gain. Two dB compressed power data at 95 GHz yields 15.3 dBm (224 mW/mm) and PAEs up to 22.8%. Increasing temperature up to 80°C results in output power and PAE degradation of only 0.43 dB and 2.6 percentage points, respectively. These promising results are on the path to 100-300 mW MHEMT power amplifiers at W-band with improved manufacturability over InP HEMT. [C1896]

#### "Performance of AlGaIn/GaN HEMTs for 2.8 GHz and 10 GHz power amplifier applications"

AlGaIn/GaN high electron mobility transistors (HEMTs) have demonstrated great potential for microwave power transmitter applications as required by phased array radar and wireless base stations. In this paper, we report on state-of-the-art power density generated from large gate periphery AlGaIn/GaN HEMTs. At 2.8 GHz, 7 W/mm gate periphery (14.7 W total) was obtained under pulsed conditions from 2.1 mm gate periphery devices and 5 W/mm (42 W total) pulsed power was demonstrated from 244.2 mm gate periphery devices. At 10 GHz, 9.2 W/mm (13.8 W total) power was obtained under pulsed conditions from 1.5 mm gate periphery devices with drain bias up to 55 V. The 444.2 mm (16.8 mm<sup>2</sup>) multiple-die hybrid power amplifiers at 2.8 GHz and 441.5 mm (6 mm<sup>2</sup>) multiple-die package at 10 GHz were also evaluated. [C1897]

#### "A complete self-defined empirical model for enhancement-mode AlGaAs/InGaAs pHEMTs"

We propose a complete self-defined empirical large-signal and noise including model for enhancement-mode AlGaAs/InGaAs pHEMTs. This model achieves excellent fitting of the DC transconductance,  $g_m$ , which considers the difference of the drain-to-source conductance between DC and RF measurements. In addition, for a full prediction at various biases, all parameters of the model are characterized against the gate-to-source and drain-to-source voltages. In consequence, the predictions of the power and IM3 are very accurate. Additionally, it can also predict the NFmin and  $\Gamma_{opt}$  points well using the noise parameters by calculating the thermal noise of the equivalent circuit model. This noise figure prediction including model is not always available from the commonly used conventional pHEMT models. [C1898]

#### "25.5 to 76.5GHz active frequency tripler for automotive radar applications"

This paper discusses the development of a 25.5 GHz to 76.5 GHz single stage active frequency tripler for automotive radar applications. With an input drive level of 17 dBm at  $f/3$ , the frequency triplers tested demonstrated an output power level of 0 dBm from 73 to 82 GHz. The frequency tripler was subsequently cascaded with a 25.5 GHz VCO to demonstrate a 76.5 GHz VCO. [C1899]

#### "Monolithic coplanar 77 GHz balanced HEMT mixer with very small chip size"

A balanced HEMT mixer for 76-77 GHz car radar applications has been designed and fabricated on a 6 inch GaAs production line. The monolithic circuit has a very small chip size of only 0.56 mm<sup>2</sup>. With 2 dBm of LO power, a conversion loss below 11 dB was measured in the 76-77 GHz band. The results demonstrate that the single-device concept used in the circuit design is suitable for very compact monolithic millimeter-wave mixers. [C1900]

#### "A W-band monolithic medium power amplifier"

This paper summarizes the design and measured performance of a MMIC power amplifier for W-band. The chip was fabricated on a 50  $\mu$ m GaAs substrate using 0.1  $\mu$ m AlGaAs/InGaAs/GaAs pseudomorphic-HEMT technology. Measurements show that it has small-signal gain of  $19 \pm 1$  dB from 72 to 95 GHz. During scalar measurements with moderate heat-sinking, the chip delivered more than 100 mW between 75 and 93 GHz, with a corresponding large signal gain of 11 dB. Such an amplifier is widely useful in millimeter-wave applications requiring moderately high power over broad frequency ranges, including emerging wireless communication systems in W-band. [C1901]

#### "A new scaleable low frequency noise model for field-effect transistors used in resistive mixers"

A new scaleable low-frequency noise model for cold-FETs ( $U_{ds} \approx 0$  V) is proposed. The model was tested using the Fujitsu HEMT FHC40LG in resistive mixer circuits where low-frequency noise (1/f-noise and generation-recombination noise) occurs due to the self-mixing process. Describing the noise of the FET channel as resistance fluctuations the model explains the existence of noise in absence of a DC current. A method for implementing resistance noise in common CAE programs is also shown. The model yields excellent-agreement with simulation results. [C1902]

#### "A Ka-band class F MMIC amplifier design utilizing adaptable knowledge-based neural network"

### modeling techniques"

This paper describes the first implementation of an adaptable knowledge-based neural network (AKBNN) model in a high efficiency class F MMIC (monolithic microwave integrated circuit) amplifier design at Ka-band in a 0.25  $\mu\text{m}$  GaAs PHEMT technology. A single-stage amplifier based upon the AKBNN model employed shows comparable results to measured performance of a gain of 7.5 dB, a PAE of 35%, and an output power of 17 dBm. [C1903]

### "An antenna switch MMIC using E/D mode p-HEMT for GSM/DCS/PCS/WCDMA bands application"

A monolithic antenna switch IC using enhancement and depletion (E/D)-mode AlGaAs/InGaAs pseudomorphic high electron mobility transistors (p-HEMTs) has been developed for GSM/DCS/PCS/WCDMA band digital mobile communication systems. This antenna switch MMIC achieves a low insertion loss and small chip size using a single pole double throw (SPDT) switch for GSM and single pole 4 throw (SP4T) switch for other band configurations, as well as internal logic circuits with an E/D mode p-HEMTs process. This MMIC achieves an insertion loss of 0.21dB at 915MHz and 0.53dB at 1785MHz. The isolation to the RX ports is more than 30 dB, and the input power at 0.1 dB compression is over 36 dBm at +2.7 V operation. [C1904]

### "ANN model for AlGaIn/GaN HEMTs constructed from near-optimal-load large-signal measurements"

AlGaIn/GaN HEMTs have a high potential for high-power applications at microwave frequencies. We developed a behavioural model corresponding to the operation condition as how this device will be used in power amplifiers, i.e., at a high output load. The model is based on time-domain large-signal measurements, and the representation format is an artificial neural network (ANN). AlGaIn/GaN devices on sapphire are known to be temperature sensitive. Therefore, we also consider the incorporation of the self-heating effect in the behavioural model description. [C1905]

### "Large signal modeling of AlGaIn/GaN HEMTs with $P_{\text{sat}} > 4$ W/mm at 30 GHz suitable for broadband power applications"

Large signal modeling and investigations of an AlGaIn/GaN HEMT processed on SiC with  $I_g = 150$  nm are performed with respect to broadband amplifiers up to 30 GHz. Output power values of 3.4 W or 4.25 W/mm at 18 GHz and  $P_{\text{out}} = 1.6$  W, equivalent to 4 W/mm at 30 GHz, are measured. The device modeling shows good agreement of the measured and modeled power sweeps at 10 GHz and 30 GHz. The large signal simulations show the suitability of AlGaIn/GaN HEMTs for multi-band amplifiers in the K-band. [C1906]

### "Mechanism of power density degradation due to trapping effects in AlGaIn/GaN HEMTs"

AlGaIn/GaN HEMTs are promising devices for very high power applications. These transistors present high breakdown voltages and have already shown their ability to operate at high temperature. But their power performances are limited because of the presence of traps within the material, decreasing the drain current density. In order to predict the loss of power density and quantify trapping effects, simulations need to be performed with a suitable model, which accounts for these parasitic trapping effects. This paper deals with the characterization, modeling and simulation of trapping effects and power behavior of a 1 mm GaN device on a SiC substrate. Experimental results are compared to the simulations. [C1907]

### "Asymmetrically recessed (ASR) 0.13 $\mu\text{m}$ In<sub>0.65</sub>GaAs HEMT's using double-deck shaped (DDS) gate technology"

In this paper, we fabricated a 0.13  $\mu\text{m}$  ASR gate In<sub>0.65</sub>GaAs P-HEMT by inserting additional dummy gate line and using DDS gate structure. The fabricated device showed excellent DC and RF characteristics with a improvement in output conductance ( $G_{\text{ds}}$ ) and maximum oscillation frequency ( $f_{\text{max}}$ ). These results demonstrate that an ASR gate structure for high performance 100 nm scale InP P-HEMT. [C1908]

### "Low-frequency noise characteristics of AlSb/InAsSb HEMTs as a function of temperature and illumination"

Measurements of the low-frequency noise characteristics of AlSb/InAsSb HEMTs as a function of temperature and illumination are reported in this paper. The primary focus in this paper is on devices in which a digital alloy superlattice of InAs/InSb was used to form an InAsSb channel. This appears to be related to the lower stress in this channel, which is matched to AlSb. [C1909]

### "Enhanced functionality in GaN and SiC devices by using novel processing"

Some examples of recent advances in enhancing or adding functionality to GaN and SiC devices through the use of novel processing techniques are discussed. The first example is the use of ion implantation to incorporate transition metals such as Mn, Cr and Co at atomic percent levels in the wide bandgap semiconductors to produce room temperature ferromagnetism. A discussion is given of the phase space within which single-phase material can be obtained and the requirements for demonstrating the presence of a true dilute magnetic semiconductor. The ability to make GaN and SiC ferromagnetic leads to the possibility of magnetic devices with gain, spin fets operating at low voltages and spin polarized light emitters. The second example is the use of novel oxides such as  $\text{Sc}_2\text{O}_3$  and  $\text{MgO}$  as gate dielectrics or surface passivants on GaN. True inversion behavior has been demonstrated in gated MOS-GaN diodes with implanted n-regions supplying the minority carriers need for inversion. These oxide layers also effectively mitigate current collapse in AlGaN/GaN HEMTs through their passivation of surface states in the gate-drain region. The third example is the use of laser drilling to make through-wafer via holes in SiC, sapphire and GaN. The ablation rate is sufficiently high that this maskless, serial process appears capable of achieving similar throughput to the more conventional approach of plasma etching of vias. The fourth example is the use of either ungated AlGaN/GaN HEMTs or simple GaN and SiC Schottky diodes as sensors for chemicals, biogens, radiation, combustion gases or strain. The sensitivity of either the channel carrier density or the barrier height to changes in surface condition make these materials systems ideal for compact, robust sensors capable of operating at elevated temperatures. [C1910]

### "High performance GaN HEMTs at 40 GHz with power density of 2.8W/mm"

In this article we report record power densities in GaN HEMTs operating at 40 GHz. Devices fabricated with 0.18  $\mu\text{m}$  long e-beam gates showed a power density of 2.82 W/mm and a gain of 5.8 dB at 40 GHz. This record performance was obtained due to a combination of a high power gain, negligible RF dispersion, and a high breakdown voltage. [C1911]

### "A 174 W high-efficiency GaN HEMT power amplifier for W-CDMA base station applications"

AlGaN/GaN high electron mobility transistors (HEMTs) have been developed for current-collapse-free operation at high drain bias voltages. The newly designed single-chip GaN HEMT amplifier for W-CDMA base station applications achieves a record CW output power of 150 W with a high power-added efficiency (PAE) of 54% at 2.1 GHz. The amplifier, combined with a digital pre-distortion (DPD) system, also demonstrates a state of the art efficiency of 40% with an adjacent channel leakage power ratio (ACLR) of less than -50 dBc for 4-carrier W-CDMA signals and reaches the saturated peak power level of 174 W with a drain supply voltage of 63 V. We prove for the first time that the AlGaN/GaN HEMT amplifier can completely fulfill the W-CDMA system requirement. [C1912]

### "Low-frequency noise characteristics of 0.13 $\mu\text{m}$ In<sub>0.65</sub>GaAs p-HEMT under the influence of impact ionization induced hole current"

The paper presents the investigation of the low-frequency noise characteristics of D-mode and E-mode 0.13  $\mu\text{m}$  In<sub>0.65</sub>GaAs p-HEMT under influence of impact ionisation induced gate hole current. The D-mode p-HEMT having a InP Schottky gate showed Lorentzian low-frequency noise components and drift of corner frequency due to drain bias change, while the InAlAs gate E-mode p-HEMT showed no change in behaviour due to the reduction of gate hole current. [C1913]

### "Improved quantization of 2DEG of p-HEMT"

The heterostructure potential of a tri-gate depleted mode p-HEMT was modeled for conventional and tailored field operation conditions. The set of energy levels in quantum wells under same bias on all gates were compared with parameters of p-HEMT, when the bias on the gates are varied. To make electron flow in p-HEMT with more coherent energy is documented by modeling and confirmed by experimental measurements of I-V curves and gain. [C1914]

### "A metamorphic high electron-mobility transistor with reflowed submicron T-gate for high-speed optoelectronics applications"

A metamorphic high electron-mobility transistor (HEMT) manufactured with reflowed submicron T-gate using e-beam lithography for high-speed optoelectronics applications is developed. The In<sub>0.53</sub>Al<sub>0.47</sub>As/InGaAs HEMT uses In<sub>x</sub>Al<sub>1-x</sub>As as the buffer layer between GaAs substrate and the InP lattice-matched HEMT structure. The T-gate developed has a gate length of 160  $\mu\text{m}$ . The fabricated metamorphic HEMT has a saturation drain



current of 280 mA/mm and a transconductance of 840 mS/mm at  $V_{DS} = 1.2$  V. Noise figure for 160  $\mu\text{m}$  gate-width device is less than 1 dB and the associated gain is up to 14 dB at 18 GHz. The device demonstrates a cut-off frequency  $f_{To}$  of 150 GHz and a maximum frequency  $f_{MAXup}$  to 350 GHz. The metamorphic HEMT developed has the potential for high-speed optoelectronics applications. [C1915]

#### "Low-frequency noise in laser-debonded GaN films"

Low-frequency noise was measured from laser-debonded HVPE-grown GaN films. Substantial increase in the noise was seen for the 5  $\mu\text{m}$  thick films, indicating generation of localized states due to laser illumination. For the 20  $\mu\text{m}$  thick films, low-frequency noise measured from the debonded sample is found to be similar to the control sample, indicating the material degradation is limited to the region close to the GaN-sapphire interface. [C1916]

#### "6.2 E In<sub>0.2</sub>Al<sub>0.8</sub>Sb/InAs<sub>0.7</sub>Sb<sub>0.3</sub> HEMTs for low voltage high-frequency applications"

The paper presents the performance of In<sub>0.2</sub>Al<sub>0.8</sub>Sb/InAs<sub>0.7</sub>Sb<sub>0.3</sub>HEMTs that are fabricated for the first time in a uniform alloy of InAs<sub>0.7</sub>Sb<sub>0.3</sub> as the channel layer with adjacent In<sub>0.2</sub>Al<sub>0.8</sub>Sb barrier layers, with a lattice constant of 6.2E. The paper also presents the cross-sectional view of the material structure used in the fabrication process, X-ray analysis spectrum of the material structure, diffraction peaks of the layers, drain characteristics of HEMT and gate transfer characteristics as a function of gate bias. The addition of Sb to the InAs channel offers the possibility of improvement in low-voltage high-frequency applications. [C1917]

#### "High performance AlGaIn/GaN HEMTs with a field plated gate structure"

Record performance at 4 GHz has been obtained by using field plated AlGaIn/GaN HEMTs. For devices on sapphire substrate, high power density (12 W/mm) as well as high efficiency (58%) have been measured. Devices on SiC substrate yielded power density up to 18.8 W/mm and efficiency up to 74% (with 6 W/mm). Excellent linearity performance was also achieved: while maintaining a carrier to third-order intermodulation ratio of 30 dBc device yielded 2.4 W/mm with 53% PAE. [C1918]

#### "Influence of layer structure and surface passivation on performance of AlGaIn/GaN HEMTs on Si and SiC substrates"

In this work, results of the comparative study of unpassivated and passivated AlGaIn/GaN HEMTs which were grown on Si and SiC substrates and which consisted of intentionally undoped and doped layer structures. The doped structures consists of an undoped AlGaIn spacer, Si-doped AlGaIn carrier supply and an undoped AlGaIn barrier layer. A100-150 nm thick SiO<sub>2</sub> and SiN are used as passivation layers. The induced charge, carrier density of used layer structures before and after passivation are studied. DC performance and small signal characterization of HEMT are also studied. It has been shown here that the AlGaIn/GaN HEMT performance is improved and impact of passivation is less pronounced if a doped layer structure is used instead of undoped one. [C1919]

#### "High frequency InAs-channel HEMTs for low power ICs"

InAs-channel HEMTs with improved breakdown characteristics were realized by using AlInAs barriers for enhanced hole confinement. A performance of  $f_t > 300$  GHz at  $V_{ds} = 0.7$  V has been achieved for depletion mode devices. As an important step towards enhancement mode operation, we fabricated devices with charge compensation by p-type doping. Devices with  $V_g = -0.35$  V and  $f_t = 20$  GHz were realized. These results, in conjunction with the sub-micron device development, show promise for a low-power highspeed IC technology. [C1920]

#### "An ultra low phase noise W-band GaAs-based PHEMT MMIC CPW VCO"

A W-band voltage control oscillator (VCO) using 0.1m AlGaAs/InGaAs/GaAs PHEMT MMIC technology with ultra low phase noise is presented. This VCO demonstrated an operation frequency centered at 97 GHz with a tuning range of 2GHz and an output power of 1 mW. The measured single side-band phase noise is -88 dBc/Hz at 1 MHz offset. To the best of our knowledge, this phase noise performance is not only the best among the previously reported results for HEMT MMIC VCO at this frequency, but also rivals those for most VCOs using HBTs. [C1921]

#### "Envelope currents method with extended dynamic range for the simulation of nonlinear communication circuits"

A novel approach to analyze the effects of nonlinear distortion in communication circuits is reported based on a recursive algorithm. In each iteration a time-varying linear circuit excited by appropriate nonlinear currents obtained from an expansion of the nonlinearity is analyzed. This procedure has been applied to a common-source HEMT amplifier excited with a single tone and results show a very fast convergence together with a high dynamic range. The technique was used in the evaluation of the spectral regrowth and constellation distortion of a QPSK signal with raised cosine and root raised cosine conforming pulses produced by the amplifier at 5.8 GHz. [C1922]

#### **"Low cost 5-bit phase shifter for DBS phased array antennas"**

A low cost patent pending 5-bit digital phase shifter has been developed for application in DBS receiving phased array antennas. New simplified loaded line architecture of less significant bit is proposed. The new circuit mitigates PCB technology limitations and reduces the number of switching components, which are low cost discrete p-HEMT FETs. TRL measurement technique was employed for extraction of the cold FET two states parameters. The digital 5-bit phase shifter operates in full satellite TV band from 10.7 to 12.75 GHz and has following main parameters: insertion loss 6dB, insertion loss deviation  $\pm 1.4$ dB, average RMS phase error  $3^\circ$  and worst-case input/output return loss 11dB. The control of the device is CMOS(5V) compatible with setting time less than 70ns. [C1923]

#### **"Millimetre wave VCOs with wide electronic tuning range for synthesised radios"**

A series of new and very compact local oscillators for point-to-multipoint (PMP) and point-to-point (PtP) radio link systems has been developed in the 26 GHz to 36 GHz frequency range. The oscillators mainly consist of a GaAs-pHEMT microwave monolithic integrated circuit (MMIC) and a planar ring resonator (RR). Three MMICs have been designed to cover the whole frequency range. The ring resonator operates at harmonic frequencies. An innovative fully automated active laser-trimming procedure is used to adjust the centre frequency, the varactor tuning sensitivity, the electronic tuning range, respectively, and the electrical line length between the MMIC and the ring resonator. The laser tuneable frequency range is larger than 10% without any significant deterioration of the oscillator's characteristics. The maximum electronic tuning range can be adjusted by laser-trimming to values of more than 2.5% of the centre frequency. A typical single-band phase noise value of approx. -108 dBc/Hz is achieved at an offset frequency of 1MHz. The temperature drift of the oscillator frequency is typ. 9 ppm/K. [C1924]

#### **"A filter synthesis method applied to millimeter-wave distributed switch design"**

A filter synthesis method based on the image-parameter theory is applied to the design of millimeter-wave distributed switches. The method provides accurate closed-form equations for circuit element calculation. With this set of equations, the required performance can be easily achieved within a close tolerance of required specifications. A distributed SPDT MMIC is implemented with the pHEMT process to confirm the proposed method. The measured insertion loss is less than 3.1 dB and the isolation is better than 40 dB from 15 GHz to 50 GHz, which confirm the proposed method. [C1925]

#### **"A dynamic bias control technique of PHEMT SSPA for optimised PAE and EVM applied to MQAM satellite communication systems"**

This paper presents a method for the optimisation of both PAE and EVM of a millimeter wave power amplifier applied here to MQAM modulations. A first key point lies in that both input and output biasing voltages of the SSPA are dynamically controlled versus the RF power level associated with the symbol to be transmitted. The leading idea here is that the dynamic biasing control is designed and implemented to keep fixed AM/AM and AM/PM conversion values while RF input power level changes. By doing so, the power gain of the PAs can be dynamically tuned to a fixed power gain corresponding to the compression gain behaviour for which the PAE is optimum either at low, medium and high input RF power level. As a main consequence, PAE performances can be drastically improved (from 1% to 20% at Ka band) as compared to classical back-off solutions and optimised while keeping a very good EVM. A Ka band hybrid amplifier has been developed using an  $8 \times 75 \mu\text{m}$  Power PHEMT. The proposed linearisation technique is validated by comparisons between measured PAE and EVM on the SSPA when a fixed bias and a controlled bias are used. [C1926]

#### **"600V AlGaIn/GaN power-HEMT: design, fabrication and demonstration on high voltage DC-DC converter"**

A 600 V class AlGaIn/GaN power HEMT was designed for high voltage power electronics application such as power supplies and motor drives. The fabricated device was demonstrated in a DC-DC down converter circuit,

showing the future possibility of high efficiency and high frequency operations of AlGaIn/GaN power HEMTs.

[C1927]

### "Electrical degradation mechanisms of RF power GaAs PHEMTs"

In this research, we have carried out a systematic investigation of the electrical degradation of RF power PHEMTs. By examining devices with different geometries as well as a variety of test structures, our research confirms previous observations of degradation under the gate of the device. We have also identified for the first time a mechanism that affects the source. Additionally, we convincingly show that impact ionization (II) is not directly responsible for drain degradation. Instead, we find that a hot-electron (HE)-induced chemical reaction at the surface of the drain, coupled with contact degradation appear to be the mechanisms responsible for the drain damage. [C1928]

### "Improvement of circuit-speed of HEMTs IC by reducing the parasitic capacitance"

We developed a novel process technology to remove the dielectric substance around gate electrodes to decrease parasitic capacitance. The process enabled us to increase the operating speed of the integrated circuit without causing any process damage. As a result, we achieved 90 GHz operation of a static T-FF circuit using InP-HEMT technology. This is the fastest T-FF, consisting of a FET, reported to date. We also showed the excellent potential of this technology for fabricating ultra-high speed ICs. [C1929]

### "Technology for millimetre wave radiometers"

Technology for millimetre wave radiometers is discussed. Distinction between coherent and incoherent detection is also addressed. As an example, a detail of the 70 GHz ultra low noise and high stability receivers for the European Space Agency (ESA) Planck Mission is given. These receivers are part of the low frequency instrument (LFI). The LFI receivers will make use of monolithic microwave integrated circuit (MMIC) and the key components are the low-noise amplifiers (LNA). Indium phosphide (InP) technology has been used for manufacturing the HEMT and PIN diode MMICs. Recently complete elegant breadboard model (EBB) of LFI 70 GHz receivers have demonstrated a 30 K noise temperature with 16 GHz bandwidth and a 1/f knee frequency of 30 MHz. Described radiometer modules form flexible basis for constructing radiometers with many pixels for millimetre wave imaging and remote sensing applications. [C1930]

### "AlGaIn/GaN HEMTs on SiC: towards power operation at V-band"

The operation of AlGaIn/GaN HEMTs on SiC substrate at V-band frequencies (50-75 GHz) is discussed. Both common source and dual-gate AlGaIn/GaN HEMTs on SiC substrate are optimized and investigated by active and passive load-pull measurements. At 60 GHz, a power density of  $\geq 0.5$  W/mm can be measured for a small common source AlGaIn/GaN HEMT limited so far by the available input power of the newly developed load-pull system. A common source HEMT with  $W_g=0.18$  mm yields a power density of 1.9 W/mm at 40 GHz and a linear power gain of  $\geq 5$  dB at 60 GHz, while several dual-gate AlGaIn/GaN HEMTs of  $W_g=0.18$  mm and 0.36 mm yield MSG/MAG values  $\geq 12$  dB at 60 GHz. [C1931]

### "3.5-watt AlGaIn/GaN HEMTs and amplifiers at 35 GHz"

Sub-0.2- $\mu$ m AlGaIn/GaN HEMTs were successfully scaled to 1.05 mm gate-width with minor gain reduction. On-chip single-stage amplifiers exhibited gains of 8 dB and 7.5 dB, as well as output powers of 3.6 W and 3.5 W, at 30 GHz and 35 GHz, respectively. This multi-watt output power at millimeter-wave frequencies well exceeded previous state-of-the-art for a GaN HEMT and is comparable to that from 6-7 times larger GaAs-based devices. [C1932]

### "State-space modelling of slow-memory effects based on multisine vector measurements"

Non-linear microwave devices and circuits often exhibit slow-memory effects. When subjected to two-tone, or more general multisine excitations, the characteristics of these devices and circuits depend on the offset frequency between the tones. Since modulated excitations are an integral part of telecommunication systems, models aimed for circuit and system design should be able to accurately represent slow-memory behaviour. In this work, we develop a modelling procedure based on the state-space modelling approach to accurately incorporate these slow-memory effects. The technique is experimentally demonstrated on a high electron mobility transistor (HEMT). [C1933]

### "Investigation of quantum effects in monolithic integrated circuits based on RTDs and HEMTs with

### **a quantum hydrodynamic transport model"**

This paper describes the first reported numerical simulations of monolithic integrated circuits of resonant tunneling structures and high electron mobility transistors based on  $\text{In}_{0.53}\text{Ga}_{0.47}\text{As}/\text{In}_{0.52}\text{Al}_{0.48}\text{As}/\text{InP}$  with a quantum hydrodynamic transport model (QHD-Model). For the numerical investigations the device simulator SIMBA is used, which is capable to handle complex device geometries as well as various physical models represented by certain sets of partial differential equations. As a new feature the involvement of a quantum potential is implemented to include quantum mechanical transport phenomena in different quantum size devices. The coupled solution of this quantum correction potential with a hydrodynamic transport model allows to model resonant tunneling of electrons through potential barriers and particle build up in potential wells. Different structure variations, especially the resonant tunneling diode area and the gate width of the HEMT structure show variable modulations in the output characteristics of the monolithic integrated device. [C1934]

### **"HEMTs with ultrahigh cutoff frequency"**

We succeeded in fabricating ultra-short 30-nm-gate InP-based high electron mobility transistors (HEMTs) with an extremely high current gain cutoff frequency ( $f_T$ ) of 547 GHz. The superior high-speed performance of our InP-HEMTs was mainly due to their optimized gate-recess structures. We investigated the effect of lateral gate-recess length on  $f_T$  with the asymmetric gate-recess technique, and clarified the impact of source- and drain-side recess lengths on their high-speed performance from the viewpoint of electron velocity and source resistance. We also demonstrated the importance of parasitic resistances, which were no longer negligible in these ultra-high-speed InP-HEMTs. [C1935]

### **"Direct-Coupled DC-40 GHz Amplifier for High-Speed Data Communication System"**

The millimeter wave transport over fiber needs more and more bandwidth according to SONET norm which must be able to propagate baseband modulated digital signal. This paper presents a modulator driver which is a direct-coupled amplifier to overcome the frequency limitations due to the link capacitors. A two stages DC-40 GHz GaAs P-HEMT amplifier including a level shift cell has been designed using the real frequency synthesis method. [C1936]

### **"A 94 GHz RF Electronics Subsystem for the CloudSat Cloud Profiling Radar"**

The CloudSat spacecraft, scheduled for launch in 2004, will carry the 94 GHz Cloud Profiling Radar (CPR) instrument. The design, assembly and test of the flight Radio Frequency Electronics Subsystem (RFES) for this instrument has been completed and is presented here. The RFES consists of an Upconverter (which includes an Exciter and two Drive Amplifiers (DA's)), a Receiver, and a Transmitter Calibrator assembly. Some key performance parameters of the RFES are as follows: dual 100 mW pulse-modulated drive outputs at 94 GHz, overall Receiver noise figure [C1937]

### **"Large-signal state-space model for Ge-based MHEMTs: construction and validation by an amplifier in multilayer thin-film technology"**

We construct a large-signal state-space model for thin-film metamorphic HEMTs based on germanium, directly from time-domain large-signal measurements. These thin-film HEMTs are used in a feedback amplifier circuit, designed as a multichip module with deposited thin layers (MCM-D) on glass. For the first time, we show that this type of state-space model can accurately predict the large-signal behaviour of a feedback amplifier. [C1938]

### **"Optically powered small e-field probes with integrated JFET- and HEMT-preamplifiers"**

Miniaturized electro-optical e-field probes (6times5times5mm<sup>3</sup>) based on a VCSEL as transmitter are presented. An integrated preamplifier based on a JFET (for the lower) and a HEMT (for the upper frequency range) increases the probe sensitivity and avoids the high pass filter characteristics of the original probe concept. The probes can be used in air as well as in liquids. They allow the e-field measurement both in the time and frequency domain with bandwidths up to the GHz range. With the HEMT sensor, a very high sensitivity of 90mV/m/radicHz in air was achieved. A possibility for sensitivity improvement by more than 20dB is presented [C1939]

### **"High conversion gain millimeter-wave optoelectronic mixer based on InAlAs/InGaAs metamorphic HEMT"**

We experimentally investigate the InAlAs/InGaAs metamorphic HEMT (m-HEMT) on GaAs substrate as a millimeter-wave optoelectronic mixer. The maximum internal conversion gain of 18.17 dB is obtained with 0 dBm



local oscillator (LO) power. The m-HEMT exhibits a wide LO frequency range which is well extended to the millimeter-wave band. We also measured the spurious free dynamic range of the m-HEMT as an optoelectronic mixer, whose value is about 96 dBHz<sup>23</sup>/[C1940]

#### "High-directivity photonic emitter for 10-Gbit/s wireless link"

We present a high-directivity photonic emitter with a high-gain antenna and a waveguide-output photodiode module. The photodiode module is integrated with UTC-PDs and HEMT amplifiers. A wireless link with the emitter achieved 10-Gbit/s data transmission. [C1941]

#### "Frequency and breakdown properties of AlGaN/GaN HEMTs"

AlGaN/GaN heterostructure transistors show potential in high frequency high-power applications because of their high breakdown voltages and high electron saturation velocities. The operating drain voltage, limiting the maximum RF output power, should be lower than breakdown voltage of the device. The frequency and breakdown properties of the AlGaN/GaN heterostructure transistors have been studied. [C1942]

#### "Self-heating effect on device characteristics of GaN/AlGaN HEMTs: 2D Monte Carlo device simulation"

Mechanism of self-heating in GaN/AlGaN HEMT and an influence of lattice-temperature rise on device characteristics are investigated theoretically. A novel simulation technique is applied, where a local temperature-dependent carrier transport is calculated by employing a Monte Carlo (MC) particle technique in combination with a heat flow calculation. The devices on substrates of three different materials, i.e., silicon carbide (SiC), sapphire (Al<sub>2</sub>O<sub>3</sub>) and silicon (Si), are studied and compared. A heat generation concentrates on the drain side of the area under gate, which is mainly coming from intra-valley scatterings of electrons in  $\Gamma$  and U valleys under high electric field. It is suggested that the SiC and the Si substrates are of great advantage to reduction of the self-heating effect on device characteristics because of their higher thermal conductivities, in comparison with the Al<sub>2</sub>O<sub>3</sub> substrate. [C1943]

#### "AlGaN-GaN HEMTs: material, device, circuit technology and applications"

The enabling features and performance of GaN based HEMTs as a high power, high bandwidth semiconductor technology are presented. Progress on materials development includes the development of AlGaN and AlN barrier HEMTs with room temperature electron mobility exceeding 2000 cm<sup>2</sup>/V-s. Trap free GaN HEMT devices with >10 W/mm power density and devices with >70 % efficiency are presented. Operation at >200 °C is reported. Simultaneous linearity and efficiency under class B is presented followed by discussion of mm-wave power performance. Finally, device scaling resulting in a total power >100 Watts and GaN HEMT circuit demonstrations are presented including mm-wave amplifier with >3 Watts at 30 GHz and 35 GHz. [C1944]

#### "AGaAs PHEMT Distributed Amplifier with Low Group Delay Time Variation for 40 GBit/s Optical Systems"

A four stage distributed amplifier MMIC with 11.2 dB  $\Gamma_B \pm 1.0$  dB gain and a bandwidth exceeding 50GHz has been demonstrated in a commercially available 0.15 $\mu$ m pseudomorphic GaAs HEMT technology. Group delay time variation from 1.5GHz to 40GHz equals to  $\Gamma_B \pm 3.5$  ps. When used as preamplifier, biasing can be applied from a single 5.2V supply via the reverse drain load without the need for an expensive external RF-coil for decoupling. The resulting overall power consumption is less than 230mW. The noise figure was measured to be between 5.1 dB and 3.0dB in the band from 3 GHz to 17 GHz. The output voltage swing of the 20GHz fundamental at the 1-dB gain compression is 2.1V, this makes the circuit also suitable as preamplifier for a modulator driver. [C1945]

#### "Simulation and Analytical Calculation of the Noise Figure in HEMT Gate Mixers"

A simplified analytic expression is developed to predict the noise performance of HEMT gate mixers. A nonlinear model of noise was given for theoretical study and implanted in ADS simulator. A contribution of each noise source was presented in this paper. This study is applied to a millimeter-wave HEMT gate mixer. The LO, RF and IF frequencies chosen for this test were 24.5, 28.5 and 4 GHz respectively. Good agreement is obtained between analytical calculation, simulation and experimental noise figure in single side band NFSSB. [C1946]

#### "A SiGe HEMT Mixer IC with Low Conversion Loss"

The authors present the first SiGe HEMT mixer integrated circuit. The active mixer stage, operating up to 10GHz

RF, has been designed and realized using a 0.1  $\mu\text{m}$  gate length transistor technology. The design is based on a new large-signal simulation model developed for the SiGe HEMT. Good agreement between simulation and measurement is reached. The mixer exhibits 4.0dB and 4.7dB conversion loss when down-converting 3.0GHz and 6.0GHz signals, respectively, to an intermediate frequency of 500MHz using high-side injection of 5dBm local oscillator power. Conversion loss is less than 8dB for RF frequencies up to 10GHz with a mixer linearity of  $\sim 8\text{dBm}$  input related 1dB compression point. [C1947]

#### "An Ultra Low Phase Noise W-Band GaAs-Based PHEMT MMIC CPW VCO"

A W-band voltage control oscillator (VCO) using 0.1-  $\mu\text{m}$  AlGaAs/InGaAs/GaAs PHEMT MMIC technology with ultra low phase noise is presented. This VCO demonstrated an operation frequency centered at 97 GHz with a tuning range of 2 GHz and an output power of 1 mW. The measured single side-band phase noise is -88 dBc/Hz at 1MHz offset. To the best of our knowledge, this phase noise performance is not only the best among the previously reported results for HEMT MMIC VCO at this frequency, but also rivals those for most VCOs using HBTs. [C1948]

#### "Rigorous modeling of high-speed semiconductor devices"

We present the state-of-the-art in simulation for industrial heterostructure devices based on SiGe/Si and III-V compound semiconductors. The work includes a detailed comparison of device simulators and current transport models to be used, and addresses critical modeling issues. Results from two-dimensional hydrodynamic analyses of Heterojunction Bipolar transistors (HBTs) and High Electron Mobility Transistors (HEMTs) with Minimos-NT are presented in good agreement with measured data. The examples are chosen to demonstrate technologically important issues which can be addressed and solved by device simulation. [C1949]

#### "DC-40 GHz amplifier for high-speed optical communications designed with the real frequency technique"

Synchronous optical network (SONET/SDH) requirements for 40 Gbps links impose transmitter drivers to provide a high and linear voltage swing to the modulator from a few kilohertz to 40 GHz. This paper presents a two stage DC-40 GHz GaAs P-HEMT amplifier including a level shift part for DC-coupling. The design synthesis method uses the real frequency technique. [C1950]

#### "Feedback Amplifier based on an Embedded HEMT in Thin-film Multilayer MCM-D Technology"

In this paper a feedback amplifier circuit integrated in MCM-D (MultiChip Module with Deposited thin films) on glass technology is presented. The active device of the amplifier is a thin-film Ge (germanium) -based HEMT. The HEMT is embedded in the bottom dielectric layer of the MCM-D. The combination of passive MCM-D technology and HEMTs on Ge allows for efficient semimonolithic integration of active devices and realization of MCMs with embedded passive and active components for amplifier circuits. [C1951]

#### "A new consideration of correlation between external noise sources in HEMT two-temperature model"

We consider the correlation between equivalent gate and drain noise sources in the two-temperature model to demonstrate a better compatibility between measured noise parameters ( $y_{opt}$ ,  $R_n$ ,  $F_{min}$ ) and the results from simulation. The originality of the contribution lies in considering correlation between external input and output equivalent noise temperatures ( $T_{in}$  and  $T_{out}$ ) for a transistor. Danneville's model has been used with two additional constants (real and imaginary parts of correlation) which has a better agreement with measurements. A two stage MMIC compatible HEMT low noise amplifier at Ka-band, which could be used for local multipoint distribution systems (LMDS) and fixed satellite services (FSS), has been designed and the effect on its noise figure of noise sources' correlation has been considered. A low noise amplifier in Ka-band has been designed, and the proposed model applied to it. The results of the simulation have been compared in three cases. [C1952]

#### "Design of a 49-GHz AlSb/InAs HEMT monolithic grid oscillator"

An AlSb/InAs HEMT monolithic grid oscillator is designed using full-wave electromagnetic techniques. Simulations predict an oscillation frequency of 49 GHz with a loop gain of 1.4, which is within 10% of the loop gain corresponding to optimum feedback. [C1953]

#### "1/f Noise Optimum for Field-Effect Transistors in Single-Ended Resistive Mixers"

The low-frequency noise in single-ended resistive FET mixers is investigated with respect to the influence of the

gate-source voltage. Using a simple broadband mixer with a Fujitsu HEMT, measurement and simulation results are compared yielding good agreement. Two mechanisms exist that create  $1/f$ -noise: The self-mixing process and the self-mixing current. Both cancel each other, i.e., there is a gate bias where a flicker noise minimum appears. The location of this minimum can be controlled with the DC output impedance. [C1954]

### "Envelope Currents Method with Extended Dynamic Range for the Simulation of Nonlinear Communication Circuits"

A novel approach to analyze the effects of non-linear distortion in communication circuits is reported based on a recursive algorithm. In each iteration a time-varying linear circuit excited by appropriate nonlinear currents obtained from an expansion of the nonlinearity is analyzed. This procedure has been applied to a common-source HEMT amplifier excited with a single tone and results show a very fast convergence together with a high dynamic range. The technique was used in the evaluation of the spectral regrowth and constellation distortion of a QPSK signal with raised cosine and root raised cosine conforming pulses produced by the amplifier at 5.8 GHz [C1955]

### "Low cost 5-bit Phase Shifter for DBS Phased Array Antennas"

A low cost patent pending 5-bit digital phase shifter has been developed for application in DBS receiving phased array antennas. New simplified loaded line architecture of less significant bit is proposed. The new circuit mitigates PCB technology limitations and reduces the number of switching components, which are low cost discrete p-HEMT FETs. TRL measurement technique was employed for extraction of the cold FET two states parameters. The digital 5-bit phase shifter operates in full satellite TV band from 10.7 to 12.75 GHz and has following main parameters: insertion loss 6 dB, insertion loss deviation  $\Gamma_B \pm 1.4$  dB, average RMS phase error  $3\Gamma_B$  ° and worst-case input/output return loss 11 dB. The control of the device is CMOS(5V) compatible with setting time less than 70 ns. [C1956]

### "Technology for Millimetre Wave Radiometers"

Technology for millimetre wave radiometers is discussed. Distinction between coherent and incoherent detection is also addressed. As an example, details of the 70 GHz ultra low noise and high stability receivers for the European Space Agency (ESA) Planck Mission is given. These receivers are part of the Low Frequency Instrument (LFI). The LFI receivers will make use of Monolithic Microwave Integrated Circuits (MMIC) and the key components are the Low-Noise Amplifiers (LNA). Indium Phosphide (InP) technology has been used for manufacturing the HEMT and PIN diode MMICs. Recently complete Elegant Breadboard Model (EBB) of LFI 70 GHz receivers have demonstrated a 30 K noise temperature with 16 GHz bandwidth and a  $1/f$  knee frequency of 30 mHz. Described radiometer modules form flexible basis for constructing radiometers with many pixels for millimetre wave imaging and remote sensing applications. [C1957]

### "Wideband cryogenic on-wafer measurements at 20-295 K and 50-110 GHz"

A measurement system has been developed for cryogenic on-wafer characterization at 50-110 GHz. The measurement system allows on-wafer S-parameter measurements of active and passive devices at this frequency range. The S-parameters of active devices can be measured as function of frequency, temperature, and bias conditions. As an example of cryogenic on-wafer measurements, measured S-parameters of InP HEMTs are presented at temperatures of 20, 80, 160, and 295 K and in the frequency range of 50-110 GHz. [C1958]

### "Improved fabrication process for obtaining high power density AlGaIn/GaN HEMTs"

An improved process for fabricating high power density AlGaIn/GaN HEMTs is now presented. Previously, a silicon nitride passivation layer has been shown to improve the power performance of AlGaIn/GaN HEMTs by minimizing surface related dispersion effects. Typically, this passivation layer has been deposited during the final stages of the fabrication process, with the device active area exposed to various potentially harmful plasmas and chemical treatments. In the new process, a high quality silicon nitride layer is deposited early in the fabrication process, serving to both protect the AlGaIn surface from damage and to minimize dispersion related phenomena. In addition, the silicon nitride layer provides an opportunity for forming well defined field-plated gate structures.  $0.6 \mu\text{m} \times 150 \mu\text{m}$  gate devices built with this process have demonstrated state-of-the-art CW output power and power added efficiency of  $>15.6$  W/mm and 44% respectively at 10 GHz, when operated at 60 V drain voltage. [C1959]

### "Low standby leakage current power amplifier module made with junction PHEMT technology"

A true enhancement-mode junction pseudomorphic HEMT (JPHEMT) with a high threshold voltage ( $V_{th}$ ) of +0.5 V was developed for single-supply power amplifiers. The novel JPHEMT exhibits an extremely low standby leakage current. The leakage current at 25°C is  $2.24 \times 10^{-10}$  A/mm and even at 85°C is  $8.64 \times 10^{-9}$  A/mm. It is suggested that the leakage current is the lowest among reported enhancement-mode FETs. Moreover, the novel JPHEMT exhibits a high turn-on voltage ( $V_F$ ) of 1.3 V at 1 mA/mm, which is 100 mV higher than that of a conventional JPHEMT. The PA module performance for 1.95 GHz W-CDMA systems, under conditions of  $V_{DS}$  of 3.5 V and an adjacent channel leakage power ratio (ACLR) of -37 dBc, demonstrated an output power ( $P_{out}$ ) of 26.5 dBm, an associated gain (Gain) of 26 dB and a power added efficiency (PAE) of 47%. The standby leakage current at gate-to-source voltage ( $V_{GS}$ ) of 0 V was less than 1  $\mu$ A even at 85°C. This high RF-performance, with extremely low leakage current results, indicate that the novel JPHEMT has single-supply amplifier capability. [C1960]

#### "Metamorphic AlSb/InAs HEMT for low-power, high-speed electronics"

Metamorphic high electron mobility transistors (HEMT) on GaAs substrates, with InAs channels and 0.1- $\mu$ m metal gates, have demonstrated 5 to 10 times lower power dissipation for equivalent  $f_{T}$  over conventional InAlAs/InGaAs lattice-matched HEMTs and MHEMTs. Our AlSb/InAs HEMTs exhibit transconductances higher than 1 S/mm at drain biases as low as 0.2 V, while maintaining measured  $f_T$  results greater than 200 GHz and  $f_{MAX}$  results approaching 200 GHz. We have achieved low power X-band MMIC low-noise amplifiers with greater than 7 dB/stage peak gain from 12-14 GHz and 6 mW/stage DC power dissipation. [C1961]

#### "A highly integrated quad-band GSM TX-front-end-module"

In this paper, we describe a highly integrated, quad-band (UGSM/EGSM/DCS/PCS), transmit, front-end module (TX-FEM) integrating power amplifiers, a PA controller, T/R switches, a switch controller, a dual-band directional detector/coupler, a diplexer, matching networks and harmonic filters in a single, 50  $\Omega$  input and output, 941041.5mm package. The module employs InGaP/GaAs HBT, AlGaAs/InGaAs/AlGaAs PHEMT, GaAs Schottky/passive, and Si Schottky/bipolar/CMOS semiconductor technologies and to the authors' best knowledge demonstrates the highest level of integration for a TX-FEM ever reported. The module utilizes the excellent performance and ruggedness characteristics of the Skyworks fourth generation HBT process and features 34 dBm  $P_{out}$  with 45% PAE GSM and 31 dBm  $P_{out}$  and 36% PAE DCS/PCS performance, while meeting a VSWR > 20:1 open loop ruggedness spec. [C1962]

#### "DARPA's program on Antimonide Based Compound Semiconductors (ABCS)"

The objective of DARPA's ABCS (Antimonide Based Compound Semiconductors) Program is to demonstrate low power dissipation, high frequency integrated circuits (up to 5000 components per chip) exploiting the high mobility and small bandgaps of 6.1 eV semiconductors. This talk will present an overview of the program and then discuss some exciting new results. [C1963]

#### "Ultra-low-noise amplifier for the ranges 0.5-1, 1-2, 2-4 GHz: design peculiarities"

Ultra-low-noise amplifiers, having noise temperature 10-20 K under moderate (uncryogenic) cooling, for the ranges 0.5-1, 1-2, 2-4 GHz are presented. The design peculiarities aimed to the most effective realization of modern PHEMTs potential are described. Relying on obtained experimental data prediction, it is shown that noise temperature of uncooled broadband amplifiers may be reduced down to 10 K over 0.3 to 3 GHz band. [C1964]

#### "High performance 50 nm T-gate In<sub>0.52</sub>Al<sub>0.48</sub>As/In<sub>0.53</sub>Ga<sub>0.47</sub>As metamorphic high electron mobility transistors"

We report the performance of 50 nm gate length metamorphic GaAs HEMTs with maximum transconductance ( $g_m$ ) of 1520 mS/mm and current cut-off frequency ( $f_T$ ) of 350 GHz, to our knowledge the highest  $g_m$  and  $f_T$  of a GaAs-based HEMT transistor. The devices were fabricated with a novel UVIII/PMMA T-gate resist stack and a non-selective "digital" wet etch gate recess technology which results in a highly uniform, high yield sub-100 nm HEMT technology. [C1965]

#### "A 3.3 V self-biased 2.4-2.5GHz high linearity PHEMT MMIC power amplifier"

A 3.3V single voltage self-biased 2.4GHz-2.5GHz high linearity AlGaAs/InGaAs/GaAs PHEMT MMIC power amplifier for wireless local-area network (WLAN's) applications (dual channel for 802.11a/b combination systems) is demonstrated. This two-stage amplifier is designed to fully match for a 50 ohm input and output impedance. In this process, a backside via-ground method is not used, so it can offer very low cost for the production of wireless LAN IC. With only a 3.3V drain voltage, the amplifier has achieved 30dB small-signal gain,



23.5dBm 1 dB gain compression power with 24.2% power-added efficiency (PAE). In addition, high linearity with 37.2dBm third-order intercept point at frequency of 2.45GHz is achieved. For this power amplifier MMIC, the WLAN requirements of power amplifiers including aspects of high efficiency, high gain, high linearity and operation at 2.4GHz ISM band are procured. [C1966]

#### "Backgating, high-current and breakdown characterisation of AlGa<sub>N</sub>/Ga<sub>N</sub> HEMTs on silicon substrates"

The backgating effect, as well as breakdown and high-current performance, of AlGa<sub>N</sub>/Ga<sub>N</sub> HEMTs on silicon substrates are studied. The material structure of the investigated devices differs in the thickness of the stress-relaxing intermediate layer sequence ( 1  $\mu$ m and 2.5  $\mu$ m thick). It is shown that the transistor backgating effect is reduced for the thicker sequence. Similarly, the reverse gate current is two orders of magnitude lower and the gate-drain breakdown voltage increases substantially in devices with the thicker sequence. An increase from 40 V to 160 V of the HEMT blocking capability, measured under electrostatic discharge-like conditions, is also observed. [C1967]

#### "Nonlinear model of high electron mobility transistor"

A new nonlinear HEMT model is presented. The model is based on a well-known small-signal model and includes a nonlinear description of some typically nonlinear components. A parameter extraction algorithm based on processing S-parameter and noise figure data measurements has been developed. [C1968]

#### "Self-aligned 0.12 $\mu$ m T-gate In<sub>0.53</sub>Ga<sub>0.47</sub>As/In<sub>0.52</sub>Al<sub>0.48</sub>As HEMT technology utilising a non-annealed ohmic contact strategy"

An InGaAs/InAlAs based HEMT structure, lattice matched to an InP substrate, is presented in which drive current and transconductance has been optimized through a double-delta doping strategy. Together with an increase in channel carrier density, this allows the use of a non-annealed ohmic contact process. HEMT devices with 120 nm standard and self-aligned T-gates were fabricated using the non-annealed ohmic process. At DC, self-aligned and standard devices exhibited transconductances of up to 1480 and 1100 mS/mm respectively, while both demonstrated current densities in the range 800 mA/mm. At RF, a cutoff frequency  $f_{T0}$  of 190 GHz was extracted for the self-aligned device. The DC characteristics of the standard devices were then calibrated and modelled using a compound semiconductor Monte Carlo device simulator. MC simulations provide insight into transport within the channel and illustrate benefits over a single delta doped structure. [C1969]

#### "10 Gb/s modulator driver IC with ultra high gain and compact size using composite lumped-distributed amplifier approach"

In this paper, a 10 Gb/s modulator driver MMIC is presented using a composite lumped-distributed amplifier approach, which allows a very compact chip size with ultra high gain and high output voltage swing. The chip size is further reduced using double-input distributed amplifier topology. The designed modulator driver is fabricated using a depletion-mode 0.15  $\mu$ m GaAs pHEMT process. The chip size is as small as 1.1 mm<sup>2</sup>. Measured small-signal gain is as high as 31.5 dB with 3 dB bandwidth of 15.0 GHz and good input/output return losses. The measured eye diagram shows clear eye open and output voltage swing of 7.4 V<sub>pp</sub> at the input of 10 Gb/s 223-1 pseudorandom NRZ data. The input swing is 0.22 V<sub>pp</sub>. To the knowledge of the authors, this result is among the highest gain per chip area with high output voltage swing for 10 Gb/s modulator driver ICs. [C1970]

#### "InP HEMT IC technology for 40 Gbit/s and beyond"

InP-based HEMT integrated circuit (IC) technology has contributed much to the research and development of highspeed optical communications systems and microwave/millimeter-wave wireless systems. This paper describes recent progress in our InP HEMT IC technology for 40 Gbit/s optical communications systems and discusses future prospects for 100 Gbit/s and beyond. [C1971]

#### "77 GHz low noise amplifier for automotive radar applications"

This paper discusses the design, fabrication, and testing of a three-stage microstrip pHEMT low noise amplifier (LNA) for automotive radar applications. The LNA goals were 4.5 dB noise figure and greater than 12 dB of gain at 76-77 GHz. The LNA as fabricated provides 10 dB of gain over the 70-78 GHz frequency range, with 4 dB noise figure at 77 GHz and better than 5 dB noise figure over the 75-79 GHz band. Based on a review of comparable work to date, the noise figure demonstrated at 77 GHz with this LNA surpasses that achievable with other low noise amplifiers. [C1972]

### "Highly linear and compact MMW phased array transmitters [CMMIC power amplifiers]"

In this paper, we describe more extensive linearity measurements (OIP3, NPR, ACPR) of multistage compact MMIC power amplifiers for future phased array transmitters at MMW frequencies. As an example, extremely high 500 mW/mm P1dB with 24% PAE at P1dB (peak PAE of 30% at Psat) and greater than 4 W/mm OIP3 were achieved on a 24-27 GHz HEMT MMIC with a compact size of 5.88 mm<sup>2</sup>. ACPR (-37 to -40 dB) and NPR tests (>18 dB at OBO of 4.5 dB) confirm the linearity and power capability of the technology. These MMICs provide leveraging performance for highly linear single beam and multibeam phased arrays for satellite, airborne and ground communication links. [C1973]

### "High dynamic range, triple gate-based compact DC-40 GHz variable attenuator MMIC for Ka-band variable gain amplifier ICs"

The design and performance of a compact DC-40 GHz variable attenuator MMIC are reported in this paper. Using our standard 4-inch 0.25- $\mu$ m GaAs power PHEMT technology, this T-type attenuator exhibits more than 30-dB dynamic range, with a nominal insertion loss of 4 dB over the DC-40 GHz band. By using triple-gate FETs, typical input power compression of more than 10 to 20 dBm is achieved with a die area of only 1 mm<sup>2</sup> (0.94x1.12 mm<sup>2</sup>) and better overall performance. This MMIC is 30% smaller than any previously reported analog attenuators operating in the DC-40 GHz frequency range. This attenuator is used as well in a variable gain amplifier (VGA), specifically designed for Ka-band LMDS and VSAT radios. From 24 to 32 GHz, the VGA MMIC demonstrates a maximum gain of 32 dB, with more than 35-dB dynamic range and 24-dBm output power at 1-dB gain compression. [C1974]

### "A 80-Gbit/s D-type flip-flop circuit using InP HEMT technology"

80 Gbit/s operation of a static D-type flip-flop (D-FF) circuit was achieved using InP-based HEMT technology with a cut-off frequency of 245 GHz and a transconductance of 1500 mS/mm. To generate 80 GHz differential clock signals from the single phase one in the circuit, a rat-race circuit was placed in front of the clock buffer. The power supply voltage was -5.7 V and power consumption was 1.2 W. Its performance was measured using a selector module that we developed. The results showed that the D-FF operated at 80 Gbit/s, which was more than half as much again as speeds reported to date. [C1975]

### "A 18-45 GHz double-balanced mixer with integrated LO amplifier and unique suspended broadside-coupled balun"

An ultra wide band double-balanced mixer with integrated LO buffer amplifier has been developed using 0.15 $\mu$ m depletion mode PHEMT technology. The mixer employs a unique broadside-coupled balun for superior 18-45 GHz bandwidth and overcomes many of the disadvantages of edge coupled transmission lines in microstrip or stripline. The mixer utilizes GaAs HEMT S-D diode mixing and integrates LO power amplifier to ease the drive requirements typically associated with this type of mixing. The LO amplifier has a distributed input stage and sequential traditional common source FETs for efficient power amplification. The LO can also be sub-harmonically pumped for 2 $\times$  frequency multiplication as well as fundamentally driven. The result is a mixer capable of -10 dB conversion gain for up or down mixing across many commercial frequency bands for 18-45 GHz. LO power requires only 0 dBm. [C1976]

### "Gate optimization of AlGaIn/GaN HEMTs using WSi, Ir, Pd, and Ni Schottky contacts"

High electron mobility transistors (HEMTs) were fabricated from AlGaIn/GaN on semi-insulating SiC substrates with WSi, Ir, Pd, and Ni Schottky contacts. The devices had 0.30  $\mu$ m T-gates with a total width of 300  $\mu$ m. Devices with Ir gates had the highest measured Schottky barrier and the best small-signal performance of all gate metal combinations attempted. These devices yielded maximum drain current densities of 1.03 A/mm, peak transconductances of 252 mS/mm, unity current gain cutoff frequencies of 46 GHz, and maximum frequencies of oscillation at 64 GHz. Power measurements of these same devices produced 6.5 W/mm with PAE of 32% at 10 GHz CW when optimizing for power. [C1977]

### "A 55 GHz HEMT monolithic voltage controlled sources"

Three mm-wave sources are described based on GaAs MMIC PHEMT technology. Different configurations of active 28-56 GHz doubler are used into the oscillator's chains. [C1978]

### "Optical receiver module using an InP HEMT transimpedance amplifier for over 40 Gbit/s"

We developed an optical receiver module for over 40 Gbit/s that uses two ultra-high-speed device technologies: an InP HEMT transimpedance amplifier (TIA) and a uni-travelling-carrier photodiode (UTC-PD). We introduced a new design criterion for the interface between the PD and TIA in order to obtain sufficient bandwidth. We confirmed error-free operation of the optical receiver module for a 50 Gbit/s non-return-to-zero optical input signal. [C1979]

#### **"A high spectral purity GaAs PHEMT MMIC balanced frequency quadrupler"**

The balanced configuration 7-28 GHz frequency quadrupler is described and compared with a single ended quadrupler at the same input frequencies. [C1980]

#### **"Modeling of the excitation of terahertz plasma oscillations in a HEMT by ultrashort optical pulses"**

Device models for the HEMT-based THz source are developed: an all-analytical model and a model in which the electron systems in the channel is considered analytically in the linear approximation, whereas the transport of the photogenerated electrons and holes is treated invoking an ensemble Monte Carlo particle simulation. Using these models, the frequency-dependent currents and device responsivity as functions of the structural parameters, gate voltage, and energy of the absorbed optical photons are calculated. An example of the dependences calculated for HEMTs with the fundamental plasma frequency  $f_P = 1$  THz and different values of the electron mobility  $\mu$  in the channel is performed. [C1981]

#### **"Feedback amplifier based on an embedded HEMT in thin-film multilayer MCM-D technology"**

In this paper a feedback amplifier circuit integrated in MCM-D (MultiChip Module with Deposited thin films) on glass technology is presented. The active device of the amplifier is a thin-film Ge (germanium) -based HEMT. The HEMT is embedded in the bottom dielectric layer of the MCM-D. The combination of passive MCM-D technology and HEMTs on Ge allows for efficient semimonolithic integration of active devices and realization of MCMs with embedded passive and active components for amplifier circuits. [C1982]

#### **"Simulation and analytical calculation of the noise figure in HEMT gate mixers"**

A simplified analytic expression is developed to predict the noise performance of HEMT gate mixers. A nonlinear model of noise was given for theoretical study and implanted in ADS simulator. A contribution of each noise source was presented in this paper. This study is applied to a millimeter-wave HEMT gate mixer. The LO, RF and IF frequencies chosen for this test were 24.5, 28.5 and 4 GHz respectively. Good agreement is obtained between analytical calculation, simulation and experimental noise figure in single side band NFSSB,. [C1983]

#### **"Single supply, high linearity, high efficient PHEMT power devices and amplifier for 2 GHz & 5 GHz WLAN applications"**

A single supply, high linearity, high efficient power devices and amplifier MMIC is implemented utilizing high performance of quasi-enhanced power PHEMT technology. The PHEMT power device features  $V_{th} = -0.65$  V,  $V_{bdg} = 26$  V,  $I_{max} = 144$  mA/mm at  $V_{gs} = 0.2$  V,  $G_m = 340$  mS/mm. When matched on-wafer compromise between power and efficiency, the OIP3 at peak IP3 is 40.5 dBm for 2 GHz and 37.0 dBm for 5.8 GHz, respectively. The power amplifier achieves at 5.8 GHz  $P_{out} = 27$  dBm with associated PAE=45 % at 5 V under  $V_{gs} = 0$  V,  $G_L = 14.5$  dB, OIP3=37.5 dBm. [C1984]

#### **"A chip-scale packaged amplifier MMIC using broadband hot-via transitions"**

The performance of RF hot-via transitions for use in chip-scale package (CSP) MMICs are presented. This is illustrated with the realization of a low noise amplifier MMIC using optimized hot-vias. Based on our standard 0.25- $\mu$ m GaAs low-noise PHEMT process, with BCB coating and backside metallization, this 2-stage low noise microstrip amplifier mounted with bumps on a carrier substrate achieved a linear gain of 15 dB over the 15- to 32 GHz frequency range. To the author's knowledge, this is the first demonstration of chip-scale packaged active MMICs using hot-via transitions. [C1985]

#### **"Integration of Bax Sr1-x TiO3 thin films with AlGaIn/GaN HEMT circuits"**

AlGaIn/GaN HEMTs have attracted considerable interest as power devices in microwave applications, promising greater than a tenfold increase in power-density as compared with GaAs devices. Similarly, BaxSr1-xTiO3(BST) thin films have been investigated for microwave circuit application because of their high dielectric constants, high tunability, relatively low loss, and fast switching speed. BST-based varactors are especially attractive for high power RF circuits since they can sustain relatively large AC fields, unlike diode technologies. Additionally due to

its high dielectric constant, BST is a candidate for every compact MMIC DC blocking capacitors, promising a 100-fold reduction in capacitor area as compared with SiN and SiO<sub>2</sub> capacitors. In this paper, we will provide a valid method of process integration for future active GaN circuit design and fabrication using BST capacitors. A C-band MMIC oscillator in GaN HEMT technology has been designed with BST capacitors as DC blocking capacitors. [C1986]

#### **"Dual band monolithic AGC amplifier for space applications based on a commercial 0.2 $\mu$ m PHEMT technology"**

This paper reports the design and measurement of a dual band monolithic AGC amplifier to be used in transmit/receive modules for Telemetry, Tracking and Control (TTC) of satellite systems. The amplifier is also included in a multifunction Monolithic Microwave Integrated Circuit, MMIC, containing frequency converters. The block diagram of this chip is shown. The goal of the work is to reduce the number, size, and consequently, the cost of the circuitry actually in use, whilst maintaining performance, through the use of mature GaAs PHEMT technology. Issues such as circuit topologies, dc power consumption, circuit area minimization and optimization are all important factors that are addressed during the design. [C1987]

#### **"Ka-band coplanar low-noise amplifier design with power PHEMTs"**

The design of a coplanar lownoise amplifier (LNA) is presented in this paper. Pseudomorphic high electron mobility transistors (PHEMTs), optimized for power applications, are used in order to evaluate the potentiality of this technology for mixed-mode applications. The three stages amplifier noise figure is lower than 2.6 dB on the 27-31 GHz frequency band with a 20 dB power gain. [C1988]

#### **"A novel distributed multicell multistage amplifier structure"**

A novel distributed multicell multistage amplifier structure is presented in this paper. This approach enables the design of multicell multistage power amplifiers based on distributed transistor arrays (multicells). Measured data of 40-device monolithic power amplifiers in the frequency hands 25-30GHz and 28-34GHz are also presented. The amplifiers have a small-signal gain of -15dB, a 1dB gain compression at output power (P<sub>1dB</sub>) of 32dBm and output intercept point (OICP<sub>3</sub>) of 38dBm. Measured results are compared with computed data. [C1989]

#### **"A GaAs PHEMT distributed amplifier with low group delay time variation for 40 GBit/s optical systems"**

A four stage distributed amplifier MMIC with 11.2 dB $\pm$ 1.0 dB gain and a bandwidth exceeding 50 GHz has been demonstrated in a commercially available 0.15  $\mu$ m pseudomorphic GaAs HEMT technology. Group delay time variation from 1.5 GHz to 40 GHz equals to  $\pm$ 3.5 ps. When used as preamplifier, biasing can be applied from a single 5.2 V supply via the reverse drain load without the need for an expensive external RF-coil for decoupling. The resulting overall power consumption is less than 230 mW. The noise figure was measured to be between 5.1dB and 3.0 dB in the band from 3 GHz to 17 GHz. The output voltage swing of the 20 GHz fundamental at the 1-dB gain compression is 2.1 V, this makes the circuit also suitable as preamplifier for a modulator driver. [C1990]

#### **"Direct-coupled DC-40 GHz amplifier for high-speed data communication system"**

The millimeter wave transport over fiber needs more and more bandwidth according to SONET norm which must be able to propagate baseband modulated digital signal. This paper presents a modulator driver which is a direct-coupled amplifier to overcome the frequency limitations due to the link capacitors. A two stages DC-40 GHz GaAs P-HEMT amplifier including a level shift cell has been designed using the real frequency synthesis method. [C1991]

#### **"A 94 GHz RF Electronics Subsystem for the CloudSat Cloud Profiling Radar"**

The CloudSat spacecraft, scheduled for launch in 2004, will carry the 94 GHz Cloud Profiling Radar (CPR) instrument. The design, assembly and test of the flight Radio Frequency Electronics Subsystem (RFES) for this instrument has been completed and is presented here. The RFES consists of an Upconverter (which includes an Exciter and two Drive Amplifiers (DA's)), a Receiver, and a Transmitter Calibrator assembly. Some key performance parameters of the RFES are as follows: dual 100 mW pulse-modulated drive outputs at 94 GHz, overall Receiver noise figure [C1992]

#### **"1/f noise optimum for field-effect transistors in single-ended resistive mixers"**



The low-frequency noise in single-ended resistive FET mixers is investigated with respect to the influence of the gate-source voltage. Using a simple broadband mixer with a Fujitsu HEMT, measurement and simulation results are compared yielding good agreement. Two mechanisms exist that create  $1/f$ -noise: The self-mixing process and the self-mixing current. Both cancel each other, i.e., there is a gate bias where a flicker noise minimum appears. The location of this minimum can be controlled with the DC output impedance. [C1993]

#### "Flip-chip integration of power HEMTs: a step towards a GaN MMIC technology"

In this paper, flip-chip integration is demonstrated as a method for faster progress towards a GaN MMIC technology by separating the development of active devices and passive matching circuits. This approach offers distinct advantages in the verification of passive components realized on a 2" SiC substrate. A proven 0.3  $\mu\text{m}$  GaAs PHEMT technology was used for the transistors that allowed to reproducibly verify both, the flip-chip transitions and the behaviour of the coplanar SiC structures. As an example, three X-band amplifiers in flip-chip technology are presented that demonstrate the feasibility of the technology. [C1994]

#### "A simplified approach for quasi-linear power amplifier distortion evaluation"

The paper presents a simplified approach for the evaluation of mild distortion in highly linear power amplifiers (PA) for microwave communications. In particular, it is shown how intermodulation distortion (IMD) can be accurately predicted on the basis of a single-tone power-swept Harmonic Balance analysis instead of using two-tone or multi-tone analyses leading to time-consuming and computationally expensive iterative PA design procedures. Moreover, simple equations provided in the paper show that common design specifications given in terms of maximum acceptable IMD are conveniently converted into constraints on a suitable non linearity index, involving both AM/AM and AM/PM amplifier characteristics. Experimental validation is provided in the paper on the basis of a 50  $\Omega$ -loaded GaAs 600  $\mu\text{m}$ -PHEMT based power amplifier simulated with Agilent ADS. [C1995]

#### "A SiGe HEMT mixer IC with low conversion loss"

The authors present the first SiGe HEMT mixer integrated circuit. The active mixer stage, operating up to 10 GHz RF, has been designed and realized using a 0.1  $\mu\text{m}$  gate length transistor technology. The design is based on a new large-signal simulation model developed for the SiGe HEMT. Good agreement between simulation and measurement is reached. The mixer exhibits 4.0 dB and 4.7 dB conversion loss when down-converting 3.0 GHz and 6.0 GHz signals, respectively, to an intermediate frequency of 500 MHz using high-side injection of 5 dBm local oscillator power. Conversion loss is less than 8 dB for RF frequencies up to 10 GHz with a mixer linearity of -8.8 dBm input related 1 dB compression point. [C1996]

#### "Recent advances in GaN HEMT development"

GaN HEMTs show great potential for RF applications. This paper provides an overview on the current status of GaN HEMT technology. It discusses the relevant properties of the AlGaIn/GaN material system. Describes the evolution of GaN HEMTs during the last 10 years, and highlights the state of the art performance of these transistors. A comparison with competing HEMT type is made and the prospects of commercial GaN HEMTs are discussed. [C1997]

#### "A low noise composite-channel metamorphic HEMT for wireless communication application"

A composite-channel metamorphic high electron mobility transistor (MHEMT) was developed for low noise high linearity application. The MHEMT was grown by molecular beam epitaxy (MBE) on GaAs substrates with InAlAs graded buffer. The composite-channel layers in the MHEMT include a top In<sub>0.55</sub>Ga<sub>0.45</sub>As layer, a middle In<sub>0.67</sub>Ga<sub>0.33</sub>As layer, and a bottom In<sub>0.55</sub>Ga<sub>0.45</sub>As layer. The design of this structure provides better electron confinement in the channel with less impact ionization as compared to conventional dual delta doped MHEMTs. This results in devices with higher linearity and drain to gate voltage as compared to the conventional metamorphic HEMTs. The 0.25  $\times$  160  $\mu\text{m}^2$  device with the novel channel structure exhibits a maximum frequency of oscillation  $f_{\text{max}}$  of 290 GHz and a current gain cut-off frequency  $f_{\text{tof}}$  of 110 GHz. The noise figure of the device at 6 GHz is 0.23 dB and an associated gain was 15.06 dB. The IP<sub>3</sub> of the device at 6 GHz is 18.67 dBm. The composite channel metamorphic HEMT shows great potential for high linearity and low noise application at high frequencies. [C1998]

#### "L-band, high efficiency 25 watt power amplifier using PHEMT for base station system"

In this paper, a 1.9 GHz watt high power amplifier using AlGaAs/InGaAs/GaAs PHEMT device for PHS base station applications is demonstrated. This amplifier utilizes a pre-matched FET which is composed of only a single 50 mm FET device and a MIS capacitor in a CuW flange package with other matching circuits on the FR4

PCB. Under 10 Volts and a 4 A dc bias condition, the amplifier has achieved 12.5 dB small-signal gain, 43.7 dBm 1 dB gain compression power with 43% power-added efficiency (PAE) and 44 dBm saturated output power with 41% PAR. In addition, high linearity with 53 dBm third-order intercept point is achieved. The ACP at 600 KHz offset from 1.906 GHz when operating at 39 dBm output power with  $\pi/4$ -DQPSK signal is better than 71 dBc. [C1999]

#### "Modelling of the trap related parasitic effects in metamorphic HEMT on GaAs substrate"

An investigation has been carried out on InAlAs/InGaAs metamorphic HEMTs on GaAs substrate dedicated to high performance amplifiers inserted in receiver as well as transmitter blocks of long distance and high bit rate optical links. This paper presents experimental results on parasitic effects, related to trapping/detrapping mechanisms (particularly gate lag, drain lag and kink effect). Trap signatures have been measured. The gate and drain lags impact is revealed to be different before or after the kink effect zone. These phenomena are detrimental both for digital and analogue applications of III-V field effect transistors. Models of these two effects, established according measurements and taking into account these impact changes, have been developed with ADS software in order to be inserted in the M-HEMT model. [C2000]

#### "High breakdown voltage In<sub>0.52</sub>Al<sub>0.48</sub>As/In<sub>0.53</sub>Ga<sub>0.47</sub>As metamorphic HEMT using In<sub>x</sub>Ga<sub>1-x</sub>P graded buffer"

Metamorphic In<sub>0.52</sub>Al<sub>0.48</sub>As/In<sub>0.53</sub>Ga<sub>0.47</sub>As HEMT grown on GaAs with In<sub>x</sub>Ga<sub>1-x</sub>P ( $x=0.48 \rightarrow 1$ ) graded buffer layer is reported. In this design the In<sub>0.53</sub>Ga<sub>0.47</sub>As channel layer was grown on top of the InGaP graded buffer directly without an InAlAs buffer as in the conventional design. The device shows high breakdown voltage: the measured on-state and off-state breakdown voltage are 11 V and 23 V, respectively, at a gate current of 0.1 mA/mm. The impact ionization rate and its dependence on temperature is also measured and analyzed, and the possible mechanism of the high breakdown voltage achieved is discussed. The metamorphic HEMT shows promising performance for its potential in power applications. [C2001]

#### "A tunable active MMIC filter for on-chip X-band radar receiver front-ends"

A 7.9-9.7 GHz tunable active monolithic microwave integrated circuit (MMIC) filter intended future on-chip X-band radar receiver front-ends is presented together with measured and simulated results. Typical measured filter data over the agile frequency band show a maximum gain of 11-16 dB, a noise figure of 6 dB, an input-referred third order intercept point of 0 dBm and 20-23 dB of out-of-band rejection at 2 GHz below the filter center frequency [C2002]

#### "InP HEMT and HBT applications beyond 200 GHz"

InP HEMT and InP HBT offer significant performance advantages for applications that range from microwave and millimeter-wave to fast digital and optoelectronic circuits. The improved transport characteristics, high transconductance, and optical integration properties of these devices hold great benefit for wireless and fiber-optic communications, radar, passive imaging and radiometer systems. We present an overview of recent results for InP devices and integrated circuits, including the current status of TRW's InP HEMT and HBT device and MMIC performance. The migration to new materials and process technology will enable volume production capability for high-performance applications to 200 GHz and beyond. [C2003]

#### "Improvement of the high frequency performance of HEMTs by bufferless technology"

By means of a 2D Monte Carlo simulation of 50-nm-gate lattice matched AlInAs/InGaAs HEMTs, we show the benefits of using bufferless technology in terms of improvement of the cutoff frequency and noise characteristics. We have found an increase of approximately a 15% in  $f_c$ ,  $f_{\text{tand}}$  and  $f_{\text{max}}$ . Moreover, though only a slight reduction of 0.2 dB in the minimum noise figure is obtained, the bufferless HEMT shows an important decrease of the noise resistance (almost 5  $\Omega$ ) and a 2.3 dB increase of the associated gain at 94 GHz [C2004]

#### "Low noise characteristics of double-doped In<sub>0.52</sub>Al<sub>0.48</sub>As/In<sub>0.53</sub>Ga<sub>0.47</sub>As power metamorphic HEMT on GaAs substrate with wide head T-shaped gate"

The 0.2  $\mu\text{m}$  gate-length power MHEMTs with the wide head T-shaped gate are characterized for DC, microwave, and noise performance. The MHEMT device shows the DC output characteristics having an extrinsic transconductance of 700 mS/mm and a threshold voltage of -0.92 V. The  $f_{\text{T}}$  and  $f_{\text{max}}$  obtained for the 0.2  $\mu\text{m}$  and 100  $\mu\text{m}$  MHEMT device are 120 GHz and 230 GHz, respectively. The MHEMTs exhibit the minimum noise figure,  $\text{NF}_{\text{min}}$ , of 1.26 dB and associated gain of 8.6 dB at 30 GHz. The  $\text{NF}_{\text{min}}$  measured at 35 GHz is 1.45 dB with associated gain of 7.5 dB. This noise data is first reported for power MHEMT devices with InGaAs channel

of 53% In. These excellent noise characteristics can be explained by the drastic reduction of gate resistance owing to the T-shaped gate with a wide head of about 1.2  $\mu\text{m}$  and the improved device performance. [C2005]

#### **"Innovative nitride passivation of 0.1 $\mu\text{m}$ InGaAs/InAlAs/InP HEMTs using high-density inductively coupled plasma CVD (HD-ICP-CVD)"**

A novel nitride passivation of 0.1  $\mu\text{m}$  InGaAs/InAlAs/InP HEMTs using high-density inductively coupled plasma CVD (HD-ICP-CVD) is reported. The nitride films deposited by HD-ICP-CVD have a lower wet HF etch rate (high density) and lower hydrogen concentration than those deposited by PECVD. A reduction of surface leakage current after passivation was observed; resulting in an approximate 40% improvement of off-state reverse breakdown voltage over that of PECVD passivated devices. The increase in breakdown voltage implies a potential improvement in power performance at millimeter wave frequency. A successful demonstration of HD-ICP-CVD passivated InP HEMTs promises adoption of HD-ICP-CVD nitride deposition for the next-generation InP HEMT passivation technique. [C2006]

#### **"High reliability of 0.07 $\mu\text{m}$ pseudomorphic InGaAs/InAlAs/InP HEMT MMICs on 3-inch InP substrates"**

The high-reliability performance of G-band (180 GHz) MMIC amplifiers fabricated using 0.07  $\mu\text{m}$  T-gate pseudomorphic InGaAs/InAlAs/InP HEMTs on 3-inch wafers is reported. Low noise amplifiers were life-tested at two-temperatures ( $T_1 = 200^\circ\text{C}$  and  $T_2 = 215^\circ\text{C}$ ) and stressed at  $V_{\text{dsof}} 1\text{ V}$  and  $I_{\text{dsof}} 250\text{ mA/mm}$  in a  $\text{N}_2$  ambient. The activation energy is as high as 1.7 eV, achieving a projected median-time-to-failure (MTTF)  $\approx 24106$  hours at a channel temperature of  $125^\circ\text{C}$ . MTTF was determined by 2-temperature constant current stress using  $|\Delta G_{\text{mp}}| > 20\%$  as the failure criteria. This is the first demonstration of the high reliability of 0.07  $\mu\text{m}$  pseudomorphic InGaAs/InAlAs/InP HEMT MMICs on a 3-inch InP production process. This result demonstrates a robust 0.07  $\mu\text{m}$  pseudomorphic InGaAs/InAlAs/InP HEMT production technology for G-band applications. [C2007]

#### **"Breakdown dynamics and RF-breakdown in InP-based HEMTs"**

In this paper, two approaches to enhance the breakdown voltage in InP-based lattice matched HEMTs (InP-LMHEMTs) have been investigated by means of a Monte Carlo simulator. In the first we have studied the effects of channel thickness on the breakdown dynamics. On-state breakdown calculations show that channel shrinking results in an enhancement of breakdown voltages. This study shows a frequency dependence of breakdown voltage which is relevant for power RF device applications. In the second approach the effect of a body contact (BC) to quench the breakdown effects and increase the breakdown voltage in InP-LMHEMTs is reported. On-state and off-state breakdown results show that the BC prevents holes generated by impact ionization (II) from accumulating in the channel and the buffer, inhibiting the parasitic bipolar effect (PBE). This improves the breakdown behavior and extends the range of the usable drain voltages. [C2008]

#### **"Monte Carlo study of electron transport in AlSb/InAs HEMT structures"**

A Monte Carlo model of in-plane electron transport in InAs/AlSb heterostructures is presented. Special attention has been paid to the effects of nonparabolicity, which are crucial for such a narrow gap system. Electron states are obtained from a Ben Daniel-Duke equation with energy-dependent effective mass. The effect of band mixing on scattering rates is included, at an approximate level, through the use of a "Bloch overlap factor". It has been shown that neglecting this factor leads to a strong underestimation of electron mobility, whereas our model gives realistic values. We have studied a standard single well structure and a more sophisticated double well structure. In the latter case, the electron transfer between the two coupled wells has been discussed. [C2009]

#### **"Use of a system simulator to study the influence of InP-HEMT excess gate current on 40 Gbits/s fiber optic system performances"**

The optical system performances are strongly related to the micro-optoelectronic device parameters inserted into the transmitter and receiver blocks. These blocks contain InP photonic and GaAs or InP electron devices (principally HEMTs or FETs). It has been previously demonstrated that the hybrid or monolithic integration used to assemble these devices (in OEICs) suffer from various intrinsic and process dependent parasitic effects. It could be very interesting to analyze the impact of these misfunctionings on the optical link performances taking into account the network requests. The evaluation of device parameters by means of breadboard (testbed) equipments is time consuming and cost effective, especially if iterative measurements are required. The emergence of system simulators drastically makes easier this evaluation. In this contribution, we report results on the use of an optical system simulator (COMSIS) to study the impact of one of the OEICs misfunctionings on optical system performances. [C2010]

### "Solid-state 8 GHz transient signal digitizer characterization"

A new technique leading to an accurate sampling of single shot high frequency signals is described. This technique provides 20 GHz sampling of electrical pulses up to 8 GHz bandwidth with a 60 dB dynamic range. The prototype of a transient digitizer involving this new principle is tested, with the goal of a new product development. We present the theory of the sampling operations, the outline of the prototype, the design and fabrication of an innovative set of specific GaAs MMICs, the assembling of the complete system and the first results obtained in performance characterization [C2011]

### "Compact LNA and VCO 3-D MMICs using commercial GaAs PHEMT technology for V-band single-chip TRX MMIC"

This paper presents compact V-band low-noise amplifier (LNA) and Ka-band voltage-control oscillator (VCO) 3-D MMICs for a V-band highly-integrated single-chip transceiver MMIC. 3-D MMICs are fabricated through the cooperation of commercial foundry GaAs pHEMT and 3-D interconnection processes. The LNA (chip size is 0.75 mm<sup>2</sup>) achieves 15 dB gain and better than 3.3 dB noise figure from 50 GHz to 60 GHz. The VCO (chip size of 0.52 mm<sup>2</sup>) achieves 11.5 dBm output power, 3.8 GHz oscillation frequency tuning range, and a phase noise of -102 dBc/Hz at 1 MHz offset and 28.6 GHz output signal. The cooperation 3-D MMIC technology with a high-performance commercial foundry technology promises low-cost, compact, and high performance millimeter-wave MMICs [C2012]

### "A 60 GHz millimeter-wave MMIC chipset for broadband wireless access system front-end"

This paper presents a complete 60 GHz millimeter-wave MMIC chipset for broadband wireless access system. This chipset consists of a low noise amplifier, a power amplifier, an up-converter, a down-converter, a quadrupler and an SPDT switch. Frequency range of these MMICs is from 55 GHz to 64 GHz, this frequency covers the entire 60 GHz application band [C2013]

### "Ku-band low noise MMIC amplifier with bias circuit for compensation of temperature dependence and process variation"

In this paper, a Ku-band low-noise MMIC amplifier is presented, which is equipped with a bias circuit that compensates not only temperature dependence of the FETs' gain but also gain variation between chips due to process variations. The Ku-band low noise MMIC amplifier with proposed gate-bias circuit was designed and manufactured. It was proved that the proposed bias circuit reduced the temperature dependence of the two-stage MMIC amplifier's gain from 1.4 dB/100 K to 1.0 dB/100 K. The chip area consumed for the bias circuit is less than 10% of the total chip size of 1.17 mm<sup>2</sup>. The gain variation between chips was reduced to 0.25 dB in RMS. This amplifier is suitable for active phased array applications [C2014]

### "A 7.9-9.7 GHz on-chip radar receiver front-end for future adaptive X-band smart skin array antennas"

In this paper, we present a 7.9-9.7 GHz on-chip radar receiver front-end intended for a digital beamforming X-band smart skin phased array antenna. This agile single-chip receiver front-end could potentially enable a significant size and cost reduction of the microwave receiver modules in such an adaptive frequency hopping radar system. Measured results show a close to adequate performance [C2015]

### "Design of an LTCC integrated tri-band direct conversion receiver front-end module"

This paper presents the results of a front-end receiver module integrating GSM/DCS/PCS band select functions and a direct conversion IC on a low temperature cofired ceramic (LTCC) substrate. The front-end-module (FEM) integrated a SP3T GaAs PHEMT switch for band selection, three SAW filters for pre-selection, and a direct conversion IC for down conversion of the RF signal. Integrated passives included a PCS balun, direct conversion IC matching elements and structures to improve the performance of differential SAW filters. The LTCC module contained 24 embedded passives and 15 surface mount components integrated on a 328 mil/4586 mil, 19-layer multi-layer integrated circuit (MLIC). Receiver sensitivity was better than -114 dBm, the system noise figure was less than 9 dB, and the return loss characteristics measured at the antenna input port were better than 10 dB for all three bands. EM simulation was used to achieve first pass design success and the modeling approach yielded excellent agreement between measured and simulated results [C2016]

### "A 60 GHz MMIC chipset for 1-Gbit/s wireless links"



This paper describes the development of a MMIC chipset for 60 GHz; radio links and radars. The chipset includes a low noise amplifier, an image rejection mixer, a frequency quadrupler, and a power amplifier. All were optimized to work together as a 1-Gbit/s radio link in the unlicensed 59 GHz to 64 GHz wireless band, although most are suitable for any application from 55 GHz to 70 GHz. These MMICs are fabricated in Agilent's advanced e-beam PHEMT process and have been demonstrated in fully operational 1-Gbit/s radio-links in field testing [C2017]

#### "A 94 GHz single-chip FMCW radar module for commercial sensor applications"

A single-chip 94 GHz frequency modulated continuous wave (FMCW) radar module has been developed for high resolution sensing under adverse conditions and environments. The monolithic microwave integrated circuit (MMIC) includes a varactor tuned VCO with injection port, very compact transmit and receive amplifiers and a single-ended resistive mixer. To enable bidirectional operation of a single transmit-receive antenna a combination of a Wilkinson divider and a Lange coupler was integrated. The circuit features coplanar technology and cascode HEMTs for compact size and low cost. These techniques result in a particularly small over-all chip-size of only 243 mm<sup>2</sup>. The packaged 94 GHz FMCW radar sensor achieved a tuning range of 6 GHz, an output power of 1 mW and a conversion loss of 5 dB. The RF performance of the radar module was successfully verified by real-time monitoring the time flow of a gas-assisted injection molding process [C2018]

#### "A 38/76 GHz automotive radar chip set fabricated by a low cost PHEMT technology"

Two complex transmit MMICs have been developed for the conversion of a 38 GHz VCO signal to 76 GHz. They consist of a 38 GHz driver amplifier, a frequency doubler and 76 GHz output amplifiers. These MMICs achieve a saturated output power of 14 dBm at 76 GHz and a maximum conversion gain of 9 dB and 12 dB, respectively. The transmit chips are supplemented by a 38 GHz voltage-controlled oscillator with 1.5 GHz tuning bandwidth and 10 dBm output power. The developed MMICs are designed for flip-chip mounting and have been fabricated by a production oriented PHEMT technology. They are suited for low cost automotive radar systems [C2019]

#### "A comparison of W-band monolithic resistive mixer architectures"

Three W-band resistive mixer architectures have been designed and their performance compared and contrasted. The mixers were fabricated using 0.1  $\mu\text{m}$  gate length InP HEMT technology for improved conversion loss performance compared to GaAs pHEMT. In particular, a state of art 94 GHz sub-harmonic resistive mixer is reported with 9.5 dB conversion loss when operated with a LO drive level of 2 dBm [C2020]

#### "A highly integrated MMIC chipset for 60 GHz broadband wireless applications"

A full and flexible MMIC (monolithic microwave integrated circuit) chipset has been developed for 60 GHz broadband wireless applications. It is based on several circuits operating in the 55-65 GHz frequency range. The MMICs have been fabricated on commercially available 0.25 and 0.15  $\mu\text{m}$  GaAs pHEMT processes. The chipset is focused on a MMIC multifunction chip (MFC) including a sub-harmonic mixer and an LO buffer allowing carrier 24LO suppression and image rejection. Several frequency multipliers by 2, 3 and 4 have been produced for the LO supply chain and use balancing topologies leading to fundamental or even-harmonics suppression improvement. Finally, a complete family of low noise/medium power amplifiers is described. All the circuits have been designed in order to ease integration, to reduce size and to achieve the cost requirements for such systems [C2021]

#### "A 36 W CW AlGaIn/GaN-power HEMT using surface-charge-controlled structure"

We describe high power 36 W CW operation at 30 V using AlGaIn/GaN HEMTs on SiC. Surface-charge-controlled structure, consisting of n-type doped thin GaN cap layer on AlGaIn/GaN HEMT structure, is used to obtain high gate-drain breakdown voltage and to reduce current collapse. By optimizing threshold voltage of this structure, we obtained a maximum drain current of 1 A/mm and a gate-drain breakdown voltage over 200 V. A 24-mm-wide-gate chip showed output power of 45.6 dBm (36 W) at 2.2 GHz with a liner gain of 9.7 dB [C2022]

#### "Applications of SiC MESFETs and GaN HEMTs in power amplifier design"

Very high power densities have been shown for both SiC MESFET and GaN HEMT devices. Both of these active devices benefit from the high breakdown voltages afforded by their wide-bandgap semiconductor properties. The GaN device also benefits from current densities as high as 1 A/mm. This high power density, along with good efficiency and linearity, provide an excellent base for future military and commercial power amplifier applications. High power densities are possible using narrow band power-matching networks. Although the gain-bandwidth limitation is exacerbated due to the high-impedance load lines required, high power design is possible even over

multi-octave bandwidths [C2023]

### "InP-based HEMT technologies toward 100 Gbit/s ICs"

This paper describes HEMT IC technology developed at NTT for 50 Gbit/s ICs, which are the key components in 40 Gbit/s optical communications systems these days. We have successfully integrated state-of-the-art HEMTs and achieved stable operation of D-FFs at over 50 Gbit/s with high yield and uniformity. It also discusses the potential of the technology for achieving 100 Gbit/s-class ICs and clarifies the HEMT performance requirements. The target performance of HEMTs is a gmof over 1.4 S/mm with an fTof over 280 GHz. Scaling down of HEMTs and reducing their parasitic capacitance are the major issues in achieving 100 Gbit/s operations. [C2024]

### "3.2 W/mm, 71% PAE AlGaIn/GaN HEMT operation at 20 GHz"

Summary form only given. In this paper we report record AlGaIn/GaN HEMT operation at 20 GHz. The 500  $\mu\text{m}$  total gate periphery devices exhibited a continuous wave output power of 3.2 W/mm with a gain of 5.2 dB and an associated power aided efficiency of 71%. To the best of our knowledge, these are the highest reported output power and PAE results for AlGaIn/GaN HEMT devices operating at 20 GHz. AlGaIn/GaN HEMTs offer increased breakdown, thermal conductivity, electron sheet carrier densities, and saturated electron velocities in comparison to existing group III-V technologies making them well suited for robust operation at frequencies through Ka-band. In order for this material system to meet the requirements for satellite communications and high performance radar, K-band operation is required. The results in this paper show promise for AlGaIn/GaN HEMT operation at 20 GHz. The device layers for this study were grown by MOCVD on SiC. 0.15  $\mu\text{m}$  Pt/Au T-gates in a 2  $\mu\text{m}$  source-drain channel were fabricated with electron beam lithography. The devices were passivated with silicon nitride and two levels of interconnect metal including airbridges for external connection. [C2025]

### "Modeling transconductance- and capacitance-voltage characteristics of AlGaAs/GaAs HEMTs"

A new simple and accurate analytical model for the transconductance-voltage and capacitance-voltage characteristics of AlGaAs/GaAs HEMT devices is presented. It is suitable for use in device simulation programs. The model is based on a simple formulation of the sheet carrier concentration in the two-dimensional electron gas (2-DEG) in the HEMT. The model takes into account the parasitic conduction in the AlGaAs. The model gives very good agreement with measured transconductance and capacitance characteristics for different HEMT devices. [C2026]

### "AlGaIn/GaN current aperture vertical electron transistors"

Describes AlGaIn/GaN current aperture vertical electron transistor (CAVET) structures. A CAVET consists of a source region separated from a drain region by an insulating layer containing a narrow aperture which is filled with conducting material. A device mesa is formed by reactive ion etching, and source contacts are deposited on either side of the aperture. The drain metal contacts the n-doped region below the aperture. Electrons flow from the source contacts through the aperture into the n-type base region and are collected at the drain. A Schottky gate, located directly above the aperture, is used to modulate the current passing through the aperture. In a CAVET, because the virtual drain (or pinched off region) is located underneath the gate, charge does not accumulate at the gate edge, so no large fields near the gate edge are present. Instead, our simulations show that the high field region in a CAVET is buried in the bulk. The CAVET therefore has the potential to support large source-drain voltages, since surface related breakdown is eliminated. [C2027]

### "High power hybrid and MMIC amplifiers using wide-bandgap semiconductor devices on semi-insulating SiC substrates"

An overview of hybrid and monolithic high-power microwave amplifiers using SiC MESFET and GaN HEMT active devices is presented. High power densities of 5.2 W/mm and 63% power added efficiency (PAE) have been demonstrated for SiC MESFETs at 3.5 GHz. This performance has driven the development of wide-bandwidth MMIC amplifiers, which have yielded 37 W of pulsed power at 3.5 GHz. GaN HEMTs on SiC substrates can achieve these high performance levels at frequencies where SiC cannot operate. At 10 GHz, a 12-mm GaN HEMT hybrid amplifier achieved a CW output power level of 38 W with an associated gain of 8 dB and PAE of 29%, complementing a previous pulsed result of 50.1 W. MMIC amplifiers have also been demonstrated using GaN-on-SiC technology. At 16 GHz, a two-stage GaN HEMT MMIC wide-bandwidth amplifier was capable of a peak power level of 24.2 watts with an associated gain of 12.8 dB and PAE of 22%. Recently, a 6-mm single-stage narrow-band MMIC amplifier has produced 32 watts of pulsed power at 10 GHz with an associated gain of 8.3 dB and a PAE of 35.3%. Finally, to validate progress in scaling unit cell performance to large devices, we have demonstrated 103 W of CW power from a single GaN HEMT transistor at

2 GHz with an associated drain efficiency of 52%. [C2028]

#### "AlGaIn/GaN HEMTs grown by MBE on semi-insulating HVPE GaN templates"

Summary form only given. Attempts to circumvent the low thermal conductivity of sapphire substrates by including in a device structure a thick (15  $\mu\text{m}$ ) GaN buffer grown by HVPE between the sapphire substrate and the MBE device layer stack. The heat generated in the device close to the surface of the structure is spread laterally in the HVPE buffer, increasing the effective thermal area of the device, and lowering the thermal impedance of the HEMT device. In contrast to SiC, the sapphire substrate technology is mature and affordable. Principally, both MBE and HVPE growth may be scaled up in area to grow on readily available large diameter sapphire substrates. [C2029]

#### "High performance of InGaP/InGaAs enhanced-mode PHEMT structures by gas source molecular beam epitaxy"

Single-supply-voltage enhanced-mode PHEMTs have been attracted more and more attention recently due to its applications in new generation wireless communication and automotive radar. Precise control over the gate groove deep etching process is a key issue for E-mode PHEMTs. According to the excellent etch selectivity of  $\text{In}_{0.49}\text{Ga}_{0.51}\text{P}/\text{GaAs}$ , we expect it may be a suitable material for E-mode PHEMT. In this article, GSMBE grown InGaP/GaAs E-mode PHEMT structures and E-mode PHEMT and related LNA circuits have been investigated. Results on the optimized structure design, growth conditions for materials and devices in particularly on the precise control InGaP composition, composition uniformity, and the P/As atomic mixing at the interface of InGaP/GaAs over the material growth process are presented. [C2030]

#### "Device Research Conference (Cat. No.02TH8606)"

First Page of the Article [C2031]

#### "High indium metamorphic HEMT on a GaAs substrate"

Metamorphic growth of device structures on GaAs substrates has advanced rapidly in recent years. High quality electronic and optical devices have been demonstrated. Also long-term reliability has been achieved with low noise MHEMT devices. Most of the development emphasis has been with structures conventionally grown on InP substrates. This work is motivated by the lower cost, larger diameter, and greater robustness of GaAs substrates compared to InP substrates. However an important characteristic of metamorphic growth is the degree of freedom in choosing the  $\text{In}_x(\text{GaAl})_{1-x}\text{As}$  composition and consequently the lattice constant between GaAs and InAs. Consequently new device structures can be achieved which are not possible by pseudomorphic growth on either GaAs or InP substrates. In this effort, solid source MBE was used to grow metamorphic HEMT structures with high indium content. For the conventional MHEMT, the indium concentration is graded to  $\text{In}_{0.52}\text{Al}_{0.48}\text{As}$  to expand the lattice constant to that of InP. Here the indium content was graded to  $\text{In}_{0.64}\text{Al}_{0.36}\text{As}$  to achieve a larger lattice constant than InP. The resulting surface roughness was examined by AFM. For a  $25\text{ }\mu\text{m} \times 25\text{ }\mu\text{m}$  area, the RMS roughness was 12E which is very similar to the roughness present in the conventional MHEMT with less indium content. [C2032]

#### "Interface roughness scattering of electrons in a [411]A $\text{In}_{0.53}\text{Ga}_{0.47}\text{As}/\text{In}_{0.52}\text{Al}_{0.48}\text{As}$ HEMT structure with super-flat interfaces"

InP-based InGaAs/InAlAs high electron mobility transistors (HEMTs) have demonstrated excellent high-frequency and low-noise performance due to their high saturation velocity of electrons in an InGaAs channel layer. Recently, we have reported that effectively atomically flat InGaAs/InAlAs interfaces over a wafer-size area ["[411]A super-flat interfaces"] can be formed in lattice-matched and pseudomorphic InGaAs/InAlAs quantum wells (QWs) grown on [411] A-oriented InP substrates by molecular beam epitaxy (MBE), and the highest mobility (90,500  $\text{cm}^2/\text{Vs}$  with two dimensional electron gas (2DEG) concentration of  $3.14 \times 10^{12} \text{cm}^{-2}$  at 77 K) of 2DEG for InGaAs/InAlAs HEMT structures was achieved in the [411]A pseudomorphic InGaAs/InAlAs HEMT structure. In this study, we have investigated the low temperature (20 K) 2DEG mobility in the lattice-matched InGaAs/InAlAs HEMT structure grown on the [411]A InP substrate with changing  $N_{\text{sub}}$  gate-biasing, and we found that interface roughness scattering in the [411]A sample was much smaller than that of an usual [100] sample. [C2033]

#### "P-GaN/AlGaIn/GaN high electron mobility transistors"

Despite the considerable improvement in GaN-technology and material quality, RF-dispersion is still one of the main issues hampering device progress. RF-dispersion affects device output power and device power added

efficiency (PAE) due to a reduction in saturation current and an increase in knee voltage at high frequencies and high biases. Surface passivation, using silicon nitride, has been found to mitigate RF-dispersion and microwave power degradation (B.M. Green et al, IEEE Electron Dev. Lett., vol. 21, pp. 268-270, 2000; S.C. Binari et al, IEEE Trans Electron. Dev., vol. 48, pp. 465-471, 2001; R. Vetury et al, ibid., vol. 48, pp. 560-566, 2001). This paper discusses a novel AlGaIn/GaN high electron mobility transistor (HEMT) device structure which has been developed to reduce RF-dispersion prior to silicon nitride passivation. The device structure uses a p-doped GaN cap layer to screen surface potential changes (regardless of origin) from affecting the gate-drain access region resistance, reducing the amount of RF-dispersion in the device. The epilayers of AlGaIn/GaN devices were grown by metal organic chemical vapor deposition (MOCVD) on a c-plane sapphire substrate. Sheet electron concentration and electron Hall mobility of the as-grown wafer were  $1.35 \times 10^{13} \text{ cm}^{-2}$  and  $1,475 \text{ cm}^2/\text{V}\cdot\text{s}$  at room temperature. [C2034]

### "Submicron enhancement-mode AlGaIn/GaN HEMTs"

Most recent GaN-based HEMT technology has been focused toward microwave power applications. In this work, we report DC and RF characteristics of the first E-mode AlGaIn/GaN HEMTs fabricated down to  $0.2 \mu\text{m}$  gatelength, and having an f<sub>tr</sub> reaching 25 GHz. Further improvement of E-mode GaN HEMTs could open potential applications for mixed-signal ICs with a high dynamic range. [C2035]

### "Power amplifiers for 60 GHz WLAN applications"

This paper presents MMIC power amplifiers for 60 GHz broadband radio applications. These amplifiers have been fabricated using a commercially available  $0.15 \mu\text{m}$  GaAs pseudomorphic HEMT technology. The output compression point of the prototype three stage single ended amplifier was +15 dBm and the small signal gain, 12 dB. The improved version achieved 15.5 dB linear gain and +14 dBm compression point using 3 V supply voltage. [C2036]

### "InP HEMT-based, cryogenic, wideband LNAs for 4-8 GHz operating at very low DC-power"

We present cryogenic broadband amplifiers for 4-8 GHz with very low dc-power consumption and low noise. Two different amplifiers were designed and manufactured, one of which was based on in-house InP devices and the other on commercial GaAs devices. When cooled to 15 K, the InP-based amplifier shows an input noise temperature of 3.9 K at a dc-power consumption of 3.7 mW. The GaAs-based amplifier shows an input noise temperature of 6.5 K at a dc-power consumption of 23 mW. [C2037]

### "Influence of growth conditions on the structural, optical and electrical quality of MBE grown InAlAs/InGaAs metamorphic HEMTs on GaAs"

InAlAs/InGaAs metamorphic HEMTs on GaAs have demonstrated low noise figures and high output powers with obvious advantages over structures grown on InP substrates. Indeed, from a processing viewpoint, the GaAs substrate is less brittle, less expensive, available in size up to 6 inches in diameter and then it is preferred for the production of high performance monolithic integrated circuits. Furthermore, the metamorphic scheme allows one to arbitrary choose the indium content in the InAlAs/InGaAs layers, which is a supplementary degree of freedom for the optimization of the active layers. Various buffer layers have been developed to accommodate the lattice mismatch between the active layers and the substrate. Production tools allows the growth of ternary as well as quaternary graded buffer layers; although the growth of a ternary alloy is more simple, it still requires the optimization of growth parameters like temperatures and arsenic fluxes. The layers presented here are based on thick InAlAs with a graded indium content from 1%-10% to 49% and terminated with an inverse step to obtain a highly relaxed  $\text{In}_{0.42}\text{Al}_{0.58}\text{As}/\text{In}_{0.43}\text{Ga}_{0.57}\text{As}$  structure. In the present work, the quality of the metamorphic HEMT structures is investigated by varying the growth parameters for the graded buffer layer as well as for the active layers. The structural quality is studied with high resolution X-ray diffraction, transmission electron microscopy (TEM) and atomic force microscopy, while the optical quality and the electrical quality of the HEMTs are studied with photoluminescence and Hall effect measurements respectively. [C2038]

### "0.1 $\mu\text{m}$ InP HEMT devices and MMICs for cryogenic low noise amplifiers from X-band to W-band"

We present the TRW  $0.1 \mu\text{m}$  InP HEMT MMIC production technology that has been developed and used for state-of-the-art cryogenic LNA applications. The  $0.1 \mu\text{m}$  InP HEMT devices typically show cutoff frequency above 200 GHz and transconductance above  $1000 \text{ mS/mm}$ . Aspects of device design and fabrication are presented which impact important parameters including the InP HEMT device gain, gate leakage current, and parasitic capacitance. One example of state-of-the-art cryogenic MMIC performance is a W-band cryogenic MMIC LNA operated at 20 degrees Kelvin that shows above 23 dB gain and a noise temperature of 30 to 40 K (0.45 to 0.6 dB noise figure) over the band of 80-105 GHz. [C2039]



### "A 48 GHz monolithically integrated frequency tripler with InP HEMTs"

We present a single-device 16-48 GHz frequency tripler realized with a 0.2  $\mu\text{m}$  InP HEMT process using coplanar waveguide technology. The fabricated circuit presents a maximum third harmonic conversion gain of -10.5 dBm, a maximum output power of -9 dBm, a first harmonic suppression of more than 25 dB, and a peak third harmonic conversion efficiency of 5.5%. This characteristics make it a suitable candidate for the generation of a stable high-frequency local oscillator. [C2040]

### "Importance of gate-recess structure to the cutoff frequency of ultra-high-speed InGaAs/InAlAs HEMTs"

We have succeeded in developing 30-nm-gate lattice-matched InGaAs/InAlAs HEMTs with an extremely high cutoff frequency  $f_{\text{tof}}$  472 GHz, the highest value yet reported for any transistor. The superior high-speed characteristics of our HEMT were mainly due to a much reduced lateral gate-recess length while maintaining a small gate-to-channel distance, which enhanced the average electron velocity under the gate. We fabricated asymmetrically recessed-gate HEMTs to separately investigate the effect of source- and drain-side recess lengths on  $f_t$ , and clarified that the drain-side recess is more critical to a superior  $f_t$ . Monte Carlo simulation results were consistent with the experimental observations [C2041]

### "Aluminium oxide technology for millimeter wave devices"

In this paper we present the results of the design and research of millimetre-wave amplifiers which had been manufactured on aluminium oxide substrates of a new type. The design of the amplifier is carried out based on calculated parameters offered by an equivalent scheme and measured V-I characteristics of the HEMT. The transition processes determining the mode of amplification in the HEMT amplifier have been simulated. The achieved parameters of multistage amplifiers are as follows:  $G_p=26$  dB,  $NF=2.1$  dB at  $f=28\ldots31$  GHz and  $G_p=24$  dB,  $NF=2.4$  dB at  $f=33.5\ldots36$  GHz. [C2042]

### "High speed electronics for lightwave communications"

In this talk, we will examine how semiconductor IC technologies such as CMOS devices, ASICs, HEMTs, HBTs, will impact the performance of these functional blocks at 40 Gbps as well as the future prospective of utilizing these IC technologies to realize transceivers to transport data rate in the 100+ Gbps regime. [C2043]

### "A novel dispersion compensation scheme based on phase comparison between two SSB signals generated from a spectrally filtered CS-RZ signal"

We proposed a novel dispersion compensation scheme based on relative phase detection of two SSB components of CS-RZ transmission code. These two components have NRZ pulse shape. Chromatic dispersion was detected by using 43-Gbit/s comparator HEMT ICs. The proposed technique successfully detected signs of chromatic dispersion and has sensitivity of 0.16-ps/nm/mV. Furthermore, the use of SSB-DD technique enabled us to achieve a wider dispersion tolerance (65-ps/nm) than that of a conventional CS-RZ signal. [C2044]

### "An ultra-wideband GaAs pHEMT driver amplifier for fiber optic communications at 40 Gb/s and beyond"

We have developed a GaAs pHEMT amplifier IC that can drive 40 Gb/s modulators requiring 4 V signals. The excellent amplitude flatness and phase linearity is exhibited both in small-signal S-parameter and in-fixture eye pattern measurements. The 78 GHz 3-dB bandwidth will drive the development of systems with bit-rates higher than 40 Gb/s and modulation formats such as RZ which require electrical components with very high bandwidths. [C2045]

### "A 24 GHz PHEMT-based oscillator"

Presents a systematic nonlinear procedure for designing microwave oscillators utilising a nonlinear PHEMT model, the negative resistance approach and the describing function concept. The procedure is applied in the design of a 24 GHz oscillator which is then realised in hybrid technology. Measurement results show -6% shift in the frequency but an acceptable agreement in the output power. A detailed analysis shows that the frequency shift arises mainly from inadequate CAD models in the K-band, for the microstrip components employed in the design. [C2046]

## "DC and 1/f noise characterization of cryogenically cooled pseudomorphic HEMT's"

First Page of the Article [C2047]

## "Phase noise amplitude distribution as indicator of origin of random phase perturbation in a test oscillator"

In this paper, we present an analysis of phase noise distribution. Phase noise, of a designed and realized test oscillator, as a consequence of low frequency (LF) noise up-conversion was simulated. The analysis shows that low frequency noise sources, which are inside the oscillator transistor, give the pure Gaussian distribution of phase noise and LF noise sources located outwith the transistor change this distribution. This behavior could be explained by the influence of the transistor and the transistor's package impedance, which contribute to the signal delay. The microwave test oscillator is designed and realized with AlGaAs/InGaAs HEMTs. [C2048]

## "Ultra low-power VCO based on InP-HEMT and heterojunction interband tunnel diode for wireless application"

The monolithic integration of tunneling diodes (TDs) with other semiconductor devices such as HEMTs or HBTs, creates novel quantum functional nonlinear devices and circuits with unique properties: the Negative Differential Resistance (NDR) and the extremely low DC power consumption. In this paper we present an InP-HEMT/TD based voltage controlled oscillator operating in the 6 GHz band suitable for wireless applications. The circuit draws a current of 1.75 mA at 500 mV and generates an output power of -16 dBm. The maximum tuning range is 150 MHz and the single sideband-to-carrier ratio (SSCR) is of -105 dBc/Hz at 5 MHz [C2049]

## "Sheet density of electrons in spacer layer of AlGaIn/GaN MODFET: calculating and analysing"

The finite barrier height at an AlGaIn/GaN heterointerface causes the nonvanishing probability of penetration of electrons into it. Therefore a nonzero carrier concentration appears also in the spacer layer of an AlGaIn/GaN MODFET. The existence of that charge has not been yet quantitatively considered, but its influence is observed on high gate polarisation in AlGaAs/GaAs heterostructures. Theoretical investigation of surface concentration in this layer for various gate voltages has shown an increasing characteristic if the gate voltage is increased. The comparison between surface concentration in the spacer layer and in the channel suggests that the former cannot be considered negligible, especially for higher values of gate voltage, when it becomes comparable with the latter. The possible consequences of this effect on device operation undoubtedly deserves to be examined (at least as the influence of parasitic capacitances, if the considerably degraded mobility of these electrons compared to the mobility of channel carriers is accepted beforehand). [C2050]

## "Wide band gap electronic devices"

The feature sizes of silicon devices approach values where fundamental physics limitations lead to diminishing returns on investment in further scaling, and wide band gap semiconductor materials look increasingly attractive for many applications, where high electron mobility, high current carrying capabilities, a high thermal conductivity, high temperature operation, and a high breakdown field make them superior to silicon and III-V semiconductor technology. GaN-based devices have demonstrated high-temperature operation with little or no degradation up to 300°C. The most spectacular results have been obtained for AlGaIn/GaN microwave power High Electron Mobility Transistors (HEMTs) that yielded over to 11 W/mm power at 10 GHz. The maximum density of the two-dimensional electron gas at the GaN/AlGaIn heterointerface or in GaN/AlGaIn quantum well structures can exceed  $2 \times 10^{13} \text{ cm}^{-2}$ , which is an order of magnitude higher than for traditional GaAs/AlGaAs heterostructures. Very large piezoelectric constants of AlN and GaN can be used in piezoelectric and pyroelectric sensors and could be taken advantage for enhancing the sheet carrier concentration and reducing leakage current in conventional electronic devices. Recently proposed Strain Energy Band Engineering and Pulsed Atomic Epitaxy techniques should allow us to independently control strain and lattice mismatch by using AlInGaIn/GaN heterostructures and should find important applications in power devices. SiO<sub>2</sub>/AlGaInN/GaN Metal Oxide Semiconductor Heterostructure Field Effect Transistors (MOSHFETs) and SiN/AlGaInN/GaN Metal Insulator Semiconductor Heterostructure Field Effect Transistors (MISHFETs) have exhibited performance superior to that of conventional AlGaIn/GaN devices and hold promise for power applications. GaN epitaxial layers can be grown on SiC, which allows us to combine superior transport properties of GaN with a high thermal conductivity of SiC. All this gives hope that electronic devices based on GaN will reach the same prominence as GaN-based blue and white, and UV light emitters. [C2051]

## "AlGaIn/GaN HEMTs on sapphire"

This paper presents the recent progress in the development of fabrication processes and device performance of

recessed as well as non recessed AlGaIn/GaN HEMTs at the University of Illinois. Maximum drain current density as high as 1.31 A/mm, record high extrinsic transconductance of 402 mS/mm, unity gain cut-off frequency ( $f_T$ ) of 107 GHz, and maximum frequency of oscillation ( $f_{max}$ ) of 148 GHz were demonstrated for recessed AlGaIn/GaN HEMTs with a gate length of 0.15  $\mu\text{m}$  grown by MOCVD. Results for MBE-grown devices are also presented.

[C2052]

#### "High performance voltage controlled bi-directional amplifiers in support of component reuse for large aperture phase array"

The objective of this paper is to provide a novel and innovative solution to reduce the projected high parts count for large aperture phase array (>100,000 elements). Bi-directional amplifiers are ideal for this application since RF amplification, in either transmit or receive directions, are controlled through bias thus eliminating the need for lossy switches that degrades the system noise figure performance. In addition, the size, weight, and cost of the transceiver module can be greatly reduced since only one amplifier is required. Two bidirectional amplifiers are presented here in both common gate and common-source configurations [C2053]

#### "A monolithic, 2 to 18 GHz upconverter"

This paper describes the design and evaluation of an upconverter IC for Electronic Surveillance Measures (ESM) applications. The purpose of the IC is to enable a signal anywhere in the 2-18GHz frequency band to be converted to 21-23GHz for subsequent downconversion to an IF suitable for digitisation. The required LO range is 23-41GHz. The RF, LO and IF ports of the IC are all single ended but the internal mixer is balanced at all ports and single-ended to differential conversion is realised on-chip, using novel broadband active and passive balun structures. The IC has been fabricated on the Triquint Semiconductor Texas' 0.25 $\mu\text{m}$  PHEMT process and has a measured conversion loss of 7dB to 14GHz, rising to 10dB by 18GHz. Input return loss is better than 12dB from 2 to 18GHz and LO rejection is over 30dB [C2054]

#### "Miniaturized and broadband V-band balanced frequency doubler for highly integrated 3-D MMIC"

This paper presents a compact V-band balanced frequency doubler 3-D MMIC with broadband performance. The MMIC was fabricated by combining a commercial 0.15  $\mu\text{m}$  GaAs pHEMT technology with the 3-D MMIC technology. A fabricated frequency doubler MMIC, which occupies 0.92 mm<sup>2</sup>, achieves 2.5-dBm output power and more than 15-dB fundamental signal suppression over 50-GHz to 68-GHz (30% bandwidth) for an 8-dBm input signal. A transmit MMIC, intended for 50-GHz application, realizes a 10-dBm output power and 40-dB isolation in an area of 1.48 mm<sup>2</sup>, it is supported by input and output buffer amplifiers. These fabricated MMICs are very effective in realizing compact and highly integrated single-chip transceiver MMICs. Furthermore, they can be re-used for various V-band applications, resulting in significant cost reduction [C2055]

#### "40-GHz MMICs for optical modulator driver applications"

This paper presents the simulated and measured performance of 50 kHz to 40 GHz distributed amplifier MMICs. The chips were fabricated in a double-doped AlGaAs/InGaAs/AlGaAs p-HEMT technology and designed using a microstrip configuration. The driver MMIC achieves 40-GHz bandwidth and provides 6.6 V<sub>p</sub>-p which is ideal for lithium niobate optical modulator driver applications [C2056]

#### "A 50-Gbit/s 1:4 demultiplexer IC in InP-based HEMT technology"

We have developed a 50-Gb/s 1:4 demultiplexer (DEMUX) integrated circuit with a wide phase margin of 108 degrees in 0.13- $\mu\text{m}$  InP-based HEMT technology. To increase the phase margin, we designed the data and clock distribution with the aim of achieving high symmetry and eliminating multiple reflections. The measured performance of the fabricated 1:4 DEMUX was suitable for practical use in 50-Gbit/s-class applications [C2057]

#### "A 0.15- $\mu\text{m}$ GaAs MHEMT transimpedance amplifier IC for 40-Gb/s applications"

The design and performance of a 0.15- $\mu\text{m}$  MHEMT transimpedance amplifier IC suitable for 40-Gb/s receiver applications is presented. Experimental results for the circuit demonstrate 263 $\Omega$  of transimpedance and 42.6 GHz 3dB-bandwidth with 0.075 pF of photodiode capacitance connected at the input. The IC dissipates 180 mW of power from a single +6V supply and has a die area of 0.72 mm<sup>2</sup> [C2058]

#### "Monolithic Ka-band VCO with wide tuning range"

This paper reports on the design procedure and measurement results of a Ka-band MMIC VCO utilizing a 0.15  $\mu\text{m}$  T-gate GaAs P-HEMT technology. A balanced buffer amplifier is also developed for assurance of output

power higher than 10 dBm. The VCO with center frequency of 35 GHz exhibits a tuning range of up to 3 GHz and typical output power of 10 dBm at 35 GHz without the amplifier. The best measured phase noise at 1MHz offset is -106 dBc/Hz. The buffer amplifier exhibits a typical gain of 5.9 dB with 15dBm output power. A large coupler is used for a good matching between the VCO and amplifier. [C2059]

#### "Access to microsystem technology: the CMP services solution"

CMP aims at providing Universities, Research Laboratories and Industries with the possibility to have their integrated circuits projects fabricated for prototyping and low volume production. Presently, users are serviced for CMOS double layer poly/double layer metal (DLP/DLM) 0.8  $\mu$ , DLM/TLM 0.6  $\mu$ , DLP/4LM 0.35  $\mu$ , SLP/6LM 0.18  $\mu$  and 0.12  $\mu$ , BiCMOS DLP/DLM 0.8  $\mu$ , SiGe BiCMOS DLP/DLM 0.8  $\mu$  and 5 LM 0.35  $\mu$ , and HEMT GaAs 0.2  $\mu$ . About 40 multi-project runs are offered per year. Micro Electro Mechanical Systems (MEMS) are provided in standard CMP runs in CMOS DLP/DLM 0.8  $\mu$ m and DLM/TLM 0.6  $\mu$ , BiCMOS DLP/DLM 0.8  $\mu$  and HEMT GaAs 0.2  $\mu$ , using compatible front-side bulk micro-machining. MUMPS process is offered as a surface micro-machining allowing one to integrate MEMS only microstructures. This paper describes the services available, focusing on the most advanced IC processes and on the MEMS processes. [C2060]

#### "A 43Gb/s full-rate-clock 4:1 multiplexer in InP-based HEMT technology"

First Page of the Article [C2061]

#### "An overview of efficiency enhancements with application to linear handset power amplifiers"

A consequence of high spectral efficiency provided by second and third generation cellular systems is the requirement for linear power amplifiers in the transmitter unit of the mobile handset. The battery nature of the mobile phone emphasizes high amplifier efficiency for extending talk time and battery life. This represents an inherent trade-off between amplifier efficiency and linearity. Recent efforts have focused on considering alternative approaches with the goal of improving the efficiency/linearity performance trade-off compared to traditional single-ended Class A/B topologies. Some alternative approaches are examined here [C2062]

#### "Ku-band MMIC's in low-cost, SMT compatible packages"

MM-wave components are very expensive due to the high package and assembly cost. This paper describes a 0.25  $\mu$ m PHEMT Ku-band 2-watt PA, and a 2.2 dB NF LNA MMIC in a low-cost SMT package (\$2.00). The package has excellent thermal resistance, 0.5 C/W, return loss (20 dB), and input/output isolation (40 dB), from DC-40 GHz. We believe this is the first time such a package design has been published [C2063]

#### "A broadband monolithic S-band class-E power amplifier"

This paper describes what is believed to be the first successful design and fabrication of a highly efficient broadband monolithic class-E power amplifier that operates at S-band and employs a 0.3  $\mu$ m  $\times$  1000  $\mu$ m PHEMT device. The amplifier measured performance shows a peak Power Added Efficiency (PAE) of 90% and a peak output power of greater than 23 dBm at 3.25 GHz [C2064]

#### "A 90Gb/s 2:1 multiplexer IC in InP-based HEMT technology"

First Page of the Article [C2065]

#### "Evolution of DC and RF degradation induced by high-temperature accelerated lifetest of pseudomorphic GaAs and InGaAs/InAlAs/InP HEMT MMICs"

The evolution of DC and microwave degradation induced by three-temperature accelerated lifetest of pseudomorphic GaAs and InGaAs/InAlAs/InP HEMTs was investigated. Reliability investigations were performed on monolithic microwave integrated circuit (MMIC) amplifiers fabricated using 0.1  $\mu$ m T-gate pseudomorphic GaAs and InGaAs/InAlAs/InP HEMTs. Operating at accelerated life test conditions, MMIC amplifiers were lifetested at three-temperatures (T1=255°C, T2=270°C and T3=285°C for 0.1  $\mu$ m GaAs PHEMT; T1=215°C, T2=230°C and T3=250°C for 0.1  $\mu$ m InGaAs/InAlAs/InP HEMT). High reliability performance with  $|\Delta S_{21}| > 1.0$  dB as the failure criteria was achieved on both technologies. From the 3-temperature lifetest, while GaAs PHEMT MMICs have activation energy of 1.7 eV, InGaAs/InAlAs/InP HEMT MMICs exhibit the activation energy of 2 eV. The difference is due to the distinct degradation mechanisms, which cause the S21 degradation. For GaAs PHEMTs, S21 degradation is mainly induced by the gradual gate metal sinking through the high-temperature lifetest; on the other hand, for InGaAs/InAlAs/InP HEMTs, the increase of access resistance on the source and drain regions causes the S21 degradation. Nevertheless, MTTF at Tchannel=125°C of



pseudomorphic GaAs and InGaAs/InAlAs/InP HEMTs is higher than 14108 hours. This is state-of-the-art of reliability performance reported on both technologies. From this study, the understanding of degradation evolution leads to the different approaches to improving the high-temperature reliability performance on pseudomorphic GaAs and InGaAs/InAlAs/InP HEMTs. [C2066]

#### "Microwave III-V semiconductors for telecommunications and prospective of the III-V industry"

The microwave III-V semiconductor IC technology (primarily GaAs) has emerged as a powerful enabling technology for wireless and optical communications in the past 5 years. It has been dominating, or making substantial penetration into, the market for handset power amplifiers and switches, advanced wireless LAN RF front-ends and various other key RF components for broadband wireless, wireless infrastructure, satellite telecommunications, high data rate fiber optical communications and automotive radar applications. The microwave III-V semiconductor IC industry has grown dramatically in the past 2-3 years. It is worth noting that the majority of the recently formed GaAs fabs are located in Taiwan. Their intent is to provide pure-play foundry services following the silicon foundry business model developed by TSMC and UMC. In this presentation, we discuss the key components of III-V microwave transistors (HBT, pHEMT and MESFET etc.) and their RFICs/MMICs, their electrical performance, major applications, market status, trends and opportunities. We define the current status for the global III-V semiconductor industry, the rapidly growing GaAs MMIC fab industry in Taiwan and its advantages for providing a one-stop, total solution for wireless and optical communication components customers. [C2067]

#### "Innovative nitride passivation for pseudomorphic GaAs HEMTs and impact on device performance"

A novel low temperature nitride deposition technique using high-density inductively coupled plasma chemical vapor deposition (HD-ICP-CVD) to passivate 0.15  $\mu\text{m}$  pseudomorphic GaAs HEMTs has been developed for the first time.  $\text{SiH}_4/\text{N}_2$  chemistries are used in HD-ICP-CVD for nitride deposition instead of  $\text{SiH}_4/\text{NH}_3/\text{N}_2$  in plasma-enhanced CVD (PECVD). HD-ICP-CVD nitride films have a lower wet BOE etch rate and lower hydrogen concentration than those of nitride films deposited by PECVD. Nitride films with high density and low hydrogen concentration provide a potential improvement of hermeticity and reliability, which are crucial for MMIC insertion in the commercial arena. Furthermore, HD-ICP-CVD passivated devices exhibit better performance combinations of reverse breakdown voltage, transconductance, and cutoff frequency than those of PECVD passivated devices. The results achieved here warrant the application of HD-ICP-CVD for next-generation nitride passivation in compound semiconductor technologies. [C2068]

#### "A 43 Gb/s full-rate-clock 4:1 multiplexer in InP-based HEMT technology"

A 43 Gb/s 4:1 multiplexer in 0.13  $\mu\text{m}$  InP-based HEMT technology contains a 52 Gb/s static D-FF and a phase adjuster giving the D-FF 360° effective phase margin. Microwave techniques and optimization of layout enable 43 Gb/s operation with 43 GHz full-rate clock. Power dissipation is 7.9 W at -5.2 V [C2069]

#### "A 90Gb/s 2:1 multiplexer IC in InP-based HEMT technology"

A 90Gb/s 2:1 multiplexer IC uses 0.13  $\mu\text{m}$ -gate InP-based HEMT technology. Parallel 2-ch input data are serialized. The differential outputs are 0.7Vpp. The 1.94x1.8mm<sup>2</sup> die consumes 1.3W from a -5.2V supply [C2070]

#### "A fully-integrated broadband amplifier MMIC employing a novel chip size package"

In this work, using a novel RF-CSP, a broadband amplifier MMIC including all the matching and biasing components was developed for Ku and K band applications. To integrate DC biasing components on the MMIC, an STO (SrTiO<sub>3</sub>) capacitor was employed. By employing an anisotropic conductive film for the RF-CSP, the MMIC fabrication process became very simple and cost effective. The packaged amplifier MMIC exhibited good RF performance in a wide frequency range. This work is the first report for fully-integrated Ku or K band MMICs which have all the biasing and matching components [C2071]

#### "A GaAs MHEMT distributed amplifier with 300-GHz gain-bandwidth product for 40-Gb/s optical applications"

A distributed amplifier with greater than 13.4 dB gain and 65 GHz bandwidth has been demonstrated using 0.15  $\mu\text{m}$  metamorphic GaAs HEMT technology. The amplifier has an average noise figure of 3.1 dB from 2-40 GHz and an output 1-dB compression point of 11 dBm at 22 GHz. The group delay variation from 1 to 40 GHz is  $\pm 7.5$  ps. The amplifier may be biased with a single supply voltage, and consumes only 105 mW. With these characteristics, the amplifier is ideally suited for 40-Gb/s optical networks [C2072]

### "A set of integrated circuits for 60 GHz radio front-end"

This paper describes results obtained within the MMIC research activity at the Helsinki University of Technology (HUT). These MMICs were developed for a 60 GHz broadband radio front-end. A set of circuits is reported including power, low noise amplifiers, mixers and signal generation circuits. They have been fabricated with a commercially available 0.15  $\mu\text{m}$  GaAs pseudomorphic HEMT technology. Finally, the performance of the circuits was measured at 60 GHz frequency: The power amplifier has 14 dBm output compression point and 15.5 dB small signal gain. The low noise amplifier exhibits 24 dB of gain with 3.5 dB noise figure and the up-conversion mixer circuit has 12.7 dB of conversion loss [C2073]

### "InGaP PHEMTs for 3.5GHz W-CDMA applications"

In this paper we present DC, small signal, and power characteristics of an InGaP PHEMT device using InGaP as barrier layer material. A comparison of intrinsic  $G_m$ ,  $R_{ds}$ ,  $C_{gs}$ , and  $C_{gd}$  with an AlGaAs PHEMT device showed that the InGaP PHEMT is very promising for microwave and RF linear power amplification. Operating from 12 V supplies, a 15.4 mm InGaP PHEMT device achieved 29.5 dBm output power with 12.1 dB associated gain and 25.6% power-added-efficiency at 3.5 GHz, while meeting the -40 dBc ACPR specification under W-CDMA stimulus [C2074]

### "RF performance and thermal analysis of AlGaIn/GaN power HEMTs in presence of self-heating effects"

Power, linearity and noise performance of AlGaIn/GaN power HEMTs are measured at different gate-to-source bias conditions in order to study the influence of self-heating on RF performance. Additionally, a load-pull system, capable of measuring intermodulation distortion products under pulsed mode of operation, is implemented for the first time. This new system is used to investigate the impact of self-heating on power device linearity. Also, for the first time, the effect of the RF drive on thermal effects and power added efficiency (PAE) is investigated. This forms the basis of more accurate nonlinear models. Finally, thermal simulations of 2-finger GaN FETs are performed under pulsed and continuous regimes to determine the temperature distribution caused by a 5W/mm power dissipation density [C2075]

### "Novel technique for determining bias, temperature and frequency dependence of FET characteristics"

A novel measurement of the dynamics of HEMT and MESFET behavior permits classification of dispersion effects and identifies operating regions that they affect. This reveals a simple structure to the otherwise complicated dynamic behavior that has concerned circuit designers. With this insight, it is possible to predict biases, temperatures and frequencies that dispersion will or will not affect. It is interesting to note that, for some devices, dispersion effects can be seen to exist at microwave frequencies and may therefore contribute to intermodulation distortion [C2076]

### "A 2-18 GHz wideband high dynamic range receiver MMIC"

In this paper, a 2 to 18 GHz wideband receiver MMIC for EW applications is presented. The receiver comprises a balanced cascode travelling wave LNA, a wideband active balun and a cold-FET ring mixer. The MMIC was fabricated using the TriQuint GaAs pHEMT process, using 0.25  $\mu\text{m}$  gate length devices. The measured conversion gain is greater than 7.8 dB between 3 GHz and 20 GHz. The RF input return loss is better than 10 dB between 3 GHz and 21.5 GHz. The receiver requires a drain bias voltage of 5 V and draws a drain current of approximately 260 mA. This wideband receiver is believed to be the first fully integrated single-chip receiver MMIC covering the 2 to 18 GHz frequency band [C2077]

### "Ku-band MMIC's in low-cost, SMT compatible packages"

mm-wave components are very expensive due to the high package and assembly cost. This paper describes a 0.25  $\mu\text{m}$  PHEMT Ku-band 2-watt PA, and a 2.2 dB NF LNA MMIC in a low-cost SMT package (\$2.00). The package has excellent thermal resistance, 0.5 C/W, return loss (20 dB), and input/output isolation (40 dB), from DC-40 GHz. We believe this is the first time such a package design is published [C2078]

### "Ultra low-power VCO based on InP-HEMT and heterojunction interband tunnel diode for wireless application"

The monolithic integration of tunneling diodes (TDs) with other semiconductor devices such as HEMTs or HBTs,

creates novel quantum functional nonlinear devices and circuits with unique properties: the Negative Differential Resistance (NDR) and the extremely low DC power consumption. In this paper we present an InP-HEMTTD based voltage controlled oscillator operating in the 6 GHz band suitable for wireless applications. The circuit draws a current of 1.75 mA at 500 mV and generates an output power of -16 dBm. The maximum tuning range is 150 MHz and the single sideband-to-carrier ratio (SSCR) is of -105 dBc/Hz at 5 MHz [C2079]

#### **"Enhancement mode PHEMT low noise amplifier with LNA linearity control (IP3) and mitigated bypass switch"**

A new LNA has been designed using single supply enhancement mode PHEMT process for WCDMA and other wireless application up to 6 GHz. The LNA has direct CMOS logic controllable integrated bypass-mitigated switch and LNA linearity (IP3) control switch. Two different kind of logic controls (0/3 V, 3/0 V) switch has been design for bypass-mitigated switch. In high linearity mode the LNA draws 8.5 mA current and has 15 dB gain, 1 dB noise figure, -6 dBm IP1dB, 7.3 dBm IIP3 with I/O return loss >11 dB. In low linearity mode the LNA draws 3.5 mA current and has 14 dB gain, 1.1 dB noise figure, -6.5 dBm IP1dB, 2 dBm IIP3 with I/O return loss >11 dB. The LNA bypass-mitigated switch has <3.5 dB insertion loss and NF, I/O return loss >11 dB and draws negligible current with 3/0 V logic, ~200  $\mu$ A for 0/3 V logic. Due to well-behaved match of LNA in High Linearity/Low Linearity/Bypass modes, this LNA has minimum mismatch effect for duplexers; and filters in a receiver system [C2080]

#### **"A 3-33 GHz PHEMT MMIC distributed drain mixer"**

A compact wide-band GaAs PHEMT MMIC distributed drain mixer covering RF frequencies from 3 to 33 GHz is reported. The measured results show that the conversion loss of the distributed drain mixer is better than 4 dB over the frequency range at an LO power of 13 dBm without IF amplification. Using the matching circuit in the output of the FETs, LO-to-IF and LO-to-RF isolations are better than 19 dB from 3 to 33 GHz. This mixer utilizes a simple distributed topology with single-gate HEMTs and achieves very broad band performance comparable to cascode or dual-gate distributed mixers. The overall chip size of this MMIC is only 1.741 mm<sup>2</sup> [C2081]

#### **"Ka-band direct digital receiver using 0.25 $\mu$ m GaAs PHEMTs"**

A new direct conversion wideband (26 GHz-28.5 GHz) six-port millimeter wave receiver using MMIC technology is proposed to meet the needs of mass-market wireless communications. This six-port receiver is designed to operate without the need for precise power reading and the use of digital signal processor (DSP) that is usually required in other receivers. The proposed receiver architecture is chosen to satisfy requirements of hardware receiver used in QPSK communications. The receiver contains one MMIC module consisting of a wide band six-port junction with four RF Schottky detectors, a receiver front-end and a base band module composed of video amplifiers and I&Q decoder. The maximum bit rate, at least 100 Mbs, is determined solely by the limiting speed of ancillary video amplifiers and analogue decoder. This new hardware receiver is proposed as a robust, rugged, low cost receiver for use in wide Ka-band wireless mass market QPSK communications such as LMDS services that are a prime example of communication equipment requiring such receivers. BER results are presented in the presence of noise and local oscillator (LO) phase shift [C2082]

#### **"A broadband, push-pull power MMIC operating at K/Ka-band frequencies"**

A 2-stage, push-pull power MMIC operating over the 20 to 36 GHz band is presented. With a P1dB and PSAT of 0.51 W and 0.78 W respectively, this IC has demonstrated a 1-dB power bandwidth, at a minimum output power of 28 dBm, that extends from 22 to 31 GHz. This result represents the highest combination of output power and bandwidth reported from a power MMIC operating at K/Ka-band frequencies. The size of this IC with integrated baluns is a compact 1.5  $\times$  3.75 mm<sup>2</sup> [C2083]

#### **"Intercept point behavior of Ka-band GaAs high power amplifiers"**

Intermodulation distortion (IMD) and output intercept point (OIP) behavior due to output power saturation, thermal effects and bias conditions were investigated for AlGaAs/InGaAs/GaAs pHEMT power amplifiers at Ka-Band frequencies. A power amplifier with a chip size of 3.3 mm<sup>2</sup> and a saturated output power of more than 27 dBm from 37-41 GHz, and a 3 mm<sup>2</sup> high gain compact dual-gate power amplifier with an output power saturation of 27 dBm at 35 GHz were designed. Intermodulation distortion for these two power amplifiers was compared. In order to separate fundamental effects from measurement induced phenomena, the principle accuracy of multi-tone measurement systems that are based on scalar spectrum analyzers was reviewed [C2084]

#### **"50 GHz high output voltage distributed amplifiers for 40 Gb/s EO modulator driver application"**

Both single-ended and differential distributed amplifiers were developed using 0.15  $\mu\text{m}$  GaAs power PHEMT for 40 Gb/s EO modulator driver circuits. The single-ended approach has achieved 12 dB gain up to 50 GHz, greater than 5 dB gain control range and output voltage  $>6.5$  Vp-p measured at 10 Gb/s. Power transfer data shows Psat of 20 dBm at 40 GHz, which translates to 6.3 Vp-p swing at 40 GHz. The differential approach has achieved 8 dB gain up to 45 GHz and differential output voltage of 9 Vp-p measured at 10 Gb/s. These amplifiers are suitable for use in fiber-optic communication systems [C2085]

#### "Characteristics of microwave power GaN HEMTs on 4-inch Si wafers"

We present the design and development of AlGaIn/GaN high electron mobility transistors (HEMTs) fabricated on a 4-inch Si wafer. The GaN HEMT devices demonstrate a maximum drain current of 900 mA/mm, a peak  $g_{\text{mof}}$  of 300 mS/mm, and a microwave output power density of 1.5 W/mm. To the best of the authors' knowledge, these are the best results reported on GaN HEMTs on 4-inch Si wafers [C2086]

#### "Output harmonic termination techniques for AlGaIn/GaN HEMT power amplifiers using active integrated antenna approach"

In this paper, effects of output harmonic terminations on PAE and output power of AlGaIn/GaN HEMT power amplifier are investigated. Using a traditional method of harmonic termination, we observe a substantial increase in PAE and output power. Further, we demonstrate the high efficiency AlGaIn/GaN HEMT power amplifier with harmonic termination characteristics by using the active integrated antenna approach. For the microstrip-based AlGaIn/GaN HEMT power amplifier, large signal measurements and comparisons of PAE and output power were done in class-AB operation with and without output harmonic terminations. For the antenna integrated power amplifier using an AlGaIn/GaN HEMT with 1 mm gate periphery, output power of 30 dBm and peak PAE of 55 % with a power gain of 14 dB were achieved at a drain voltage of 18 V and a gate voltage of -2.8 V [C2087]

#### "1 and 2 watt MMIC power amplifiers for commercial K/Ka-band applications"

Two ICs, specifically designed for commercial applications at K/Ka-band frequencies, are presented. These ICs provide 1 and 2 watts of linear power respectively, gain levels of typically 17 dB and a power added efficiency of 25% at the 1 dB gain compression point. While the RF performance parameters are not state-of-the-art, these compact chips establish new levels for power density, i.e. the ratio of output power to chip area. This figure of merit is particularly important for the cost sensitive commercial market [C2088]

#### "0.25 $\mu\text{m}$ pHEMT 40Gb/s E/O modulator drivers"

The development of two high voltage, 40 Gb/s E/O modulator driver ICs is described. Both were designed with a Distributed Amplifier (DA) topology utilizing a 0.25 $\mu\text{m}$  GaAs pHEMT production process. The modulator drivers exhibit 6 dB of small signal gain, greater than 42 GHz of 3-dB bandwidth, and better than 6.5-Vpp output swing [C2089]

#### "A 6 watt LDMOS broadband high efficiency distributed power amplifier fabricated using LTCC technology"

A novel new approach in designing high efficiency power distributed amplifiers for broadband wireless applications has been developed. This synthesis technique allows the designer to achieve power added efficiencies, during class B operation, greater than 50% while still preserving the low VSWR and broadband characteristics of distributed structures. The performance of these newly designed amplifiers can yield the same PAE and power output performance of narrow band, single-ended, reactively matched amplifiers, without the high sensitivity to manufacturing variations. This synthesis technique has been applied to develop LDMOS and PHEMT distributed power amplifiers for cellular base stations and portable communication applications [C2090]

#### "High efficiency wideband 6 to 18 GHz PHEMT power amplifier MMIC"

Design and performance of a power amplifier that has established new benchmarks for 6 to 18 GHz power is reported. The amplifier achieved 7.5 Watts max, 5.4 Watts average, 4 Watts min with 36 % max, 22 % average PAE and 12 dB of power gain from 6 to 18 GHz. This output power, bandwidth, and efficiency is superior to the best previously reported results. The amplifier is implemented in a fully selective 0.15  $\mu\text{m}$  double recess power PHEMT process [C2091]

#### "A 40 GHz-band fully monolithic VCO with a one-wave length microstrip resonator for accurate oscillation frequency"



A 40 GHz-band fully monolithic VCO with a one-wavelength microstrip resonator (MSR) associated with a dumping resistor is presented. Employing a one-wavelength MSR, high setting accuracy of oscillation frequency can be obtained, and it is a very effective method to improve yield of millimeter wave MMIC oscillator. Also the one-wavelength MSR with a dumping resistor is proposed for suppression of parasitic oscillation. In analytical approach, variation of oscillation frequency is less than 150 MHz over  $C_{gs}/C_{ds}$  / $C_{dg}$  variation of  $\pm 10\%$  in worst case. The measured VCO tuning range is 493 MHz and it is much wider than the variation of oscillation frequency caused by process variations [C2092]

#### **"A 15 watt PFP GaAs PHEMT MMIC power amplifier for 3G wireless transmitter applications"**

This work describes a wide-bandwidth highly integrated MMIC linear power amplifier implemented with high voltage GaAs PHEMT device technology targeting 3G wireless infrastructure applications. The MMIC amplifier exhibits 34 dB small signal gain, less than 0.5 dB gain variation across the UMTS frequency band centered at 2.14 GHz, and a peak-envelope power in excess of 15 W when biased with a 12 volt supply. Under a 64 traffic channel single carrier W-CDMA signal (test model 1, with a 11 dB peak-to-average signal ratio), the amplifier achieves 2W average output power and 17% power added efficiency at an ACPR of -40 dBc. Under a 9-channel single carrier IS-95 forward-link signal, the amplifier achieves 4 W average power at an efficiency of 25% at an ACPR of -38 dBc. The MMIC amplifier is highly integrated consisting of 3-gain stages, input and interstage matching circuits, and output pre-matching-all contained on the GaAs IC. The use of on-chip pre-matching for the output load line greatly simplifies and reduces off chip component matching elements and their tolerances. To the author's best knowledge, this amplifier represents the highest power and efficiency reported to date for a GaAs PHEMT amplifier realized at this level of integration [C2093]

#### **"Uncertainty estimation and optimal extraction of intrinsic FET small signal model parameters"**

In this paper, analytical expressions for the sensitivities in the parameters of a standard intrinsic FET small signal model are derived with respect to variations in the S-parameters. The sensitivities are used to estimate the uncertainty in extracted model parameters. The theories are applied to measurements made on a commercial HEMT device. Using models for the measurement uncertainties allows the model parameter uncertainties to be studied versus frequency and bias. As a result, optimal, minimum uncertainty parameter extraction can be performed independent of the bias voltage and without prior knowledge of the FET device characteristics. Thus making it suitable for implementation in automatic multi-bias extraction programs [C2094]

#### **"MBE growth of high quality AlGaIn/GaN HEMTs on resistive Si[111] substrate with RF small signal and power performances"**

For high-power and high-frequency electronic applications, the III-V nitride layers are usually grown on sapphire or silicon carbide substrates. However, the development of these applications on silicon substrates has obvious technological advantages (cost, integration). In the present work, AlGaIn/GaN heterostructures are grown on a resistive [111] silicon substrate (4000-10000  $\Omega \cdot \text{cm}$ ) in a reactive molecular beam epitaxy system using ammonia (Riber Compact 21). The structural quality of the epilayers as well as electrical properties have been investigated. AlGaIn/GaN HEMT devices with different gate lengths and source to drain spacings have been realized in order to investigate their static characteristics and RF power performances. [C2095]

#### **"InP HEMT and HBT technology and applications"**

InP HEMT and InP HBT offer significant performance advantages for applications that range from microwave and millimeter-wave to fast digital and optoelectronic circuits. The improved transport characteristics, high transconductance, and optical integration properties of these devices hold great benefit for wireless and fiber-optic communications, radar, passive imaging and radiometer systems. We present an overview of recent results for InP devices and integrated circuits, including the current status of TRW's, InP HEMT and HBT device and MMIC performance. The migration to new materials and process technology will enable volume production capability for high-performance applications to 200 GHz and beyond. [C2096]

#### **"Monte Carlo study of the breakdown of an AlInAs/GaInAs HEMT on InP with an InP etch stop layer"**

This paper deals with the evaluation of AlInAs/GaInAs HEMTs (high electron mobility transistors) with an InP etch stop layer (IESL) for power applications in the millimeter and submillimeter wave ranges. We use a 2D Monte Carlo model in order to analyze the capability of the device to handle high voltage with small gate length. [C2097]

### "Ultra-high-speed IC and OEIC technologies beyond 40 Gbit/s"

This paper describes ultra-high-speed IC and OEIC technologies beyond 40 Gbit/s using InP-based microelectronics. 0.1- $\mu\text{m}$  gate-length InP HEMT IC technology for 40 Gbit/s/channel systems and OEIC technologies for future 100-Gbit/s class optical receivers are reviewed [C2098]

### "Recent test results of a flight X-band solid-state power amplifier utilizing GaAs MESFET, HFET, and PHEMT technologies"

In support of the MErcury Surface, Space ENvironment, GEochemistry, and Ranging (MESSENGER) spacecraft that The Johns Hopkins University Applied Physics Laboratory (JHU/APL) is currently building under NASA's Discovery Program, an onboard telecommunication system has been designed and will be assembled at JHU/APL. One of the main components of the system is an X-band solid-state power amplifier (SSPA) operating at 8.433 GHz that supports various downlink antennae including an eight-element phased array. This SSPA subsystem is comprised of over 40 hybrid devices, each of which along with internal matching circuits contains one of the following five different GaAs part types manufactured by Triquint Semiconductor, Inc.: (1) 8810 Metal-Semiconductor Field Effect Transistor (MESFET) Gain Block Amplifier Microwave Monolithic Integrated Circuit (MMIC), (2) 4230 Heterostructure Field Effect Transistor (HFET) Amplifier, (3) 4240 HFET Amplifier, (4) 9083 Pseudomorphic High-Electron-Mobility Transistor (pHEMT) High Power Amplifier MMIC, and (5) 6336 MESFET Phase Shifter MMIC. The hybrid package has been custom-designed at JHU/APL specifically for spaceborne applications. In this paper, we will discuss the 168-hour burn-in and 1000-hour life tests for the hybrids that have been undergoing device screening and space qualification testing. For the approximately 140 samples that were screened in the burn-in test, there were minor shifts in certain device parameters such as the 1-dB compression and power gain, although the DC drain and gate currents showed negligible changes. Such initial parameter shifts are typical of devices settling into their stable long-term useful-life behaviors. At present, the life test is in progress and interim test results will be presented. All preliminary indications point to sufficient device reliability for the MESSENGER space mission. This work demonstrates the viability of employing a blend of proven (MESFET) and recently matured (PHEMT and HFET) technologies for space hardware. [C2099]

### "Reliability evaluation on dual-etch-stop InGaAs PHEMTs"

Pseudomorphic high electron mobility transistor (PHEMT) technology has been widely used in microwave switches and power amplifiers (PAs) for telecommunication applications. Because of its higher charge density and greater saturated electron velocity in InGaAs channel compared with GaAs used in MESFETs, the PHEMT exhibits lower insertion loss in switch, and higher power gain and added efficiency in PA operations. However, due to the 2-D nature of InGaAs channel in PHEMT, most of its electrical parameters are much more sensitive to the recess depth in comparison with that from traditional MESFET technology. The use of etch-stop material under the gate metal will greatly improve the precise control of gate recess and simplify process steps. This paper presents the results and detailed analysis of on-wafer-level accelerated DC and RF biased stress test and three-temperature thermal stress lifetest on our 0.9  $\mu\text{m}$  Dual-Etch-Stop (DES) PHEMT process. High-temperature-operating-life (HTOL) test on single-pole-double-throw (SPDT) switch products using this DES PHEMT process has also been performed. Our report describes the reliability experiments and compares the reliability results of this new DES PHEMT process against the standard non-etch-stop (NES) PHEMT baseline material. Statistical analysis derived an activation energy  $E_a = 1.4$  eV and an MTTF >107hours at 125°C. [C2100]

### "Experimental and numerical analysis of gate- and drain-lag phenomena in AlGaAs/InGaAs PHEMTs"

Gate- and drain-lag phenomena are investigated in AlGaAs-InGaAs pseudomorphic HEMTs by comparing experimental transient and pulsed characteristics with simulated ones. A consistent interpretation for experimental data is provided, relying on the assumption that acceptor-like surface traps are present at the ungated surface between gate and source/drain contacts. [C2101]

### "Influence of silicon nitride passivation on DC and RF behaviour of InP HEMTs"

In this paper, the influence of silicon nitride ( $\text{Si}_3\text{N}_4$ ) passivation on the DC and RF behaviour of a delta-doped InP based HEMT is examined. For operation stability and better reliability of MMICs using HEMTs, devices must be coated with a passivating, dielectric layer.  $\text{Si}_3\text{N}_4$  is an excellent candidate for use as a passivation layer since it can also be used as MIM capacitor dielectric for InP MMIC fabrication. After passivation, a shift in the threshold voltage of the transistor is noticed, together with an increase in transconductance. However, the passivation layer increases the parasitic capacitances and thus the RF performance of the device drops. [C2102]

### "Improving baseband performance of four-cascaded single stage distributed amplifiers for high speed optical communication"

This paper demonstrates an improved four cascaded single stage distributed amplifier, which operates over the frequency range from DC to 20 GHz. Simulation results show that the proposed circuit offers superior baseband performance over the existing cascaded single stage distributed amplifier topology. In addition, it provides 10 dB higher gain than the conventional distributed amplifier using the same amount of active devices. [C2103]

### "Solid-state RF power amplifiers: status and perspective"

Solid-state power electronics has been developed for the last 50 years. Germanium, silicon, gallium arsenide, indium phosphide and their related compounds are, or have been, studied over this period. Wide band gap semiconductors are now new players in this field. This paper tries to give an overview of this strategic field, especially focused on the compound devices. Wide band gap devices are very suitable for extremely high power amplifier applications and GaAs-like components could not compete for the highly demanding applications, but classical III-V devices will still occupy the market field requiring low to medium power level and high power efficiencies. [C2104]

### "GaN devices for microwave applications [CFET/HEMT]"

AlGaIn/GaN field effect transistors offer spectacular improvements in performance compared to conventional III-V components. In particular they are well suited to applications requiring high levels of output power and are capable of producing RF output power levels approaching 12 W/mm of gate periphery with power added efficiency close to theoretical limits. This paper describes the current status of GaN based FETs and discusses circuit functions and system applications that can benefit from this disruptive technology. [C2105]

### "Role of FET size in the optimization of MMIC nonlinear performance"

One of the main advantages of MMIC technology is the possibility of making a full use of scaling properties to improve performance. The majority of approaches which apply device-scaling only attend to linear criteria, without considering the improvement that could be achieved in nonlinear performance, like intermodulation distortion. In this paper, nonlinear design criteria are proposed to help in the selection of HEMT gate-width in MMICs, which are applied to several circuits, including a differential amplifier, a doubly balanced mixer and a single FET resistive mixer. [C2106]

### "Comparison of surface passivation on films for reduction of current collapse in AlGaIn/GaN high electron mobility transistors"

Three different passivation layers (SiNx, MgO and Sc2O3) were examined for their effectiveness in mitigating surface-state-induced current collapse in AlGaIn/GaN high electron mobility transistors (HEMTs). The plasma-enhanced chemical vapor deposited SiNx produced 80-85% recovery of the drain-source current, independent of whether SiH4/NH3 or SiD4/ND3 plasma chemistries were employed. Both the Sc2O3 and MgO produced essentially complete recovery of the current in GaN-cap HEMT structures and 80-95% recovery in AlGaIn-cap structures. The Sc2O3 had superior long-term stability, with no change in HEMT behavior over 5 months aging. [C2107]

### "Impact ionization in high performance AlGaIn/GaN HEMTs"

We report compelling evidence of impact ionization in high-performance AlGaIn/GaN HEMTs. Relevant to the present paper, these devices also show excellent low-leakage DC properties that contain signatures of impact ionization in the output and sub-threshold characteristics. Temperature and bias dependent data are presented to support the identification of impact ionization in the devices. [C2108]

### "AlGaIn/GaN HEMT high-power and low-noise performance at $f \geq 20$ GHz"

Reports on the power and noise performance of AlGaIn/GaN HEMTs in the K (18-27 GHz) band. At 20 GHz, a record CW output power of 2 W with an associated gain of 8 dB and PAE of 33% has been achieved on an 8-finger 0.2  $\mu\text{m}$  × 500  $\mu\text{m}$  device. Minimum noise figure of 1.4 dB has been achieved on a 0.15  $\mu\text{m}$  × 200  $\mu\text{m}$  device at 26 GHz. The data demonstrate the viability of AlGaIn/GaN HEMTs for high-frequency power and LNA applications. [C2109]

### "Packaging of microwave integrated circuits operating beyond 100 GHz"

Several methods of packaging high speed (75-330 GHz) InP HEMT MMIC devices are discussed. Coplanar

wirebonding is presented with measured insertion loss of less than 0.5 dB and return loss better than -17 dB, from DC to 110 GHz. A motherboard/daughterboard packaging scheme is presented which supports minimum loss chains of MMICs using this coplanar wirebonding method.. Split-block waveguide packaging approaches are presented in G-band (140-220 GHz) with two types of MMIC-waveguide transitions: E-plane probe and antipodal finline. [C2110]

#### "High linearity, robust, AlGaIn-GaN HEMTs for LNA and receiver ICs"

AlGaIn-GaN HEMTs have not only been identified as the technology of choice for next generation high-power, high frequency applications but recently have also garnered interest for low noise receiver applications. In this paper, we discuss the noise figure and linearity of robust GaN HEMTs for LNA integrated circuits. GaN HEMTs with a low noise figure of 0.75 dB at X-band are presented. We believe this is the first comprehensive report combining all major requirements of a robust LNA-receiver technology: low noise figure, high linearity and high survivability. [C2111]

#### "AlGaIn/GaN-HEMTs for power applications up to 40 GHz"

A 0.15  $\mu\text{m}$  T-gate AlGaIn/GaN-HEMT 2-inch technology has been developed. Transistors with 120  $\mu\text{m}$  gatewidth show a peak transconductance of 300 mS/mm and cut-off frequencies  $f_{\text{tand}}$   $f_{\text{max}}$  of 65 GHz and 149 GHz, respectively. Large periphery 720  $\mu\text{m}$  gatewidth devices are capable of CW operation up to 40 GHz yielding an output power of 0.91 W and a linear gain of 6 dB at 35 GHz. To the authors' knowledge these results represent the highest absolute power level so far achieved with a GaN-HEMT in the Ka-band. [C2112]

#### "Hot electron effects on undoped AlGaIn/GaN high electron mobility transistors"

Summary form only given. In this work, we report on the effects of hot electron stress on the degradation of undoped Al<sub>0.3</sub>Ga<sub>0.7</sub>GaN power HEMT's with SiN passivation, consisting of a decrease in the drain current, an increase in the parasitic drain and source resistance, and a shift in threshold voltage. The stressed devices suffered from aggravated drain current slump (DC to RF dispersion). Pulsed I-V measurements and current-mode deep level transient spectroscopy (DLTS) suggested possible changes in surface charge profiles occurred during hot electron stress test. The nature of degradation under hot electron stress was irreversible. [C2113]

#### "Reliability of 100 nm silicon nitride capacitors in an InP HEMT MMIC process"

A reliability study has been conducted on capacitors made with 100 nm of silicon nitride, in an InP HEMT MMIC fabrication process. Special wafers were fabricated, containing 1482 200  $\mu\text{m}$   $\times$  200  $\mu\text{m}$  capacitors each, and these were probed automatically. They were subject to ramped-voltage stress and the breakdown voltages recorded. On a typical wafer the vast majority of the breakdown voltages are between 50 and 90 V. In addition, I-V curves were measured on a small number of specimens from 0 V up to breakdown. This was done in two regimes: above 25 V with a conventional setup, and below 25 V with an ultra-low-current measurement system. These were done at 25°C and 175°C above 25 V, and at 25°C only below 25 V. These were fitted well with a model for the conductivity, consisting of an ohmic conduction at low voltages and Frenkel-Poole conduction at high voltages. Parameters of the fits included thermal activation energies, the voltage acceleration factor in the Frenkel-Poole model, and  $d_{\text{eff}}$ , the effective thickness of the dielectric at the thinnest point. Analysis invoked the time-dependent dielectric breakdown model, which provides the time to failure as a function of the  $d_{\text{eff}}$ , while  $d_{\text{eff}}$  can be found from the ramped-voltage measurements. From the 10 wafers that have been probed so far, the mean of the distribution of failure times (at 1.5 V, 40°C) is above 5  $\times$  10<sup>7</sup> hrs, and the distribution becomes insignificant below 2  $\times$  10<sup>6</sup> hrs. Further, the probability of failure in 10 years at 1.5 V, 40°C is much less than 1 in 14,600. This indicates that 100 nm silicon nitride capacitors in this technology have good reliability. [C2114]

#### "Creation of current collapse in GaN HEMTs due to short-term DC bias stress"

Summary form only given. Gallium nitride HEMTs have recently received significant attention for microwave high-power solid state applications, and have demonstrated record output power densities. Significant work is still required, however, for GaN HEMTs to become a viable technology. One area of current investigation is that of device stability. In the work reported here, we studied the effect of short term bias on the DC characteristics of several GaN HEMT wafers. A current collapse effect was found to be induced in some, but not all, of the devices after stress, apparently caused by the generation of trapping centers. This effect was observed for material grown by both MOCVD and MBE; and for a limited number of devices, it appears that silicon nitride passivation can suppress this effect. [C2115]

#### "Excitation of plasma oscillations and terahertz photomixing in high-electron mobility transistor"



We consider the excitation of plasma oscillations in the channel of a high-electron mobility transistor by transient near infrared radiation. This effect results in the pertinent excitation of the electric current in the external circuit that can be used for generation of terahertz electromagnetic radiation. [C2116]

#### "Metamorphic optical receiver components"

GaAs based metamorphic HEMT (MHEMT) technology has emerged as an attractive, low cost alternative to InP HEMTs. The strain-induced imperfections caused by high indium content layers on GaAs are eliminated in metamorphic devices by providing a properly grown lattice-matching buffer between the substrate and active device layers. Metamorphic device technology has now expanded to optical receiver components and shows performance suitable for 40 Gb/s digital and analog optical links. [C2117]

#### "Performance of InGaP/InGaAs/GaAs camel-gate single $\delta$ -doping pHEMT"

A newly designed single delta-doped InGaP/InGaAs/GaAs pseudomorphic HEMT with n+-GaAs/p+-InGaP/n-InGaP camel gate structure has been first fabricated and demonstrated. For a  $14100 \mu\text{m}^2$  device, the experimental results show an extrinsic transconductance of 85 mS/mm and a saturation current density of 425 mA/mm. Significantly, due to the p-n depletion from p+-InGaP gate to channel region and the presence of  $\Delta E_c$  at InGaP/InGaAs heterostructure, the turn-on voltage of gate is larger than 1.7 V. In addition, an extremely broad gate voltage swing larger than 3 V with above 80% maximum gm is obtained. The unit current cutoff frequency  $f_{T\text{and}}$  and maximum oscillation frequency  $f_{\text{max}}$  are up to 18 and 30 GHz, respectively. [C2118]

#### "The photo-controlled MOBILE's with RTD/HPT structure"

In this paper, by replacing the HEMT with a phototransistor in the MOBILE'S, we can get a novel optoelectronic functional device, which presents the function of both photocurrent switching and photo-current latching. Furthermore, basing on photo-current latching behavior, various photo-controlled basis logic gate elements such as Delayed Flip-Flop (DFF) can be designed and fabricated. [C2119]

#### "Internal waveform probing of HBT and HEMT MMIC power amplifiers"

In this paper, a practical MMIC internal waveform probing technique has been developed. The technique can be used for model extraction, design verification, process diagnosis, and reliability assessment, as demonstrated in the above. [C2120]

#### "Time domain RF characterisation of a thin-film metamorphic HEMT under modulated backside illumination"

It is shown in this paper how the opto-electrical interaction of a microwave device can be characterized by combining a large-signal network analyzer set-up with a modulated laser module. The concept is demonstrated by measuring a "thin film" M(etamorphic) HEMT under modulated optical (1550 nm laser light) illumination. The advantage of this approach is that the time-domain characteristics of the electrical currents, generated by the modulated laser light, can be visualised and analysed. [C2121]

#### "MMIC development for Local Multipoint Distribution Service (LMDS)"

This paper covers a few Monolithic Microwave Integrated Circuit (MMIC) design using the Gallium Arsenide (GaAs) pseudomorphic high electron mobility transistor (p-HEMT) technology to be used in Local Multipoint Distribution Service (LMDS) system. Three different sections describe in brief the design approach and methodology involved in each RF circuit design especially in stabilizing circuitry and meeting the small and large signal specifications. [C2122]

#### "High breakdown InGaP/InGaAs tunneling real space transfer HEMT"

A novel  $\delta$ -doped InGaP/InGaAs/AlGaAs tunneling real-space transfer high electron mobility transistor (TRST-HEMT) has been successfully fabricated by low-pressure metal organic chemical vapor deposition. Three-terminal N-shaped negative differential resistance (NDR) phenomenon due to the hot electrons real-space transfer (RST) at high electric field is observed. Two-terminal gate-to-drain breakdown voltage is more than 40 V. High three-terminal on-state breakdown voltage as high as 19.2 V and broad plateau of current valley as high as 15 V are achieved. [C2123]

#### "W-Band GaAs HEMT MMIC Subharmonically Pumped Diode Mixers with 20 GHz IF Bandwidth"

Two subharmonically pumped (SHP) diode mixers are designed for wideband W-band RF frequencies, fixed LO frequency operation. These mixers are fabricated on a 4-mil substrate using 0.1- $\Gamma$ B $\Gamma$ m GaAs MMIC process. Both simulation and test results show that the mixers are with 12.25 and 11.75 dB average conversion losses, respectively. Both mixers have IF bandwidth wider than 20 GHz. The conversion loss flatness of the symmetric circuit is within  $\Gamma$ B $\pm$ 1.25 dB. To our knowledge, these are the state-of-the-art result on low-conversion-loss wideband MMIC SHP diode mixers. [C2124]

### "A Highly Linear Circularly Polarized Active Antenna With Gain Control"

In this paper, a novel highly linear circularly polarized active antenna with gain control is presented. A printed patch is used as the output 90 $\Gamma$ B $^\circ$  hybrid in a HEMT balanced amplifier, whose branches provide gain control based on a new biasing strategy. Low intermodulation distortion (IMD) and reduced DC power consumption are assured along The proposed radiating structure could be efficiently integrated in arrays, particularly if some amplitude aperture distribution were required and some complex modulation format were to be transmitted. [C2125]

### "Characteristics of GaAs HEMTs with Flip-Chip Interconnections"

A GaAs HEMT with flip-chip interconnections has been developed. There are various ground current passes for the HEMT on surface of the GaAs chip in this assembly structure, each pass depending on the transmission line type for the chip. We evaluated the high-frequency characteristics of the HEMT TEGs with flip-chip interconnection for three types of the transmission lines: with a microstrip line (MSL), with a coplanar waveguide (CPW), and with an inverted microstrip line (IMSL). All three types of TEGs had similar values of a maximum available power gain (MAG) at 30 GHz. However, the IMSL-type TEG, which had superior characteristics in high-frequency ranges of more than 30 GHz, was chosen as the most suitable type. The IMSL-type TEG had an MAG of 10.02 dB and a Rollett stability factor K of 1.20 at 30 GHz. [C2126]

### "LT (Al)GaAs and Al(Ga)As/AlAsSb oxides for electronic applications"

Research into various areas of III-V electronics is presented. GaAs MESFETs passivated with LT Al<sub>x</sub>Ga<sub>1-x</sub>As showed increased breakdown voltages (V<sub>bkd</sub>=43V) over standard devices (V<sub>bkd</sub>=8V). MESFETs and pHEMTs fabricated with insulating oxide buffers (GaAs-On-Insulator) produced world record power-added efficiencies (PAE=88%). Recently, research has been oriented towards collector-up with oxide current confinement layers for high gain, high speed performance. [C2127]

### "Electrical isolation of n-GaAs by proton implantation-effects of doping implant, isolation implant and implant temperature"

An effective and reliable technology for device isolation in III-V semiconductors is an essential requirement for the better efficiency and throughput of a number of commercial devices such as ICs, HBTs, HEMT, lasers, LEDs and MMICs. We report on the effects of doping implants, variable doses for isolation implants and variable substrate temperature during implantation on the achieved electrical isolation in n-type GaAs layers using proton bombardment. The starting material was prepared using multi-energy 28Si ion implantation into semiinsulating GaAs at various doses to form n-type GaAs layers of different initial sheet carrier concentration. The isolation was obtained by proton irradiation at a suitable energy to place the peak of the damage distribution well inside the semi-insulating GaAs substrate and a constant level of damage in the near surface device region. Isolation implants were performed at variable doses from 10<sup>12</sup>- 10<sup>16</sup>ions-cm<sup>-2</sup>at room temperature (RT). One particular set of samples was implanted with variable doses at liquid nitrogen temperature and temperatures ranging from RT to 300 $^\circ$ C. The threshold dose to convert a conductive layer to a highly resistive one and respective sheet resistivities are found to be different for different initial sheet carrier concentration. The stability and value of isolation is also dependent on the implant temperature. Hot implants at 250 or 300 $^\circ$ C, due to their enhanced dynamic annealing and nature of formed trap structures during implantation show better stability of isolation values for a range of doses without any post-implant annealing. The as-implanted sheet resistivity achieved in hot implantation cases is comparable to semi-insulating GaAs resistivities. These results are important in order to choose the right isolation-implant conditions for stable and efficient isolation in device structures. [C2128]

### "Experimental/numerical investigation on current collapse in AlGaIn/GaN HEMT's"

Rf current collapse is investigated in AlGaIn/GaN HEMT's by means of pulsed, transient, and small-signal measurements. Numerical device simulations are presented, showing that the concomitant presence, at the ungated device surface, of polarization-induced charges and hole traps can explain, without invoking any other hypothesis, all dispersion effects observed experimentally. [C2129]

### "Improved intermodulation distortion profile of AlGaIn/GaN HEMT at high drain bias voltage"

We demonstrate, for the first time, the excellent linearity characteristics of AlGaIn/GaN HEMTs at drain bias voltages up to 30 V, class AB operation, at 1.9 GHz. AlGaIn/GaN HEMTs with a drain periphery of 1 mm, grown on SiC substrates, exhibit a third-order intermodulation distortion (IM3) of -34.7 dBc for an output power level of 26 dBm, 8 dB back-off from saturation power ( $P_{sat}$ ), at drain bias voltage of 30 V. Furthermore, we will show the linearity characteristics dependence on  $V_{ds}$  and describe that superior linearity profile can be obtained with AlGaIn/GaN HEMTs at high drain voltage bias. [C2130]

### "AlGaIn/GaN HEMTs on SiC operating at 40 GHz"

The operation of AlGaIn/GaN HEMTs on SiC in the Ka-band is analyzed with respect to the achievable output power between 35 GHz and 40 GHz. 150 nm gate length AlGaIn/GaN HEMTs are investigated by active load-pull measurements. Further, small-signal and noise analysis are performed with regard to the use at Ka-band and robust receiver applications. [C2131]

### "Broad-band optical receiver for multigigabit-per-second (40Gb/s) optical communication systems"

This paper presents the design and characterization of a high-bandwidth transimpedance GaAs MMIC receiver suitable for 40 Gbps data transmission rates. The circuit was implemented on a MMIC PH15 process from United Monolithic Semiconductors (UMS). This process features 0.13  $\mu\text{m}$  pseudomorphic transistors (0.135  $\mu\text{m}$  PHEMT) with low resistance, good reliability and an  $f_{tof}$  approximately 100 GHz. This circuit presents a 49 dB $\Omega$  gain, low noise figure and wide bandwidth considering detector input capacitance in excess of 100 fF. An analysis involving noise, stability and the influence of bond-wire inductance on the overall circuit behaviour was performed. Input capacitance tolerance and output impedance matching conditions were evaluated. On-going on-wafer characterisation results are also presented and compared with simulation data, showing good agreement. [C2132]

### "Signal and noise improvement of a distributed FET mixer"

A traveling wave distributed mixer is studied. It is shown that increasing the drain-source capacitances in a distributed FET mixer simultaneously improves its conversion gain and noise figure. Besides, it is shown that proper loading of input and output elements can improve the device performance. The simulation results are well matched with the measurements and also with the results of the existing certified simulators. [C2133]

### "Linearity and gain characteristics of AlGaIn/GaN HEMTs"

AlGaIn/GaN HEMTs exhibited high cut-off frequencies at low current levels, which enabled linear operation at close to class-B biases. When biased at 35V and 40mA/mm (4% of channel current), excellent linearity performance including simultaneous 3rd order intermodulation (IM3) of -30dBc and PAE of 40% was obtained at 4 GHz, with only -2.6dB back off. However, the gain reduction at high current levels made class-A operation less favorable. These gain characteristics are believed to be related to the ratio of the effective electron mass ( $m_e$ ) over the conduction band discontinuity ( $\Delta E_c$ ) of AlGaIn/GaN. [C2134]

### "A simplified noise modeling of mm-wave FETs"

A simple procedure for finding the noise parameters of MESFETs and HEMTs is discussed. The influence of gate width on the equivalent noise temperature of HEMTs is studied. This is the basis of width scaling and is applicable in high power FETs. Also the influence of drain current on the noise performance of FETs is discussed. This matter is useful in accurate noise modeling of mm-wave ICs. [C2135]

### "Large-signal modeling of HEMT device based on neural network"

In this article, a neural network model using Levenberg-Marquart algorithm and hyperbolic tangent activation function is developed to simulate three nonlinear parameters for HEMT device. Compared with BP neural network, this ANN model can accelerate convergence. The example shows that the developed ANN model possesses higher accuracy and good generalization. It can be applied to device modeling efficiently. [C2136]

### "Improving large-signal FET/HEMT model accuracy by optimization of diode response"

In this paper, a simple technique for measuring and modeling the response of the gate-source and gate-drain diodes in a large-signal FET/HEMT model is presented. Measurements are conducted on an ATF36163 PHEMT transistor, and significant improvement in a large-signal model for the PHEMT is achieved by optimizing the

response of the diode models. The significance of the gate-source and gate-drain diodes in large-signal modeling is discussed. [C2137]

#### "100-Gbit/s logic IC using 0.1- $\mu$ m-gate-length InAlAs/InGaAs/InP HEMTs"

High-speed electrical multiplexing and demultiplexing are keys in optical fiber communication systems. In the last few years, multiplexing operations at over 80 Gbit/s have been reported for selector ICs using InP HEMT and InP HBT technologies. The record operating speed is, however, still 90 Gbit/s, which was characterized only by means of a waveform observation on digitizing sampling oscilloscope. This paper describes 100-Gbit/s multiplexing and demultiplexing error-free logic operations in InP HEMT technology. [C2138]

#### "Optimization of PHEMT geometry for power applications"

Impact ionization is generally taken as a phenomenon, responsible for breakdown in Pseudomorphic High Electron Mobility Transistor (PHEMT). Tuning and modeling the impact ionization phenomenon in PHEMT as a function of device design parameters can serve an effective optimization vehicle for the device manufacturer. The aims of this work are: a) developing a methodology for measuring and modeling impact ionization phenomena in PHEMT, b) developing an empirical model relating the device design parameters to impact ionization, using the methodology above. [C2139]

#### "40 Gbit/s high performances GaAs pHEMT high voltage modulator driver for long haul optical fiber communications"

In this paper, we describe the development of high gain and high voltage 40 Gb/s modulator driver ICs. Both chips were designed with a double-distributed amplifier topology using a 0.15  $\mu$ m GaAs pHEMT technology process. The modulator driver exhibits 26 dB of small signal gain over 50 GHz of 3 dB bandwidth and provides more than 7.5 Vpp output swing in a 50  $\Omega$  load to drive LiNbO<sub>3</sub> modulators. [C2140]

#### "1.4-THz gain-bandwidth product InP-HEMTs preamplifier using an improved Cherry-Hooper topology"

We have developed an InP-HEMT differential-ended broadband preamplifier with THz-class gain-bandwidth product by using an improved Cherry-Hooper topology. The key to achieving the high performance preamplifier is to use a mismatching technique, which expands the impedance difference between gain stages. Using this technique, we achieved 64 dB $\Omega$  transimpedance gain with a 40 GHz bandwidth, and its gain-bandwidth product reached 1.42 THz—the highest yet reported for 40 Gbit/s preamplifiers. [C2141]

#### "1.7-W 50-Gbit/s InP HEMT 4:1 multiplexer IC with a multi-phase clock architecture"

Low-power and high-speed operation of a 4:1 multiplexer IC with a multi-phase clock architecture is reported. The architecture features a toggle-type flip-flop (TFF) that generates a four-phase clock, and a series-gated 4:1 selector (SEL). The fabricated IC using InP HEMTs operates at 50 Gbit/s error-free with 1.71-W power consumption and 1-Vpp output amplitude. The power consumption is less than 1/3 that of a conventional tree-type InP HEMT 4:1 multiplexer IC and is achieved without any reduction of operation speed and output amplitude. [C2142]

#### "Direct up-conversion MMIC with RF bandwidth of 4 to 12 GHz"

The design and performance of a novel direct up-conversion MMIC is described. The circuit accepts analog differential or single-ended signals from a DAC, forms a sampling pulse from the DAC clock, and creates a time domain waveform that is a pulse doublet train amplitude modulated by the DAC input. The appropriate spectral line is then obtained via bandpass filtering. This approach minimizes cost, volume, power, and weight by eliminating the requirement for a local oscillator. The MMIC is implemented in a fully selective 0.15  $\mu$ m double recess PHEMT process. [C2143]

#### "A 16 GHz MMIC image-rejection resistive mixer with InP HEMTs"

In this paper we present a monolithically integrated image-rejection resistive mixer that shifts a signal in the 1-2 GHz band up to the 14-15 GHz band using a 16 GHz local oscillator (LO). The circuit was realized with our 0.2  $\mu$ m InP HEMT in-house process using a coplanar-waveguide technology. The fabricated circuit presents a peak conversion gain of -7.3 dBm for 2 dBm LO power, an LO suppression of 20 dB and an upper-sideband rejection of more than 17 dB. This performance is excellent if compared to the best reported results for InP HEMT resistive mixers. [C2144]



### "An 8-Watt 3.5 GHz power amplifier with tunable matching"

A high power 3-stage, S-band power amplifier MMIC implemented with a partially matched output stage is presented. This MMIC PA achieves 39 dBm output power and greater than 25% power added efficiency using 0.6  $\mu\text{m}$  PHEMT technology. Small-signal performance matches very well with modeled predictions. The amplifier is exceptionally stable under varying loads, has a bandwidth of several 100 MHz and is easily matched and tuned about the 3.5 GHz band with a simple output matching technique using chip caps, bond wires and duroid transmission lines. [C2145]

### "Simulations of quantum transport in HEMT using density gradient model"

In this paper, quantum transport simulations for AlGaAs/InGaAs HEMT devices based on the density gradient model are presented. It is shown that size quantization effects have a pronounced influence on the electrical characteristics. [C2146]

### "Gallium nitride (GaN) HEMT's: progress and potential for commercial applications"

This paper focuses on the development of 100 mm gallium nitride HEMT technology at RF Micro Devices and the utilization of GaN transistors for commercial applications such as power amplifiers, power switches and low-noise power oscillators. [C2147]

### "50-Gbit/s 4-bit multiplexer/demultiplexer chip-set using InP HEMTs"

This paper reports on the 50-Gbit/s 4:1 multiplexer (MUX) and 1:4 demultiplexer (DMUX) chip-set using InP HEMTs. In order to achieve high and wide-range bit-rate operation, timing design inside the ICs was precisely executed. The packaged MUX and DMUX achieved 50 Gbit/s back-to-back error-free operation for 231-1 pseudo-random bit streams (PRBS). Furthermore, the MUX operated from 4 to 50 Gbit/s with  $>1$  Vpp output amplitude, and the DMUX exhibited  $>180$ -degrees phase margin from 4 to 50 Gbit/s for 231-1 PRBS. [C2148]

### "A 4-Watt X-band compact coplanar high power amplifier MMIC with 18-dB gain and 25-% PAE"

The performance of a compact coplanar (CPW) microwave monolithic integrated circuit (MMIC) amplifier with high output power in the X-band is presented. Based on our 0.3- $\mu\text{m}$  gate length GaAs power PHEMT process on 4" wafer, this two-stage amplifier, having a chip size of 16 mm<sup>2</sup>, averages 4 Watts CW and 25-% PAE in the X-band, with more than 18-dB linear gain. Peak output powers of P-1dB = 36.3 dBm (4.3 Watts) and Psat of 36.9 dBm (4.9 Watt) at 10 GHz with a power added efficiency of 35 % were also measured. Compared to previously reported X-band coplanar HPA, this represents a chip size reduction of 20 %, comparable to the size of compact state-of-the-art microstrip PAs. [C2149]

### "X-band successive detection log amplifier/limiter MMIC implemented in 0.15 $\mu\text{m}$ double recess PHEMT"

Design and performance of an X-band successive detection log amplifier/limiter MMIC covering 8 to 12 GHz is reported. The three-stage amplifier is a cascadeable block providing 20 dB nominal gain, 5.5 dB noise figure, +7 dBm limited output, [C2150]

### "A high gain-bandwidth product InP HEMT distributed amplifier with 92 GHz cut-off frequency for 40 Gbit/s applications and beyond"

The design, fabrication and characteristics of a coplanar distributed ultra broadband amplifier are presented. The circuit is fabricated using a composite channel InP CC-HEMT high breakdown voltage technology developed in Alcatel OPTO+. It exhibits an average gain of 13 dB over a 92 GHz -3dB cut-off frequency that corresponds to a state of the art gain-bandwidth product of 410 GHz for baseband amplifier ICs. It still presents 8 dB gain at 110 GHz. Such an amplifier is a good candidate for 40 and 80 Gbit/s optoelectronic driver modules applications. We discuss the use of coplanar waveguide lines and low impedance bias microstrip transmission lines in such a design. We also highlight the need of largest bandwidths for 40 Gbit/s eye diagram quality and the needed gain-bandwidth product for 80 Gbit/s ETDM communications. [C2151]

### "A four-stage Ku-band 1 watt PHEMT MMIC power amplifier"

In this paper, a Ku-band 1 watt AlGaAs/InGaAs/GaAs PHEMT MMIC power amplifier for VSAT ODU (outdoor unit) applications is demonstrated. This four-stage amplifier is designed to fully match for a 50 ohm input and

output impedance. With 7 V and 700 mA DC bias condition, the amplifier has achieved 30 dB small-signal gain, 30.8 dBm 1-dB gain compression power with 24.5% power-added efficiency (PAE) and 31.3 dBm saturation power with 27.5% PAE from 14 to 17 GHz. [C2152]

#### "A compact 30 GHz MMIC high power amplifier (3 W CW) in chip and packaged form"

This paper presents performance of a compact 3 W HPA (High Power Amplifier) in MMIC and packaged form at 30 GHz. A low cost high power packaged part was achieved by designing a compact MMIC and adopting a laminate substrate approach for a package. TriQuint standard 0.25  $\mu\text{m}$  PHEMT production process on 50  $\mu\text{m}$  substrate technology was used for a compact MMIC PA design. The output power at P1 dB (CW measurement) of MMIC and packaged parts are 34.9 dBm and 34.5 dBm with associated gain of 21.5 dB. These results are the highest CW-power and gain reported for a single MMIC and packaged part at Ka-band. [C2153]

#### "GaAs IC Symposium. IEEE Gallium Arsenide Integrate Circuit Symposium. 24th Annual Technical Digest 2002 (Cat. No.02CH37354)"

First Page of the Article [C2154]

#### "Growth of shallow InAs HEMTs with metamorphic buffer"

Shallow InAs inserted-channel heterostructures are fabricated on GaAs with electron system only 19.5 nm below the surface and mobility of 160000  $\text{cm}^2/\text{Vs}$ . An additional superlattice grown prior to the metamorphic buffer is established for defect reduction. [C2155]

#### "GaN power switching device growth by plasma assisted molecular beam epitaxy"

Newly fabricated junction field effect transistors (JFETs) and high electron mobility transistors (HEMTs) based on gallium nitride (GaN) substrates are presented. The devices, grown with plasma assisted molecular beam epitaxy (PAMBE), are to be used for power switching applications. Very high quality p- and n-type films were grown. Some test results are shown for surface smoothness and for successfully processed Schottky diodes [C2156]

#### "1 watt broad Ka-band ultra small high power amplifier MMICs using 0.25- $\mu\text{m}$ GaAs PHEMTs"

We report the design and performance of ultra compact high power amplifier MMICs for Ka-band applications. Using a production 4-inch 0.25- $\mu\text{m}$  GaAs PHEMT technology, in combination with appropriate compact circuit topologies, these power amplifiers achieved on wafer, a linear gain of more than 18 dB over the 26-36 GHz frequency range, with an output power at 1 dB gain compression of P-1 dB=29.5 dBm (900 mW) and a saturated output power above 1 watt (30.1 dBm), for a chip size of only 2.25  $\text{mm}^2$  (1.25 $\times$ 1.8  $\text{mm}^2$ ). To our knowledge, this is the highest output power and gain densities per chip area (i.e. 400-440  $\text{mW}/\text{mm}^2$  and 8  $\text{dB}/\text{mm}^2$ ) ever reported at Ka-band for any GaAs PHEMT MMIC power amplifier. [C2157]

#### "A 3-V fully differential distributed limiting driver for 40 Gb/s optical transmission systems"

A fully differential 40 Gb/s electroabsorption modulator driver is presented. Based on a distributed limiting architecture, the circuit can supply up to 3.0 V peak-to-peak per side in a 50  $\Omega$  load at data rates as high as 44 Gb/s. Both the input and output are internally matched to 50  $\Omega$  and exhibit return loss of better than 10 dB up to 50 GHz. Additional features of the driver include the use of a single -5.2 V supply, output swing control (1.7 to 3.0 Vpp per side), DC output offset control (-0.15 V to -1.1 V) and pulse width control (30% to 70%). [C2158]

#### "An over 110-GHz InP HEMT flip-chip distributed baseband amplifier with inverted microstrip line structure for optical transmission systems"

We successfully developed state of the art InP HEMT distributed amplifiers by using inverted microstrip line technology. For one, we achieved a gain of 14.5 dB and a 94-GHz 3-dB bandwidth resulting in a gain-bandwidth product of 500 GHz, and for the other we achieved a gain of 7.5 dB and a 3-dB bandwidth of over 110 GHz. This technology also demonstrates the capability of fabricating ultra-broadband packaged ICs with flip-chip assembly for operation up to the W-band. To our knowledge, these results represent the highest gain bandwidth product and the widest bandwidth for distributed amplifiers reported to date. [C2159]

#### "Impact of RF stress on dispersion and power characteristics of AlGaIn/GaN HEMTs"

The impact of RF stress on dispersion and power characteristics of AlGaIn/GaN HEMTs are reported. Reduced drain current ( 67  $\text{mA}/\text{mm}$  in the saturation region) and similar output power and power-added efficiency were

found after RF stress. Transconductance dispersion is small before and after RF stress while output resistance dispersion reduces after RF stress. Tests performed under UV light suggest that the observed results may be attributed to trapping in the AlGaIn/GaN HEMT layers. [C2160]

#### "Monolithic integration of In<sub>0.53</sub>Ga<sub>0.47</sub>As photodiodes and In<sub>0.53</sub>Ga<sub>0.47</sub>As/In<sub>0.52</sub>Al<sub>0.48</sub>As HEMTs on GaAs substrates for long wavelength OEIC applications"

Metamorphic long wavelength double heterojunction photodiodes with In<sub>0.53</sub>Ga<sub>0.47</sub>As photo-absorption layer and In<sub>0.53</sub>Ga<sub>0.47</sub>As/In<sub>0.52</sub>Al<sub>0.48</sub>As metamorphic HEMTs were realized on the same GaAs substrate. The photodiodes exhibited high speed and low leakage characteristics and the performance of HEMTs beneath the photodiode layers were also comparable to those fabricated on HEMT-only heterostructures. [C2161]

#### "0.1 $\mu$ m InGaAs/InAlAs/InP HEMT MMICs-a flight qualified technology"

0.1  $\mu$ m InGaAs/InAlAs/InP HEMT MMIC technology on 3-inch InP substrates has been qualified in the categories of three-temperature lifetest, gamma radiation, RF survivability, electrostatic discharge, via-hole baking, and H<sub>2</sub>poisoning. The three-temperature lifetest (T<sub>1</sub>= 215°C, T<sub>2</sub>= 230°C and T<sub>3</sub>= 250°C) of 0.1  $\mu$ m InGaAs/InAlAs/InP HEMT MMICs in a N<sub>2</sub> ambient demonstrates an activation energy (E<sub>a</sub>) as high as 1.9 eV, achieving a projected median-time-to-failure (MTF)  $\approx$  14108 hours at a 125°C junction temperature. Gamma radiation up to 5 mega RAD dose does not induce any degradation of DC/RF characteristics. Electrostatic discharge (ESD) shows destructive voltage up to 100 Volts. Furthermore, 0.1  $\mu$ m InP HEMTs exhibit less sensitivity to H<sub>2</sub> exposure than 0.1  $\mu$ m GaAs pseudomorphic HEMTs. The qualification results demonstrate the readiness of 0.1  $\mu$ m InGaAs/InAlAs/InP MMICs technology for flight applications. [C2162]

#### "Dependence of power and efficiency of AlGaIn/GaN HEMTs on the load resistance for class B bias"

The material properties of GaN and the AlGaIn/GaN heterostructure such as high breakdown field and high sheet charge density, allow AlGaIn/GaN HEMTs to be operated at significantly higher drain bias voltages as compared to other III-V compound semiconductor FETs. As expected, larger RF voltage and current swings result in higher normalized output power at microwave frequencies. AlGaIn/GaN HEMTs are capable of generating output power density in excess of 10 W/mm in the X-band, which is at least an order of magnitude larger than what is obtainable with GaAs FETs. In this paper, we discuss the effect of the load impedance on measured output power (P<sub>out</sub>) and efficiency ( $\eta$ ) at various drain bias conditions in class B mode. Dynamic loadlines; extracted at the device's output are used for analysis of the trade-off between voltage and current swings at different load resistances and its effect on output power and efficiency. [C2163]

#### "AlGaIn/GaN HEMTs grown by molecular beam epitaxy on sapphire, SiC, and HVPE GaN templates"

Molecular beam epitaxy of GaN and related alloys is becoming a rival to the more established metalorganic vapor phase epitaxy. Excellent control of impurity, interface abruptness, and in situ monitoring of the growth are driving the increase in quality of MBE epilayers. We have developed nucleation schemes with plasma-assisted MBE on three types of substrates, consisting of sapphire, semi-insulating (SI-) SiC, and HVPE SI-GaN templates on sapphire. While sapphire and SI-SiC are established substrates for the growth of AlGaIn/GaN HEMT epilayers, HVPE GaN templates may provide a path to low-cost large-diameter substrates for electronic devices. We compare device results of HEMTs fabricated on these substrates. As a metric for device performance, the saturated RF power output in class A operation is measured at 2 GHz. We achieved a saturated power density of 2.2 W/mm from HEMTs on sapphire, 1.1 W/mm from HEMTs on HVPE GaN templates on sapphire, and 6.3 W/mm. from HEMTs on semi-insulating 6H-SiC substrates. The difference in output power can be attributed to self-heating due to insufficient thermal conductivity of the sapphire substrate, and to trapping in the compensation-doped HVPE template. [C2164]

#### "Simulations of high linearity and high efficiency of class B power amplifiers in GaN HEMT technology"

We describe the design and simulation of highly linear and highly efficient common source class B power amplifiers. Efficient broadband class B push-pull amplifiers are not feasible at microwave frequencies as baluns with desired broadband even-mode impedance are unavailable. We find, however, that a single-ended class B amplifier with bandpass filtering has an equivalent efficiency and linearity. Simulations of class B designs predict a power added efficiency (PAE) of 48% with 40 dBc of third order intermodulation product (IMD3) performance when biased close to the pinch-off voltage. [C2165]

### "92 GHz cut-off frequency InP double channel HEMT based coplanar distributed amplifier for 40 Gbit/s applications and beyond"

In this paper, we present the design, fabrication and measurements of an ultra broad band amplifier with 92 GHz cut-off frequency intended for ETDM transmission applications over 40 Gbit/s. The circuit is based on InP double channel HEMT technology developed in OPTO+ to get high frequency-breakdown voltage product. We will discuss the use of coplanar wave-guide lines and low impedance bias micro-strip transmission lines in such a design. We will also highlight the need of largest bandwidths for 40 Gbit/s eye diagram quality and the needed gain bandwidth for 80 Gbit/s ETDM communications. [C2166]

### "30 years of accomplishments in compound semiconductor materials and devices attributable to Prof. Lester F. Eastman"

To those that best know him, Prof. Eastman is not only one of the most congenial academicians in the world, but is a walking encyclopedia of knowledge relating to compound semiconductor materials, structures, and devices. Moreover, he is always most willing to enthusiastically share the details of his knowledge. His personal contributions to the field are multitudinous. He has mentored over 110 successful Ph.D. candidates. Eighteen of these have founded new businesses, 19 have become academicians, 16 have become directors, managers, CEOs, or VPs in industry, one is currently the associate director of the FBI, and 3 have already retired. Three hundred and eighty seven of his over 700 papers have been cited in the Science Citation Index, with 9 of them having over 100 citations each. His earliest cited paper was published in 1964. In this paper, several of his traits and accomplishments along with their impact on his students, the DoD, the scientific community, and our standard of living are highlighted. Projections are also made of future impacts. [C2167]

### "Design of GaN/AlGaIn HEMT class-E power amplifier considering trapping and thermal effects"

A microwave class-E power amplifier using AlGaIn/GaN HEMT as the switching device is reported by incorporating trapping and thermal effects in the large-signal device model. The load network of the class-E amplifier is designed by considering more realistic exponential decay of the drain current during fall time and finite quality factor of the resonant circuit to incorporate the nonidealities of the active device and passive components. With 9 V supply voltage, calculated output power and power conversion efficiency are 89 mW and 58% at 1GHz which decrease to 84 mW and 54% at 3.8 GHz, respectively for a GaN/Al<sub>0.30</sub>Ga<sub>0.70</sub>N HEMT with gate width of 50  $\mu$ m. [C2168]

### "MMIC compatible AlSb/InAs HEMT with stable AlGaSb buffer layers"

In this paper, we present state-of-the-art  $f_{T\max}$  results of 130 GHz, and 110 GHz for AlSb/InAs HEMTs with AlGaSb/AlSb metamorphic buffer layers that demonstrate InAs-channel HEMTs that are stable with exposure to air and are compatible with standard MMIC production processes. [C2169]

### "AlGaAsSb/InGaAs/AlGaAsSb metamorphic HEMTs"

Deep quantum well In<sub>0.8</sub>Ga<sub>0.2</sub>As/AlGaAsSb MHEMTs on GaAs are described. The step-graded AlGaAsSb strain-relief buffer layer provided a high-quality surface for growth of the MHEMT layers. AlGaAsSb barrier layers offer flexibility in choosing the channel composition and the barrier height. Typical Hall mobilities were 11,000 cm<sup>2</sup>/V-sec at 300 K for carrier concentrations of  $2.4 \times 10^{12}$  cm<sup>-2</sup>. Extrinsic DC transconductance of 820 mS/mm was obtained for an MHEMT with a 0.15  $\mu$ m/64  $\mu$ m gate. Typical extrinsic unity current gain cutoff,  $f_t$ , was 173 GHz with maximum frequency of oscillation,  $f_{max}$ , of 474 GHz. Aside from layer growth, the MHEMTs were fabricated using only small changes from conventional GaAs PHEMT processing. This technology promises affordable production costs for high performance millimeter-wave low noise amplifiers. [C2170]

### "Silicon-germanium power devices at low temperatures for deep-space applications"

Silicon-germanium heterostructure. based 1-watt n-channel metal-oxide-semiconductor modulation-doped field effect transistors (MOS-MODFETs) with 6  $\mu$ m gate lengths and 1 mm total gate widths have been designed, fabricated and tested from 300 K to 90 K. The devices were fabricated by an ion-implanted process and employ a low-temperature thermal oxide and PECVD deposited oxide as the gate insulator. The devices showed a saturation current of approximately 77 mA at  $V_{DS}=14$  V,  $V_{GS}=5$  V at 90 K, corresponding to a power dissipation of 1 W. Because they employ oxide as a gate dielectric, the devices have a low gate leakage current of  $I_{GS}=10$  V. [C2171]

### "Advanced large-signal modeling of GaN-HEMTs"



For improved non-linear modeling of AlGaIn/GaN high electron mobility transistors, a large-signal model originally developed for GaAs-based devices has been extended by introduction of a thermal sub-circuit to account for self-heating. Thereby, DC output characteristics which typically show negative output conductance at a high dissipating power level are well reproduced. Since self-heating also effects the transconductance, which is related to S<sub>21</sub> at RF conditions, the comparison of broadband S-parameter simulations and measurements revealed significant improvement when using the extended model. First experimental and theoretical investigations on the transient behavior at pulsed conditions are finally presented. [C2172]

#### "Microwave power SiC MESFETs and GaN HEMTs"

We have fabricated SiC MESFETs with more than 60 W of output power at 450 MHz from single 21.6 mm gate periphery devices (2.9 W/mm) and 27 W of output power at 3 GHz from single 14.4 mm SiC MESFET devices (1.9 W/mm). We have also demonstrated more than 6.7 W/mm CW power from 400  $\mu$ m GaN/AlGaIn HEMT devices for X band (10 GHz) applications. These excellent device performances have been attributed to the improved substrate and epitaxial film quality, optimized device thermal management, and enhanced device fabrication technologies. The substrates and epitaxial films from different sources were compared and some showed significant less SiC substrate micropipes confirmed by X-ray topography and epitaxial defects characterized by optical defect mapping. [C2173]

#### "Three decades of our graduate research and education in compound semiconductor materials and devices"

In the 37 years of activity in Cornell University's research on compound semiconductor materials and devices, much has been discovered, and many students have been educated. The materials include GaAs, AlGaAs, InGaAs, InAlAs, InGaP, GaN, AlGaIn, and InN. The devices have included microwave MESFETs, HEMTs, and HBTs, as well as semiconductor lasers for high speed modulation. The students and results have been hired and transferred to industry, where they have made strong contributions to devices for radar and communication. [C2174]

#### "MSM diodes based on an AlGaIn/GaN HEMT layer structure for varactor and photodiode application"

The electrical and optoelectronic properties of MSM diodes that are based on an AlGaIn/GaN HEMT layer system are investigated. Device fabrication uses standard HEMT processing steps, allowing integration in HEMT circuits without the need of sophisticated growth or etching techniques. The CMAX/CMIN ratio can be tuned by electrode geometry in contrast to conventional varactor diode concepts. Capacitance ratios up to 100 have been reached that exceed best values for published heterostructure varactor diodes. RF optimized devices with 0.5  $\mu$ m electrode length exhibit cut-off frequencies up to 86 GHz. Optoelectronic measurements show the potential of the device as MSM photodetector. [C2175]

#### "Investigation of current collapse in doped and undoped AlGaIn/GaN HEMTs"

The origin of the current collapse which is present in HEMTs on AlGaIn/GaN heterostructures is assigned to deep level states in the layer system. Using photoionization spectroscopy we investigated these levels in doped and undoped HEMT structures on sapphire. In both HEMTs we found two different trap energies of about 3.2 eV and 2.9 eV. By varying the gate voltage we found that a decrease of the gate bias leads to an increased occupation of trap states involved in the current collapse, which indicates that the concentration of trapped donor surface states has a strong influence on the current collapse. [C2176]

#### "A new MMIC sampling phase detector design for space applications"

A new GaAs MMIC sampling phase detector (SPD) has been designed and tested. The authors new SPD design concept gives solutions to the trade-off between phase detection and RF/IF isolation. Moreover, it eases command signal generation and conforms to space level specifications. [C2177]

#### "Signal and noise neural models of pHEMTs"

Low-noise pHEMT transistors, that have excellent performances at microwave frequencies, can be described by their scattering and noise parameters. In this paper, a pHEMT neural model, based on multilayer perceptron neural networks is proposed. The obtained neural models can predict transistor's signal and noise performances very efficiently and accurately for a broad range of bias conditions in the operating frequency range. [C2178]

### "Phase noise in heterojunction field effect transistor amplifiers"

We present phase modulation (PM) noise results in linear high electron mobility transistor (HEMT) amplifiers at different bias conditions at carrier frequencies of 1 GHz and 2 GHz. Our measurements show that the noise at a carrier frequency of 1 GHz is higher than at 2 GHz as expected. It was also found that the dependence of PM noise with drain voltage and drain current varied when different transistors were used. The best PM noise obtained for a HEMT amplifier was  $L(10 \text{ Hz}) \approx -132 \text{ dBc/Hz}$  at a carrier frequency of 1 GHz and  $L(10 \text{ Hz}) \approx -127 \text{ dBc/Hz}$  at a carrier frequency of 2 GHz. [C2179]

### "RF small-signal and power characterization of AlGaIn/GaN HEMTs"

S-parameter and load pull measurements are used to characterize the properties of AlGaIn/GaN HEMTs grown on sapphire or silicon substrates. From the small signal data it follows that the cut-off frequencies  $f_{\text{T}}$  and  $f_{\text{max}}$  increase with the number of fingers, i.e. with the gate width, because of reduced contribution of parasitics to the total gate capacitance. Load-pull measurement setup is described and results of the output power, gain and PAE at 7 GHz are shown. [C2180]

### "High power monolithic AlGaIn/GaN HEMT oscillator"

A monolithic X-band oscillator, based on AlGaIn/GaN HEMT with 1.5 mm total gate periphery, has been designed, fabricated and characterized. The oscillator delivers 1.7 W at 9.556 GHz into 50 ohm load when biased at  $V_{\text{ds}}=30 \text{ V}$  and  $V_{\text{gs}}=-5 \text{ V}$ , with a DC-to-RF efficiency of 16%. Phase noise was estimated to be  $-87 \text{ dBc/Hz}$  at 100 kHz offset and 30 kHz bandwidth. Experimental results show great promise for AlGaIn/GaN HEMT MMIC technology to be used in future high power microwave source applications. [C2181]

### "The effect of gamma-irradiation on the operating parameters of group III nitrides-based field effect transistors"

The influence of gamma ray irradiation on the properties of AlGaIn/GaN based HEMTs has been investigated. It is shown that after being irradiated by gamma-quanta with a total dose of 109 rad the devices preserve their operational ability. [C2182]

### "Proceedings IEEE Lester Eastman Conference on High Performance Devices (Cat. No.02CH37365)"

First Page of the Article [C2183]

### "Suppression of drain conductance dispersion in InP-based HEMTs for broadband optical communication systems"

Demonstrated InP-based HEMTs without drain conductance ( $g_d$ ) frequency dispersion for broadband optical communication systems. It was possible to markedly suppress the  $g_d$  dispersion by using composite channel and double-doped structures rather than a conventional HEMT structure. Furthermore, we clarified that hole generation time by impact ionization determines the frequency range of the  $g_d$  dispersion in a conventional InP-based HEMT by investigating the  $g_d$  dispersion over a wide range of frequencies (100 Hz-20 GHz) [C2184]

### "The history and future of GaAs devices in commercial wireless products"

After years of development and utilization for low volume, high performance military and space based systems, GaAs MESFET first made a major impact in the commercial wireless markets in the early 1990s. Over the next decade, evolution of commercial wireless products led to critical roles for III-V based p-HEMT and HBT as well. Technology trends and specifications of proposed future wireless systems will similarly affect the role of GaAs devices in the coming decade. The performance characteristics of GaAs devices that led to their utilization in current and past systems as well as potential future roles for these devices are discussed [C2185]

### "Bias-dependent performance of high-power AlGaIn/GaN HEMTs"

Large-signal behavior with a fixed load and varying supply voltages was proposed for characterizing the quality of AlGaIn/GaN HEMTs. Improved devices demonstrated constantly high PAEs of 56-62% at 8 GHz throughout a wide voltage range from 10 to 40 V. These 300- $\mu\text{m}$ -wide devices also generated 3.1-W output power with only 3.4-dB gain compression at 45 V, which translates to 10.3-W/mm power density; the highest for any FET of the same size [C2186]

### "Semiconductor technologies for high speed optical networking"

For high speed TDM optical links, high speed physical layer electronics provides critical interface between the local electronic data traffic and high speed optoelectronic devices. We examine the impact of several high speed compound semiconductor IC technologies such as SiGe, GaAs, and InP, on the performance of optoelectronic transceivers at data rate of 40 Gbps and 100+ Gbps regime. In this paper, we utilize a 40 Gbps optoelectronics transceiver as an example to illustrate the advantages and limitations of these compound semiconductor IC technologies [C2187]

### "40 Gbit/s reshaping amplifier cell"

The design of a 40 Gbit/s reshaping amplifier cell with 6 dB gain and a 2 V output signal for ETDM transmission system is presented. The switching-speed of the structure is improved, as well as the reshaping and the limiting effects, by optimising the transistor sizes, DC operating points and the layout design. The chip is fabricated in a GaAs p-HEMT technology with typical  $f_t$  of about 95 GHz, using microstrip transmission lines. Careful layout analysis is performed to optimise propagation phenomena and to minimise interconnection parasitic elements [C2188]

### "A measurement based gate current model for GaAs MESFET's and HEMT's including self-heating and impact ionization"

We present a new gate current model to improve the simulation accuracy of power MESFET and HEMT characteristics. The model is designed to meet the demands of a circuit designer. By the use of a polynomial fit it predicts the gate current within the usual voltage range of an amplifier load line with the highest accuracy. In addition, this leads to a much better simulator convergence than the conventional exponential fit. It also includes the critical on-state breakdown effects that are overlooked by usual gate current models. The model is split into two parts, one equation describes the current caused by tunneling and thermionic emission and another equation describes the impact ionization current. This gives insight into the device physics and allows independent thermal modeling of both effects [C2189]

### "Efficient construction of a large-signal behavioural HEMT model from automated vectorial large-signal measurements"

Large-signal models for microwave devices are classically derived via a small-signal detour using S-parameter measurements. Due to the recent advances in the metrology area of vectorial large-signal measurements, several novel modelling methodologies circumventing this small-signal detour are being developed. An important aspect that these methods have in common is the minimisation of the number of required measurements. As in the case of S-parameter measurements, the goal of the large-signal measurements is to adequately cover the predefined operating region of the device-under-test. In this work, we present a method that enables us to automatically calculate the excitation signals to be applied in order to efficiently cover the ( $V_1$ ,  $V_2$ ) voltage plane of two-port microwave devices. We illustrate this method on a HEMT, where we obtained a significant (>90%) reduction in measurements. Finally, we show that this limited set of vectorial large-signal measurements is sufficient to construct an accurate time-domain behavioural model [C2190]

### "Modeling the temperature noisy performance of low-noise III-V microwave devices down to cryogenic levels"

We performed research work on the effects of temperature by investigating the, DC behavior, the small signal and the noise performance of HEMT and HBT at microwave frequencies by means of different experimental systems down to cryogenic levels. The measurement data were then employed to extract temperature-dependent noisy models to be implemented in commercial CAD software. Here we report the results of the modeling procedure with a special concern for the noise performance whose knowledge is of primary importance in the design of ultra high sensitivity receivers [C2191]

### "Varactor diodes based on an AlGaIn/GaN HEMT layer structure"

We report the fabrication and characterization of MSM diodes on an AlGaIn/GaN HEMT layer system for varactor applications. Device fabrication uses standard HEMT processing steps, allowing an integration in HEMT circuits without the need of sophisticated growth or etching techniques. The  $C_{MAX}/C_{MIN}$  ratio can be tuned by electrode geometry in contrast to conventional varactor diode concepts. Capacitance-voltage measurements exhibit  $C_{MAX}/C_{MIN}$  ratios up to 100. These results exceed best values for published heterostructure varactor diodes. Fabrication of AlGaIn/GaN HEMTs on the same layer system with identical technology prove the potential for monolithic integration [C2192]

### "Wide bandgap semiconductor devices and MMICs for RF power applications"

High power densities of 5.2 W/mm and 63% power added efficiency (PAE) have been demonstrated for SiC MESFETs at 3.5 GHz. Wide bandwidth MMICs have also been demonstrated with SiC MESFETs, yielding 37 W at 3.5 GHz. Even higher power densities have been obtained with GaN HEMTs, showing up to 12 W/mm under pulsed conditions. Hybrid amplifiers using GaN HEMTs on SiC substrates have demonstrated a pulsed output power level of 50.1 W, with 8 dB gain and PAE of 28% at 10 GHz, and CW power levels of 36 W have also been obtained. A wide bandwidth GaN MMIC amplifier had a peak pulsed power level of 24.2 watts, with a gain of 12.8 dB and PAE of 22% at 16 GHz [C2193]

### "Ohmic contacts to n-type AlGaIn and nitride HEMT epilayers"

The authors examine the influence of a variety of processing variables on the specific contact resistance of Ti/Al/Pt/Au ohmic contacts to n-type AlGaIn, and we study the effect of replacing Ti with V when fabricating ohmic contacts to n-type AlGaIn/GaN HEMT epilayers. The replacement of Ti with V allows the annealing temperature for formation of low resistance ohmic contacts to be decreased by 150 °C [C2194]

### "Etching issues in etching compound and Si-based device fabrication"

Summary form only given. Ion-induced damage is an important issue in III-V and Si-Ge devices. The principal cause of damage is the introduction of traps and point defects by ions penetrating into the semiconductor. At the low ion energies used in modern process technology (100 eV say) the bulk of the ions remain on or within a few nm of surfaces. However, some ions channel along the  $\langle 111 \rangle$  direction and so penetrate into the semiconductor to a depth of 30 to 50 nm. In HEMT's with  $f_T$  greater than 100 GHz, the active current carrying layer is only 30 to 50 nm below the surface. In compound semiconductor it is usually impossible to anneal such damage away. An analytic model of this channelling has been developed and its accuracy checked by measuring the penetration of ions produced by a very low energy implantation. An important finding is that while atomic ions (e.g. Cl<sup>+</sup>) can channel and so cause damage molecular ions (e.g. Cl<sup>2+</sup>) do not. This can be used to predict processes that will be suitable for low damage [C2195]

### "III-V nitride-based two terminal devices for high power, high-frequency applications"

III-V Nitride devices have demonstrated impressive high frequency, power and noise performance. Basic transport studies have also been performed theoretically and experimentally in these materials and are primarily driven by the need for better understanding of High Electron Mobility Transistor (HEMT) properties. Although further investigations are necessary to fully understand the transport properties of III-V Nitride devices, the studies reported so far suggest the possibility of realizing two-terminal Negative Differential Resistance (NDR) diodes based on these materials. In this paper, the transport characteristics of III-V Nitrides are reviewed first, followed by a presentation of the expected high frequency and power performance. The technology necessary for realizing nitride NDR devices is discussed and first experimental characteristics are reported [C2196]

### "Modeling electron mobility in MBE-grown InAs/AlSb thin films for HEMT applications using neural networks"

Statistical experimental design was used to explore the effects of the HEMT channel growth parameters on device performance. A 22full-factorial central composite circumscribed Box-Wilson design with three center points was implemented. The growth parameters under investigation were the channel growth temperature and interface formation, both of which greatly impact device operation. Interface formation was defined as the method used to form the InAs/AlSb interface [C2197]

### "RF performance of GaN/AlGaIn HEMT amplifier"

An exact time-domain technique to analyze the RF performance considering the thermal effects of the GaN/AlGaIn HEMT amplifier is reported. The maximum output power of 28 dBm at a power gain of 8.2 dB, and power added efficiency (PAE) of 19% with low frequency gain of 11 dB at an operating frequency of 2 GHz, reported for a 1  $\mu$ m/500  $\mu$ m Al<sub>0.15</sub>Ga<sub>0.85</sub>N/GaN HEMT are in excellent agreement with theoretical calculations. The calculated third-order intermodulation (IM3) and carrier-to-IM3 ratio are -16.5 dB and 13.5 dBc, respectively, at the peak operating power/PAE at 2 GHz. With output power decreasing to 16 dBm at 2 GHz the above quantities are -37 dB and 22.5 dBc, respectively [C2198]

### "Gain compression in GaN HEMT amplifiers"



Volterra series analysis is used to determine linear and nonlinear gain, output power of a GaN HEMT amplifier. Gain compression defined as the difference between linear and nonlinear gain is reported for varying temperatures. Measured 1-dB gain compression of 17.5 dBm for a  $1.45 \times 10^5 \mu\text{m}$  Al<sub>0.15</sub>Ga<sub>0.85</sub>N/GaN HEMT at 300 K and at 2 GHz is in excellent agreement with the calculated value of 17 dBm. With the operating frequency increasing from 1 GHz to 6 GHz the 1-dB gain compression point decreases from 20.5 dBm to 13.8 dBm at 300 K. At 2 GHz the 1-dB gain compression point decreases from 17.5 dBm at 300 K to 6.5 dBm at 600 K [C2199]

#### "17-36 GHz broadband PHEMT MMIC power amplifier for point-to-multipoint applications"

A broadband MMIC power amplifier operating from 17 to 36 GHz is developed for point-to-multipoint applications using  $0.25 \mu\text{m}$  AlGaAs/InGaAs/GaAs pseudomorphic high electron mobility transistor (PHEMT). The amplifier is fully monolithic, with all matching, biasing, and DC block circuitry included on the chip. Operated under 5 V power supply, the two-stage balanced power amplifier has 11 dB small-signal gain with a 3 dB bandwidth from 17 to 36 GHz. The output powers at 1 dB compression are 20 dBm at 26 and 28 GHz and greater than 23 dBm at 30.5 GHz. [C2200]

#### "1.6 w/mm, 26% PAE AlGaN/GaN HEMT operation at 29GHz"

Summary form only given. In this paper, we report the first GaN HEMT power device to operate at 29 GHz. The  $0.2 \mu\text{m}$  T-gate AlGaN/GaN HEMT with a  $120 \mu\text{m}$  total gate periphery exhibited a pulsed output power of 1.6 W/mm with a gain of 6.7 dB and an associated power aided efficiency of 26% at 29 GHz. The epitaxial layers were grown by MOCVD on SiC [C2201]

#### "Effects of surface traps on breakdown voltage and switching speed of GaN power switching HEMTs"

As a competitive candidate for power switching electronics, GaN has slightly wider bandgap, higher electric strength, and higher saturated velocity than SiC. An insulating-gate structure GaN HEMT with a breakdown voltage of 1.3 kV was fabricated with a specific on-resistance of  $1.7 \text{ m}\Omega\cdot\text{cm}^2$ . State-of-the-art power device figure of merit of  $\text{VBR}_2/\text{Ron} = 9.94 \times 10^8 [\text{V}^2\cdot\Omega^{-1}\text{cm}^{-2}]$  was achieved on this device. Device analysis shows that the surface traps play a dominant role in breakdown voltage and switching speed. High switching speed was realized on the kilo-volts devices by adoption of double gate dielectrics [C2202]

#### "Numerical simulation of DC characteristic of InP/InGaAs based optically controlled HEMT"

A new analytical formula of DC characteristics is presented. It shows excellent agreement with experimental data. For the conditions of  $V_{\psi}=1.4 \text{ V}$  and  $V_r=1.0 \text{ V}$ , the channel conductance  $g_{\text{dis}}$  is  $3.09 \times 10^{-2} \text{ mS/mm}$ , the transconductance  $g_{\text{mis}}$  is  $22.2 \text{ mS/mm}$ , and the cut-off frequency  $f_{\text{Ti}}$  is 16.3 GHz. The mechanism of optically controlled HEMT is explored. Under stable illumination, it shows good agreement with experimental data. The optical responsivity of HEMT is up to  $11.4 \text{ A/W}$ . [C2203]

#### "Measurement and simulation of IM distortion in high mobility transistors"

This paper reports the characterisation of intermodulation (IM) distortion in high electron mobility transistors (HEMTs). The second- and third-order IM products in HEMT common-source amplifiers are measured and simulated comprehensively. The comparison of measured and simulated IM products as a function of gate-source voltage, drain-source voltage, input level as well as load impedance are reported. Excellent agreement between measurements and simulations is achieved. [C2204]

#### "Gate width optimization of PHEMT MMIC LNA for low power consumption"

We have developed C-band LNAs of a very low noise and of a very low power dissipation by using a commercially standard  $0.25 \mu\text{m}$  T gate PHEMT technology. A 2-stage MMIC LNA of very low noise figure as low as 0.76 dB and gain of 16 dB at 5.4 GHz has been implemented using a minimum input matching network. Also an LNA of very low power consumption as small as 18 mW with 3 V power supply has been implemented using an optimization of gate width and circuit topology. [C2205]

#### "Optimization of AlGaN/GaN HEMT performance"

Performance optimization of AlGaN/GaN HEMTs on sapphire or silicon substrates is presented. Firstly, the Round-HEMT technology, which is simple in processing and allows fast feedback between structure growth and device properties, is presented. It is shown that different device performance ( $I_{\text{dss}}=130\text{-}360 \text{ mA/mm}$  and  $g_{\text{m,ext}}=79\text{-}132 \text{ mS/mm}$ ) is obtained on structures with nearly identical 2DEG properties ( $G_{\text{ch}} = 1 \text{ mS}$ ). An

improvement of the DC behavior is obtained for RF-optimized i.e. linear HEMTs ( $I_{dss}=603$  mA/mm and  $g_{m,ext}=236$  mS/mm). High-frequency measurements show a  $f_T=35$  GHz and  $f_{max}=70$  GHz for  $L_G=300$  nm and  $W_G=100$   $\mu$ m. Finally, first results we obtained on AlGaIn/GaN HEMTs grown on Si substrates are presented. The Round-HEMTs with 300 nm gate length exhibit a saturation current of 820 mA/mm, a good pinch-off and a peak extrinsic transconductance of 110 mS/mm. The highest saturation current reported so far for AlGaIn/GaN/Si HEMTs and static output characteristics up to 20 V demonstrate that the devices are capable of handling 16 W/mm of static heat dissipation without any degradation of their performance [C2206]

### "Push-push oscillators for 94 and 140 GHz applications using standard pseudomorphic GaAs HEMTs"

Millimeter wave harmonic oscillators taking advantage of the push-push principle are demonstrated, allowing the use of the second harmonic of the oscillators to extend the applicable frequency range of standard pseudomorphic HEMTs to 94 and 140 GHz. Two configuration schemes are realized. An improved approach using a drain-connected pair of oscillators for efficient and compact circuit design and high output power is presented. Using this approach, oscillators at 94 GHz and 135 GHz were developed, with more than 0 dBm and -2 dBm output power and a high suppression of the fundamental signal of 38 dBc and 20 dBc, respectively. All MMICs were realized in a standard 0.13  $\mu$ m pHEMT technology using optical stepper lithography [C2207]

### "Monolithic 38 GHz coplanar feedback VCOs fabricated by a production PHEMT technology"

A set of coplanar 38 GHz voltage-controlled oscillators has been developed. The oscillators are based on a feedback topology and consist of a two-stage amplifier, a frequency selective feedback network, and a voltage-controlled phase shifter. The monolithic circuits also include a buffer stage and were fabricated by a production-oriented PHEMT technology. By employing different feedback networks and phase shifters according to a building block concept, several versions with tuning bandwidths between 0.6 GHz and 1.3 GHz have been realized. The oscillators show a high tuning linearity and an almost constant output power of typically 12 dBm [C2208]

### "Compact MMIC active inductor"

An active inductor implementation suitable for microwave and millimeter wave applications is introduced. The circuit is very simple, compact and can be easily realized in a floating configuration. Simulations, based on Philips smart library ED0D2AH, show that the component can have a quality factor in excess of 100 at 22 GHz with a current consumption of 5.5 mA @ 2.5 V bias. A monolithic implementation in PHEMT technology is reported and discussed [C2209]

### "185 GHz monolithic amplifier in InGaAs-InAlAs transferred-substrate HBT technology"

We report a single-stage tuned amplifier that exhibits a peak small signal gain of 3.0 dB at 185 GHz. To the best of our knowledge, this is the first reported HBT result for a tuned amplifier at this frequency, and the gain-per-stage compares favorably with results from HEMT technologies. The amplifier was designed in a transferred-substrate HBT technology that has exhibited record values of extrapolated  $f_{max}(>1$  THz) [C2210]

### "Performance of a 1.2 THz frequency tripler using a GaAs frameless membrane monolithic circuit"

The first ever planar Schottky diode multiplier working over a THz will be presented in this paper. A tunerless 1.2 THz waveguide frequency tripler has been designed, fabricated and tested. The frequency multiplier consists of a 3 micron-thick GaAs frameless-membrane monolithic circuit, mounted in a split waveguide-block, which includes a built-in Picket-Potter horn. The 1.2 THz membrane tripler is driven by a 400 GHz solid-state chain composed of HEMT based power amplifiers followed by two tunerless planar diode frequency doublers. At room temperature, output power up to 80 microwatts was measured at 1126 GHz with a peak-efficiency of 0.9% and a 3 dB bandwidth of about 3.5%. The output power of the multiplier chain increased dramatically with a decrease of the ambient temperature-up to 195 microwatts was measured at 120 K. When further cooled to 50 K the chain delivers power levels as high as 250 microwatts. To the best of our knowledge, this is the first demonstration of a fully planar multiplier chain at these frequencies, along with performance that supercedes current state-of-the-art performance of whisker-contacted sources [C2211]

### "Conditions for broadband MMIC voltage-controlled oscillators based on theory and experiments"

A systematic study of maximally broadband VCO designs is undertaken. The theoretical investigations lead to the practical realization of two fully monolithically integrated VCOs based on reflection-type and feedback design techniques. Employing efficient diode tuning, the practical implementations of PHEMT-MMICs exhibit a variation

of output frequency of 30% and 45%, respectively [C2212]

### **"High-power broadband AlGaIn/GaN HEMT MMICs on SiC substrates"**

Broadband, high power cascode AlGaIn/GaN HEMT MMIC amplifiers with high gain and power-added efficiency (PAE) have been fabricated on high-thermal conductivity SiC substrates. A cascode gain cell exhibiting 5 W of power at 8 GHz with a small signal gain of 19 dB was realized. A broadband amplifier MMIC using these cascode cells in conjunction with a lossy-match input matching network was designed, fabricated, and evaluated, showing a useful operating range of DC-8 GHz with an output power of 5-7.5 W and a PAE of 20-33% respectively. A nonuniform distributed amplifier (NDA) based on this same process yielded an output power of 3-6 W over a DC-8 GHz bandwidth with an associated PAE of 13-31% [C2213]

### **"New design method of non-uniform distributed power amplifiers. Application to a single stage 1 W PHEMT MMIC"**

A new design methodology of non-uniform distributed power amplifiers is reported in this paper. This method is based on analytical expressions of the optimum input and output artificial lines making up the non-uniform distributed power amplifier. These relationships are based on the optimum load line requirement for power operation. To validate the proposed design methodology, a non-uniform distributed power amplifier has been manufactured at the TriQuint Semiconductor foundry using a 0.25  $\mu\text{m}$  power PHEMT process. This single stage MMIC amplifier is made of six non-uniform cells and demonstrates 1 W output power with 7 dB associated gain and 20% PAE over multi-octave bandwidth [C2214]

### **"20-30 GHz broadband MMIC power amplifiers with compact flat gain PHEMT cells"**

20-30 GHz band MMICs have been successfully developed using two types of novel compact size flat gain PHEMT cells that have flat maximum available gain and sufficient stabilities over a wide frequency range of 20-30 GHz. One type is a feedback type. The other has an equalizer circuit at the gate of a PHEMT. The MMIC delivers gains of over 18 dB and P1dB of over 22 dBm. These results show this method is very effective in designing broadband MMICs [C2215]

### **"A K-band subharmonic down-converter in a GaAs metamorphic HEMT process"**

In this paper, we present the first implementation of a K-band subharmonic down-converter fabricated in a 0.18- $\mu\text{m}$  GaAs Metamorphic High Electron Mobility Transistor (MHEMT) process. The low noise and high gain characteristics of the MHEMTs at K-band allow for the integration of a single-stage amplifier with a subharmonic mixer resulting in low-power broadband performance. The subharmonic mixer exhibits conversion loss of 13 dB and IIP3 of +8 dBm from 23 to 30 GHz. With the addition of the amplifier, the down-converter exhibits a conversion loss of 3 dB, noise figure of 5 dB, and IIP3 of -5 dBm from 26 to 30 GHz. The single-stage amplifier exhibits InP-like performance with gain of 11 dB, NF of 1.5 dB, and dc power consumption of 15 mW [C2216]

### **"A new balanced amplifier using 6-port power divider"**

A new balanced amplifier using the 6-port power divider is proposed. The power divider used in this balanced amplifier has a totally planar structure, and needs no internal resistor and termination. The measured insertion loss of the 2-port back-to-back power divider/combiner for the balanced amplifier is around 0.7 dB, which is a reasonable value at 10 GHz. In power measurement, the 1 dB output power compression point of the proposed balanced amplifier is twice that of the single-ended amplifier as predicted. The measured performances show that the proposed amplifier can be applied as a new balanced amplifier [C2217]

### **"Adjustment of a temperature compensated Ka-band ring resonator VCO using fully automated laser-trimming"**

A new Ka-band voltage controlled oscillator (VCO) using a planar ring resonator (RR) and a GaAs PHEMT microwave monolithic integrated circuit (MMIC) is presented. The resonator operates at harmonic frequencies and is manufactured on a temperature stable calcium magnesium titanate substrate using photolithographic thin-film processes. An innovative fully automated active laser-trimming procedure is used to adjust the frequency of the free-running oscillator as well as the varactor tuning sensitivity. In addition, automated laser-trimming is used to equalize the electrical length between the ring resonator and the MMIC. High unloaded quality factors of more than 350 have been obtained for the harmonic ring resonator. With these high quality factors a single side-band phase noise of better than -110 dBc/Hz is achieved at an offset frequency of 1 MHz. In addition, the frequency tuning range of the laser-trimming procedure is larger than 10% without any significant change of the VCO's characteristics such as phase noise and varactor tuning sensitivity. The typical temperature drift of the oscillator

frequency is less than 4 ppm/K. We use a RR-VCO with an electrical length of four wavelengths, which is phase-locked to an external reference, as a local oscillator in our latest microwave Point-to-Multipoint (PMP) transceivers [C2218]

#### "Design techniques of reducing chip area and highly integrated MMIC for W-band application"

In this paper, several novel techniques for minimizing chip area are presented. In order to demonstrate these features, we have developed a three stage W-band amplifier. This MMIC exhibits more than 15 dB gain from 75 GHz to 90 GHz, and size of this MMIC is less than 0.5 mm<sup>2</sup>. We have also designed and fabricated a single chip 77 GHz T/R MMIC for automotive radar. This MMIC includes 25 active circuits in one chip, and size of this MMIC is less than 8.5 mm<sup>2</sup> [C2219]

#### "A monolithically integrated bacteriorhodopsin/GaAs MODFET bio-photoreceiver"

We report the first monolithic integration of selectively deposited bacteriorhodopsin (bR), acting as a photodetector, with a GaAs-based modulation doped field effect transistor (MODFET). The photovoltage developed across the bR is applied across the gate of the FET. In essence, the large photovoltage developed across bR is converted to a photocurrent. We believe these sensors will be extremely useful for imaging arrays and artificial vision applications [C2220]

#### "AlGaIn/GaN microwave power transistors for S band"

Multifinger power transistors have been fabricated using AlGaIn/GaN grown on insulating SiC by MOVPE. Using a 1  $\mu$ m gate length device,  $f_{Tof}$  10 GHz and  $f_{MAXof}$  24 GHz were found for a 1 mm wide device. A total power of 10 W pulsed was obtained for a 10 mm wide device at 2.8 GHz [C2221]

#### "Investigation of self-heating effects in AlGaIn-GaN HEMTs"

Self-heating effects in AlGaIn-GaN HEMTs grown on sapphire are studied exploiting transistor DC characterization methods. A negative differential output resistance is observed for high power levels accompanied by a transistor transconductance decrease. An analytical formula for a source-drain current drop as a function of a parasitic source resistance is proposed to explain this behavior. The transistor source resistance is determined experimentally at different elevated temperatures to construct channel temperature vs. dissipated power transfer characteristics. It is found that the HEMT channel temperature increases rapidly with dissipated power and reaches values of ~200°C at 2.6 W/mm. The transistor thermal impedance was determined to be 67°CmmW<sup>-1</sup> [C2222]

#### "Novel asymmetric gate-recess engineering for sub-millimeter-wave InP-based HEMTs"

A self-aligned asymmetric gate-recess structure for ultra-high speed InGaAs-InAlAs high electron mobility transistors (HEMTs) is successfully fabricated. A 50 nm T-shaped-gate HEMT with a longer drain-side recess exhibits a much-improved maximum oscillation frequency ( $f_{max}$ ) of 503 GHz, while retaining a similarly high current-gain cutoff frequency ( $f_t$ ) of 307 GHz compared to that with a conventional symmetric recess structure. This result indicates reduced electric field between gate and drain while keeping a small source resistance ( $R_s$ ) in the developed asymmetrically recessed HEMT [C2223]

#### "Ka band power pHEMT technology for space power flip-chip assembly"

This paper proposes a released power pHEMT process for flip-chip mounting. The potential of this flip-chip process is demonstrated for power and low-noise applications in Ka-band [C2224]

#### "65-145 GHz InP MMIC HEMT medium power amplifiers"

In this paper, we present two MMIC power amplifier designs utilizing InP HEMT technology. The first amplifier covers two full waveguide bands, WR10 (75-110 GHz) and WR8 (90-140 GHz), yielding a maximum output power of at least 25 mW between 65-140 GHz. The second design is optimized for the WR10 waveguide band and provides at least 13 dB of large signal gain over 75-110 GHz, and an output power of 40-50 mW [C2225]

#### "Simple model for dynamic range estimate of GaAs amplifiers"

The method to estimate the dynamic range of low bias power low noise GaAs amplifiers for portable radio communication equipment is presented. The method uses the extension of a simple linear noise model of the microwave FET, major components of which are bias dependent. Both noise figure and intermodulation distortion



of an amplifier may be predicted with this model and the dynamic range is easily calculated as a function of bias current and transistor width. The model unifies small signal and nonlinear properties in a form suitable for manual computation [C2226]

### "InGaP PHEMTs for wireless power applications"

This paper shows that we have successfully fabricated a InGaP PHEMT device with a tight threshold voltage distribution of 22 mV by using InGaP as barrier layer material. Fabricated device performance is similar to our standard AlGaAs PHEMT for low voltage operation. A 15 mm device delivers 30 dBm output power, 10.2 dB associated gain, and 67% power added efficiency at 1 dB compression point while operated at 3.5 V and 1.9 GHz [C2227]

### "Study of self-heating effects in GaN HEMTs"

Pulsed RF and I-V characterizations are performed on power GaN HEMTs. These measurements are carried out at different temperatures for the first time to understand self-heating effects and to investigate the possibility of improving heat dissipation mechanisms. These measurements are the basis for robust large-signal models [C2228]

### "Dynamic Large-Signal I-V Analysis and Non-Linear Modelling of Algan/Gan HEMTS"

For AlGaIn/GaN high electron mobility transistors (HEMTs), the voltage and current waveforms at CW large-signal operation at 5 GHz have been reconstructed from experimental magnitude and phase information on fundamental and higher harmonics of transmitted and reflected signals. To compare with the DC behaviour, the clipped waveforms have accurately been analysed to recover the dynamic output characteristics in view of dispersion effects related to self-heating. In conjunction with small-signal S-parameter data, the large-signal experimental results have been used in an attempt to apply a HEMT large-signal model, showing satisfactory agreement of simulated and measured characteristics at least in regions where self-heating is not much pronounced. [C2229]

### "Reliability of metamorphic HEMTs on GaAs substrates"

Metamorphic HEMT (MHEMT) technology enables the growth of high indium content channels on GaAs substrates, giving them the performance of InP HEMTs. MHEMT growth techniques use a graded alloy composition layer structure, permitting channel In contents exceeding 25% without strain. Potential applications include 40 Gb/sec fiber as well as LNAs for LMDS and satellite communication. Many such applications place stringent requirements on reliability with Belcore standards requiring 106hrs Mean Time to Failure (MTTF) at 125C for power devices. Satellite applications require a LNA projected failure-free service of 15-30 years at 80C, which implies an 80C MTTF of approximately 107hours. Naturally, one will ask "Is MHEMT technology reliable?" From the results of our ongoing work, we show MHEMT reliability to be similar to InP HEMTs' with 106hours MTTF at 125C. [C2230]

### "Analysis of HEMT Time-Evolution Characteristics"

A novel transient measurement of the time-evolution of drain characteristics is analyzed to separate thermal and trapping dispersions. The procedure extracts isothermal characteristics from the measured data and parameterizes thermal dispersion. A significant dispersion effect in the isothermal characteristics is then linked to leakage currents that are related to drain potential. The effect of impact ionization is also evident in the data. This analysis provides information necessary to formulate bias- and rate-dependent models of HEMTs. [C2231]

### "CMP provides the access to advanced low cost manufacturing"

CMP aims at providing universities, research laboratories and industries with the possibility of having their integrated circuit projects fabricated for prototyping and low volume production. Presently, users are serviced for CMOS double layer poly/double layer metal (DLP/DLM) 0.8  $\mu\text{m}$ , DLM/TLM 0.6  $\mu\text{m}$ , DLP/4LM 0.35  $\mu\text{m}$ , SLP/6LM 0.25  $\mu\text{m}$ , SLP/6LM 0.18  $\mu\text{m}$ , BiCMOS DLP/DLM 0.8  $\mu\text{m}$ , SiGe HBT 0.8  $\mu\text{m}$  DLP/DLM, SiGe HBT 0.35  $\mu\text{m}$  SLP/5LM and GaAs HEMT 0.2  $\mu\text{m}$ . About 40 multi-project runs are offered per year. Micro Electro Mechanical Systems (MEMS) are also provided in standard CMP runs in CMOS DLP/DLM 0.8  $\mu\text{m}$  and 0.6  $\mu\text{m}$ , BiCMOS DLP/DLM 0.8  $\mu\text{m}$  and HEMT GaAs 0.2  $\mu\text{m}$ , using compatible front-side bulk micro-machining. MUMPS is offered as a surface micro-machining process, allowing one to integrate MEMS only microstructures. Finally, the main processes for Multi-Chip Modules (MCMs) are also available through CMP. [C2232]

### "High Dynamic-Range and Very Low Noise K-Band p-HEMT LNA MMIC for LMDS and Satellite Communication"

An excellent noise figure and high linearity, K-band p-HEMT LNA MMIC, that incorporates single-bias configuration and negative feedback circuit, has been developed for LMDS (Local Multi-point Distribution Service) and satellite communication. The third order intercept point (IP3) of this MMIC is 20 dBm, while output power at 1-dB gain compression is 8.5 dBm. The IP3 and noise figure is 19.5 +/Г,Вi 1 dBm and 1.8 +/Г,Вi 0.2 dB, respectively, at frequencies between 24 and 32 GHz. The die size of the MMIC is 1.9 mm<sup>2</sup>. This MMIC shows a potential reliable application in high-speed wireless access system. [C2233]

### "Effect of gate metal on reliability of metamorphic HEMTs"

The influence of the gate metal on the reliability of metamorphic InAlAs/InGaAs HEMTs with a gate length of 0.12 μm was studied by biased accelerated life tests in air and in nitrogen. By replacing the Ti-Pt-Au gate by Pt-Ti-Pt-Au we found that the life time at 220°C can be increased at least by a factor of two. An activation energy of 1.5 eV and a life time of 1.14106h at 125°C in air were derived for MHEMTs with Pt-Ti-Pt-Au gate. [C2234]

### "Quantitative analysis of microwave frequency multiplication in MESFET/HEMT devices"

This paper provides an in-depth analysis of the principles of harmonic frequency generation utilizing microwave MESFET/HEMT transistor models. The technique employs an in-depth computer oriented and quantitative analysis. The effects of bias, drive voltage, and load on the harmonic output of an ideal transistor model are explored [C2235]

### "A compact MMIC SPDT switch for 60 GHz applications"

This paper presents a GaAs MMIC SPDT switch for 60 GHz applications. Insertion loss and isolation of the switch was measured to be 1 dB and 20 dB, respectively. The circuit uses only two passive HEMT devices in shunt configuration making it very compact, reciprocal and with a high power performance [C2236]

### "Effects of active microwave device parameters on microwave harmonic frequency generators"

Modern microwave and RF systems are increasingly utilizing internal frequency upconversion techniques. This paper develops improved methods of designing active microwave frequency multipliers utilizing MESFET and HEMT devices. The methods extend and improve the accuracy of classical techniques developed over the past few years [C2237]

### "Frequency Dependence of HEMT Under Optical Illumination"

An analysis of the AC characteristics of Al-GaAs/GaAs HEMT under illumination with modulated light has been carried out for small signal condition. A new model for the photovoltage calculation is outlined. The effect of the signal frequency on the photoconductive current is evaluated, the results show that photoconductive current is very small and can be neglected in calculation. The frequency dependence of photovoltage along with 2-DEG charge density, drain-source current and transconductance of the device have been studied analytically for HEMT structure. [C2238]

### "Single optical clock pulse generator for processing ultrafast asynchronous optical packets"

A new scheme for generating a single optical clock pulse from an ultrafast asynchronous optical packet is proposed and a 6.6-ps pulse is demonstrated. The scheme uses an InP OEIC, a gain-switched LD, and a pulse compressor, and is applicable to a self-serial-to-parallel conversion system. [C2239]

### "Relating Dynamics of FET Behavior to Operating Regions"

Dispersion effects and the operating regions they effect are identified in a HEMT and a MESFET. Large-signal pulse and small-signal RF measurements reveal a simple structure to the otherwise complicated dynamic behavior of the FETs. A simple model demonstrates how heating, impact ionization, and leakage currents can contribute to this behavior and that each has an effect in specific regions of bias and operating frequency. It is possible to identify operating conditions that will or will not be affected by dispersion with measurements over a wide range of frequencies from dc to microwave and a range of terminal potentials. [C2240]

### "Monolithic Millimeter-Wave Source Incorporating Planar Surface Wave Assisted Antenna"

A monolithic 120 GHz free-space, continuous-wave source capable of providing 12.6 dBm of EIRP at 18% DC-

to-EIRP conversion efficiency is presented. We utilize both the excellent high frequency performance of the InP based HEMT technology developed by HRL along with the newly developed surface wave assisted antenna concept. Because the antenna itself prefers to be fabricated on a high dielectric constant substrate, monolithic integration with MMIC circuits becomes straightforward [C2241]

#### "A New Empirical Gate Capacitance Model for PHEMT and MESFET Transistors"

This work deals with a nonlinear model for the gate-source capacitance CGS (VGS, VDS) and gate-drain capacitance CGD (VGS, VDS) of GaAs MESFET, HEMT and PHEMT transistors. An analytical bias dependent expression for modeling the CGS (VGS, VDS) and CGD (VGS, VDS) capacitances is developed. The CGS (VGS, VDS) and CGD (VGS, VDS) experimental values are obtained using a multibias extraction of the small signal equivalent circuit procedure. Good agreement between modeled and experimental data, as a function of gate-source and drain-source bias, is obtained. The main feature of the proposed nonlinear model is that no optimization is needed to achieve a good fit of modeled to experimental data. [C2242]

#### "High Speed Circuits Based on HEMT Technology for Optical/Wireless Communication and Sensor Systems"

{no data available} [C2243]

#### "Automatically Controlled Coverage of the Voltage Plane of Quasi-Unilateral Devices"

We developed a systematic procedure to efficiently cover the (V1, V2) voltage plane of two-port microwave devices. The method is restricted to (quasi-)unilateral devices, because we assume that the V1(t) does not change when applying an additional a2 travelling voltage wave. By choosing the adequate magnitude and phase of this a2 signal, the V2 of interest can be constructed. We illustrate this method on a HEMT and show that, for the used experimental conditions, only 27 vectorial large-signal measurements are sufficient to cover the (V1, V2) operating region of the device. This is a significant reduction in the number of required measurements for non-linear model generation, in comparison to the classical approach based on multi-bias broadband S-parameter measurements. [C2244]

#### "W-Band On-Wafer Noise Parameter Measurements"

Several current and planned space missions for earth observation and astronomy require very low noise receivers at W-band. Key components in W-band low noise receivers are the InP low noise amplifiers (LNA). The design of LNAs is a greatly dependent at the availability of good noise models for the devices used in the LNAs. To characterise devices at W-band an on-wafer noise parameter set-up has been developed and is presented here. Using the set-up the noise parameters of an InP HEMT in the frequency band 79-94 GHz have been measured. These are the first reported noise parameter measurements of active devices at W-band. The measurement set-up is based on the cold-source method. [C2245]

#### "Millimeter-wave Active MMIC Frequency Multipliers"

In this paper, a novel theoretical comparison of MESFET and HEMT performances as frequency multipliers for different harmonic orders is presented. Additionally, three W-band single-ended coplanar PHEMT MMIC multipliers (a doubler, a tripler and a quadrupler) are reported. The experimental results show state-of-the art performance and verify the theoretical conclusions. [C2246]

#### "Design and characterization of a monolithic amplifier for millimeter wave"

This paper focuses on design and characterization of integrated circuits working in the millimeter wave. The circuit consists of a monolithic amplifier, aimed for wireless indoor communications at 60 GHz. A calibration kit has also been developed in order to perform proper measurement on wafer. [C2247]

#### "Non-Linear Characterization and Simulation of a Travelling Wave Amplifier"

A large-signal characterization for a travelling wave amplifier (TWA) is presented based on measurements with a non-linear vector network analyzer. The TWA is a four stage CPW design fabricated in a 0.15  $\mu\text{m}$  GaAs HEMT process. The measurement results are compared with simulations in the frequency domain and in the power domain up to the fifth harmonic. Over all a good agreement has been achieved. The model for the transistors, implemented as user-defined model in Agilent ADS, is suitable for large signal designs, especially for high output voltage swings required for drivers of optical modulators. [C2248]

### "Low 1/f Noise 30 GHz Broadband Amplifiers for the Differential Radiometers of the Planck Surveyor Mission."

A radiometer Back End Module based on broadband low noise amplifiers and band pass filters is presented. Low noise amplifiers are multistage HEMT MMIC chips. A 20% of bandwidth at 30 GHz have been achieved. The passband is fixed by coupled lines microstrip filters. A complete module containing two identical branches of amplification and filtering stages with a gain greater than 30 dB has been developed. The low 1/f noise behavior of gain fluctuations allows the module to be used as the Back End Module for the differential radiometers in the European Scientific mission Planck. Details of the MMIC chips and filters assembly as well as experimental results are included. [C2249]

### "A High Gain-Bandwidth Baseband GaAs P-HEMT Matrix Distributed Amplifier IC with a Shifted Second Tier Structure"

A new matrix distributed amplifier has been proposed, in which the second tier has been shifted to the output load. It was intended to increase the amplifications from the later shunt arms of the center line whose voltages are always larger than that of the earlier ones, so that the overall gain could be improved without compromising with the bandwidth. In addition, a new bias scheme was also employed that extended the gain down to the extremely low frequency and resulted in a first baseband matrix distributed amplifier. The proposed design has been verified by using a 0.25  $\mu\text{m}$  self-aligned gate GaAs P-HEMT coplanar IC process, and yielded a gain of 18.5dB from 0-30 GHz, which was 3dB higher than that of the conventional design. [C2250]

### "A monolithic K-band MMIC receiver"

This paper presents the designs and measurement results of a K-band monolithic microwave integrated circuit (MMIC) receiver, including a low noise amplifier and a singly balanced mixer. The MMIC chips are fabricated with a 0.15- $\mu\text{m}$  gate-length pseudomorphic (PM) GaAs-based HEMT MMIC technology, carried out by a commercially available foundry [C2251]

### "An extended RF non-linear model for power prediction of AlGaAs/InGaAs pHEMT's"

A modified Curtice non-linear model for pHEMTs, capable of modeling the current-voltage characteristics, drain-source resistances, gate-source and gate-drain capacitances, is developed. Parameter extraction is based on dual delta-doped pseudomorphic HEMTs on GaAs substrates. Measured and modeled dc I-V, S-parameters, and power performance are compared and demonstrate a great improvement from conventional non-linear models. [C2252]

### "2.4 V-operated enhancement mode PHEMT with 32 dBm output power and 61% power efficiency"

2.4 V operated enhancement-mode pseudomorphic high electron mobility transistors (E-PHEMTs) with high output power and power-added-efficiency (PAE) have been developed. With optimally designed epitaxial structure and gate recess process, the E-PHEMT shows high power performance and high power gain. Under 2.4 V bias at 1.9 GHz, the E-PHEMT shows maximum output power of 32.25 dBm and maximum power-added efficiency of 61.45% with linear power gain of 13.93 dB when the device was tuned for maximum output power match. When tuned for maximum output power added efficiency, the E-PHEMT can achieve a maximum PAE of 78.51%. The developed E-PHEMT with superior power performance is one of the candidates for power amplifiers used for 2.4 V-operated 3G wireless communication system [C2253]

### "A novel technique for accurate noise modelling"

Recent MESFET and HEMT noise models have derived all four noise parameters,  $F_{\text{min}}$ ,  $R_n$ ,  $\text{mag}(\text{Gopt})$ , and  $\text{ang}(\text{Gopt})$ , and generally show good (but not excellent) agreement with all of them. This paper describes a novel correction technique developed and incorporated in the existing Fukui model. This modified model not only shows excellent agreement with measured data but also has been successfully applied in MMIC designs. The correction factor is applicable to any generic model equations. [C2254]

### "V-band MMIC low-noise amplifier design based on distributed active device model"

A V-band two stage MMIC low-noise amplifier using 0.15  $\mu\text{m}$  pHEMT based on a distributed active device model has been designed. This model is successful in constructing the equivalent circuit of HEMT that cannot be scaled from a standard HEMT model. An MMIC amplifier based on the distributed model and careful EM simulation exhibits a maximum gain of 9.6 dB and a minimum noise figure of 3.6 dB at 61 GHz. This results indicate that the distributed HEMT model is effective for the design V-band MMIC low noise amplifiers [C2255]



### "Indium phosphide HEMT and HBT production for microwave and millimeter-wave applications"

Indium phosphide HEMT and HBT offer significantly improved performance for microwave and millimeter-wave applications compared to gallium arsenide HEMT and HBT. Both low-noise and power amplifiers benefit from the improved transport characteristics and high transconductance of these devices. Velocium and TRW are transitioning production capability from GaAs to InP products using 100 mm substrates to leverage InP's improved telecommunications performance [C2256]

### "High power density and large voltage swing of enhancement-mode Al<sub>0.5</sub>Ga<sub>0.5</sub>As/InGaAs pHEMTs for 3.5 V L-band applications"

High power density and large voltage swing Al<sub>0.5</sub>Ga<sub>0.5</sub>As/InGaAs enhancement-mode pHEMTs operating under  $V_{ds} = 3.5$  V for L-band application have been developed. In the study, we improve the current density and the gate voltage operation region of the devices by increasing the Al mole fraction of  $Al_xGa_{1-x}As$  to  $x = 0.5$ . The developed  $1.0\ \mu m$  long and  $1\ mm$  width gate FETs exhibit a  $V_{th} = +0.24$  V and an  $I_{max}$  of 286 mA/mm. The maximum output power at 1.9 GHz operation is 95 mW/mm, with a linear power gain of 18.7 dB, and a power-added efficiency of 60 %. These characteristics demonstrate the great potential of E-pHEMTs for high power microwave device applications [C2257]

### "GaN/AlGaN HEMT microwave class-E power amplifier"

We report the first GaN/AlGaN microwave class-E power amplifier. A physics-based nonlinear model of the GaN/AlGaN HEMT is used instead of the switching models of the active device considered in previous works. The expressions of load network components of the class-E amplifier are derived considering exponential decay of the drain current during fall time and finite quality factor of the resonant circuit to incorporate the nonidealities of the active device and passive components. The class-E amplifier has been simulated using the Cadence circuit simulator using different HEMT structures. Calculated output power and power conversion efficiency are 93 mW and 72% at 1 GHz that decreases to 69 mW and 68% at 11 GHz, respectively for a  $1\ \mu m \times 150\ \mu m$  GaN/Al<sub>0.25</sub>Ga<sub>0.75</sub>N HEMT. For a  $0.12\ \mu m \times 100\ \mu m$  GaN/Al<sub>0.20</sub>Ga<sub>0.80</sub>N HEMT the corresponding quantities are 131 mW, 82%, 87 mW and 77%, respectively [C2258]

### "A broadband GaN push-pull distributed microwave power amplifier"

We have demonstrated a broadband GaN push-pull amplifier that used two  $1.5\ mm$  AlGaN/GaN HEMTs and a new balun. The balun structure is based on the compensation approach suggested by Marchand, which is preferred for low loss, broadband, and high frequency operation [C2259]

### "Recent advances in AlSb/InAs HEMTs for high-speed electronics"

Future high-speed receiver and logic applications that require lightweight power supplies, long battery lifetime, improved efficiency, or high component density will require transistors that consume less power. AlSb/InAs HEMTs have intrinsic advantages for these high-speed, low-power-consumption applications due to the attractive material properties of this heterojunction material system that include high values of mobility, channel conductivity, and peak electron velocity at low electric field. For example, intrinsic  $f_T$  values of 250 GHz have been obtained at  $V_{DS} = 600$  mV and an  $f_{ToF}$  of 90 GHz has been measured at  $V_{DS} = 100$  mV. Furthermore, simulations of logic circuits that combine the HEMTs with resonant tunneling diodes show a power dissipation of only 0.3 mW/gate at 20 Gb/s when biased at 400 mV. The potential payoffs associated with this material system are, however, dependent on further improvements in the technology. In this talk, the current status of the design, fabrication, and characterization of Sb-based HEMTs at NRL will be presented including  $1/f$  noise characterization, the use of an InAsSb channel and a TiW/Au gate metalization, and their integration with RITDs [C2260]

### "In<sub>0.5</sub>Ga<sub>0.5</sub>P/In<sub>0.22</sub>Ga<sub>0.78</sub>As/GaAs pseudomorphic high electron mobility transistor with gate oxide layer for improving on-state and off-state breakdown voltages"

We report, for the first time to our knowledge, the characteristics of In<sub>0.5</sub>Ga<sub>0.5</sub>P/In<sub>0.22</sub>Ga<sub>0.78</sub>As/GaAs p-HEMTs with a 50 E gate oxide layer implemented by the liquid phase oxidation of GaAs. This enhances the on-state and off-state breakdown voltages compared to those of p-HEMT without a gate oxide layer, permitting a trade-off between channel current driving capability and both breakdown voltages [C2261]

### "Investigation of on-state breakdown in InAlAs/InGaAs HEMTs"

By performing Monte Carlo simulations of submicron InAlAs/InGaAs HEMTs on InP, we have calculated consistently the DC, RF, and on-state breakdown characteristics, which are in close agreement with measured data. Our calculations reveal for open-channel conditions the occurrence of impact ionization not only in the channel but also in the cap layer of our device due to a short gate-drain recess length. Furthermore, the breakdown dynamics has been studied by performing calculations of the y-parameters for operating the HEMT under high ionization conditions. Our results describe a significant frequency dependence of the small-signal elements in the conventional equivalent circuit model of the FET [C2262]

#### **"Device and circuit optimization of PHEMT MMIC LNA for low power consumption"**

This paper presents a low power PHEMT monolithic LNA for C-band applications. A two-stage PHEMT MMIC low noise amplifier with power consumption of 18 mW, low noise figure as low as 1.7 dB with gain 18 dB at 5.8 GHz, has been designed using S- and noise parameters and large signal model. The input return loss and output return loss are better than -17 dB and -20 dB at 5.8 GHz, while drawing only 6 mA from a 3 V supply. This PHEMT MMIC LNA has superior DC power performance while still maintaining low noise figure, compared with other HEMT LNAs at the frequency range [C2263]

#### **"Novel approach to a consistent large-signal and small-signal modeling of power PHEMTs"**

A new method is presented to address the Gm and Gds dispersion in large-signal power PHEMT modeling. Instead of using a single DC current source or two current sources for DC and RF respectively, three 4-D sources as functions of V<sub>do</sub>, V<sub>go</sub>, V<sub>gs</sub>, and V<sub>ds</sub>, are introduced to model DC current, RF Gm and RF Gds independently. A model constructed based on the new approach shows consistency in predicting large-signal performance and small-signal S-parameter response over a wide bias range. The model is verified by comparing the modeled DC, RF Gm and RF Gds, bias-dependent S-parameter, power performance as well as device port waveforms at power driving condition [C2264]

#### **"A Ka-band compact 1 watt power amplifier using a Platy-TRL matching method"**

A fully-matched two-stage power amplifier MMIC has been successfully developed operating with the frequency range from 27 GHz to 29 GHz. Platy-transmission lines with low characteristic impedance have been utilized for matching at an intermediate stage and an output one in order to accomplish a compact chip area. Four HEMTs have been combined at an output stage in the developed MMIC. A difference in load impedance at each input port is suppressed by two short stubs in the final output circuit. The stubs are also effective for coincidence of through-phases between four input ports and an output port of the final output circuit. The amplifier has a linear gain of 8 dB and an output power of greater than 30 dBm at 29 GHz. The ultra compact chip area of 1.6 Ч 1.8 mm<sup>2</sup> has been achieved using the platy-TRL matching method (PTMM). The developed MMIC using the PTMM will be able to be applied to a higher output power amplifier as a basic cell that has an output power of 1 watt [C2265]

#### **"A low noise and low power dissipation downconverter MMIC for DBS applications"**

In this work, using 0.2  $\mu$ m GaAs modulation doped FET (MODFET) technology, a high performance DBS downconverter MMIC was developed for direct broadcasting satellite (DBS) applications. Without an LNA, the downconverter MMIC showed a very low noise of 4.8 dB, which is 5 dB lower than conventional circuits. A low LO power of -10 dBm was required for normal DBS operation of the downconverter MMIC, which reduced the power consumption to 175 mW via removal of the LO amplifier on the MMIC. The LO leakage power at IF output was suppressed to a level lower than -30 dBm, which removes a bulky LO rejection filter from the board. The fabricated chip, which includes a mixer, IF amplifiers, and LO rejection filter, exhibits a small size of 0.84Ч0.9 mm<sup>2</sup> [C2266]

#### **"A fully integrated broadband amplifier with 161% 3-dB bandwidth"**

A broadband, low voltage supply, fully integrated monolithic amplifier using GaAs high electron mobility transistors is described. At 2 V power supply, it has 14.5  $\pm$  0.4 dB of gain from 1 through 6 GHz. The 3-dB bandwidth is from 800 MHz to 7.4 GHz. The bandwidth is 161%. More than 15 dB gain is attainable if the supply voltage is increased to 3 V [C2267]

#### **"Ka-band monolithic GaAs PHEMT low noise and driver amplifiers"**

This paper presents the designs and measurement results of two monolithic microwave integrated circuit (MMIC) amplifiers. The driver amplifier demonstrated a measured gain of 8-11 dB from 9 to 25 GHz with a measured output P<sub>1dB</sub> of 12 dBm at 13.2 GHz. The LNA shows a linear gain of 28 dB with 3-dB noise figure from 25 to 35

GHz. The MMIC chips are fabricated with a 0.15- $\mu\text{m}$  gate-length pseudomorphic (PM) GaAs-based HEMT MMIC technology carried out by commercially available foundry [C2268]

#### "Gain profiles for conditionally stable and unconditionally stable amplifiers"

Gain profiles along the line joining the USC (unit Smith chart) center and the SC (stability circle) center for conditionally stable and unconditionally amplifiers are important for amplifier design. SC intersects the USC at two invariant points if  $|k| < 1$ . K, B and D factors can be used to classify the gain profiles. This paper illustrates the gain profiles along the line joining the USC center and SC center for different K, B and D factors [C2269]

#### "High reliability of 0.1 $\mu\text{m}$ MMIC amplifiers on both AlGaAs/InGaAs/GaAs and InGaAs/InAlAs/InP HEMTs"

The high-reliability performance of MMIC amplifiers fabricated using 0.1  $\mu\text{m}$  T-gate on both AlGaAs/InGaAs/GaAs and InGaAs/InAlAs/InP HEMTs is reported. Operating at an accelerated life test condition, two-stage balanced MMIC amplifiers were lifetested at three-temperatures ( $T_1=255^\circ\text{C}$ ,  $T_2=270^\circ\text{C}$  and  $T_3=285^\circ\text{C}$  for GaAs HEMT;  $T_1=215^\circ\text{C}$ ,  $T_2=230^\circ\text{C}$  and  $T_3=250^\circ\text{C}$  for InP HEMT) in an either air or  $\text{N}_2$  ambient. For GaAs HEMT technology, the activation energy ( $E_a$ ) is as high as 1.7 eV, achieving a projected median-time-to-failure (MTF)  $> 64109$  hours at  $125^\circ\text{C}$  junction temperature. For InP HEMT technology, the activation energy ( $E_a$ ) is greater than 2 eV, achieving a projected median-time-to-failure (MTF)  $> 14109$  hours at  $125^\circ\text{C}$  junction temperature. MTF was determined by 3T constant current stress using  $|\Delta S_{21}| > 1.0$  dB as the failure criteria. The results demonstrate the high reliability of MMIC amplifiers fabricated using 0.1  $\mu\text{m}$  T-gate on both AlGaAs/InGaAs/GaAs and InGaAs/InAlAs/InP HEMTs based on small-signal microwave characteristics of HEMT MMICs [C2270]

#### "Advanced GaAs MMIC technology development at WIN Semiconductors corporation"

WIN Semiconductors has successfully developed and demonstrated high performance and highly manufacturable HBT and pHEMT technologies in a short period of time. This indicates the advanced GaAs MMIC technology development is taking shape in Taiwan. WIN Semiconductors is dedicated to continuing the development efforts and to providing best GaAs technologies to the community [C2271]

#### "Broadband bidirectional active MMIC power splitter and combiner for feed networks"

We present a number of broadband, 2-18 GHz, active MMICs intended for use in broadband active distribution networks. These networks are often part of a radar transmit or receive array antenna and are often passive and lossy structures. The possibility of gain in the distribution network reduces the need for additional amplification and can improve the system dynamic behaviour as well as noise performance. The MMICs considered in this paper are an active power splitter an active power combiner and a bidirectional power splitter/combiner. The circuits have been fabricated using a 0.2  $\mu\text{m}$  GaAs PHEMT foundry process from OMMIC. Measured results show good agreement with simulations [C2272]

#### "A 20-40 GHz monolithic doubly-balanced mixer using modified planar Marchand baluns"

A 20-40 GHz doubly-balanced mixer was designed for high-speed wireless communications. In the design, a modified planar Marchand balun was employed to have wide bandwidth while keeping compact size. The circuit was implemented with TRW 0.15  $\mu\text{m}$  PHEMT foundry and the chip takes 2.542  $\text{mm}^2$ . The simulated conversion loss is 10 dB, and port-to-port isolation greater than 50 dB from 20 to 40 GHz. Measurement was also conducted [C2273]

#### "Monolithic Ka-band even-harmonic quadrature resistive mixer for direct conversion receivers"

This paper describes the design and measured performance of a Ka-band even-harmonic quadrature mixer which employs PHEMT resistive mixer elements. By employing the even-harmonic technique, with local oscillator at half the RF input frequency, the mixer is better suited for direct conversion receiver application. The chip operates in the 30 to 40 GHz range and has been used to successfully demodulate a 4 Mb/s 16-QAM signal at 38 GHz [C2274]

#### "Large signal bias-dependent modeling of PHEMTs by pulsed measurements"

A bias-dependent large signal model and corresponding parameter extraction procedures are presented to characterize PHEMT devices by pulsed measurements. Two nonlinear current sources and few additional parameters are used to model bias-dependence of the drain current. Results show that the method discussed in

this paper can be applied to model the large signal behavior of PHEMTs from DC to RF at any bias points [C2275]

#### "A 1-chip RF transceiver MMIC for ETC with surface via-hole isolation technique"

An RF Transmitter Receiver MMIC (TX-RX MMIC) with 16-pin plastic package has been developed for 5.8 GHz Japanese Electronic Toll Collection system (ETC). The MMIC contains following RF blocks; local buffer amplifier, variable attenuator, ASK modulator, power amplifier, low-noise amplifier, down-converter, local switch and antenna switch. We have developed the new Surface Via-Hole (SVH) isolation technique to integrate all RF circuits into single chip. The double hetero-junction modulation doped FETs (MODFETs) and SrTiO<sub>3</sub>(STO) MIM capacitors are also developed to realize a single voltage operation and small chip size. By using SVH isolation technique, low carrier leakage of -43 dBm, high on/off ratio of 39.6 dB at 5.84 GHz and low total current of 150 mA are achieved, and the practical small chip size (2.25×1.25 mm<sup>2</sup>) is realized [C2276]

#### "A 1.7 mA low noise amplifier with integrated bypass switch for wireless 0.05-6 GHz portable applications"

An ultra low current low noise amplifier with an integrated bypass switch has been developed using PHEMT technology. The LNA/Sw uses only 1.7 mA when powered and less than 1 uA when bypassed. It is usable from 50 MHz to 6 GHz. This enables portable systems such as Bluetooth, Home RF, PDAs, wireless LANs. The LNA provides 15 dB gain, 1.8 dB noise figure with 50  $\Omega$  load at the output and  $\Gamma_{opt}$  at the input. Bypass mode provides 5 dB insertion loss into the same I/O match. The LNA and bypass switch with associated control circuitry are integrated into a single RFIC and housed in the miniature SOT package. This LNA/Sw provides lower current and easier usage with comparable NF, Gain, and bandwidth than previously reported products [C2277]

#### "Design of an LTCC switch diplexer front-end module for GSM/DCS/PCS applications"

This paper presents the results of an antenna switch/filter module integrating GSM/DCS/PCS diplexer functions and Rx/Tx antenna switching on a low temperature co-fired ceramic (LTCC) substrate. Although the RF front-end module (FEM) was configured for dual-band (GSM/DCS) applications, the high pass filter function was designed to operate in the PCS band as well. Harmonic filtering was included in the diplexer design, which reduced the filtering requirements for the power amplifier. The 50-ohm in/out FEM utilized GaAs PHEMT switches and associated bias passives surface mounted on the LTCC substrate. S-parameter characterization of the FEM demonstrated excellent insertion and return loss characteristics. For GSM, the return and insertion losses measured at 912 MHz were better than 28 dB and less than 1.7 dB, respectively. Similarly, for DCS applications, the return and insertion losses at 1.77 GHz were better than 19 dB and less than 1.5 dB, respectively. In both cases, the design approach yielded excellent agreement between measured and simulated results [C2278]

#### "Dual-band/tri-mode receiver IC for N- and W-CDMA systems using 6"-PHEMT technology"

A dual-band/tri-mode receiver IC for CDMA based mobile systems has been fabricated using our 6"-PHEMT production line, comprising the complete RF front end and one IF stage. The first LNA stage exhibits an input IP<sub>3</sub> of +8 dBm and a noise figure of 1.0 dB, the overall gain of the complete receiver is 26.0 dB. The current consumption only is 17 mA, for a minimum LO power demand of -7 dBm [C2279]

#### "Characterization techniques for temperature-dependent experimental analysis of microwave transistors"

In our research work the effects of temperature on DC behavior, small signal and noise performance of several low-noise transistors at microwave frequencies were investigated by means of different experimental systems down to cryogenic levels. We here present the results of such an extensive investigation together with the details of the experimental procedures followed. The on-wafer cooling set-up was designed and realized in our lab and it exhibited a very good performance characterized by fast settling times. Clear self-heating effects were observed in DC behavior of on-wafer pseudomorphic HEMT's tested over the 220-320 K temperature range [C2280]

#### "An accurate analytical model of the AlGaAs/GaAs high electron mobility transistor (HEMT)"

A new and accurate analytical model for the AlGaAs/GaAs high electron mobility transistor (HEMT) or MODFET is presented. This model uses a polynomial expression to model the dependence of sheet carrier concentration ( $n_2$ ) in the two-dimensional electron gas on gate voltage ( $V_G$ ). It takes into account parasitic conduction in the



AlGaAs layer by including a MESFET operation. It also includes the effects of the extrinsic source and drain resistances. Based on this model, analytical drain current-voltage equations suitable for computer simulation are derived. Calculated results show excellent agreement with measured characteristics, much closer than previous other models [C2281]

### "Semiconductor device reliability in extreme high temperature space environments"

Reliability at high temperatures is one of the most important problems for electronic components operating in extreme space environments. High temperature operation not only reduces the performance of electronic devices, but also greatly shortens their lifetime. The electronic devices are usually designed for room temperature performance. In this paper a review is made of high temperature reliability testing of solid-state electronic components. To date, most of this work has been concerned with high temperature stressing, usually for short periods of time (less than 100 hours) to demonstrate stability. Comprehensive high temperature reliability studies will be required to field high temperature devices for future space exploration [C2282]

### "CMP: the access to advanced low cost manufacturing"

Summary form only given, as follows. CMP aims at providing Universities, Research Laboratories and industries with the possibility to have their integrated circuits projects fabricated for prototyping and low volume production. Presently, users are serviced for CMOS double layer poly/double layer metal (DLP/DLM) 0.8  $\mu$ , DLM/TLM 0.6  $\mu$ , DLP/4LM 0.35  $\mu$ , SLP/6LM 0.25  $\mu$ , SLP/6LM 0.18  $\mu$ , BiCMOS DLP/DLM 0.8  $\mu$ , SiGe HBT 0.8  $\mu$  DLP/DLM, SiGe HBT 0.35  $\mu$  SLP/5LM and GaAs HEMT 0.2  $\mu$ . About 40 multi-project runs are offered per year. Micro Electro Mechanical Systems (MEMS) are also provided in standard CMP runs in CMOS DLP/DLM 0.8  $\mu$  0.6  $\mu$ , BiCMOS DLP/DLM 0.8  $\mu$  and HEMT GaAs 0.2  $\mu$ , using compatible front-side bulk micro-machining. MUMPS process is offered as a surface micromachining allowing one to integrate MEMS only microstructures. Finally, the main processes for Multi-Chip Modules (MCMs) are also accessible through CMP. CMP has introduced very advanced processes during the 3 last years: 0.25  $\mu$ m CMOS in 1997, 0.18  $\mu$ m CMOS in 1999, 0.5  $\mu$ m Silicon On Sapphire in 2000, and the 0.35  $\mu$ m HBT BiCMOS in 2001. Those processes represent a challenge for CAD design, applications, and training. We will present the process and design-kits features for those advanced technologies, and give some results on the dissemination and support activity at CMP. Accessing advanced and state of the art processes gives to the academic/research community a high quality of engineering education and a high quality of research. [C2283]

### "Cryogenic, X-band and Ka-band InP HEMT based LNAs for the Deep Space Network"

Exploration of the Solar System with automated spacecraft that are more than ten astronomical units from Earth requires very large antennae employing extremely sensitive receivers. A key figure of merit in the specification of the spacecraft-to-earth telecommunications link is the ratio of the antenna gain to operational noise temperature (G/Top) of the system. The Deep Space Network (DSN) receivers are cryogenic, low-noise amplifiers (LNAs). InP HEMT LNA modules are demonstrating noise temperatures less than ten times the quantum noise limit (10 hf/k) from 1 to 100 GHz. To date, the lowest noise LNA modules developed for the DSN have demonstrated noise temperatures of under 4 K at 8.4 GHz and 11 K at 32 GHz. The development and demonstration of cryogenic, InP HEMT based front-end amplifiers for the DSN requires accurate component and module characterization, and modeling from 1 to 100 GHz at physical temperatures down to and below 12 K, because of the broad band frequency response of InP HEMTs. The characterization and modeling begins with the HEMT chip, proceeds to the multi-stage HEMT LNA module, and culminates with the complete front-end cryogenic receiver package for the antenna. This paper presents an overview of this development process with emphasis on comparison between modeled and measured results at 8.4 GHz. Results are shown for devices, LNA modules, front-end receiver packages employing these modules, and antennae employing these packages [C2284]

### "Design and performance of a highly integrated wideband active downconverter MMIC"

The design and performance of a highly integrated wideband downconverter MMIC is described. The circuit utilizes 0.25  $\mu$ m pHEMT technology and a high density interconnect (HDI) process to yield a single ended, double balanced active downconverter with a 1 mm<sup>2</sup> die area. The circuit is self biased and draws 17-24 mA from a single 3-5 V positive supply. Diode level shifting is employed to achieve a direct coupled IF output. Measured performance of the MMIC demonstrates 10 GHz 3 dB-RF bandwidth and positive conversion gain through 18 GHz [C2285]

### "High performance AlGaIn/GaN HEMTs with recessed gate on sapphire substrate"

A high performance AlGaIn/GaN high electron mobility transistor (HEMT) with recessed gate is successfully

fabricated on a sapphire substrate. In order to realize a high performance HEMT, it is very important not only to improve the 2-dimensional electron gas (2DEG) but also to reduce the parasitic resistance. However, the increase of aluminum content in AlGa<sub>N</sub> to produce a high density 2DEG results in poor ohmic contact, as well known. In our recessed gate structure, an ohmic contact with low resistivity can be formed on n-GaN with high electron density. This is grown on an AlGa<sub>N</sub> layer with high aluminum content. We describe the fabrication and illustrate the performance of the AlGa<sub>N</sub>/Ga<sub>N</sub> HEMT with recessed gate and conclude that it is a promising device for high power and high frequency applications [C2286]

#### "Hyperspectral imaging of breakdown in InAlAs/InGaAs HEMTs: a comparative study"

Although InAlAs/InGaAs HEMTs offer promise for high-speed, high power applications, both offstate and on-state breakdown voltages in this material system tend to be poor. One promising avenue for understanding breakdown is the study of photon emission. Previous examinations of emission in this material system and in the AlGaAs material system have generally been limited to investigations of a single device. In this work we will present a comparative investigation of emission at breakdown in a set of InAlAs/InGaAs HEMTs that includes devices with a wide range of doping levels. Such a comparison allows us to understand better the tradeoffs in device design, as well as helping us to identify when/if different breakdown mechanisms may be at play [C2287]

#### "Excellent DC characteristics of HEMTs on semi-insulating silicon carbide substrate"

Summary form only given. The epitaxial layers of Al<sub>0.26</sub>Ga<sub>0.74</sub>N/GaN were grown by MOCVD with a good uniformity and carrier mobility of 1281 cm<sup>2</sup>/Vs at room temperature. High electron mobility transistor (HEMT) have been fabricated using AlGa<sub>N</sub>/Ga<sub>N</sub> heterostructure on semi-insulating silicon carbide substrate. The fabricated 2.2 μm gate length Al<sub>0.26</sub>Ga<sub>0.74</sub>N/GaN HEMTs exhibited high transconductance 287 mS/mm with high drain current density 857 mA/mm. This is the first report with highest transconductance so far achieved for 2.2 μm gate length AlGa<sub>N</sub>/Ga<sub>N</sub> HEMTs. Good IDS-VDS characteristics of a 2.2 μm gate length and 15 μm gate width HEMT, yielding a maximum current density of 867 mA/mm and a record extrinsic transconductance of 287 mS/mm for the gate voltage of 0.2 V. From the transfer characteristics, the observed maximum drain-source current density is 1100 mA/mm for the gate and drain voltage of 3.8 and 10 V. The I-V characteristic is noteworthy for its minimal current decrease at large dissipation levels due to self-heating. Owing to the excellent thermal conductivity of the SiC substrate, the current density decreases during the sweep (857 mA/mm to 833 mA/mm) by only 2.8% when the drain bias is increases to 20 V. The self-heating effect is high for sapphire based device structures [C2288]

#### "Linearity of high Al-content AlGa<sub>N</sub>/Ga<sub>N</sub> HEMTs"

This work will address the advancements in the linearity of AlGa<sub>N</sub>/Ga<sub>N</sub> HEMTs. This is the first reported linearity result for high-Al content devices, and it is the first reported result of linearity for nitride-based HEMTs under both transmitter and receiver types of conditions. When the device technology matures, it will have commercial and military applications in wireless base stations, satellite communications, and radar [C2289]

#### "Terahertz plasma-wave excitation in 80-nm gate-length GaAs MESFET by photomixing long-wavelength CW laser sources"

The resonance frequency can be externally controlled which offers tunability of oscillation. The THz plasma resonant phenomena, however, has only been measured by illuminating a AlGaAs/GaAs HEMT with a single 2.5-THz gas laser source and there has been no experimental reports on the resonance frequency dependence. This paper demonstrates the first experiment on GaAs MESFETs [C2290]

#### "Chaos generator MMIC's using resonant tunneling diodes"

Recently, applications of chaos, which is often observed in nonlinear circuits, have been studied intensively in the field of information processing and communication systems. Using resonant tunneling devices to make such nonlinear circuits has many advantages, for example, simplicity in circuit, high operation frequency and low power consumption. In this paper, we report the demonstration of high-frequency operations of the chaos generator microwave monolithic ICs consisting of an RTD and a high electron mobility transistor (HEMT) [C2291]

#### "40-Gbit/s D-type flip-flop and multiplexer circuits using InP HEMT"

We developed a novel design technique for a D-type flip-flop (D-FF) circuit that is based on a small-signal-equivalent circuit approach. This technique provides the best condition to operate the D-FF at a high frequency. Using this technique, we fabricated a master-slave D-FF using a 0.15-μm InP HEMT technology. We achieved 40-Gbit/s operation with clear-eye-waveform patterns and reduced jitter [C2292]

### "Temperature dependence of intermodulation and linearity in GaN based devices"

Gain, intermodulation distortion of an AlGaIn/GaN device operating at RF, have been analyzed using a general Volterra series representation. The circuit model to represent the GaN FET is obtained from a physics based analysis. Theoretical current-voltage characteristics are in excellent agreement with the experimental data. For a  $1\ \mu\text{m} \times 500\ \mu\text{m}$  Al<sub>0.15</sub>Ga<sub>0.85</sub>N/GaN FET, the calculated output power, power added efficiency and gain are 25 dBm, 13% and 10.1 dB, respectively at 15 dBm input power and are in excellent agreement with the experimental data. The output referred third order intercept point IP<sub>3</sub> is 39.9 dBm at 350 K and 33 dBm at 650 K. These are in agreement with the simulated results from Cadence which are 39.34 dBm and 35.7 dBm, respectively. At 10 GHz, third order intermodulation distortion IM<sub>3</sub> for 10 dBm output power is -88 dB at 350 K and -82 dB at 650 K. At 350 K IM<sub>3</sub> is -97 dB at 5 GHz and -88 dB at 10 GHz. For the same frequencies IM<sub>3</sub> increased to -90 dB and -82 dB, respectively, at 650 K [C2293]

### "Noise characteristics of highly strained InGaP/InGaAs p-HEMTs grown on patterned substrates by using compound-source MBE"

In this paper, we report on the low-frequency and microwave noise characteristics of the highly strained InGaP/In<sub>0.33</sub>Ga<sub>0.67</sub>As p-HEMTs grown on patterned substrate and the conventional InGaP/In<sub>0.22</sub>Ga<sub>0.78</sub>As p-HEMTs grown on non-patterned substrate [C2294]

### "Monolithic integration of InAlAs/InGaAs enhancement and depletion (E/D)-mode metamorphic HEMTs on GaAs substrate"

Except for a few studies on enhancement (E)-mode metamorphic HEMTs, most of the research studies so far however focused on depletion (D)-mode HEMTs. In view of excellent performance of D-mode devices, it is compelling to investigate E-mode devices as well. Moreover, once discrete devices are established, it becomes very much interesting to look into the monolithic integration of E- and D-mode devices as it finds an extensive application for ultra-high speed and low power digital circuits. To the best of our knowledge, there are no published results on monolithic integration of metamorphic E/D HEMTs so far. In this paper, we present results on monolithically integrated metamorphic In<sub>0.52</sub>Al<sub>0.48</sub>As/In<sub>0.53</sub>Ga<sub>0.47</sub>As E/D HEMTs on GaAs substrate with gate-lengths down to 0.13  $\mu\text{m}$  [C2295]

### "A flip-flop based on monolithic integration of InAs/AlSb/GaSb RITDs and InAlAs/InGaAs/InP HEMTs"

We report for the first time the demonstration of logic circuits based on the monolithic integration of high-speed submicron gate length InAlAs/InGaAs/InP HEMTs with InAs/AlSb/GaSb RITDs. An inverting D flip-flop was implemented using the MOBILE circuit architecture [C2296]

### "High reliability of 0.1 $\mu\text{m}$ InGaAs/InAlAs/InP HEMT MMICs on 3-inch InP substrates"

The high-reliability performance of K-band MMIC amplifiers fabricated with 0.1  $\mu\text{m}$  gate length InGaAs/InAlAs/InP HEMTs on 3-inch wafers using a high volume production process technology is reported. Operating at an accelerated life test condition of  $V_{\text{ds}}=1.5\ \text{V}$  and  $I_{\text{ds}}=150\ \text{mA/mm}$ , two-stage balanced amplifiers were life tested at two-temperatures ( $T_1=230^\circ\text{C}$ , and  $T_2=250^\circ\text{C}$ ) in nitrogen ambient. The activation energy ( $E_a$ ) is as high as 1.5 eV, achieving a projected median-time-to-failure (MTF) $>14106$  hours at a  $125^\circ\text{C}$  junction temperature. MTF was determined by 2T constant current stress using  $|\Delta S_{21}|>1.0\ \text{dB}$  as the failure criteria. This is the first report of high reliability 0.1  $\mu\text{m}$  InGaAs/InAlAs/InP HEMT MMICs based on small-signal microwave characteristics. This result demonstrates a reliable InGaAs/InAlAs/InP HEMT production technology [C2297]

### "Proceedings of the 2001 SBMO/IEEE MTT-S International Microwave and Optoelectronics Conference. (Cat. No.01TH8568)"

First Page of the Article [C2298]

### "On optical gain mechanisms in a 2DEG photodetector"

Discusses the gain mechanisms in an optical detector based on a modulation doped heterojunction. It is shown that, in this gate-less HEMT device, varying the density of the mobile electron gas produces large differences in optical responsivity. The observed behavior is explained on the basis of a internal variation of the Fermi level, similar to a photovoltaic gating effect. [C2299]

### "Fully physical time-dependent compact thermal modelling of complex non linear 3-dimensional systems for device and circuit level electro-thermal CAD"

An fully analytical spectral domain decomposition approach to solution of the nonlinear time-dependent heat diffusion equation in complex volumes is introduced. Its application to device/circuit level electro-thermal simulation on CAD timescales is illustrated. The full treatment in coupled electro-thermal CAD of thermal nonlinearity due to temperature dependent diffusivity is described. Thermal solutions are presented in the form of thermal impedance matrix expressions for thermal subsystems. These include double Fourier series solutions for rectangular multilayers, which are an order of magnitude faster to evaluate than existing semi-analytical Fourier solutions based on DFT-FFT. They also include double Fourier series solutions for arbitrarily distributed volume heat sources and sinks, constructed without use of Green's function techniques, and for rectangular volumes with prescribed fluxes on all faces. These analytical solutions allow treatment of arbitrary device structures without invoking conventional numerical methods. They provide minimal boundary condition independent compact thermal models, allowing CAD timescale coupled electro-thermal solution for complex systems, without requiring lumped element RC network extraction or node reduction. The time-independent thermal resistance matrix description of device structure is illustrated by a fully physical, coupled electro-thermal study of the interaction of substrate thickness and surface convection in power HEMTs. The thermal time-dependent implementation is illustrated by circuit level harmonic balance simulation of a 343 MMIC amplifier array [C2300]

### "Conference Proceedings. 2001 International Conference on Indium Phosphide and Related Materials. 13th IPRM (Cat. No.01CH37198)"

The following topics were dealt with: long wavelength lasers; HBTs and novel devices; MBE growth; optical device processing; nanostructures; novel optical materials and devices; optoelectronic devices; epitaxial growth; processing; high speed optical modulators; HEMTs; integrated photonic devices; photonic crystals [C2301]

### "Characterization of parasitics in microwave devices by comparing S and noise parameter measurements with two different on wafer calibration techniques"

This paper presents a procedure for an accurate characterization of parasitic effects of terminal pads in microwave devices. This procedure is based on the measurement of S and noise parameters of the device with two different sets of calibration standards, and simplifies the process of extracting the parasitic elements of the small signal equivalent circuit [C2302]

### "2.4 V-operated enhancement-mode power PHEMTs for personal handy-phone system application"

Enhancement-mode pseudomorphic high electron mobility transistors (E-PHEMTs) were developed for low voltage wireless communication applications. Under drain bias of 3.6 V, the device delivered a high output power density of 265.25 mW/mm (29.5 dBm) with a power-added-efficiency (PAE) of 50.54%. Under 1.9 GHz pi/4-shifted quadrature phase shift keying (QPSK) modulation signal, the 3.36 mm devices meet personal handy-phone system (PHS) specification at an output power level of 22.42 dB with PAE of 35.12% under 2.4 V drain bias. The E-PHEMTs developed are adequate for low-voltage-operated PHS application. [C2303]

### "Noise performance and bias-dependence of Si/SiGe HBT's at microwave frequencies"

The results of an investigation on the bias-dependence of the noise performance of Si/SiGe HBT's over the 5-25 GHz frequency range are reported. The noise parameters  $\Gamma_{\text{opt}}$  and  $R_{\text{opt}}$  have been derived from a model analysis based on measurements of the device scattering parameters and minimum noise figure  $F_{\text{min}}$ . The noise behaviour of the HBT and its bias dependence is compared with that of low-noise HEMT's and advanced polysilicon BJT's previously characterised and modelled in our lab. [C2304]

### "Low temperatures in RTP"

Even though RTP was originally designed for temperatures from 700 to 1200°C the processes with lower temperatures gain more and more importance. Steady state temperatures down to 300°C makes temperature control from 200°C necessary. This processes occur in silicon and in compound semiconductor production. In GaAs production low temperature processes are used for alloying metal to achieve lowest contact resistances. For this applications we used the graphite box supplied for the Mattson SHS2800CS. Together with the special low temperature pyrometer setup. Temperatures can be controlled down to 200°C. But the correct temperature profile is not easy to achieve. This is coming from the fact that the wafer can be heated rapidly, but not cooled rapidly. This will lead to a overshoot, 7°C in this specific example. To solve this problem a short open loop step was introduced. This method is used in production as a standard now. The alloying of the contacts for HBT and



HEMT production using this methods will be presented. [C2305]

#### "Design and fabrication of low noise MODFET for 30-60 GHz band"

Described in this paper are unified design and electronic lithography-based technology of production of low-noise Schottky FETs. HEMT and PHEMT series for 3-60 GHz frequency band have been manufactured. [C2306]

#### "Design and performance of Gilbert cell mixer MMICs with GaAs PHEMT technology"

The design and performance of a Gilbert cell mixer, using GaAs PHEMT technology is presented. It was designed to operate as a down converter, with an RF frequency of 1.9 GHz, a LO of 2.0 GHz and IF of 100 MHz. A voltage gain of over 11.8 dB and an input reflection coefficient of smaller than -14 dB, without a matching network, were obtained. [C2307]

#### "The radiation firmness of the GaAs-AlGaAs HEMT ohmic contacts"

The results of investigation of the effect of  $\gamma$ -radiation on the GaAs-AlGaAs field-effect transistors ohmic contacts specific contact resistivity are presented. The surface microrelief investigations and their correlation with the ohmic contacts parameters are presented. Investigations were carried out for two structure types subjected to various thermal treatment. It was shown that  $\gamma$ -radiation may be used for parameters improvement; the radiation limit was determined. [C2308]

#### "Advances in InP HEMT technology for high frequency applications"

This paper reviews the remarkable progress being made in the development of InP HEMT devices and circuits for high frequency analog applications. Despite possessing superior performance, widespread use of InP HEMTs has to date been hindered by their relatively high cost (as compared with GaAs-based devices). However, the commercialization of HEMTs with high-indium-content InGaAs channels now appears to be inevitable due to recent progress on two parallel fronts-the development of metamorphic HEMTs (MHEMTs) and the scaling of InP substrates to larger sizes (4 and 6-inch) [C2309]

#### "A model for hydrogen-induced piezoelectric effect in InP HEMTs and GaAs PHEMTs"

We have developed a model for the impact of the hydrogen-induced piezoelectric effect on the threshold voltage of InP HEMTs and GaAs PHEMTs. We have used 2D finite element simulations to calculate the mechanical stress caused by a gate that has expanded due to hydrogen-absorption. This has allowed us to map the piezo-electric charge distribution in the semiconductor heterostructure. We used a simple electrostatics model to calculate the impact of this piezo-electric polarization charge on the threshold voltage. We have found that the model explains experimentally observations of hydrogen-induced threshold voltage shifts, both in InP HEMTs and in GaAs PHEMTs [C2310]

#### "Fabrication technology and device performance of sub-50-nm-gate InP-based HEMTs"

Sub-50-nm-gate InAlAs/InGaAs high electron mobility transistors (HEMTs) lattice-matched to InP substrates were fabricated. Our method of fabrication includes the two-step-recess gate technology and a low temperature process, applied at below 300°C. We succeeded in fabricating ultra-short 25-nm-long T-shaped-gates. RF measurements showed that the cutoff frequency  $f_{\text{ToF}}$  of a 25-nm-gate HEMT is 396 GHz, and this is the highest value yet reported for any type of transistor [C2311]

#### "AlSb/InAs HEMTs with a TiW/Au gate metalization"

We report on the fabrication and characteristics of AlSb/InAs HEMTs with a TiW/Au gate metalization. Prior to the metal evaporation, the usual oxygen plasma surface pretreatment was adjusted to minimize damage. These HEMTs exhibit decreased gate leakage current in the low drain bias region and similar microwave performance compared to previous HEMTs fabricated from the same material with a Cr/Au gate metal. The HEMTs were found to be thermally stable up to 180°C when heat treated in a H<sub>2</sub>/N<sub>2</sub> ambient. TiW/Au diode test structures fabricated on similar HEMT material were thermally stable up to 270°C [C2312]

#### "Stable and uniform InAlAs/InGaAs HEMT ICs for 40-Gbit/s optical communication systems"

We developed thermally stable InAlAs/InGaAs HEMTs which have uniform offset-voltage in differential amplifiers. The standard deviation of their offset-voltages is only 6.2 mV, and their threshold voltage changes by less than 11 mV when they are annealed for 60 minutes at 330°C. These properties are essential for the operation of 40-

Gbit/s optical communication circuits [C2313]

### "High speed optical fiber communication ICs based on InP HEMT"

High-speed integrated circuit technology is the key to realizing large-capacity optical fiber communication systems. This paper describes the present status of 0.1- $\mu\text{m}$ -gate InP HEMT ICs for the next-generation 40-Gbit/s/ch. systems. As an advanced IC technology, this paper also describes a 40-Gbit/s OEIC that is monolithically fabricated with a uni-traveling-carrier photodiode and the 0.1- $\mu\text{m}$  InP HEMTs [C2314]

### "A comparison of deep level effects on the DC characteristics of $\text{In}_x\text{Ga}_{1-x}\text{P}/\text{In}_{0.20}\text{Ga}_{0.80}\text{As}/\text{GaAs}$ and $\text{Al}_{0.24}\text{Ga}_{0.76}\text{As}/\text{In}_{0.20}\text{Ga}_{0.80}\text{As}/\text{GaAs}$ high electron mobility transistors grown by solid source MBE"

Deep Level Transient Spectroscopy (DLTS) has been used to characterise the deep levels in  $\text{In}_x\text{Ga}_{1-x}\text{P}/\text{In}_{0.20}\text{Ga}_{0.80}\text{As}/\text{GaAs}$  ( $0.40 \leq x \leq 0.48$ ) pseudomorphic high electron mobility transistors (pHEMT) grown by solid source molecular beam epitaxy (SSMBE). Three different pHEMT devices were investigated, with a single InGaP barrier layer, double InGaP barrier layers and strained InGaP barrier layers. Only one electron trap in the InGaP barrier layer was detected in each of the devices. The activation energy of the electron trap is 0.39 eV for the single barrier layer device, 0.40 eV for the double barrier layer device and 0.57 eV for the strained barrier layer device. The trap concentrations are  $7.22 \times 10^{18} \text{cm}^{-3}$ ,  $2.38 \times 10^{20} \text{cm}^{-3}$  and  $5.02 \times 10^{20} \text{cm}^{-3}$ , respectively. The current-voltage (I-V) characteristics and transconductance of the devices were measured at 300 K, 77 K and 30 K. The drain saturation current becomes smaller due to the carriers being captured by the defects, and the transconductance becomes higher due to an increase in carrier mobility in the channel as the temperature was lowered from 300 K to 30 K. No devices showed any collapse in the I-V characteristic or persistent photoconductivity (PPC) at low temperature, suggesting that the trap in the InGaP layer does not have a DX centre-like characteristic. A comparison was made with  $\text{Al}_{0.24}\text{Ga}_{0.76}\text{As}/\text{In}_{0.20}\text{Ga}_{0.80}\text{As}/\text{GaAs}$  pHEMTs. Only one electron trap was detected in the  $\text{Al}_{0.24}\text{Ga}_{0.76}\text{As}$  layers of the latter pHEMTs. The trap concentration is  $1.72 \times 10^{20} \text{cm}^{-3}$ . Drain current collapse at temperature below 77 K at low drain bias and persistent photoconductivity (PPC) effect were evident, indicating the presence of DX centers in the  $\text{Al}_{0.24}\text{Ga}_{0.76}\text{As}$  layers [C2315]

### "0.06 $\mu\text{m}$ gate length metamorphic $\text{In}_{0.52}\text{Al}_{0.48}\text{As}/\text{In}_{0.53}\text{Ga}_{0.47}\text{As}$ HEMTs on GaAs with high $f_T$ and $f_{\text{MAX}}$ "

State-of-the art metamorphic  $\text{In}_{0.52}\text{Al}_{0.48}\text{As}/\text{In}_{0.53}\text{Ga}_{0.47}\text{As}$  HEMTs on a GaAs substrate with 60 nanometer gate length is reported. The DC and microwave performance were investigated. Typical drain-to-source current  $I_{\text{ds}}$  of 600 mA/mm and extrinsic transconductance of 850 mS/mm were obtained with our devices. Cutoff frequency  $f_T$  and maximum oscillation frequency  $f_{\text{max}}$  are 260 GHz and 490 GHz respectively. To our knowledge, these frequency performances are the highest ever reported for HEMTs on GaAs substrate [C2316]

### "0.1 $\mu\text{m}$ enhancement-mode pseudomorphic InGaAs/InAlAs/InP HEMT"

We present state-of-the-art performance of 0.1  $\mu\text{m}$  enhancement-mode (E-mode) pseudomorphic InGaAs/InAlAs/InP HEMTs fabricated on 3-inch wafers in a production environment. The E-mode HEMTs have a cutoff frequency of 210 GHz, transconductance of 1180 mS/mm, and less than 1 mA/mm  $I_{\text{dss}}$  (drain current at a gate bias of zero volts), measured at a drain bias of 1 V. The device characteristics make the E-mode HEMTs suitable candidates for ultra-high-speed digital and analog applications. Low noise amplifiers utilizing E-mode HEMTs, which were fabricated on 3-inch wafers in TRW's InP production line, demonstrated excellent repeatability, performance, yield and uniformity [C2317]

### "A 60 GHz high power composite channel GaInAs/InP HEMT on InP substrate with $\text{LG} = 0.15 \mu\text{m}$ "

We have improved power performance by studying three different GaInAs/InP composite channel structures. Also, different gate to drain extension devices have been processed. By using composite channel devices, we benefit from the better ionization threshold energy of InP compared to GaInAs (1.69 eV against 0.92 eV). The difference of conduction band offset between the two materials ( $\Delta E_C = 0.2 \text{ eV}$ ) makes possible electron transfer from GaInAs to InP layers with the same electronic properties. New process technologies have been applied to compare these structures. The gate current resulting from the impact ionization phenomena is reduced to 30  $\mu\text{A}$  at  $V_{\text{DS}} = 4.5 \text{ V}$  for a large extension device, which constitute the best result among the three structures. Also, we improve power performances at 60 GHz by reducing the GaInAs channel width and substituting delta doping by bulk doping. The best device performance is 422 mW/mm at  $V_{\text{DS}} = 3 \text{ V}$  and  $V_{\text{GS}} = 0.7 \text{ V}$  [C2318]

### "Effect of phosphine plasma treatment on protection from Si passivation in AlInAs/InGaAs HEMT due to F atoms"

A process technology to suppress diffusing fluorine (F) atoms into the AlInAs layer at elevated temperature is investigated using AlInAs/InGaAs HEMT wafers grown on InP substrates. Removal of F atoms adsorbed on the AlInAs surface and formation of a barrier layer to suppress F diffusion are attempted by a plasma process. It is demonstrated by SIMS measurements that diffusion of F atoms is suppressed even after annealing at 400°C for the AlInAs layer treated successively with phosphine plasma at room temperature and 250°C. Hall measurements also reveal that a reduction in the two dimensional electron gas density is suppressed [C2319]

### "High-speed operation of a novel frequency divider using resonant tunneling chaos circuit"

This paper demonstrates high-frequency operation of a frequency divider IC composed of a resonant tunneling diode and a high electron mobility transistor. This circuit is based on the long-period behavior of the nonlinear circuits generating chaos. We investigate the effects of the input frequency, the bias voltage, and the input amplitude on the operation to discuss the operating margins. It is also shown that the dividing ratio can be selected by changing the input amplitude [C2320]

### "Demonstration of push-pull operation of AlGaIn/GaN HEMTs on SiC"

We report the first demonstration of Class B push-pull operation of AlGaIn/GaN HEMTs on SiC substrates, thereby taking advantage of lower thermal dissipation while achieving linear operation and allowing higher power density in large-area devices. This lower thermal dissipation can be achieved because of the potentially higher power-added-efficiency (PAE) of Class B operation, relative to Class A operation [C2321]

### "A V-Band MMIC SPDT passive HEMT switch using impedance transformation networks"

A V-Band MMIC single pole double throw (SPDT) switch using GaAs PHEMT process is designed, fabricated and tested. In contrast to the conventional resonant-type switch design method, this passive FET switch circuit utilizes impedance transformation to compensate the drain-source capacitance effect for the off-state in millimeter-wave frequency range. This SPDT switch has a measured isolation better than 30 dB for the off-state and 4 dB insertion loss for the on-state from 53 GHz to 61 GHz. The isolation performance of this design approach outmatches previously published FET switches in this frequency range [C2322]

### "High isolation V-band SPDT switch MMIC for high power use [CHEMTs application]"

This paper presents design and performance of a V-band SPDT switch MMIC for high power use. The switch design utilizes distributed 5-shunt diodes. The developed SPDT switch shows an isolation of greater than 32 dB and an insertion loss of less than 1.8 dB in a broadband frequency range from 50 GHz to 70 GHz. Input and output return losses are better than 9 dB in ON-state. The chip size is 2.65 mm  $\times$  1.33 mm. The power-handling capability was confirmed to be higher than 10 dBm of input power at 60 GHz. To our knowledge, this total broadband performance of high isolation and low insertion loss, as well as the high power-handling capability is the best among V-band SPDT switch MMICs so far [C2323]

### "A 1.7 mA low noise amplifier with integrated bypass switch for wireless 0.05-6 GHz portable applications"

An ultra low current low noise amplifier with an integrated bypass switch has been developed using PHEMT technology. The LNA/Sw uses only 1.7 mA when powered and less than 1 A when bypassed. It is usable from 50 MHz to 6 GHz. This enables portable systems such as Bluetooth, Home RF, PDAs, wireless LANs. The LNA provides 15 dB gain, 1.8 dB noise figure with 50  $\Omega$  load at the output and  $\Gamma_{opt}$  at the input. Bypass mode provides 5 dB insertion loss into the same I/O match. The LNA and bypass switch with associated control circuitry are integrated into a single RFIC and housed in the miniature SOT package. This LNA/Sw provides lower current and easier usage with comparable NF, gain, and bandwidth than previously reported products [C2324]

### "A measurement based distributed low frequency noise HEMT model: application to design of millimeter wave automotive radar chip sets"

A fully measurement based extraction procedure of a distributed low-frequency nonlinear noise model of a PHEMT is proposed. This model describes accurately the distributed nature under the device gate which allows a good noise behavior prediction in nonlinear circuits. It is used to simulate successfully noise characteristics of MMICs for FMCW automotive radar at 77 GHz. The simulated and experimental results on two different source-

chips: a VCO and DRO have been compared and we demonstrate the accuracy of the noise model which results in being independent of the application [C2325]

#### "A simple bias dependant LF FET noise model for CAD"

Extensive multi-bias low frequency noise (LFN) measurements were performed on MESFET, HEMT and InP HEMT devices in order to obtain a simple bias dependent LF noise model usable in CAD tools and consistent with small and large signal models and high frequency noise models. The model was experimentally evaluated with a 10 GHz DRO and good correspondence was obtained between the modelled and measured LFN [C2326]

#### "A high-performance GaAs SP3T switch for digital cellular systems"

A high-performance GaAs SP3T switch has been developed using asymmetrical design of the transmit and receive paths. A combination of stacked FETs and multi-gate PHEMT FETs with high breakdown voltages and large peripheries was implemented in this design. Insertion loss of less than 0.8 dB and isolation greater than 25 dB to 2 GHz were obtained. With a positive 3-V control voltage, power handling of the device exceeded 34 dBm while maintaining second and third harmonic levels better than 65 dBc [C2327]

#### "High gain PHEMT frequency doubler for 76 GHz automotive radar"

A one-stage 38.25/76.5 GHz frequency doubler has been developed with a maximum conversion gain of 1 dB. The doubler achieves a saturated output power of 9 dBm for 12 dBm input power. Two complex transmit MMICs consisting of a 38 GHz amplifier, the frequency doubler and 76 GHz amplifiers with increased output power of 14 dBm and 10 dB conversion gain have been developed for automotive applications [C2328]

#### "A monolithic HEMT diode balanced mixer for 100-140 GHz"

We report the design and evaluation of a broadband, balanced mixer for 100-140 GHz using a HEMT MMIC process on a 75  $\mu\text{m}$  InP substrate. The circuit uses Schottky diodes as mixing elements. It demonstrates a conversion loss of  $15 \pm 2$  dB from 100-130 GHz with 5 dBm LO drive at 80 GHz. Measurements indicate a wide IF bandwidth extending beyond 50 GHz. This is the first demonstration of a monolithic HEMT diode balanced mixer in this frequency range [C2329]

#### "A family of Q, V and W-band monolithic resistive mixers"

This paper presents the design, fabrication, and testing results of Q, V, and W-band monolithic broadband resistive mixers for measurement instruments. Low conversion loss and good flatness of the frequency response across a wide frequency range were achieved using an InGaP-InGaAs HEMT biased in the resistive mode. Three mixers in Q, V, and W-band show similar excellent measured performance. Q and V-band mixers were designed using two Lange couplers. The Q-band mixer exhibits a conversion loss of 11.7 dB and a loss flatness of 1.2 dB for 11 GHz IF frequency over 42-56 GHz RF frequency band. The V-band mixer exhibits a conversion loss of 12.8 dB and a loss flatness of 1.0 dB for 18 GHz IF frequency over 56-72 GHz RF frequency band. On the other hand, the W-band mixer using a 180-degree balun, shows a conversion loss of 10.6 dB and a loss flatness of 1.2 dB for 30 GHz IF frequency over a 72-84 GHz RF frequency band [C2330]

#### "An ultra broad band reflection type 180° phase shifter with series and parallel LC circuits"

An ultra broad band reflection type 180° phase shifter is proposed. It is composed of a 3-dB Lange coupler and a pair of novel reflective terminating circuits. The reflective terminating circuit switches two states of series and parallel LC circuits and it can achieve a 180° phase difference independently of frequency. Using a simplified circuit model without parasitic circuit elements, we have derived the determining condition of circuit elements to achieve 180° phase difference for all frequencies. The fabricated reflective terminating circuit MMIC has achieved a phase difference of  $183 \pm 3^\circ$  over 0.5 to 30 GHz. The 180° phase shifter MMIC has demonstrated a phase shift of  $187 \pm 7^\circ$  over 0.5 to 20 GHz band [C2331]

#### "Improved three-dimensional GaAs inductors"

This paper clarifies the state-of-the-art GaAs inductors fabricated using three-dimensional (3-D) MMIC technology. A novel 3-D inductor is proposed and evaluated experimentally. Our 4.9 nH inductance achieves a peak Q factor of 35.93 with a resonant frequency of 8.07 GHz. To the knowledge of the authors, this performance is the highest yet reported for GaAs on-chip inductors. A 0.6-4 GHz band LNA is fabricated using 0.15  $\mu\text{m}$  GaAs PHEMT devices ( $f_{\text{max}}=120$  GHz) and the 3-D inductors. The fabricated LNA offers 12.3 dB gain and a noise figure under 1.5 dB with a d.c. power consumption of 27.84 mW [C2332]



### **"Thermal transients in microwave active devices and their influence on intermodulation distortion"**

A fully physical transient thermal model is used to investigate the effects of temperature on the intermodulation distortion performance of microwave devices. A 24 mm, 60 finger PHEMT is used to compare measurements with predictions from the model. Results are in very good agreement and are a strong indication of thermally induced intermodulation distortion [C2333]

### **"Global electrothermal CAD of complex nonlinear 3-D systems based on a fully physical time-dependent compact thermal model"**

An original spectral domain decomposition approach is presented for the time-dependent thermal modelling of complex, nonlinear, 3-dimensional systems. This fully analytical approach immediately gives rise to compact models of nonlinear distributed thermal subsystems, without requiring approximation by a lumped element RC network, or nodal reduction. In combination with any thermally self-consistent models of analogue, digital, RF and microwave, microelectromechanical or photonic devices, it supplies a CAD timescale description of mutual thermal interaction between power dissipating and temperature sensitive elements. It therefore has the potential for thermal description of the whole system-in-package. In combination with microwave circuit simulator, Transim (NCSU), the thermal model is applied to the self-consistent global electrothermal harmonic balance simulation of a spatial power combining power FET array. The model is validated by comparison of electrothermal simulation of a power HEMT against experimentally obtained thermal images [C2334]

### **"Ku-band Quadri-SSPA for Stentor satellite transmit active antenna"**

This paper presents the architecture and the performance of a Ku-band Quadri-SSPA (4 RF amplifying channels) developed in the frame of Stentor French technological satellite for transmit active antenna application. Major technical advances in terms of technological features and RF performance (output power capabilities, DC power consumption and linearity) over a 13 unit lot (52 single SSPA) are highlighted [C2335]

### **"Scalable large-signal device model for high power-density AlGaIn/GaN HEMTs on SiC"**

A scalable device model for high-power, large periphery AlGaIn-GaN HEMTs on SiC has been developed which includes device self-heating. The parameterized model coefficients were evaluated using S-parameters obtained from isothermal bias contours and pulsed I-V measurements. Model scaling with device size was examined by comparing with measurements for peripheries from 0.25 mm to 1.5 mm. The scaled model showed good agreement with measured S-parameters and power sweep data [C2336]

### **"E-PHEMT, single supply, high efficient power amplifiers for GSM and DCS applications"**

This paper presents power amplifier MMICs for GSM and DCS applications using a newly developed 0.5  $\mu\text{m}$  enhancement mode power PHEMT process. An Automatic Bias Control (ABC) circuit is implemented on-chip to achieve high PAE. A Voltage Variable Attenuator (VVA) is also designed and fabricated on-chip to adjust the input power level and the overall gain. Under a low single supply voltage of 3.2 V the GSM PA provides 35 dBm output power with 55% PAE, and the DCS PA delivers 33 dBm with 40% PAE. Both chips are housed in 20-pin 4 mm $\times$ 4 mm Miniature Leadless Packages (MLP) [C2337]

### **"A single supply high performance PA MMIC for GSM handsets using quasi-enhancement mode PHEMT"**

A 3-stage GaAs FET power amplifier MMIC utilizing a quasi-enhancement mode PHEMT process has been developed for single supply GSM applications. The MMIC operates from a 3.2 V power supply and at 900 MHz, provides 35.5 dBm output power and 63.0% power added efficiency. Another 3 stage MMIC designed for DCS-1800, which at 1750 MHz provides 33.2 dBm output power with 61.1% PAE, is also presented [C2338]

### **"A power PHEMT device technology for broadband wireless access"**

An unmatched power InGaAs PHEMT transistor in a ceramic package has been developed for broadband wireless access (BWA) applications. Operating at 3.5 GHz, from 12 V supplies, a typical device delivers more than 40 dBm of peak envelope power at -30 dBc IMD with drain efficiencies as high as 58% in class AB mode. Under the stringent W-CDMA spec of -40 dBc adjacent channel power (with 11.2 dB peak-to-average signal ratio), a small signal gain of 9.5 dB and linear power in excess of 31.5 dBm with 36% efficiency is obtained in class AB mode. Our paper presents the device technology, and the DC and RF performance under W-CDMA and two-tone excitation [C2339]

### "A novel high efficiency multioctave amplifier using cascaded reactively terminated single-stage distributed amplifiers for EW system applications"

This paper demonstrates the design of a high efficiency amplifier employing a novel concept of cascaded reactively terminated single-stage distributed amplifier (CRTSSDA). In addition, CRTSSDA produces an available power gain significantly higher than conventional distributed amplifiers using the same number of active devices. Three-CRTSSDAs were designed and fabricated for EW application. The novel amplifier achieved an associated gain above 26 dB with flatness of  $\pm 0.5$  dB, an average power added efficiency in excess of 27% at an output power of 25 dBm over the 2-18 GHz band with an efficiency peak of 30% at 12 GHz [C2340]

### "Two-tone intermodulation distortion simulations in the time domain using a quasi-2D physical pHEMT model"

The need for both linear and efficient pHEMTs for modern wireless handsets necessitates a thorough understanding of the origins of intermodulation distortion at the device level. For the first time, two-tone time domain simulations of a microwave pHEMT using a quasi-two-dimensional physical device model in a CAD environment are presented. The model fully accounts for device-circuit interaction and is validated experimentally for a two-tone experiment around 5 GHz [C2341]

### "Monolithic 6W Ka-band high power amplifier"

The design and performance of a fully monolithic 6W Ka-band power amplifier is outlined. Excellent agreement between modeled and measured performance was demonstrated. This 3-stage power amplifier, which power combines 16 FETs on the third stage, is fully matched on chip to 50 $\Omega$  at the input and output wire bond pads. Performance achieved ~20.5 dB gain from 24-32 GHz with a peak power of >6W and PAE of ~21%. This performance was achieved using a 0.1  $\mu$ m power PHEMT process. To the authors knowledge, this is the highest output power demonstrated from a single device in this frequency band [C2342]

### "40-Gbit/s D-type flip-flop and multiplexer circuits using InP HEMT"

We developed a novel design technique for a D-type flip-flop (D-FF) circuit that is based on a small-signal-equivalent circuit approach. This technique provides the best condition to operate the D-FF at a high frequency. Using this technique, we fabricated a master-slave D-FF using a 0.15- $\mu$ m InP HEMT technology. We achieved 40-Gbit/s operation with clear-eye-waveform patterns and reduced jitter [C2343]

### "Temperature dependence of intermodulation and linearity in GaN based devices"

The gain and intermodulation distortion of an AlGaIn-GaN device operating at RF, have been analyzed using a general Volterra series representation. The circuit model to represent the GaN FET is obtained from a physics based analysis. Theoretical current-voltage characteristics are in excellent agreement with the experimental data. For a 1  $\mu$ m $\times$ 500  $\mu$ m Al<sub>0.15</sub>Ga<sub>0.85</sub>N-GaN FET, the calculated output power, power added efficiency and gain are 25 dBm, 13% and 10.1 dB, respectively at 15 dBm input power and are in excellent agreement with the experimental data. The output referred third order intercept point IP3 is 39.9 dBm at 350 K and 33 dBm at 650 K. These are in agreement with the simulated results from Cadence which are 39.34 dBm and 35.7 dBm, respectively. At 10 GHz, third order intermodulation distortion IM3 for 10 dBm output power is -88 dB at 350 K and -82 dB at 650 K. At 350 K IM3 is -97 dB at 5 GHz and -88 dB at 10 GHz. For the same frequencies IM3 increased to -90 dB and -82 dB, respectively, at 650 K [C2344]

### "A 14-Vpp 10 Gbit/s E/O modulator driver IC"

The development of a high voltage, wideband E/O modulator driver IC is described. The DC coupled, single-ended amplifier exhibits a 3 dB-bandwidth of 11.5 GHz, 9.5 dB small signal gain, and 14-Vpp output voltage swing. The IC utilizes a 0.25  $\mu$ m pHEMT production process and provides sufficient bandwidth and output power for 10 Gbit/s high voltage E/O modulator applications [C2345]

### "Phase conjugation array using subharmonically injection locked self-oscillating mixers"

A novel approach is developed and tested for achieving phase conjugation. Using anti-symmetric pair of subharmonically injection locked self-oscillating mixers (SILSOM), which oscillate at  $\omega$ , an input signal at  $\omega/2$  will be converted to its conjugated signal. No external RF source is needed for LO pumping, and the input and output signals will be the same frequency due to the locking phenomenon of the oscillators. The proposed phase conjugation array finds its application in a retro-directive antenna array [C2346]

### "Optical control on HEMT devices"

Theoretical work for the DC characteristics of depletion mode Al<sub>0.3</sub>Ga<sub>0.7</sub>As/GaAs HEMTs under optical illumination is presented. Both the photoconductive effect, which increases the 2-DEG channel electron concentration, and the photovoltaic effect in the gate junction are discussed. Analysis of the effect of optical control on the gain of a HEMT amplifier and the optical tuning of a HEMT oscillator are further described [C2347]

### "Advances in InP HEMT technology for high frequency applications"

This paper presents an overview of the rapid progress being made in the development of InP HEMT devices and circuits for high frequency analog applications. Although widespread use of InP HEMTs has to date been limited by their comparatively high cost, commercialization now appears to be inevitable due to recent progress on two parallel fronts-the development of metamorphic HEMTs (MHEMTs) and the scaling of InP substrates to larger sizes (4- and 6-inch) [C2348]

### "An 850 nm wavelength monolithic integrated photoreceiver with a single-power-supplied transimpedance amplifier based on GaAs PHEMT technology"

An 850 nm wavelength monolithic integrated photoreceiver with a novel single-power-supplied transimpedance amplifier is reported based on 0.8  $\mu$ m depleted GaAs PHEMT technology. The IC consists of an MSM photodetector and a transimpedance amplifier with a 50 ohm-matched differential output. The MSM PD on the chip shows a dark current of 2.0 nA as well as a responsivity of 0.30 A/W under a bias of 3.5 V. The TIA shows a transimpedance gain of more than 58 dB $\Omega$  with a -3 dB bandwidth of 2.0 GHz. Opening eye diagrams are demonstrated at bit-rates of 1.25 Gbit/s and 2.5 Gbit/s under a +5 V supply [C2349]

### "Ultra low noise 2.5 Gbit/s 3.3V transimpedance amplifier with automatic gain control"

We present a high performance 2.5 Gb/s Transimpedance Amplifier (TIA) with the lowest input noise current ever reported at 3.3 V. Typical use is as a low noise preamplifier for lightwave receiver modules in optical fiber with an exceptionally good sensitivity and high gain. The circuit features a very small chip size, differential outputs, very low power consumption and built in Automatic Gain Control (AGC) to allow operation over a wide dynamic range. We have used an advanced enhancement-depletion mode PHEMT process to fabricate the device. This type of process offers the designer the flexibility and options required to obtain both a very good noise figure and low power consumption [C2350]

### "A millimeter wave monolithic VCO with an integrated HEMT as a varactor"

A voltage controlled oscillator (VCO) is one of the key components in millimeter wave systems for FM or FSK modulation, frequency tuning and phase locked sources, etc. MMIC VCOs with integrated varactor for frequency control or modulation is useful for such functions. The main problem is to integrate the varactor with a standard technological process. One possibility is the use of a cold HEMT as a diode. Drain and source are connected and the non-linearity  $C_{gs}$  is only depending upon the voltage  $V_{gs}$  ( $=V_{ds}$ ). Capacitance ratio and quality factor can then be optimized in relation to the gate length. A short gate length provides a low capacitance ratio, but high quality factor. The purpose of this work is to develop a monolithic VCO with improved frequency variation linearity and with simplified fabrication process, by applying high  $f_{max}$  0.1  $\mu$ m gate HEMT both as an active element and as a varactor [C2351]

### "Dynamics of microwave FET behaviour"

The article discusses dispersion in the dynamic characteristics of microwave HEMTs, and the application of a pulsed-bias measurement system. Thermal effects and non-thermal effects are analysed [C2352]

### "Influence of impact ionization stresses on AlGaAs-InGaAs HEMT performances"

Pseudomorphic HEMTs are widely used in medium power applications. Users are concerned by the reliability of PHEMT-based technologies submitted to RF overdrive. In particular, III-V FETs may suffer from impact ionization effect and surface related mechanisms. The small-signal response of interface states at passivated III-V semiconductor surfaces has been measured over a wide frequency range from 1 Hz to microwave frequencies (Iizuka et al, 1997). During RF operation, impact ionization mechanisms often occur in the channel and their influence on the reliability of devices is not well known. In this work, the effect of life-tests performed on PHEMTs biased in the impact ionization regime with or without thermal stress has been analyzed by monitoring the evolution of DC electrical characteristics and their temperature dependence. The reverse gate current is measured as a function of temperature to observe the behavior of surface traps located at the drain edge of the

gate in access regions. Correlation between drain current transients, temperature dependence of the reverse gate current and the on-state breakdown loci is discussed to evaluate both the influence of surface traps on electrical parameters and their evolution after aging [C2353]

#### "A compact K-band transceiver module for broadband wireless and LMDS applications"

This paper describes a compact, self-contained, gallium arsenide (GaAs) monolithic microwave integrated circuit (MMIC) based, millimeter-wave transceiver module developed at Northrop Grumman. Transceiver characteristics and results of a previous broadband wireless access (BRA) system deployment using the MMIC transceiver are reported [C2354]

#### "Neural models of microwave transistor noise parameters based on bias conditions and S-parameters"

This paper presents the results of neural networks application in microwave transistor noise modeling. The neural networks are used to model noise parameters dependence on bias conditions and frequency. In order to improve the modeling, S-parameters are included as inputs of neural models. Once trained, the developed model can be used to predict noise parameters without additional knowledge about noise parameters or any additional computational effort [C2355]

#### "Highly linear low voltage GaAs pHEMT MMIC switches for multimode wireless handset applications"

A true 3 V highly linear low loss single pole five throw (SP5T) switch for multimode wireless handset applications is presented. By using advanced Filtronic pHEMT technology with extremely low leakage current and low channel resistance it is possible to achieve very low harmonic levels at maximum GSM power levels ( $P_{2ND} < -35$  dBm at  $P_{IN} = 34.5$  dBm) by using four FETs in series and yet still achieve insertion losses of 0.5 dB at 900 MHz. Increasing the number of FETs also allows for 24 dB of isolation to be achieved at 900 MHz [C2356]

#### "Extremely high P1dB MMIC amplifiers for Ka-band applications"

In this paper we describe single stage and two-stage MMIC power amplifier data at Ka-band. An extremely high P1dB power density of 700 mW/mm and 571 mW/mm were measured for the 1-stage and 2-stage GaAs HEMT MMIC amplifiers respectively. When biased for optimal IP3, 4.5 W/mm and 2.1 W/mm were achieved respectively. The performance of the latter 2-stage MMIC PA is achieved in a very compact design of 4.08 mm<sup>2</sup> total MMIC area. These are believed to be among the best numbers reported for linear power amplifiers at Ka-band [C2357]

#### "Low noise AlGaIn/GaN MODFETs with high breakdown and power characteristics"

AlGaIn/GaN MODFETs (0.25 $\times$ 200  $\mu$ m<sup>2</sup>) with low noise, high breakdown and power characteristics have been evaluated. A noise figure of 1.9 dB with 16.2 dB associated gain was obtained at a quiescent point of  $I_{DS} = 30$  mA and  $V_{DS} = 10$  V at 10 GHz. The maximum power measured was 22.9 dBm ( $\sim 1$  W/mm) and PAE was 21.9% at 8.4 GHz at the same bias condition. In addition, a maximum breakdown voltage ( $V_{BD}$ ) of  $\sim 115$  V at  $I_D = 20$   $\mu$ A and  $I_G \sim 30$   $\mu$ A was measured. A MODFET noise model and its correlation with gate leakage current are also investigated [C2358]

#### "Comparisons of technologies and MMICS results for military needs"

During the last 3 years, the French MoD has supported technology developments and/or specific MMICs designs for power amplification from S-band to Ku-band (i.e. 18 GHz), for radar and electronic warfare applications. Our objective in this paper, is to present and analyse the results obtained on three X-band power amplifiers using different GaAs technologies and designs with a view to meeting the same specifications target. To our knowledge, this is the first time a concrete comparison is conducted on three different state-of-the art technologies, simultaneously taking into account, technology, reliability issues and microwave measurements of MMICs [C2359]

#### "Super low noise InGaP gated PHEMT"

Very high performance InGaP/InGaAs/GaAs PHEMT is demonstrated. The fabricated InGaP gated PHEMT device with 0.25 $\times$ 160  $\mu$ m<sup>2</sup> of gate dimension shows a 304 mA/mm of saturation drain current at  $V_{GS} = 0$  V,  $V_{DS} = 2$  V and a 320 mS/mm of extrinsic transconductance. Noise figure at 12 GHz is measured to be 0.46 dB with a 13 dB associated gain. With such a high gain and low noise, the drain-to-gate breakdown can be as high as 10 V.



Standard deviation in the threshold voltage of 22 mV across a 4-inch wafer can be achieved using a highly selective wet recess etching process [C2360]

#### "Low-k BCB passivated Al<sub>0.5</sub>Ga<sub>0.5</sub>As/In<sub>0.15</sub>Ga<sub>0.85</sub>As enhancement-mode pHEMTs"

A high power-added efficiency Al<sub>0.5</sub>Ga<sub>0.5</sub>As/InGaAs enhancement-mode pHEMTs with benzocyclobutene (BCB) passivated layer are fabricated and characterized. This passivation technology takes advantages of the low dielectric permittivity (2.7) and a low loss tangent (0.0008), which simplifies the passivation process for microwave power device. In this work, we not only suppress the drain-source breakdown voltage but also improve the device power performance under a high input power swing by using a BCB passivation layer. The passivated 1.0  $\mu$ m-long gate pHEMTs exhibit a higher off-state performance than unpassivated ones. The maximum output power under a 2.4 GHz operation is 118 mW/mm, with a linear power gain of 11.1 dB, and a power-added efficiency of 60%. These characteristics demonstrate a great potential for BCB passivated E-mode pHEMTs on the large-signal microwave power device applications [C2361]

#### "InP and GaAs components for 40 Gbps applications"

We have developed a number of products for 40 Gbps applications, including GaAs and InP HEMT modulator drivers, InP-based monolithically integrated PIN-TIA circuits, InP double heterojunction HBT TIAs, and high responsivity dual-absorption PIN diodes. A number of other products are currently in development, including a number of InP DHBT digital circuits [C2362]

#### "A monolithic X-band class-E power amplifier"

This paper describes what is believed to be the first successful design and fabrication of a broadband monolithic high efficiency class-E driver amplifier that operates at X-band and employs a 0.3  $\mu$ m  $\times$  600  $\mu$ m pHEMT device. The amplifier's measured performance shows a peak Power Added Efficiency (PAE) of 63% at 10.6 GHz and a constant output power of greater than 24 dBm together with a gain of 10 dB over 9-11 GHz [C2363]

#### "45 GHz distributed amplifier with a linear 6-Vp-p output for a 40 Gb/s LiNbO<sub>3</sub> modulator driver circuit"

We developed a coplanar waveguided-type distributed amplifier for a LiNbO<sub>3</sub> modulator driver (LN driver) using double-doped AlGaAs/InGaAs/AlGaAs-pseudomorphic High Electron Mobility Transistors (p-HEMTs). By using a stabilization and impedance control technique, we obtained a 45 GHz bandwidth for coplanar waveguided (CPW) lines with a 600  $\mu$ m thick substrate and 54 GHz bandwidth for grounded coplanar waveguided (GCPW) lines with a 75  $\mu$ m thick substrate, and a linear 6-Vp-p output at 40 Gb/s. These results indicate that our circuit design technique is suitable for use in fiber-optic communication systems [C2364]

#### "A DC-45 GHz metamorphic HEMT traveling wave amplifier"

Metamorphic HEMT (MHEMT) technology is capable of providing InP based HEMT performance at GaAs based HEMT levels of manufacturability and cost. This makes the MHEMT an attractive alternative for low noise, high frequency, and wide bandwidth applications. The authors describe the performance of a DC-45 GHz MHEMT traveling wave amplifier (TWA) that is well suited for broadband applications such as 40 Gb/s fiber-optic receivers. The amplifier provides a typical noise figure of 2 dB and output powers in excess of 3 dBm [C2365]

#### "Low noise hybrid amplifier using AlGaIn/GaN power HEMT devices"

This work reports on efforts to demonstrate AlGaIn/GaN Low Noise Amplifiers (LNAs) in epitaxial material designed to build power transistors. The hybrid LNA circuit produced a noise figure of 3 dB, a gain of 8.5 dB, an input return loss of -6.5 dB and an output return loss of -9 dB at 4 GHz. Further, devices in an enhanced process have improved noise characteristics and more realizable match conditions. These device enhancements will enable robust X-band LNA demonstrations [C2366]

#### "High reliability of 0.1 $\mu$ m InGaAs/InAlAs/InP HEMT MMICs on 3-inch InP production process"

The high-reliability performance of K-band MMIC amplifiers fabricated using 0.1  $\mu$ m T-gate InGaAs/InAlAs/InP HEMTs on 3-inch wafers using a high volume production process is reported. Operating at an accelerated life test condition of  $V_{ds}$ =1.2 V and  $I_{ds}$ =150 mA/mm, two-stage balanced amplifiers were life tested at three temperatures ( $T_1$ =215°C,  $T_2$ =230°C and  $T_3$ =250°C) in a N<sub>2</sub> ambient. The activation energy ( $E_a$ ) is as high as 2 eV, achieving a projected median-time-to-failure (MTF) >14108 hours at a 125°C junction temperature. MTF was determined by 3-temperature constant current stress using  $|\Delta S_{21}| > 1.0$  dB as the failure criteria. This is the

first demonstration of 3-temperature high reliability 0.1  $\mu\text{m}$  InGaAs/InAlAs/InP HEMT based on small-signal microwave characteristics of HEMT MMIC. This result demonstrates a robust InGaAs/InAlAs/InP HEMT production technology [C2367]







#### "High reliability non-hermetic 0.1 $\mu\text{m}$ GaAs pseudomorphic HEMT MMIC amplifiers"

High reliability performance of a Q-band low-noise MMIC amplifier fabricated using 0.1  $\mu\text{m}$  production AlGaAs/InGaAs/GaAs HEMT process technology is reported. Operating at an accelerated DC bias condition of  $V_{ds}=4.2\text{ V}$  and  $I_{ds}=150\text{ mA/mm}$ , two-stage balanced amplifiers were lifetested at three temperatures ( $T_{\text{ambient}}=255^{\circ}\text{C}$ ,  $T_{\text{ambient}}=270^{\circ}\text{C}$ , and  $T_{\text{ambient}}=285^{\circ}\text{C}$ ) in air ambient. After stress, MMIC amplifiers were brought down to room temperature and small-signal microwave characteristics were measured. Failure time for each temperature was determined using  $\Delta S_{21}=-1.0\text{ dB}$  measured at room temperature as the failure criteria. The activation energy ( $E_a$ ) is 1.7 eV, achieving a projected median-time-to-failure (MTF) of 64109 hours at a  $125^{\circ}\text{C}$  junction temperature. This is the state-of-art of 0.1  $\mu\text{m}$  HEMT reliability based on  $S_{21}$  failure criteria of MMIC amplifiers under DC stress at high junction temperature in air ambient. This result demonstrates a robust HEMT technology which is immune to the stress effects of high electric field under high temperature operation, and demonstrates the suitability of the HEMTs for non-hermetic commercial applications [C2368]

#### "High-quality MOCVD AlGaIn/GaN structure for HEMT applications"

In this work we report on the epitaxial growth and characterization of high-quality MOCVD AlGaIn/GaN structure grown on sapphire substrates specifically studied for HEMTs performances optimization. Various technological issues, concerning material properties and device technology, must be properly tailored to fully exploit the potential of such devices. The high quality of the obtained active material lead to HEMT device showing improved performance in terms of breakdown voltage, device isolation and reverse leakage current. Particularly the low defect density and the high resistivity, obtained by using as crystallization layer AlN deposited at high temperature for the growth of the GaN layer, have lead to an effective 2DEG carrier concentration of  $8 \times 10^{12}\text{ cm}^{-2}$  with related mobility of  $1700\text{ cm}^2/\text{Vs}$  and a very high breakdown voltage devices ( $V_{bd} > 150\text{ V}$ ), permitting also excellent active device isolation and limited reverse leakage current [C2369]

## СПИСОК ЛИТЕРАТУРЫ

- C1158.** Dan An. High Performance 94 GHz Resistive Mixer Using GaAs Metamorphic HEMT Technology. / Dan An, Bok-Hyung Lee, Byeong-Ok Lim, Mun-Kyo Lee, Sung-Chan Kim, Hyun-Chang Park, Jin-Koo Rhee. // 2006. The 1st European Microwave Integrated Circuits Conference. - Manchester, 10-13 Sept. 2006. - P. 375-378. 
- C1159.** Sung-Chan Kim. Wideband and High Gain Cascode Amplifier using Metamorphic HEMT for Millimeter-wave Applications. / Sung-Chan Kim, An D., Bok-Hyung Lee, Mun-Kyo Lee, Dong-Hoon Shin, Jin-Koo Rhee. // 2006. The 1st European Microwave Integrated Circuits Conference. - Manchester, 10-13 Sept. 2006. - P. 371-374. 
- C1160.** Holm M.A. Charge Effects and Transient Simulation of p-HEMT Meander Gate Switches. / Holm M.A., Cameron N.L., Brookbanks D.M. // 2006. The 1st European Microwave Integrated Circuits Conference. - Manchester, 10-13 Sept. 2006. - P. 367-370. 
- C1161.** Sang-Gyu Park. A Ka-band MMIC Oscillator Using a Miniaturized CPW 1-D PBG Structure. / Sang-Gyu Park, Jeong-Hoon Kim, Myeung-Su Kim, Sung-Won Kim, Kwang-Seok Seo, Won-Bae Kim, Jong-In Song. // 2006. The 1st European Microwave Integrated Circuits Conference. - Manchester, 10-13 Sept. 2006. - P. 332-335. 
- C1162.** Dong Min Kang. A W-band MMIC One-Chip Set for Automotive Radar Sensor by using a 0.15 $\mu\text{m}$  mHEMT Process. / Dong Min Kang, Ju Yeon Hong, Jae Yeob Shim, Hyung Sup Yoon, Kyung Ho Lee. // 2006. The 1st European Microwave Integrated Circuits Conference. - Manchester, 10-13 Sept. 2006. - P. 328-331. 
- C1163.** Benbakhti B. Study of Field Plate AlGaIn/GaN HEMTs by Means of a 2D-Hydrdynamic Model for Power Applications. / Benbakhti B., Rousseau M., De Jaeger J.C. // 2006. The 1st European Microwave Integrated Circuits Conference. - Manchester, 10-13 Sept. 2006. - P. 363-366. 

- C1164.** Sakai R. Studies of InGaAs layers growth by metalorganic chemical vapor deposition for InP-HEMTs; Effects of trimethylindium and triethylindium. / Sakai R., Uchida M., Araki G. // 2006. The 1st European Microwave Integrated Circuits Conference. - Manchester, 10-13 Sept. 2006. - P. 360-362. ↑
- C1165.** Gao S. Microwave Class-F and Inverse Class-F Power Amplifiers Designs using GaN Technology and GaAs pHEMT. / Gao S., Butterworth P., Sambell A., Sanabria C., Xu H., Heikman S., Mishra U., York R.A. // 2006. The 1st European Microwave Integrated Circuits Conference. - Manchester, 10-13 Sept. 2006. - P. 493-496. ↑
- C1166.** Madjar A. GaN HEMT Performance-Measurements and Simulations of a 3.6 mm Device from Cree. / Madjar A., Turski Z., Yifei Li. // 2006. The 1st European Microwave Integrated Circuits Conference. - Manchester, 10-13 Sept. 2006. - P. 487-489. ↑
- C1167.** Bessemoulin A. Compact K-band Watt-level GaAs PHEMT Power Amplifier MMIC with integrated ESD protection. / Bessemoulin A., McCulloch M.G., Alexander A., McCann D., Mahon S.J., Harvey J.T. // 2006. The 1st European Microwave Integrated Circuits Conference. - Manchester, 10-13 Sept. 2006. - P. 517-520. ↑
- C1168.** Dadello A. 44-GHz High Power and Driver Microstrip Amplifier MMICs using 6-inch 0.15- $\mu$ m PHEMTs. / Dadello A., Fattorini A., Mahon S.J., Bessemoulin A., Harvey J.T. // 2006. The 1st European Microwave Integrated Circuits Conference. - Manchester, 10-13 Sept. 2006. - P. 483-486. ↑
- C1169.** Stiebler W.C. A Non-Quasi-Static, Relaxation-Time Small-Signal HEMT Model Compatible with Large-Signal Modeling. 2006. The 1st European Microwave Integrated Circuits Conference. - Manchester, 10-13 Sept. 2006. - P. 387-390. ↑
- C1170.** Kuan-Yu Chen. GaAs Power pHEMT Characterization for Extracting Nonlinear Parameters of Drain Current by Harmonic Measurement. / Kuan-Yu Chen, Chien-Chang Huang. // 2006. The 1st European Microwave Integrated Circuits Conference. - Manchester, 10-13 Sept. 2006. - P. 429-432. ↑
- C1171.** Martin-Guerrero T.M. Frequency domain-based approach for nonlinear quasi-static FET model extraction from large-signal waveform measurements. / Martin-Guerrero T.M., Banos-Polglase J.D., Camacho-Penalosa C., Fernandez-Barciela M., Morgan D.G., Tasker P.J. // 2006. The 1st European Microwave Integrated Circuits Conference. - Manchester, 10-13 Sept. 2006. - P. 441-444. ↑
- C1172.** van Wanum M. Generic robust LVCMOS-compatible control logic for GaAs HEMT switches. / van Wanum M., van der Bent G., Rodenburg M., de Hek A.P. // 2006. The 1st European Microwave Integrated Circuits Conference. - Manchester, 10-13 Sept. 2006. - P. 83-86. ↑
- C1173.** Sung-Won Kim. 77GHz Low Noise Sub Block MMICs with 120 nm In<sub>0.4</sub>AlAs/In<sub>0.35</sub>GaAs Metamorphic HEMTs. / Sung-Won Kim, Dong-Hwan Kim, Jin-Churl Her, Kyung-Chul Jang, Woo-Yeol Choi, Young-Woo Kwon, Kwang-Seok Seo. // 2006. The 1st European Microwave Integrated Circuits Conference. - Manchester, 10-13 Sept. 2006. - P. 103-106. ↑
- C1174.** Kelly M. 4-8 GHz Low Noise Amplifiers using metamorphic HEMT Technology. / Kelly M., Angelov I., Starski J.P., Wadefalk N., Zirath H. // 2006. The 1st European Microwave Integrated Circuits Conference. - Manchester, 10-13 Sept. 2006. - P. 118-121. ↑
- C1175.** Ui N. A 100W Class-E GaN HEMT with 75% Drain Efficiency at 2GHz. / Ui N., Sano S. // 2006. The 1st European Microwave Integrated Circuits Conference. - Manchester, 10-13 Sept. 2006. - P. 72-74. ↑
- C1176.** Romanini P. Very High Performance GaN HEMT devices by Optimized Buffer and Field Plate Technology. / Romanini P., Peroni M., Lanzieri C., Cetronio A., Calori M., Passaseo A., Poti B., Chini A., Mariucci L., Di Gaspare A., Teppati V., Camarchia V. // 2006. The 1st European Microwave Integrated Circuits Conference. - Manchester, 10-13 Sept. 2006. - P. 61-64. ↑
- C1177.** Uren M.J. Control of Short-Channel Effects in GaN/AlGaIn HFETs. / Uren M.J., Hayes D.G., Balmer R.S., Wallis D.J., Hilton K.P., Maclean J.O., Martin T., Roff C., McGovern P., Benedikt J., Tasker P.J. // 2006. The 1st European Microwave Integrated Circuits Conference. - Manchester, 10-13 Sept. 2006. - P. 65-68. ↑
- C1178.** Jin-Cherl Her. Enhanced Schottky Gate and Pulsed IV Characteristics of AlGaIn-GaN HEMT on Si with Gate-annealing and SiNX Passivation. / Jin-Cherl Her, Sung-Won Kim, Kyung-Chul Jang, Gyung-Seon Seol, Min-Koo Han, Jae-Eung Oh, Kwang-Seok Seo. // 2006. The 1st European Microwave Integrated Circuits

Conference. - Manchester, 10-13 Sept. 2006. - P. 69-71. ↑

**C1179.** Rafael-Valdivia G. New drain current model for MESFET/HEMT devices based on pulsed measurements. / Rafael-Valdivia G., Brady R., Brazil T.J. // 2006. The 1st European Microwave Integrated Circuits Conference. - Manchester, 10-13 Sept. 2006. - P. 289-291. ↑

**C1180.** Mengistu E.S. A Large-Signal Model of GaN HEMTs for Linear High Power Amplifier Design. / Mengistu E.S., Kompa G. // 2006. The 1st European Microwave Integrated Circuits Conference. - Manchester, 10-13 Sept. 2006. - P. 292-295. ↑

**C1181.** Vasallo B.G. Monte Carlo Comparison Between InP-Based Double-Gate and Standard HEMTs. / Vasallo B.G., Wichmann N., Bollaert S., Cappy A., Gonzalez T., Pardo D., Mateos J. // 2006. The 1st European Microwave Integrated Circuits Conference. - Manchester, 10-13 Sept. 2006. - P. 304-307. ↑

**C1182.** Kamitsuna H. An 8FrB—8 Switch Matrix MMIC Integrating Eight InP-HEMT SP8T Switches for 10-Gbit/s Systems. / Kamitsuna H., Yamane Y., Tokumitsu M., Sugahara H., Enoki T. // 2006. The 1st European Microwave Integrated Circuits Conference. - Manchester, 10-13 Sept. 2006. - P. 281-284. ↑

**C1183.** Schuh P. Advanced High Power Amplifier Chain for X-Band T/R-Modules based on GaN MMICs. / Schuh P., Leberer R., Sledzik H., Oppermann M., Adelseck B., Brugger H., Quay R., Mikulla M., Weimann G. // 2006. The 1st European Microwave Integrated Circuits Conference. - Manchester, 10-13 Sept. 2006. - P. 241-244. ↑

**C1184.** Orenco G. Advanced Neural Network Techniques for GaN-HEMT Dynamic Behavior Characterization. / Orenco G., Colantonio P., Giannini F., Pirola M., Camarchia V., Guerrieri S.D. // 2006. The 1st European Microwave Integrated Circuits Conference. - Manchester, 10-13 Sept. 2006. - P. 249-252. ↑

**C1185.** Adahl A. A novel high purity, highly efficient, broadband MMIC frequency multiplier implemented in metamorphic HEMT technology. / Adahl A., Zirath H. // 2006. The 1st European Microwave Integrated Circuits Conference. - Manchester, 10-13 Sept. 2006. - P. 273-276. ↑

**C1186.** Fujii K. Constant Linearity Variable Gain Traveling Wave Amplifier MMIC for 1 to 26.5 GHz Applications. / Fujii K., Morkner H. // 2006. The 1st European Microwave Integrated Circuits Conference. - Manchester, 10-13 Sept. 2006. - P. 521-524. ↑

**C1187.** Schuberth C. Load Pull Characterization of GaN/AlGaIn HEMTs. / Schuberth C., Arthaber H., Mayer M.L., Magerl G., Quay R., van Raay F. // 2006 International Workshop on Integrated Nonlinear Microwave and Millimeter-Wave Circuits. - Aveiro, 30-31 Jan. 2006. - P. 180-182. ↑

**C1188.** Chenhui Jiang. Conversion Matrix Analysis of GaAs HEMT Active Gilbert Cell Mixers. / Chenhui Jiang, Johanson T.K., Krozer V. // 2006 International Workshop on Integrated Nonlinear Microwave and Millimeter-Wave Circuits. - Aveiro, 30-31 Jan. 2006. - P. 94-97. ↑

**C1189.** Philippon A. Design Method and New Architecture of Sub-Harmonic Balanced Cold FET Mixer for MVDS Applications. / Philippon A., Campovecchio M., Nallatamby J.C., Butterworth P., Quere R. // 2006 International Workshop on Integrated Nonlinear Microwave and Millimeter-Wave Circuits. - Aveiro, 30-31 Jan. 2006. - P. 90-93. ↑

**C1190.** Ding J. Multiphysics Simulation of Electromagnetic Shielding and Thermal Stressing within Ceramic and Silicon Multilayer Packages for RF Applications. / Ding J., Linton D., Armstrong M., Mitchell N., Fusco V. // 2006. 1st Electronics Systemintegration Technology Conference. - Dresden, 5-7 Sept. 2006. - Vol. 1. - P. 679-683. ↑

**C1191.** Fujii K. Constant Linearity Variable Gain Traveling Wave Amplifier MMIC for 1 to 26.5 GHz Applications. / Fujii K., Morkner H. // 2006. 36th European Microwave Conference. - Manchester, 10-15 Sept. 2006. - P. 1747-1750. ↑

**C1192.** Kawano Y. Sub-10 ps Pulse Generator with Biphasic Modulation Function in 0.13- $\mu$ m InP HEMT. / Kawano Y., Nakasha Y., Suzuki T., Ohki T., Takahashi T., Makiyama K., Hirose T., Joshin K. // 2006. 36th European Microwave Conference. - Manchester, 10-15 Sept. 2006. - P. 1821-1824. ↑

**C1193.** Kawano Y. Sub-10 ps Pulse Generator with Biphasic Modulation Function in 0.13- $\mu$ m InP HEMT. /



Kawano Y., Nakasha Y., Suzuki T., Ohki T., Takahashi T., Makiyama K., Hirose T., Joshin K. // 2006. EuRAD 2006. 3rd European Radar Conference. - Manchester, 13-15 Sept. 2006. - P. 342-345. ↑

**C1194.** Stegmayer G. RF Dynamic Behavioral Model Suitable for GaN-HEMT Devices. / Stegmayer G., Pirola M., Camarchia V., Orenco G., Colantonio P., Serino A. // 2006 International Workshop on Integrated Nonlinear Microwave and Millimeter-Wave Circuits. - Aveiro, 30-31 Jan. 2006. - P. 9-12. ↑

**C1195.** Cabria L. Taking Advantage of PHEMT Nonlinear Behavior for RFID Applications. / Cabria L., Garcia J.A., Tazon A., Mediavilla A. // 2006 International Workshop on Integrated Nonlinear Microwave and Millimeter-Wave Circuits. - Aveiro, 30-31 Jan. 2006. - P. 42-45. ↑

**C1196.** Colantonio P. Class F design criteria validation through non linear load pull simulation. / Colantonio P., Giannini F., Limiti E., Ticconi A. // 2006 International Workshop on Integrated Nonlinear Microwave and Millimeter-Wave Circuits. - Aveiro, 30-31 Jan. 2006. - P. 30-33. ↑

**C1197.** Ahmed A. Measurements of Envelope Frequency Dependent Nonlinearity in GaN HEMT Power Device. / Ahmed A., Bunz B., Srinidhi E.R., Kompa G. // 2006 International Workshop on Integrated Nonlinear Microwave and Millimeter-Wave Circuits. - Aveiro, 30-31 Jan. 2006. - P. 48-51. ↑

**C1198.** Pena R. Bias Selection for Conversion and Linearity Optimization in a GaN HEMT Resistive Mixer. / Pena R., Garcia J.A., Brana A., Jimenez A., Munoz E. // 2006 International Workshop on Integrated Nonlinear Microwave and Millimeter-Wave Circuits. - Aveiro, 30-31 Jan. 2006. - P. 84-87. ↑

**C1199.** Camarchia V. GaN HEMT Technology Development Assessment through Nonlinear Characterization. / Camarchia V., Guerrieri S.D., Pirola M., Teppati V., Ghione G. // 2006 International Workshop on Integrated Nonlinear Microwave and Millimeter-Wave Circuits. - Aveiro, 30-31 Jan. 2006. - P. 64-67. ↑

**C1200.** Madero-Ayora M.J. Phase Characterization of Intermodulation Products Including Electrothermal Memory Effects. / Madero-Ayora M.J., Reina-Tosina J., Crespo-Cadenas C. // 2006 International Workshop on Integrated Nonlinear Microwave and Millimeter-Wave Circuits. - Aveiro, 30-31 Jan. 2006. - P. 56-59. ↑

**C1201.** Colantonio P. Power Amplifier Design Strategy to null IMD asymmetry. / Colantonio P., Giannini F., Giofre R., Limiti E., Nanni A. // 2006. 36th European Microwave Conference. - Manchester, 10-15 Sept. 2006. - P. 1304-1307. ↑

**C1202.** Zeeb D.M. A High-Performance 14.4 to 19.7 GHz Power Detector Fabricated with Flip-Chip Technology. 2006. 36th European Microwave Conference. - Manchester, 10-15 Sept. 2006. - P. 1621-1624. ↑

**C1203.** Sarfraz M. 30-Watt Power Amplifier for 3.5GHz WiMAX Base station Application. / Sarfraz M., Akkul M. // 2006. 36th European Microwave Conference. - Manchester, 10-15 Sept. 2006. - P. 1706-1708. ↑

**C1204.** Mizuno S. Novel Instability-Probing Simulation for Power Amplifiers. / Mizuno S., Naito K., Tateno Y., Sano S., Tokumitsu T. // 2006. 36th European Microwave Conference. - Manchester, 10-15 Sept. 2006. - P. 1284-1287. ↑

**C1205.** Masud M.A. Comparative investigation between a single ended and a balanced IF VGA. / Masud M.A., Zirath H. // 2006. 36th European Microwave Conference. - Manchester, 10-15 Sept. 2006. - P. 220-223. ↑

**C1206.** Kawakami K. A Switch-Type Power Amplifier and Its Application to a CDMA Cellphone. / Kawakami K., Kusunoki S., Kobayashi T., Hashizume M., Shimada M., Hatsugai T., Koimori T., Kozakai O. // 2006. 36th European Microwave Conference. - Manchester, 10-15 Sept. 2006. - P. 348-351. ↑

**C1207.** Samoska L. A G-Band 160 GHz T/R Module Concept for Planetary Landing Radar. / Samoska L., Pekka Kangaslahti, Pukala D., Sadowy G., Pollard B., Hodges R. // 2006. 36th European Microwave Conference. - Manchester, 10-15 Sept. 2006. - P. 757-760. ↑

**C1208.** Gao S. Microwave Class-F and Inverse Class-F Power Amplifiers Designs using GaN Technology and GaAs pHEMT. / Gao S., Butterworth P., Sambell A., Sanabria C., Xu H., Heikman S., Mishra U., York R.A. // 2006. 36th European Microwave Conference. - Manchester, 10-15 Sept. 2006. - P. 1719-1722. ↑

**C1209.** Steven M. Currie. Proton Tolerance of InAs Based HEMT and DHBT Devices. / Steven M. Currie, Nathan E. Harff, Robert G. Pittelkow, Paul W. Marshall, Joshua Bergman, Berinder Brar, Jonathan B. Hacker,

Augusto Gutierrez, Cedric Monier, Barry K. Gilbert, Erik S. Daniel. // 2006 IEEE Radiation Effects Data Workshop. - Ponte Vedra, FL, July 2006. - P. 66-71. ↑

**C1210.** Bessemoulin A. Compact K-band Watt-level GaAs PHEMT Power Amplifier MMIC with integrated ESD protection. / Bessemoulin A., McCulloch M.G., Alexander A., McCann D., Mahon S.J., Harvey J.T. // 2006. 36th European Microwave Conference. - Manchester, 10-15 Sept. 2006. - P. 1743-1746. ↑

**C1211.** Wurfl J. Advances in GaN-based discrete power devices for L- and X-band applications. / Wurfl J., Behtash R., Lossy R., Liero A., Heinrich W., Trankle G., Hirche K., Fischer G. // 2006. 36th European Microwave Conference. - Manchester, 10-15 Sept. 2006. - P. 1716-1718. ↑

**C1212.** Dadello A. 44-GHz High Power and Driver Microstrip Amplifier MMICs using 6-inch 0.15- $\mu$ m PHEMTs. / Dadello A., Fattorini A., Mahon S.J., Bessemoulin A., Harvey J.T. // 2006. 36th European Microwave Conference. - Manchester, 10-15 Sept. 2006. - P. 1709-1712. ↑

**C1213.** Henriquez Stanley L. An Efficient and Accurate Approach for Characterizing Non-Linear Capacitance in MESFET/HEMT Devices. / Henriquez Stanley L., Karangu Caroline, Ogunniyi Aderinto J., White Carl. // 2006 IEEE Sarnoff Symposium. - Princeton, NJ, 27-28 March 2006. - P. 1-4. ↑

**C1214.** Madjar A. GaN HEMT Performance-Measurements and Simulations of a 3.6 mm Device from Cree. / Madjar A., Turski Z., Yifei Li. // 2006. 36th European Microwave Conference. - Manchester, 10-15 Sept. 2006. - P. 1713-1715. ↑

**C1215.** Pichonat E. Temperature analysis of AlGaIn/GaN High-Electron-Mobility Transistors using micro-Raman scattering spectroscopy and Transient Interferometric Mapping. / Pichonat E., Kuzmik J., Bychikhin S., Pogany D., Poisson M.A., Grimbert B., Gaquiere C. // 2006. The 1st European Microwave Integrated Circuits Conference. - Manchester, 10-13 Sept. 2006. - P. 54-57. ↑

**C1216.** Abielmona S. A Low Phase Noise Microwave Oscillator with a Miniaturized LTCC Resonator for SIP Design. / Abielmona S., Roy L. // 2006. IEEE MTT-S International Microwave Symposium Digest. - San Francisco, CA, 11-16 June 2006. - P. 589-592. ↑

**C1217.** Wooyeol Choi. A V-band MMIC Self Oscillating Mixer Active Integrated Antenna Using a Push-Pull Patch Antenna. / Wooyeol Choi, Changyul Cheon, Youngwoo Kwon. // 2006. IEEE MTT-S International Microwave Symposium Digest. - San Francisco, CA, 11-16 June 2006. - P. 630-633. ↑

**C1218.** Therrien R. AlGaIn/GaN HFETs on Si Substrates for WiMAX Applications. / Therrien R., Singhal S., Chaudhari A., Nagy W., Marquart J., Johnson J.W., Hanson A.W., Riddle J., Rajagopal P., Preskenis B., Zhitova O., Williamson J., Kizilyalli I.C., Linthicum K.J. // 2006. IEEE MTT-S International Microwave Symposium Digest. - San Francisco, CA, 11-16 June 2006. - P. 710-713. ↑

**C1219.** Rafael-Valdivia G. Single function drain current model for MESFET/HEMT devices including pulsed dynamic behavior. / Rafael-Valdivia G., Brady R., Brazil T.J. // 2006. IEEE MTT-S International Microwave Symposium Digest. - San Francisco, CA, 11-16 June 2006. - P. 473-476. ↑

**C1220.** Tessmann A. A Compact W-Band Dual-Channel Receiver Module. / Tessmann A., Kuri M., Riessle M., Massler H., Zink M., Reinert W., Bronner W., Leuther A. // 2006. IEEE MTT-S International Microwave Symposium Digest. - San Francisco, CA, 11-16 June 2006. - P. 85-88. ↑

**C1221.** Kawano Y. An RF Chipset for Impulse Radio UWB Using 0.13  $\mu$ m InP-HEMT Technology. / Kawano Y., Nakasha Y., Yokoo K., Masuda S., Takahashi T., Hirose T., Oishi Y., Hamaguchi K. // 2006. IEEE MTT-S International Microwave Symposium Digest. - San Francisco, CA, 11-16 June 2006. - P. 316-319. ↑

**C1222.** Shinohara K. Ultra-High-Speed Low-Noise InP-HEMT Technology. / Shinohara K., Chen P.S., Bergman J., Kazemi H., Brar B., Watanabe I., Matsui T., Yamashita Y., Endoh A., Hikosaka K., Mimura T., Hiyamizu S. // 2006. IEEE MTT-S International Microwave Symposium Digest. - San Francisco, CA, 11-16 June 2006. - P. 337-340. ↑

**C1223.** Darwish A.M. 4-Watt Ka-Band AlGaIn/GaN Power Amplifier MMIC. / Darwish A.M., Boutros K., Luo B., Huebschman B., Viveiros E., Hung H.A. // 2006. IEEE MTT-S International Microwave Symposium Digest. - San Francisco, CA, 11-16 June 2006. - P. 730-733. ↑

- C1224.** Kirby P.L. W-Band Oscillator on Metamorphic HEMT. / Kirby P.L., Herrick K., Alm R., Luque N.A., Rodriguez A., Dunleavy L.P., Papapolymerou J. // 2006. IEEE MTT-S International Microwave Symposium Digest. - San Francisco, CA, 11-16 June 2006. - P. 735-738. ↑
- C1225.** Soubercaze-Pun G. Design of a X-band GaN oscillator: from the low frequency noise device characterization and large signal modeling to circuit design. / Soubercaze-Pun G., Tartarin J.G., Bary L., Rayssac J., Morvan E., Grimberty B., Delage S.L., De Jaeger J.-C., Graffeuil J. // 2006. IEEE MTT-S International Microwave Symposium Digest. - San Francisco, CA, 11-16 June 2006. - P. 747-750. ↑
- C1226.** Schuh P. 20W GaN HPAs for Next Generation X-Band T/R-Modules. / Schuh P., Leberer R., Sledzik H., Oppermann M., Adelseck B., Brugger H., Behtash R., Leier H., Quay R., Kiefer R. // 2006. IEEE MTT-S International Microwave Symposium Digest. - San Francisco, CA, 11-16 June 2006. - P. 726-729. ↑
- C1227.** Vetry R. Performance and RF Reliability of GaN-on-SiC HEMT's using Dual-Gate Architectures. / Vetry R., Shealy J.B., Green D.S., McKenna J., Brown J.D., Gibb S.R., Leverich K., Garber P.M., Poulton M.J. // 2006. IEEE MTT-S International Microwave Symposium Digest. - San Francisco, CA, 11-16 June 2006. - P. 714-717. ↑
- C1228.** Ui N. A 45% Drain Efficiency, -50dBc ACLR GaN HEMT Class-E Amplifier with DPD for W-CDMA Base Station. / Ui N., Sano S. // 2006. IEEE MTT-S International Microwave Symposium Digest. - San Francisco, CA, 11-16 June 2006. - P. 718-721. ↑
- C1229.** Maekawa A. A 500W Push-Pull AlGaIn/GaN HEMT Amplifier for L-Band High Power Application. / Maekawa A., Yamamoto T., Mitani E., Sano S. // 2006. IEEE MTT-S International Microwave Symposium Digest. - San Francisco, CA, 11-16 June 2006. - P. 722-725. ↑
- C1230.** Jarndal A. Accurate Large-Signal Modeling of AlGaIn-GaN HEMT Including Trapping and Self-Heating Induced Dispersion. / Jarndal A., Bunz B., Kompa G. // 2006. ISPSD 2006. IEEE International Symposium on Power Semiconductor Devices and IC's. - Naples, 4-8 June 2006. - P. 1-4. ↑
- C1231.** Angelini A. Evaluation of GaN HEMT Technology Development Through Nonlinear Characterization. / Angelini A., Camarchia V., Cappelluti F., Donati Guerrieri S., Pirola M., Bonani F., Serino A., Ghione G. // 2006. ISPSD 2006. IEEE International Symposium on Power Semiconductor Devices and IC's. - Naples, 4-8 June 2006. - P. 1-4. ↑
- C1232.** Inada M. Low Specific On-Resistance AlGaIn/GaN HEMT on Sapphire Substrate. / Inada M., Yagi S., Yamamoto Y., Piao G., Shimizu M., Okumura H., Arai K. // 2006. ISPSD 2006. IEEE International Symposium on Power Semiconductor Devices and IC's. - Naples, 4-8 June 2006. - P. 1-4. ↑
- C1233.** Mrunal A.K. Power amplifier linearization using a diode. / Mrunal A.K., Shirasgaonkar M., Patrikar R.M. // 2006. MELECON 2006. IEEE Mediterranean Electrotechnical Conference. - Malaga, 16-19 May 2006. - P. 173-176. ↑
- C1234.** Gao Y. Feasibility Study of AlGaIn/GaN HEMT for Multi-megahertz DC/DC Converter Applications. / Gao Y., Huang A.Q. // 2006. IPEMC 2006. CES/IEEE 5th International Power Electronics and Motion Control Conference. - Shanghai, 14-16 Aug. 2006. - Vol. 2. - P. 1-3. ↑
- C1235.** Lai R. 0.07  $\mu$ m InP HEMT MMIC Technology for G-band Power Amplifiers. / Lai R., Huang P., Grundbacher R., Farkas D., Cavus A., Liu P.H., Chin P., Chou Y.C., Barsky M., Tsai R., Raja R., Oki A. // 2006. International Conference on Indium Phosphide and Related Materials Conference Proceedings. 7-11 May 2006. - P. 39-41. ↑
- C1236.** Marinkovic Z. Efficient ANN based noise modeling of microwave FETs against temperature. / Marinkovic Z., Pronic-Rancic O., Markovic V. // 2006. MELECON 2006. IEEE Mediterranean Electrotechnical Conference. - Malaga, 16-19 May 2006. - P. 153-156. ↑
- C1237.** Ma B.Y. Ultra-Low-Power Wideband High Gain InAs/AlSb HEMT Low-Noise Amplifiers. / Ma B.Y., Hacker J.B., Bergman J., Nagy G., Sullivan G., Chen P., Brar B. // 2006. IEEE MTT-S International Microwave Symposium Digest. - San Francisco, CA, 11-16 June 2006. - P. 73-76. ↑
- C1238.** Masuda S. Very Compact High-gain Broadband Low-noise Amplifier in InP HEMT Technology. / Masuda S., Ohki T., Hirose T. // 2006. IEEE MTT-S International Microwave Symposium Digest. - San

Francisco, CA, 11-16 June 2006. - P. 77-80. ↑

**C1239.** Yu-Lung Tang. Full Ka-band High Performance InP MMIC LNA Module. / Yu-Lung Tang, Wadefalk N., Morgan M.A., Weinreb S. // 2006. IEEE MTT-S International Microwave Symposium Digest. - San Francisco, CA, 11-16 June 2006. - P. 81-84. ↑

**C1240.** Roenker K.P. An Introductory Course in Nanoelectronics at the Senior/Graduate Level. 2006. IEEE-NANO 2006. Sixth IEEE Conference on Nanotechnology. 17-20 June 2006. - Vol. 1. - P. 406-409. ↑

**C1241.** Seung-Chul Lee. High Performance AlGaIn/GaN HEMT Switches Employing 500°C Oxidized Ni/Au Gate for Very Low Leakage Current and Improvement of Uniformity. / Seung-Chul Lee, Jiyong Lim, Min-Woo Ha, Jin-Cherl Her, Chong-Man Yun, Min-Koo Han. // 2006. ISPSD 2006. IEEE International Symposium on Power Semiconductor Devices and IC's. - Naples, 4-8 June 2006. - P. 1-4. ↑

**C1242.** Boutros K.S. GaN Switching Devices for High-Frequency, KW Power Conversion. / Boutros K.S., Chandrasekaran S., Luo W.B., Mehrotra V. // 2006. ISPSD 2006. IEEE International Symposium on Power Semiconductor Devices and IC's. - Naples, 4-8 June 2006. - P. 1-4. ↑

**C1243.** Mashkantsev V.G. The Perspective Structures for Microwave Heterotransistors for Communication Techniques. / Mashkantsev V.G., Kalinin S.V. // 2006. Proceedings. 7th Annual 2006 International Workshop and Tutorials on Electron Devices and Materials. - Erlagol, Altai, 1-5 July 2006. - P. 24-26. ↑

**C1244.** Gunnarsson S.E. Single-Chip 60 GHz Transmitter and Receiver MMICs in a GaAs mHEMT Technology. / Gunnarsson S.E., Karnfelt C., Zirath H., Kozhuharov R., Kuylenstierna D., Fager C., Alping A. // 2006. IEEE MTT-S International Microwave Symposium Digest. - San Francisco, CA, 11-16 June 2006. - P. 801-804. ↑

**C1245.** Deal W.R. A Low Power/Low Noise MMIC Amplifier for Phased-Array Applications using InAs/AlSb HEMT. / Deal W.R., Tsai R., Lange M.D., Boos J.B., Bennett B.R., Gutierrez A. // 2006. IEEE MTT-S International Microwave Symposium Digest. - San Francisco, CA, 11-16 June 2006. - P. 2051-2054. ↑

**C1246.** Coffie R. Impact of AlN Interlayer on Reliability of AlGaIn/GaN HEMTS. / Coffie R., Chen Y.C., Smorchkova I., Wojtowicz M., Chou Y.C., Heying B., Oki A. // IEEE International Reliability Physics Symposium Proceedings, 2006. 44th Annual. - San Jose, CA, 26-30 March 2006. - P. 99-102. ↑

**C1247.** K.S. Zhuravlev. Molecular Beam Epitaxy of Heterostructures on the Basis of III-V Materials for UHF Transistors. / K. S. Zhuravlev, A. I. Toropov, V. G. Mansurov. // 2006. CriMiCO '06. 16th International Crimean Conference Microwave and Telecommunication Technology. - Sevastopol, Crimea, Sept. 2006. - Vol. 2. - P. 589-590. ↑

**C1248.** Fung A.K. On-Wafer Vector Network Analyzer Measurements in the 220-325 GHz Frequency Band. / Fung A.K., Dawson D., Samoska L., Lee K., Oleson C., Boll G. // 2006. IEEE MTT-S International Microwave Symposium Digest. - San Francisco, CA, 11-16 June 2006. - P. 1931-1934. ↑

**C1249.** Kyoung-Joon Cho. 40 W Gallium-Nitride Microwave Doherty Power Amplifier. / Kyoung-Joon Cho, Wan-Jong Kim, Jong-Heon Kim, Stapleton S.P. // 2006. IEEE MTT-S International Microwave Symposium Digest. - San Francisco, CA, 11-16 June 2006. - P. 1895-1898. ↑

**C1250.** Byk E. Plastic Packaged High Linearity Low Noise Amplifier for 12-30GHz Multi-band Telecom Applications. / Byk E., Quentin P., Camiade M., Tranchant S. // 2006. IEEE MTT-S International Microwave Symposium Digest. - San Francisco, CA, 11-16 June 2006. - P. 1903-1906. ↑

**C1251.** Ganesello F. 65 nm RFCMOS technologies with bulk and HR SOI substrate for millimeter wave passives and circuits characterized up to 220 GHz. / Ganesello F., Gloria D., Montusclat S., Raynaud C., Boret S., Clement C., Dambrine G., Lepilliet S., Saguin F., Scheer P., Benech P., Fournier J.M. // 2006. IEEE MTT-S International Microwave Symposium Digest. - San Francisco, CA, 11-16 June 2006. - P. 1927-1930. ↑

**C1252.** Brehm G.E. Trends in Microwave/Millimeter-Wave Front-End Technology. 2006. The 1st European Microwave Integrated Circuits Conference. - Manchester, 10-13 Sept. 2006. - P. 1-4. ↑

**C1253.** Wichmann N. InP-Based InAlAs/InGaAs Double-Gate Transistors Beyond Conventional HEMT's Limitations. / Wichmann N., Bollaert S., Vasallo B.G., Wallart X., Dambrine G., Cappy A. // 2006. The 1st



European Microwave Integrated Circuits Conference. - Manchester, 10-13 Sept. 2006. - P. 25-28. ↑

**C1254.** Schlechtweg M. Millimeter-Wave Front-End Components in Metamorphic HEMT Technology. / Schlechtweg M., Kallfass I., Tessmann A., Schworer C., Leuther A. // 2006. The 1st European Microwave Integrated Circuits Conference. - Manchester, 10-13 Sept. 2006. - P. 31-34. ↑

**C1255.** Miguel N. Pimenta. Novel Encoder and Correlator for Optical Code Division Multiple Access Networks. / Miguel N. Pimenta, Izzat Darwazeh. // 2006. LEOS 2006. 19th Annual Meeting of the IEEE Lasers and Electro-Optics Society. - Montreal, Que., Oct. 2006. - P. 422-423. ↑

**C1256.** I.M. Abolduyev. X-Band Power AlGaIn/GaN HEMT. / I. M. Abolduyev, N. B. Gladysheva, A. A. Dorofeev, V. M. Minnebaev, A. A. Tchernyavsky. // 2006. CriMiCO '06. 16th International Crimean Conference Microwave and Telecommunication Technology. - Sevastopol, Crimea, Sept. 2006. - Vol. 1. - P. 179. ↑

**C1257.** I.M. Abolduyev. L-Band Low Noise AlGaIn/GaN HEMT. / I. M. Abolduyev, N. B. Gladysheva, A. A. Dorofeev, V. M. Minnebaev, A. A. Tchernyavsky. // 2006. CriMiCO '06. 16th International Crimean Conference Microwave and Telecommunication Technology. - Sevastopol, Crimea, Sept. 2006. - Vol. 1. - P. 180. ↑

**C1258.** M.V. Cherkashin. Visual Design of 1.5-2.5 GHz MMIC Low-Noise Amplifier. / M. V. Cherkashin, L. I. Babak. // 2006. CriMiCO '06. 16th International Crimean Conference Microwave and Telecommunication Technology. - Sevastopol, Crimea, Sept. 2006. - Vol. 1. - P. 213-214. ↑

**C1259.** Chen G. A Reliable Low Gate Bias Model Extraction Procedure for AlGaIn/GaN HEMTs. / Chen G., Kumar V., Schwindt R., Adesida I. // 2006. IEEE MTT-S International Microwave Symposium Digest. - San Francisco, CA, 11-16 June 2006. - P. 1097-1100. ↑

**C1260.** Kenney J.S. Identification of RF Power Amplifier Memory Effect Origins using Third-Order Intermodulation Distortion Amplitude and Phase Asymmetry. / Kenney J.S., Fedorenko P. // 2006. IEEE MTT-S International Microwave Symposium Digest. - San Francisco, CA, 11-16 June 2006. - P. 1121-1124. ↑

**C1261.** Schuh P. Linear broadband GaN MMICs for Ku-band Applications. / Schuh P., Leberer R., Sledzik H., Schmidt D., Oppermann M., Adelseck B., Brugger H., Quay R., van Raay F., Seelmann-Eggebert M., Kiefer R., Bronner W. // 2006. IEEE MTT-S International Microwave Symposium Digest. - San Francisco, CA, 11-16 June 2006. - P. 1324-1326. ↑

**C1262.** Colomb F.Y. A 3-Watt Q-Band GaAs pHEMT Power Amplifier MMIC For High Temperature Operation. / Colomb F.Y., Platzker A. // 2006. IEEE MTT-S International Microwave Symposium Digest. - San Francisco, CA, 11-16 June 2006. - P. 897-900. ↑

**C1263.** Huang P. A 20-mW G-band Monolithic Driver Amplifier Using 0.07- $\mu$ m InP HEMT. / Huang P., Lai R., Grundbacher R., Gorospe B. // 2006. IEEE MTT-S International Microwave Symposium Digest. - San Francisco, CA, 11-16 June 2006. - P. 806-809. ↑

**C1264.** Nishikawa K. 0.4 V, 5.6 mW InP HEMT V-band Low-Noise Amplifier MMIC. / Nishikawa K., Enoki T., Sugitani S., Toyoda I. // 2006. IEEE MTT-S International Microwave Symposium Digest. - San Francisco, CA, 11-16 June 2006. - P. 810-813. ↑

**C1265.** Mahon S.J. A Novel Non-Uniform Distributed Amplifier/Attenuator for Millimetre-wave Transmitter MMICs. 2006. IEEE MTT-S International Microwave Symposium Digest. - San Francisco, CA, 11-16 June 2006. - P. 814-817. ↑

**C1266.** Fujii K. Single supply 1W Ku-band Power Amplifier Based on 0.25 $\mu$ m E-mode PHEMT. / Fujii K., Morkner H. // 2006. IEEE MTT-S International Microwave Symposium Digest. - San Francisco, CA, 11-16 June 2006. - P. 1855-1858. ↑

**C1267.** Shuoqi Chen. A 1/2 Watt High Linearity and Wide Bandwidth PHEMT Driver Amplifier MMIC for Millimeter-Wave Applications. / Shuoqi Chen, Sabyasachi Nayak. // 2006. IEEE MTT-S International Microwave Symposium Digest. - San Francisco, CA, 11-16 June 2006. - P. 1863-1866. ↑

**C1268.** Murata H. Optical mixing in InP-based high-electron mobility transistors by use of a focused laser beam. / Murata H., Kobayashi N., Okamura Y., Kosugi T., Enoki T. // 2006 and 2006 Quantum Electronics and Laser Science Conference. CLEO/QELS 2006. Conference on Lasers and Electro-Optics. - Long Beach, CA, 21-

26 May 2006. - P. 1-2. ↑

**C1269.** Sandhiya P. A Ka Band, Low Power Dissipation, High Spectral Purity GaAs pHEMT MMIC X4 Multiplier. / Sandhiya P., Mayock J.G.E., Buck C. // 2006. IEEE MTT-S International Microwave Symposium Digest. - San Francisco, CA, 11-16 June 2006. - P. 1513-1516. ↑

**C1270.** Shiojima K. AlGaIn/GaN Dual-Gate HEMT Mixers for 24 GHz Pulse-Modulation. / Shiojima K., Makimura T., Kosugi T., Suemitsu T., Shigekawa N., Hiroki M., Yokoyama H. // 2006. IEEE MTT-S International Microwave Symposium Digest. - San Francisco, CA, 11-16 June 2006. - P. 1331-1334. ↑

**C1271.** van Raay F. X-Band High-Power Microstrip AlGaIn/GaN HEMT Amplifier MMICs. / van Raay F., Quay R., Kiefer R., Bronner W., Seelmann-Eggebert M., Schlechtweg M., Mikulla M., Weimann G. // 2006. IEEE MTT-S International Microwave Symposium Digest. - San Francisco, CA, 11-16 June 2006. - P. 1368-1371. ↑

**C1272.** Powell J.R. MMIC and Module Design and Performance for Millimetric Transceiver Front-ends for Transport Applications. / Powell J.R., Munday P.D., Tang W.H.A., Hunt R.C., Gunton D.J. // 2006. IEEE MTT-S International Microwave Symposium Digest. - San Francisco, CA, 11-16 June 2006. - P. 1497-1500. ↑

**C1273.** Liao C.C. Comparing High Mobility InGaAs FETs with Si and GOI Devices. / Liao C.C., Kao H.L., Chin A., Yu D.S., Li M.-F., Zhu C., Mcalister S.P. // 2006 64th Device Research Conference. - State College, PA, USA, June 2006. - P. 85-86. ↑

**C1274.** Chou Y.C. Gate Sinking Effect of 0.1  $\mu\text{m}$  InP HEMT MMICs Using Pt/Ti/Pt/Au. / Chou Y.C., Lai R., Leung D., Kan Q., Farkas D., Eng D., Wojtowicz M., Chin P., Block T., Oki A. // 2006 International Conference on Indium Phosphide and Related Materials Conference Proceedings. - Princeton, NJ, 2006. - P. 188-191. ↑

**C1275.** Tae-Woo Kim. Sub-threshold characteristics of the 0.2  $\mu\text{m}$  capless InP/In/sub 0.52/Al/sub 0.48/As/In/sub 0.53/Ga/sub 0.47/As p-HEMTs having a self-aligned gate. / Tae-Woo Kim, Seong June Jo, Seung Heon Shin, Jae-Hyung Jang, Jong-In Song. // 2006 International Conference on Indium Phosphide and Related Materials Conference Proceedings. - Princeton, NJ, 2006. - P. 309-312. ↑

**C1276.** Mateos J. Ultra fast Gunn effect at THz frequencies in HEMTs. / Mateos J., Perez S., Pardo D., Gonzalez T. // 2006 International Conference on Indium Phosphide and Related Materials Conference Proceedings. - Princeton, NJ, 2006. - P. 313-316. ↑

**C1277.** Kwang-Seok Seo. Nanometer Scale InGaAs HEMT Technology for Ultra High Speed IC. / Kwang-Seok Seo, Dae-Hyun Kim. // 2006 International Conference on Indium Phosphide and Related Materials Conference Proceedings. - Princeton, NJ, 2006. - P. 30-35. ↑

**C1278.** Dae-Hyun Kim. The Impact of Side-Recess Spacing on the Logic Performance of 50 nm InGaAs HEMTs. / Dae-Hyun Kim, del Alamo J.A., Jae-Hak Lee, Kwang-Seok Seo. // 2006 International Conference on Indium Phosphide and Related Materials Conference Proceedings. - Princeton, NJ, 2006. - P. 177-180. ↑

**C1279.** Thayne I. 50nm GaAs mHEMTs and MMICs for Ultra-Low Power Distributed Sensor Network Applications. / Thayne I., Elgaid K., Holland M., McLelland H., Moran D., Thoms S., Stanley C. // 2006 International Conference on Indium Phosphide and Related Materials Conference Proceedings. - Princeton, NJ, 2006. - P. 181-184. ↑

**C1280.** Kang I.H. Low-Frequency-Noise Characteristic of Quasi-Enhancement-Mode HEMT Using a Selectively Hydrogen-Pretreatment. / Kang I.H., Kim S.C., Bahng W., Kim N.K. // 2006 25th International Conference on Microelectronics. - Belgrade, 2006. - P. 279-282. ↑

**C1281.** Kang I.H. Accurate Noise Modeling of HEMT for Low-Noise Applications. / Kang I.H., Kim S.C., Bahng W., Kim N.K. // 2006 25th International Conference on Microelectronics. - Belgrade, 2006. - P. 294-297. ↑

**C1282.** Balsi M. Validation of a statistical non-linear model of GaAs HEMT MMIC's by hypothesis testing and principal components analysis. / Balsi M., Centurelli F., Marietti P., Scotti G., Tommasino P., Trifiletti A., Valente G. // 2006. ISCAS 2006. Proceedings. 2006 IEEE International Symposium on Circuits and Systems. - Island of Kos, 2006. - P. 4 P.-4638. ↑

**C1283.** Malmkvist M. Effect of Schottky layer thickness on DC, RE and noise of 70-nm gate length InP HEMTs. / Malmkvist M., Borg M., Shumin Wang, Grahn J. // 2006 International Conference on Indium Phosphide

and Related Materials Conference Proceedings. - Princeton, NJ, 2006. - P. 329-331. ↑

**C1284.** Pajona O. Electrical models for detrimental effects in metamorphic HEMTs. / Pajona O., Aupetit-Berthelemot C., Dumas J.M. // 2006 International Conference on Indium Phosphide and Related Materials Conference Proceedings. - Princeton, NJ, 2006. - P. 332-335. ↑

**C1285.** Sugiyama H. Metal-organic vapor-phase epitaxy growth of InP using triethylphosphine with phosphine as phosphorous source. / Sugiyama H., Sakai R., Araki G. // 2006 International Conference on Indium Phosphide and Related Materials Conference Proceedings. - Princeton, NJ, 2006. - P. 391-394. ↑

**C1286.** G.H. Jessen. AlGaIn/GaN HEMT on Diamond Technology Demonstration. / G. H. Jessen, J. K. Gillespie, G. D. Via, A. Crespo, D. Langley, J. Wasserbauer, F. Faili, D. Francis, D. Babic, F. Ejeckam, S. Guo, I. Eliashevich. // 2006. CSIC 2006. IEEE Compound Semiconductor Integrated Circuit Symposium. - San Antonio, TX, Nov. 2006. - P. 271-274. ↑

**C1287.** {no data available}. 2006 ROCS Workshop. 2006. [Reliability of Compound Semiconductors] ROCS Workshop. - San Antonio, TX, 12-12 Nov. 2006. - P. i. ↑

**C1288.** Roland Shaw. Performance Characterization, Repeatability, and Consistency of X-Band GaN HEMTs Prior to High Temperature RF Reliability Testing. / Roland Shaw, David Sanderlin, Jansen DeJulio. // 2006. [Reliability of Compound Semiconductors] ROCS Workshop. - San Antonio, TX, Nov. 2006. - P. 3-20. ↑

**C1289.** Noriyuki Watanabe. High-quality InAlN/GaN high electron mobility transistors on Si (111) by metalorganic chemical vapor deposition. / Noriyuki Watanabe, Haruki Yokoyama, Masanobu Hiroki, Yasuhiro Oda, Takashi Kobayashi, Takuma Yagi. // 2006. CSIC 2006. IEEE Compound Semiconductor Integrated Circuit Symposium. - San Antonio, TX, Nov. 2006. - P. 257-260. ↑

**C1290.** Ruonan Wang. A Planar Integration Process for E/D-mode AlGaIn/GaN HEMT DCFL Integrated Circuits. / Ruonan Wang, Yong Cai, Zhiqun Cheng, C. W. Tang, Kei May Lau, Kevin J. Chen. // 2006. CSIC 2006. IEEE Compound Semiconductor Integrated Circuit Symposium. - San Antonio, TX, Nov. 2006. - P. 261-264. ↑

**C1291.** Kazutaka Takagi. X-band AlGaIn/GaN HEMT with over 80W Output Power. / Kazutaka Takagi, Kazutoshi Masuda, Yasushi Kashiwabara, Hiroyuki Sakurai, Keiichi Matsushita, Shinji Takatsuka, Hisao Kawasaki, Yoshiharu Takada, Kunio Tsuda. // 2006. CSIC 2006. IEEE Compound Semiconductor Integrated Circuit Symposium. - San Antonio, TX, Nov. 2006. - P. 265-268. ↑

**C1292.** Mohd Nizam Osman. The Impact of Multiple-Gated Layout on the Drain-Source Current of pseudomorphic-HEMTs. / Mohd Nizam Osman, Zaiki Awang, Syamsuri Yaakob, Mohamed Razman Yahya, Abdul Fatah Awang Mat. // 2006. RFM 2006. International RF and Microwave Conference. - Putra Jaya, 12-14 Sept. 2006. - P. 201-204. ↑

**C1293.** Abdul Manaf Hashim. Interdigital-Gated HEMT Structure for High Frequency Devices. / Abdul Manaf Hashim, Seiya Kasai, Tamotsu Hashizume, Hideki Hasegawa. // 2006. RFM 2006. International RF and Microwave Conference. - Putra Jaya, 12-14 Sept. 2006. - P. 262-266. ↑

**C1294.** Idham M N.F. Effect of Indium Content in the Channel on the Electrical Performance of Metamorphic High Electron Mobility Transistors. / Idham M N.F., Ahmad Ismat A.I., Rasidah S., Asban D., Razman Y M., Abdul Fatah A.M. // 2006. ICSE '06. IEEE International Conference on Semiconductor Electronics. - Kuala Lumpur, Oct. 29 2006-Dec. 1 2006. - P. 743-746. ↑

**C1295.** A. Faqir. Physical Investigation of High-Field Degradation Mechanisms in GaN/AlGaIn/GaN HEMTs. / A. Faqir, A. Chini, G. Verzellesi, F. Fantini, F. Rampazzo, G. Meneghesso, E. Zanoni, J. Bernat, P. Kordos. // 2006. [Reliability of Compound Semiconductors] ROCS Workshop. - San Antonio, TX, Nov. 2006. - P. 25-31. ↑

**C1296.** Chou Y.C. The Effect of Gate Current on the Degradation of GaAs PHEMT MMICs. / Chou Y.C., Luo B.-W., Leung D., Kan Q., Biedenbender M., Bhorania R., Lai R., Eng D., Farkas D., Chin P., Wojtowicz M., Block T., Oki A. // 2006. [Reliability of Compound Semiconductors] ROCS Workshop. - San Antonio, TX, 12-12 Nov. 2006. - P. 111-114. ↑

**C1297.** Mahyuddin N.M. Modeling of a 10GHz Dielectric Resonator Oscillator in ADS. / Mahyuddin N.M., Ain M.F., Hassan S.I.S., Singh M. // 2006. RFM 2006. International RF and Microwave Conference. - Putra Jaya, ↑

12-14 Sept. 2006. - P. 106-110. ↑

**C1298.** King-Yuen Wong. 6C-5 Planar Integration of SAW Filter with HEMT on AlGaIn/GaN Heterostructure Using Fluoride-based Plasma Treatment. / King-Yuen Wong, Tang W.C.W., Kei May Lau, Chen K.J. // 2006. IEEE Ultrasonics Symposium. - Vancouver, BC, 2-6 Oct. 2006. - P. 281-284. ↑

**C1299.** Kang-Sung Lee. Fabrication of 35-nm zigzag T-gate Al<sub>0.25</sub>Ga<sub>0.75</sub>As/In<sub>0.2</sub>Ga<sub>0.8</sub>As/GaAs pHEMTs. / Kang-Sung Lee, Young-Su Kim, Yun-Ki Hong, Yoon-Ha Jeong. // 2006. NMDC 2006. IEEE Nanotechnology Materials and Devices Conference. - Gyeongju, 22-25 Oct. 2006. - Vol. 1. - P. 112-113. ↑

**C1300.** Colantonio P. New Design Approach to minimise IMD Asymmetry and IM3 products in Microwave FETs. / Colantonio P., Giannini F., Limiti E., Nanni A. // 2006. MIKON 2006. International Conference on Microwaves, Radar & Wireless Communications. - Krakow, 22-24 May 2006. - P. 13-17. ↑

**C1301.** Aziz M.A. Theoretical Study of The Charge Control in AlGaIn/GaN HEMTs. / Aziz M.A., El-Abd A. // 2006. NRSC 2006. Proceedings of the Twenty Third National Radio Science Conference. - Menoufiya, 14-16 March 2006. - Vol. 0. - P. 1-7. ↑

**C1302.** Shchepetov A. Plasma Wave HEMTs for THz applications. / Shchepetov A., Roelens Y., Bollaert S., Cappy A., Dyakonova N., Knap W., Lusakowski J., Teppe F., El Fatimy A., Dyakonov M. // 2006. IRMMW-THz 2006. Joint 31st International Conference on Infrared Millimeter Waves and 14th International Conference on Terahertz Electronics. - Shanghai, 18-22 Sept. 2006. - P. 136. ↑

**C1303.** Hu W.D. Current Collapse Simulation of GaN HEMTs. / Hu W.D., Chen X.S., Quan Z.J., Xia C.S., Lu W. // 2006. IRMMW-THz 2006. Joint 31st International Conference on Infrared Millimeter Waves and 14th International Conference on Terahertz Electronics. - Shanghai, 18-22 Sept. 2006. - P. 255. ↑

**C1304.** Tan S. Electrical control of ballistic spin-dependent conductance through magneto-electric barriers in the 2D-electron gas of GaAs heterostructure. / Tan S., Jalil M., Kumar S., Teo K., Zheng Y., Liew T. // 2006. INTERMAG 2006. IEEE International Magnetism Conference. - San Diego, CA, 8-12 May 2006. - P. 122. ↑

**C1305.** Bryan L.B. Parasitic Effects on Harmonic Reflection in Active Microwave Frequency Triplers. / Bryan L.B., Di Giulio D.K., Johnson J.E., Branner G.R. // 2006. MWSCAS 06. 49th IEEE International Midwest Symposium on Circuits and Systems. - San Juan, 6-9 Aug. 2006. - Vol. 2. - P. 679-683. ↑

**C1306.** Sanusi R. Modeling of Polyimide MIM Capacitors for Applications in Planar Monolithic Microwave Integrated Circuits. / Sanusi R., Rahim A.I.A., Osman M.N., Kushairi N., Rasmi A., Muhammad N.F.I., Yahya M.R., Mat A.F.A. // 2006. ICSE '06. IEEE International Conference on Semiconductor Electronics. - Kuala Lumpur, Oct. 29 2006-Dec. 1 2006. - P. 1030-1033. ↑

**C1307.** El-Abd A. New I-V Model For AlGaIn/GaN HEMT At Large Gate Bias. / El-Abd A., Aziz M.A., Shalby A.A., Khamis S. // 2006. ICSE '06. IEEE International Conference on Semiconductor Electronics. - Kuala Lumpur, Oct. 29 2006-Dec. 1 2006. - P. 1010-1014. ↑

**C1308.** Aziz M.M.A. Extraction of the Small-Signal Equivalent Circuit Elements in HEMTs. 2006. NRSC 2006. Proceedings of the Twenty Third National Radio Science Conference. - Menoufiya, 14-16 March 2006. - Vol. 0. - P. 1-6. ↑

**C1309.** Chia-Yuan Chang. High-Performance In<sub>0.52</sub>Al<sub>0.48</sub>As/In<sub>0.6</sub>Ga<sub>0.4</sub>As Power Metamorphic HEMT for Ka-Band Applications. / Chia-Yuan Chang, Chang E.Y., Yi-Chung Lien, Miyamoto Y., Szu-Hung Chen, Li-Hsin Chu. // 2006. ICSE '06. IEEE International Conference on Semiconductor Electronics. - Kuala Lumpur, Oct. 29 2006-Dec. 1 2006. - P. 422-424. ↑

**C1310.** Norman Fadhil Idham M. Device Characteristics of HEMT Structures based on Backgate Contact Method. / Norman Fadhil Idham M., Nurul Afzan O., Soetedjo H., Ahmad Ismat A.R., Sabtu I., Mohamed Razman Y., Abdul Fatah A.M. // 2006. ICSE '06. IEEE International Conference on Semiconductor Electronics. - Kuala Lumpur, Oct. 29 2006-Dec. 1 2006. - P. 740-742. ↑

**C1311.** Micovic M. GaN HFET for W-band Power Applications. / Micovic M., Kurdoghlian A., Hashimoto P., Hu M., Antcliffe M., Willadsen P.J., Wong W.S., Bowen R., Milosavljevic I., Schmitz A., Wetzel M., Chow D.H. // 2006. IEDM '06. International Electron Devices Meeting. - San Francisco, CA, 11-13 Dec. 2006. - P. 1-3. ↑

↑



- C1312.** Zhao Weifeng. Monolithic integration of thermally stable enhancement-mode and depletion-mode InAlAs/InGaAs/InP HEMTs utilizing Ir-gate and Ag-ohmic contact technologies. / Zhao Weifeng, Jin Niu, Chen Guang, Wang Liang, Adesida Ilesanmi. // 2006. IEDM '06. International Electron Devices Meeting. - San Francisco, CA, 11-13 Dec. 2006. - P. 1-4. ↑
- C1313.** Dae-Hyun Kim. Scaling Behavior of In<sub>0.7</sub>Ga<sub>0.3</sub>As HEMTs for Logic. / Dae-Hyun Kim, del Alamo J.A. // 2006. IEDM '06. International Electron Devices Meeting. - San Francisco, CA, 11-13 Dec. 2006. - P. 1-4. ↑
- C1314.** Adesida I. Processes and Device Technologies for AlGaN/GaN High Electron Mobility Transistors. / Adesida I., Kumar V., Mohammed F., Wang L., Basu A., Kim D.-H., Lanford W. // 2006. IEDM '06. International Electron Devices Meeting. - San Francisco, CA, 11-13 Dec. 2006. - P. 1-4. ↑
- C1315.** Wu Y.-F. An Internally-matched GaN HEMT Amplifier with 550-watt Peak Power at 3.5 GHz. / Wu Y.-F., Wood S.M., Smith R.P., Sheppard S., Allen S. T., Parikh P., Milligan J. // 2006. IEDM '06. International Electron Devices Meeting. - San Francisco, CA, 11-13 Dec. 2006. - P. 1-3. ↑
- C1316.** Moon J.S. High PAE 1mm AlGaN/GaN HEMTs for 20 W and 43% PAE X-band MMIC Amplifiers. / Moon J.S., Wong D., Antcliffe M., Hashimoto P., Hu M., Willadsen P., Micovic M., Moyer H.P., Kurdoghlian A., MacDonald P., Wetzel M., Bowen R. // 2006. IEDM '06. International Electron Devices Meeting. - San Francisco, CA, 11-13 Dec. 2006. - P. 1-2. ↑
- C1317.** Zaman S. Intermodulation Behaviour of a Transient Trapping Model. / Zaman S., Parker A. // 2006. ICECE '06. International Conference on Electrical and Computer Engineering. - Dhaka, 19-21 Dec. 2006. - P. 29-32. ↑
- C1318.** Xinyan Gao. The Optimum Design of A Broad Band Low Noise Amplifier. / Xinyan Gao, Wenkai Xie. // 2006. IRMMW-THz 2006. Joint 31st International Conference on Infrared Millimeter Waves and 14th International Conference on Terahertz Electronics. - Shanghai, 18-22 Sept. 2006. - P. 92. ↑
- C1319.** Ho-Young Kim. Wave guide type photo receiver module with 20 dB amplifier at 60 GHz millimeter wave frequency band. / Ho-Young Kim, Seon-Eui Hong, Myung-Suk Oh, Dong-Young Kim, En-Soo Nam, Young-Jun Chong, Hyun-Kyu Yu. // 2006. IRMMW-THz 2006. Joint 31st International Conference on Infrared Millimeter Waves and 14th International Conference on Terahertz Electronics. - Shanghai, 18-22 Sept. 2006. - P. 95. ↑
- C1320.** Uemoto Y. A Normally-off AlGaN/GaN Transistor with Ron A=2.6mΩcm<sup>2</sup> and BVds =640V Using Conductivity Modulation. / Uemoto Y., Hikita M., Ueno H., Matsuo H., Ishida H., Yanagihara M., Ueda T., Tanaka T., Ueda D. // 2006. IEDM '06. International Electron Devices Meeting. - San Francisco, CA, 11-13 Dec. 2006. - P. 1-4. ↑
- C1321.** Suh C. S. High-Breakdown Enhancement-Mode AlGaN/GaN HEMTs with Integrated Slant Field-Plate. / Suh C. S., Dora Y., Fichtenbaum N., McCarthy L., Keller S., Mishra U. K. // 2006. IEDM '06. International Electron Devices Meeting. - San Francisco, CA, 11-13 Dec. 2006. - P. 1-3. ↑
- C1322.** Medjdoub F. Can InAlN/GaN be an alternative to high power / high temperature AlGaN/GaN devices?. / Medjdoub F., Carlin J.-F., Gonschorek M., Feltn E., Py M.A., Ducatteau D., Gaquiere C., Grandjean N., Kohn E. // 2006. IEDM '06. International Electron Devices Meeting. - San Francisco, CA, 11-13 Dec. 2006. - P. 1-4. ↑
- C1323.** Wataru Saito. High Voltage and High Switching Frequency Power-Supplies using a GaN-HEMT. / Wataru Saito, Ichiro Omura, Tomokazu Domon, Kunio Tsuda. // 2006. CSIC 2006. IEEE Compound Semiconductor Integrated Circuit Symposium. - San Antonio, TX, Nov. 2006. - P. 253-256. ↑
- C1324.** Steven Gao. MMIC Class-F Power Amplifiers using Field-Plated AlGaN/GaN HEMTs. / Steven Gao, Hongtao Xu, Umesh K. Mishra, Robert A. York. // 2006. CSIC 2006. IEEE Compound Semiconductor Integrated Circuit Symposium. - San Antonio, TX, Nov. 2006. - P. 81-84. ↑
- C1325.** Ching-Hung Chiu. A 3-34 GHz GaAs PHEMT Distributed Mixer with Low DC Power Consumption. / Ching-Hung Chiu, Kung-Hao Liang, Hong-Yeh Chang, Yi-Jen Chan. // 2006. CSIC 2006. IEEE Compound Semiconductor Integrated Circuit Symposium. - San Antonio, TX, Nov. 2006. - P. 73-76. ↑
- C1326.** Michael V. Aust. Wideband Dual-Gate GaN HEMT Low Noise Amplifier for Front-End Receiver Electronics. / Michael V. Aust, Arvind K. Sharma, Yao-Chung Chen, Michael Wojtowicz. // 2006. CSIC 2006.

IEEE Compound Semiconductor Integrated Circuit Symposium. - San Antonio, TX, Nov. 2006. - P. 89-92. ↑

**C1327.** J.P. Conlon. GaN Wide Band Power Integrated Circuits. / J. P. Conlon, N. Zhang, M. J. Poulton, J. B. Shealy, R. Vetury, D. S. Green, J. D. Brown, S. Gibb. // 2006. CSIC 2006. IEEE Compound Semiconductor Integrated Circuit Symposium. - San Antonio, TX, Nov. 2006. - P. 85-88. ↑

**C1328.** W.R. Deal. Demonstration of a Sub-Millimeter Wave Integrated Circuit (S-MMIC) using InP HEMT with a 35-nm Gate. / W. R. Deal, S. Din, V. Radisic, J. Padilla, X.B. Mei, W. Yoshida, P.H. Liu, J. Uyeda, M. Barsky, T. Gaier, A. Fung, L. Samoska, R. Lai. // 2006. CSIC 2006. IEEE Compound Semiconductor Integrated Circuit Symposium. - San Antonio, TX, Nov. 2006. - P. 33-36. ↑

**C1329.** Mikko Karkkainen. Coplanar 94 GHz Metamorphic HEMT Low Noise Amplifiers. / Mikko Karkkainen, Mikko Varonen, Kari A. I. Halonen, Mikko Kantanen, Timo Karttaavi, Rainer Weber, Arnulf Leuther, Matthias Seelmann-Eggebert, Tapani Narhi. // 2006. CSIC 2006. IEEE Compound Semiconductor Integrated Circuit Symposium. - San Antonio, TX, Nov. 2006. - P. 29-32. ↑

**C1330.** Sang-Min Nam. A Ka-band High Power Frequency Doubler in SMT Package. / Sang-Min Nam, Frank Traut, Joe Cuggino. // 2006. CSIC 2006. IEEE Compound Semiconductor Integrated Circuit Symposium. - San Antonio, TX, Nov. 2006. - P. 61-64. ↑

**C1331.** M. Passlack. High Mobility III-V Mosfet Technology. / M. Passlack, R. Droopad, K. Rajagopalan, J. Abrokwhah, P. Zurcher, P. Fejes. // 2006. CSIC 2006. IEEE Compound Semiconductor Integrated Circuit Symposium. - San Antonio, TX, Nov. 2006. - P. 39-42. ↑

**C1332.** Wen-Ren Lee. A high-efficiency, broadband and high output power PHEMT balanced K-band doubler with integrated balun. / Wen-Ren Lee, Shih-Fong Chao, Zuo-Min Tsai, Pin-Cheng Huang, Chun-Hsien Lien, Jeng-Han Tsai, Huei Wang. // 2006. APMC 2006. Asia-Pacific Microwave Conference. - Yokohama, 12-15 Dec. 2006. - P. 763-766. ↑

**C1333.** Kiwon Lee. Improved DC and RF performance of high power AlGaIn/GaN HEMTs with a novel inner field-plate. / Kiwon Lee, Kwangui Ko, Sungsik Lee, Kyoungsoon Yang. // 2006. APMC 2006. Asia-Pacific Microwave Conference. - Yokohama, 12-15 Dec. 2006. - P. 1019-1022. ↑

**C1334.** Chi-shien Lee. Ka-band flip-chip assembled power amplifier. / Chi-shien Lee, Wei-kuo Huang, Che-ming Wang, Yue-ming Hsin, Tsung-Jung Yeh. // 2006. APMC 2006. Asia-Pacific Microwave Conference. - Yokohama, 12-15 Dec. 2006. - P. 718-721. ↑

**C1335.** Yu-Lin Zou. A high performance Ka-band push-push oscillator design using finite ground cpw structure. / Yu-Lin Zou, I-Shan Chen, Hwann-Kaeo Chiou. // 2006. APMC 2006. Asia-Pacific Microwave Conference. - Yokohama, 12-15 Dec. 2006. - P. 751-754. ↑

**C1336.** R.J. Trew. The Physics of Reliability for High Voltage AlGaIn/GaN HFET's. / R.J. Trew, Y. Liu, W.W. Kuang, G.L. Bilbro. // 2006. CSIC 2006. IEEE Compound Semiconductor Integrated Circuit Symposium. - San Antonio, TX, Nov. 2006. - P. 103-106. ↑

**C1337.** David Schmelzer. A GaN HEMT Class F Amplifier at 2 GHz with >80 % PAE. / David Schmelzer, Stephen I. Long. // 2006. CSIC 2006. IEEE Compound Semiconductor Integrated Circuit Symposium. - San Antonio, TX, Nov. 2006. - P. 96-99. ↑

**C1338.** Joshin K. Recent progress of high power GaN-HEMT for wireless application. / Joshin K., Kikkawa T. // 2006. APMC 2006. Asia-Pacific Microwave Conference. - Yokohama, 12-15 Dec. 2006. - P. 1027-1032. ↑

**C1339.** Kobayashi K.W. High linearity-wideband PHEMT Darlington amplifier with +40 dBm IP3. 2006. APMC 2006. Asia-Pacific Microwave Conference. - Yokohama, 12-15 Dec. 2006. - P. 1035-1038. ↑

**C1340.** Zhong Shichang. 8-Watt internally matched GaAs power amplifier at 16-16.5GHz. / Zhong Shichang, Chen Tangsheng, Lin Gang, Li Fuxiao. // 2006. ICSICT '06. 8th International Conference on Solid-State and Integrated Circuit Technology. - Shanghai, 23-26 Oct. 2006. - P. 887-889. ↑

**C1341.** Qiu Z.J. Electrical properties of metamorphic In<sub>0.52</sub>Al<sub>0.48</sub>As/In<sub>0.65</sub>Ga<sub>0.35</sub>As HEMT's on GaAs substrate. / Qiu Z.J., Liu R., Zhang S.L., Gui Y.S., Cui L.J., Zeng Y.P., Chu J.H. // 2006. ICSICT '06. 8th International Conference on Solid-State and Integrated Circuit Technology. - Shanghai, 23-26 Oct. 2006. - P. 887-889. ↑

875-877. ↑

**C1342.** Zhiyong Ma. MOCVD grown AlGaIn/GaN HEMT structure with compositionally step-graded AlGaIn barrier layer. / Zhiyong Ma, Xiaoliang Wang, Guoxin Hu, Junxue Ran, Xinhua Wang, Baozhu Wang, Weijun Luo, Jianpin Li. // 2006. ICSICT '06. 8th International Conference on Solid-State and Integrated Circuit Technology. - Shanghai, Oct. 2006. - P. 917-919. ↑

**C1343.** Li Chengzhan. Effect of Passivation on Increasing of AlGaIn/GaN HEMT Gate Reverse Leakage. / Li Chengzhan, Liu Jian, Liu Xinyu, Liu Guoguo, Liu Dan, Chen Xiaojuan, He Zhijing. // 2006. ICSICT '06. 8th International Conference on Solid-State and Integrated Circuit Technology. - Shanghai, Oct. 2006. - P. 908-910. ↑

**C1344.** Yeong-Her Wang. Liquid Phase Oxidation on GaAs-based Transistor Applications. / Yeong-Her Wang, Kuan-Wei Lee. // 2006. ICSICT '06. 8th International Conference on Solid-State and Integrated Circuit Technology. - Shanghai, 23-26 Oct. 2006. - P. 849-852. ↑

**C1345.** Palacios T. 50 nm AlGaIn/GaN HEMT Technology for mm-wave Applications. / Palacios T., Fichtenbaum N., Keller S., Denbaars S.P., Mishra U.K. // 2006 64th Device Research Conference. - State College, PA, USA, June 2006. - P. 99-100. ↑

**C1346.** Sheng-Hui Lu. Effect of Source-Connected Field Plate on Electric Field Distribution and Breakdown Voltage in AlGaIn/GaN HEMTs. / Sheng-Hui Lu, Wei Zhou, Di Yan, Jian-Xin Xia, Mo-Hua Yang. // 2006. ICSICT '06. 8th International Conference on Solid-State and Integrated Circuit Technology. - Shanghai, Oct. 2006. - P. 860-862. ↑

**C1347.** Yuan-Zheng Yue. Study of Surface Passivation with Different a-SiN<sub>x</sub>B:H Films Effect on AlGaIn/GaN HEMTs. / Yuan-Zheng Yue, Yue Hao, Jin-Cheng Zhang, Qian Feng. // 2006. ICSICT '06. 8th International Conference on Solid-State and Integrated Circuit Technology. - Shanghai, Oct. 2006. - P. 857-859. ↑

**C1348.** John W. Palmour. Energy Efficient Wide Bandgap Devices. 2006. CSIC 2006. IEEE Compound Semiconductor Integrated Circuit Symposium. - San Antonio, TX, Nov. 2006. - P. 4-7. ↑

**C1349.** {no data available}. 2006 IEEE CSIC Symposium. 2006. CSIC 2006. IEEE Compound Semiconductor Integrated Circuit Symposium. - San Antonio, TX, Nov. 2006. - P. i. ↑

**C1350.** Toshihiko Kosugi. 120-GHz Tx/Rx Waveguide Modules for 10-Gbit/s Wireless Link System. / Toshihiko Kosugi, Masami Tokumitsu, Koichi Murata, Takatomo Enoki, Hiroyuki Takahashi, Akihiko Hirata, Tadao Nagatsuma. // 2006. CSIC 2006. IEEE Compound Semiconductor Integrated Circuit Symposium. - San Antonio, TX, Nov. 2006. - P. 25-28. ↑

**C1351.** Michael Schlechtweg. From 100 GHz to Terahertz Electronics-Activities in Europe. / Michael Schlechtweg, Axel Tessmann. // 2006. CSIC 2006. IEEE Compound Semiconductor Integrated Circuit Symposium. - San Antonio, TX, Nov. 2006. - P. 8-11. ↑

**C1352.** Luo Weijun. Structure Optimization of Field-Plate AlGaIn/GaN HEMTs. / Luo Weijun, Wei Ke, Chen Xiaojuan, Li Chengzhan, Liu Xinyu, Wang Xiaoliang. // 2006. ICSICT '06. 8th International Conference on Solid-State and Integrated Circuit Technology. - Shanghai, Oct. 2006. - P. 926-928. ↑

**C1353.** Qian Luo. Investigation of Surface Charging Effects in AlGaIn/GaN HEMT by a New Measurement Method. / Qian Luo, Jiangfeng Du, Mohua Yang, Shenghui Lu, Wei Zhou, Jianxin Xia, Qi Yu. // 2006. ICSICT '06. 8th International Conference on Solid-State and Integrated Circuit Technology. - Shanghai, Oct. 2006. - P. 923-925. ↑

**C1354.** Choi Y.C. Effects of an Fe-doped GaN Buffer in AlGaIn/GaN Power HEMTs on Si Substrate. / Choi Y.C., Eastman L.F., Pophristic M. // 2006. ESSDERC 2006. Proceeding of the 36th European Solid-State Device Research Conference. - Montreux, 19-21 Sept. 2006. - P. 282-285. ↑

**C1355.** Junxue Ran. Characteristics of InGaIn Channel HEMTs Grown by MOCVD. / Junxue Ran, Xiaoliang Wang, Guoxin Hu, Weijun Luo, Zhiyong Ma, Jianping Li, Cuimei Wang, Junxi Wang, Yiping Zeng, Jinmin Li, Xinyu Liu, Jian Liu, Zhijing He. // 2006. ICSICT '06. 8th International Conference on Solid-State and Integrated Circuit Technology. - Shanghai, Oct. 2006. - P. 929-931. ↑

**C1356.** Kevin W. Kobayashi. A Novel E-mode PHEMT Linearized Darlington Cascode Amplifier. 2006. CSIC

2006. IEEE Compound Semiconductor Integrated Circuit Symposium. - San Antonio, TX, Nov. 2006. - P. 153-156. ↑

**C1357.** Ming-Yih Kao. High Performance Dual Recess 0.15- $\mu\text{m}$  pHEMT for Multi-Function MMIC Applications. / Ming-Yih Kao, Sabyasachi Nayak, Rached Hajji, Hillyard S.E., Ketterson A.A. // 2006. CSIC 2006. IEEE Compound Semiconductor Integrated Circuit Symposium. - San Antonio, TX, 12-15 Nov. 2006. - P. 129-132. ↑

**C1358.** W.R. Deal. Broadband Dual-Gate Balanced Low Noise Amplifiers. / W. R. Deal, M. Biedenbender, P.H. Liu, C. Namba, S. Chen, M. Sergeant, J. Uyeda, M. Siddiqui, R. Lai, B. Allen. // 2006. CSIC 2006. IEEE Compound Semiconductor Integrated Circuit Symposium. - San Antonio, TX, Nov. 2006. - P. 169-172. ↑

**C1359.** C.H. Lin. A Fully Matched Ku-band 9W PHEMT MMIC High Power Amplifier. / C. H. Lin, H. Z. Liu, C. K. Chu, H. K. Huang, Y. H. Wang, C. C. Liu, C. H. Chang, C. L. Wu, C. S. Chang. // 2006. CSIC 2006. IEEE Compound Semiconductor Integrated Circuit Symposium. - San Antonio, TX, Nov. 2006. - P. 165-168. ↑

**C1360.** T. Ashley. Indium Antimonide Based Technology for RF Applications. / T. Ashley, L. Buckle, M. T. Emeny, M. Fearn, D. G. Hayes, K. P. Hilton, R. Jefferies, T. Martin, T. J. Phillips, J. Powell, A. W. H. Tang, D. Wallis, P. J. Wilding. // 2006. CSIC 2006. IEEE Compound Semiconductor Integrated Circuit Symposium. - San Antonio, TX, Nov. 2006. - P. 121-124. ↑

**C1361.** Malmros A. A comparison of cryogenically cooled pseudomorphic and lattice matched InP HEMTs: Implementation in an ultra-low noise amplifier. / Malmros A., Wadefalk N., Starski P., Grahn J. // 2006. APMC 2006. Asia-Pacific Microwave Conference. - Yokohama, 12-15 Dec. 2006. - P. 177-180. ↑

**C1362.** Takahashi H. Tunable coplanar filter for F-band wireless receivers. / Takahashi H., Kosugi T., Hirata A., Murata K., Nagatsuma T. // 2006. APMC 2006. Asia-Pacific Microwave Conference. - Yokohama, 12-15 Dec. 2006. - P. 15-18. ↑

**C1363.** Vassil Palankovski. Field-Plate Optimization of AlGaIn/GaN HEMTs. / Vassil Palankovski, Stanislav Vitanov, Rudiger Quay. // 2006. CSIC 2006. IEEE Compound Semiconductor Integrated Circuit Symposium. - San Antonio, TX, Nov. 2006. - P. 107-110. ↑

**C1364.** Angelov I. Large-signal modelling and comparison of AlGaIn/GaN HEMTs and SiC MESFETs. / Angelov I., Andersson K., Schreurs D., Xiao D., Rorsman N., Desmaris V., Sudow M., Zirath H. // 2006. APMC 2006. Asia-Pacific Microwave Conference. - Yokohama, 12-15 Dec. 2006. - P. 279-282. ↑

**C1365.** Lee J.-W. A high power performance 60 GHz push-push oscillator MMIC in metamorphic HEMT technology. / Lee J.-W., Kim S.-W., Seol G.-S., Seo K.-S. // 2006. APMC 2006. Asia-Pacific Microwave Conference. - Yokohama, 12-15 Dec. 2006. - P. 453-456. ↑

**C1366.** Crespo-Cadenas C. Volterra series approach to behavioral modeling: Application to an FET amplifier. / Crespo-Cadenas C., Reina-Tosina J., Madero-Ayora M.J. // 2006. APMC 2006. Asia-Pacific Microwave Conference. - Yokohama, 12-15 Dec. 2006. - P. 445-448. ↑

**C1367.** Jae Shin Kim. High-efficiency GaN/AlGaIn HEMT oscillator operating at L-band. / Jae Shin Kim, Wenhsing Wu, Jianshan Lin, Verma A., Soohwan Jang, Ren F., Pearton S., Fitch R., Gillespie J. // 2006. APMC 2006. Asia-Pacific Microwave Conference. - Yokohama, 12-15 Dec. 2006. - P. 631-634. ↑

**C1368.** Ferndahl M. Residual and oscillator phase noise in GaAs metamorphic HEMTs. / Ferndahl M., Zirath H. // 2006. APMC 2006. Asia-Pacific Microwave Conference. - Yokohama, 12-15 Dec. 2006. - P. 472-475. ↑

**C1369.** Jianfeng Xu. Numerical investigation on thermal characteristics of GaN HFETs for high power applications. / Jianfeng Xu, Wen-Yan Yin, Junfa Mao. // 2006. APMC 2006. Asia-Pacific Microwave Conference. - Yokohama, 12-15 Dec. 2006. - P. 433-436. ↑

**C1370.** Jonathan J. Lynch. Low Noise Direct Detection Sensors for Millimeter Wave Imaging. / Jonathan J. Lynch, Joel N. Schulman, Harris P. Moyer. // 2006. CSIC 2006. IEEE Compound Semiconductor Integrated Circuit Symposium. - San Antonio, TX, Nov. 2006. - P. 215-218. ↑

**C1371.** Kyoungwoon Kim. A 77 GHz Transceiver for Automotive Radar System Using a 120nm In<sub>0.4</sub>AlAs/In<sub>0.35</sub>GaAs Metamorphic HEMTs. / Kyoungwoon Kim, Wooyeol Choi, Sungwon Kim, Gyungseon Seol, Kwangseok Seo, Youngwoo Kwon. // 2006. CSIC 2006. IEEE Compound Semiconductor Integrated Circuit



Symposium. - San Antonio, TX, Nov. 2006. - P. 201-204. ↑

**C1372.** Chow Y.H. A 1V, 0.9dB noise-figure high linearity LNA MMIC for concurrent GPS handset application. / Chow Y.H., Tan T.L., Won-Kyu Kim. // 2006. APMC 2006. Asia-Pacific Microwave Conference. - Yokohama, 12-15 Dec. 2006. - P. 401-404. ↑

**C1373.** Keon-Shik Kong. Ka-band MMIC high power amplifier (4W at 30GHz) with record compact size. / Keon-Shik Kong, Nguyen B., Nayak S., Ming-Yih Kao. // 2005. CSIC '05. IEEE Compound Semiconductor Integrated Circuit Symposium. 30 Oct.-2 Nov. 2005. - P. 4 ↑

**C1374.** Beall J.M. ESD protection for pHEMT MMIC amplifiers. / Beall J.M., Drandova G.I. // 2005. CSIC '05. IEEE Compound Semiconductor Integrated Circuit Symposium. 30 Oct.-2 Nov. 2005. - P. 4 ↑

**C1375.** Chini A. Fabrication and characterization of N-face AlGaIn/GaN/AlGaIn HEMTs. / Chini A., Rajan S., Wong M., Fu Y., Speck J.S., Mishra U.K. // 2005. DRC '05. 63rd Device Research Conference Digest. - Santa Barbara, CA, 22-22 June 2005. - Vol. 1. - P. 63-64. ↑

**C1376.** Adivarahan V. High-power stable field-plated AlGaIn-GaN MOSHFETs. / Adivarahan V., Koudymov A., Rai S., Yang J., Simin G., Asif Khan M., Fareed Q., Gaska R. // 2005. DRC '05. 63rd Device Research Conference Digest. - Santa Barbara, CA, 22-22 June 2005. - Vol. 1. - P. 177-178. ↑

**C1377.** Thibodeau E. Design of a microwave channelized active filter for MMIC. / Thibodeau E., Boone F. // 2005. Canadian Conference on Electrical and Computer Engineering. - Saskatoon, Sask., 1-4 May 2005. - P. 1543-1546. ↑

**C1378.** Moon J.S. Planar tunneling-coupled field-effect transistor for low-power mixed-signal applications. / Moon J.S., Wang K.C., Rajavel R., Bui S., Wong D., Chow D., Jenson J. // 2005. DRC '05. 63rd Device Research Conference Digest. - Santa Barbara, CA, 22-22 June 2005. - Vol. 1. - P. 261-262. ↑

**C1379.** Abolduyev I.M. AlGaIn/GaN power HEMT for Ka-band. / Abolduyev I.M., Gladysheva N.B., Dorofeev A.A., Matveev Y.A., Minnebaev V.M., Tchemyavsky A.A. // 2005 15th International Crimean Conference Microwave & Telecommunication Technology. 12-16 Oct. 2005. - Vol. 1. - P. 170 Vol. 1. ↑

**C1380.** Cherkashin M.V. Computer-aided design of ultrawide-band MMIC amplifier. / Cherkashin M.V., Eyllier D., Babak L.I., Billonnet L., Jarry B. // 2005 15th International Crimean Conference Microwave & Telecommunication Technology. - Sevastopol, Crimea, 16-16 Sept. 2005. - Vol. 2. - P. 427-428. ↑

**C1381.** Vasil'ev V.L. Millimeter wave HEMTs of R&PC &Istok&Gt;. / Vasil'ev V.L., Zemliakov V.E., Maleev N.A., Zhukov A.E., Vasil'ev A.P., Mikhlin V.S., Ustinov V.M. // 2005 15th International Crimean Conference Microwave & Telecommunication Technology. 12-16 Oct. 2005. - Vol. 1. - P. 171-172. ↑

**C1382.** Kim S. Enhancement-mode InAlAs/InGaAs/InP HEMTs with Ir-based gate metallization. / Kim S., Adesida I. // 2005. DRC '05. 63rd Device Research Conference Digest. - Santa Barbara, CA, 22-22 June 2005. - Vol. 1. - P. 259-260. ↑

**C1383.** Boutros K.S. Vertically-scaled 100nm T-gate AlGaIn/GaN HEMTs with 125GHz  $f_{sub T}$  and 174GHz  $f_{sub MAX}$ . / Boutros K.S., Luo W.B., Shinohara K. // 2005. DRC '05. 63rd Device Research Conference Digest. - Santa Barbara, CA, 22-22 June 2005. - Vol. 1. - P. 183-184. ↑

**C1384.** Palacios T.J. AlGaIn/GaN HEMTs with an InGaIn-based back-barrier. / Palacios T.J., Chakraborty A., Keller S., DenBaars S.P., Mishra U.K. // 2005. DRC '05. 63rd Device Research Conference Digest. - Santa Barbara, CA, 22-22 June 2005. - Vol. 1. - P. 181-182. ↑

**C1385.** Dora Y. Switching characteristics of high-breakdown voltage AlGaIn/GaN HEMTs. / Dora Y., Suh C., Chakraborty A., Heikman S., Chandrasekaran S., Mehrotra V., Mishra U.K. // 2005. DRC '05. 63rd Device Research Conference Digest. - Santa Barbara, CA, 22-22 June 2005. - Vol. 1. - P. 191-192. ↑

**C1386.** Tsai R. 260 GHz FT, 280 GHz f<sub>MAX</sub> AISb/InAs HEMT technology. / Tsai R., Lange M., Lee L.J., Nam P., Namba C., Liu P.H., Sandhu R., Grundbacher R., Deal W., Gutierrez A. // 2005. DRC '05. 63rd Device Research Conference Digest. June 20-22, 2005. - Vol. 1. - P. 257-258. ↑

**C1387.** Cappy A. New HEMT structures for THz applications. / Cappy A., Widmann N., Bolaert S., Wallart X.,

Knap W. // 2005. DRC '05. 63rd Device Research Conference Digest. - Santa Barbara, CA, 22-22 June 2005. - Vol. 1. - P. 255-256. ↑

C1388. Aust M.V. A highly efficient Q-band MMIC 2.8 Watt output power amplifier based on 0.15μm InGaAs/GaAs pHEMT process technology. / Aust M.V., Sharma A.K., Fordham O., Grundbacher R., To R., Tsai R., Lai R. // 2005. CSIC '05. IEEE Compound Semiconductor Integrated Circuit Symposium. 30 Oct.-2 Nov. 2005. - P. 4 ↑

C1389. Varanasi R.K. Prediction of harmonic tuning performance in pHEMTs. / Varanasi R.K., Baylis C.P. II, Dunleavy L.P., Clausen W. // 2005. WAMICON 2005. The 2005 IEEE Annual Conference Wireless and Microwave Technology. 2005. - P. 4 ↑

C1390. Aguilar M.E. Noise behavior of buried channel SiGe HFETs for high speed circuit's applications. / Aguilar M.E., Rodriguez M., Lopez-Bonilla J.L., Crozat P., Hackbarth T., Herzog J.H., Aniel F. // 2005 2nd International Conference on Electrical and Electronics Engineering. 7-9 Sept. 2005. - P. 419-423. ↑

C1391. Streit D.C. The future of compound semiconductors for aerospace and defense applications. / Streit D.C., Gutierrez-Aitken A., Wojtowicz M., Lai R. // 2005. CSIC '05. IEEE Compound Semiconductor Integrated Circuit Symposium. 30 Oct.-2 Nov. 2005. - P. 4 ↑

C1392. Varonen M. Metamorphic HEMT amplifier for K- and Ka-band applications. / Varonen M., Karkkainen M., Kangaslahti P., Halonen K. // 2005. Proceedings of the 2005 European Conference on Circuit Theory and Design. 28 Aug.-2 Sept. 2005. - Vol. 1. - P. 1/253. ↑

C1393. Grundbacher R. A 150-215 GHz InP HEMT low noise amplifier with 12 dB gain. / Grundbacher R., Raja R., Lai R., Chou Y.C., Nishimoto M., Gaier T., Dawson D., Liu P.H., Barsky M., Oki A. // 2005. International Conference on Indium Phosphide and Related Materials. - Glasgow, Scotland, 8-12 May 2005. - P. 613-616. ↑

C1394. Buhrow B.H. A low power AlSb/InAs HEMT X-band low noise amplifier. / Buhrow B.H., Sokolov V., Riemer P.J., Harff N.E., Tsai R., Gutierrez-Aitken A., Gilbert B.K., Daniel E.S. // 2005. International Conference on Indium Phosphide and Related Materials. - Glasgow, Scotland, 8-12 May 2005. - P. 617-620. ↑

C1395. Caddemi A. Artificial neural network-based procedure for cryogenic microwave noise characterization of HEMT's. / Caddemi A., Catalfamo F., Donato N. // 2005. CIMSIA. 2005 IEEE International Conference on Computational Intelligence for Measurement Systems and Applications. 20-22 July 2005. - P. 285-289. ↑

C1396. Suzuki T. A novel 50-Gbit/s NRZ-RZ converter with retiming function using InP HEMT technology. / Suzuki T., Kawano Y., Nakasha Y., Takahashi T., Makiyama K., Hirose T. // 2005. CSIC '05. IEEE Compound Semiconductor Integrated Circuit Symposium. 30 Oct.-2 Nov. 2005. - P. 4 ↑

C1397. Wu Y.-F. Field-plated GaN HEMTs and amplifiers. / Wu Y.-F., Saxler A., Moore M., Wisleder T., Mishra U.K., Parikh P. // 2005. CSIC '05. IEEE Compound Semiconductor Integrated Circuit Symposium. 30 Oct.-2 Nov. 2005. - P. 4 ↑

C1398. Zirath H. MMIC-oscillator designs for ultra low phase noise. / Zirath H., Jacobsson H., Bao M., Ferndahl M., Kozhuharov R. // 2005. CSIC '05. IEEE Compound Semiconductor Integrated Circuit Symposium. 30 Oct.-2 Nov. 2005. - P. 4 ↑

C1399. Mahon S. A family of 1, 2 and 4-watt power amplifier MMICs for cost effective VSAT ground terminals. / Mahon S., Dadello A., Harvey J., Bessemoulin A. // 2005. CSIC '05. IEEE Compound Semiconductor Integrated Circuit Symposium. 30 Oct.-2 Nov. 2005. - P. 4 ↑

C1400. Xu H. High-efficiency class-E power amplifier using field-plated GaN HEMTs. / Xu H., Gao S., Heikman S., Mishra U.K., York R.A. // 2005. CSIC '05. IEEE Compound Semiconductor Integrated Circuit Symposium. 30 Oct.-2 Nov. 2005. - P. 4 ↑

C1401. Kikkawa T. Highly uniform AlGaIn/GaN power HEMT on a 3-inch conductive N-SiC substrate for wireless base station application. / Kikkawa T., Imanishi K., Kanamura M., Joshin K. // 2005. CSIC '05. IEEE Compound Semiconductor Integrated Circuit Symposium. 30 Oct.-2 Nov. 2005. - P. 4 ↑

C1402. Kobayashi K.W. Improved efficiency, IP3-bandwidth and robustness of a microwave Darlington amplifier using 0.5μm ED PHEMT and a new circuit topology. 2005. CSIC '05. IEEE Compound Semiconductor

Integrated Circuit Symposium. 30 Oct.-2 Nov. 2005. - P. 4 ↑

**C1403.** Darwish A.M. Temperature behavior of AlGaIn/GaN on SiC HEMTs. / Darwish A.M., Huebschman B., Del Rosario R., Viveiros E., Hung H.A. // 2005. CSIC '05. IEEE Compound Semiconductor Integrated Circuit Symposium. 30 Oct.-2 Nov. 2005. - P. 4 ↑

**C1404.** Osadchuk V.S. The magnetic controlled autogenerator superhigh frequencies. / Osadchuk V.S., Osadchuk A.V. // 2005 15th International Crimean Conference Microwave & Telecommunication Technology. - Sevastopol, Crimea, 16-16 Sept. 2005. - Vol. 2. - P. 449-450. ↑

**C1405.** Gunnarsson S. A 60 GHz MMIC pHEMT image reject mixer with integrated ultra wideband IF hybrid and 30 dB of image rejection ratio. / Gunnarsson S., Kuylenskierna D., Zirath H. // 2005. APMC 2005. Asia-Pacific Conference Proceedings Microwave Conference Proceedings. 4-7 Dec. 2005. - Vol. 1. - P. 4 ↑

**C1406.** I-Yu Chen. An novel L-shape active leaky-wave antenna with power combining and scanning capability. / I-Yu Chen, Chien-Jen Wang, Jou C.F. // 2005. APMC 2005. Asia-Pacific Conference Proceedings Microwave Conference Proceedings. 4-7 Dec. 2005. - Vol. 1. - P. 4 ↑

**C1407.** Liu Y. Temperature dependence of DC and microwave characteristics of InGaAs/InP composite channel HEMTs. / Liu Y., Wang H., Radhakrishnan K., Ng G.I., Yongzhong Xiong. // 2005. Proceedings. 2005 IEEE International Workshop on Radio-Frequency Integration Technology: Integrated Circuits for Wideband Communication and Wireless Sensor Networks. 30 Nov.-2 Dec. 2005. - P. 207-210. ↑

**C1408.** Afsar M.N. Measurements of Complex Permittivity and Loss Tangent of Silicon Carbide at Millimeter Wavelengths. / Afsar M.N., Shu Chen, Yong Wang, Sakdatorn D. // 2005. IMTC 2005. Proceedings of the IEEE Instrumentation and Measurement Technology Conference. - Ottawa, Ont., 16-19 May 2005. - Vol. 3. - P. 1975-1978. ↑

**C1409.** Ferndahl M. Broadband 7 GHz VCO in mHEMT technology. / Ferndahl M., Zirath H. // 2005. APMC 2005. Asia-Pacific Conference Proceedings Microwave Conference Proceedings. 4-7 Dec. 2005. - Vol. 2. - P. 4 ↑

**C1410.** Huq H.F. Analysis of Temperature Model on Device Characteristics for AlGaIn/GaN MODFET for High Power Electronics. / Huq H.F., Alam M.T., Islam S.K. // 2005 International Semiconductor Device Research Symposium. - Bethesda, MD, 7-9 Dec. 2005. - P. 250-251. ↑

**C1411.** Liu D. 0.25μm In<sub>0.52</sub>Al<sub>0.48</sub>As/In<sub>0.53</sub>Ga<sub>0.47</sub>As/InAs<sub>0.3</sub>P<sub>0.7</sub> composite channel HEMTs with an ft of 115GHz. / Liu D., Hudait M., Lin Y., Kim H., Ringel S.A., Lu W. // 2005. APMC 2005. Asia-Pacific Conference Proceedings Microwave Conference Proceedings. 4-7 Dec. 2005. - Vol. 2. - P. 3 ↑

**C1412.** Sano H. A 1.8-2.3GHz wideband and compact power amplifier module using AlGaIn/GaN HEMTs. / Sano H., Otake K., Tateno Y., Adachi N., Mizuno S., Kawano A., Nikaido J., Sano S. // 2005. APMC 2005. Asia-Pacific Conference Proceedings Microwave Conference Proceedings. 4-7 Dec. 2005. - Vol. 2. - P. 4 ↑

**C1413.** Alum M.T. Analytical Modeling and Simulation of V<sub>sub th</sub> and V<sub>sub tl</sub> of the Delta-Doped MOS-Gate Si/SiGe HEMT. / Alum M.T., Rahman T., Islam S.K., Hasanuzzaman M. // 2005 International Semiconductor Device Research Symposium. - Bethesda, MD, 7-9 Dec. 2005. - P. 336-337. ↑

**C1414.** Hashim A.M. Basic Study of Plasma Wave Interactions in GaAs Interdigital- Gated HEMT Devices from Microwave up to THz Frequencies. / Hashim A.M., Kasai S., Hasegawa H., Hashizume T. // 2005 International Semiconductor Device Research Symposium. - Bethesda, MD, 7-9 Dec. 2005. - P. 450-451. ↑

**C1415.** Faraclas E.W. AlGaIn/GaN HEMTs: Experiment and Simulation of DC Characteristics. / Faraclas E.W., Webster R.T., Anwar A.F.M. // 2005 International Semiconductor Device Research Symposium. - Bethesda, MD, 7-9 Dec. 2005. - P. 252-253. ↑

**C1416.** Yagi S. High Breakdown Voltage AlGaIn/GaN MIS-HEMT with SiN and TiO<sub>2</sub> Gate Insulator. / Yagi S., Shimizu M., Inada M., Yamamoto Y., Guanxi Piao, Yano Y., Okumura H. // 2005 International Semiconductor Device Research Symposium. Dec. 7-9, 2005. - P. 280-281. ↑

**C1417.** Schlechtweg M. Advanced mm-wave ICs and applications. / Schlechtweg M., Tessmann A., Leuther A., Schworer C., Massler H., Mikulla M., Walther M., Riessle M. // 2005. Proceedings. 2005 IEEE International Workshop on Radio-Frequency Integration Technology: Integrated Circuits for Wideband Communication and

Wireless Sensor Networks. 30 Nov.-2 Dec. 2005. - P. 46-49. ↑

**C1418.** Liu Z.H. Microwave noise characteristics of AlGaIn/GaN HEMTs on high-resistivity silicon substrate. / Liu Z.H., Arulkumaran S., Ng G.I., Cheong W.C., Zeng R., Bu J., Wang H., Radhakrishnan K., Tan C.H. // 2005. Proceedings. 2005 IEEE International Workshop on Radio-Frequency Integration Technology: Integrated Circuits for Wideband Communication and Wireless Sensor Networks. 30 Nov.-2 Dec. 2005. - P. 127-130. ↑

**C1419.** Prokopuk N. Development of GaN-based micro chemical sensor nodes. / Prokopuk N., Kyung-Ah Son, George T., Moon J.S. // 2005 IEEE Sensors. - Irvine, CA, Oct. 30 2005-Nov. 3 2005. - P. 4 ↑

**C1420.** Rufer L. SAW chemical sensors based on AlGaIn/GaN piezoelectric material system: acoustic design and packaging considerations. / Rufer L., Torres A., Mir S., Alam M.O., Lalinsky T., Chan Y.C. // 2005. EMAP 2005. International Symposium on Electronics Materials and Packaging. 11-14 Dec. 2005. - P. 204-208. ↑

**C1421.** Marinkovic Z. Bias dependent scalable noise models of MESFETs/HEMTs based on neural networks. / Marinkovic Z., Pronic O., Markovic V., Randelovic J. // 2005. 7th International Conference on Telecommunications in Modern Satellite, Cable and Broadcasting Services. 28-30 Sept. 2005. - Vol. 2. - P. 377-380. ↑

**C1422.** Deh K. Microwave circuit models using the structured genetic algorithm. / Deh K., Prasad S., Colantonio P., Rocco G. // 2005. 7th International Conference on Telecommunications in Modern Satellite, Cable and Broadcasting Services. 28-30 Sept. 2005. - Vol. 2. - P. 367-372. ↑

**C1423.** Jiang N. Stability of preamplifier in 84-116 GHz receiver. / Jiang N., Claude S., Wood I., Niranjana P., Garcia D., Yeung K., Dindo P., Szeto K., Welle P., Rodrigues G., Derald D., Erickson D., Duncan D., Leckie B., Pfleger M. // 2005. IRMMW-THz 2005. The Joint 30th International Conference on Infrared and Millimeter Waves and 13th International Conference on Terahertz Electronics. 19-23 Sept. 2005. - Vol. 1. - P. 205-206. ↑

**C1424.** Ocvetic H. Comparison of Hetero and Mono FET and BT Structures Hrvoje Ocvetic, Tomislav Svedek. / Ocvetic H., Svedek T. // 2005. 7th International Conference on Telecommunications in Modern Satellite, Cable and Broadcasting Services. - Nis, 28-30 Sept. 2005. - Vol. 2. - P. 597-600. ↑

**C1425.** Gusenkova A.V. Selective wet etching process for AlGaAs/InGaAs pHEMT fabrication. / Gusenkova A.V., Maleev N.A., Mikhlin., Zhukov A.E., Vasil'ev A.P., Shulenkova A.S. // 2005 15th International Crimean Conference Microwave & Telecommunication Technology. - Sevastopol, Crimea, 16-16 Sept. 2005. - Vol. 2. - P. 659-660. ↑

**C1426.** Buvaylik E.V. New avalanche breakdown model for nonuniform electric fields. / Buvaylik E.V., Martynov Y.B., Pogorelova E.W. // 2005 15th International Crimean Conference Microwave & Telecommunication Technology. - Sevastopol, Crimea, 16-16 Sept. 2005. - Vol. 2. - P. 478-479. ↑

**C1427.** Sadi T. Thermally self-consistent Monte Carlo simulation of InGaAs/AlGaAs HEMTs. / Sadi T., Kelsall R., Pilgrim N. // 2005 High Frequency Postgraduate Student Colloquium. 5-6 Sept. 2005. - P. 43-46. ↑

**C1428.** {no data available}. The Tenth High Frequency Postgraduate Student Colloquium (IEEE Cat. No. 05TH8848). 2005 High Frequency Postgraduate Student Colloquium. 5-6 Sept. 2005. - {no data available}. ↑

**C1429.** Zhijun Wei. Verification of a generalized nonlinear FET/HEMT modeling through a class A power amplifier design. / Zhijun Wei, Johnson J., Branner G.R. // 2005. 48th Midwest Symposium on Circuits and Systems. - Covington, KY, 7-10 Aug. 2005. - P. 939-942. ↑

**C1430.** Huq H.F. Self-aligned AlGaIn/GaN MODFET with liquid phase deposited oxide gate for microwave power applications. / Huq H.F., Islam S.K. // 2005. 48th Midwest Symposium on Circuits and Systems. - Covington, KY, 7-10 Aug. 2005. - P. 611-614. ↑

**C1431.** Lange M.D. Ultra-low-power HEMT and HBT devices and circuit demonstrations. / Lange M.D., Cavus A., Tsai R.S., Monier C., Deal W.R., Chan B., Cox A.C., Pascua D.G., Sandhu R.S., Hsing R., Poust B.D., Kraus J.L., Nam P.S., Lee L.J., Li D., Gutierrez-Aitken A.L., Noori A.M., Hayashi S.L., Goorsky M.S. // 2005 International Semiconductor Device Research Symposium. - Bethesda, MD, 7-9 Dec. 2005. - P. 145-146. ↑

**C1432.** Krokidis G. A Fully 2-dimensional Poisson-Schrodinger modeling of the HEMT: Effects of short gate lengths. / Krokidis G., Xanthakis J.P., Uzunoglu N. // 2005 International Semiconductor Device Research



Symposium. Dec. 7-9, 2005. - P. 36-37. ↑

**C1433.** Huei Wang. Researches and applications of monolithic millimeter-wave integrated circuits at National Taiwan University. 2005. IRMMW-THz 2005. The Joint 30th International Conference on Infrared and Millimeter Waves and 13th International Conference on Terahertz Electronics. 19-23 Sept. 2005. - Vol. 2. - P. 622-623. ↑

**C1434.** Claude S. The Band 3 receiver (84-116 GHz) for ALMA. / Claude S., Dindo P., Erickson D., Jiang F., Yeung K., Derdall D., Duncan D., Garcia D., Henke D., Leckie B., Lichtenberger A., Niranjana P., Pan S.-K., Pflieger M., Rodrigues G., Szeto K., Welle P., Caputa K. // 2005. IRMMW-THz 2005. The Joint 30th International Conference on Infrared and Millimeter Waves and 13th International Conference on Terahertz Electronics. 19-23 Sept. 2005. - Vol. 2. - P. 407-408. ↑

**C1435.** Ryzhii V. Terahertz Photomixing in Heterostructure Device Based on Integration of High-Electron Mobility Transistor and Quantum-Well Infrared Photodetector. / Ryzhii V., Ryzhii M., Khmyrova I., Otsuji T., Shur M.S. // 2005. MWP 2005. International Topical Meeting on Microwave Photonics. 12-14 Oct. 2005. - P. 347-350. ↑

**C1436.** Jha A.R. High-power GaN-HEMT devices operating at MM-wave frequencies. 2005. IRMMW-THz 2005. The Joint 30th International Conference on Infrared and Millimeter Waves and 13th International Conference on Terahertz Electronics. 19-23 Sept. 2005. - Vol. 2. - P. 640-641. ↑

**C1437.** Kallfass I. One single traveling-wave MMIC for highly linear broadband mixers and variable gain amplifiers. / Kallfass I., Purtova T., Schumacher H., Brokmeier A., Ludwig W. // 2005 IEEE MTT-S International Microwave Symposium Digest. 12-17 June 2005. - P. 4 ↑

**C1438.** Nishikawa K. Low-voltage and broadband V-band InP HEMT frequency doubler MMIC. / Nishikawa K., Toyoda I., Tsunekawa K., Enoki T., Sugitani S. // 2005 IEEE MTT-S International Microwave Symposium Digest. 12-17 June 2005. - P. 4 ↑

**C1439.** Denis D. Design of power FETs based on coupled electro-thermal-electromagnetic modeling. / Denis D., Hunter I.C., Snowden C.M. // 2005 IEEE MTT-S International Microwave Symposium Digest. 12-17 June 2005. - P. 4 ↑

**C1440.** Yeong-Chang Chou. Hot carrier effect on power performance in GaAs PHEMT MMIC power amplifiers. / Yeong-Chang Chou, Grunbacher R., Lai R., Allen B.R., Osgood B., Sharma A., Quin Kan, Leung D., Eng D., Chin P., Block T., Oki A. // 2005 IEEE MTT-S International Microwave Symposium Digest. 12-17 June 2005. - P. 4 ↑

**C1441.** Vinas L.P. Current performance of high speed transistors. / Vinas L.P., Llorens D.B. // 2005 Spanish Conference on Electron Devices. 2-4 Feb. 2005. - P. 111-113. ↑

**C1442.** Tirado J.M. Numerical 2D simulation of surface states effects in AlGaIn/GaN HEMT and GaN MESFET devices. / Tirado J.M., Sanchez de Rojas J.L., Izpura J.I. // 2005. 5th IEEE Conference on Nanotechnology. 11-15 July 2005. - P. 531-532. ↑

**C1443.** Siddiqui M.A. S-band low noise amplifier for TT&C receiver in LEO satellites. 2005. RAST 2005. Proceedings of 2nd International Conference on Recent Advances in Space Technologies. 9-11 June 2005. - P. 426-431. ↑


**C1444.** Vasallo B.G. Influence of kink effect on the dynamic and noise performance of short-channel InAlAs/InGaAs HEMTs. / Vasallo B.G., Mateos J., Pardo D., Gonzalez T. // 2005 Spanish Conference on Electron Devices. 2-4 Feb. 2005. - P. 123-126. ↑


**C1445.** Adachi N. High temperature operation of AlGaIn/GaN HEMT. / Adachi N., Tateno Y., Mizuno S., Kawano A., Nikaido J., Sano S. // 2005 IEEE MTT-S International Microwave Symposium Digest. 12-17 June 2005. - P. 4 ↑


**C1446.** Kamo Y. A C-band AlGaIn/GaN HEMT with Cat-CVD SiN passivation developed for an over 100 W operation. / Kamo Y., Kunii T., Takeuchi H., Yamamoto Y., Totsuka M., Shiga T., Minami H., Kitano T., Miyakuni S., Oku T., Inoue A., Matsuda Y., Ishikawa T., Nanjo T., Chiba H., Suita M., Oishi T., Abe Y., Tsuyama Y., Shirahana R., Ohtsuka H., Iyomasa K., Yamanaka K., Hieda M., Nakayama M., Takagi T., Marumoto K. // 2005 IEEE MTT-S International Microwave Symposium Digest. 12-17 June 2005. - P. 4 ↑


- C1447.** Herrick K.J. W-band metamorphic HEMT with 267 mW output power. / Herrick K.J., Brown K.W., Rose F.A., Whelan C.S., Kotce J., Laroche J.R., Yiwen Zhang. // 2005 IEEE MTT-S International Microwave Symposium Digest. 12-17 June 2005. - P. 4 ↑
- C1448.** Amasuga H. A high power density TaN/Au T-gate pHEMT with high humidity resistance for Ka-Band applications. / Amasuga H., Goto S., Shiga T., Totsuka M., Kunii T., Oku T., Ishikawa T., Matsuda Y. // 2005 IEEE MTT-S International Microwave Symposium Digest. 12-17 June 2005. - P. 4 ↑
- C1449.** Jianjun Gao. Nonlinear HEMT modeling using artificial neural network technique. / Jianjun Gao, Lei Zhang, Jianjun Xu, Qi-jun Zhang. // 2005 IEEE MTT-S International Microwave Symposium Digest. 12-17 June 2005. - P. 4 ↑
- C1450.** Raffo A. Improvement of PHEMT intermodulation prediction through the accurate modelling of low-frequency dispersion effects. / Raffo A., Vannini G., Santarelli A., Traverso P.A., Pagani M., Palomba F., Scappaviva F., Filicori F. // 2005 IEEE MTT-S International Microwave Symposium Digest. 12-17 June 2005. - P. 4 ↑
- C1451.** Vetury R. High power, high efficiency, AlGaIn/GaN HEMT technology for wireless base station applications. / Vetury R., Wei Y., Green D.S., Gibb S.R., Mercier T.W., Leverich K., Garber P.M., Poulton M.J., Shealy J.B. // 2005 IEEE MTT-S International Microwave Symposium Digest. 12-17 June 2005. - P. 4 ↑
- C1452.** Nagy W. 150 W GaN-on-Si RF power transistor. / Nagy W., Singhal S., Borges R., Johnson J.W., Brown J.D., Therrien R., Chaudhari A., Hanson A.W., Riddle J., Booth S., Rajagopal P., Piner E.L., Linthicum K.J. // 2005 IEEE MTT-S International Microwave Symposium Digest. 12-17 June 2005. - P. 4 ↑
- C1453.** Kang-Sung Lee. Sub-50 nm T-gate pseudomorphic HEMTs using low temperature development method. / Kang-Sung Lee, Kyung-Taek Lee, Young-Su Kim, Yoon-Ha Jeong. // 2005. 5th IEEE Conference on Nanotechnology. 11-15 July 2005. - P. 832-835. ↑
- C1454.** Lan E. High power density InGaP PHEMTs for 26 V operation. / Lan E., Green B.M., Li P., Hartin O., Fisher P., Maurer D., Piel P.M., Knappenberger B., Hooper R., de Baca M.C., Miller M., Weitzel C.E. // 2005. Digest of Papers. 2005 IEEE Radio Frequency integrated Circuits (RFIC) Symposium. 12-14 June 2005. - P. 375-378. ↑
- C1455.** Chun San Chu. A novel RF high-Q metal-semiconductor-metal planar inter-digitated varactor based on double-channel AlGaIn/GaN HEMT structure. / Chun San Chu, Yugang Zhou, Chen K.J., Kei May Lau. // 2005. Digest of Papers. 2005 IEEE Radio Frequency integrated Circuits (RFIC) Symposium. 12-14 June 2005. - P. 385-388. ↑
- C1456.** Ueda H. High current operation of GaN power HEMT. / Ueda H., Sugimoto M., Uesugi T., Fujishima O., Kachi T. // 2005. Proceedings. ISPSD '05. The 17th International Symposium on Power Semiconductor Devices and ICs. 23-26 May 2005. - P. 311-314. ↑
- C1457.** Ping Wing Lai. A 5 GHz pHEMT transformer-coupled VCO. / Ping Wing Lai, Long S.I. // 2005. Digest of Papers. 2005 IEEE Radio Frequency integrated Circuits (RFIC) Symposium. 12-14 June 2005. - P. 135-138. ↑
- C1458.** Meneghesso G. Hot-electron-stress degradation in unpassivated GaN/AlGaIn/GaN HEMTs on SiC. / Meneghesso G., Pierobon R., Rampazzo F., Tamiazzo G., Zanoni E., Bernat J., Kordos P., Basile A.F., Chim A., Verzellesi G. // 2005. Proceedings. 43rd Annual. 2005 IEEE International Reliability Physics Symposium. April 17-21, 2005. - P. 415-422. ↑
- C1459.** Chou Y.C. Hot carrier reliability in GaAs PHEMT MMIC power amplifiers. / Chou Y.C., Gmundbacher R., Lai R., Li G.P., Kan Q., Yu M., Callejo L., Leung D., Eng D., Block T., Oki A. // 2005. Proceedings. 43rd Annual. 2005 IEEE International Reliability Physics Symposium. April 17-21, 2005. - P. 590-591. ↑
- C1460.** Yasuda E. An ultra-low distortion 3P2T antenna switch MMIC for dual-band W-CDMA applications. / Yasuda E., Hidaka K., Nakatsuka T., Watanabe A., Tara K. // 2005. Digest of Papers. 2005 IEEE Radio Frequency integrated Circuits (RFIC) Symposium. 12-14 June 2005. - P. 455-458. ↑
- C1461.** Kohama K. An antenna switch MMIC for GSM/UMTS handsets using E/D-mode JPHEMT technology. / Kohama K., Nakamura M., Onodera K., Wada S., Tamari S., Mizunuma Y. // 2005. Digest of Papers. 2005 IEEE ↑


Radio Frequency integrated Circuits (RFIC) Symposium. 12-14 June 2005. - P. 509-512. 


**C1462.** Bosch W. Low cost X-band power amplifier MMIC fabricated on a 0.25  $\mu\text{m}$  GaAs pHEMT process. / Bosch W., Mayock J.G.E., O'Keefe M.F., McMonagle J. // 2005 IEEE International Radar Conference. 9-12 May 2005. - P. 22-26. 


**C1463.** Tan S.G. Single spin-FET for programmable logic gates. / Tan S.G., Jalil M.B.A., Kumar B., Teo K.L., Liew T., Chong T.C. // 2005. INTERMAG Asia 2005. Digests of the IEEE International Magnetics Conference. 4-8 April 2005. - P. 1209-1210. 


**C1464.** Eguchi K. A design of 10-GHz delta-sigma modulator using a 4-level differential resonant-tunneling quantizer. / Eguchi K., Chibashi M., Waho T. // 2005. Proceedings. 35th International Symposium on Multiple-Valued Logic. 19-21 May 2005. - P. 43-47. 


**C1465.** Patro S.K. On the design and performance of a balanced-cascade LNA for FDD-WCDMA direct-conversion node-B RF receiver. 2005. ICPWC 2005. 2005 IEEE International Conference on Personal Wireless Communications. 23-25 Jan. 2005. - P. 339-342. 


**C1466.** Xinzhong Duo. A concurrent multi-band LNA for multi-standard radios. / Xinzhong Duo, Li-Rong Zheng, Ismail M., Tenhunen H. // 2005. ISCAS 2005. IEEE International Symposium on Circuits and Systems. 23-26 May 2005. - P. 3982-3985. 


**C1467.** Edenhofer P. Active frequency selective surfaces for antenna applications electronically to control phase distribution and reflective/transmissive amplification. / Edenhofer P., Alpaslan A. // 2005. IEEE/ACES International Conference on Wireless Communications and Applied Computational Electromagnetics. 3-7 April 2005. - P. 237-240. 


**C1468.** Muramatsu N. A novel oscillation circuit using a resonant-tunneling diode. / Muramatsu N., Okazaki H., Waho T. // 2005. ISCAS 2005. IEEE International Symposium on Circuits and Systems. 23-26 May 2005. - P. 2341-2344. 


**C1469.** Palumbo G. Optimized design of source coupled logic gates in GaAs HEMT technology. / Palumbo G., Tommasino P., Trifiletti A. // 2005. ISCAS 2005. IEEE International Symposium on Circuits and Systems. 23-26 May 2005. - P. 3583-3586. 


**C1470.** Hyung Sup Yoon. Extremely low noise characteristics of 0.1  $\mu\text{m}$   $\Gamma$ -gate power metamorphic HEMT on GaAs substrate. / Hyung Sup Yoon, Jin Hee Lee, Jae Yeob Shim, Ju Yeon Hong, Dong Min Kang, Kyung Ho Lee. // 2005. International Conference on Indium Phosphide and Related Materials. 8-12 May 2005. - P. 133-136. 

**C1471.** Leuther A. Metamorphic 50 nm InAs-channel HEMT. / Leuther A., Weber R., Dammann M., Schlechtweg M., Mikulla M., Walther M., Weimann G. // 2005. International Conference on Indium Phosphide and Related Materials. 8-12 May 2005. - P. 129-132. 

**C1472.** Elgaid K. Low noise high performance 50nm T-gate metamorphic HEMT with cut-off frequency  $f_T$  of 440 GHz for millimeterwave imaging receivers applications. / Elgaid K., Moran D., McLelland H., Holland M., Thayne I.G. // 2005. International Conference on Indium Phosphide and Related Materials. 8-12 May 2005. - P. 141-143. 

**C1473.** Medjdoub F. Power potentiality at 94 GHz of InP HEMTs with large band gap channels. / Medjdoub F., Zaknoute M., Wallart X., Theron D. // 2005. International Conference on Indium Phosphide and Related Materials. 8-12 May 2005. - P. 137-140. 

**C1474.** Dong Min Kang. A 77GHz automotive radar MMIC chip set fabricated by a 0.15  $\mu\text{m}$  MHEMT technology. / Dong Min Kang, Ju Yeon Hong, Jae Yeob Shim, Jin Hee Lee, Hyung Sup Yoon, Kyung Ho Lee. // 2005 IEEE MTT-S International Microwave Symposium Digest. 12-17 June 2005. - P. 4 

**C1475.** Chow Y.H. A miniature dual-band low-noise amplifier module for IEEE 802.11 b/g/a WLAN applications. / Chow Y.H., Chong T., Hasan Z., Loh C.C., Tan T.L., Chew E.C. // 2005 IEEE MTT-S International Microwave Symposium Digest. 12-17 June 2005. - P. 4 

**C1476.** Grahn J. InGaAs-InAlAs-InP HEMT technology for ultra-high frequency and ultra-low noise

performance. / Grahn J., Starski P., Malmkvist M., Fridman M., Malmros A., Wang S., Mellberg A., Zirath H. // 2005. International Conference on Indium Phosphide and Related Materials. 8-12 May 2005. - P. 124-128. ↑

**C1477.** Wolf G. A metamorphic GaAs HEMT distributed amplifier with 50 GHz bandwidth and low noise for 40 Gbits/s. / Wolf G., Happy H., Demichel S., Leblanc R., Blache F., Lefevre R., Dambrine G. // 2005 IEEE MTT-S International Microwave Symposium Digest. 12-17 June 2005. - P. 3 ↑

**C1478.** Elgaid K. Low noise W-band MMIC amplifier using 50nm InP technology for millimeterwave receivers applications. / Elgaid K., McLelland H., Stanley C.R., Thayne I.G. // 2005. International Conference on Indium Phosphide and Related Materials. - Glasgow, Scotland, 8-12 May 2005. - P. 523-525. ↑

**C1479.** Yuwei Liu. Microwave noise characteristics of InP-based high electron mobility transistors with InGaAs channel and InGaAs/InP composite channel: a comparative study. / Yuwei Liu, Hong Wang, Rong Zeng. // 2005. International Conference on Indium Phosphide and Related Materials. - Glasgow, Scotland, 8-12 May 2005. - P. 437-439. ↑

**C1480.** Nakajima S. Compound semiconductor IC's. 2005. International Conference on Indium Phosphide and Related Materials. - Glasgow, Scotland, 8-12 May 2005. - P. 603-608. ↑

**C1481.** Lai R. Production InP MMICs for low cost, high performance applications. / Lai R., Grundbacher R., Sawdai D., Uyeda J., Biedenbender M., Barsky M., Gutierrez-Aitken A., Cavus A., Chin P., Liu P.H., Bhorania R., Streit D., Oki A. // 2005. International Conference on Indium Phosphide and Related Materials. - Glasgow, Scotland, 8-12 May 2005. - P. 598-602. ↑

**C1482.** Vasallo B.G. Kink effect in InAlAs/InGaAs short-channel HEMTs: influence on the dynamic and noise performance. / Vasallo B.G., Mateos J., Pardo D., Gonzalez T. // 2005. International Conference on Indium Phosphide and Related Materials. 8-12 May 2005. - P. 188-191. ↑

**C1483.** Grundbacher R. 0.1µm InGaAs/InAlAs/InP HEMT low noise amplifiers with compact stacked cascode design and its de-bias effect induced failure (DBIF). / Grundbacher R., Chou Y.C., Raja R., Lai R., Leung D., Kan Q., Schreyer G., Zell G., Eng D., Liu P.H., Block T., Oki A. // 2005. International Conference on Indium Phosphide and Related Materials. 8-12 May 2005. - P. 181-184. ↑

**C1484.** Chou Y.C. Degradation mechanism and reliability improvement of InGaAs/InAlAs/InP HEMTs using new gate metal electrode technology. / Chou Y.C., Grundbacher R., Leung D., Lai R., Kan Q., Eng D., Liu P.H., Block T., Oki A. // 2005. International Conference on Indium Phosphide and Related Materials. 8-12 May 2005. - P. 223-226. ↑

**C1485.** Borg M. Vertical scaling of gate-to-channel distance for a 70 nm InP pseudomorphic HEMT technology. / Borg M., Grahn J., Wang S., Mellberg A., Zirath H. // 2005. International Conference on Indium Phosphide and Related Materials. 8-12 May 2005. - P. 204-207. ↑

**C1486.** Kamitsuna H. A miniaturized wideband 4x4 switch matrix IC using four InP-HEMT SP4T switches. / Kamitsuna H., Yamane Y., Tokumitsu M., Sugahara H., Muraguchi M. // 2005 IEEE MTT-S International Microwave Symposium Digest. 12-17 June 2005. - P. 4 ↑

**C1487.** Noda M. A 20 GHz MOD-made BST thin film tunable phase shifter for phase adjustment of digital 360-degree PHEMT phase shifter. / Noda M., Sasaki Y., Popovici D., Okuyama M., Komaru M. // 2005 IEEE MTT-S International Microwave Symposium Digest. 12-17 June 2005. - P. 4 ↑

**C1488.** Andersson K. A general procedure for extraction of bias dependent dynamic self heating model parameters. / Andersson K., Fager C., Pedro J.C. // 2005 IEEE MTT-S International Microwave Symposium Digest. 12-17 June 2005. - P. 4 ↑

**C1489.** Kim-Lien Ngo-Wah. A V-band eight-way combined solid-state power amplifier with 12.8 Watt output power. / Kim-Lien Ngo-Wah, Goel J., Yeong-Chang Chou, Grundbacher R., Lai R., Nassour G., Divish E., Schreyer G., Whitney K., Oki A. // 2005 IEEE MTT-S International Microwave Symposium Digest. 12-17 June 2005. - P. 4 ↑

**C1490.** Hongtao Xu. High power GaN oscillators using field-plated HEMT structure. / Hongtao Xu, Sanabria C., Heikman S., Keller S., Mishra U.K., York R.A. // 2005 IEEE MTT-S International Microwave Symposium Digest. 12-17 June 2005. - P. 4 ↑



- C1491.** Hacker J.B. An ultra-low power InAs/AlSb HEMT W-band low-noise amplifier. / Hacker J.B., Bergman J., Nagy G., Sullivan G., Kadow C., Lin H.-K., Gossard A.C., Rodwell M., Brar B. // 2005 IEEE MTT-S International Microwave Symposium Digest. 12-17 June 2005. - P. 4 ↑
- C1492.** Sangsub Song. The flip-chip mounted MMIC technology using the modified MCM-D substrate for compact and low-cost W-band transceiver. / Sangsub Song, Sungwon Kim, Sungjin Yeon, Sangho Park, Ju-Yong Lee, Sanghyo Lee, Wooyeol Choi, Youngwoo Kwon, Kwang-Seok Seo. // 2005 IEEE MTT-S International Microwave Symposium Digest. 12-17 June 2005. - P. 4 ↑
- C1493.** Wei C.-J. Large-signal PHEMT switch model, which accurately predicts harmonics and two-tone inter-modulation distortion. / Wei C.-J., Klimashov A., Zhu Y., Lawrence E., Tkachenko G. // 2005 IEEE MTT-S International Microwave Symposium Digest. 12-17 June 2005. - P. 4 ↑
- C1494.** Kettle D. A lattice matched InP chip set for a Ka band radiometer. / Kettle D., Roddis N., Sloan R. // 2005 IEEE MTT-S International Microwave Symposium Digest. 12-17 June 2005. - P. 4 ↑
- C1495.** Gunnarsson S.E. A 60 GHz MMIC dual-quadrature mixer in pHEMT technology for ultra wideband IF signals and high LO to RF isolation. / Gunnarsson S.E., Zirath H. // 2005 IEEE MTT-S International Microwave Symposium Digest. 12-17 June 2005. - P. 4 ↑
- C1496.** Samoska L. Medium power amplifiers covering 90-130 GHz for the ALMA telescope local oscillators. / Samoska L., Bryerton E., Morgan M., Thacker D., Saini K., Boyd T., Pukala D., Peralta A., Hu M., Schmitz A. // 2005 IEEE MTT-S International Microwave Symposium Digest. 12-17 June 2005. - P. 4 ↑
- C1497.** Ryu K.K. MMIC HEMT switch for switch matrix of satellite communication system. / Ryu K.K., Shin D.H., Yom I.B., Lee M.Q., Park J.H., Lee S.P. // 2005 IEEE MTT-S International Microwave Symposium Digest. 12-17 June 2005. - P. 4 ↑
- C1498.** Gunyan D.B. Double-balanced, hybrid mixer with multi-decade bandwidth. 2005 IEEE MTT-S International Microwave Symposium Digest. 12-17 June 2005. - P. 4 ↑
- C1499.** Crespo-Cadenas C. Phase characterization of two-tone intermodulation distortion. / Crespo-Cadenas C., Reina-Tosina J., Madero-Ayora M.J. // 2005 IEEE MTT-S International Microwave Symposium Digest. 12-17 June 2005. - P. 4 ↑
- C1500.** Jarndal A. A new small signal model parameter extraction method applied to GaN devices. / Jarndal A., Kompa G. // 2005 IEEE MTT-S International Microwave Symposium Digest. 12-17 June 2005. - P. 4 ↑
- C1501.** Tessmann A. Metamorphic 94 GHz power amplifier MMICs. / Tessmann A., Leuther A., Schwoerer C., Massler H. // 2005 IEEE MTT-S International Microwave Symposium Digest. 12-17 June 2005. - P. 4 ↑
- C1502.** Jeng-Han Tsai. A 44-GHz high-linearity MMIC medium power amplifier with a low-loss built-in linearizer. / Jeng-Han Tsai, Hong-Yeh Chang, Pei-Si Wu, Tian-Wei Huang, Huei Wang. // 2005 IEEE MTT-S International Microwave Symposium Digest. 12-17 June 2005. - P. 4 ↑
- C1503.** Ziqiang Yang. The design of a Ka-band two-stage monolithic low noise amplifier. / Ziqiang Yang, Tao Yang, Jun Xie, Ruimin Xu. // 2005. APMC 2005. Asia-Pacific Conference Proceedings Microwave Conference Proceedings. 4-7 Dec. 2005. - Vol. 2. - P. 3 ↑
- C1504.** Seong-Sik Myoung. Low noise and high linearity LNA based on InGaP/GaAs HBT for 5.3 GHz WLAN. / Seong-Sik Myoung, Sang-Hoon Cheon, Jong-Gwan Yook. // 2005. EGAAS 2005. European Gallium Arsenide and Other Semiconductor Application Symposium. - Paris, 3-4 Oct. 2005. - P. 89-92. ↑
- C1505.** Wolf G. A metamorphic GaAs HEMT distributed amplifier with 50 GHz bandwidth and low noise for 40 Gbits/s optical receivers. / Wolf G., Demichel S., Leblanc R., Blache F., Lefevre R., Dambrine G., Happy H. // 2005. EGAAS 2005. European Gallium Arsenide and Other Semiconductor Application Symposium. - Paris, 3-4 Oct. 2005. - P. 93-95. ↑
- C1506.** Shohat J. High efficiency 10 Gb/s optical modulator driver amplifier using a power pHEMT technology. / Shohat J., Robertson I.D., Nightingale S.J. // 2005. EGAAS 2005. European Gallium Arsenide and Other Semiconductor Application Symposium. - Paris, 3-4 Oct. 2005. - P. 129-132. ↑

- C1507.** Bessemoulin A. High gain 110-GHz low noise amplifier MMICs using 120-nm metamorphic HEMTs and coplanar waveguides. / Bessemoulin A., Fellon P., Gruenenpuett J., Massler H., Reinert W., Kohn E., Tessmann A. // 2005. EGAAS 2005. European Gallium Arsenide and Other Semiconductor Application Symposium. - Paris, 3-4 Oct. 2005. - P. 77-80. ↑
- C1508.** de Hek A.P. A cost-effective 10 Watt X-band high power amplifier and 1 Watt driver amplifier chip-set. / de Hek A.P., van der Bent G., van Wanum M., van Vliet F.E. // 2005. EGAAS 2005. European Gallium Arsenide and Other Semiconductor Application Symposium. - Paris, 3-4 Oct. 2005. - P. 37-40. ↑
- C1509.** Bessemoulin A. Compact and broadband microstrip power amplifier MMIC with 400-mW output power using 0.15- $\mu\text{m}$  GaAs PHEMTs. / Bessemoulin A., Mahon S., Dadello A., McCulloch G., Harvey J. // 2005. EGAAS 2005. European Gallium Arsenide and Other Semiconductor Application Symposium. - Paris, 3-4 Oct. 2005. - P. 41-44. ↑
- C1510.** Colantonio P. Investigation of IMD asymmetry in microwave FETs via Volterra series. / Colantonio P., Giannini F., Limiti E., Nanni A. // 2005. EGAAS 2005. European Gallium Arsenide and Other Semiconductor Application Symposium. - Paris, 3-4 Oct. 2005. - P. 53-56. ↑
- C1511.** Malmkvist M. A W-band MMIC amplifier using 70-nm gate length InP HEMT technology. / Malmkvist M., Mellberg A., Grahn J. // 2005. EGAAS 2005. European Gallium Arsenide and Other Semiconductor Application Symposium. - Paris, 3-4 Oct. 2005. - P. 165-168. ↑
- C1512.** Yamanaka K. S and C band over 100 W GaN HEMT 1-chip high power amplifiers with cell division configuration. / Yamanaka K., Iyomasa K., Ohtsuka H., Nakayama M., Tsuyama Y., Kunii T., Kamo Y., Takagi T. // 2005. EGAAS 2005. European Gallium Arsenide and Other Semiconductor Application Symposium. - Paris, 3-4 Oct. 2005. - P. 241-244. ↑
- C1513.** Karnfelt C. A high purity 60 GHz-band single chip /spl times/8 multiplier with low phase noise. / Karnfelt C., Kozhuharov R., Zirath H. // 2005. EGAAS 2005. European Gallium Arsenide and Other Semiconductor Application Symposium. - Paris, 3-4 Oct. 2005. - P. 253-256. ↑
- C1514.** Maas A.P.M. A low-noise X-band microstrip VCO with 2.5 GHz tuning range using a GaN-on-SiC p-HEMT. / Maas A.P.M., van Vliet F.E. // 2005. EGAAS 2005. European Gallium Arsenide and Other Semiconductor Application Symposium. - Paris, 3-4 Oct. 2005. - P. 257-260. ↑
- C1515.** van Heijningen M. Ka-band AlGaIn/GaN HEMT high power and driver amplifier MMICs. / van Heijningen M., van Vliet F.E., Quay R., van Raay F., Kiefer R., Muller S., Krausse D., Seelmann-Eggebert M., Mikulla M., Schlechtweg M. // 2005. EGAAS 2005. European Gallium Arsenide and Other Semiconductor Application Symposium. - Paris, 3-4 Oct. 2005. - P. 237-240. ↑
- C1516.** Sanghyun Seo. A wideband balanced AlGaIn/GaN HEMT MMIC low noise amplifier for transceiver front-ends. / Sanghyun Seo, Pavlidis D., Jeong-Sun Moon. // 2005. EGAAS 2005. European Gallium Arsenide and Other Semiconductor Application Symposium. - Paris, 3-4 Oct. 2005. - P. 225-228. ↑
- C1517.** De Jaeger J.C. Noise assessment of AlGaIn/GaN HEMTs on Si or SiC substrates: application to X-band low noise amplifiers. / De Jaeger J.C., Delage S.L., Dambrine G., Di Forte Poisson M.A., Hoel V., Lepilliet S., Grimbert B., Morvan E., Mancuso Y., Gauthier G., Lefrancois A., Cordier Y. // 2005. EGAAS 2005. European Gallium Arsenide and Other Semiconductor Application Symposium. - Paris, 3-4 Oct. 2005. - P. 229-232. ↑
- C1518.** van Raay F. A microstrip X-band AlGaIn/GaN power amplifier MMIC on s.i. SiC substrate. / van Raay F., Quay R., Kiefer R., Fehrenbach W., Bronner W., Kuri M., Benkhelifa F., Massler H., Muller S., Mikulla M., Schlechtweg M., Weimann G. // 2005. EGAAS 2005. European Gallium Arsenide and Other Semiconductor Application Symposium. - Paris, 3-4 Oct. 2005. - P. 233-236. ↑
- C1519.** Masud M.A. A 45 dB variable gain low noise MMIC amplifier. / Masud M.A., Zirath H., Kelly M. // 2005 European Microwave Conference. 4-6 Oct. 2005. - Vol. 3. - P. 4 ↑
- C1520.** Colantonio P. A C-band high efficiency second harmonic tuned hybrid power amplifier in GaN technology. / Colantonio P., Giannini F., Giofre R., Limiti E., Serino A., Peroni M., Romanini P., Proietti C. // 2005 European Microwave Conference. 4-6 Oct. 2005. - Vol. 3. - P. 4 ↑
- C1521.** Florian C. A Ku band monolithic power amplifier for TT&C applications. / Florian C., Cignani R., Vannini

G., Comparini M.C. // 2005 European Microwave Conference. 4-6 Oct. 2005. - Vol. 3. - P. 4 ↑

**C1522.** De Meyer S. Modeling of a 4-18GHz 6W flip-chip integrated power amplifier based on GaN HEMTs technology. / De Meyer S., Philippon A., Campovecchio M., Charbonniaud C., Piotrowicz S., Floriot D., Quere R. // 2005 European Microwave Conference. 4-6 Oct. 2005. - Vol. 3. - P. 4 ↑

**C1523.** Krozer V. Wideband monolithic microwave integrated circuit frequency converters with GaAs mHEMT technology. / Krozer V., Johansen T.K., Djurhuus T., Vidkjaer J. // 2005 European Microwave Conference. 4-6 Oct. 2005. - Vol. 3. - P. 4 ↑

**C1524.** Wiegner D. Multistage broadband amplifiers based on GaN HEMT technology for 3G/4G base station applications with extremely high bandwidth. / Wiegner D., Merk T., Seyfried U., Tempi W., Merk S., Quay R., van Raay F., Walcher H., Massler H., Seelmann-Eggebert M., Reiner R., Moritz R., Kiefer R. // 2005 European Microwave Conference. 4-6 Oct. 2005. - Vol. 3. - P. 4 ↑

**C1525.** Bunz B. Influence of envelope impedance termination on RF behaviour of GaN HEMT power devices. / Bunz B., Ahmed A., Kompa G. // 2005 European Microwave Conference. 4-6 Oct. 2005. - Vol. 3. - P. 4 ↑

**C1526.** Kholdoun Torki. CMP service for prototyping and low volume production. / Kholdoun Torki, Bernard Courtois. // 2005. ASICON 2005. 6th International Conference On ASIC. - Shanghai, 24-30 Oct. 2005. - Vol. 2. - P. 1073-1076. ↑

**C1527.** {no data available}. Title page. 2005. EGAAS 2005. European Gallium Arsenide and Other Semiconductor Application Symposium. - Paris, 3-4 Oct. 2005. - P. i. ↑

**C1528.** Geok Ing Ng. Are we there yet?-a metamorphic HEMT and HBT perspective. / Geok Ing Ng, Radhakrishnan K., Hong Wang. // 2005. EGAAS 2005. European Gallium Arsenide and Other Semiconductor Application Symposium. - Paris, 3-4 Oct. 2005. - P. 13-19. ↑

**C1529.** Mishra U.K. Status of AlGaIn/GaN HEMT technology-a UCSB perspective. 2005. EGAAS 2005. European Gallium Arsenide and Other Semiconductor Application Symposium. - Paris, 3-4 Oct. 2005. - P. 21-27. ↑

**C1530.** Lijun Xue. Numerical Simulation of Al<sub>x</sub>Ga<sub>1-x</sub>N/AlN/GaN HEMT. / Lijun Xue, Yan Wang, Ming Liu, Changqing Xie, Chengzhan Li, Zhijing He, Yang Xia. // 2005 IEEE Conference on Electron Devices and Solid-State Circuits. 19-21 Dec. 2005. - P. 799-802. ↑

**C1531.** Nagatsuma T. Sub-Terahertz Wireless Communications Technologies. / Nagatsuma T., Hirata A., Sato Y., Yamaguchi R., Takahashi H., Kosugi T., Tokumitsu M., Sugahara H., Furuta T., Ito H. // 2005. ICECom 2005. 18th International Conference on Applied Electromagnetics and Communications. - Dubrovnik, 12-14 Oct. 2005. - P. 1-4. ↑

**C1532.** Keshavarzi M.R. Investigation of the Transmission Line Loss on the Performance of the HBT\_HEMT Matrix Amplifier. / Keshavarzi M.R., Abdipour A., Mohammadi A., Moradi G. // 2005. ICECom 2005. 18th International Conference on Applied Electromagnetics and Communications. - Dubrovnik, 12-14 Oct. 2005. - P. 1-4. ↑

**C1533.** Wolf G. A metamorphic GaAs HEMT-distributed amplifier with 50 GHz bandwidth and low noise for 40 Gbits/s photoreceiver. / Wolf G., Happy H., Demichel S., Leblanc R., Blache F., Lefevre R., Dambrine G. // 2005. MAPE 2005. IEEE International Symposium on Microwave, Antenna, Propagation and EMC Technologies for Wireless Communications. - Beijing, 8-12 Aug. 2005. - Vol. 1. - P. 27-29. ↑

**C1534.** Manan V. A dual band (10/16 GHz) p-HEMT VCO. / Manan V., Long S.I. // 2005. EGAAS 2005. European Gallium Arsenide and Other Semiconductor Application Symposium. - Paris, 3-4 Oct. 2005. - P. 261-264. ↑

**C1535.** Maekawa A. A 100 W high-efficiency GaN HEMT amplifier for S-band wireless system. / Maekawa A., Nagahara M., Yamamoto T., Sano S. // 2005. EGAAS 2005. European Gallium Arsenide and Other Semiconductor Application Symposium. - Paris, 3-4 Oct. 2005. - P. 497-500. ↑

**C1536.** Bhatnagar M. A low cost SMT integrated frequency doubler and power amplifier for 30 GHz DBS uplink applications. / Bhatnagar M., Morkner H. // 2005. EGAAS 2005. European Gallium Arsenide and Other

Semiconductor Application Symposium. - Paris, 3-4 Oct. 2005. - P. 561-564. ↑

**C1537.** Schworer C. A 150 to 220 GHz balanced doubler MMIC using a 50 nm metamorphic HEMT technology. / Schworer C., Roca Y.C., Leuther A., Tessmann A., Seelmann-Eggebert M., Massler H., Schlechtweg M., Weimann G. // 2005. EGAAS 2005. European Gallium Arsenide and Other Semiconductor Application Symposium. - Paris, 3-4 Oct. 2005. - P. 565-568. ↑

**C1538.** Maas A.P.M. 60 GHz GaAs MMIC mixers with integrated LO buffer. / Maas A.P.M., Hoogland J.A. // 2005. EGAAS 2005. European Gallium Arsenide and Other Semiconductor Application Symposium. - Paris, 3-4 Oct. 2005. - P. 465-468. ↑

**C1539.** Florian C. A V band singly balanced diode mixer for space application. / Florian C., Scappaviva F., Feudale M., Monaco V.A., Filicori F. // 2005. EGAAS 2005. European Gallium Arsenide and Other Semiconductor Application Symposium. - Paris, 3-4 Oct. 2005. - P. 441-444. ↑

**C1540.** Martin-Guerrero T.M. Frequency domain-based extraction method of one-port device's non-linear state functions from large-signal measurements. / Martin-Guerrero T.M., Camacho-Penalosa C. // 2005. EGAAS 2005. European Gallium Arsenide and Other Semiconductor Application Symposium. - Paris, 3-4 Oct. 2005. - P. 449-452. ↑

**C1541.** Zamanillo J.M. A realistic large-signal microwave PHEMT transistors model for SPICE. / Zamanillo J.M., Ingelmo H., Perez-Vega C., Mediavilla A. // 2005. EGAAS 2005. European Gallium Arsenide and Other Semiconductor Application Symposium. - Paris, 3-4 Oct. 2005. - P. 453-456. ↑

**C1542.** Daoud S.M. A novel wideband MMIC voltage controlled attenuator with a bandpass filter topology. / Daoud S.M., Shastry P.N. // 2005. EGAAS 2005. European Gallium Arsenide and Other Semiconductor Application Symposium. - Paris, 3-4 Oct. 2005. - P. 629-632. ↑

**C1543.** De Meyer S. Modelling of a 4-18 GHz 6 W flip-chip integrated power amplifier based on GaN HEMTs technology. / De Meyer S., Philippon A., Campovecchio M., Charbonniaud C., Piotrowicz S., Floriot D., Quere R. // 2005. EGAAS 2005. European Gallium Arsenide and Other Semiconductor Application Symposium. - Paris, 3-4 Oct. 2005. - P. 657-660. ↑

**C1544.** Masud M.A. A 45 dB variable gain low noise MMIC amplifier. / Masud M.A., Zirath H., Kelly M. // 2005. EGAAS 2005. European Gallium Arsenide and Other Semiconductor Application Symposium. - Paris, 3-4 Oct. 2005. - P. 669-672. ↑

**C1545.** Florian C. A Ku band monolithic power amplifier for TT&C applications. / Florian C., Cignani R., Vannini G., Comparini M.C. // 2005. EGAAS 2005. European Gallium Arsenide and Other Semiconductor Application Symposium. - Paris, 3-4 Oct. 2005. - P. 677-680. ↑

**C1546.** Bunz B. Influence of envelope impedance termination on RF behaviour of GaN HEMT power devices. / Bunz B., Ahmed A., Kompa G. // 2005. EGAAS 2005. European Gallium Arsenide and Other Semiconductor Application Symposium. - Paris, 3-4 Oct. 2005. - P. 649-652. ↑

**C1547.** Jin-Cheol Jeong. GaAs MMICs for use in upconverter module for Ka-band OBS satellite transponders. / Jin-Cheol Jeong, Dong-Pil Chang, Dong-hwan Shin, In-Bok Yom. // 2005. EGAAS 2005. European Gallium Arsenide and Other Semiconductor Application Symposium. - Paris, 3-4 Oct. 2005. - P. 633-636. ↑

**C1548.** Krozer V. Wideband monolithic microwave integrated circuit frequency converters with GaAs mHEMT technology. / Krozer V., Johansen T.K., Djurhuus T., Vidjaer J. // 2005. EGAAS 2005. European Gallium Arsenide and Other Semiconductor Application Symposium. - Paris, 3-4 Oct. 2005. - P. 637-640. ↑

**C1549.** Wiegner D. Multistage broadband amplifiers based on GaN HEMT technology for 3G/4G base station applications with extremely high bandwidth. / Wiegner D., Merk T., Seyfried U., Tempi W., Merk S., Quay R., van Raay F., Walcher H., Massler H., Seelmann-Eggebert M., Reiner R., Moritz R., Kiefer R. // 2005. EGAAS 2005. European Gallium Arsenide and Other Semiconductor Application Symposium. - Paris, 3-4 Oct. 2005. - P. 641-644. ↑

**C1550.** Hafele M. A GaAs distributed amplifier with an output voltage of 8.5 V/sub PP/ for 40 Gb/s modulators. / Hafele M., Trasser A., Beilenhoff K., Schumacher H. // 2005. EGAAS 2005. European Gallium Arsenide and Other Semiconductor Application Symposium. - Paris, 3-4 Oct. 2005. - P. 345-348. ↑



- C1551.** Pei-Si Wu. A millimeter-wave ultra-compact broadband diode mixer using modified Marchand balun. / Pei-Si Wu, Chin-Shen Lin, Tian-Wei Huang, Huei Wang, Yu-Chi Wang, Chan-Shin Wu. // 2005. EGAAS 2005. European Gallium Arsenide and Other Semiconductor Application Symposium. - Paris, 3-4 Oct. 2005. - P. 349-352. ↑
- C1552.** Krishnamurthy L. A comparative study of active and passive GaAs microwave couplers. / Krishnamurthy L., Sun Q., Vo V.T., Parkinson G., Paul D.K., Williams K., Rezazadeh A.A. // 2005. EGAAS 2005. European Gallium Arsenide and Other Semiconductor Application Symposium. - Paris, 3-4 Oct. 2005. - P. 353-356. ↑
- C1553.** Holm M.A. Advanced meander gate p-HEMT model for accurate harmonic modeling of switch MMIC designs. / Holm M.A., Brookbanks D.M. // 2005. EGAAS 2005. European Gallium Arsenide and Other Semiconductor Application Symposium. - Paris, 3-4 Oct. 2005. - P. 317-320. ↑
- C1554.** Pavlidis D. AlGaIn/GaN high electron mobility transistor (HEMT) reliability. / Pavlidis D., Valizadeh P., Hsu S.H. // 2005. EGAAS 2005. European Gallium Arsenide and Other Semiconductor Application Symposium. - Paris, 3-4 Oct. 2005. - P. 265-268. ↑
- C1555.** Tartarin J.-G. Low frequency and linear high frequency noise performances of AlGaIn/GaN grown on SiC substrate. / Tartarin J.-G., Soubercaze-Pun G., Bary L., Chambon C., Gribaldo S., Llopis O., Escotte L., Plana R., Delage S., Gaquiere C., Graffeul J. // 2005. EGAAS 2005. European Gallium Arsenide and Other Semiconductor Application Symposium. - Paris, 3-4 Oct. 2005. - P. 277-280. ↑
- C1556.** Angelov I. On the large-signal modelling of AlGaIn/GaN HEMTs and SiC MESFETs. / Angelov I., Desmaris V., Dynefors K., Nilsson P.A., Rorsman N., Zirath H. // 2005. EGAAS 2005. European Gallium Arsenide and Other Semiconductor Application Symposium. - Paris, 3-4 Oct. 2005. - P. 309-312. ↑
- C1557.** Shih-Fong Chao. Compact W-band SPQT MMIC switch using traveling wave concept. / Shih-Fong Chao, Zuo-Min Tsai, Kun-You Lin, Huei Wang. // 2005. EGAAS 2005. European Gallium Arsenide and Other Semiconductor Application Symposium. - Paris, 3-4 Oct. 2005. - P. 357-360. ↑
- C1558.** Clausen M.C. Advanced manufacturing techniques for next generation power FET Technology. / Clausen M.C., McMonagle J. // 2005. EGAAS 2005. European Gallium Arsenide and Other Semiconductor Application Symposium. - Paris, 3-4 Oct. 2005. - P. 429-432. ↑
- C1559.** Camarchia V. A comprehensive class A to B power and load-pull characterization of GaN HEMTs on SiC and sapphire substrates. / Camarchia V., Guerrieri S.D., Pirola M., Teppati V., Ghione G., Peroni M., Lanzieri C. // 2005. EGAAS 2005. European Gallium Arsenide and Other Semiconductor Application Symposium. - Paris, 3-4 Oct. 2005. - P. 4 ↑
- C1560.** Wei-Chien Chen. A 38-48-GHz miniature MMIC subharmonic mixer. / Wei-Chien Chen, Shih-Yu Chen, Jeng-Han Tsai, Tian-Wei Huang, Huei Wang. // 2005. EGAAS 2005. European Gallium Arsenide and Other Semiconductor Application Symposium. - Paris, 3-4 Oct. 2005. - P. 437-440. ↑
- C1561.** Kallfass I. Verification of a frequency dispersion model in the performance of a GaAs pHEMT travelling-wave MMIC. / Kallfass I., Zhang C., Grunenputt J., Teyssandier C., Schumacher H. // 2005. EGAAS 2005. European Gallium Arsenide and Other Semiconductor Application Symposium. - Paris, 3-4 Oct. 2005. - P. 381-384. ↑
- C1562.** Gauthier G. KORRIGAN-a comprehensive initiative for GaN HEMT technology in Europe. / Gauthier G., Mancuso Y., Murgadella F. // 2005. EGAAS 2005. European Gallium Arsenide and Other Semiconductor Application Symposium. - Paris, 3-4 Oct. 2005. - P. 361-363. ↑
- C1563.** Larheche H. Progress in microwave GaN HEMT grown by MBE on silicon and Smart Cut/spl trade/engineered substrates for high power applications. / Larheche H., Faure B., Richtarch C., Letertre F., Langer R., Bove P. // 2005. EGAAS 2005. European Gallium Arsenide and Other Semiconductor Application Symposium. - Paris, 3-4 Oct. 2005. - P. 369-371. ↑
- C1564.** van Raay F. High power/high bandwidth GaN MMICs and hybrid amplifiers: design and characterization. / van Raay F., Quay R., Kiefer R., Walcher H., Kappeler O., Seelmann-Eggebert M., Muller S., Schlechtweg M., Weimann G. // 2005. EGAAS 2005. European Gallium Arsenide and Other Semiconductor Application Symposium. - Paris, 3-4 Oct. 2005. - P. 373-376. ↑

**C1565.** Jin-Cheol Jeong. GaAs MMICs for use in upconverter module for Ka-band OBS satellite transponders. / Jin-Cheol Jeong, Dong-Pil Chang, Dong-hwan Shin, In-Bok Yom. // 2005 European Microwave Conference. 4-6 Oct. 2005. - Vol. 3. - P. 4 ↑

**C1566.** Chusseau L. THz active devices and applications: a survey of recent researches. / Chusseau L., Lampin J.F., Bollaert S., Duvillaret L., Mangeney J. // 2005 European Microwave Conference. 4-6 Oct. 2005. - Vol. 1. - P. 4 ↑

**C1567.** Hafele M. GaAs distributed amplifiers with up to 350 GHz gain-bandwidth product for 40 Gb/s LiNbO<sub>3</sub> modulator drivers. / Hafele M., Beilenhoff K., Schumacher H. // 2005 European Microwave Conference. 4-6 Oct. 2005. - Vol. 1. - P. 4 ↑

**C1568.** Virdee B.S. Efficient HFET power amplifier. / Virdee B.S., Virdee A.S. // 2005 European Microwave Conference. 4-6 Oct. 2005. - Vol. 1. - P. 4 ↑

**C1569.** Gao S. Microwave class-F power amplifier design including input harmonic terminations. / Gao S., Butterworth P., Ooi S., Sambell A. // 2005. APMC 2005. Asia-Pacific Conference Proceedings Microwave Conference Proceedings. 4-7 Dec. 2005. - Vol. 5. - P. 4 ↑

**C1570.** Tsung-Yu Yang. A compact Ka-band power amplifier using finite-ground coplanar waveguide design. / Tsung-Yu Yang, Li-Chih Pai, Hwann-Kaeo Chiou. // 2005. APMC 2005. Asia-Pacific Conference Proceedings Microwave Conference Proceedings. 4-7 Dec. 2005. - Vol. 5. - P. 4 ↑

**C1571.** Guoli Qu. Intrinsic dependence of intermodulation distortion in HEMTs. / Guoli Qu, Parker A.E., Guangchun Zhang. // 2005. APMC 2005. Asia-Pacific Conference Proceedings Microwave Conference Proceedings. 4-7 Dec. 2005. - Vol. 5. - P. 4 ↑

**C1572.** Bhattacharya A. Advanced high performance MMICs for satellite transponder. / Bhattacharya A., Bhavsar M., Thakkar J., Srivastava S.M., Garg V.K. // 2005. APMC 2005. Asia-Pacific Conference Proceedings Microwave Conference Proceedings. 4-7 Dec. 2005. - Vol. 5. - P. 4 ↑

**C1573.** Karnfelt C. High gain active microstrip antenna for 60 GHz WLAN. / Karnfelt C., Hallbjorner P., Zirath H., Ligander P., Boustedt K., Alping A. // 2005 European Microwave Conference. 4-6 Oct. 2005. - Vol. 1. - P. 4 ↑

**C1574.** Kanamura M. An over 100 W n-GaN/n-AlGaIn/GaN MIS-HEMT power amplifier for wireless base station applications. / Kanamura M., Kikkawa T., Iwai T., Imanishi K., Kubo T., Joshin K. // 2005. IEDM Technical Digest. IEEE International Electron Devices Meeting. - Washington, DC, 5-5 Dec. 2005. - P. 572-575. ↑

**C1575.** Lossy R. High power, high AlGaIn/GaN-HEMTs with novel powerbar design. / Lossy R., Liero A., Wurfl J., Trankle G. // 2005. IEDM Technical Digest. IEEE International Electron Devices Meeting. - Washington, DC, 5-5 Dec. 2005. - P. 580-582. ↑

**C1576.** Wu Y.-F. 8-watt GaN HEMTs at millimeter-wave frequencies. / Wu Y.-F., Moore M., Saxler A., Wisleder T., Mishra U.K., Parikh P. // 2005. IEDM Technical Digest. IEEE International Electron Devices Meeting. - Washington, DC, 5-5 Dec. 2005. - P. 583-585. ↑

**C1577.** Kappeler O. An AlGaIn/GaN push-pull HEMT amplifier with 400 MHz bandwidth and 100 W peak output power. / Kappeler O., Quay R., van Raay F., Kiefer R., Reiner R., Walcher H., Muller S., Mikulla M., Schlechtweg M., Weimann G., Wiegner D., Seyfried U., Tempi W. // 2005. IEDM Technical Digest. IEEE International Electron Devices Meeting. - Washington, DC, 5-5 Dec. 2005. - P. 385-386. ↑

**C1578.** Iwai T. Thermal and source bumps utilizing carbon nanotubes for flip-chip high power amplifiers. / Iwai T., Shioya H., Kondo D., Hirose S., Kawabata A., Sato S., Nihei M., Kikkawa T., Joshin K., Awano Y., Yokoyama N. // 2005. IEDM Technical Digest. IEEE International Electron Devices Meeting. - Washington, DC, 5-5 Dec. 2005. - P. 257-260. ↑

**C1579.** Zhenchuan Yang. GaN on patterned silicon (GPS) technique for GaN-based integrated microsensors. / Zhenchuan Yang, Ruonan Wang, Deliang Wang, Baoshun Zhang, Chen K.J., Kei May Lau. // 2005. IEDM Technical Digest. IEEE International Electron Devices Meeting. - Washington, DC, 5-5 Dec. 2005. - P. 298-301. ↑

- C1580.** Ueda D. AlGaIn/GaN devices for future power switching systems. / Ueda D., Murata T., Hikita M., Nakazawa S., Kuroda M., Ishida H., Yanagihara M., Inoue K., Ueda T., Uemoto Y., Tanaka T., Egawa T. // 2005. IEDM Technical Digest. IEEE International Electron Devices Meeting. - Washington, DC, 5-5 Dec. 2005. - P. 377-380. ↑
- C1581.** Zhiqun Cheng. Monolithic integrated C-band low noise amplifier using AlGaIn/graded-AlGaIn/GaN HEMTs. / Zhiqun Cheng, Yong Cai, Jie Liu, Yugang Zhou, Kei May Lau, Chen K.I. // 2005. APMC 2005. Asia-Pacific Conference Proceedings Microwave Conference Proceedings. 4-7 Dec. 2005. - Vol. 2. - P. 4 ↑
- C1582.** Ziqiang Yang. A 2 GHz high isolation DPDT switch MMIC. / Ziqiang Yang, Tao Yang, Yu You, Ruimin Xu. // 2005. APMC 2005. Asia-Pacific Conference Proceedings Microwave Conference Proceedings. 4-7 Dec. 2005. - Vol. 2. - P. 3 ↑
- C1583.** Ming-Fong Lei. A 100-120 GHz quadruple-LO pumped harmonic diode mixer using standard GaAs based 0.15- $\mu$ m PHEMT process. / Ming-Fong Lei, Huei Wang. // 2005. APMC 2005. Asia-Pacific Conference Proceedings Microwave Conference Proceedings. 4-7 Dec. 2005. - Vol. 2. - P. 3 ↑
- C1584.** Korolev A.M. Low-noise pHEMT amplifier operating at extra-low supply voltage and power. / Korolev A.M., Shulga V.M. // 2005. APMC 2005. Asia-Pacific Conference Proceedings Microwave Conference Proceedings. 4-7 Dec. 2005. - Vol. 2. - P. 4 ↑
- C1585.** Hsien-Chin Chiu. Enhancement- and depletion-mode InGaP/InGaAs pHEMTs on 6-inch GaAs substrate. / Hsien-Chin Chiu, Chia-Shih Cheng, Yuan-Jui, Shih, Chan-Shin Wu. // 2005. APMC 2005. Asia-Pacific Conference Proceedings Microwave Conference Proceedings. 4-7 Dec. 2005. - Vol. 2. - P. 4 ↑
- C1586.** Gao S. Microwave class-E GaN power amplifiers. / Gao S., Xu H., Heikman S., Mishra U., York R.A. // 2005. APMC 2005. Asia-Pacific Conference Proceedings Microwave Conference Proceedings. 4-7 Dec. 2005. - Vol. 2. - P. 4 ↑
- C1587.** Kang-Ho Lee. High linearity SPDT switch for dual band wireless LAN applications. / Kang-Ho Lee, Zhejun Jin, Kyung-Heon Koo. // 2005. APMC 2005. Asia-Pacific Conference Proceedings Microwave Conference Proceedings. 4-7 Dec. 2005. - Vol. 2. - P. 4 ↑
- C1588.** Min Han. V-band CPW balanced medium power amplifier for 60 GHz wireless LAN application. / Min Han, Sung-Woon Moon, Seok-Gyu Choi, Tae-Jong Baek, Byeung-Ok Lim, Dan An, Mi-ra Kim, Sam-Dong Kim, Jin-Koo Rhee. // 2005. APMC 2005. Asia-Pacific Conference Proceedings Microwave Conference Proceedings. 4-7 Dec. 2005. - Vol. 2. - P. 3 ↑
- C1589.** Qin Y. Broadband high efficiency circularly polarized active integrated antenna. / Qin Y., Gao S., Elsdon M., Sambell A. // 2005. APMC 2005. Asia-Pacific Conference Proceedings Microwave Conference Proceedings. 4-7 Dec. 2005. - Vol. 3. - P. 4 ↑
- C1590.** Cabral P.M. Dynamic AM-AM and AM-PM behavior in microwave PA circuits. / Cabral P.M., Pedro J.C., Carvalho N.B. // 2005. APMC 2005. Asia-Pacific Conference Proceedings Microwave Conference Proceedings. 4-7 Dec. 2005. - Vol. 4. - P. 4 ↑
- C1591.** Chen I.-Y. An Novel L-shape Active Leaky-Wave Antenna with power combining and scanning capability. / Chen I.-Y., Chien-Jen Wang, Jou C.F. // 2005. APMC 2005. Asia-Pacific Conference Proceedings Microwave Conference Proceedings. 4-7 Dec. 2005. - Vol. 4. - P. 1-4. ↑
- C1592.** Kawano A. High-efficiency and wide-band single-ended 200W GaN HEMT power amplifier for 2.1 GHz W-CDMA base station application. / Kawano A., Adachi N., Tateno Y., Mizuno S., Ui N., Nikaido J., Sano S. // 2005. APMC 2005. Asia-Pacific Conference Proceedings Microwave Conference Proceedings. 4-7 Dec. 2005. - Vol. 3. - P. 4 ↑
- C1593.** Parvesh. Effect of temperature on current voltage characteristics of lattice mismatched Al<sub>m</sub>Ga<sub>1-m</sub>N/GaN HEMTs. / Parvesh, Pandeyb S., Haldarc S., Gupta M., Gupta R.S. // 2005. APMC 2005. Asia-Pacific Conference Proceedings Microwave Conference Proceedings. 4-7 Dec. 2005. - Vol. 3. - P. 4 ↑
- C1594.** Yuwei Liu. Microwave noise in InP/InGaAs composite channel high electron mobility transistors (HEMTs). / Yuwei Liu, Hong Wang, Rong Zeng. // 2005. APMC 2005. Asia-Pacific Conference Proceedings Microwave Conference Proceedings. 4-7 Dec. 2005. - Vol. 3. - P. 3 ↑

- C1595.** Yut-Hoong Chow. Design of a wideband active-buffered mixer in enhancement-mode GaAs pHEMT technology. / Yut-Hoong Chow, Lim-Guan Yew, Haji-Mokhtar Fuad, Ooi B., Vice M. // 2005. APMC 2005. Asia-Pacific Conference Proceedings Microwave Conference Proceedings. 4-7 Dec. 2005. - Vol. 3. - P. 4 ↑
- C1596.** Saito W. 380v/1.9A GaN power-HEMT: current collapse phenomena under high applied voltage and demonstration of 27.1 MHz class-E amplifier. / Saito W., Kuraguchi M., Takada Y., Tsuda K., Domon T., Omura I., Yamaguchi M. // 2005. IEDM Technical Digest. IEEE International Electron Devices Meeting. - Washington, DC, 5-5 Dec. 2005. - P. 586-589. ↑
- C1597.** Cherkashin M.V. Design of 2-10 GHz feedback MMIC LNA using >technique. / Cherkashin M.V., Eyllier D., Babak L.I., Billonnet L., Jarry B., Zaitsev D.A., Dyagilev A.V. // 2005 European Microwave Conference. 4-6 Oct. 2005. - Vol. 2. - P. 4 ↑
- C1598.** Zamanillo J.M. Optical ports: next generation of MMIC control devices?. / Zamanillo J.M., Portilla J., Navarro C., Perez-Vega C. // 2005 European Microwave Conference. 4-6 Oct. 2005. - Vol. 2. - P. 4 ↑
- C1599.** Inkwon Ju. Ultra broadband DC to 40 GHz 5-bit pHEMT MMIC digital attenuator. / Inkwon Ju, Youn-Sub Noh, In-Bok Yom. // 2005 European Microwave Conference. 4-6 Oct. 2005. - Vol. 2. - P. 4 ↑
- C1600.** Barajas E. Low noise high linearity ultra broadband monolithic amplifier using travelling-wave gain stages. / Barajas E., Aja B., de la Fuente M.L., Pascual J.P., Artal E. // 2005 European Microwave Conference. 4-6 Oct. 2005. - Vol. 2. - P. 4 ↑
- C1601.** Maekawa A. A 100W high-efficiency GaN HEMT amplifier for S-Band wireless system. / Maekawa A., Nagahara M., Yamamoto T., Sano S. // 2005 European Microwave Conference. 4-6 Oct. 2005. - Vol. 3. - P. 4 ↑
- C1602.** Schworer C. A 150 to 220 GHz balanced doubler MMIC using a 50 nm metamorphic HEMT technology. / Schworer C., Campos Roca Y., Leuther A., Tessmann A., Seelmann-Eggebert M., Massler H., Schlechtweg M., Weiman G. // 2005 European Microwave Conference. 4-6 Oct. 2005. - Vol. 3. - P. 4 ↑
- C1603.** Mehdi M. A novel technique for obtaining LO and RF (LSB) rejection in 25-40 GHz microwave up conversion mixers based on the concepts of distributed and double balanced mixing. / Mehdi M., Rumelhard C., Polleux J.L., Lefebvre B. // 2005 European Microwave Conference. 4-6 Oct. 2005. - Vol. 3. - P. 4 ↑
- C1604.** Bhatnagar M. A low cost SMT integrated frequency doubler and power amplifier for 30GHz DBS uplink applications. / Bhatnagar M., Morkner H. // 2005 European Microwave Conference. 4-6 Oct. 2005. - Vol. 3. - P. 4 ↑
- C1605.** Daoud S.M. A novel wideband MMIC voltage controlled attenuator with a bandpass filter topology. / Daoud S.M., Shastry P.N. // 2005 European Microwave Conference. 4-6 Oct. 2005. - Vol. 3. - P. 4 ↑
- C1606.** Matsuzaki H. Laterally scaled down tiered-edge ohmic structure of InP-based HEMTs for 2-S/mm<sup>2</sup>/sub m/ and 500-GHz f/sub T/. / Matsuzaki H., Maruyama T., Kosugi T., Takahashi H., Tokumitsu M., Enoki T. // 2005. IEDM Technical Digest. IEEE International Electron Devices Meeting. - Washington, DC, 5-5 Dec. 2005. - P. 775-778. ↑
- C1607.** Villanueva A.A. Non-uniform degradation behavior across device width in RF power GaAs PHEMTs. / Villanueva A.A., del Alamo J.A., Hisaka T., Hayashi K., Somerville M. // 2005. IEDM Technical Digest. IEEE International Electron Devices Meeting. - Washington, DC, 5-5 Dec. 2005. - P. 783-786. ↑
- C1608.** Yong Cai. Monolithic integration of enhancement-and depletion-mode AlGaIn/GaN HEMTs for GaN digital integrated circuits. / Yong Cai, Zhiqun Cheng, Wilson Chak Wah Tang, Chen K.J., Kei May Lau. // 2005. IEDM Technical Digest. IEEE International Electron Devices Meeting. - Washington, DC, 5-5 Dec. 2005. - P. 4 P.-774. ↑
- C1609.** Dae-Hyun Kim. Performance evaluation of 50 nm In/sub 0.7/Ga/sub 0.3/As HEMTs for beyond-CMOS logic applications. / Dae-Hyun Kim, del Alamo J.A., Jae-Hak Lee, Kwang-Seok Seo. // 2005. IEDM Technical Digest. IEEE International Electron Devices Meeting. - Washington, DC, 5-5 Dec. 2005. - P. 767-770. ↑
- C1610.** Sozza A. Evidence of traps creation in GaN/AlGaIn/GaN HEMTs after a 3000 hour on-state and off-state hot-electron stress. / Sozza A., Dua C., Morvan E., diForte-Poisson M.A., Delage S., Rampazzo F., Tazzoli A., Danesin F., Meneghesso G., Zanoni E., Curutchet A., Malbert N., Labat N., Grimbart B., De Jaeger J.-C. //



2005. IEDM Technical Digest. IEEE International Electron Devices Meeting. - Washington, DC, 5-5 Dec. 2005. - P. 4 P.-593. ↑

**C1611.** Palacios T. Ge-spacer technology in AlGaIn/GaN HEMTs for mm-wave applications. / Palacios T., Snow E., Pei Y., Chakraborty A., Keller S., DenBaars S.P., Mishra U.K. // 2005. IEDM Technical Digest. IEEE International Electron Devices Meeting. - Washington, DC, 5-5 Dec. 2005. - P. 3 P.-789. ↑

**C1612.** Detratti M. A 4.5 GHz 3-4 dual-modulus frequency divider IC in GaAs technology. / Detratti M., Cabo J., Pascual J.P., Herrera A. // 2005 European Microwave Conference. 4-6 Oct. 2005. - Vol. 2. - P. 4 ↑

**C1613.** Chi-Yang Chang. A 1.5 to 37 GHz ultra-broadband MMIC Mouw's star mixer. / Chi-Yang Chang, Ching-Ku Liao, Dow-Chih Niu. // 2005 European Microwave Conference. 4-6 Oct. 2005. - Vol. 2. - P. 4 ↑

**C1614.** Yu H. Ion implantation for unalloyed ohmic contacts to AlGaIn/GaN HEMTs. / Yu H., McCarthy L., Rajan S., Keller S., Denbaars S.P., Speck J.S., Mishra U.K. // 2004. 62nd DRC. Conference Digest [Includes 'Late News Papers' volume] Device Research Conference. 21-23 June 2004. - P. 37-38. ↑

**C1615.** Wu Y.-F. Linearity performance of GaN HEMTs with field plates. / Wu Y.-F., Saxler A., Wisleder T., Moore M., Smith R.P., Sheppard S., Chavarkar P.M., Parikh P. // 2004. 62nd DRC. Conference Digest [Includes 'Late News Papers' volume] Device Research Conference. 21-23 June 2004. - P. 35-36. ↑

**C1616.** Tsai R. 275 GHz fMAX, 220 GHz fT AlSb/InAs HEMT technology. / Tsai R., Boos J.B., Bennett B.R., Lange M., Grundbacher R., Namba C., Liu P.H., Lee J., Barsky M., Gutierrez A. // 2004. 62nd DRC. Conference Digest [Includes 'Late News Papers' volume] Device Research Conference. 21-23 June 2004. - P. 12-13. ↑

**C1617.** Jung-Hui Tsai. Device linearity enhancement of InGaP/InGaAs/GaAs camel-gate p-channel pseudomorphic high electron mobility transistor. / Jung-Hui Tsai, Shao-Yen Chiu, Ying-Cheng Chu, King-Poul Zhu. // 2004. IWJT '04. The Fourth International Workshop on Junction Technology. 15-16 March 2004. - P. 217-219. ↑

**C1618.** Shen L. Improved high power thick-GaN-capped AlGaIn/GaN HEMTs without surface passivation. / Shen L., Buttari D., Heikman S., Chini A., Coffie R., McCarthy L., Chakraborty A., Keller S., DenBaars S.P., Mishra U.K. // 2004. 62nd DRC. Conference Digest [Includes 'Late News Papers' volume] Device Research Conference. 21-23 June 2004. - P. 39-40. ↑

**C1619.** Palacios T. Use of multichannel heterostructures to improve the access resistance and fT linearity in GaN-based HEMTs. / Palacios T., Chini A., Buttari D., Heikman S., Keller S., Denlaars S.P., Mishra U.K. // 2004. 62nd DRC. Conference Digest [Includes 'Late News Papers' volume] Device Research Conference. 21-23 June 2004. - P. 41-42. ↑

**C1620.** Yifeng Wu. Will the velocity of GaN HEMTs ever overshoot? [mm-wave frequencies]. 2004. 62nd DRC. Conference Digest [Includes 'Late News Papers' volume] Device Research Conference. 21-23 June 2004. - P. 191 vol.1. ↑

**C1621.** Tan S.W. An economic method for fabrication sub-quarter- $\mu\text{m}$  gate doped-channel FET's by photolithography. / Tan S.W., Chen W.T., Chu M.Y., Lour W.S. // 2004. IWJT '04. The Fourth International Workshop on Junction Technology. 15-16 March 2004. - P. 213-216. ↑

**C1622.** Bergman J. Low-voltage, high-performance InAs/AlSb HEMTs with power gain above 100 GHz at 100 mV drain bias. / Bergman J., Nagy G., Sullivan G., Ikhlassi A., Brar B. // 2004. 62nd DRC. Conference Digest [Includes 'Late News Papers' volume] Device Research Conference. 21-23 June 2004. - P. 243-244. ↑

**C1623.** Matulionis A. Comparative analysis of hot-phonon effects in nitride and arsenide channels for HEMTs. 2004. 62nd DRC. Conference Digest [Includes 'Late News Papers' volume] Device Research Conference. 21-23 June 2004. - P. 145-146. ↑

**C1624.** Sanabria C. Influence of the heterostructure design on noise figure of AlGaIn/GaN HEMTs. / Sanabria C., Xu H., Palacios T., Chakraborty P., Heikman S., Mishra U.K., York R.A. // 2004. 62nd DRC. Conference Digest [Includes 'Late News Papers' volume] Device Research Conference. 21-23 June 2004. - P. 43-44. ↑

**C1625.** Dae-Hyun Kim. A new two-step recess technology using SiNx passivation and Pt-buried gate process and its application to 0.15  $\mu\text{m}$  Al<sub>0.6</sub>InAs/In<sub>0.65</sub>GaAs HEMTs. / Dae-Hyun Kim, Kang-Min Lee, Jae-Hak Lee,

Kwang-Seok Seo. // 2004. 62nd DRC. Conference Digest [Includes 'Late News Papers' volume] Device Research Conference. 21-23 June 2004. - P. 69-70. ↑

C1626. Palacios T. Influence of the access resistance in the rf performance of mm-wave AlGaIn/GaN HEMTs. / Palacios T., Rajan S., Shen L., Chakraborty A., Heikman S., Keller S., DenBaars S.P., Mishra U.K. // 2004. 62nd DRC. Conference Digest [Includes 'Late News Papers' volume] Device Research Conference. 21-23 June 2004. - P. 75-76. ↑

C1627. Arfaei F. The influence of HEMT nonlinear distributed modeling on transient performance of microwave circuits. / Arfaei F., Berenji K., Abdipour A., Mohammadi A. // 2004. MIKON-2004. 15th International Conference on Microwaves, Radar and Wireless Communications. 17-19 May 2004. - Vol. 1. - P. 118-121. ↑

C1628. Manshadi F. NASA ultra low noise X-band microwave feeds for deep space communication. 2004. MIKON-2004. 15th International Conference on Microwaves, Radar and Wireless Communications. 17-19 May 2004. - Vol. 2. - P. 733-736. ↑

C1629. Qin Y. Design of low cost broadband class-E power amplifier using low voltage supply. / Qin Y., Gao S., Sambell A. // 2004 High Frequency Postgraduate Student Colloquium. 6-7 Sept. 2004. - P. 101-106. ↑

C1630. Xinzhong Duo. On-chip versus off-chip passives in multi-band radio design. / Xinzhong Duo, Torikka T., Li-Rong Zheng, Ismail M., Tenhunen H. // 2004. ESSCIRC 2004. Proceeding of the 30th European Solid-State Circuits Conference. 21-23 Sept. 2004. - P. 327-330. ↑

C1631. Camprini M. Ultra low DC power consumption In-P HITFET based differential oscillator. / Camprini M., Cidronali A., Magrini I., Collodi G., Costanzo L., Manes G. // 2004. MELECON 2004. Proceedings of the 12th IEEE Mediterranean Electrotechnical Conference. 12-15 May 2004. - Vol. 1. - P. 171-174. ↑

C1632. Sippel J.C. A physics-based analytical model of a GaN/AlGaIn HEMT incorporating spontaneous and piezoelectric polarization. / Sippel J.C., Islam S.S., Mukhejee S.S. // 2004. Canadian Conference on Electrical and Computer Engineering. 2-5 May 2004. - Vol. 3. - P. 1401-1404. ↑

C1633. Donato N. Microwave characterization and modeling of packaged HEMTs by a direct extraction procedure at cryogenic temperatures. / Donato N., Caddemi A., Crupi G., Calandra E. // 2004. IMTC 04. Proceedings of the 21st IEEE Instrumentation and Measurement Technology Conference. 18-20 May 2004. - Vol. 3. - P. 2208-2211. ↑

C1634. {no data available}. Device Research Conference (IEEE Cat. No.04TH8724). 2004. 62nd DRC. Conference Digest [Includes 'Late News Papers' volume] Device Research Conference. 21-23 June 2004. - {no data available}. ↑

C1635. Mishra U.K. Gallium nitride electronics: Watt is the limit? [summary of GaN semiconductor devices]. 2004. 62nd DRC. Conference Digest [Includes 'Late News Papers' volume] Device Research Conference. 21-23 June 2004. - P. 3-5. ↑

C1636. Chini A. Effect of gate recessing on linearity characteristics of AlGaIn/GaN HEMTs. / Chini A., Buttari D., Coffie R., Shen L., Palacios T., Heikman S., Chakraborty A., Keller S., Mishra U.K. // 2004. 62nd DRC. Conference Digest [Includes 'Late News Papers' volume] Device Research Conference. 21-23 June 2004. - P. 33-34. ↑

C1637. Ito H. Pre-amplifier-integrated uni-traveling-carrier photodiode module with a rectangular waveguide-output port for operation in the 120-GHz band. / Ito H., Furuta T., Hirata A., Kosugi T., Muramoto Y., Tokumitsu M., Nagatsuma T., Ishibashi T. // 2004. LEOS 2004. The 17th Annual Meeting of the IEEE Lasers and Electro-Optics Society. 7-11 Nov. 2004. - Vol. 1. - P. 128-129. ↑

C1638. Shirt Fun Ooi. High efficiency class-F power amplifier design. / Shirt Fun Ooi, Gao S., Sambell A., Smith D., Butterworth P. // 2004 High Frequency Postgraduate Student Colloquium. 6-7 Sept. 2004. - P. 113-118. ↑

C1639. Hing Weng Seng. Implementing RF signal limiter with heterojunction devices. / Hing Weng Seng, Sloan R., Williams K. // 2004 High Frequency Postgraduate Student Colloquium. 6-7 Sept. 2004. - P. 195-198. ↑

C1640. Chang-Soon Choi. Millimeter-wave optoelectronic mixers based on InP HEMT. / Chang-Soon Choi,

Woo-Young Choi. // 2004. LEOS 2004. The 17th Annual Meeting of the IEEE Lasers and Electro-Optics Society. 7-11 Nov. 2004. - Vol. 1. - P. 126-127. ↑

**C1641.** Kanaya K. A 76 GHz high performance subharmonic mixer MMIC using low 1/f noise diodes for automotive radars. / Kanaya K., Aihara Y., Katoh T., Komaru M., Matsuda Y. // 2004. IEEE Compound Semiconductor Integrated Circuit Symposium. 24-27 Oct. 2004. - P. 260-263. ↑

**C1642.** Bryant D.T. Integrated LNA-sub-harmonic mixer for 77 GHz automotive radar applications using GaAs pHEMT technology. / Bryant D.T., Eye R.A., Carroll J.M., Allen D. // 2004. IEEE Compound Semiconductor Integrated Circuit Symposium. 24-27 Oct. 2004. - P. 257-259. ↑

**C1643.** Bessemoulin A. Hot-via interconnects: a step toward surface mount chip scale packaged MMICs up to 110 GHz. / Bessemoulin A., Gaessler C., Gruenenpuett C., Reig B. // 2004. IEEE Compound Semiconductor Integrated Circuit Symposium. 24-27 Oct. 2004. - P. 237-240. ↑

**C1644.** Kikkawa T. Recent progress and future prospects of GaN HEMTs for base-station applications. 2004. IEEE Compound Semiconductor Integrated Circuit Symposium. 24-27 Oct. 2004. - P. 17-20. ↑

**C1645.** Root D.E. Device modeling for III-V semiconductors-an overview. / Root D.E., Iwamoto M., Wood J. // 2004. IEEE Compound Semiconductor Integrated Circuit Symposium. 24-27 Oct. 2004. - P. 279-282. ↑

**C1646.** Poppe M. Microwave mixers based on a novel zero bias diode. / Poppe M., Kleen D., Janson H., Zirath H., Adahl A. // 2004. IEEE Compound Semiconductor Integrated Circuit Symposium. 24-27 Oct. 2004. - P. 264-267. ↑

**C1647.** Hacker J.B. Monolithic GaAs PHEMT MMICs integrated with RF MEMS switches. / Hacker J.B., Kim M., Mihailovich R.E., DeNatale J.F. // 2004. IEEE Compound Semiconductor Integrated Circuit Symposium. 24-27 Oct. 2004. - P. 229-232. ↑

**C1648.** Inoue Y. A 90-GHz InP-HEMT lossy match amplifier with a 20-dB gain using a broadband matching technique. / Inoue Y., Sato M., Kawano Y., Masuda S., Ohki T., Makiyama K., Takahashi T., Shigematsu H., Hirose T. // 2004. IEEE Compound Semiconductor Integrated Circuit Symposium. 24-27 Oct. 2004. - P. 145-148. ↑

**C1649.** Kosugi T. 120-GHz Tx/Rx chipset for 10-Gbit/s wireless applications using 0.1 μm-gate InP HEMTs. / Kosugi T., Tokumitsu M., Enoki T., Muraguchi M., Hirata A., Nagatsuma T. // 2004. IEEE Compound Semiconductor Integrated Circuit Symposium. 24-27 Oct. 2004. - P. 171-174. ↑

**C1650.** Kunii T. A high reliability GaN HEMT with SiN passivation by Cat-CVD. / Kunii T., Totsuka M., Kamo Y., Yamamoto Y., Takeuchi H., Shimada Y., Shiga T., Minami H., Kitano T., Miyakuni S., Nakatsuka S., Inoue A., Oku T., Nanjo T., Oishi T., Ishikawa T., Matsuda Y. // 2004. IEEE Compound Semiconductor Integrated Circuit Symposium. 24-27 Oct. 2004. - P. 197-200. ↑

**C1651.** Suzuki T. Design and InP HEMT Technology for ultra-high speed digital ICs with beyond 80-Gbit/s operation. / Suzuki T., Kawano Y., Nakashima Y., Takahashi T., Makiyama K., Hirose T., Takikawa M. // 2004. IEEE Compound Semiconductor Integrated Circuit Symposium. 24-27 Oct. 2004. - P. 211-214. ↑

**C1652.** Schwindt R.S. Temperature-dependence of a GaN-based HEMT monolithic X-band low noise amplifier. / Schwindt R.S., Kumar V., Aktas O., Lee J.W., Adesida I. // 2004. IEEE Compound Semiconductor Integrated Circuit Symposium. 24-27 Oct. 2004. - P. 201-203. ↑

**C1653.** Kamitsuna H. A fast low-power 444 switch IC using InP HEMTs for 10-Gbit/s systems. / Kamitsuna H., Yamane Y., Tokumitsu M., Sugahara H., Muraguchi M. // 2004. IEEE Compound Semiconductor Integrated Circuit Symposium. 24-27 Oct. 2004. - P. 97-100. ↑

**C1654.** Tessmann A. A 220 GHz metamorphic HEMT amplifier MMIC. / Tessmann A., Leuther A., Massler H., Kuri M., Schwoerer C., Schlechtweg M., Weimann G. // 2004. IEEE Compound Semiconductor Integrated Circuit Symposium. 24-27 Oct. 2004. - P. 297-300. ↑

**C1655.** Krutov A.V. Low noise hybrid-monolithic amplifier with PHEMT transistors. / Krutov A.V., Rebrov A.S. // 2004. CriMico 2004. 2004 14th International Crimean Conference on Microwave and Telecommunication Technology. 13-17 Sept. 2004. - P. 96-97. ↑

- C1656.** Osadchuk V.S. Optically controlled active generator for superhigh frequencies. / Osadchuk V.S., Osadchuk A.V. // 2004. CriMico 2004. 2004 14th International Crimean Conference on Microwave and Telecommunication Technology. 13-17 Sept. 2004. - P. 110-111. ↑
- C1657.** Klimova A.V. The temperature model limits for high electron mobility transistors. 2004. CriMico 2004. 2004 14th International Crimean Conference on Microwave and Telecommunication Technology. 13-17 Sept. 2004. - P. 155-156. ↑
- C1658.** Ihara K. The temperature dependency of a GaAs pHEMT wideband IQ modulator IC. 2004 IEEE Radio and Wireless Conference. 19-22 Sept. 2004. - P. 223-225. ↑
- C1659.** Albasha L. Novel control architecture for JPHEMT power amplifiers achieving high efficiency EDGE application. / Albasha L., Clifton J.C., Lawrenson A., Eaton A. // 2004 IEEE Radio and Wireless Conference. 19-22 Sept. 2004. - P. 343-346. ↑
- C1660.** Ma long. Self-consistent numerical model and optimization of two-dimensional electron gases for AlGaIn/GaN HEMT. / Ma long, Wang yan, Yu Zhiping, Tian lilin. // 2004. IWJT '04. The Fourth International Workshop on Junction Technology. 15-16 March 2004. - P. 190-193. ↑
- C1661.** Yemtsev P.A. High electron mobility transistor small signal model. / Yemtsev P.A., Sunduchkov I.K., Sunduchkov K.S., Shelkovnikov B.N. // 2004. CriMico 2004. 2004 14th International Crimean Conference on Microwave and Telecommunication Technology. 13-17 Sept. 2004. - P. 161-163. ↑
- C1662.** Krutov A.V. An experimental extraction of low noise field effect transistor's linear equivalent circuit and noise model. / Krutov A.V., Rebrov A.S. // 2004. CriMico 2004. 2004 14th International Crimean Conference on Microwave and Telecommunication Technology. 13-17 Sept. 2004. - P. 164-165. ↑
- C1663.** Thayne I. Very high performance 50 nm T-gate III-V HEMTs enabled by robust nanofabrication technologies. / Thayne I., Cao X., Moran D., Boyd E., Elgaid K., McLelland H., Holland M., Thoms S., Stanley C. // 2004. 4th IEEE Conference on Nanotechnology. 16-19 Aug. 2004. - P. 95-97. ↑
- C1664.** Deal W. A 110-GHz AlSb/InAs MMIC amplifier. / Deal W., Tsai R., Lange M., Grundbacher R., Lee L.J., Padmanabhan K., Liu P.H., Namba C., Nam P., Gutierrez A., Bennett B.R., Boos J.B. // 2004. IEEE Compound Semiconductor Integrated Circuit Symposium. 24-27 Oct. 2004. - P. 301-304. ↑
- C1665.** Yamakawa S. Quantum corrected full-band cellular Monte Carlo simulation of AlGaIn/GaN HEMTs. / Yamakawa S., Goodnick S.M., Aboud S., Saraniti M. // 2004. IWCE-10 2004. Abstracts. 10th International Workshop on Computational Electronics. 24-27 Oct. 2004. - P. 53-54. ↑
- C1666.** Won Ko. High-gain direct-coupled matrix distributed amplifier using active feedback topology. / Won Ko, Youngwoo Kwon. // 2004. IEEE Compound Semiconductor Integrated Circuit Symposium. 24-27 Oct. 2004. - P. 309-312. ↑
- C1667.** Limacher R. Broadband low-noise amplifiers for K- and Q-bands using 0.2  $\mu\text{m}$  InP HEMT MMIC technology. / Limacher R., Megej A., Scoca L., Zaugg T., Meier H., Orzati A., Bachtold W. // 2004. IEEE Compound Semiconductor Integrated Circuit Symposium. 24-27 Oct. 2004. - P. 305-308. ↑
- C1668.** {no data available}. Session TU1C: Advances in Low Noise HEMT Technology. 2004 IEEE MTT-S International Microwave Symposium Digest. 6-11 June 2004. - Vol. 1. - P. 147. ↑
- C1669.** Rice P. A 10 GHz dielectric resonator oscillator using GaN technology. / Rice P., Moore M., Barnes A.R., Uren M.J., Malbert N., Labat N., Sloan R. // 2004 IEEE MTT-S International Microwave Symposium Digest. 6-11 June 2004. - Vol. 3. - P. 1497-1500. ↑
- C1670.** Hongtao Xu. Low phase-noise 5 GHz AlGaIn/GaN HEMT oscillator integrated with Bax Sr<sub>1-x</sub> TiO<sub>3</sub> thin films. / Hongtao Xu, Sanabria C., Pervez N.K., Keller S., Mishra U.K., York R.A. // 2004 IEEE MTT-S International Microwave Symposium Digest. 6-11 June 2004. - Vol. 3. - P. 1509-1512. ↑
- C1671.** Grundbacher R. High performance and high reliability InP HEMT low noise amplifiers for phased-array applications. / Grundbacher R., Yeong-Chang Chou, Lai R., Kwan Ip, Kam S., Barsky M., Hayashibara G., Leung D., Eng D., Tsai R., Nishimoto M., Block T., Po-Hsin Liu, Oki A. // 2004 IEEE MTT-S International Microwave Symposium Digest. 6-11 June 2004. - Vol. 1. - P. 157-160. ↑



- C1672.** Ellis G.A. Wideband AlGaIn/GaN HEMT MMIC low noise amplifier. / Ellis G.A., Jeong-Sun Moon, Wong D., Micovic M., Kurdoghlian A., Hashimoto P., Ming Hu. // 2004 IEEE MTT-S International Microwave Symposium Digest. 6-11 June 2004. - Vol. 1. - P. 153-156. ↑
- C1673.** Heins M.S. X-band GaAs mHEMT LNAs with 0.5 dB noise figure. / Heins M.S., Carroll J.M., Kao M., Delaney J., Campbell C.F. // 2004 IEEE MTT-S International Microwave Symposium Digest. 6-11 June 2004. - Vol. 1. - P. 149-152. ↑
- C1674.** Behtash R. Coplanar AlGaIn/GaN HEMT power amplifier MMIC at X-band. / Behtash R., Tobler H., Berlec F.-J., Ziegler V., Leier H., Adelseck B., Martin T., Balmer R.S., Pavlidis D., Jansen R.H., Neuburger M., Schumacher H. // 2004 IEEE MTT-S International Microwave Symposium Digest. 6-11 June 2004. - Vol. 3. - P. 1657-1659. ↑
- C1675.** Gu Z. Low insertion loss and high linearity PHEMT SPDT and SP3T switch ICs for WLAN 802.11 a/b/g applications. / Gu Z., Johnson D., Belletete S., Fryklund D. // 2004. Digest of Papers. 2004 IEEE Radio Frequency Integrated Circuits (RFIC) Symposium. 6-8 June 2004. - P. 505-508. ↑
- C1676.** Won Ko. A GaAs-based 3-40 GHz distributed mixer with cascode FET cells. / Won Ko, Youngwoo Kwon. // 2004. Digest of Papers. 2004 IEEE Radio Frequency Integrated Circuits (RFIC) Symposium. 6-8 June 2004. - P. 413-416. ↑
- C1677.** Kamitsuna H. A 10 Gbit/s switch matrix MMIC using InP HEMTs with a logic-level-independent interface. / Kamitsuna H., Kitabayashi H., Matsuzaki H., Tokumitsu M., Muraguchi M. // 2004. Digest of Papers. 2004 IEEE Radio Frequency Integrated Circuits (RFIC) Symposium. 6-8 June 2004. - P. 325-328. ↑
- C1678.** Haibo Long. L-simulator: a magPEEC-based new CAD tool for simulating magnetic-enhanced IC inductors of 3D arbitrary geometry. / Haibo Long, Zhenghe Feng, Haigang Feng, Wang A., Tianling Ren. // 2004. ISCAS '04. Proceedings of the 2004 International Symposium on Circuits and Systems. 23-26 May 2004. - Vol. 5. - P. V-233-V-237-233. ↑
- C1679.** Chang-Ho Lee. A novel DP4T antenna switch for dual-band WLAN applications. / Chang-Ho Lee, Banerjee B., Laskar J. // 2004. Digest of Papers. 2004 IEEE Radio Frequency Integrated Circuits (RFIC) Symposium. 6-8 June 2004. - P. 571-574. ↑
- C1680.** Shuoqi Chen. A Ka/Q-band 2 Watt MMIC power amplifier using dual recess 0.15  $\mu\text{m}$  PHEMT process. / Shuoqi Chen, Nayak S., Ming-Yih Kao, Delaney J. // 2004 IEEE MTT-S International Microwave Symposium Digest. 6-11 June 2004. - Vol. 3. - P. 1669-1672. ↑
- C1681.** Mellberg A. Cryogenic 2-4 GHz ultra low noise amplifier. / Mellberg A., Wadefalk N., Angelov I., Choumas E., Kollberg E., Rorsman N., Starski P., Stenarson J., Zirath H. // 2004 IEEE MTT-S International Microwave Symposium Digest. 6-11 June 2004. - Vol. 1. - P. 161-163. ↑
- C1682.** {no data available}. 2004 IEEE MTT-S International Microwave Symposium Digest (IEEE Cat. No.04CH37535). 2004 IEEE MTT-S International Microwave Symposium Digest. 6-11 June 2004. - Vol. 3. - P. 0\_1. ↑
- C1683.** Chang-Soon Choi. Characteristics of InP HEMT harmonic optoelectronic mixers and their application to 60 GHz radio-on-fiber systems. / Chang-Soon Choi, Hyo-Soon Kang, Dae-Hyun Kim, Kwang-Seok Seo, Woo-Young Choi. // 2004 IEEE MTT-S International Microwave Symposium Digest. 6-11 June 2004. - Vol. 1. - P. 401-404. ↑
- C1684.** Ming-Fong Lei. Design and analysis of a miniature W-band MMIC subharmonically pumped resistive mixer. / Ming-Fong Lei, Pei-Si Wu, Tian-Wei Huang, Huei Wang. // 2004 IEEE MTT-S International Microwave Symposium Digest. 6-11 June 2004. - Vol. 1. - P. 235-238. ↑
- C1685.** Piel P.-M. A 26 volts, 45 Watts GaAs pHEMT for 2 GHz WCDMA applications. / Piel P.-M., Miller M., Green B. // 2004 IEEE MTT-S International Microwave Symposium Digest. 6-11 June 2004. - Vol. 3. - P. 1363-1366. ↑
- C1686.** Akkul M. 50 watt MMIC power amplifier design for 2 GHz applications. / Akkul M., Sarfraz M., Mayock J., Bosch W. // 2004 IEEE MTT-S International Microwave Symposium Digest. 6-11 June 2004. - Vol. 3. - P. 1355-1358. ↑

- C1687.** Kikkawa T. An over 200-W output power GaN HEMT push-pull amplifier with high reliability. / Kikkawa T., Maniwa T., Hayashi H., Kanamura M., Yokokawa S., Nishi M., Adachi N., Yokoyama M., Tateno Y., Joshin K. // 2004 IEEE MTT-S International Microwave Symposium Digest. 6-11 June 2004. - Vol. 3. - P. 1347-1350. ↑
- C1688.** Lynch J. Design and analysis of a W-band multiplier chipset. / Lynch J., Entchev E., Lyons B., Tessman A., Massler H., Leuther A., Schlechtweg M. // 2004 IEEE MTT-S International Microwave Symposium Digest. 6-11 June 2004. - Vol. 1. - P. 227-230. ↑
- C1689.** Nagatsuma T. Millimeter-wave photonic integrated circuit technologies for high-speed wireless communications applications. / Nagatsuma T., Hirata A., Harada M., Ishii H., Machida K., Minotani T., Ito H., Kosugi T., Shibata T. // 2004. Digest of Technical Papers. ISSCC. 2004 IEEE International Solid-State Circuits Conference. 15-19 Feb. 2004. - P. 448-449. ↑
- C1690.** DeNatale J. Reconfigurable RF circuits based on integrated MEMS switches. 2004. Digest of Technical Papers. ISSCC. 2004 IEEE International Solid-State Circuits Conference. 15-19 Feb. 2004. - P. 310-311. ↑
- C1691.** Suzuki T. Under 0.5W 50Gb/s full-rate 4:1MUX and 1:4 DEMUX in 0.13μm InP HEMT technology. / Suzuki T., Takahashi T., Makiyama K., Sawada K., Nakasha Y., Hirose T., Takikawa M. // 2004. Digest of Technical Papers. ISSCC. 2004 IEEE International Solid-State Circuits Conference. 15-19 Feb. 2004. - P. 234-525. ↑
- C1692.** Chi-Hsueh Wang. A Q-band miniaturized uniplanar MMIC HEMT mixer. / Chi-Hsueh Wang, Yo-Shen Lin, Huei Wang, Chun Hsiung Chen. // 2004 IEEE MTT-S International Microwave Symposium Digest. 6-11 June 2004. - Vol. 1. - P. 187-190. ↑
- C1693.** Suzuki T. 144-Gbit/s selector and 100-Gbit/s 4:1 multiplexer using InP HEMTs. / Suzuki T., Nakasha Y., Takahashi T., Makiyama K., Hirose T., Takikawa M. // 2004 IEEE MTT-S International Microwave Symposium Digest. 6-11 June 2004. - Vol. 1. - P. 117-120. ↑
- C1694.** Cabral P.M. New nonlinear device model for microwave power GaN HEMTs. / Cabral P.M., Pedro J.C., Carvalho N.B. // 2004 IEEE MTT-S International Microwave Symposium Digest. 6-11 June 2004. - Vol. 1. - P. 51-54. ↑
- C1695.** Sungjae Lee. Numerical noise model for the AlGaIn/GaN HEMT. / Sungjae Lee, Webb K.J. // 2004 IEEE MTT-S International Microwave Symposium Digest. 6-11 June 2004. - Vol. 2. - P. 1057-1060. ↑
- C1696.** Upshur J.I. Advanced non-linear model for accurate prediction of harmonically terminated power amplifier performance. / Upshur J.I., White C., Bayne M.E. Jr., Davis B., Walker L. Jr., Reece M.A., Thompson W.L. II, Cheng S., Wallis R.E. // 2004 IEEE MTT-S International Microwave Symposium Digest. 6-11 June 2004. - Vol. 2. - P. 1077-1080. ↑
- C1697.** Chang-Ho Lee. Novel T/R switch architectures for MIMO applications. / Chang-Ho Lee, Banerjee B., Laskar J. // 2004 IEEE MTT-S International Microwave Symposium Digest. 6-11 June 2004. - Vol. 2. - P. 1137-1140. ↑
- C1698.** Green B.M. A high power density 26 V GaAs pHEMT technology. / Green B.M., Lan E., Li P., Hartin O., Gaw C.A., CdeBaca M., Johnson E.M., Klingbeil L.S., Fisher P., Kim J., Maurer D., Knappenberger B., Miller M., Weitzel C.E. // 2004 IEEE MTT-S International Microwave Symposium Digest. 6-11 June 2004. - Vol. 2. - P. 817-820. ↑
- C1699.** Cha S. Wideband AlGaIn/GaN HEMT low noise amplifier for highly survivable receiver electronics. / Cha S., Chung Y.H., Wojtowicz M., Smorchkova I., Allen B.R., Yang J.M., Kagiwada R. // 2004 IEEE MTT-S International Microwave Symposium Digest. 6-11 June 2004. - Vol. 2. - P. 829-831. ↑
- C1700.** Akkul M. High efficiency power amplifier input/output circuit topologies for base station and WLAN applications. / Akkul M., Roberts M., Walker V., Bosch W. // 2004 IEEE MTT-S International Microwave Symposium Digest. 6-11 June 2004. - Vol. 2. - P. 843-846. ↑
- C1701.** Kaper V. Signal generation, control and frequency conversion AlGaIn/GaN HEMT MMICs. / Kaper V., Thompson R., Prunty T., Shealy J.R. // 2004 IEEE MTT-S International Microwave Symposium Digest. 6-11 June 2004. - Vol. 2. - P. 1145-1148. ↑

- C1702.** Andrenko A. Microwave resistive and dielectric planar antennas with conical radiation patterns. / Andrenko A., Ivanchenko I., Korolev A., Popenko N. // 2004. MSMW 04. The Fifth International Kharkov Symposium on Physics and Engineering of Microwaves, Millimeter, and Submillimeter Waves. 21-26 June 2004. - Vol. 2. - P. 674-676. ↑
- C1703.** Korolev A.M. Ultra-low-noise cooled microwave PHEMT amplifiers for radio astronomy applications. / Korolev A.M., Shulga V.M. // 2004. MSMW 04. The Fifth International Kharkov Symposium on Physics and Engineering of Microwaves, Millimeter, and Submillimeter Waves. 21-26 June 2004. - Vol. 2. - P. 894-895. ↑
- C1704.** Dobes J. Using modified GaAs FET model function for the accurate representation of PHEMTs and varactors. 2004. MELECON 2004. Proceedings of the 12th IEEE Mediterranean Electrotechnical Conference. 12-15 May 2004. - Vol. 1. - P. 35-38. ↑
- C1705.** Hettak K. A novel uniplanar 44 GHz MMIC subharmonic mixer using CPW series stubs. / Hettak K., Verver C.J., Morin G.A., Stubbs M.G. // 2004 IEEE MTT-S International Microwave Symposium Digest. 6-11 June 2004. - Vol. 2. - P. 1157-1160. ↑
- C1706.** Qi Zhang. Fully monolithic 8 watt Ku-band high power amplifier. / Qi Zhang, Brown S.A. // 2004 IEEE MTT-S International Microwave Symposium Digest. 6-11 June 2004. - Vol. 2. - P. 1161-1164. ↑
- C1707.** Jong Hwan Jeon. A novel dual band transmitter for WLAN 802.11 a/g applications. / Jong Hwan Jeon, Jae Hong Choi, Sung Min Kang, Tae Yong Kim, Won Choi, Kyung Heon Koo. // 2004 IEEE MTT-S International Microwave Symposium Digest. 6-11 June 2004. - Vol. 2. - P. 1285-1288. ↑
- C1708.** Brinkhoff J. Charge trapping and intermodulation in HEMTs. / Brinkhoff J., Parker A.E. // 2004 IEEE MTT-S International Microwave Symposium Digest. 6-11 June 2004. - Vol. 2. - P. 799-802. ↑
- C1709.** Lyons M.R. Design of low-cost 4W & 6W MMIC high power amplifiers for Ka-band modules. / Lyons M.R., Grondahl C.D., Daoud S.M. // 2004 IEEE MTT-S International Microwave Symposium Digest. 6-11 June 2004. - Vol. 3. - P. 1673-1676. ↑
- C1710.** Bhunia A. High heat flux cooling solutions for thermal management of high power density gallium nitride HEMT. / Bhunia A., Boutros K., Chung-Lung Chen. // 2004. ITherm '04. The Ninth Intersociety Conference on Thermal and Thermomechanical Phenomena in Electronic Systems. 1-4 June 2004. - Vol. 2. - P. 75-81. ↑
- C1711.** Kazemi H. An ultra-low power integrated T/R module for space-based radar technology. / Kazemi H., Hacker J.B., Xin H., Grace M., Norvell B., Higgins K., Gilbert M. // 2004. Proceedings of the IEEE Radar Conference. 26-29 April 2004. - P. 6-8. ↑
- C1712.** Nakasha Y. An 80 Gbit/s 1:2 demultiplexer in InP-based HEMT technology. / Nakasha Y., Suzuki T., Kano H., Kawano Y., Takahashi T., Makiyama K., Hirose T., Takikawa A. // 2004. Digest of Papers. 2004 IEEE Radio Frequency Integrated Circuits (RFIC) Symposium. 6-8 June 2004. - P. 321-324. ↑
- C1713.** Sano K. InP-based optical system ICs operating at 40 Gbit/s and beyond. / Sano K., Murata K., Fukuyama H., Tsunashima S., Ishii K., Kurishima K., Matsuzaki H., Enoki T., Tokumitsu M., Sugahara H., Muraguchi M. // 2004. Digest of Papers. 2004 IEEE Radio Frequency Integrated Circuits (RFIC) Symposium. 6-8 June 2004. - P. 313-316. ↑
- C1714.** Raphael S. Electrothermal models of transistors based on finite element analysis for radar applications. / Raphael S., Christophe C., Philippe D., Raymond Q. // 2004. ITherm '04. The Ninth Intersociety Conference on Thermal and Thermomechanical Phenomena in Electronic Systems. 1-4 June 2004. - Vol. 2. - P. 515-522. ↑
- C1715.** Boutros K.S. A study of output power stability of GaN HEMTs on SiC substrates. / Boutros K.S., Rowell P., Brar B. // 2004. 42nd Annual. 2004 IEEE International Reliability Physics Symposium Proceedings. 25-29 April 2004. - P. 577-578. ↑
- C1716.** Yang J.M. Affordable high performance InP X-band transceiver module for large aperture phased array applications. / Yang J.M., Aust M., Chung Y., Lee W., Stokes R., Dupery R., Lai R., Gorospe B., Kagiwada R. // 2004 IEEE MTT-S International Microwave Symposium Digest. 6-11 June 2004. - Vol. 3. - P. 1761-1763. ↑
- C1717.** Delcourt S. A nonuniform thermal de-embedding approach for cryogenic on-wafer high-frequency

noise measurements. / Delcourt S., Dambrine G., Bourzgui N.E., Lepilliet S., Laporte C., Fraysse J.-P., Maignan M. // 2004 IEEE MTT-S International Microwave Symposium Digest. 6-11 June 2004. - Vol. 3. - P. 1809-1812. ↑

**C1718.** Freeman J.C. Channel temperature model for microwave AlGaIn/GaN power HEMTs on SiC and sapphire. 2004 IEEE MTT-S International Microwave Symposium Digest. 6-11 June 2004. - Vol. 3. - P. 2031-2034. ↑

**C1719.** Chou Y.C. Degradation mechanism of GaAs PHEMT power amplifiers under elevated temperature lifetest with RF-overdrive. / Chou Y.C., Lai R., Grundbacher R., Yu M., Leung D., Callejo L., Eng D., Okazaki D., Yamane B., Kiyono K., Kan Q., Oki A. // 2004. 42nd Annual. 2004 IEEE International Reliability Physics Symposium Proceedings. 25-29 April 2004. - P. 463-468. ↑

**C1720.** Adesida I. GaN electronics with high electron mobility transistors. / Adesida I., Kumar V., Lee J.-W., Kuliev A., Schwindt R., Lanford W. // 2004. 24th International Conference on Microelectronics. 16-19 May 2004. - Vol. 1. - P. 89-96. ↑

**C1721.** van Vliet F.E. Fully-integrated core chip for X-band phased array T/R modules. / van Vliet F.E., de Boer A. // 2004 IEEE MTT-S International Microwave Symposium Digest. 6-11 June 2004. - Vol. 3. - P. 1753-1756. ↑

**C1722.** Kim Dae-Hyun. High  $f_T$  0.05  $\mu\text{m}$  In<sub>0.52</sub>AlAs/In<sub>0.53</sub>GaAs HEMT's with strained 5 nm InAs sub-channel on InP substrate. / Kim Dae-Hyun, Noh Hun-Hee, Lee Kang-Min, Lee Jae.-Hak., Wei Feng, Xiaogang Xie, Quangang Du, Jian Jiang, Seo Kwang-Seok. // 2004. 16th IPRM. 2004 International Conference on Indium Phosphide and Related Materials. 31 May-4 June 2004. - P. 558-559. ↑

**C1723.** Yuwei Liu. Photoluminescence and electrical properties of InGaAs/InP composite channel metamorphic HEMT structures subjected to rapid thermal annealing. / Yuwei Liu, Hong Wang, Yongzhong Xiong. // 2004. 16th IPRM. 2004 International Conference on Indium Phosphide and Related Materials. 31 May-4 June 2004. - P. 606-608. ↑

**C1724.** Chou Y.C. The de-bias effect of gate current in InP HEMT MMICs. / Chou Y.C., Truong M., Leung D., Grundbacher R., Lai R., Eng D., Block T., Oki A. // 2004. 16th IPRM. 2004 International Conference on Indium Phosphide and Related Materials. 31 May-4 June 2004. - P. 393-396. ↑

**C1725.** Malmkvist M. A 50-nm gate length InP pseudomorphic HEMT implemented in an MMIC broadband feedback amplifier. / Malmkvist M., Mellberg A., Grahn J., Rorsman N., Zirath H. // 2004. 16th IPRM. 2004 International Conference on Indium Phosphide and Related Materials. 31 May-4 June 2004. - P. 386-388. ↑

**C1726.** Chou Y.C. Tradeoff of DC/RF performance versus reliability in 0.1  $\mu\text{m}$  InP HEMTs. / Chou Y.C., Grundbacher R., Leung D., Lai R., Eng D., Liu P.H., Block T., Oki A. // 2004. 16th IPRM. 2004 International Conference on Indium Phosphide and Related Materials. 31 May-4 June 2004. - P. 389-392. ↑

**C1727.** Pierobon R. Study of breakdown dynamics in InAlAs/InGaAs/InP HEMTs with gate length scaling down to 80 nm. / Pierobon R., Rampazzo F., Clonfero F., De Pellegrin T., Bertazzo M., Meneghesso G., Zanoni E., Suemitsu T., Enoki T. // 2004. 16th IPRM. 2004 International Conference on Indium Phosphide and Related Materials. 31 May-4 June 2004. - P. 823-826. ↑

**C1728.** Shinohara K. Nanogate InP-HEMT technology for ultrahigh-speed performance. / Shinohara K., Yamashita Y., Endoh A., Watanabe I., Hikosaka K., Mimura T., Hiyamizu S., Matsui T. // 2004. 16th IPRM. 2004 International Conference on Indium Phosphide and Related Materials. 31 May-4 June 2004. - P. 721-726. ↑

**C1729.** Chou Y.C. Degradation analysis of 0.1  $\mu\text{m}$  InP HEMTs using low frequency noise characterization. / Chou Y.C., Guan H., Li G.P., Lai R., Grundbacher R., Leung D., Eng D., Block T., Oki A. // 2004. 16th IPRM. 2004 International Conference on Indium Phosphide and Related Materials. 31 May-4 June 2004. - P. 619-622. ↑

**C1730.** Schlechtweg M. Millimeter-wave and mixed-signal integrated circuits based on advanced metamorphic HEMT technology. / Schlechtweg M., Leuther A., Tessman A., Schworer C., Massler H., Reinert W., Lang M., Nowotny U., Kappeler O., Walther M., Losch R. // 2004. 16th IPRM. 2004 International Conference on Indium Phosphide and Related Materials. 31 May-4 June 2004. - P. 609-614. ↑

**C1731.** Hara N. Improvement in reliability of InP-based HEMTs by suppressing impact ionization. / Hara N., Okamoto N., Imanishi K., Sawada K., Takahashi T., Makiyama K., Takikawa M. // 2004. 16th IPRM. 2004



International Conference on Indium Phosphide and Related Materials. 31 May-4 June 2004. - P. 615-618. ↑

**C1732.** Dae-Hyun Kim. High performance of 0.15μm quasi enhancement-mode (E-mode) In<sub>0.4</sub> GaAs/In<sub>0.4</sub> AlAs metamorphic HEMTs on GaAs substrate using new triple-gate technology. / Dae-Hyun Kim, Hun-Hee Noh, Suk-Jin Kim, Jae-Hak Lee, Ki-Woong Chung, Kwang-Seok Seo. // 2004. 16th IPRM. 2004 International Conference on Indium Phosphide and Related Materials. 31 May-4 June 2004. - P. 374-377. ↑

**C1733.** Chee-Leong Tan. Investigation of drain current transient in InP-based high electron mobility transistors (HEMTs). / Chee-Leong Tan, Hong Wang, Radhakrishnan K., Wai-Chye Cheong, Jing Bu. // 2004. 16th IPRM. 2004 International Conference on Indium Phosphide and Related Materials. 31 May-4 June 2004. - P. 213-214. ↑

**C1734.** Der-Wei Tu. Metamorphic HEMT and its application. 2004. 16th IPRM. 2004 International Conference on Indium Phosphide and Related Materials. 31 May-4 June 2004. - P. 283. ↑

**C1735.** Cheng-Kuo Lin. Characteristics of In<sub>x</sub> Al<sub>1-x</sub> As/In<sub>x</sub> Ga<sub>1-x</sub> As (x=50%, 60%) metamorphic HEMTs on GaAs substrates. / Cheng-Kuo Lin, Jing-Chang Wu, Wen-Kai Wang, Yi-Jen Chan. // 2004. 16th IPRM. 2004 International Conference on Indium Phosphide and Related Materials. 31 May-4 June 2004. - P. 205-208. ↑

**C1736.** Elgaid K. Integration of a novel, high quality Si<sub>3</sub> N<sub>4</sub> metal insulator metal (MIM) capacitors deposited by (ICP-CVD) at room temperature with 50 nm T-gate InP-HEMTs to realise monolithic millimetre-wave integrated circuits (MMMICs). / Elgaid K., McLelland H., Cao X., Thayne I.G. // 2004. 16th IPRM. 2004 International Conference on Indium Phosphide and Related Materials. 31 May-4 June 2004. - P. 183-186. ↑

**C1737.** Cheng-Kuo Lin. Investigation of enhancement-mode metamorphic InAlAs/InGaAs HEMTs by Schottky metal diffusion. / Cheng-Kuo Lin, Jing-Chang Wu, Wen-Kai Wang, Yi-Jen Chan. // 2004. 16th IPRM. 2004 International Conference on Indium Phosphide and Related Materials. 31 May-4 June 2004. - P. 198-201. ↑

**C1738.** Dae-Hyun Kim. Passivation study for In<sub>0.4</sub> AlAs/In<sub>0.65</sub> GaAs HEMTs by UHV RPECVD grown SiN<sub>x</sub> dielectrics and their impact on I-V kink and low-frequency dispersion phenomena. / Dae-Hyun Kim, Hun-Hee Noh, Sung-Sun Choi, Jae-Hak Lee, Kwang-Seok Seo. // 2004. 16th IPRM. 2004 International Conference on Indium Phosphide and Related Materials. 31 May-4 June 2004. - P. 354-357. ↑

**C1739.** Tae-Woo Kim. Low-frequency transconductance dispersion characteristics of 0.13μm In<sub>0.65</sub> GaAs p-HEMTs with side-recessed InAlAs and InP surface. / Tae-Woo Kim, Dae-Hyun Kim, In-Ho Kang, Jeong-Hoon Kim, Kwang-Seok Seo, Jong-In Song. // 2004. 16th IPRM. 2004 International Conference on Indium Phosphide and Related Materials. 31 May-4 June 2004. - P. 370-373. ↑

**C1740.** Fastenau J.M. Strain relaxation and dislocation filtering in metamorphic HBT and HEMT structures grown on GaAs substrates by MBE. / Fastenau J.M., Lubyshv D., Fang X.-M., Doss C., Wu Y., Liu W.K., Bals S., Griffith Z., Kim Y.-M., Rodwell M.J.W. // 2004. 16th IPRM. 2004 International Conference on Indium Phosphide and Related Materials. 31 May-4 June 2004. - P. 346-349. ↑

**C1741.** Grundbacher R. High performance millimeter wave 0.1 μm InP HEMT MMIC LNAs fabricated on 100 mm wafers. / Grundbacher R., Uyeda J., Lai R., Umemoto D., Liu P.H., Barsky M., Cavus A., Lee L.J., Chen J., Gonzalez J., Chen S., Block T., Oki A. // 2004. 16th IPRM. 2004 International Conference on Indium Phosphide and Related Materials. 31 May-4 June 2004. - P. 284-287. ↑

**C1742.** Wichmann N. InAlAs/InGaAs double-gate HEMTs with high extrinsic transconductance. / Wichmann N., Duszynski I., Bollaert S., Wallart X., Cappy A. // 2004. 16th IPRM. 2004 International Conference on Indium Phosphide and Related Materials. 31 May-4 June 2004. - P. 295-298. ↑


**C1743.** Uchiyama H. Control of plasma induced fluorine damage in P-HEMT using InSb barrier layer. / Uchiyama H., Taniguchi T., Kudo M. // 2004. 16th IPRM. 2004 International Conference on Indium Phosphide and Related Materials. 31 May-4 June 2004. - P. 727-730. ↑


**C1744.** Parish G. AlGaIn/GaN High Electron Mobility Transistors with Improved Carrier Transport. / Parish G., Umana-Membreno G.A., Jolley S.M., Buttari D., Keller S., Nener B.D., Mishra U.K. // 2004 Conference on Optoelectronic and Microelectronic Materials and Devices. - Brisbane, Qld., 8-8 Dec. 2004. - P. 29-32. ↑


**C1745.** Jha S.K. Studies of Hot-Electron Degradation in GaN HEMTs with Varying Gate Recess Depths. / Jha S.K., Leung B.H., Surya C., Schweizer H., Pilkhuhn M.H. // 2004 Conference on Optoelectronic and





Microelectronic Materials and Devices. - Brisbane, Qld., 8-8 Dec. 2004. - P. 33-36. 


**C1746.** {no data available}. 2004 Conference on Optoelectronic and Microelectronic Materials and Devices-COMMAD 04 Proceedings. 2004 Conference on Optoelectronic and Microelectronic Materials and Devices. - Brisbane, Qld., 8-8 Dec. 2004. - P. i. 


**C1747.** Shouxuan Xie. High linearity GaN HEMT power amplifier with pre-linearization gate diode. / Shouxuan Xie, Paidi V., Heikman S., Likun Shen, Chini A., Mishra U.K., Rodwell M.J.W., Long S.I. // 2004. Proceedings. IEEE Lester Eastman Conference on High Performance Devices. 4-6 Aug. 2004. - P. 223-228. 


**C1748.** Parikh P. GaN HEMTs: material, device, circuit technology and applications. / Parikh P., Wu Y.-F., Moore M., Chavarkar P., Wisleder T., Mishra U.K., Sheppard S., Smith R.P., Saxler A., Alien S., Milligan J., Palmour J. // 2004. International Meeting for Future of Electron Devices. 26-28 July 2004. - P. 41-42. 


**C1749.** Guan L.H. The etching of GaAs, AlGaAs and InGaAs in different chemicals in p-HEMT mesa layers. / Guan L.H., Yusof A., Dolah A., Sazli Jusoh M., Yahya M.R., Majlis B.Y. // 2004. ICSE 2004. IEEE International Conference on Semiconductor Electronics. 7-9 Dec. 2004. - P. 4 


**C1750.** Rahim A.I.A. Design of GaAs-based pseudomorphic HEMTs by 2D device simulations. / Rahim A.I.A., Muhammad N.F.I., Sanusi R., Yahya M.R. // 2004. ICSE 2004. IEEE International Conference on Semiconductor Electronics. 7-9 Dec. 2004. - P. 5 


**C1751.** Kharuddin K.N.M. Comparison study of uniformly-doped and delta-doped Al<sub>0.22</sub>Ga<sub>0.78</sub>As/In<sub>0.22</sub>Ga<sub>0.78</sub>As pseudomorphic HEMTs. / Kharuddin K.N.M., Yeop Majlis B. // 2004. ICSE 2004. IEEE International Conference on Semiconductor Electronics. 7-9 Dec. 2004. - P. 4 


**C1752.** {no data available}. 2004 IEEE International Conference on Semiconductor Electronics (IEEE Cat. No.04EX917C). 2004. ICSE 2004. IEEE International Conference on Semiconductor Electronics. 7-9 Dec. 2004. - {no data available}. 


**C1753.** Kharuddin K.N.M. Electrical characteristics of Al<sub>0.22</sub>Ga<sub>0.78</sub>As/In<sub>0.22</sub>Ga<sub>0.78</sub>As PHEMT with gate length in nano regime. / Kharuddin K.N.M., Majlis B.Y. // 2004. ICSE 2004. IEEE International Conference on Semiconductor Electronics. 7-9 Dec. 2004. - P. 5 


**C1754.** Wu Y.-F. Noise characteristics of field-plated GaN HEMTs. / Wu Y.-F., Moore M., Wisleder T., Chavarkar P.M., Parikh P., Saxler A. // 2004. Proceedings. IEEE Lester Eastman Conference on High Performance Devices. 4-6 Aug. 2004. - P. 192-194. 


**C1755.** Zili Xie. Growth and characteristics of InP/In<sub>x</sub>Ga<sub>1-x</sub>As/In<sub>0.53</sub>Ga<sub>0.47</sub>As HEMTs. / Zili Xie, Jai Qiu, Juan Sun. // 2004. SIMC-XIII-2004. 13th International Conference on Semiconducting and Insulating Materials. 20-25 Sept. 2004. - P. 242-246. 

**C1756.** Rajan S. MBE-grown AlGaIn/GaN HEMTs on SiC. / Rajan S., Chakraborty A., Mishra U.K., Poblencz C., Waltereit P., Speck J.S. // 2004. Proceedings. IEEE Lester Eastman Conference on High Performance Devices. 4-6 Aug. 2004. - P. 108-113. 

**C1757.** Patro S.K. Design and performance of a ultra-low-NF, high gain, linear LNA for 3GPP wireless node-B application. 2004. Proceedings of the IEEE INDICON 2004. First India Annual Conference. 20-22 Dec. 2004. - P. 118-122. 

**C1758.** Zhenghe Feng. Simulation and design of 3D geometric RF IC inductors by novel modeling techniques with magPEEC plus FastCap. / Zhenghe Feng, Haibo Long. // 2004. Proceedings. ICCEA 2004. 2004 3rd International Conference on Computational Electromagnetics and Its Applications. 1-4 Nov. 2004. - P. PS/17. 

**C1759.** Palankovski V. Numerical simulation of selected semiconductor devices. / Palankovski V., Selberherr S. // 2004. 27th International Spring Seminar on Electronics Technology: Meeting the Challenges of Electronics Technology Progress. 13-16 May 2004. - Vol. 1. - P. 122-125. 

**C1760.** Ye P.D. GaN MOS-HEMT using atomic layer deposition Al<sub>2</sub>O<sub>3</sub> as gate dielectric and surface passivation. / Ye P.D., Yang B., Ng K.K., Bude J., Wilk G.D., Halder S., Hwang J.C.M. // 2004. Proceedings. IEEE Lester Eastman Conference on High Performance Devices. 4-6 Aug. 2004. - P. 167-172. 

**C1761.** Hongtao Xu. A new field-plated GaN HEMT structure with improved power and noise performance. /

Hongtao Xu, Sanabria C., Chini A., Yun Wei, Heikman S., Keller S., Mishra U.K., York R.A. // 2004.

Proceedings. IEEE Lester Eastman Conference on High Performance Devices. 4-6 Aug. 2004. - P. 186-191. ↑

**C1762.** Neuburger M. Unstrained InAlN/GaN HEMT structure. / Neuburger M., Zimmermann T., Kohn E., Dadgar A., Schulze F., Krtischil A., Gunther M., Witte H., Blasing J., Krost A., Daumiller I., Kunze M. // 2004.

Proceedings. IEEE Lester Eastman Conference on High Performance Devices. 4-6 Aug. 2004. - P. 161-166. ↑

**C1763.** Chu K.K. Stable high power GaN-on-GaN HEMT. / Chu K.K., Chao P.C., Windyka J.A. // 2004.

Proceedings. IEEE Lester Eastman Conference on High Performance Devices. 4-6 Aug. 2004. - P. 114-120. ↑

**C1764.** Vitusevich S.A. Low frequency noise parameters in an AlGaIn/GaN heterostructure with 33% and 75% Al mole fraction. / Vitusevich S.A., Danylyuk S.V., Klein N., Petrychuk M.V., Belyaev A.E., Vertiatichikh A., Eastman L.F. // 2004. Proceedings. IEEE Lester Eastman Conference on High Performance Devices. 4-6 Aug. 2004. - P. 138-144. ↑

**C1765.** Limacher R. 4-12 GHz InP HEMT-based MMIC low-noise amplifier. / Limacher R., Auf der Maur M., Meier H., Megej A., Orzati A., Bachtod W. // 2004. 16th IPRM. 2004 International Conference on Indium Phosphide and Related Materials. 31 May-4 June 2004. - P. 28-31. ↑

**C1766.** Wichmann N. 100nm InAlAs/InGaAs double-gate HEMT using transferred substrate. / Wichmann N., Duszynski I., Bollaert S., Mateos J., Wallart X., Cappy A. // 2004. IEDM Technical Digest. IEEE International Electron Devices Meeting. 13-15 Dec. 2004. - P. 1023-1026. ↑

**C1767.** Dae-Hyun Kim. Suppression of kink phenomenon in ultra-high-speed strained InAs- inserted E-mode HEMTs with a new 0.1  $\mu\text{m}$  Y-shaped Pt-buried gate and their impacts on device performance. / Dae-Hyun Kim, Tae-Woo Kim, Hun-Hee Noh, Jae-Hak Lee, Wei Feng, Xiaogang Xie, Quangang Du, Jiang Jian, Jong-In Song, Kwang-Seok Seo. // 2004. IEDM Technical Digest. IEEE International Electron Devices Meeting. 13-15 Dec. 2004. - P. 1027-1030. ↑

**C1768.** del Alamo J.A. Thermal, electrical and environmental reliability of InP HEMTs and GaAs PHEMTs. / del Alamo J.A., Villanueva A.A. // 2004. IEDM Technical Digest. IEEE International Electron Devices Meeting. 13-15 Dec. 2004. - P. 1019-1022. ↑

**C1769.** Kanamura M. A 100-W high-gain AlGaIn/GaN HEMT power amplifier on a conductive n-SiC substrate for wireless base station applications. / Kanamura M., Kikkawa T., Joshin K. // 2004. IEDM Technical Digest. IEEE International Electron Devices Meeting. 13-15 Dec. 2004. - P. 799-802. ↑

**C1770.** Jie Liu. Al<sub>0.3</sub>Ga<sub>0.7</sub>N/Al<sub>0.05</sub>Ga<sub>0.95</sub>N/GaN composite-channel HEMTs with enhanced linearity. / Jie Liu, Yugang Zhou, Rongming Chu, Yong Cai, Chen K.J., Kei May Lau. // 2004. IEDM Technical Digest. IEEE International Electron Devices Meeting. 13-15 Dec. 2004. - P. 811-814. ↑

**C1771.** Miyoshi M. Growth and characterization of AlGaIn/AlN/GaN HEMTs on 100-mm-diameter epitaxial AlN/sapphire templates. / Miyoshi M., Imanishi A., Ishikawa H., Egawa T., Asai K., Mouri M., Shibata T., Tanaka M., Oda O. // 2004. IEDM Technical Digest. IEEE International Electron Devices Meeting. 13-15 Dec. 2004. - P. 1031-1034. ↑

**C1772.** Hyun-Goo Kim. Construction of the Korean VLBI network (KVN). / Hyun-Goo Kim, Seog-Tae Han, Young-Chol Minh. // 2004. Proceedings. 2004 Asia-Pacific Radio Science Conference. 24-27 Aug. 2004. - P. 409-411. ↑

**C1773.** Varonen M. Millimetre wave metamorphic HEMT amplifiers. / Varonen M., Karkkainen M., Kantanen M., Karttaavi T., Kangaslahti P., Halonen K. // 2004. Proceedings Norchip Conference. 8-9 Nov. 2004. - P. 8-11. ↑

**C1774.** Otsuji T. A novel terahertz plasma-wave photomixer with resonant-cavity enhanced structure. / Otsuji T., Hanabe M., Shigenobu J., Takahashi S., Sano E. // 2004. Conference Digest of the 2004 Joint 29th International Conference on Infrared and Millimeter Waves, 2004 and 12th International Conference on Terahertz Electronics. 27 Sept.-1 Oct. 2004. - P. 331-332. ↑

**C1775.** Wu Y.-F. High-gain microwave GaN HEMTs with source-terminated field-plates. / Wu Y.-F., Moore M., Wisleder T., Chavarkar P.M., Mishra UK, Parikh P. // 2004. IEDM Technical Digest. IEEE International Electron Devices Meeting. 13-15 Dec. 2004. - P. 1078-1079. ↑

- C1776.** Tessmann A. Millimeter-wave circuits based on advanced metamorphic HEMT technology. / Tessmann A., Leuther A., Schworer C., Massler H., Reinert W., Walther M., Losch R., Schlechtweg M. // 2004. Conference Digest of the 2004 Joint 29th International Conference on Infrared and Millimeter Waves, 2004 and 12th International Conference on Terahertz Electronics. 27 Sept.-1 Oct. 2004. - P. 165-166. ↑
- C1777.** Pavlidis D. Recent advances in III-V nitride electronic devices. 2004. IEDM Technical Digest. IEEE International Electron Devices Meeting. 13-15 Dec. 2004. - P. 795-798. ↑
- C1778.** Jha A.R. Advances in III-V transistors (HEMTs and HBTs) for mm-wave applications. 2004. EDMO 2004. 12th International Symposium on Electron Devices for Microwave and Optoelectronic Applications. 8-9 Nov. 2004. - P. 5-8. ↑
- C1779.** Negra R. Switched-mode high-efficiency Ka-band MMIC power amplifier in GaAs pHEMT technology. / Negra R., Bachtold W. // 2004. EDMO 2004. 12th International Symposium on Electron Devices for Microwave and Optoelectronic Applications. 8-9 Nov. 2004. - P. 15-18. ↑
- C1780.** Wang F. Characteristics of low noise 800MHz amplifier at cryogenic temperature. / Wang F., Zhang X.P., Gao L.M., Wei B., Cao B.S., Gao B.X. // Proceedings Microwave and Millimeter Wave Technology, 2004. ICMMT 4th International Conference on. 18-21 Aug. 2004. - P. 991-994. ↑
- C1781.** Ain M.F. Design of 2 GHz quasi-lumped element oscillator. / Ain M.F., Hassan S.I.S. // 2004. RFM 2004. Proceedings RF and Microwave Conference. 5-6 Oct. 2004. - P. 13-16. ↑
- C1782.** Song Di. Simulation of the temperature injection PHEMT. / Song Di, Lu Chang-zhi, Cai Xiao-dan. // Proceedings Microwave and Millimeter Wave Technology, 2004. ICMMT 4th International Conference on. 18-21 Aug. 2004. - P. 531-535. ↑
- C1783.** Szczepaniak Z.R. Analysis of microwave X-band HEMT limiters based on self-limiting effect. / Szczepaniak Z.R., Arvaniti A. // 2004. EDMO 2004. 12th International Symposium on Electron Devices for Microwave and Optoelectronic Applications. 8-9 Nov. 2004. - P. 19-22. ↑
- C1784.** Liu H.Z. High linearity power amplifier for PHS base station using a 50 mm AlGaAs/InGaAs/GaAs PHEMT. / Liu H.Z., Huang H.K., Wang C.C., Wang Y.H., Chang C.H., Wu W., Wu C.L., Chang C.S. // 2004. Proceedings. The 2004 IEEE Asia-Pacific Conference on Circuits and Systems. 6-9 Dec. 2004. - Vol. 1. - P. 105-108. ↑
- C1785.** Yeong-Jia Chen. In<sub>0.425</sub>Al<sub>0.575</sub>As/In<sub>0.65</sub>Ga<sub>0.35</sub>As metamorphic HEMT on GaAs. / Yeong-Jia Chen, Zhou-Bin Wang, Ke-Hua Su, Wei-Chou Hsu. // 2004. Proceedings. IVESC 2004. The 5th International Vacuum Electron Sources Conference. 6-10 Sept. 2004. - P. 372-374. ↑
- C1786.** Chen-Kuo Chu. A 3.5GHz 2W MMIC power amplifier using AlGaAs/InGaAs/GaAs PHEMTs. / Chen-Kuo Chu, Hou-Kuei Huang, Hong-Zhi Liu, Ray-Jay Chiu, Che-Hung Lin, Chih-Cheng Wang, Yeong-Her Wang, Chuan-Chien Hsu, Wang Wu, Chang-Luen Wu, Chian-Sern Chang. // 2004. Proceedings. The 2004 IEEE Asia-Pacific Conference on Circuits and Systems. 6-9 Dec. 2004. - Vol. 1. - P. 101-104. ↑
- C1787.** Masuda S. 110GHz high-gain flip-chip InP HEMT amplifier with resin encapsulation on an organic substrate. / Masuda S., Kira H., Hirose T. // 2004. 34th European Microwave Conference. 11-15 Oct. 2004. - Vol. 1. - P. 81-84. ↑
- C1788.** Bunz B. Broadband HEMT-based frequency tripler for use in active multi-harmonic load-pull system. / Bunz B., Kompa G. // 2004. 34th European Microwave Conference. 11-15 Oct. 2004. - Vol. 1. - P. 193-196. ↑
- C1789.** Changzhi Lu. The temperature characteristics of AlGaN/GaN double heterostructure HEMTs. / Changzhi Lu, Shiwei Feng, Dongfeng Wang, Xiudian Zhu, Zhifang Fan, Morkoc H. // 2004. Proceedings. 7th International Conference on Solid-State and Integrated Circuits Technology. 18-21 Oct. 2004. - Vol. 3. - P. 2284-2286. ↑
- C1790.** Lijun Xue. Investigation on the sources of 2DEG in Al<sub>x</sub>Ga<sub>1-x</sub>N/GaN HEMT. / Lijun Xue, Ming Liu, Yan Wang, Yang Xia, Zhijing He, Long Ma, Lihui Zhang, Baoqin Chen, Zhiping Yu. // 2004. Proceedings. 7th International Conference on Solid-State and Integrated Circuits Technology. 18-21 Oct. 2004. - Vol. 2. - P. 1011-1014. ↑



- C1791.** Wang D. Recent advances in CDMA power amplifier module developments. / Wang D., Xinwei Wang, Ping Li, Tang A., Souchuns C., Wen Chen, McNamara B., Xudong Wang, Li Liu, Apel T., Pavio R., Canfiel J. // 2004. Proceedings. 7th International Conference on Solid-State and Integrated Circuits Technology. 18-21 Oct. 2004. - Vol. 2. - P. 1236-1241. ↑
- C1792.** Cao X. High yield, high uniformity, high performance 50 nm T-gate In<sub>0.52</sub>Al<sub>0.48</sub>As/In<sub>0.70</sub>Ga<sub>0.30</sub>As HEMT process. / Cao X., Thoms S., Stanley C., Thayne L. // 2004. Proceedings. 7th International Conference on Solid-State and Integrated Circuits Technology. 18-21 Oct. 2004. - Vol. 3. - P. 2249-2252. ↑
- C1793.** Barker J.M. Studies of high field transport in GaN/AlGaIn heterostructures. / Barker J.M., Ferry D.K., Goodnick S.M., Koleske D.D., Allerman A., Shul R.J. // 2004. Proceedings. 7th International Conference on Solid-State and Integrated Circuits Technology. 18-21 Oct. 2004. - Vol. 3. - P. 2261-2264. ↑
- C1794.** Shapoval S. Instability of the induced potential distribution in undoped AlGaIn/GaN HEMTs and SiC transistor structures. / Shapoval S., Sirotkin V., Kovalchuk A., Zemlyakov V., Yakimov E., Gudkov V. // 2004. Proceedings. 7th International Conference on Solid-State and Integrated Circuits Technology. 18-21 Oct. 2004. - Vol. 3. - P. 2277-2279. ↑
- C1795.** Murata K. InP-based IC technologies for 100-Gbit/s and beyond. / Murata K., Sano K., Enoki T., Sugahara H., Tokumitsu M. // 2004. 16th IPRM. 2004 International Conference on Indium Phosphide and Related Materials. 31 May-4 June 2004. - P. 10-15. ↑
- C1796.** Umedam Y. High-speed series-connected voltage-balancing pulse driver using InP HEMTs. / Umedam Y., Kanda A., Sano K., Murata K., Sugahara H. // 2004. 16th IPRM. 2004 International Conference on Indium Phosphide and Related Materials. 31 May-4 June 2004. - P. 16-19. ↑
- C1797.** Kim S. High performance of W-band MMICs using 60 nm InGaAs HEMT technology. / Kim S., Song S., Choi W., Lee S., Ko W., Kwon Y., Seo K. // 2004. 16th IPRM. 2004 International Conference on Indium Phosphide and Related Materials. 31 May-4 June 2004. - P. 20-23. ↑
- C1798.** Marso M. MSM varactor diodes based on AlGaIn/GaN/SiC HEMT layer structures. / Marso M., Bernat J., Javorka P., Fox A., Wolter M., Kordos P. // 2004. ASDAM 2004. The Fifth International Conference on Advanced Semiconductor Devices and Microsystems. Oct. 17-21, 2004. - P. 151-154. ↑
- C1799.** {no data available}. 2004 International Conference on Indium Phosphide and Related Materials. 16th IPRM (IEEE Cat. No.04CH37589). 2004. 16th IPRM. 2004 International Conference on Indium Phosphide and Related Materials. 31 May-4 June 2004. - {no data available}. ↑
- C1800.** Jin Hee Lee. 0.15 μm gate length MHEMT technology for 77 GHz automotive radar applications. / Jin Hee Lee, Hyung Sup Yoon, Jae Yeob Shim, Ju Yeon Hong, Dong Min Kang, Hae Cheon Kim, Kyung Ik Cho, Kyung Ho Lee, Boo Woo Kim. // 2004. 16th IPRM. 2004 International Conference on Indium Phosphide and Related Materials. 31 May-4 June 2004. - P. 24-27. ↑
- C1801.** Ismail N. Methodology to compare on-state breakdown loci of GaAs FET's. / Ismail N., Malbert N., Labat N., Touboul A., Muraro J.-L. // 2004. ICM 2004 Proceedings. The 16th International Conference on Microelectronics. 6-8 Dec. 2004. - P. 258-261. ↑
- C1802.** Hisaka T. Degradation mechanisms of GaAs PHEMTs in high humidity conditions. / Hisaka T., Aihara Y., Nogami Y., Sasaki H., Uehara Y., Yoshida N., Hayashi K. // 2004. [Reliability of Compound Semiconductors] ROCS Workshop. 24 Oct. 2004. - P. 81-88. ↑
- C1803.** Sghaier N. Current instabilities and deep level investigation on AlGaIn/GaN HEMT's on silicon and sapphire substrates. / Sghaier N., Yacoubi N., Bluet J.M., Souifi A., Guillot G., Gaquiere C., De Jaeger J.C. // 2004. ICM 2004 Proceedings. The 16th International Conference on Microelectronics. 6-8 Dec. 2004. - P. 672-675. ↑
- C1804.** Shoujun Yang. 0.15 μm PHEMT 80 Gb/s selector. / Shoujun Yang, Zhigong Wang, En Zhu, Jun Feng, Minzhen Xiong. // 2004. Proceedings. 7th International Conference on Solid-State and Integrated Circuits Technology. 18-21 Oct. 2004. - Vol. 3. - P. 2246-2248. ↑
- C1805.** Chou Y.C. The effect of elevated temperature lifetest on low frequency noise performance in GaAs PHEMT dual gate MMICs [LNA example]. / Chou Y.C., Callejo L., Bledenbender M., Lee K., Allen B., Lal R., Kan

Q., Grundbacher R., Leung D., Eng D., Block T., Okl A. // 2004. [Reliability of Compound Semiconductors] ROCS Workshop. 24 Oct. 2004. - P. 69-79. ↑

C1806. Pingshan Wang. Transient analysis of nonlinear microwave circuits using small-signal scattering parameters. / Pingshan Wang, Kaper V.S., Richard S.J., Kan E.C. // 2003 IEEE Radio Frequency Integrated Circuits (RFIC) Symposium. 8-10 June 2003. - P. 361-364. ↑

C1807. Tosaka H. An antenna switch MMIC using E/D mode p-HEMT for GSM/DCS/PCS/WCDMA bands application. / Tosaka H., Fujii T., Miyakoshi K., Ikenaka K., Takahashi M. // 2003 IEEE Radio Frequency Integrated Circuits (RFIC) Symposium. 8-10 June 2003. - P. 519-522. ↑

C1808. Kuo-Liang Deng. Novel high gain and broadband GaAs MMIC distributed amplifiers with traveling-wave gain stages. / Kuo-Liang Deng, Tian-Wei Huang, Huei Wang. // 2003 IEEE Radio Frequency Integrated Circuits (RFIC) Symposium. 8-10 June 2003. - P. 325-328. ↑

C1809. {no data available}. 61st Device Research Conference. Conference Digest (Cat. No.03TH8663). 2003 Device Research Conference. 23-25 June 2003. - {no data available}. ↑

C1810. Mohammad-Taheri M. The effect of dispersion on the bandwidth of distributed amplifier. / Mohammad-Taheri M., Elmasry M.I. // 2003. IEEE CCECE 2003. Canadian Conference on Electrical and Computer Engineering. 4-7 May 2003. - Vol. 3. - P. 1593-1596. ↑

C1811. Kaper V. Time-domain characterization of nonlinear operation of an AlGaIn/GaN HEMT. / Kaper V., Tilak V., Green B., Thompson R., Prunty T., Eastman L.F., Shealy J.R. // Spring 2003. 61st ARFTG Conference Digest. 13 June 2003. - P. 97-102. ↑

C1812. Virdee B.S. Single-ended amplifier that substantially improves PAE and ultra-broadband performance. / Virdee B.S., Virdee A.S. // 2003 IEEE Radio Frequency Integrated Circuits (RFIC) Symposium. 8-10 June 2003. - P. 691-693. ↑

C1813. Chang-Kun Park. Ku-band low noise amplifier with using short-stub ESD protection. / Chang-Kun Park, Min-Gun Kim, Chung-Han Kim, Songcheol Hong. // 2003 IEEE Radio Frequency Integrated Circuits (RFIC) Symposium. 8-10 June 2003. - P. 671-674. ↑

C1814. Tayel M.B. Characterization of high electron mobility transistor under different temperatures. / Tayel M.B., Rashed S.A. // 2003. NRSC 2003. Proceedings of the Twentieth National Radio Science Conference. 18-20 March 2003. - P. D10-1-7. ↑

C1815. Tatu S.O. New results on MMIC six-port's used in Ka band direct conversion receivers. / Tatu S.O., Moldovan E., Brehm G., Ke Wu, Bosio R.G. // 2003 IEEE Radio Frequency Integrated Circuits (RFIC) Symposium. 8-10 June 2003. - P. 523-526. ↑

C1816. Hui S.C. A multilayer active hybrid-ring using ground-slot coupling technique. / Hui S.C., Ooi B.-L., Leong M.S., Kooi P.S. // 2003 IEEE Radio Frequency Integrated Circuits (RFIC) Symposium. 8-10 June 2003. - P. 651-654. ↑

C1817. Naiqian Zhang. Large area GaN HEMT power devices for power electronic applications: switching and temperature characteristics. / Naiqian Zhang, Mehrotra V., Chandrasekaran S., Moran B., Likun Shen, Mishra U., Etzkorn E., Clarke D. // 2003. PESC '03. 2003 IEEE 34th Annual Power Electronics Specialist Conference. 15-19 June 2003. - Vol. 1. - P. 233-237. ↑

C1818. Jia-Liang Chen. Design of a 20-to-40 GHz bandpass MMIC amplifier. / Jia-Liang Chen, Sheng-Fuh Chang, Cherng-Cherng Liu, Hsi-Wei Kuo. // 2003 IEEE MTT-S International Microwave Symposium Digest. 8-13 June 2003. - Vol. 2. - P. 1275-1278. ↑

C1819. Tsukahara Y. Millimeter-wave MMIC switches with pHEMT cells reduced parasitic inductance. / Tsukahara Y., Katoh T., Notani Y., Ishida T., Ishikawa T., Komaru M., Matsuda Y. // 2003 IEEE MTT-S International Microwave Symposium Digest. 8-13 June 2003. - Vol. 2. - P. 1295-1298. ↑

C1820. Andersson K. C-band linear resistive wide bandgap FET mixers. / Andersson K., Desmaris V., Eriksson J., Rorsman N., Zirath H. // 2003 IEEE MTT-S International Microwave Symposium Digest. 8-13 June 2003. - Vol. 2. - P. 1303-1306. ↑

- C1821.** Suzuki T. A 100-Gbit/s 2:1 multiplexer in InP HEMT technology. / Suzuki T., Nakasha Y., Sakoda T., Sawada K., Takahashi T., Makiyama K., Hirose T., Takigawa M. // 2003 IEEE MTT-S International Microwave Symposium Digest. 8-13 June 2003. - Vol. 2. - P. 1173-1176. ↑
- C1822.** Sano K. 1.4-W 50-Gbit/s InP HEMT 1:4 demultiplexer IC with a multi-phase clock architecture. / Sano K., Murata K., Kitabayashi H., Sugitani S., Sugahara H., Enoki T. // 2003 IEEE MTT-S International Microwave Symposium Digest. 8-13 June 2003. - Vol. 2. - P. 1181-1184. ↑
- C1823.** Roux P. Single ended to differential MHEMT transimpedance amplifier with 66 dB-Ω differential transimpedance and 50 GHz bandwidth. / Roux P., Baeyens Y., Houtsmā V., Leven A., Weiner J., Benz A., Chen Y.K. // 2003 IEEE MTT-S International Microwave Symposium Digest. 8-13 June 2003. - Vol. 2. - P. 1193-1196. ↑
- C1824.** Garcia J.A. A zero-bias single-device balanced E-PHEMT mixer with conversion gain for RFID applications. / Garcia J.A., Malaver E., Cabria L. // 2003 IEEE MTT-S International Microwave Symposium Digest. 8-13 June 2003. - Vol. 2. - P. 1311-1314. ↑
- C1825.** Baeyens Y. Compact high-gain lumped differential 40 Gb/s driver amplifiers in production 0.15 μm PHEMT technology. / Baeyens Y., Paschke P., Houtsmā V., Leven A., Hocke R., Weisser S., Roux P., Chen Y.K. // 2003 IEEE Radio Frequency Integrated Circuits (RFIC) Symposium. 8-10 June 2003. - P. 67-70. ↑
- C1826.** Kikkawa T. High-power and high-efficiency AlGaIn/GaN HEMT operated at 50 V drain bias voltage. / Kikkawa T., Nagahara M., Adachi N., Yokokawa S., Kato S., Yokoyama M., Kanamura M., Yamaguchi Y., Hara N., Joshin K. // 2003 IEEE Radio Frequency Integrated Circuits (RFIC) Symposium. 8-10 June 2003. - P. 167-170. ↑
- C1827.** Ezzeddine A.K. The high voltage/high power FET (HiVP). / Ezzeddine A.K., Huang H.C. // 2003 IEEE Radio Frequency Integrated Circuits (RFIC) Symposium. 8-10 June 2003. - P. 215-218. ↑
- C1828.** Won-Young Uhm. A high performance V-band monolithic quadruple sub-harmonic mixer. / Won-Young Uhm, Woo-Suk Sul, Hyo-Jong Han, Sung-Chan Kim, Han-Sin Lee, Dan An, Sam-Dong Kim, Dong-Hoon Shin, Hyung-Moo Park, Jin-Koo Rhee. // 2003 IEEE MTT-S International Microwave Symposium Digest. 8-13 June 2003. - Vol. 2. - P. 1319-1322. ↑
- C1829.** Dellier S. 40 GHz MMIC driver of electro-absorption modulator for high-speed optical pulse generation. / Dellier S., Blache F., Campovecchio M., de La Grandiere D., Vuye S., Quere R., Burie J.R. // 2003 IEEE MTT-S International Microwave Symposium Digest. 8-13 June 2003. - Vol. 2. - P. 1347-1350. ↑
- C1830.** Chang-Soon Choi. A millimeter-wave harmonic optoelectronic mixer based on InAlAs/InGaAs metamorphic HEMT. / Chang-Soon Choi, Woo-Young Choi, Dae-Hyun Kim, Kwang-Seok Seo. // 2003 IEEE MTT-S International Microwave Symposium Digest. 8-13 June 2003. - Vol. 2. - P. 1383-1386. ↑
- C1831.** Endoh A. InP HEMTs: physics, applications, and future. / Endoh A., Yamashita Y., Shinohara K., Higashiwaki M., Hikosaka K., Matsui T., Hiyaizumi S., Mimura T. // 2003 Device Research Conference. 23-25 June 2003. - P. 5-8. ↑
- C1832.** Chou Y.C. On the investigation of gate metal interdiffusion in GaAs HEMTs. / Chou Y.C., Leung D., Lai R., Grundbacher R., Liu P.H., Biedenbender M., Kan Q., Eng D., Wojtowicz M., Oki A. // 2003. 25th Annual Technical Digest 2003. IEEE Gallium Arsenide Integrated Circuit (GaAs IC) Symposium. 9-12 Nov. 2003. - P. 63-66. ↑
- C1833.** Vice M. A 0.5-3 GHz high linearity enhancement mode pHEMT mixer with square wave drive and sum terminating diplexer. 2003. 25th Annual Technical Digest 2003. IEEE Gallium Arsenide Integrated Circuit (GaAs IC) Symposium. 9-12 Nov. 2003. - P. 52-55. ↑
- C1834.** Cola A. Novel heterostructure MSM photodetectors for Gigabit Ethernet. / Cola A., Nabet B., Chen X., Quaranta F., Cataldo A., Lomascolo M., Taurino A., Currie M. // 2003. IMOC 2003. Proceedings of the 2003 SBMO/IEEE MTT-S International Microwave and Optoelectronics Conference. 20-23 Sept. 2003. - Vol. 1. - P. 75-79. ↑
- C1835.** Wren M. The effect of the gate Schottky diode on pHEMT power amplifier performance. / Wren M., Brazil T.J. // 2003 High Frequency Postgraduate Student Colloquium. 8-9 Sept. 2003. - P. 52-55. ↑

- C1836.** Zirath H. Development of 60 GHz front end circuits for high data rate communication systems in Sweden and Europe. 2003. 25th Annual Technical Digest 2003. IEEE Gallium Arsenide Integrated Circuit (GaAs IC) Symposium. 9-12 Nov. 2003. - P. 93-96. ↑
- C1837.** Hisaka T. Degradation mechanism of PHEMT under large signal operation. / Hisaka T., Nogami Y., Sasaki H., Hasuike A., Yoshida N., Hayashi K., Sonoda T., Villanueva A.A., del Alamo J.A. // 2003. 25th Annual Technical Digest 2003. IEEE Gallium Arsenide Integrated Circuit (GaAs IC) Symposium. 9-12 Nov. 2003. - P. 67-70. ↑
- C1838.** Gu Z. A 2.3 V PHEMT power SP3T antenna switch IC for GSM handsets. / Gu Z., Johnson D., Belletete S., Frykund D. // 2003. 25th Annual Technical Digest 2003. IEEE Gallium Arsenide Integrated Circuit (GaAs IC) Symposium. 9-12 Nov. 2003. - P. 48-51. ↑
- C1839.** Zolper J.C. Status, challenges, and future opportunities for compound semiconductor electronics. 2003. 25th Annual Technical Digest 2003. IEEE Gallium Arsenide Integrated Circuit (GaAs IC) Symposium. 9-12 Nov. 2003. - P. 3-6. ↑
- C1840.** Smith P.M. Progress in GaAs metamorphic HEMT technology for microwave applications. / Smith P.M., Dugas D., Chu K., Nichols K., Duh K.G., Fisher J., Mt Pleasant L., Xu D., Gunter L., Vera A., Lender R., Meharry D. // 2003. 25th Annual Technical Digest 2003. IEEE Gallium Arsenide Integrated Circuit (GaAs IC) Symposium. 9-12 Nov. 2003. - P. 21-24. ↑
- C1841.** Caddemi A. Circuit modeling of low-noise microwave transistors: its role in supporting a complete device characterization. 2003. TELSIKS 2003. 6th International Conference on Telecommunications in Modern Satellite, Cable and Broadcasting Service. 1-3 Oct. 2003. - Vol. 2. - P. 549-556. ↑
- C1842.** Caddemi A. A robust approach for the direct extraction of HEMT circuit elements vs. bias and temperature. / Caddemi A., Donato N., Crupi G. // 2003. TELSIKS 2003. 6th International Conference on Telecommunications in Modern Satellite, Cable and Broadcasting Service. 1-3 Oct. 2003. - Vol. 2. - P. 557-560. ↑
- C1843.** Kao Y. 10 Gb/s soliton generation for ULH transmission using a wideband GaAs pHEMT amplifier. / Kao Y., Leven A., Baeyens Y., Chen Y., Grosz D., Bannon F., Fang W., Kung A., Maywar D., Lakoba T., Agarwal A., Banerjee S., Wood T. // 2003. OFC 2003 Optical Fiber Communications Conference. 23-28 March 2003. - P. 674-675. ↑
- C1844.** Nishikawa K. V-band fully-integrated TX/RX single-chip 3-D MMICs using commercial GaAs pHEMT technology for high-speed wireless applications. / Nishikawa K., Piernas B., Nakagawa T., Araki K., Cho K. // 2003. 25th Annual Technical Digest 2003. IEEE Gallium Arsenide Integrated Circuit (GaAs IC) Symposium. 9-12 Nov. 2003. - P. 97-100. ↑
- C1845.** Shen L. Temperature dependence of the current-voltage characteristics of AlGaIn/GaN HEMT. / Shen L., Chini A., Coffie R., Buttari D., Heikman S., Keller S., Mishra U. // 2003 Device Research Conference. 23-25 June 2003. - P. 63-64. ↑
- C1846.** Jung-Hoon Song. Generation of coherent GHz acoustic phonons in AlGaIn/GaN microwave field effect transistors. / Jung-Hoon Song, Qiang Zhang, Patterson W. III, Nurmikko A.V., Uren M.J., Hilton K.P., Balmer R.S., Martin T. // 2003 Device Research Conference. 23-25 June 2003. - P. 65-66. ↑
- C1847.** Shinohara K. 550 GHz-ft pseudomorphic InP-HEMTs with reduced source-drain resistance. / Shinohara K., Yamashita Y., Endoh A., Watanabe I., Hikosaka K., Mimura T., Hiyamizu S., Matsui T. // 2003 Device Research Conference. 23-25 June 2003. - P. 145-146. ↑
- C1848.** Zhang A.P. Self-heating effects in AlGaIn/GaN high-power HEMTs. / Zhang A.P., Rowland L.B., Kaminsky E.B., Tilak V., Allen A.F., Edward B.J. // 2003 Device Research Conference. 23-25 June 2003. - P. 15-16. ↑
- C1849.** Lee C. Ka-band CW power performance by AlGaIn/GaN HEMTs on SiC. / Lee C., Jinwei Yang, Asif Khan M., Saunier P. // 2003 Device Research Conference. 23-25 June 2003. - P. 17-18. ↑
- C1850.** Waechtler T. High power AlGaIn/GaN HEMTs grown by plasma-assisted MBE operating at 2 to 25 GHz. / Waechtler T., Manfra M.J., Weimann N.G. // 2003 Device Research Conference. 23-25 June 2003. - P.



61-62. ↑

**C1851.** Ohno Y. Effect of surface passivation on breakdown of AlGaIn/GaN HEMTs. / Ohno Y., Nakao T., Kishimoto S., Maezawa K., Mizutani T. // 2003. International Symposium on Compound Semiconductors. 25-27 Aug. 2003. - P. 169-170. ↑

**C1852.** Fujishiro H.I. Self-heating effect on device characteristics of GaN/AlGaIn HEMTs: 2D Monte Carlo device simulation. / Fujishiro H.I., Mikami N., Takei T., Izawa M., Moku T., Ohtuka K. // 2003. International Symposium on Compound Semiconductors. 25-27 Aug. 2003. - P. 171-172. ↑

**C1853.** Magno R. High speed, low power electronics using Sb-based semiconductors. / Magno R., Boos J.B., Bennett B.R., Ikossi K., Glaser E.R., Papanicolaou N.A., Anconca M.G., Tinkham B.P., Kruppa W., Park D., Shanabrook B.V., Mittereder J., Chang W., Hobart K.D., Bass R., Dietrich H.B., Mohny S.E., Wang S., Robinson J., Tsai R., Barsky M., Gutierrez A. // 2003. International Symposium on Compound Semiconductors. 25-27 Aug. 2003. - P. 175-176. ↑

**C1854.** Vertiatchikh A. Frequency and breakdown properties of AlGaIn/GaN HEMTs. / Vertiatchikh A., Schaff W.J., Eastman L.F. // 2003. International Symposium on Compound Semiconductors. 25-27 Aug. 2003. - P. 53-54. ↑

**C1855.** Parikh P. AlGaIn-GaN HEMTs: material, device, circuit technology and applications. / Parikh P., Wu Y.-F., Chavarkar P., Moore M., Mishra U.K., Sheppard S., Smith R.P., Saxler A., Duc J., Pribble W., Milligan J., Palmour J. // 2003. International Symposium on Compound Semiconductors. 25-27 Aug. 2003. - P. 165-166. ↑

**C1856.** Eastman L.F. Scattering limitations on electron transit velocity in AlGaIn/GaN HEMTs. / Eastman L.F., Matulionis A., Vertiatchikh A. // 2003. International Symposium on Compound Semiconductors. 25-27 Aug. 2003. - P. 167-168. ↑

**C1857.** Madureira M.A.M. Broad-band transimpedance amplifier for multigigabit-per-second (40 Gbps) optical communication systems in 0.135  $\mu\text{m}$  PHEMT technology. / Madureira M.A.M., Monteiro P.M.P., Aguiar R.L., Violas M., Gloanec M., Leclerc E., Lefebvre B. // 2003. ISCAS '03. Proceedings of the 2003 International Symposium on Circuits and Systems. 25-28 May 2003. - Vol. 1. - P. I-409-I-412-409. ↑

**C1858.** Kumar S. Enhancement mode GaAs PHEMT LNA with linearity control (IP3) and phased matched mitigated bypass switch and differential active mixer. / Kumar S., Vice M., Morkner H., Lam W. // 2003 IEEE MTT-S International Microwave Symposium Digest. 8-13 June 2003. - Vol. 3. - P. 1577-1580. ↑

**C1859.** Tessmann A. A coplanar 94 GHz low-noise amplifier MMIC using 0.07  $\mu\text{m}$  metamorphic cascode HEMTs. / Tessmann A., Leuther A., Schwoerer C., Massler H., Kudzusz S., Reinert W., Schlechtweg M. // 2003 IEEE MTT-S International Microwave Symposium Digest. 8-13 June 2003. - Vol. 3. - P. 1581-1584. ↑

**C1860.** Kao M. Metamorphic HEMT technology for millimeter-wave and 40-Gb/s fiber-optics applications. / Kao M., Beam E.A. III, Yun T., Campbell C.F., Heins M.S., Saunier P., Delaney J.B., Eye R.A. // 2003. International Conference on Indium Phosphide and Related Materials. 12-16 May 2003. - P. 361-364. ↑

**C1861.** Tanaka T. Growth of AlInAs using low-oxygen-content metalorganic precursors and application to HEMT structures. / Tanaka T., Tokudome K., Miyamoto Y. // 2003. International Conference on Indium Phosphide and Related Materials. 12-16 May 2003. - P. 393-396. ↑

**C1862.** Chou Y.C. On the development of automatic assembly line for InP HEMT MMICs. / Chou Y.C., Barsky M., Grundbacher R., Lai R., Leung D., Bonnin R., Akbany S., Tsui S., Kan Q., Eng D., Oki A. // 2003. International Conference on Indium Phosphide and Related Materials. 12-16 May 2003. - P. 476-479. ↑

**C1863.** Shih-Chieh Yen. An Nth-harmonic oscillator using an N-push coupled oscillator array with voltage-clamping circuits. / Shih-Chieh Yen, Tah-Hsiung Chu. // 2003 IEEE MTT-S International Microwave Symposium Digest. 8-13 June 2003. - Vol. 3. - P. 2169-2172. ↑

**C1864.** Lei Zhao. A 1 watt, 3.2 VDC, high efficiency distributed power PHEMT amplifier fabricated using LTCC technology. / Lei Zhao, Pavo A., Thompson W. // 2003 IEEE MTT-S International Microwave Symposium Digest. 8-13 June 2003. - Vol. 3. - P. 2201-2204. ↑

**C1865.** Tanahashi N. A W-band ultra low noise amplifier MMIC using GaAs pHEMT. / Tanahashi N., Kanaya

K., Matsuzuka T., Katoh I., Notani Y., Ishida T., Oku T., Ishikawa T., Komaru M., Matsuda Y. // 2003 IEEE MTT-S International Microwave Symposium Digest. 8-13 June 2003. - Vol. 3. - P. 2225-2228. ↑

**C1866.** Dawson D. Cryogenic measurements of 183 GHz MMIC low noise amplifiers. / Dawson D., Gaier T., Raja R., Nishimoto M., Lai R., Wells M. // 2003 IEEE MTT-S International Microwave Symposium Digest. 8-13 June 2003. - Vol. 3. - P. 1585-1587. ↑

**C1867.** Merkle T. A n-state time-domain measurement test-bench for characterization of intermodulation distortion on device level. / Merkle T., Ramberger S., Kuri M., van Raay F. // 2003 IEEE MTT-S International Microwave Symposium Digest. 8-13 June 2003. - Vol. 3. - P. 1643-1646. ↑

**C1868.** I-Jen Chen. A V-band GaAs HEMT uniplanar monolithic integrated antenna and receiver front end. / I-Jen Chen, Huei Wang, Powen Hsu. // 2003 IEEE MTT-S International Microwave Symposium Digest. 8-13 June 2003. - Vol. 3. - P. 2023-2026. ↑

**C1869.** Webster R.T. Impact ionization in AlGaAsSb/InGaAs/GaAsSb metamorphic HEMTs. / Webster R.T., Anwar A.F.M., Heaton J.L., Nichols K., Duncan S. // 2003. International Conference on Indium Phosphide and Related Materials. 12-16 May 2003. - P. 233-234. ↑

**C1870.** Dae-Hyun Kim. Schottky barrier height enhancement for In<sub>0.52</sub> AlAs layer by using in-situ Ar plasma pre-treatment and its application to In<sub>0.52</sub> AlAs/In<sub>0.53</sub> GaAs/InP HEMT's. / Dae-Hyun Kim, Young-Ho Kim, Jae-Eung Oh, Kwang-Seok Seo. // 2003. International Conference on Indium Phosphide and Related Materials. 12-16 May 2003. - P. 102-105. ↑

**C1871.** Robin F. InP HEMT-based CPW amplifiers for 94 and 110 GHz. / Robin F., Orzati A., Limacher R., Meier H., Bachtold W. // 2003. International Conference on Indium Phosphide and Related Materials. 12-16 May 2003. - P. 110-113. ↑

**C1872.** Mittereder J.A. Current collapse induced in AlGaN/GaN HEMTs by short-term DC bias stress. / Mittereder J.A., Binari S.C., Klein P.B., Roussos J.A., Katzer D.S., Storm D.F., Koleske D.D., Wickenden A.E., Henry R.L. // 2003. 41st Annual. 2003 IEEE International Reliability Physics Symposium Proceedings. 30 March-4 April 2003. - P. 320-323. ↑

**C1873.** Fukai Y.K. Bias acceleration model of drain resistance degradation in InP-based HEMTs. / Fukai Y.K., Sugitani S., Enoki T., Kitabayashi H., Makimura T., Yamane Y., Muraguchi M. // 2003. 41st Annual. 2003 IEEE International Reliability Physics Symposium Proceedings. 30 March-4 April 2003. - P. 324-328. ↑

**C1874.** Dae-Hyun Kim. Damage-free SiO<sub>2</sub>/SiN<sub>x</sub> side-wall gate process and its application to 40 nm InGaAs/InAlAs HEMT's with 65% InGaAs channel. / Dae-Hyun Kim, Suk-Jin Kim, Young-Ho Kim, Kwang-Seok Seo. // 2003. International Conference on Indium Phosphide and Related Materials. 12-16 May 2003. - P. 61-64. ↑

**C1875.** Sawada K. Fabrication of 0.1 μm-gate InP HEMTs using i-line lithography. / Sawada K., Makiyama K., Takahashi T., Nozaki K., Igarashi M., Kon J., Hara N. // 2003. International Conference on Indium Phosphide and Related Materials. 12-16 May 2003. - P. 65-68. ↑

**C1876.** Wichmann N. Double-gate HEMTs on transferred substrate. / Wichmann N., Duszynski I., Parenty T., Bollaert S., Mateos J., Wallart X., Cappy A. // 2003. International Conference on Indium Phosphide and Related Materials. 12-16 May 2003. - P. 118-121. ↑

**C1877.** Leuther A. 70 nm low-noise metamorphic HEMT technology on 4 inch GaAs wafers. / Leuther A., Tessmann A., Dammann M., Reinert W., Schlechtweg M., Mikulla M., Walther M., Weimann G. // 2003. International Conference on Indium Phosphide and Related Materials. 12-16 May 2003. - P. 215-218. ↑

**C1878.** Herrick K.J. W-band power metamorphic HEMT technology on GaAs. / Herrick K.J., Whelan C.S., Marsh P.F., Lardizabal S. // 2003. International Conference on Indium Phosphide and Related Materials. 12-16 May 2003. - P. 231-232. ↑

**C1879.** Seow Boon-Eu. A high isolation enhancement mode GaAs PHEMT buffer amplifier. / Seow Boon-Eu, Nguyen Lan, Vice M., Chan E., Chow Yut-Hoong. // 2003. NCTT 2003 Proceedings. 4th National Conference on Telecommunication Technology. 14-15 Jan. 2003. - P. 58-62. ↑

**C1880.** Gonzalez A.F. Comparison of bistable circuits based on resonant-tunneling diodes. / Gonzalez A.F.,

Mazumder P. // 2003. Proceedings. 16th International Conference on VLSI Design. 4-8 Jan. 2003. - P. 493-498.



**C1881.** Hyung Sup Yoon. 0.15  $\mu\text{m}$  gate length InAlAs/InGaAs power metamorphic HEMT on GaAs substrate with extremely low noise characteristics. / Hyung Sup Yoon, Jin Hee Lee, Jae Yeob Shim, Ju Yeon Hong, Dong Min Kang, Woo Jin Chang, Hae Cheon Kim, Kyoung Ik Cho. // 2003. International Conference on Indium Phosphide and Related Materials. 12-16 May 2003. - P. 114-117.

**C1882.** Udomoto J. A 38/77 GHz MMIC transmitter chip set for automotive applications. / Udomoto J., Matsuzuka T., Chaki S., Kanaya K., Katoh T., Notani Y., Hisaka T., Oku T., Ishikawa T., Komaru M., Matsuda Y. // 2003 IEEE MTT-S International Microwave Symposium Digest. 8-13 June 2003. - Vol. 3. - P. 2229-2232.

**C1883.** Matsuzuka T. A 19 GHz low phase noise HFET VCO MMIC. / Matsuzuka T., Kawakami K., Aihara Y., Ishikawa T., Komaru M., Matsuda Y. // 2003 IEEE MTT-S International Microwave Symposium Digest. 8-13 June 2003. - Vol. 2. - P. 725-728.

**C1884.** Cidronali A. Extraction of conversion matrices for P-HEMTs based on vectorial large-signal measurements. / Cidronali A., Gupta K.C., Jargon J., Remley K.A., DeGroot D., Manes G. // 2003 IEEE MTT-S International Microwave Symposium Digest. 8-13 June 2003. - Vol. 2. - P. 777-780.

**C1885.** Colomb F.Y. 2 and 4 watt Ka-band GaAs PHEMT power amplifier MMICs. / Colomb F.Y., Platzker A. // 2003 IEEE MTT-S International Microwave Symposium Digest. 8-13 June 2003. - Vol. 2. - P. 843-846.

**C1886.** Hui S.C. A multilayer active hybrid-ring using ground-slot coupling technique. / Hui S.C., Ban-Leong Ooi, Leong M.S., Kooi P.S. // 2003 IEEE MTT-S International Microwave Symposium Digest. 8-13 June 2003. - Vol. 1. - P. A137-A140.

**C1887.** Chang-Kun Park. Ku-band low noise amplifier with using short-stub ESD protection. / Chang-Kun Park, Min-Gun Kim, Chung-Han Kim, Songcheol Hong. // 2003 IEEE MTT-S International Microwave Symposium Digest. 8-13 June 2003. - Vol. 1. - P. A157-A160.

**C1888.** Virdee B.S. Single-ended amplifier that substantially improves PAE and ultra-broadband performance. / Virdee B.S., Virdee A.S. // 2003 IEEE MTT-S International Microwave Symposium Digest. 8-13 June 2003. - Vol. 1. - P. A177-A179.

**C1889.** Pei-Si Wu. An 18-71 GHz multi-band and high gain GaAs MMIC medium power amplifier for millimeter-wave applications. / Pei-Si Wu, Tian-Wei Huang, Huei Wang. // 2003 IEEE MTT-S International Microwave Symposium Digest. 8-13 June 2003. - Vol. 2. - P. 863-866.

**C1890.** Dan An. High conversion gain V-band quadruple subharmonic mixer using cascode structure. / Dan An, Sung Chan Kim, Woo Suk Sul, Hyo Jong Han, Han Shin Lee, Won Young Uhm, Hyung Moo Park, Sam Dong Kim, Dong Hoon Shin, Jin Koo Rhee. // 2003 IEEE MTT-S International Microwave Symposium Digest. 8-13 June 2003. - Vol. 2. - P. 911-914.

**C1891.** Varonen M. Integrated power amplifier for 60 GHz wireless applications. / Varonen M., Karkkainen M., Kangaslahti P., Porra V. // 2003 IEEE MTT-S International Microwave Symposium Digest. 8-13 June 2003. - Vol. 2. - P. 915-918.

**C1892.** Shuoqi Chen. A balanced 2 watt compact PHEMT power amplifier MMIC for Ka-band applications. / Shuoqi Chen, Reese E., Keon-Shik Kong. // 2003 IEEE MTT-S International Microwave Symposium Digest. 8-13 June 2003. - Vol. 2. - P. 847-850.

**C1893.** Shimura T. A high power density, 6W MMIC for Ku/K-Band applications. / Shimura T., Satoh T., Hasegawa Y., Fukaya J. // 2003 IEEE MTT-S International Microwave Symposium Digest. 8-13 June 2003. - Vol. 2. - P. 851-854.

**C1894.** Fujii K. E-PHEMT, single supply, power amplifier for Ku band applications. / Fujii K., Morkner H. // 2003 IEEE MTT-S International Microwave Symposium Digest. 8-13 June 2003. - Vol. 2. - P. 859-862.

**C1895.** Tatu S.O. New results on MMIC six-port's used in Ka band direct conversion receivers. / Tatu S.O., Moldovan E., Gailon B., Ke Wu, Bosisio R.G. // 2003 IEEE MTT-S International Microwave Symposium Digest. 8-13 June 2003. - Vol. 1. - P. A9-A12.

- C1896.** Herrick K.J. 95 GHz metamorphic HEMT power amplifiers on GaAs. / Herrick K.J., Lardizabal S.M., Marsh P.F., Whelan C.S. // 2003 IEEE MTT-S International Microwave Symposium Digest. 8-13 June 2003. - Vol. 1. - P. 137-140. ↑
- C1897.** Zhang A.P. Performance of AlGaIn/GaN HEMTs for 2.8 GHz and 10 GHz power amplifier applications. / Zhang A.P., Rowland L.B., Kaminsky E.B., Kretchmer J.W., Tilak V., Allen A.F., Edward B.J. // 2003 IEEE MTT-S International Microwave Symposium Digest. 8-13 June 2003. - Vol. 1. - P. 251-254. ↑
- C1898.** Wang W.K. A complete self-defined empirical model for enhancement-mode AlGaAs/InGaAs pHEMTs. / Wang W.K., Lin C.K., Wu C.C., Chan Y. // 2003 IEEE MTT-S International Microwave Symposium Digest. 8-13 June 2003. - Vol. 1. - P. 443-446. ↑
- C1899.** Allen D. 25.5 to 76.5GHz active frequency tripler for automotive radar applications. / Allen D., Bryant D., Gaiewski W. // 2003 IEEE MTT-S International Microwave Symposium Digest. 8-13 June 2003. - Vol. 3. - P. 2233-2236. ↑
- C1900.** Siweris H.J. Monolithic coplanar 77 GHz balanced HEMT mixer with very small chip size. / Siweris H.J., Tischer H. // 2003 IEEE MTT-S International Microwave Symposium Digest. 8-13 June 2003. - Vol. 1. - P. 125-128. ↑
- C1901.** Morgan M. A W-band monolithic medium power amplifier. / Morgan M., Weinreb S. // 2003 IEEE MTT-S International Microwave Symposium Digest. 8-13 June 2003. - Vol. 1. - P. 133-136. ↑
- C1902.** Margraf M. A new scaleable low frequency noise model for field-effect transistors used in resistive mixers. / Margraf M., Boeck G. // 2003 IEEE MTT-S International Microwave Symposium Digest. 8-13 June 2003. - Vol. 1. - P. 559-562. ↑
- C1903.** Reece M.A. A Ka-band class F MMIC amplifier design utilizing adaptable knowledge-based neural network modeling techniques. / Reece M.A., White C., Penn J., Davis B., Bayne M.Jr., Richardson N., Thompson W.I.I., Walker L. // 2003 IEEE MTT-S International Microwave Symposium Digest. 8-13 June 2003. - Vol. 1. - P. 615-618. ↑
- C1904.** Tosaka H. An antenna switch MMIC using E/D mode p-HEMT for GSM/DCS/PCS/WCDMA bands application. / Tosaka H., Fujii T., Miyakoshi K., Ikenaka K., Takahashi M. // 2003 IEEE MTT-S International Microwave Symposium Digest. 8-13 June 2003. - Vol. 1. - P. A5-A8. ↑
- C1905.** Schreurs D. ANN model for AlGaIn/GaN HEMTs constructed from near-optimal-load large-signal measurements. / Schreurs D., Verspecht J., Vandamme E., Vellas N., Gaquiere C., Germain M., Borghs G. // 2003 IEEE MTT-S International Microwave Symposium Digest. 8-13 June 2003. - Vol. 1. - P. 447-450. ↑
- C1906.** van Raay F. Large signal modeling of AlGaIn/GaN HEMTs with  $P_{sat} > 4$  W/mm at 30 GHz suitable for broadband power applications. / van Raay F., Quay R., Kiefer R., Schlechtweg M., Weimann G. // 2003 IEEE MTT-S International Microwave Symposium Digest. 8-13 June 2003. - Vol. 1. - P. 451-454. ↑
- C1907.** De Meyer S. Mechanism of power density degradation due to trapping effects in AlGaIn/GaN HEMTs. / De Meyer S., Charbonniaud C., Quere R., Campovecchio A., Lossy R., Wurfl J. // 2003 IEEE MTT-S International Microwave Symposium Digest. 8-13 June 2003. - Vol. 1. - P. 455-458. ↑
- C1908.** Dae-Hyun Kim. Asymmetrically recessed (ASR) 0.13 $\mu$ m In<sub>0.65</sub> GaAs HEMT's using double-deck shaped (DDS) gate technology. / Dae-Hyun Kim, Seong-Jin Yeon, Jae-Hak Lee, Kwang-Seok Seo. // 2003 International Semiconductor Device Research Symposium. 10-12 Dec. 2003. - P. 184-185. ↑
- C1909.** Kruppa W. Low-frequency noise characteristics of AlSb/InAsSb HEMTs as a function of temperature and illumination. / Kruppa W., Boos J.B., Bennett B.R., Tinkham B.P. // 2003 International Semiconductor Device Research Symposium. 10-12 Dec. 2003. - P. 194-195. ↑
- C1910.** Pearton S.J. Enhanced functionality in GaN and SiC devices by using novel processing. / Pearton S.J., Abernathy C.R., Gila B.P., Ren F., Zavada J.M., Chu S.N.G. // 2003 International Semiconductor Device Research Symposium. 10-12 Dec. 2003. - P. 302. ↑
- C1911.** Boutros K. High performance GaN HEMTs at 40 GHz with power density of 2.8W/mm. / Boutros K., Regan M., Rowell P., Gotthold D., Birkhahn R., Brar B. // 2003. IEDM '03 Technical Digest. IEEE International



Electron Devices Meeting. 8-10 Dec. 2003. - P. 12.5.1-12.5.2. ↑

**C1912.** Joshin K. A 174 W high-efficiency GaN HEMT power amplifier for W-CDMA base station applications. / Joshin K., Kikkawa T., Hayashi H., Maniwa T., Yokokawa S., Yokoyama M., Adachi N., Takikawa M. // 2003. IEDM '03 Technical Digest. IEEE International Electron Devices Meeting. 8-10 Dec. 2003. - P. 12.6.1-12.6.3. ↑

**C1913.** Tae-Woo Kim. Low-frequency noise characteristics of 0.13  $\mu\text{m}$  In<sub>0.65</sub>GaAs p-HEMT under the influence of impact ionization induced hole current. / Tae-Woo Kim, Dae-Hyun Kim, In-Ho Kang, Jeong-Hoon Kim, Kwang-Seok Seo, Jong-In Song. // 2003 International Semiconductor Device Research Symposium. 10-12 Dec. 2003. - P. 182-183. ↑

**C1914.** Gudimetta S. Improved quantization of 2DEG of p-HEMT. / Gudimetta S., Mil'shtein S. // 2003 International Semiconductor Device Research Symposium. 10-12 Dec. 2003. - P. 524-525. ↑

**C1915.** Yi-Chung Lien. A metamorphic high electron-mobility transistor with reflowed submicron T-gate for high-speed optoelectronics applications. / Yi-Chung Lien, Edward Yi Chang, Li-Xing Chu, Huang-Choung Chang, Cheng-Shih Lee, Szu-Hung Chen, Yueh-Ching Lin, Huang-Ming Lee. // Proceedings of the Sixth Chinese Symposium Optoelectronics. 12-14 Sept. 2003. - P. 281-283. ↑

**C1916.** Chan C.P. Low-frequency noise in laser-debonded GaN films. / Chan C.P., Leung B.H., Loke Y.H., Man H.C., Yue T.M., Surya C. // 2003 IEEE Conference on Electron Devices and Solid-State Circuits. 16-18 Dec. 2003. - P. 83-86. ↑

**C1917.** Papanicolaou N.A. 6.2 E In<sub>0.2</sub>Al<sub>0.8</sub>Sb/InAs<sub>0.7</sub>Sb<sub>0.3</sub> HEMTs for low voltage high-frequency applications. / Papanicolaou N.A., Tinkham B.P., Boos J.B., Bennett B.R., Bass R., Park D. // 2003 International Semiconductor Device Research Symposium. 10-12 Dec. 2003. - P. 352. ↑

**C1918.** Chini A. High performance AlGaIn/GaN HEMTs with a field plated gate structure. / Chini A., Buttari D., Coffie R., Shen L., Heikman S., Chakraborty A., Keller S., Mishra U.K. // 2003 International Semiconductor Device Research Symposium. 10-12 Dec. 2003. - P. 434-435. ↑

**C1919.** Bernat J. Influence of layer structure and surface passivation on performance of AlGaIn/GaN HEMTs on Si and SiC substrates. / Bernat J., Javorka P., Wolter M., Fox A., Marso M., Kordos P. // 2003 International Semiconductor Device Research Symposium. 10-12 Dec. 2003. - P. 437-438. ↑

**C1920.** Royter Y. High frequency InAs-channel HEMTs for low power ICs. / Royter Y., Elliott K.R., Deelman P.W., Rajavel R.D., Chow D.H., Milosavljevic I., Fields C.H. // 2003. IEDM '03 Technical Digest. IEEE International Electron Devices Meeting. 8-10 Dec. 2003. - P. 30.7.1-30.7.4. ↑

**C1921.** Ping-Yu Chen. An ultra low phase noise W-band GaAs-based PHEMT MMIC CPW VCO. / Ping-Yu Chen, Zou-Min Tsai, Shey-Shi Lu, Huei Wang. // 2003. 33rd European Microwave Conference. 7-9 Oct. 2003. - Vol. 2. - P. 503-506. ↑

**C1922.** Crespo-Cadenas C. Envelope currents method with extended dynamic range for the simulation of nonlinear communication circuits. / Crespo-Cadenas C., Reina-Tosina J. // 2003. 33rd European Microwave Conference. 7-9 Oct. 2003. - Vol. 2. - P. 769-772. ↑

**C1923.** Kamenopolsky S.D. Low cost 5-bit phase shifter for DBS phased array antennas. 2003. 33rd European Microwave Conference. 7-9 Oct. 2003. - Vol. 2. - P. 801-804. ↑

**C1924.** Schallner M. Millimetre wave VCOs with wide electronic tuning range for synthesised radios. / Schallner M., Kern S., Lohrmann R., Losert M., Muth K., Sommer D. // 2003. 33rd European Microwave Conference. 7-9 Oct. 2003. - Vol. 3. - P. 1187-1190. ↑

**C1925.** Sheng-Fuh Chang. A filter synthesis method applied to millimeter-wave distributed switch design. / Sheng-Fuh Chang, Jia-Liang Chen, Hsih-Wei Kuo, Han-Zen Hsu. // 2003. 33rd European Microwave Conference. 7-9 Oct. 2003. - Vol. 3. - P. 1295-1298. ↑

**C1926.** Forestier S. A dynamic bias control technique of PHEMT SSPA for optimised PAE and EVM applied to MQAM satellite communication systems. / Forestier S., Bouysse P., Quere R., Mallet A., Nebus J.M., Lapierre L. // 2003. 33rd European Microwave Conference. 7-9 Oct. 2003. - Vol. 3. - P. 1345-1348. ↑

- C1927.** Saito W. 600V AlGaIn/GaN power-HEMT: design, fabrication and demonstration on high voltage DC-DC converter. / Saito W., Takada Y., Kuraguchi M., Tsuda K., Omura I., Ogura T. // 2003. IEDM '03 Technical Digest. IEEE International Electron Devices Meeting. 8-10 Dec. 2003. - P. 23.7.1-23.7.4. ↑
- C1928.** Villanueva A.A. Electrical degradation mechanisms of RF power GaAs PHEMTs. / Villanueva A.A., del Alamos J.A., Hisaka T., Hayashi K. // 2003. IEDM '03 Technical Digest. IEEE International Electron Devices Meeting. 8-10 Dec. 2003. - P. 30.4.1-30.4.4. ↑
- C1929.** Makiyama K. Improvement of circuit-speed of HEMTs IC by reducing the parasitic capacitance. / Makiyama K., Takahashi T., Suzuki T., Sawada K., Ohki T., Nishi M., Hara N., Takikawa M. // 2003. IEDM '03 Technical Digest. IEEE International Electron Devices Meeting. 8-10 Dec. 2003. - P. 30.6.1-30.6.4. ↑
- C1930.** Tuovinen J. Technology for millimetre wave radiometers. / Tuovinen J., Hughes N., Jukkala P., Kangaslahti P., Karttaavi T., Sjoman P., Varis J. // 2003. 33rd European Microwave Conference. 7-9 Oct. 2003. - Vol. 2. - P. 883-886. ↑
- C1931.** Quay R. AlGaIn/GaN HEMTs on SiC: towards power operation at V-band. / Quay R., Tessmann A., Kiefer R., Weber R., van Raay F., Kuri M., Riessle M., Massler H., Muller S., Schlechtweg M., Weimann G. // 2003. IEDM '03 Technical Digest. IEEE International Electron Devices Meeting. 8-10 Dec. 2003. - P. 23.2.1-23.2.4. ↑
- C1932.** Wu Y.-F. 3.5-watt AlGaIn/GaN HEMTs and amplifiers at 35 GHz. / Wu Y.-F., Moore M., Saxler A., Smith P., Chavarkar P.M., Parikh P. // 2003. IEDM '03 Technical Digest. IEEE International Electron Devices Meeting. 8-10 Dec. 2003. - P. 23.5.1-23.5.3. ↑
- C1933.** Schreurs D. State-space modelling of slow-memory effects based on multisine vector measurements. / Schreurs D., Remley K.A., Myslinski M., Vandersmissen R. // 2003. Fall 2003. 62nd ARFTG Microwave Measurements Conference. 4-5 Dec. 2003. - P. 81-87. ↑
- C1934.** Hontschel J. Investigation of quantum effects in monolithic integrated circuits based on RTDs and HEMTs with a quantum hydrodynamic transport model. / Hontschel J., Kliks W., Stenzel R. // 2003 International Symposium on Compound Semiconductors: Post-Conference Proceedings. 25-27 Aug. 2003. - P. 114-117. ↑
- C1935.** Shinohara K. HEMTs with ultrahigh cutoff frequency. / Shinohara K., Matsui T., Yamashita Y., Endoh A., Hikosaka K., Mimura T., Watanabe I., Hiyamizu S. // 2003 International Symposium on Compound Semiconductors: Post-Conference Proceedings. 25-27 Aug. 2003. - P. 124-131. ↑
- C1936.** Courcelle L. Direct-Coupled DC-40 GHz Amplifier for High-Speed Data Communication System. / Courcelle L., Kerherve E., Jarry P. // 2003. 33rd European Microwave Conference. - Munich, Germany, Oct. 2003. - P. 1103-1106. ↑
- C1937.** LaBelle Remi. A 94 GHz RF Electronics Subsystem for the CloudSat Cloud Profiling Radar. / LaBelle Remi, Girard Ralph, Arbery Graham. // 2003. 33rd European Microwave Conference. - Munich, Germany, Oct. 2003. - P. 1139-1142. ↑
- C1938.** Vandersmissen R. Large-signal state-space model for Ge-based MHEMTs: construction and validation by an amplifier in multilayer thin-film technology. / Vandersmissen R., Schreurs D., Carchon G., Borghs G. // 2003. Fall 2003. 62nd ARFTG Microwave Measurements Conference. 4-5 Dec. 2003. - P. 283-289. ↑
- C1939.** Mann W. Optically powered small e-field probes with integrated JFET- and HEMT-preamplifiers. / Mann W., Petermann K. // 2003. EMC '03. 2003 IEEE International Symposium on Electromagnetic Compatibility. - Istanbul, 16-16 May 2003. - Vol. 1. - P. 445-448. ↑
- C1940.** Hyo-Soon Kang. High conversion gain millimeter-wave optoelectronic mixer based on InAlAs/InGaAs metamorphic HEMT. / Hyo-Soon Kang, Chang-Soon Choi, Woo-Young Choi, Dac-Hyun Kim, Kwang-Seok Seo. // 2003. MWP 2003 Proceedings. International Topical Meeting on Microwave Photonics. 10-12 Sept. 2003. - P. 105-108. ↑
- C1941.** Hirata A. High-directivity photonic emitter for 10-Gbit/s wireless link. / Hirata A., Kosugi T., Shibata T., Nagatsuma T. // 2003. MWP 2003 Proceedings. International Topical Meeting on Microwave Photonics. 10-12 Sept. 2003. - P. 35-38. ↑

- C1942.** Vertiatchikh A. Frequency and breakdown properties of AlGaIn/GaN HEMTs. / Vertiatchikh A., Schaff W.J., Eastman L.F., Matulionis A. // 2003 International Symposium on Compound Semiconductors: Post-Conference Proceedings. 25-27 Aug. 2003. - P. 132-137. ↑
- C1943.** Fujishiro H.I. Self-heating effect on device characteristics of GaN/AlGaIn HEMTs: 2D Monte Carlo device simulation. / Fujishiro H.I., Mikami N., Takei T., Izawa M., Moku T., Ohtuka K. // 2003 International Symposium on Compound Semiconductors: Post-Conference Proceedings. 25-27 Aug. 2003. - P. 152-157. ↑
- C1944.** Parikh P. AlGaIn-GaN HEMTs: material, device, circuit technology and applications. / Parikh P., Wu Y.-F., Chavarkar P., Moore M., Mishra U.K., Sheppard S., Smith R.P., Saxler A., Pribble W., Allen S., Milligan J., Palmour J. // 2003 International Symposium on Compound Semiconductors: Post-Conference Proceedings. 25-27 Aug. 2003. - P. 164-171. ↑
- C1945.** Hafele M. AGaAs PHEMT Distributed Amplifier with Low Group Delay Time Variation for 40 GBit/s Optical Systems. / Hafele M., Schworer C., Beilenhoff K., Schumacher H. // 2003. 33rd European Microwave Conference. - Munich, Germany, Oct. 2003. - P. 1091-1094. ↑
- C1946.** Amrouche Faiza. Simulation and Analytical Calculation of the Noise Figure in HEMT Gate Mixers. / Amrouche Faiza, Allam Rachid, Paillot Jean-Marie. // 2003. 33rd European Microwave Conference. - Munich, Germany, Oct. 2003. - P. 351-354. ↑
- C1947.** Kallfass I. A SiGe HEMT Mixer IC with Low Conversion Loss. / Kallfass I., Gruson F., Abele P., Michelakis K., Hackbarth T., Hieber K.-H., Muller J., Schumacher H. // 2003. 33rd European Microwave Conference. - Munich, Germany, Oct. 2003. - P. 407-410. ↑
- C1948.** Chen Ping-Yu. An Ultra Low Phase Noise W-Band GaAs-Based PHEMT MMIC CPW VCO. / Chen Ping-Yu, Tsai Zou-Min, Lu Shey-Shi, Wang Huei. // 2003. 33rd European Microwave Conference. - Munich, Germany, Oct. 2003. - P. 503-506. ↑
- C1949.** Palankovski V. Rigorous modeling of high-speed semiconductor devices. / Palankovski V., Selberherr S. // 2003 IEEE Conference on Electron Devices and Solid-State Circuits. 16-18 Dec. 2003. - P. 127-132. ↑
- C1950.** Courcelle L. DC-40 GHz amplifier for high-speed optical communications designed with the real frequency technique. / Courcelle L., Kerherve E., Jarry P. // 2003. ICECS 2003. Proceedings of the 2003 10th IEEE International Conference on Electronics, Circuits and Systems. 14-17 Dec. 2003. - Vol. 2. - P. 408-411. ↑
- C1951.** Vandersmissen Raf. Feedback Amplifier based on an Embedded HEMT in Thin-film Multilayer MCM-D Technology. / Vandersmissen Raf, Schreurs Dominique, Carchon Geert, Borghs Gustaaf. // 2003. 33rd European Microwave Conference. - Munich, Germany, Oct. 2003. - P. 297-300. ↑
- C1952.** Saghafi S. A new consideration of correlation between external noise sources in HEMT two-temperature model. / Saghafi S., Arfaei F. // 2003. IEEE Topical Conference on Wireless Communication Technology. 15-17 Oct. 2003. - P. 14-15. ↑
- C1953.** Song C. Design of a 49-GHz AlSb/InAs HEMT monolithic grid oscillator. / Song C., Shiroma W.A., Tsai R., Padmanabhan K., Bayuk B., Gutierrez-Aitken A. // 2003. IEEE Topical Conference on Wireless Communication Technology. 15-17 Oct. 2003. - P. 175-176. ↑
- C1954.** Margraf Michael. 1/f Noise Optimum for Field-Effect Transistors in Single-Ended Resistive Mixers. / Margraf Michael, Boeck Georg. // 2003. 33rd European Microwave Conference. - Munich, Germany, Oct. 2003. - P. 1015-1017. ↑
- C1955.** Crespo-Cadenas Carlos. Envelope Currents Method with Extended Dynamic Range for the Simulation of Nonlinear Communication Circuits. / Crespo-Cadenas Carlos, Reina-Tosina Javier. // 2003. 33rd European Microwave Conference. - Munich, Germany, Oct. 2003. - P. 769-772. ↑
- C1956.** Kamenopolsky Stanimir D. Low cost 5-bit Phase Shifter for DBS Phased Array Antennas. 2003. 33rd European Microwave Conference. - Munich, Germany, Oct. 2003. - P. 801-804. ↑
- C1957.** Tuovinen Jussi. Technology for Millimetre Wave Radiometers. / Tuovinen Jussi, Hughes Nicholas, Jukkala Petri, Kangaslahti Pekka, Karttaavi Timo, Sjoman Pekka, Varis Jussi. // 2003. 33rd European Microwave Conference. - Munich, Germany, Oct. 2003. - P. 883-886. ↑

- C1958.** Vaha-Heikkila T. Wideband cryogenic on-wafer measurements at 20-295 K and 50-110 GHz. / Vaha-Heikkila T., Varis J., Hakojarvi H., Tuovinen J. // 2003. 33rd European Microwave Conference. 7-9 Oct. 2003. - Vol. 3. - P. 1167-1170. ↑
- C1959.** Thompson R. Improved fabrication process for obtaining high power density AlGaIn/GaN HEMTs. / Thompson R., Kaper V., Prunty T., Shealy J.R. // 2003. 25th Annual Technical Digest 2003. IEEE Gallium Arsenide Integrated Circuit (GaAs IC) Symposium. 9-12 Nov. 2003. - P. 298-300. ↑
- C1960.** Saka N. Low standby leakage current power amplifier module made with junction PHEMT technology. / Saka N., Nakamura M., Shimada M., Kimura T., Motoyama H., Hase I. // 2003. 25th Annual Technical Digest 2003. IEEE Gallium Arsenide Integrated Circuit (GaAs IC) Symposium. 9-12 Nov. 2003. - P. 301-304. ↑
- C1961.** Tsai R. Metamorphic AlSb/InAs HEMT for low-power, high-speed electronics. / Tsai R., Barsky M., Boos J.B., Bennett B.R., Lee J., Papanicolaou N.A., Magno R., Namba C., Liu P.H., Park D., Grundbacher R., Gutierrez A. // 2003. 25th Annual Technical Digest 2003. IEEE Gallium Arsenide Integrated Circuit (GaAs IC) Symposium. 9-12 Nov. 2003. - P. 294-297. ↑
- C1962.** DiCarlo P. A highly integrated quad-band GSM TX-front-end-module. / DiCarlo P., Boerman S., Burton R., Chung H.-C., Evans D., Gerard M., Gering J., Khayo I., Lagrandier L., Lalicevic I., Reginella P., Sprinkle S., Tkachenko Y. // 2003. 25th Annual Technical Digest 2003. IEEE Gallium Arsenide Integrated Circuit (GaAs IC) Symposium. 9-12 Nov. 2003. - P. 280-283. ↑
- C1963.** Rosker M. DARPA's program on Antimonide Based Compound Semiconductors (ABCS). / Rosker M., Shah J. // 2003. 25th Annual Technical Digest 2003. IEEE Gallium Arsenide Integrated Circuit (GaAs IC) Symposium. 9-12 Nov. 2003. - P. 293. ↑
- C1964.** Korolev A.M. Ultra-low-noise amplifier for the ranges 0.5-1, 1-2, 2-4 GHz: design peculiarities. / Korolev A.M., Shulga V.M. // 2003. CriMiCo 2003. 13th International Crimean Conference Microwave and Telecommunication Technology. 8-12 Sept. 2003. - P. 156-158. ↑
- C1965.** Xin Cao. High performance 50 nm T-gate In<sub>0.52</sub>Al<sub>0.48</sub>As/In<sub>0.53</sub>Ga<sub>0.47</sub>As metamorphic high electron mobility transistors. / Xin Cao, Thayne I., Thoms S., Holland M., Stanley C. // 2003. ESSDERC '03. 33rd Conference on European Solid-State Device Research. 16-18 Sept. 2003. - P. 517-519. ↑
- C1966.** Chen-Kuo Chu. A 3.3 V self-biased 2.4-2.5GHz high linearity PHEMT MMIC power amplifier. / Chen-Kuo Chu, Hou-Kuei Huang, Chih-Cheng Wang, Yeong-Her Wang, Chuan Chien Hsu, Wang Wu, Chang-Luen Wu, Chian-Sern Chang. // 2003. ESSCIRC '03. Proceedings of the 29th European Solid-State Circuits Conference. 16-18 Sept. 2003. - P. 667-670. ↑
- C1967.** Kuzmik J. Backgating, high-current and breakdown characterisation of AlGaIn/GaN HEMTs on silicon substrates. / Kuzmik J., Blaho M., Pogany D., Gornik E., Alam A., Dikme Y., Heuken M., Javorka P., Marso M., Kordos P. // 2003. ESSDERC '03. 33rd Conference on European Solid-State Device Research. 16-18 Sept. 2003. - P. 319-322. ↑
- C1968.** Yemtsev P.A. Nonlinear model of high electron mobility transistor. / Yemtsev P.A., Sunduchkov I.K., Shelkovnikov B.N., Sunduchkov K.S. // 2003. CriMiCo 2003. 13th International Crimean Conference Microwave and Telecommunication Technology. 8-12 Sept. 2003. - P. 216-217. ↑
- C1969.** Moran D.A.J. Self-aligned 0.12 μm T-gate In<sub>0.53</sub>Ga<sub>0.47</sub>As/In<sub>0.52</sub>Al<sub>0.48</sub>As HEMT technology utilising a non-annealed ohmic contact strategy. / Moran D.A.J., Kalna K., Boyd E., McEwan F., McLelland H., Zhuang L.L., Stanley C.R., Asenov A., Thayne I. // 2003. ESSDERC '03. 33rd Conference on European Solid-State Device Research. 16-18 Sept. 2003. - P. 315-318. ↑
- C1970.** Jinho Jeong. 10 Gb/s modulator driver IC with ultra high gain and compact size using composite lumped-distributed amplifier approach. / Jinho Jeong, Youngwoo Kwon. // 2003. 25th Annual Technical Digest 2003. IEEE Gallium Arsenide Integrated Circuit (GaAs IC) Symposium. 9-12 Nov. 2003. - P. 149-152. ↑
- C1971.** Murata K. InP HEMT IC technology for 40 Gbit/s and beyond. / Murata K., Sano K., Fukuyama H., Yamane Y., Fukai Y.K., Kitabayashi H., Sugahara H., Enoki T. // 2003. 25th Annual Technical Digest 2003. IEEE Gallium Arsenide Integrated Circuit (GaAs IC) Symposium. 9-12 Nov. 2003. - P. 161-164. ↑
- C1972.** Eye R. 77 GHz low noise amplifier for automotive radar applications. / Eye R., Allen D. // 2003. 25th



Annual Technical Digest 2003. IEEE Gallium Arsenide Integrated Circuit (GaAs IC) Symposium. 9-12 Nov. 2003. - P. 139-142. ↑

**C1973.** Lai R. Highly linear and compact MMW phased array transmitters [MMIC power amplifiers]. / Lai R., Siddiqui M., Pitman B., Nishimoto M., Johnson K., Din S., Fordham D., Schreyer G., Grundbacher R., Callejo L., Streit D. // 2003. 25th Annual Technical Digest 2003. IEEE Gallium Arsenide Integrated Circuit (GaAs IC) Symposium. 9-12 Nov. 2003. - P. 101-104. ↑

**C1974.** Lefebvre B. High dynamic range, triple gate-based compact DC-40 GHz variable attenuator MMIC for Ka-band variable gain amplifier ICs. / Lefebvre B., Bessemoulin A., Amara H., Sevin R., Quentin P. // 2003. 25th Annual Technical Digest 2003. IEEE Gallium Arsenide Integrated Circuit (GaAs IC) Symposium. 9-12 Nov. 2003. - P. 135-138. ↑

**C1975.** Suzuki T. A 80-Gbit/s D-type flip-flop circuit using InP HEMT technology. / Suzuki T., Takahashi T., Hirose T., Takigawa M. // 2003. 25th Annual Technical Digest 2003. IEEE Gallium Arsenide Integrated Circuit (GaAs IC) Symposium. 9-12 Nov. 2003. - P. 165-168. ↑

**C1976.** Morkner H. A 18-45 GHz double-balanced mixer with integrated LO amplifier and unique suspended broadside-coupled balun. / Morkner H., Kumar S., Vice M. // 2003. 25th Annual Technical Digest 2003. IEEE Gallium Arsenide Integrated Circuit (GaAs IC) Symposium. 9-12 Nov. 2003. - P. 267-270. ↑

**C1977.** Jessen G.H. Gate optimization of AlGaIn/GaN HEMTs using WSi, Ir, Pd, and Ni Schottky contacts. / Jessen G.H., Fitch R.C., Gillespie J.K., Via G.D., Moser N.A., Yannuzzi M.J., Crespo A., Dettmer R.W., Jenkins T.J. // 2003. 25th Annual Technical Digest 2003. IEEE Gallium Arsenide Integrated Circuit (GaAs IC) Symposium. 9-12 Nov. 2003. - P. 277-279. ↑

**C1978.** Kozhuharov R. A 55 GHz HEMT monolithic voltage controlled sources. / Kozhuharov R., Masuda T., Zirath H., Lowenmark V. // 2003. 25th Annual Technical Digest 2003. IEEE Gallium Arsenide Integrated Circuit (GaAs IC) Symposium. 9-12 Nov. 2003. - P. 259-262. ↑

**C1979.** Fukuyama H. Optical receiver module using an InP HEMT transimpedance amplifier for over 40 Gbit/s. / Fukuyama H., Murata K., Sano K., Kitabayashi H., Yamane Y., Enoki T., Sugahara H. // 2003. 25th Annual Technical Digest 2003. IEEE Gallium Arsenide Integrated Circuit (GaAs IC) Symposium. 9-12 Nov. 2003. - P. 237-240. ↑

**C1980.** Masuda T. A high spectral purity GaAs PHEMT MMIC balanced frequency quadrupler. / Masuda T., Lowenmark V., Zirath H., Kozhuharov R. // 2003. 25th Annual Technical Digest 2003. IEEE Gallium Arsenide Integrated Circuit (GaAs IC) Symposium. 9-12 Nov. 2003. - P. 255-258. ↑

**C1981.** Ryzhii M. Modeling of the excitation of terahertz plasma oscillations in a HEMT by ultrashort optical pulses. / Ryzhii M., Satou A., Khmyrova I., Vyukov V., Ryzhii V., Shur M.S. // 2003. NUSOD 2003. Proceedings of the IEEE/LEOS 3rd International Conference on Numerical Simulation of Semiconductor Optoelectronic Devices. 14-16 Oct. 2003. - P. 84-85. ↑

**C1982.** Vandersmissen R. Feedback amplifier based on an embedded HEMT in thin-film multilayer MCM-D technology. / Vandersmissen R., Schreurs D., Carchon G., Borghs G. // 2003. 33rd European Microwave Conference. 7-9 Oct. 2003. - Vol. 1. - P. 297-300. ↑

**C1983.** Amrouche F. Simulation and analytical calculation of the noise figure in HEMT gate mixers. / Amrouche F., Allam R., Paillot J.M. // 2003. 33rd European Microwave Conference. 7-9 Oct. 2003. - Vol. 1. - P. 351-354. ↑

**C1984.** Min Park. Single supply, high linearity, high efficient PHEMT power devices and amplifier for 2 GHz & 5 GHz WLAN applications. / Min Park, Hokyun Ahn, Dong Min Kang, Honggu Ji, Jaekyoung Mun, Haecheon Kim, Kyoung Ik Cho. // 2003. 33rd European Microwave Conference. 7-9 Oct. 2003. - Vol. 1. - P. 371-374. ↑

**C1985.** Bessemoulin A. A chip-scale packaged amplifier MMIC using broadband hot-via transitions. / Bessemoulin A., Gaessler C., Marschall P., Quentin P. // 2003. 33rd European Microwave Conference. 7-9 Oct. 2003. - Vol. 1. - P. 289-292. ↑

**C1986.** Hongtao Xu. Integration of Bax Sr1-x TiO3 thin films with AlGaIn/GaN HEMT circuits. / Hongtao Xu, Pervez N.K., Hansen P.J., Sanabria C., Shen L., Keller S., Mishra U.K., York R.A. // 2003. EDMO 2003. The

11th IEEE International Symposium on Electron Devices for Microwave and Optoelectronic Applications. 17-18 Nov. 2003. - P. 273-278. ↑

**C1987.** Sotero S. Dual band monolithic AGC amplifier for space applications based on a commercial 0.2  $\mu\text{m}$  PHEMT technology. / Sotero S., Herrera A., Cabo J. // 2003. 33rd European Microwave Conference. 7-9 Oct. 2003. - Vol. 1. - P. 9-12. ↑

**C1988.** Long S. Ka-band coplanar low-noise amplifier design with power PHEMTs. / Long S., Escotte L., Graffeuil J., Fellon P., Roques D. // 2003. 33rd European Microwave Conference. 7-9 Oct. 2003. - Vol. 1. - P. 17-20. ↑

**C1989.** Lohrmann R. A novel distributed multicell multistage amplifier structure. / Lohrmann R., Gill H., Koch S. // 2003. 33rd European Microwave Conference. 7-9 Oct. 2003. - Vol. 1. - P. 379-382. ↑

**C1990.** Hafele M. A GaAs PHEMT distributed amplifier with low group delay time variation for 40 GBit/s optical systems. / Hafele M., Schworer C., Beilenhoff K., Schumacher H. // 2003. 33rd European Microwave Conference. 7-9 Oct. 2003. - Vol. 3. - P. 1091-1094. ↑

**C1991.** Courcelle L. Direct-coupled DC-40 GHz amplifier for high-speed data communication system. / Courcelle L., Kerherve E., Jarry P. // 2003. 33rd European Microwave Conference. 7-9 Oct. 2003. - Vol. 3. - P. 1103-1106. ↑

**C1992.** LaBelle R. A 94 GHz RF Electronics Subsystem for the CloudSat Cloud Profiling Radar. / LaBelle R., Girard R., Arbery G. // 2003. 33rd European Microwave Conference. 7-9 Oct. 2003. - Vol. 3. - P. 1139-1142. ↑

**C1993.** Margraf M. 1/f noise optimum for field-effect transistors in single-ended resistive mixers. / Margraf M., Boeck G. // 2003. 33rd European Microwave Conference. 7-9 Oct. 2003. - Vol. 3. - P. 1015-1017. ↑

**C1994.** Seemann K. Flip-chip integration of power HEMTs: a step towards a GaN MMIC technology. / Seemann K., Ramberger S., Tessmann A., Quay R., Schneider J., Riessle M., Walcher H., Kuri M., Kiefer R., Schlechtweg M. // 2003. 33rd European Microwave Conference. 7-9 Oct. 2003. - Vol. 1. - P. 383-386. ↑

**C1995.** Santarelli A. A simplified approach for quasi-linear power amplifier distortion evaluation. / Santarelli A., Paganelli R.P., Costantini A., Vannini G., Filicori F. // 2003. 33rd European Microwave Conference. 7-9 Oct. 2003. - Vol. 1. - P. 387-390. ↑

**C1996.** Kallfass I. A SiGe HEMT mixer IC with low conversion loss. / Kallfass I., Gruson F., Abele P., Michelakis K., Hackbarth T., Hieber K.-H., Muller J., Schumacher H. // 2003. 33rd European Microwave Conference. 7-9 Oct. 2003. - Vol. 1. - P. 407-410. ↑

**C1997.** Schwierz F. Recent advances in GaN HEMT development. / Schwierz F., Ambacher O. // 2003. EDMO 2003. The 11th IEEE International Symposium on Electron Devices for Microwave and Optoelectronic Applications. 17-18 Nov. 2003. - P. 204-209. ↑

**C1998.** Lu C.Y. A low noise composite-channel metamorphic HEMT for wireless communication application. / Lu C.Y., Chen K.S., Lee H.M., Chang E.Y., Chen S.H., Lin Y.C., Chen G.J. // 2003. EDMO 2003. The 11th IEEE International Symposium on Electron Devices for Microwave and Optoelectronic Applications. 17-18 Nov. 2003. - P. 87-92. ↑

**C1999.** Wang Y.H. L-band, high efficiency 25 watt power amplifier using PHEMT for base station system. / Wang Y.H., Liu H.Z., Huang H.K., Wang C.C. // 2003. EDMO 2003. The 11th IEEE International Symposium on Electron Devices for Microwave and Optoelectronic Applications. 17-18 Nov. 2003. - P. 76-82. ↑

**C2000.** Pajona O. Modelling of the trap related parasitic effects in metamorphic HEMT on GaAs substrate. / Pajona O., Aupetit-Berthelemot C., Dumas J.M. // 2003. EDMO 2003. The 11th IEEE International Symposium on Electron Devices for Microwave and Optoelectronic Applications. 17-18 Nov. 2003. - P. 151-156. ↑

**C2001.** Yuan K. High breakdown voltage  $\text{In}_{0.52}\text{Al}_{0.48}\text{As}/\text{In}_{0.53}\text{Ga}_{0.47}\text{As}$  metamorphic HEMT using  $\text{InxGa}_{1-x}\text{P}$  graded buffer. / Yuan K., Radhakrishnan K. // 2002. IPRM. 14th Indium Phosphide and Related Materials Conference. 2002. - P. 161-164. ↑

**C2002.** Malmqvist R. A tunable active MMIC filter for on-chip X-band radar receiver front-ends. / Malmqvist R.,

Gustafsson A., Alfredsson M., Ouacha A. // 2002 IEEE MTT-S International Microwave Symposium Digest. - Seattle, WA, 2002. - Vol. 3. - P. 1907-1910. ↑

C2003. Streit D. InP HEMT and HBT applications beyond 200 GHz. / Streit D., Lai R., Oki A., Gutierrez-Aitken A. // 2002. IPRM. 14th Indium Phosphide and Related Materials Conference. 2002. - P. 11-14. ↑

C2004. Mateos J. Improvement of the high frequency performance of HEMTs by bufferless technology. / Mateos J., Gonzalez T., Pardo D., Bollaert S., Wallart X., Cappy A. // 2002. IPRM. 14th Indium Phosphide and Related Materials Conference. - Stockholm, 2002. - P. 173-176. ↑

C2005. Hyung Sup Yoon. Low noise characteristics of double-doped In<sub>0.52</sub>Al<sub>0.48</sub>As/In<sub>0.53</sub>Ga<sub>0.47</sub>As power metamorphic HEMT on GaAs substrate with wide head T-shaped gate. / Hyung Sup Yoon, Jin Hee Lee, Jae Yeob Shim, Seong Jin Kim, Dong Min Kang, Ju Yeon Hong, Woo Jin Chang, Kyung Ho Lee. // 2002. IPRM. 14th Indium Phosphide and Related Materials Conference. 2002. - P. 201-204. ↑

C2006. Chou Y.C. Innovative nitride passivation of 0.1 μm InGaAs/InAlAs/InP HEMTs using high-density inductively coupled plasma CVD (HD-ICP-CVD). / Chou Y.C., Lai R., Li G.P., Nam P., Grundbacher R., Barsky M., Kim H.K., Ra Y., Oki A., Streit D. // 2002. IPRM. 14th Indium Phosphide and Related Materials Conference. 2002. - P. 315-318. ↑

C2007. Chou Y.C. High reliability of 0.07 μm pseudomorphic InGaAs/InAlAs/InP HEMT MMICs on 3-inch InP substrates. / Chou Y.C., Leung D., Lai R., Grundbacher R., Barsky M., Tsai R., Eng D., Wojtowicz M., Nishimoto M., Liu P.H., Oki A., Streit D. // 2002. IPRM. 14th Indium Phosphide and Related Materials Conference. 2002. - P. 365-368. ↑

C2008. Sleiman A. Breakdown dynamics and RF-breakdown in InP-based HEMTs. / Sleiman A., Di Carlo A., Lugli P. // 2002. IPRM. 14th Indium Phosphide and Related Materials Conference. 2002. - P. 181-184. ↑

C2009. Thobel J.-L. Monte Carlo study of electron transport in AlSb/InAs HEMT structures. / Thobel J.-L., Bonno O., Boutry H., Dessenne F. // 2002. IPRM. 14th Indium Phosphide and Related Materials Conference. 2002. - P. 185-188. ↑

C2010. Dubois A. Use of a system simulator to study the influence of InP-HEMT excess gate current on 40 Gbits/s fiber optic system performances. / Dubois A., Aupetit-Berthelemot C., Verneuil J.L., Dumas J.M. // 2002. IPRM. 14th Indium Phosphide and Related Materials Conference. 2002. - P. 197-200. ↑

C2011. Ghis A. Solid-state 8 GHz transient signal digitizer characterization. / Ghis A., Ouvrier-Buffet P., Rolland N., Benlarbi-Delai A., Rolland P.A., Glay D., Jaeger D. // 2002 IEEE MTT-S International Microwave Symposium Digest. - Seattle, WA, 2002. - Vol. 3. - P. 1673-1676. ↑

C2012. Nishikawa K. Compact LNA and VCO 3-D MMICs using commercial GaAs PHEMT technology for V-band single-chip TRX MMIC. / Nishikawa K., Piernas B., Kamogawa K., Nakagawa T., Araki K. // 2002 IEEE MTT-S International Microwave Symposium Digest. - Seattle, WA, 2002. - Vol. 3. - P. 1717-1720. ↑

C2013. Mimino Y. A 60 GHz millimeter-wave MMIC chipset for broadband wireless access system front-end. / Mimino Y., Nakamura K., Hasegawa Y., Aoki Y., Kuroda S., Tokumitsu T. // 2002 IEEE MTT-S International Microwave Symposium Digest. - Seattle, WA, 2002. - Vol. 3. - P. 1721-1724. ↑

C2014. Yamanaka K. Ku-band low noise MMIC amplifier with bias circuit for compensation of temperature dependence and process variation. / Yamanaka K., Yamauchi K., Mori K., Ikeda Y., Ikematsu H., Tanahashi N., Takagi T. // 2002 IEEE MTT-S International Microwave Symposium Digest. - Seattle, WA, 2002. - Vol. 3. - P. 1427-1430. ↑

C2015. Malmqvist R. A 7.9-9.7 GHz on-chip radar receiver front-end for future adaptive X-band smart skin array antennas. / Malmqvist R., Alfredsson M., Gustafsson A., Ouacha A. // 2002 IEEE MTT-S International Microwave Symposium Digest. - Seattle, WA, 2002. - Vol. 3. - P. 1431-1434. ↑

C2016. Lucero R. Design of an LTCC integrated tri-band direct conversion receiver front-end module. / Lucero R., Pavia A., Penunuri D., Bost J. // 2002 IEEE MTT-S International Microwave Symposium Digest. - Seattle, WA, 2002. - Vol. 3. - P. 1545-1548. ↑

C2017. Fujii K. A 60 GHz MMIC chipset for 1-Gbit/s wireless links. / Fujii K., Adamski M., Bianco P., Gunyan

D., Hall J., Kishimura R., Lesko C., Schefer M., Hessel S., Morkner H., Niedzwiecki A. // 2002 IEEE MTT-S International Microwave Symposium Digest. - Seattle, WA, 2002. - Vol. 3. - P. 1725-1728. ↑

C2018. Tessmann A. A 94 GHz single-chip FMCW radar module for commercial sensor applications. / Tessmann A., Kudzus S., Feltgen T., Riessle M., Sklarczyk C., Haydl W.H. // 2002 IEEE MTT-S International Microwave Symposium Digest. - Seattle, WA, 2002. - Vol. 3. - P. 1851-1854. ↑

C2019. Werthof A. A 38/76 GHz automotive radar chip set fabricated by a low cost PHEMT technology. / Werthof A., Siweris H.J., Tischer H., Liebl W., Jaeger G., Grave T. // 2002 IEEE MTT-S International Microwave Symposium Digest. - Seattle, WA, 2002. - Vol. 3. - P. 1855-1858. ↑

C2020. Barnes A.R. A comparison of W-band monolithic resistive mixer architectures. / Barnes A.R., Munday P., Jennings R., Moore M.T. // 2002 IEEE MTT-S International Microwave Symposium Digest. - Seattle, WA, 2002. - Vol. 3. - P. 1867-1870. ↑

C2021. Vaudesca O. A highly integrated MMIC chipset for 60 GHz broadband wireless applications. / Vaudesca O., Lefebvre B., Lehoue V., Quentin P. // 2002 IEEE MTT-S International Microwave Symposium Digest. - Seattle, WA, 2002. - Vol. 3. - P. 1729-1732. ↑

C2022. Kikkawa T. A 36 W CW AlGaIn/GaN-power HEMT using surface-charge-controlled structure. / Kikkawa T., Nagahara M., Kimura T., Yokokawa S., Kato S., Yokoyama M., Tateno Y., Horino K., Domen K., Yamaguchi Y., Hara N., Joshin K. // 2002 IEEE MTT-S International Microwave Symposium Digest. - Seattle, WA, 2002. - Vol. 3. - P. 1815-1818. ↑

C2023. Pribble W.L. Applications of SiC MESFETs and GaN HEMTs in power amplifier design. / Pribble W.L., Palmour J.W., Sheppard S.T., Smith R.P., Allen S.T., Smith T.J., Ring Z., Sumakeris J.J., Saxler A.W., Milligan J.W. // 2002 IEEE MTT-S International Microwave Symposium Digest. - Seattle, WA, 2002. - Vol. 3. - P. 1819-1822. ↑

C2024. Enoki T. InP-based HEMT technologies toward 100 Gbit/s ICs. 2002. IPRM. 14th Indium Phosphide and Related Materials Conference. 2002. - P. 439-442. ↑

C2025. Sandhu R. 3.2 W/mm, 71% PAE AlGaIn/GaN HEMT operation at 20 GHz. / Sandhu R., Wojtowicz M., Smorchkova I., Barsky M., Tsai R., Yang J.W., Wang H., Khan M.A. // 2002. 60th DRC. Conference Digest Device Research Conference. 2002. - P. 27-28. ↑

C2026. AbdelRassoul R.A. Modeling transconductance- and capacitance-voltage characteristics of AlGaAs/GaAs HEMTs. / AbdelRassoul R.A., Yakout M.A., AbdelFattah A.I., Essa S.G. // 2002. (NRSC 2002). Proceedings of the Nineteenth National Radio Science Conference. 2002. - P. 475-483. ↑

C2027. Ben-Yaacov I. AlGaIn/GaN current aperture vertical electron transistors. / Ben-Yaacov I., Seck Y.-K., Heikman S., DenBaars S.P., Mishra U.K. // 2002. 60th DRC. Conference Digest Device Research Conference. 2002. - P. 31-32. ↑

C2028. Sheppard S.T. High power hybrid and MMIC amplifiers using wide-bandgap semiconductor devices on semi-insulating SiC substrates. / Sheppard S.T., Smith R.P., Pribble W.L., Ring Z., Smith T., Allen S.T., Milligan J., Palmour J.W. // 2002. 60th DRC. Conference Digest Device Research Conference. 2002. - P. 175-178. ↑

C2029. Weimann N.G. AlGaIn/GaN HEMTs grown by MBE on semi-insulating HVPE GaN templates. / Weimann N.G., Manfra M.J., Hsu J.W.P., Pfeiffer L.N., West K.W., Lang D.V., Molnar R.J. // 2002. 60th DRC. Conference Digest Device Research Conference. 2002. - P. 33. ↑

C2030. Li A.Z. High performance of InGaP/InGaAs enhanced-mode PHEMT structures by gas source molecular beam epitaxy. / Li A.Z., Chen Y.Q., Chen J.X., Liu X.C., Chen J., Wang R.M. // 2002 International Conference on Molecular Beam Epitaxy. 2002. - P. 77-78. ↑

C2031. {no data available}. Device Research Conference (Cat. No.02TH8606). 2002. 60th DRC. Conference Digest Device Research Conference. 2002. - {no data available}. ↑

C2032. Hoke W.E. High indium metamorphic HEMT on a GaAs substrate. / Hoke W.E., Kennedy T.D., Torabi A., Whelan C.S., Marsh P.F., Leoni R.E., Xu C., Hsieh K.C. // 2002 International Conference on Molecular Beam Epitaxy. 2002. - P. 73-74. ↑



- C2033.** Watanabe I. Interface roughness scattering of electrons in a [411]A In<sub>0.53</sub> Ga<sub>0.47</sub> As/In<sub>0.52</sub> Al<sub>0.48</sub> As HEMT structure with super-flat interfaces. / Watanabe I., Kanzaki K., Kitada T., Yamamoto M., Shimomura S., Hiayamizu S. // 2002 International Conference on Molecular Beam Epitaxy. 2002. - P. 75-76. ↑
- C2034.** Coffie R. P-GaN/AlGaN/GaN high electron mobility transistors. / Coffie R., Heikman S., Buttari D., Keller S., Chini A., Shen L., Zhang N., Jimenez A., Jena D., Mishra U.K. // 2002. 60th DRC. Conference Digest Device Research Conference. 2002. - P. 25-26. ↑
- C2035.** Moon J.S. Submicron enhancement-mode AlGaN/GaN HEMTs. / Moon J.S., Wong D., Hussain T., Micovic M., Deelman P., Ming Hu, Antcliffe M., Ngo C., Hashimoto P., McCray L. // 2002. 60th DRC. Conference Digest Device Research Conference. 2002. - P. 23-24. ↑
- C2036.** Varonen M. Power amplifiers for 60 GHz WLAN applications. / Varonen M., Karkkainen M., Riska J., Kangaslahti P., Porra V. // 2002. RAWCON 2002. IEEE Radio and Wireless Conference. 2002. - P. 245-248. ↑
- C2037.** Mellberg A. InP HEMT-based, cryogenic, wideband LNAs for 4-8 GHz operating at very low DC-power. / Mellberg A., Wadefalk N., Rorsman N., Choumas E., Stenarson J., Angelov I., Starski P., Kollberg E., Grahn J., Zirath H. // 2002. IPRM. 14th Indium Phosphide and Related Materials Conference. 2002. - P. 459-462. ↑
- C2038.** Cordier Y. Influence of growth conditions on the structural, optical and electrical quality of MBE grown InAlAs/InGaAs metamorphic HEMTs on GaAs. / Cordier Y., Lorenzini P., Chauveau J.-M., Ferre D., Androussi Y., DiPersio J., Vignaud D., Codron J.-L. // 2002 International Conference on Molecular Beam Epitaxy. 2002. - P. 71-72. ↑
- C2039.** Grundbacher R. 0.1 μm InP HEMT devices and MMICs for cryogenic low noise amplifiers from X-band to W-band. / Grundbacher R., Lai R., Barsky M., Tsai R., Gaier T., Weinreb S., Dawson D., Bautista J.J., Davis J.F., Erickson N., Block T., Oki A. // 2002. IPRM. 14th Indium Phosphide and Related Materials Conference. 2002. - P. 455-458. ↑
- C2040.** Orzati A. A 48 GHz monolithically integrated frequency tripler with InP HEMTs. / Orzati A., Robin F., Meier H.P., Homan O.J., Bachtold W. // 2002. IPRM. 14th Indium Phosphide and Related Materials Conference. 2002. - P. 447-450. ↑
- C2041.** Shinohara K. Importance of gate-recess structure to the cutoff frequency of ultra-high-speed InGaAs/InAlAs HEMTs. / Shinohara K., Yamashita Y., Endoh A., Hikosaka K., Matsui T., Hiayamizu S., Mimura T. // 2002. IPRM. 14th Indium Phosphide and Related Materials Conference. - Stockholm, 2002. - P. 451-454. ↑
- C2042.** Muravjev V.V. Aluminium oxide technology for millimeter wave devices. / Muravjev V.V., Tamelo A.A., Sokol V.A., Parkun U.M. // 2002. MIKON-2002. 14th International Conference on Microwaves, Radar and Wireless Communications. 2002. - Vol. 1. - P. 271-274. ↑
- C2043.** Chen Y.K. High speed electronics for lightwave communications. / Chen Y.K., Baeyens Y., Liu C.-T., Kopf R., Chen C., Yang Y., Frackowiak J., Tate A., Leven A., Paschke P., Berger M., Weiner J., Tu K., Georgiou G., Roux P., Houstma V., Koc U. // 2002. OFC 2002 Optical Fiber Communication Conference and Exhibit. 17-22 Mar 2002. - P. 272-273. ↑
- C2044.** Hirano A. A novel dispersion compensation scheme based on phase comparison between two SSB signals generated from a spectrally filtered CS-RZ signal. / Hirano A., Kuwahara S., Miyamoto Y., Murata K. // 2002. OFC 2002 Optical Fiber Communication Conference and Exhibit. 17-22 Mar 2002. - P. 196-197. ↑
- C2045.** Heins M.S. An ultra-wideband GaAs pHEMT driver amplifier for fiber optic communications at 40 Gb/s and beyond. / Heins M.S., Carroll J.M., Kao M.-Y., Steinbeiser C.F., Landon T.R., Campbell C.F. // 2002. OFC 2002 Optical Fiber Communication Conference and Exhibit. 17-22 Mar 2002. - P. 273-274. ↑
- C2046.** Lewandowski A. A 24 GHz PHEMT-based oscillator. / Lewandowski A., Kompa G., Mwema W., Wiatr W. // 2002. MIKON-2002. 14th International Conference on Microwaves, Radar and Wireless Communications. 2002. - Vol. 2. - P. 377-380. ↑
- C2047.** Ferrante G. DC and 1/f noise characterization of crogenically cooled pseudomorphic HEMT's. / Ferrante G., Principato F., Caddemi A., Donato N., Tuccari G. // 2002. Proceedings of the 5th European Workshop on Low Temperature Electronics. 2002. - P. 117-120. ↑

- C2048.** Hadzi-Vukovic J. Phase noise amplitude distribution as indicator of origin of random phase perturbation in a test oscillator. / Hadzi-Vukovic J., Jevtic M.M., Simic D. // 2002. MIEL 2002. 23rd International Conference on Microelectronics. 2002. - Vol. 1. - P. 301-304. ↑
- C2049.** Cidronali A. Ultra low-power VCO based on InP-HEMT and heterojunction interband tunnel diode for wireless application. / Cidronali A., Collodi G., Camprini M., Nair V., Manes G., Lewis J., Goronkin H. // 2002 IEEE MTT-S International Microwave Symposium Digest. - Seattle, WA, 2002. - Vol. 1. - P. 43-46. ↑
- C2050.** Cevizovic D. Sheet density of electrons in spacer layer of AlGaIn/GaN MODFET: calculating and analysing. / Cevizovic D., Sasic R., Ramovic R. // 2002. MIEL 2002. 23rd International Conference on Microelectronics. 2002. - Vol. 2. - P. 475-478. ↑
- C2051.** Shur M.S. Wide band gap electronic devices. / Shur M.S., Gaska R., Khan A., Simin G. // 2002. Proceedings of the Fourth IEEE International Caracas Conference on Devices, Circuits and Systems. 2002. - P. D051-1-D051-8-1. ↑
- C2052.** Kumar V. AlGaIn/GaN HEMTs on sapphire. / Kumar V., Adesida I. // 2002. Proceedings of the Fourth IEEE International Caracas Conference on Devices, Circuits and Systems. 2002. - P. D048-1-D048-6-1. ↑
- C2053.** Yang J.M. High performance voltage controlled bi-directional amplifiers in support of component reuse for large aperture phase array. / Yang J.M., Chung Y.H., Nishimoto M., Lai R., Tsai R., Kagiwada R., Yang C.C. // 2002 IEEE MTT-S International Microwave Symposium Digest. - Seattle, WA, 2002. - Vol. 1. - P. 65-68. ↑
- C2054.** Devlin L.M. A monolithic, 2 to 18 GHz upconverter. / Devlin L.M., Dearn A.W., Pearson G.A., Beasley P.D.L., Morgan G.D. // 2002 IEEE MTT-S International Microwave Symposium Digest. - Seattle, WA, 2002. - Vol. 1. - P. 257-260. ↑
- C2055.** Nishikawa K. Miniaturized and broadband V-band balanced frequency doubler for highly integrated 3-D MMIC. / Nishikawa K., Piernas B., Nakagawa T., Araki K. // 2002 IEEE MTT-S International Microwave Symposium Digest. - Seattle, WA, 2002. - Vol. 1. - P. 351-354. ↑
- C2056.** Virk R.S. 40-GHz MMICs for optical modulator driver applications. / Virk R.S., Camargo E., Hajji R., Parker S., Benelbar R., Notomi S., Ohnishi H. // 2002 IEEE MTT-S International Microwave Symposium Digest. - Seattle, WA, 2002. - Vol. 1. - P. 91-94. ↑
- C2057.** Kano H. A 50-Gbit/s 1:4 demultiplexer IC in InP-based HEMT technology. / Kano H., Suzuki T., Yamaura S., Nakasha Y., Sawada K., Takahashi T., Makiyama K., Hirose T., Watanabe Y. // 2002 IEEE MTT-S International Microwave Symposium Digest. - Seattle, WA, 2002. - Vol. 1. - P. 75-78. ↑
- C2058.** Campbell C.F. A 0.15- $\mu$ m GaAs MHEMT transimpedance amplifier IC for 40-Gb/s applications. / Campbell C.F., Heins M.S., Kao M.Y., Muir M.E., Carroll J.M. // 2002 IEEE MTT-S International Microwave Symposium Digest. - Seattle, WA, 2002. - Vol. 1. - P. 79-82. ↑
- C2059.** Ryu Seonghan. Monolithic Ka-band VCO with wide tuning range. / Ryu Seonghan, Kim Huijung, Lim Joonyoul, Yim Joungyun, Kwon Woosung, Kim Bumman, Im Kyoungsoon, Kim Youngwoong, Han Seogtae. // 2002. 32nd European Microwave Conference. - Milan, Italy, 23-26 Sept. 2002. - P. 1-3. ↑
- C2060.** Charlot B. Access to microsystem technology: the CMP services solution. / Charlot B., Courtois B., Delori H., Paillotin J.-F., Torki K. // 2002. MIEL 2002. 23rd International Conference on Microelectronics. 2002. - Vol. 1. - P. 47-53. ↑
- C2061.** Nakasha Y. A 43Gb/s full-rate-clock 4:1 multiplexer in InP-based HEMT technology. / Nakasha Y., Suzuki T., Kano H., Ohya A., Sawada K., Makiyama K., Takahashi T., Nishi M., Hirose T., Takikawa M., Watanabe Y. // 2002. Digest of Technical Papers. ISSCC. 2002 IEEE International Solid-State Circuits Conference. 2002. - Vol. 2. - P. 148-442. ↑
- C2062.** Staudinger J. An overview of efficiency enhancements with application to linear handset power amplifiers. 2002 IEEE Radio Frequency Integrated Circuits (RFIC) Symposium. - Seattle, WA, 2002. - P. 45-48. ↑
- C2063.** Huang H.C. Ku-band MMIC's in low-cost, SMT compatible packages. / Huang H.C., Ezzeddine A., Darwish A., Hsu B., Williams J., Peak S. // 2002 IEEE MTT-S International Microwave Symposium Digest. -

Seattle, WA, 2002. - Vol. 1. - P. 27-30. ↑

**C2064.** Tayrani R. A broadband monolithic S-band class-E power amplifier. 2002 IEEE Radio Frequency Integrated Circuits (RFIC) Symposium. - Seattle, WA, 2002. - P. 53-56. ↑

**C2065.** Suzuki T. A 90Gb/s 2:1 multiplexer IC in InP-based HEMT technology. / Suzuki T., Nakasha Y., Takahashi T., Makiyama K., Imanishi K., Hirose T., Watanabe Y. // 2002. Digest of Technical Papers. ISSCC. 2002 IEEE International Solid-State Circuits Conference. 2002. - Vol. 2. - P. 150-443. ↑

**C2066.** Chou Y.C. Evolution of DC and RF degradation induced by high-temperature accelerated lifetest of pseudomorphic GaAs and InGaAs/InAlAs/InP HEMT MMICs. / Chou Y.C., Leung D., Lai R., Grunbacher R., Eng D., Scarpulla J., Barsky M., Liu P.H., Biedenbender M., Oki A., Streit D. // 2002. 40th Annual Reliability Physics Symposium Proceedings. 2002. - P. 241-247. ↑

**C2067.** Chan Shin Wu. Microwave III-V semiconductors for telecommunications and prospective of the III-V industry. 2002. Proceedings. International Symposium on Quality Electronic Design. 2002. - P. 223. ↑

**C2068.** Chou Y.C. Innovative nitride passivation for pseudomorphic GaAs HEMTs and impact on device performance. / Chou Y.C., Nam P., Li G.P., Kim L.K., Grunbacher R., Ahlers E., Ra Y., Xu Q., Biedenbender M.B., Oki A. // 2002. 40th Annual Reliability Physics Symposium Proceedings. 2002. - P. 235-240. ↑

**C2069.** Nakasha Y. A 43 Gb/s full-rate-clock 4:1 multiplexer in InP-based HEMT technology. / Nakasha Y., Suzuki T., Kano H., Ohya A., Sawada K., Makiyama K., Takahashi T., Nishi M., Hirose T., Takikawa M., Watanabe Y. // 2002. Digest of Technical Papers. ISSCC. 2002 IEEE International Solid-State Circuits Conference. - San Francisco, CA, 2002. - Vol. 1. - P. 190-459. ↑

**C2070.** Suzuki T. A 90Gb/s 2:1 multiplexer IC in InP-based HEMT technology. / Suzuki T., Nakasha Y., Takahashi T., Makiyama K., Imanishi K., Hirose T., Watanabe Y. // 2002. Digest of Technical Papers. ISSCC. 2002 IEEE International Solid-State Circuits Conference. - San Francisco, CA, 2002. - Vol. 1. - P. 192-193. ↑

**C2071.** Young Yun. A fully-integrated broadband amplifier MMIC employing a novel chip size package. / Young Yun, Nishijima M., Katsuno M., Ishida H., Minagawa K., Nobusada T., Tanaka T. // 2002 IEEE MTT-S International Microwave Symposium Digest. - Seattle, WA, 2002. - Vol. 1. - P. 409-412. ↑

**C2072.** Heins M.S. A GaAs MHEMT distributed amplifier with 300-GHz gain-bandwidth product for 40-Gb/s optical applications. / Heins M.S., Campbell C.F., Kao M.-Y., Muir M.E., Carroll J.M. // 2002 IEEE MTT-S International Microwave Symposium Digest. - Seattle, WA, 2002. - Vol. 2. - P. 1061-1064. ↑

**C2073.** Karkkainen M. A set of integrated circuits for 60 GHz radio front-end. / Karkkainen M., Varonen M., Riska J., Kangaslahti P., Porra V. // 2002 IEEE MTT-S International Microwave Symposium Digest. - Seattle, WA, 2002. - Vol. 2. - P. 1273-1276. ↑

**C2074.** Lan E. InGaP PHEMTs for 3.5GHz W-CDMA applications. / Lan E., Johnson E., Knappenberger B., Miller M. // 2002 IEEE MTT-S International Microwave Symposium Digest. - Seattle, WA, 2002. - Vol. 2. - P. 1039-1042. ↑

**C2075.** Nuttinck S. RF performance and thermal analysis of AlGaIn/GaN power HEMTs in presence of self-heating effects. / Nuttinck S., Gebara E., Laskar J., Wagner B., Harris M. // 2002 IEEE MTT-S International Microwave Symposium Digest. - Seattle, WA, 2002. - Vol. 2. - P. 921-924. ↑

**C2076.** Parker A.E. Novel technique for determining bias, temperature and frequency dependence of FET characteristics. / Parker A.E., Rathmell J.G. // 2002 IEEE MTT-S International Microwave Symposium Digest. - Seattle, WA, 2002. - Vol. 2. - P. 993-996. ↑

**C2077.** Bannister D.C. A 2-18 GHz wideband high dynamic range receiver MMIC. / Bannister D.C., Zelle C.A., Barnes A.R. // 2002 IEEE Radio Frequency Integrated Circuits (RFIC) Symposium. - Seattle, WA, 2002. - P. 147-149. ↑

**C2078.** Huang H.C. Ku-band MMIC's in low-cost, SMT compatible packages. / Huang H.C., Ezzeddine A., Darwish A., Hsu B., Williams J., Peak S. // 2002 IEEE Radio Frequency Integrated Circuits (RFIC) Symposium. - Seattle, WA, 2002. - P. 281-284. ↑

- C2079.** Cidronali A. Ultra low-power VCO based on InP-HEMT and heterojunction interband tunnel diode for wireless application. / Cidronali A., Collodi G., Camprini M., Nair V., Manes G., Lewis J., Goronkin H. // 2002 IEEE Radio Frequency Integrated Circuits (RFIC) Symposium. - Seattle, WA, 2002. - P. 297-300. ↑
- C2080.** Kumar S. Enhancement mode PHEMT low noise amplifier with LNA linearity control (IP3) and mitigated bypass switch. / Kumar S., Vice M., Morkner H., Wayne L. // 2002 IEEE Radio Frequency Integrated Circuits (RFIC) Symposium. - Seattle, WA, 2002. - P. 213-216. ↑
- C2081.** Kuo-Liang Deng. A 3-33 GHz PHEMT MMIC distributed drain mixer. / Kuo-Liang Deng, Huei Wang. // 2002 IEEE Radio Frequency Integrated Circuits (RFIC) Symposium. - Seattle, WA, 2002. - P. 151-154. ↑
- C2082.** Ovidiu Tatu S. Ka-band direct digital receiver using 0.25  $\mu\text{m}$  GaAs PHEMTs. / Ovidiu Tatu S., Moldovan E., Brehm G., Ke Wu, Bosisio R.G. // 2002 IEEE Radio Frequency Integrated Circuits (RFIC) Symposium. - Seattle, WA, 2002. - P. 155-158. ↑
- C2083.** Schellenberg J.M. A broadband, push-pull power MMIC operating at K/Ka-band frequencies. 2002 IEEE MTT-S International Microwave Symposium Digest. - Seattle, WA, 2002. - Vol. 2. - P. 909-912. ↑
- C2084.** Merkle T. Intercept point behavior of Ka-band GaAs high power amplifiers. / Merkle T., Tessmann A., Ramberger S. // 2002 IEEE MTT-S International Microwave Symposium Digest. - Seattle, WA, 2002. - Vol. 1. - P. 453-456. ↑
- C2085.** Yuen C. 50 GHz high output voltage distributed amplifiers for 40 Gb/s EO modulator driver application. / Yuen C., Laursen K., Duc Chu, Mar K. // 2002 IEEE MTT-S International Microwave Symposium Digest. - Seattle, WA, 2002. - Vol. 1. - P. 481-484. ↑
- C2086.** Manohar S. Characteristics of microwave power GaN HEMTs on 4-inch Si wafers. / Manohar S., Narayanan A., Keerti A., Pham A., Brown J., Borges R., Linthicum K. // 2002 IEEE MTT-S International Microwave Symposium Digest. - Seattle, WA, 2002. - Vol. 1. - P. 449-452. ↑
- C2087.** Younkyu Chung. Output harmonic termination techniques for AlGaIn/GaN HEMT power amplifiers using active integrated antenna approach. / Younkyu Chung, Hang C.Y., Shujun Cai, Yongxi Qian, Wen C.P., Wang K.L., Toh T. // 2002 IEEE MTT-S International Microwave Symposium Digest. - Seattle, WA, 2002. - Vol. 1. - P. 433-436. ↑
- C2088.** Schellenberg J.M. 1 and 2 watt MMIC power amplifiers for commercial K/Ka-band applications. 2002 IEEE MTT-S International Microwave Symposium Digest. - Seattle, WA, 2002. - Vol. 1. - P. 445-448. ↑
- C2089.** Carroll J.M. 0.25 $\mu\text{m}$  pHEMT 40Gb/s E/O modulator drivers. / Carroll J.M., Coutant A., Heins M.S., Campbell C.F., Reese E. // 2002 IEEE MTT-S International Microwave Symposium Digest. - Seattle, WA, 2002. - Vol. 1. - P. 489-492. ↑
- C2090.** Lei Zhao. A 6 watt LDMOS broadband high efficiency distributed power amplifier fabricated using LTCC technology. / Lei Zhao, Padio A., Stengel B., Thompson B. // 2002 IEEE MTT-S International Microwave Symposium Digest. - Seattle, WA, 2002. - Vol. 2. - P. 897-900. ↑
- C2091.** Komiak J.J. High efficiency wideband 6 to 18 GHz PHEMT power amplifier MMIC. / Komiak J.J., Wendell Kong, Nichols K. // 2002 IEEE MTT-S International Microwave Symposium Digest. - Seattle, WA, 2002. - Vol. 2. - P. 905-907. ↑
- C2092.** Ikematsu H. A 40 GHz-band fully monolithic VCO with a one-wave length microstrip resonator for accurate oscillation frequency. / Ikematsu H., Kawakami K., Katoh T., Itoh K. // 2002 IEEE MTT-S International Microwave Symposium Digest. - Seattle, WA, 2002. - Vol. 2. - P. 843-846. ↑
- C2093.** Staudinger J. A 15 watt PFP GaAs PHEMT MMIC power amplifier for 3G wireless transmitter applications. / Staudinger J., Sherman R., Quach T., Miller M., Frye L. // 2002 IEEE MTT-S International Microwave Symposium Digest. - Seattle, WA, 2002. - Vol. 2. - P. 617-620. ↑
- C2094.** Fager C. Uncertainty estimation and optimal extraction of intrinsic FET small signal model parameters. / Fager C., Linner P., Pedro J.C. // 2002 IEEE MTT-S International Microwave Symposium Digest. - Seattle, WA, 2002. - Vol. 2. - P. 729-732. ↑



- C2095.** Cordier Y. MBE growth of high quality AlGaIn/GaN HEMTs on resistive Si[111] substrate with RF small signal and power performances. / Cordier Y., Semond F., Lorenzini P., Grandjean N., Natali F., Damilano B., Massies J., Hoel V., Minko A., Vellas N., Gaquiere C., DeJaeger J.C., Dessertene B., Cassette S., Surrugue M., Adam D., Grattepain J.-C., Delage S.L. // 2002 International Conference on Molecular Beam Epitaxy. 2002. - P. 99-100. ↑
- C2096.** Streit D. InP HEMT and HBT technology and applications. / Streit D., Lai R., Oki A., Gutierrez-Aitken A. // 2002. EDMO 2002. The 10th IEEE International Symposium on Electron Devices for Microwave and Optoelectronic Applications. 18-19 Nov. 2002. - P. 14-17. ↑
- C2097.** Medjdoub F. Monte Carlo study of the breakdown of an AlInAs/GaInAs HEMT on InP with an InP etch stop layer. / Medjdoub F., Theron D., Dessenne F., Fauquembergue R., de Jaeger J.C. // 2002. EDMO 2002. The 10th IEEE International Symposium on Electron Devices for Microwave and Optoelectronic Applications. 18-19 Nov. 2002. - P. 57-62. ↑
- C2098.** Murata K. Ultra-high-speed IC and OEIC technologies beyond 40 Gbit/s. / Murata K., Sano K., Sugahara H., Enoki T. // 2002. ECOC 2002. 28th European Conference on Optical Communication. - Copenhagen, 8-12 Sept. 2002. - Vol. 4. - P. 1-2. ↑
- C2099.** Nhan E. Recent test results of a flight X-band solid-state power amplifier utilizing GaAs MESFET, HFET, and PHEMT technologies. / Nhan E., Sheng Cheng, Jose M.J., Fortney S.O., Penn J.E. // 2002. Proceedings GaAs Reliability Workshop. 20 Oct. 2002. - P. 37-44. ↑
- C2100.** Gao F. Reliability evaluation on dual-etch-stop InGaAs PHEMTs. 2002. Proceedings GaAs Reliability Workshop. 20 Oct. 2002. - P. 95-115. ↑
- C2101.** Basile A.F. Experimental and numerical analysis of gate- and drain-lag phenomena in AlGaAs/InGaAs PHEMTs. / Basile A.F., Mazzanti A., Manzini E., Verzellesi G., Canali C., Pierobon R., Lanzieri C. // 2002. EDMO 2002. The 10th IEEE International Symposium on Electron Devices for Microwave and Optoelectronic Applications. 18-19 Nov. 2002. - P. 63-68. ↑
- C2102.** Vandersinissen R. Influence of silicon nitride passivation on DC and RF behaviour of InP HEMTs. / Vandersinissen R., Schreurs D., Borghs G. // 2002. EDMO 2002. The 10th IEEE International Symposium on Electron Devices for Microwave and Optoelectronic Applications. 18-19 Nov. 2002. - P. 172-176. ↑
- C2103.** Ka Lun Koon. Improving baseband performance of four-cascaded single stage distributed amplifiers for high speed optical communication. / Ka Lun Koon, Zhirun Hu, Langlois P., Rezazadeh A.A. // 2002. EDMO 2002. The 10th IEEE International Symposium on Electron Devices for Microwave and Optoelectronic Applications. 18-19 Nov. 2002. - P. 254-258. ↑
- C2104.** Delage S.L. Solid-state RF power amplifiers: status and perspective. / Delage S.L., Floriot D., Brylinski C. // 2002. EDMO 2002. The 10th IEEE International Symposium on Electron Devices for Microwave and Optoelectronic Applications. 18-19 Nov. 2002. - P. 136-142. ↑
- C2105.** Uren M.J. GaN devices for microwave applications [FET/HEMT]. / Uren M.J., Barnes A.R., Martin T., Balmer R.S., Hilton K.P., Hayes D.G., Kuball M. // 2002. EDMO 2002. The 10th IEEE International Symposium on Electron Devices for Microwave and Optoelectronic Applications. 18-19 Nov. 2002. - P. 111-118. ↑
- C2106.** Crespo-Cadenas C. Role of FET size in the optimization of MMIC nonlinear performance. / Crespo-Cadenas C., Reina-Tosina J. // 2002. EDMO 2002. The 10th IEEE International Symposium on Electron Devices for Microwave and Optoelectronic Applications. 18-19 Nov. 2002. - P. 125-129. ↑
- C2107.** Luo B. Comparison of surface passivation on films for reduction of current collapse in AlGaIn/GaN high electron mobility transistors. / Luo B., Mehendru R., Kim J., Ren F., Gila B.P., Onstine A.H., Abernathy C.R., Pearton S.J., Fitch R., Gillespie J., Jenkins T., Sewell J., Via D., Crespo A., Irokawa Y. // 2002. Proceedings. IEEE Lester Eastman Conference on High Performance Devices. 6-8 Aug. 2002. - P. 477-486. ↑
- C2108.** Brar B. Impact ionization in high performance AlGaIn/GaN HEMTs. / Brar B., Boutros K., DeWames R.E., Tilak V., Shealy R., Eastman L. // 2002. Proceedings. IEEE Lester Eastman Conference on High Performance Devices. 6-8 Aug. 2002. - P. 487-491. ↑
- C2109.** Smorchkova I.P. AlGaIn/GaN HEMT high-power and low-noise performance at  $f \geq 20$  GHz. /

Smorchkova I.P., Wojtowicz M., Tsai R., Sandhu R., Barsky M., Namba C., Liu P.H., Dia R., Truong M., Ko D., Wang J., Wang H., Khan A. // 2002. Proceedings. IEEE Lester Eastman Conference on High Performance Devices. 6-8 Aug. 2002. - P. 422-427. ↑

C2110. Daniel E. Packaging of microwave integrated circuits operating beyond 100 GHz. / Daniel E., Sokolov V., Sommerfeldt S., Bublit J., Olson K., Gilbert B., Samoska L., Chow D. // 2002. Proceedings. IEEE Lester Eastman Conference on High Performance Devices. 6-8 Aug. 2002. - P. 374-383. ↑

C2111. Parikh P. High linearity, robust, AlGaIn-GaN HEMTs for LNA and receiver ICs. / Parikh P., Wu Y., Moore M., Chavarkar P., Mishra U., Neidhard R., Kehias L., Jenkins T. // 2002. Proceedings. IEEE Lester Eastman Conference on High Performance Devices. 6-8 Aug. 2002. - P. 415-421. ↑

C2112. Kiefer R. AlGaIn/GaN-HEMTs for power applications up to 40 GHz. / Kiefer R., Quay R., Muller S., Kohler K., van Raay F., Raynor B., Pletschen W., Massler H., Ramberger S., Mikulla M., Weimann G. // 2002. Proceedings. IEEE Lester Eastman Conference on High Performance Devices. 6-8 Aug. 2002. - P. 502-504. ↑

C2113. Kim H. Hot electron effects on undoped AlGaIn/GaN high electron mobility transistors. / Kim H., Vertiatichikh A., Tilak V., Thompson R.M., Prunty T., Shealy J.R., Eastman L.F. // 2002. Proceedings GaAs Reliability Workshop. 20 Oct. 2002. - P. 5-6. ↑

C2114. Rowe W.J. Reliability of 100 nm silicon nitride capacitors in an InP HEMT MMIC process. / Rowe W.J., Paine B.M., Schmitz A.E., Walden R.H., Delaney M.J. // 2002. Proceedings GaAs Reliability Workshop. 20 Oct. 2002. - P. 9-36. ↑

C2115. Mittereder J.A. Creation of current collapse in GaN HEMTs due to short-term DC bias stress. / Mittereder J.A., Binari S.C., Klein P.B., Roussos J.A., Katzer D.S., Storm D.F., Koleske D.D., Wickenden A.E., Henry R.I. // 2002. Proceedings GaAs Reliability Workshop. 20 Oct. 2002. - P. 3-4. ↑

C2116. Ryzhii V. Excitation of plasma oscillations and terahertz photomixing in high-electron mobility transistor. / Ryzhii V., Satou A., Khmyrova I., Vaccaro P.O., Aida T., Shur M. // 2002. International Topical Meeting on Microwave Photonics. 5-8 Nov. 2002. - P. 321-324. ↑

C2117. Whelan C.S. Metamorphic optical receiver components. / Whelan C.S., Leoni R.E. III, Marsh P.F., Zhang Y., Hoke W.E., Lichwala S., Lardizabal S., Hunt J., Loughton C., Grigas M., Kazior T.E. // 2002. LEOS 2002. The 15th Annual Meeting of the IEEE Lasers and Electro-Optics Society. 10-14 Nov. 2002. - Vol. 2. - P. 420-421. ↑

C2118. Jung-Hui Tsai. Performance of InGaP/InGaAs/GaAs camel-gate single  $\delta$ -doping pHEMT. 2002 Conference on Optoelectronic and Microelectronic Materials and Devices. 11-13 Dec. 2002. - P. 369-372. ↑

C2119. Huilai Liang. The photo-controlled MOBILE's with RTD/HPT structure. / Huilai Liang, Weilian Guo, Pingjuan Niu, Shilin Zhang, Ming Zhong, Haitao Qi. // 2002 Conference on Optoelectronic and Microelectronic Materials and Devices. 11-13 Dec. 2002. - P. 381-384. ↑

C2120. Hwang J.C.M. Internal waveform probing of HBT and HEMT MMIC power amplifiers. Fall 2002. 60th ARFTG Conference Digest. 5-6 Dec. 2002. - P. 111-112. ↑

C2121. Vandersmissen R. Time domain RF characterisation of a thin-film metamorphic HEMT under modulated backside illumination. / Vandersmissen R., Schreurs D., Vandenberghe S., Borghs G. // Spring 2002. 59th ARFTG Conference Digest. 7 June 2002. - P. 5. ↑

C2122. Ariffin A. MMIC development for Local Multipoint Distribution Service (LMDS). / Ariffin A., Jaafar S., Bujang S. // 2002. Proceedings. ICSE 2002. IEEE International Conference on Semiconductor Electronics. 19-21 Dec. 2002. - P. 308-313. ↑

C2123. Yen-Wei Chen. High breakdown InGaP/InGaAs tunneling real space transfer HEMT. / Yen-Wei Chen, Wei-Chou Hsu. // 2002 Conference on Optoelectronic and Microelectronic Materials and Devices. 11-13 Dec. 2002. - P. 401-404. ↑

C2124. Hwang Yuh-Jing. W-Band GaAs HEMT MMIC Subharmonically Pumped Diode Mixers with 20 GHz IF Bandwidth. / Hwang Yuh-Jing, Wang Huei, Chu Tah-Hsiung. // 2002. 32nd European Microwave Conference. - Milan, Italy, 23-26 Sept. 2002. - P. 1-4. ↑

- C2125.** Cabria L. A Highly Linear Circularly Polarized Active Antenna With Gain Control. / Cabria L., Malaver E., Garcia J. A., Tazon A., Mediavilla A., Vassallo J. // 2002. 32nd European Microwave Conference. - Milan, Italy, 23-26 Sept. 2002. - P. 1-4. ↑
- C2126.** Ono Naoko. Characteristics of GaAs HEMTs with Flip-Chip Interconnections. / Ono Naoko, Sasaki Fumio, Arai Kazuhiro, Iseki Yuji. // 2002. 32nd European Microwave Conference. - Milan, Italy, 23-26 Sept. 2002. - P. 1-4. ↑
- C2127.** Champlain J. LT (Al)GaAs and Al(Ga)As/AlAsSb oxides for electronic applications. / Champlain J., Zheng C., Mishra U. // 2002. SIMC-XII-2002. 12th International Conference on Semiconducting and Insulating Materials. 30 June-5 July 2002. - P. 121-124. ↑
- C2128.** Ahmed S. Electrical isolation of n-GaAs by proton implantation-effects of doping implant, isolation implant and implant temperature. / Ahmed S., Sealy B.J., Gwilliam R. // Ion Implantation Technology. 2002. Proceedings of the 14th International Conference on. 22-27 Sept. 2002. - P. 60-63. ↑
- C2129.** Verzellesi G. Experimental/numerical investigation on current collapse in AlGaIn/GaN HEMT's. / Verzellesi G., Pierobon R., Rampazzo F., Meneghesso G., Chini A., Mishra U.K., Canali C., Zanoni E. // 2002. IEDM '02. Digest. International Electron Devices Meeting. 2002. - P. 689-692. ↑
- C2130.** Nagahara M. Improved intermodulation distortion profile of AlGaIn/GaN HEMT at high drain bias voltage. / Nagahara M., Kikkawa T., Adachi N., Tateno Y., Kato S., Yokoyama M., Yokogawa S., Kimura T., Yamaguchi Y., Hara N., Joshin K. // 2002. IEDM '02. Digest. International Electron Devices Meeting. 2002. - P. 693-696. ↑
- C2131.** Quay R. AlGaIn/GaN HEMTs on SiC operating at 40 GHz. / Quay R., Kiefer R., van Raay F., Massler H., Ramberger S., Muller S., Dammann M., Mikulla M., Schlechtweg M., Weimann G. // 2002. IEDM '02. Digest. International Electron Devices Meeting. 2002. - P. 673-676. ↑
- C2132.** Madureira M.A.M. Broad-band optical receiver for multigigabit-per-second (40Gb/s) optical communication systems. / Madureira M.A.M., Monteiro P.M.P., Aguiar R.L., Violas M., Gloanec M., Leclerc E., Lefebvre B. // 2002. EDMO 2002. The 10th IEEE International Symposium on Electron Devices for Microwave and Optoelectronic Applications. 18-19 Nov. 2002. - P. 271-276. ↑
- C2133.** Moradi G. Signal and noise improvement of a distributed FET mixer. / Moradi G., Abdipour A., Farzaneh F. // 2002. EDMO 2002. The 10th IEEE International Symposium on Electron Devices for Microwave and Optoelectronic Applications. 18-19 Nov. 2002. - P. 284-288. ↑
- C2134.** Wu Y.-F. Linearity and gain characteristics of AlGaIn/GaN HEMTs. / Wu Y.-F., Chavarkar P.M., Moore M., Parikh P., Mishra U.K. // 2002. IEDM '02. Digest. International Electron Devices Meeting. 2002. - P. 697-699. ↑
- C2135.** Moradi G. A simplified noise modeling of mm-wave FETs. / Moradi G., Abdipour A. // 2002. Proceedings. ICMMT 2002. 2002 3rd International Conference on Microwave and Millimeter Wave Technology. 17-19 Aug. 2002. - P. 312-314. ↑
- C2136.** LingLing Sun. Large-signal modeling of HEMT device based on neural network. / LingLing Sun, YiXing Liao, XueFeng Zheng, ZhiGang Cheng, Jun Liu, Lei Zhou. // 2002. Proceedings. ICMMT 2002. 2002 3rd International Conference on Microwave and Millimeter Wave Technology. 17-19 Aug. 2002. - P. 883-886. ↑
- C2137.** Johnson J. Improving large-signal FET/HEMT model accuracy by optimization of diode response. / Johnson J., Branner G.R. // 2002. MWSCAS-2002. The 2002 45th Midwest Symposium on Circuits and Systems. 4-7 Aug. 2002. - Vol. 2. - P. II-641-II-644-641. ↑
- C2138.** Murata K. 100-Gbit/s logic IC using 0.1- $\mu$ m-gate-length InAlAs/InGaAs/InP HEMTs. / Murata K., Sano K., Kitabayashi H., Sugitani S., Sugahara H., Enoki T. // 2002. IEDM '02. Digest. International Electron Devices Meeting. 2002. - P. 937-939. ↑
- C2139.** Solodky S. Optimization of PHEMT geometry for power applications. / Solodky S., Baksht T., Shapira Y., Leibovich M., Bunin G. // 2002. The 22nd Convention of Electrical and Electronics Engineers in Israel. 1 Dec. 2002. - P. 61-62. ↑

- C2140.** Mouzannar W. 40 Gbit/s high performances GaAs pHEMT high voltage modulator driver for long haul optical fiber communications. / Mouzannar W., Jorge F., Vuye S., Dutisseuil E., Lefevre R. // 2002. 24th Annual Technical Digest Gallium Arsenide Integrated Circuit (GaAs IC) Symposium. 2002. - P. 163-166. ↑
- C2141.** Sato M. 1.4-THz gain-bandwidth product InP-HEMTs preamplifier using an improved Cherry-Hooper topology. / Sato M., Shigematsu H., Inoue Y., Arai T., Sawada K., Takahashi T., Makiyama K., Hirose T. // 2002. 24th Annual Technical Digest Gallium Arsenide Integrated Circuit (GaAs IC) Symposium. 2002. - P. 167-170. ↑
- C2142.** Sano K. 1.7-W 50-Gbit/s InP HEMT 4:1 multiplexer IC with a multi-phase clock architecture. / Sano K., Murata K., Sugitani S., Sugahara H., Enoki T. // 2002. 24th Annual Technical Digest Gallium Arsenide Integrated Circuit (GaAs IC) Symposium. 2002. - P. 159-162. ↑
- C2143.** Komiak J.J. Direct up-conversion MMIC with RF bandwidth of 4 to 12 GHz. / Komiak J.J., Kong W., Nichols K. // 2002. 24th Annual Technical Digest Gallium Arsenide Integrated Circuit (GaAs IC) Symposium. 2002. - P. 113-116. ↑
- C2144.** Orzati A. A 16 GHz MMIC image-rejection resistive mixer with InP HEMTs. / Orzati A., Robin F., Meier H.P., Bachtold W. // 2002. 24th Annual Technical Digest Gallium Arsenide Integrated Circuit (GaAs IC) Symposium. 2002. - P. 117-119. ↑
- C2145.** Rockwell S. An 8-Watt 3.5 GHz power amplifier with tunable matching. / Rockwell S., Emrick R., Bosco B., Franson S., Miller M., Johnson E., Crowder J. // 2002. 24th Annual Technical Digest Gallium Arsenide Integrated Circuit (GaAs IC) Symposium. 2002. - P. 185-188. ↑
- C2146.** Lyumkis E. Simulations of quantum transport in HEMT using density gradient model. / Lyumkis E., Mickevicius R., Penzin O., Polsky B., El Sayed K., Wettstein A., Fichtner W. // 2002. 24th Annual Technical Digest Gallium Arsenide Integrated Circuit (GaAs IC) Symposium. 2002. - P. 233-236. ↑
- C2147.** Shealy J. Gallium nitride (GaN) HEMT's: progress and potential for commercial applications. / Shealy J., Smart J., Poulton M., Sadler R., Grider D., Gibb S., Hosse B., Sousa B., Halchin D., Steel V., Garber P., Wilkerson P., Zaroff B., Dick J., Mercier T., Bonaker J., Hamilton M., Greer C., Isenhour M. // 2002. 24th Annual Technical Digest Gallium Arsenide Integrated Circuit (GaAs IC) Symposium. 2002. - P. 243-246. ↑
- C2148.** Sano K. 50-Gbit/s 4-bit multiplexer/demultiplexer chip-set using InP HEMTs. / Sano K., Murata K., Sugitani S., Sugahara H., Enoki T. // 2002. 24th Annual Technical Digest Gallium Arsenide Integrated Circuit (GaAs IC) Symposium. 2002. - P. 207-210. ↑
- C2149.** Bessemoulin A. A 4-Watt X-band compact coplanar high power amplifier MMIC with 18-dB gain and 25-% PAE. / Bessemoulin A., Quay M.R., Ramberger S., Schlechtweg M. // 2002. 24th Annual Technical Digest Gallium Arsenide Integrated Circuit (GaAs IC) Symposium. 2002. - P. 189-192. ↑
- C2150.** Komiak J.J. X-band successive detection log amplifier/limiter MMIC implemented in 0.15  $\mu\text{m}$  double recess PHEMT. / Komiak J.J., Kong W., Nichols K. // 2002. 24th Annual Technical Digest Gallium Arsenide Integrated Circuit (GaAs IC) Symposium. 2002. - P. 193-196. ↑
- C2151.** Meliani C. A high gain-bandwidth product InP HEMT distributed amplifier with 92 GHz cut-off frequency for 40 Gbit/s applications and beyond. / Meliani C., Rondeau G., Post G., Decobert J., Mouzannar W., Dutisseuil E., Lefevre R. // 2002. 24th Annual Technical Digest Gallium Arsenide Integrated Circuit (GaAs IC) Symposium. 2002. - P. 103-106. ↑
- C2152.** Liu H.Z. A four-stage Ku-band 1 watt PHEMT MMIC power amplifier. / Liu H.Z., Wang C.C., Wang Y.H., Huang J.W., Chang C.H., Wu W., Wu C.L., Chang C.S. // 2002. 24th Annual Technical Digest Gallium Arsenide Integrated Circuit (GaAs IC) Symposium. 2002. - P. 33-36. ↑
- C2153.** Kong K.K.-S. A compact 30 GHz MMIC high power amplifier (3 W CW) in chip and packaged form. / Kong K.K.-S., Boone D., King M., Nguyen B., Vernon M., Reese E., Brehm G. // 2002. 24th Annual Technical Digest Gallium Arsenide Integrated Circuit (GaAs IC) Symposium. 2002. - P. 37-39. ↑
- C2154.** {no data available}. GaAs IC Symposium. IEEE Gallium Arsenide Integrate Circuit Symposium. 24th Annual Technical Digest 2002 (Cat. No.02CH37354). 2002. 24th Annual Technical Digest Gallium Arsenide Integrated Circuit (GaAs IC) Symposium. 2002. - {no data available}. ↑



- C2155.** Heyn C. Growth of shallow InAs HEMTs with metamorphic buffer. / Heyn C., Mendach S., Sch S., Lohr S., Beyer S., Hansen W. // 2002 International Conference on Molecular Beam Epitaxy. 2002. - P. 185-186. ↑
- C2156.** Park C. GaN power switching device growth by plasma assisted molecular beam epitaxy. / Park C., Chapman P.L., Rhee S.H., Hong S.J., Zhang X., Krein P.T., Kim K. // 2002. 37th IAS Annual Meeting. Conference Record of the Industry Applications Conference. - Pittsburgh, PA, 2002. - Vol. 1. - P. 576-579. ↑
- C2157.** Bessemoulin A. 1 watt broad Ka-band ultra small high power amplifier MMICs using 0.25- $\mu$ m GaAs PHEMTs. / Bessemoulin A., Dishong J., Clark G., White D., Quentin P., Thomas H., Geiger D. // 2002. 24th Annual Technical Digest Gallium Arsenide Integrated Circuit (GaAs IC) Symposium. 2002. - P. 40-43. ↑
- C2158.** McPherson D.S. A 3-V fully differential distributed limiting driver for 40 Gb/s optical transmission systems. / McPherson D.S., Pera F., Tazlauanu A., Voinigescu S.P. // 2002. 24th Annual Technical Digest Gallium Arsenide Integrated Circuit (GaAs IC) Symposium. 2002. - P. 95-98. ↑
- C2159.** Masuda S. An over 110-GHz InP HEMT flip-chip distributed baseband amplifier with inverted microstrip line structure for optical transmission systems. / Masuda S., Hirose T., Takahashi T., Nishi M., Yokokawa S., Iijima S., Ono K., Hara N., Joshin K. // 2002. 24th Annual Technical Digest Gallium Arsenide Integrated Circuit (GaAs IC) Symposium. 2002. - P. 99-102. ↑
- C2160.** Hsu S.S.H. Impact of RF stress on dispersion and power characteristics of AlGaIn/GaN HEMTs. / Hsu S.S.H., Valizadeh P., Pavlidis D., Moon J.S., Micovic M., Wong D., Hussain T. // 2002. 24th Annual Technical Digest Gallium Arsenide Integrated Circuit (GaAs IC) Symposium. 2002. - P. 85-88. ↑
- C2161.** Jang J.H. Monolithic integration of In<sub>0.53</sub>Ga<sub>0.47</sub>As photodiodes and In<sub>0.53</sub>Ga<sub>0.47</sub>As/In<sub>0.52</sub>Al<sub>0.48</sub>As HEMTs on GaAs substrates for long wavelength OEIC applications. / Jang J.H., Cueva G., Sankaralingam R., Fay P., Hoke W.E., Adesida I. // 2002. 24th Annual Technical Digest Gallium Arsenide Integrated Circuit (GaAs IC) Symposium. 2002. - P. 55-58. ↑
- C2162.** Chou Y.C. 0.1  $\mu$ m InGaAs/InAlAs/InP HEMT MMICs-a flight qualified technology. / Chou Y.C., Leung D., Lai R., Grundbacher R., Barsky M., Kan Q., Tsai R., Eng D., Wojtowicz M., Block T., Liu P.H., Olson S., Oki A., Streit D.C. // 2002. 24th Annual Technical Digest Gallium Arsenide Integrated Circuit (GaAs IC) Symposium. 2002. - P. 77-80. ↑
- C2163.** Kaper V. Dependence of power and efficiency of AlGaIn/GaN HEMTs on the load resistance for class B bias. / Kaper V., Tilak V., Green B., Prunty T., Smart J., Eastman L.F., Shealy J.R. // 2002. Proceedings. IEEE Lester Eastman Conference on High Performance Devices. 6-8 Aug. 2002. - P. 118-125. ↑
- C2164.** Weimann N.G. AlGaIn/GaN HEMTs grown by molecular beam epitaxy on sapphire, SiC, and HVPE GaN templates. / Weimann N.G., Manfra M.J., Hsu J.W.P., Baldwin K., Pfeiffer L.N., West K.W., Chu S.N.G., Lang D.V., Molnar R.J. // 2002. Proceedings. IEEE Lester Eastman Conference on High Performance Devices. 6-8 Aug. 2002. - P. 126-133. ↑
- C2165.** Paidi V. Simulations of high linearity and high efficiency of class B power amplifiers in GaN HEMT technology. / Paidi V., Shouxuan Xie, Coffie R., Mishra U.K., Long S., Rodwell M.J.W. // 2002. Proceedings. IEEE Lester Eastman Conference on High Performance Devices. 6-8 Aug. 2002. - P. 101-107. ↑
- C2166.** Meliani C. 92 GHz cut-off frequency InP double channel HEMT based coplanar distributed amplifier for 40 Gbit/s applications and beyond. / Meliani C., Post G., Decobert J., Mouzannar W., Rondeau G., Dutisseuil E., Lefevre R. // 2002. ESSCIRC 2002. Proceedings of the 28th European Solid-State Circuits Conference. - Florence, Italy, 24-26 Sept. 2002. - P. 615-617. ↑
- C2167.** Yoder M.N. 30 years of accomplishments in compound semiconductor materials and devices attributable to Prof. Lester F. Eastman. 2002. Proceedings. IEEE Lester Eastman Conference on High Performance Devices. 6-8 Aug. 2002. - P. 34-39. ↑
- C2168.** Islam S.S. Design of GaN/AlGaIn HEMT class-E power amplifier considering trapping and thermal effects. / Islam S.S., Anwar A.F.M. // 2002. Proceedings. IEEE Lester Eastman Conference on High Performance Devices. 6-8 Aug. 2002. - P. 155-163. ↑
- C2169.** Tsai R. MMIC compatible AlSb/InAs HEMT with stable AlGaSb buffer layers. / Tsai R., Barsky N., Lee J., Boos J.B., Bennett B.R., Magno R., Namba C., Liu P.H., Gutierrez A., Lai R. // 2002. Proceedings. IEEE

Lester Eastman Conference on High Performance Devices. 6-8 Aug. 2002. - P. 276-280. ↑

**C2170.** Webster R.T. AlGaAsSb/InGaAs/AlGaAsSb metamorphic HEMTs. / Webster R.T., Anwar A.F.M., Heaton J.L., Nichols K., Duncan S. // 2002. Proceedings. IEEE Lester Eastman Conference on High Performance Devices. 6-8 Aug. 2002. - P. 315-323. ↑

**C2171.** Vijn A. Silicon-germanium power devices at low temperatures for deep-space applications. / Vijn A., Kapoor V.J. // 2002. Proceedings. IEEE Lester Eastman Conference on High Performance Devices. 6-8 Aug. 2002. - P. 270-275. ↑

**C2172.** Berroth M. Advanced large-signal modeling of GaN-HEMTs. / Berroth M., Chigaeve E., Dettmann I., Wieser N., Vogel W., Roll H., Scholz F., Schweizer H. // 2002. Proceedings. IEEE Lester Eastman Conference on High Performance Devices. 6-8 Aug. 2002. - P. 172-180. ↑

**C2173.** Zhang A.P. Microwave power SiC MESFETs and GaN HEMTs. / Zhang A.P., Rowland L.B., Kaminsky E.B., Kretchmer J.W., Beaupre R.A., Garrett J.L., Tucker J.B. // 2002. Proceedings. IEEE Lester Eastman Conference on High Performance Devices. 6-8 Aug. 2002. - P. 181-185. ↑

**C2174.** Eastman L.F. Three decades of our graduate research and education in compound semiconductor materials and devices. 2002. Proceedings. IEEE Lester Eastman Conference on High Performance Devices. 6-8 Aug. 2002. - P. 4-8. ↑

**C2175.** Marso M. MSM diodes based on an AlGaIn/GaN HEMT layer structure for varactor and photodiode application. / Marso M., Bernat J., Wolter A., Javorka P., Fox A., Kordos P. // 2002. The Fourth International Conference on Advanced Semiconductor Devices and Microsystems. 14-16 Oct. 2002. - P. 295-298. ↑

**C2176.** Wolter M. Investigation of current collapse in doped and undoped AlGaIn/GaN HEMTs. / Wolter M., Javorka P., Marso M., Carius R., Heuken M., Luth H., Kordos P. // 2002. The Fourth International Conference on Advanced Semiconductor Devices and Microsystems. 14-16 Oct. 2002. - P. 299-302. ↑

**C2177.** Desgrez S. A new MMIC sampling phase detector design for space applications. / Desgrez S., Langrez D., Delmond M., Cayrou J.-C., Cazaux J.-L. // 2002. 24th Annual Technical Digest Gallium Arsenide Integrated Circuit (GaAs IC) Symposium. 2002. - P. 259-262. ↑

**C2178.** Markovic V. Signal and noise neural models of pHEMTs. / Markovic V., Marinkovic Z. // 2002. NEUREL '02. 2002 6th Seminar on Neural Network Applications in Electrical Engineering. 2002. - P. 185-190. ↑

**C2179.** Barua S. Phase noise in heterojunction field effect transistor amplifiers. / Barua S., Van Slyke A.M., Ferre-Pikal E.S. // 2002. IEEE International Frequency Control Symposium and PDA Exhibition. 2002. - P. 710-714. ↑

**C2180.** Fox A. RF small-signal and power characterization of AlGaIn/GaN HEMTs. / Fox A., Marso M., Javorka P., Kordos P. // 2002. The Fourth International Conference on Advanced Semiconductor Devices and Microsystems. 14-16 Oct. 2002. - P. 291-294. ↑

**C2181.** Kaperm V. High power monolithic AlGaIn/GaN HEMT oscillator. / Kaperm V., Tilak V., Kim H., Thompson R., Prunty T., Smart J., Eastman L.F., Shealy J.R. // 2002. 24th Annual Technical Digest Gallium Arsenide Integrated Circuit (GaAs IC) Symposium. 2002. - P. 251-254. ↑

**C2182.** Belyaev A.E. The effect of gamma-irradiation on the operating parameters of group III nitrides-based field effect transistors. / Belyaev A.E., Konakova R.V., Petrychuk M.V., Avksentyev A.Yu., Kurakin A.M., Vitusevich S.A., Klein N., Danylyuk S.V., Danylychenko B.A. // 2002. CriMiCo 2002. 12th International Conference Microwave and Telecommunication Technology. 9-13 Sept. 2002. - P. 484-485. ↑

**C2183.** {no data available}. Proceedings IEEE Lester Eastman Conference on High Performance Devices (Cat. No.02CH37365). 2002. Proceedings. IEEE Lester Eastman Conference on High Performance Devices. 6-8 Aug. 2002. - {no data available}. ↑

**C2184.** Okamoto N. Suppression of drain conductance dispersion in InP-based HEMTs for broadband optical communication systems. / Okamoto N., Takahashi T., Imanishi K., Sawada K., Hara N. // 2001. IEDM Technical Digest. International Electron Devices Meeting. - Washington, DC, 2001. - P. 9.1.1-9.1.4. ↑

- C2185.** Golio M. The history and future of GaAs devices in commercial wireless products. / Golio M., Newgard B. // 2001 IEEE Emerging Technologies Symposium on Broadband Communications for the Internet Era Symposium digest. - Richardson, TX, 2001. - P. 63-69. ↑
- C2186.** Wu Y.-F. Bias-dependent performance of high-power AlGaIn/GaN HEMTs. / Wu Y.-F., Chavarkar P.M., Moore M., Parikh P., Mishra U.K. // 2001. IEDM Technical Digest. International Electron Devices Meeting. - Washington, DC, 2001. - P. 17.2.1-17.2.3. ↑
- C2187.** Chen Y.K. Semiconductor technologies for high speed optical networking. / Chen Y.K., Baeyens Y., Liu C.-T., Kopf R., Hamm R., Chen C., Yang Y., Frackowiak J., Tate A., Paschke P., Weiner J., Georgiou G., Roux P., Houstma V. // 2001. IEDM Technical Digest. International Electron Devices Meeting. - Washington, DC, 2001. - P. 15.1.1-15.1.3. ↑
- C2188.** Meliani C. 40 Gbit/s reshaping amplifier cell. / Meliani C., Mouzannar W., Jorge F., Lefevre R. // 2001 International Symposium on Electron Devices for Microwave and Optoelectronic Applications. - Vienna, 2001. - P. 331-334. ↑
- C2189.** Smely D. A measurement based gate current model for GaAs MESFET's and HEMT's including self-heating and impact ionization. / Smely D., Mayer M., Magerl G. // 2001 International Symposium on Electron Devices for Microwave and Optoelectronic Applications. - Vienna, 2001. - P. 223-228. ↑
- C2190.** Schreurs D. Efficient construction of a large-signal behavioural HEMT model from automated vectorial large-signal measurements. / Schreurs D., Vandenberghe S., Vandersmissen R. // 2001 International Symposium on Electron Devices for Microwave and Optoelectronic Applications. - Vienna, 2001. - P. 217-221. ↑
- C2191.** Caddemi A. Modeling the temperature noisy performance of low-noise III-V microwave devices down to cryogenic levels. / Caddemi A., Donato N., Tuccari G. // 2001 International Symposium on Electron Devices for Microwave and Optoelectronic Applications. - Vienna, 2001. - P. 267-272. ↑
- C2192.** Marso M. Varactor diodes based on an AlGaIn/GaN HEMT layer structure. / Marso M., Wolter M., Bernat J., Javorka P., Fox A., Kordos P. // 2001 International Symposium on Electron Devices for Microwave and Optoelectronic Applications. - Vienna, 2001. - P. 37-42. ↑
- C2193.** Palmour J.W. Wide bandgap semiconductor devices and MMICs for RF power applications. / Palmour J.W., Sheppard S.T., Smith R.P., Allen S.T., Pribble W.L., Smith T.J., Ring Z., Sumakeris J.J., Saxler A.W., Milligan J.W. // 2001. IEDM Technical Digest. International Electron Devices Meeting. - Washington, DC, 2001. - P. 17.4.1-17.4.4. ↑
- C2194.** Wang P.K. Ohmic contacts to n-type AlGaIn and nitride HEMT epilayers. / Wang P.K., Schweitz K.O., Pribicko T.G., Mohny S.E., Pophristic M., Gotthold D. // 2001 International Semiconductor Device Research Symposium. - Washington, DC, 2001. - P. 199-200. ↑
- C2195.** Wilkinson C.D.W. Etching issues in etching compound and Si-based device fabrication. / Wilkinson C.D.W., Rahman M. // 2001 International Microprocesses and Nanotechnology Conference. - Shimane, 2001. - P. 28. ↑
- C2196.** Pavlidis D. III-V nitride-based two terminal devices for high power, high-frequency applications. 2001 International Semiconductor Device Research Symposium. - Washington, DC, 2001. - P. 384-387. ↑
- C2197.** Triplett G. Modeling electron mobility in MBE-grown InAs/AlSb thin films for HEMT applications using neural networks. / Triplett G., May G., Brown A. // 2001 International Semiconductor Device Research Symposium. - Washington, DC, 2001. - P. 264-265. ↑
- C2198.** Anwar A.F.M. RF performance of GaN/AlGaIn HEMT amplifier. / Anwar A.F.M., Islam S.S. // 2001 International Semiconductor Device Research Symposium. - Washington, DC, 2001. - P. 209-212. ↑
- C2199.** Ahmed A. Gain compression in GaN HEMT amplifiers. / Ahmed A., Islam S.S., Anwar A.F.M. // 2001 International Semiconductor Device Research Symposium. - Washington, DC, 2001. - P. 205-208. ↑
- C2200.** Lee Y.C. 17-36 GHz broadband PHEMT MMIC power amplifier for point-to-multipoint applications. / Lee Y.C., Park C.S. // 2001. Proceedings. 6th International Conference on Solid-State and Integrated-Circuit Technology. 22-25 Oct. 2001. - Vol. 2. - P. 1320-1323. ↑

- C2201.** Sandhu R. 1.6 w/mm, 26% PAE AlGaIn/GaN HEMT operation at 29GHz. / Sandhu R., Wojtowicz M., Barsky M., Tsai R., Smorchkova I., Namba C., Liu P.H., Dia R., Truong M., Ko D., Yang J.W., Wang H., Khan M.A. // 2001. IEDM Technical Digest. International Electron Devices Meeting. - Washington, DC, 2001. - P. 17.5.1-17.5.3. ↑
- C2202.** Zhang N.-Q. Effects of surface traps on breakdown voltage and switching speed of GaN power switching HEMTs. / Zhang N.-Q., Moran B., DenBaars S.P., Mishra U.K., Wang X.W., Ma T.P. // 2001. IEDM Technical Digest. International Electron Devices Meeting. - Washington, DC, 2001. - P. 25.5.1-25.5.4. ↑
- C2203.** Fu Renwu. Numerical simulation of DC characteristic of InP/InGaAs based optically controlled HEMT. / Fu Renwu, Huang Ping, Chen Chao. // 2001. Proceedings. 6th International Conference on Solid-State and Integrated-Circuit Technology. 22-25 Oct. 2001. - Vol. 2. - P. 1352-1355. ↑
- C2204.** Guoli Qu. Measurement and simulation of IM distortion in high mobility transistors. / Guoli Qu, Parker A.E. // 2001. Proceedings. 6th International Conference on Solid-State and Integrated-Circuit Technology. 22-25 Oct. 2001. - Vol. 2. - P. 1337-1339. ↑
- C2205.** Jong Seol Yuk. Gate width optimization of PHEMT MMIC LNA for low power consumption. / Jong Seol Yuk, Byoung Gun Choi, You Sang Lee, Chul Soon Park. // 2001. Proceedings. 6th International Conference on Solid-State and Integrated-Circuit Technology. 22-25 Oct. 2001. - Vol. 2. - P. 1327-1330. ↑
- C2206.** Javorka P. Optimization of AlGaIn/GaN HEMT performance. / Javorka P., Wolter M., Alam A., Fox A., Marso M., Heuken M., Kordos P. // 2001 International Symposium on Electron Devices for Microwave and Optoelectronic Applications. - Vienna, 2001. - P. 31-36. ↑
- C2207.** Kudszus S. Push-push oscillators for 94 and 140 GHz applications using standard pseudomorphic GaAs HEMTs. / Kudszus S., Haydl W.H., Tessmann A., Bronner W., Schlechtweg M. // 2001 IEEE MTT-S International Microwave Symposium Digest. - Phoenix, AZ, 2001. - Vol. 3. - P. 1571-1574. ↑
- C2208.** Siweris H.J. Monolithic 38 GHz coplanar feedback VCOs fabricated by a production PHEMT technology. / Siweris H.J., Tischer H., Rohrer E. // 2001 IEEE MTT-S International Microwave Symposium Digest. - Phoenix, AZ, 2001. - Vol. 3. - P. 1555-1558. ↑
- C2209.** Avitabile G. Compact MMIC active inductor. / Avitabile G., Chellini B., Limiti E., Giannini F. // 2001 IEEE MTT-S International Microwave Symposium Digest. - Phoenix, AZ, 2001. - Vol. 3. - P. 1585-1588. ↑
- C2210.** Urteaga M. 185 GHz monolithic amplifier in InGaAs-InAlAs transferred-substrate HBT technology. / Urteaga M., Scott D., Mathew T., Krishnan S., Wei Y., Rodwell M.J.W. // 2001 IEEE MTT-S International Microwave Symposium Digest. - Phoenix, AZ, 2001. - Vol. 3. - P. 1713-1716. ↑
- C2211.** Maestrini A. Performance of a 1.2 THz frequency tripler using a GaAs frameless membrane monolithic circuit. / Maestrini A., Bruston J., Pukala D., Martin S., Mehdi I. // 2001 IEEE MTT-S International Microwave Symposium Digest. - Phoenix, AZ, 2001. - Vol. 3. - P. 1657-1660. ↑
- C2212.** Megej A. Conditions for broadband MMIC voltage-controlled oscillators based on theory and experiments. / Megej A., Beilenhoff K., Hartnagel H.L. // 2001 IEEE MTT-S International Microwave Symposium Digest. - Phoenix, AZ, 2001. - Vol. 3. - P. 1419-1422. ↑
- C2213.** Green B.M. High-power broadband AlGaIn/GaN HEMT MMICs on SiC substrates. / Green B.M., Tilak V., Sungjae Lee, Hyungtak Kim, Smart J.A., Webb K.J., Shealy J.R., Eastman L.F. // 2001 IEEE MTT-S International Microwave Symposium Digest. - Phoenix, AZ, 2001. - Vol. 2. - P. 1059-1062. ↑
- C2214.** Duperrier C. New design method of non-uniform distributed power amplifiers. Application to a single stage 1 W PHEMT MMIC. / Duperrier C., Campovecchio M., Roussel L., Lajugie M., Quere R. // 2001 IEEE MTT-S International Microwave Symposium Digest. - Phoenix, AZ, 2001. - Vol. 2. - P. 1063-1066. ↑
- C2215.** Sasaki Y. 20-30 GHz broadband MMIC power amplifiers with compact flat gain PHEMT cells. / Sasaki Y., Kurusu H., Hoshi H., Hisaka T., Mitsui Y. // 2001 IEEE MTT-S International Microwave Symposium Digest. - Phoenix, AZ, 2001. - Vol. 2. - P. 1067-1070. ↑
- C2216.** Matinpour B. A K-band subharmonic down-converter in a GaAs metamorphic HEMT process. / Matinpour B., Lal N., Laskar J., Leoni R.E. III., Whelan C.S. // 2001 IEEE MTT-S International Microwave



Symposium Digest. - Phoenix, AZ, 2001. - Vol. 2. - P. 1337-1339. ↑

C2217. Jong-Sik Lim. A new balanced amplifier using 6-port power divider. / Jong-Sik Lim, Soon-Young Eom, Jae-Hee Han, Seong-Hun Kim, Deok-Hee Lee, Sangwook Nam. // 2001 IEEE MTT-S International Microwave Symposium Digest. - Phoenix, AZ, 2001. - Vol. 2. - P. 1301-1304. ↑

C2218. Schallner M. Adjustment of a temperature compensated Ka-band ring resonator VCO using fully automated laser-trimming. / Schallner M., Konrath W. // 2001 IEEE MTT-S International Microwave Symposium Digest. - Phoenix, AZ, 2001. - Vol. 3. - P. 2179-2182. ↑

C2219. Mimino Y. Design techniques of reducing chip area and highly integrated MMIC for W-band application. / Mimino Y., Nakamura K., Sakamoto K., Aoki Y., Kuroda S., Tokumitsu T. // 2001 IEEE MTT-S International Microwave Symposium Digest. - Phoenix, AZ, 2001. - Vol. 3. - P. 2167-2170. ↑

C2220. Xu J. A monolithically integrated bacteriorhodopsin/GaAs MODFET bio-photoreceiver. / Xu J., Bhattacharya P., Varo G. // 2001. LEOS 2001. The 14th Annual Meeting of the IEEE Lasers and Electro-Optics Society. - San Diego, CA, 2001. - Vol. 2. - P. 833-834. ↑

C2221. Uren M.J. AlGaIn/GaN microwave power transistors for S band. / Uren M.J., Hughes B.T., Hayes D.G., Hilton K.P., Martin T., Balmer R.S., Birbeck J.C.H., Davies R.A. // 2001 International Symposium on Electron Devices for Microwave and Optoelectronic Applications. - Vienna, 2001. - P. 27-30. ↑

C2222. Kuzmik J. Investigation of self-heating effects in AlGaIn-GaN HEMTs. / Kuzmik J., Javorka P., Alam A., Marso M., Heuken M., Kordos P. // 2001 International Symposium on Electron Devices for Microwave and Optoelectronic Applications. - Vienna, 2001. - P. 21-26. ↑

C2223. Shinohara K. Novel asymmetric gate-recess engineering for sub-millimeter-wave InP-based HEMTs. / Shinohara K., Matsui T., Mimura T., Hiyaizumi S. // 2001 IEEE MTT-S International Microwave Symposium Digest. - Phoenix, AZ, 2001. - Vol. 3. - P. 2159-2162. ↑

C2224. Rogeaux E. Ka band power pHEMT technology for space power flip-chip assembly. / Rogeaux E., Frayssé J.-P., Schaffauser C., George S., Pons D., Fellon P., Geiger D., Theron D., Haese N., Verdeyme S., Quere R., Baillargeat D., Ngoya E., Long S., Escotte L. // 2001 IEEE MTT-S International Microwave Symposium Digest. - Phoenix, AZ, 2001. - Vol. 3. - P. 1895-1898. ↑

C2225. Samoska L. 65-145 GHz InP MMIC HEMT medium power amplifiers. / Samoska L., Yoke Choy Leong. // 2001 IEEE MTT-S International Microwave Symposium Digest. - Phoenix, AZ, 2001. - Vol. 3. - P. 1805-1808. ↑

C2226. Nosal Z.M. Simple model for dynamic range estimate of GaAs amplifiers. 2001 IEEE MTT-S International Microwave Symposium Digest. - Phoenix, AZ, 2001. - Vol. 3. - P. 1963-1966. ↑

C2227. Lan E. InGaP PHEMTs for wireless power applications. / Lan E., Pitts B., Mikhov M., Hartin O. // 2001 IEEE MTT-S International Microwave Symposium Digest. - Phoenix, AZ, 2001. - Vol. 3. - P. 2155-2157. ↑

C2228. Nuttinck S. Study of self-heating effects in GaN HEMTs. / Nuttinck S., Gebara E., Laskar J., Harris M. // 2001 IEEE MTT-S International Microwave Symposium Digest. - Phoenix, AZ, 2001. - Vol. 3. - P. 2151-2154. ↑

C2229. Chigaeva E. Dynamic Large-Signal I-V Analysis and Non-Linear Modelling of AlGaIn/GaN HEMTs. / Chigaeva E., Wieser N., Walther W., Grozing M., Berroth M., Roll H., Breitschadel O., Off J., Kuhn B., Scholz F., Schweizer H. // 2001. 31st European Microwave Conference. - London, England, 24-26 Sept. 2001. - P. 1-4. ↑

C2230. Marsh P.F. Reliability of metamorphic HEMTs on GaAs substrates. / Marsh P.F., Whelan C.S., Hoke W.E., Leoni R.E. III, Kazior T.E. // 2001. Proceedings GaAs Reliability Workshop. 2001. - P. 119-132. ↑

C2231. Parker Anthony E. Analysis of HEMT Time-Evolution Characteristics. / Parker Anthony E., Rathmell James G. // 2001. 31st European Microwave Conference. - London, England, 24-26 Sept. 2001. - P. 1-4. ↑

C2232. Torki K. CMP provides the access to advanced low cost manufacturing. 2001. ICM 2001 Proceedings. The 13th International Conference on Microelectronics. 29-31 Oct. 2001. - P. 20-24. ↑

C2233. Hirata M. High Dynamic-Range and Very Low Noise K-Band p-HEMT LNA MMIC for LMDS and

- Satellite Communication. / Hirata M., Mimino Y., Hasegawa Y., Fukaya J. // 2001. 31st European Microwave Conference. - London, England, 24-26 Sept. 2001. - P. 1-4. ↑
- C2234. Dammann M. Effect of gate metal on reliability of metamorphic HEMTs. / Dammann M., Leuther A., Konstanzer H., Jantz W. // 2001. Proceedings GaAs Reliability Workshop. 2001. - P. 87-88. ↑
- C2235. Johnson J. Quantitative analysis of microwave frequency multiplication in MESFET/HEMT devices. / Johnson J., Chee M., Branner G.R. // 2001. MWSCAS 2001. Proceedings of the 44th IEEE 2001 Midwest Symposium on Circuits and Systems. - Dayton, OH, 2001. - Vol. 2. - P. 760-763. ↑
- C2236. Svedin J. A compact MMIC SPDT switch for 60 GHz applications. / Svedin J., Gustafsson A. // 2001. APMC 2001. 2001 Asia-Pacific Microwave Conference. - Taipei, 2001. - Vol. 1. - P. 303-305. ↑
- C2237. Johnson J. Effects of active microwave device parameters on microwave harmonic frequency generators. / Johnson J., Branner G.R., Chee M. // 2001. MWSCAS 2001. Proceedings of the 44th IEEE 2001 Midwest Symposium on Circuits and Systems. - Dayton, OH, 2001. - Vol. 2. - P. 777-780. ↑
- C2238. Yajian Huang. Frequency Dependence of HEMT Under Optical Illumination. / Yajian Huang, Alphones Arokiaswami. // 2001. 31st European Microwave Conference. - London, England, 24-26 Sept. 2001. - P. 1-4. ↑
- C2239. Nakahara T. Single optical clock pulse generator for processing ultrafast asynchronous optical packets. / Nakahara T., Takahashi R., Takenouchi H., Suzuki H. // 2001. ECOC '01. 27th European Conference on Optical Communication. 2001. - Vol. 4. - P. 508-509. ↑
- C2240. Parker Anthony E. Relating Dynamics of FET Behavior to Operating Regions. / Parker Anthony E., Rathmell James G. // 58th ARFTG Conference Digest-Fall. - San Diego, CA, USA, Nov. 2001. - Vol. 40. - P. 1-10. ↑
- C2241. Leong Kevin M. K. H. Monolithic Millimeter-Wave Source Incorporating Planar Surface Wave Assisted Antenna. / Leong Kevin M. K. H., Radisic Vesna, Samoska Lorene, Qian Yongxi, Itoh Tatsuo. // 2001. 31st European Microwave Conference. - London, England, 24-26 Sept. 2001. - P. 1-4. ↑
- C2242. Loo-Yau J.R. A New Empirical Gate Capacitance Model for PHEMT and MESFET Transistors. / Loo-Yau J.R., Infante-Galindo R., Reynoso-Hernandez J.A. // 58th ARFTG Conference Digest-Fall. - San Diego, CA, USA, Nov. 2001. - Vol. 40. - P. 1-6. ↑
- C2243. Schlechtweg M. High Speed Circuits Based on HEMT Technology for Optical/Wireless Communication and Sensor Systems. 2001. Proceeding of the 31st European Solid-State Device Research Conference. 11-13 September 2001. - P. 89-96. ↑
- C2244. Schreurs D. Automatically Controlled Coverage of the Voltage Plane of Quasi-Unilateral Devices. / Schreurs D., Vandenberghe S., Wood J., Tufillaro N., Barford L., Root D.E. // 57th ARFTG Conference Digest-Spring. - Phoenix, AZ, USA, May 2001. - Vol. 39. - P. 1-5. ↑
- C2245. Vaha-Heikkila Tauno. W-Band On-Wafer Noise Parameter Measurements. / Vaha-Heikkila Tauno, Lahdes Manu, Tuovinen Jussi, Kantanen Mikko, Kangaslahti Pekka, Jukkala Petri, Hughes Nicholas. // 2001. 31st European Microwave Conference. - London, England, 24-26 Sept. 2001. - P. 1-4. ↑
- C2246. Campos-Roca Y. Millimeter-wave Active MMIC Frequency Multipliers. / Campos-Roca Y., Verweyen L., Fernandez-Barciela M., Curras-Francos M. C., Sanchez E., Hulsmann A., Schlechtweg M. // 2001. 31st European Microwave Conference. - London, England, 24-26 Sept. 2001. - P. 1-4. ↑
- C2247. Marzolf T. Design and characterization of a monolithic amplifier for millimeter wave. / Marzolf T., Drissi W., Zenkour L. // 2001. ICM 2001 Proceedings. The 13th International Conference on Microelectronics. 29-31 Oct. 2001. - P. 177-180. ↑
- C2248. Walthes Wolfgang. Non-Linear Characterization and Simulation of a Travelling Wave Amplifier. / Walthes Wolfgang, Berroth Manfred. // 2001. 31st European Microwave Conference. - London, England, 24-26 Sept. 2001. - P. 1-4. ↑
- C2249. Artal E. Low 1/f Noise 30 GHz Broadband Amplifiers for the Differential Radiometers of the Planck Surveyor Mission. / Artal E., Aja B., de la Fuente M. L., Palacios C., Mediavilla A., Pascual J. P., Portilla J. //

2001. 31st European Microwave Conference. - London, England, 24-26 Sept. 2001. - P. 1-4. ↑

**C2250.** Yang Sung-Gi. A High Gain-Bandwidth Baseband GaAs P-HEMT Matrix Distributed Amplifier IC with a Shifted Second Tier Structure. / Yang Sung-Gi, Seo Kwang-Seok. // 2001. 31st European Microwave Conference. - London, England, 24-26 Sept. 2001. - P. 1-4. ↑

**C2251.** Shu-Fen Wei. A monolithic K-band MMIC receiver. / Shu-Fen Wei, I-Hsiang Lin, Huei Wang. // 2001. APMC 2001. 2001 Asia-Pacific Microwave Conference. - Taipei, 2001. - Vol. 1. - P. 299-302. ↑

**C2252.** Cheng-Kuo Lin. An extended RF non-linear model for power prediction of AlGaAs/InGaAs pHEMT's. / Cheng-Kuo Lin, Yi-Jen Chan. // 2001. APMC 2001. 2001 Asia-Pacific Microwave Conference. - Taipei, Taiwan, 3-6 Dec. 2001. - Vol. 2. - P. 722-725. ↑

**C2253.** Chen S.H. 2.4 V-operated enhancement mode PHEMT with 32 dBm output power and 61% power efficiency. / Chen S.H., Chang E.Y., Lin Y.C. // 2001. APMC 2001. 2001 Asia-Pacific Microwave Conference. - Taipei, 2001. - Vol. 3. - P. 1291-1294. ↑

**C2254.** Ratna P. A novel technique for accurate noise modelling. / Ratna P., Kirty V.S.R. // 2001. APMC 2001. 2001 Asia-Pacific Microwave Conference. - Taipei, Taiwan, 3-6 Dec. 2001. - Vol. 2. - P. 730-734. ↑

**C2255.** Byung-Jun Jang. V-band MMIC low-noise amplifier design based on distributed active device model. / Byung-Jun Jang, In-Bok Yom, Seong-Pal Lee. // 2001. APMC 2001. 2001 Asia-Pacific Microwave Conference. - Taipei, 2001. - Vol. 1. - P. 25-28. ↑

**C2256.** Streit D.C. Indium phosphide HEMT and HBT production for microwave and millimeter-wave applications. / Streit D.C., Sawdai D., Grunbacher R., Tsai R., Lai R., Gutierrez-Aitken A., Oki A. // 2001. APMC 2001. 2001 Asia-Pacific Microwave Conference. - Taipei, 2001. - Vol. 1. - P. 9-14. ↑

**C2257.** Hsien-Chin Chiu. High power density and large voltage swing of enhancement-mode Al<sub>0.5</sub>Ga<sub>0.5</sub>As/InGaAs pHEMTs for 3.5 V L-band applications. / Hsien-Chin Chiu, Shih-Cheng Yang, Yi-Jen Chan. // 2001. APMC 2001. 2001 Asia-Pacific Microwave Conference. - Taipei, 2001. - Vol. 3. - P. 1203-1206. ↑

**C2258.** Islam S.S. GaN/AlGaN HEMT microwave class-E power amplifier. / Islam S.S., Anwar A.F.M. // 2001 International Semiconductor Device Research Symposium. - Washington, DC, 2001. - P. 446-449. ↑

**C2259.** Jong-Wook Lee. A broadband GaN push-pull distributed microwave power amplifier. / Jong-Wook Lee, Green B.M., Tilak V., Sungjae Lee, Shealy J.R., Eastman L.F., Webb K.J. // 2001 International Semiconductor Device Research Symposium. - Washington, DC, 2001. - P. 391-393. ↑

**C2260.** Boos J.B. Recent advances in AlSb/InAs HEMTs for high-speed electronics. / Boos J.B., Bennett B.R., Ancona M.G., Kruppa W., Park D., Yang M.J., Hobart K.D., Bracker A.S., Justh E., Mittereder J., Chang W., Turner N.H., Bass R. // 2001 International Semiconductor Device Research Symposium. - Washington, DC, 2001. - P. 554. ↑

**C2261.** Lee J.-W. In<sub>0.5</sub>Ga<sub>0.5</sub>P/In<sub>0.22</sub>Ga<sub>0.78</sub>As/GaAs pseudomorphic high electron mobility transistor with gate oxide layer for improving on-state and off-state breakdown voltages. / Lee J.-W., Kang I.-H., Kang S.-J., Jo S.-J., In S.-K., Song H.-J., Kim J.-H., Song J.-I. // 2001 International Semiconductor Device Research Symposium. - Washington, DC, 2001. - P. 634-637. ↑

**C2262.** Isler M. Investigation of on-state breakdown in InAlAs/InGaAs HEMTs. / Isler M., Schunemann K. // 2001 International Semiconductor Device Research Symposium. - Washington, DC, 2001. - P. 630-633. ↑

**C2263.** Jong Seol Yuk. Device and circuit optimization of PHEMT MMIC LNA for low power consumption. / Jong Seol Yuk, Byoung Gun Choi, Chul Soon Park. // 2001. APMC 2001. 2001 Asia-Pacific Microwave Conference. - Taipei, 2001. - Vol. 1. - P. 260-263. ↑

**C2264.** Wei C.-J. Novel approach to a consistent large-signal and small-signal modeling of power PHEMTs. / Wei C.-J., Bartle D., Tkachenko Y.A. // 2001. APMC 2001. 2001 Asia-Pacific Microwave Conference. - Taipei, 2001. - Vol. 1. - P. 252-255. ↑

**C2265.** Chaki S. A Ka-band compact 1 watt power amplifier using a Platy-TRL matching method. / Chaki S., Hisaka T., Hirai T., Sasaki Y., Sakamoto S., Mitsui Y. // 2001. APMC 2001. 2001 Asia-Pacific Microwave

Conference. - Taipei, 2001. - Vol. 1. - P. 284-287. ↑

C2266. Yun Y. A low noise and low power dissipation downconverter MMIC for DBS applications. / Yun Y., Fukuda T., Kuniyoshi T., Tanaka T., Ishikawa O. // 2001. APMC 2001. 2001 Asia-Pacific Microwave Conference. - Taipei, 2001. - Vol. 1. - P. 295-298. ↑

C2267. Wen-Chieh Wu. A fully integrated broadband amplifier with 161% 3-dB bandwidth. / Wen-Chieh Wu, Huei Wang, Hao-Hsiung Lin. // 2001. APMC 2001. 2001 Asia-Pacific Microwave Conference. - Taipei, 2001. - Vol. 1. - P. 291-294. ↑

C2268. Hua-Shan Chou. Ka-band monolithic GaAs PHEMT low noise and driver amplifiers. / Hua-Shan Chou, Chieh-Chao Liu, Chen T.H. // 2001. APMC 2001. 2001 Asia-Pacific Microwave Conference. - Taipei, 2001. - Vol. 1. - P. 139-142. ↑

C2269. Meng C.C. Gain profiles for conditionally stable and unconditionally stable amplifiers. / Meng C.C., Ni H.Y. // 2001. APMC 2001. 2001 Asia-Pacific Microwave Conference. - Taipei, 2001. - Vol. 1. - P. 33-36. ↑

C2270. Chou Y.C. High reliability of 0.1  $\mu\text{m}$  MMIC amplifiers on both AlGaAs/InGaAs/GaAs and InGaAs/InAlAs/InP HEMTs. / Chou Y.C., Leung D., Lai R., Grundbacher R., Scarpulla J., Barsky M., Eng D., Liu P.H., Biedenbender M., Oki A., Streit D.C. // 2001. APMC 2001. 2001 Asia-Pacific Microwave Conference. - Taipei, 2001. - Vol. 1. - P. 29-32. ↑

C2271. Yu-Chi Wang. Advanced GaAs MMIC technology development at WIN Semiconductors corporation. / Yu-Chi Wang, Chertouk M., Cheang P., Der-Wei Tu, Chao P.C., Chan Shin Wu. // 2001. APMC 2001. 2001 Asia-Pacific Microwave Conference. - Taipei, 2001. - Vol. 1. - P. 121-126. ↑

C2272. Alfredson M. Broadband bidirectional active MMIC power splitter and combiner for feed networks. / Alfredson M., Ouacha A., Jonsson R. // 2001. APMC 2001. 2001 Asia-Pacific Microwave Conference. - Taipei, 2001. - Vol. 1. - P. 135-138. ↑

C2273. Jia-Liang Chen. A 20-40 GHz monolithic doubly-balanced mixer using modified planar Marchand baluns. / Jia-Liang Chen, Sheng-Fuh Chang, Bo-Yuen Laue. // 2001. APMC 2001. 2001 Asia-Pacific Microwave Conference. - Taipei, 2001. - Vol. 1. - P. 131-134. ↑

C2274. Ang K.S. Monolithic Ka-band even-harmonic quadrature resistive mixer for direct conversion receivers. / Ang K.S., Chongcheawchamnan M., Kpogla D., Young P.R., Robertson I.D., Dong-sik Kim, Moon-chuel Ju, Hwa-chang Seo. // 2001. Digest of Papers. 2001 IEEE Radio Frequency Integrated Circuits (RFIC) Symposium. - Phoenix, AZ, 2001. - P. 169-172. ↑

C2275. Ooi B.L. Large signal bias-dependent modeling of PHEMTs by pulsed measurements. / Ooi B.L., Lan K., Leong M.S., Kooi K.S. // 2001. Digest of Papers. 2001 IEEE Radio Frequency Integrated Circuits (RFIC) Symposium. - Phoenix, AZ, 2001. - P. 155-157. ↑

C2276. Yamamoto S. A 1-chip RF transceiver MMIC for ETC with surface via-hole isolation technique. / Yamamoto S., Suwa A., Tanbo T., Kitazawa T., Tara K., Hagio M. // 2001. Digest of Papers. 2001 IEEE Radio Frequency Integrated Circuits (RFIC) Symposium. - Phoenix, AZ, 2001. - P. 195-198. ↑

C2277. Morkner H. A 1.7 mA low noise amplifier with integrated bypass switch for wireless 0.05-6 GHz portable applications. / Morkner H., Frank M., Yajima S. // 2001. Digest of Papers. 2001 IEEE Radio Frequency Integrated Circuits (RFIC) Symposium. - Phoenix, AZ, 2001. - P. 235-238. ↑

C2278. Lucero R. Design of an LTCC switch diplexer front-end module for GSM/DCS/PCS applications. / Lucero R., Qutteneh W., Pavia A., Meyers D., Estes J. // 2001. Digest of Papers. 2001 IEEE Radio Frequency Integrated Circuits (RFIC) Symposium. - Phoenix, AZ, 2001. - P. 213-216. ↑

C2279. McNamara B. Dual-band/tri-mode receiver IC for N- and W-CDMA systems using 6"-PHEMT technology. / McNamara B., Zhang S., Murphy M., Banzer H.M., Kapusta H., Rohrer E., Grave T., Verweyen L. // 2001. Digest of Papers. 2001 IEEE Radio Frequency Integrated Circuits (RFIC) Symposium. - Phoenix, AZ, 2001. - P. 13-16. ↑

C2280. Alina C. Characterization techniques for temperature-dependent experimental analysis of microwave transistors. / Alina C., Nicola D., Mario S. // 2001. IMTC 2001. Proceedings of the 18th IEEE Instrumentation and



Measurement Technology Conference. - Budapest, 2001. - Vol. 3. - P. 1893-1896. ↑

C2281. Yakout M.A. An accurate analytical model of the AlGaAs/GaAs high electron mobility transistor (HEMT). / Yakout M.A., AbdelRassoul R.A., AbdelFattah A.I., Essa S.G. // 2001. NRSC 2001. Proceedings of the Eighteenth National Radio Science Conference. - Mansoura, 2001. - Vol. 2. - P. 531-539. ↑

C2282. Anderson W.T. Semiconductor device reliability in extreme high temperature space environments. IEEE Proceedings. Aerospace Conference, 2001. - Big Sky, MT, 2001. - Vol. 5. - P. 2457-2462. ↑

C2283. Torki K. CMP: the access to advanced low cost manufacturing. / Torki K., Courtois B. // 2001. Proceedings. 2001 International Conference on Microelectronic Systems Education. 17-18 June 2001. - P. 6. ↑

C2284. Bautista J.J. Cryogenic, X-band and Ka-band InP HEMT based LNAs for the Deep Space Network. / Bautista J.J., Bowen J.G., Fernandez N.E., Fujiwara Z., Loreman J., Petty S., Prater J.L., Grunbacher R., Lai R., Nishimoto M., Murti M.R., Laskar J. // IEEE Proceedings. Aerospace Conference, 2001. - Big Sky, MT, 2001. - Vol. 2. - P. 2/829. ↑

C2285. Campbell C.F. Design and performance of a highly integrated wideband active downconverter MMIC. / Campbell C.F., Beall J.M. // 2001. Digest of Papers. 2001 IEEE Radio Frequency Integrated Circuits (RFIC) Symposium. - Phoenix, AZ, 2001. - P. 245-248. ↑

C2286. Sano Y. High performance AlGaN/GaN HEMTs with recessed gate on sapphire substrate. / Sano Y., Yamada T., Mita J., Kaifu K., Ishikawa H., Egawa T., Umeno M. // 2001 Device Research Conference. - Notre Dame, IN, 2001. - P. 81-82. ↑

C2287. Somerville M. Hyperspectral imaging of breakdown in InAlAs/InGaAs HEMTs: a comparative study. / Somerville M., Rameau J., Nii Moi Addo. // 2001 Device Research Conference. - Notre Dame, IN, 2001. - P. 65-66. ↑

C2288. Arulkumaran S. Excellent DC characteristics of HEMTs on semi-insulating silicon carbide substrate. / Arulkumaran S., Egawa T., Zhao G., Umeno M. // 2001 Device Research Conference. - Notre Dame, IN, 2001. - P. 91-92. ↑

C2289. Jenkins T. Linearity of high Al-content AlGaN/GaN HEMTs. / Jenkins T., Kehias L., Parikh P., Wu Y.-F., Chavarkar P., Moore M., Mishra U. // 2001 Device Research Conference. - Notre Dame, IN, 2001. - P. 201-202. ↑

C2290. Otsuji T. Terahertz plasma-wave excitation in 80-nm gate-length GaAs MESFET by photomixing long-wavelength CW laser sources. / Otsuji T., Kanamaru Y., Kitamura H., Nakae S. // 2001 Device Research Conference. - Notre Dame, IN, 2001. - P. 97-98. ↑

C2291. Maezawa K. Chaos generator MMIC's using resonant tunneling diodes. / Maezawa K., Kawano Y., Ohno Y., Kishimoto S., Mizutani T. // 2001 Device Research Conference. - Notre Dame, IN, 2001. - P. 55-56. ↑

C2292. Suzuki T. 40-Gbit/s D-type flip-flop and multiplexer circuits using InP HEMT. / Suzuki T., Kano H., Nakasha Y., Takahashi T., Imanishi K., Ohnishi H., Watanabe Y. // 2001. Digest of Papers. 2001 IEEE Radio Frequency Integrated Circuits (RFIC) Symposium. - Phoenix, AZ, 2001. - P. 291-294. ↑

C2293. Ahmed A. Temperature dependence of intermodulation and linearity in GaN based devices. / Ahmed A., Islam S.S., Anwar A.F.M. // 2001. Digest of Papers. 2001 IEEE Radio Frequency Integrated Circuits (RFIC) Symposium. - Phoenix, AZ, 2001. - P. 275-278. ↑

C2294. Jeong Hoon Kim. Noise characteristics of highly strained InGaP/InGaAs p-HEMTs grown on patterned substrates by using compound-source MBE. / Jeong Hoon Kim, Sung-June Jo, Jong-In Song. // 2001 Device Research Conference. - Notre Dame, IN, 2001. - P. 45-46. ↑

C2295. Dumka D.C. Monolithic integration of InAlAs/InGaAs enhancement and depletion (E/D)-mode metamorphic HEMTs on GaAs substrate. / Dumka D.C., Hoke W.E., Lemonias P.J., Schwindt R., Cueva G., Adesida I. // 2001 Device Research Conference. - Notre Dame, IN, 2001. - P. 49-50. ↑

C2296. Fay P. A flip-flop based on monolithic integration of InAs/AlSb/GaSb RITDs and InAlAs/InGaAs/InP HEMTs. / Fay P., Xu Y., Lu J., Bernstein G.H., Gonzalez A., Mazumder P., Chow D.H., Schulman J.N. // 2001

Device Research Conference. - Notre Dame, IN, 2001. - P. 47-48. ↑

C2297. Chou Y.C. High reliability of 0.1  $\mu\text{m}$  InGaAs/InAlAs/InP HEMT MMICs on 3-inch InP substrates. / Chou Y.C., Leung D., Scarpulla J., Lai R., Barsky M., Grundbacher R., Nishimoto M., Liu P.H., Streit D.C. // 2001. IPRM. IEEE International Conference On Indium Phosphide and Related Materials. - Nara, 2001. - P. 618-621. ↑

C2298. {no data available}. Proceedings of the 2001 SBMO/IEEE MTT-S International Microwave and Optoelectronics Conference. (Cat. No.01TH8568). 2001. IMOC 2001.Proceedings of the 2001 SBMO/IEEE MTT-S International Microwave and Optoelectronics Conference. 2001. - Vol. 1. - {no data available}. ↑

C2299. Nabet B. On optical gain mechanisms in a 2DEG photodetector. / Nabet B., Romero M.A., Cola A., Quaranta F., Cesareo M. // 2001. IMOC 2001.Proceedings of the 2001 SBMO/IEEE MTT-S International Microwave and Optoelectronics Conference. 2001. - Vol. 1. - P. 57-60. ↑

C2300. Batty W. Fully physical time-dependent compact thermal modelling of complex non linear 3-dimensional systems for device and circuit level electro-thermal CAD. / Batty W., Christoffersen C.E., David S., Panks A.J., Johnson R.G., Snowden C.M., Steer M.B. // 2001. Seventeenth Annual IEEE Symposium Semiconductor Thermal Measurement and Management. - San Jose, CA, 2001. - P. 71-84. ↑

C2301. {no data available}. Conference Proceedings. 2001 International Conference on Indium Phosphide and Related Materials. 13th IPRM (Cat. No.01CH37198). 2001. IPRM. IEEE International Conference On Indium Phosphide and Related Materials. 2001. - {no data available}. ↑

C2302. Miranda J.M. Characterization of parasitics in microwave devices by comparing S and noise parameter measurements with two different on wafer calibration techniques. / Miranda J.M., Fager C., Zirath H., Sakalas P., Munoz S., Sebastian J.L. // 2001. IMTC 2001. Proceedings of the 18th IEEE Instrumentation and Measurement Technology Conference. - Budapest, 21-23 May 2001. - Vol. 1. - P. 530-533. ↑

C2303. Chen S.H. 2.4 V-operated enhancement-mode power PHEMTs for personal handy-phone system application. / Chen S.H., Chang E.Y., Lin Y.C., Lee C.S. // 2001. IMOC 2001.Proceedings of the 2001 SBMO/IEEE MTT-S International Microwave and Optoelectronics Conference. 2001. - Vol. 1. - P. 127-129. ↑

C2304. Di Maio B. Noise performance and bias-dependence of Si/SiGe HBT's at microwave frequencies. / Di Maio B., Di Prima F. // 2001. CriMiCo 2001. 11th International Conference on Microwave and Telecommunication Technology. - Sevastopol, Crimea, Ukraine, 14-14 Sept. 2001. - P. 115-118. ↑

C2305. Gutt T. Low temperatures in RTP. Advanced Thermal Processing of Semiconductors 9th International Conference on RTP 2001. 2001. - P. 270-271. ↑

C2306. Zubkov A.M. Design and fabrication of low noise MODFET for 30-60 GHz band. / Zubkov A.M., Korablin A.S., Matveyev Y.A., Cherniavskiy A.A., Dorofeyev A.A. // 2001. CriMiCo 2001. 11th International Conference on Microwave and Telecommunication Technology. - Sevastopol, Crimea, Ukraine, 14-14 Sept. 2001. - P. 126-127. ↑

C2307. Martins E. Design and performance of Gilbert cell mixer MMICs with GaAs PHEMT technology. / Martins E., Bastida E.M., Swart J.W. // 2001. IMOC 2001.Proceedings of the 2001 SBMO/IEEE MTT-S International Microwave and Optoelectronics Conference. 2001. - Vol. 1. - P. 245-248. ↑

C2308. Konakova R.V. The radiation firmness of the GaAs-AlGaAs HEMT ohmic contacts. / Konakova R.V., Milenin V.V., Rengevych O.E., Stovpovoy M.A. // 2001. CriMiCo 2001. 11th International Conference on Microwave and Telecommunication Technology. - Sevastopol, Crimea, Ukraine, 14-14 Sept. 2001. - P. 434-436. ↑

C2309. Smith P.M. Advances in InP HEMT technology for high frequency applications. / Smith P.M., Nichols K., Kong W., MtPleasant L., Pritchards D., Lender R., Fisher J., Actis R., Dugas D., Meharry D., Swanson A.W. // 2001. IPRM. IEEE International Conference On Indium Phosphide and Related Materials. - Nara, 2001. - P. 9-14. ↑

C2310. Mertens S.D. A model for hydrogen-induced piezoelectric effect in InP HEMTs and GaAs PHEMTs. / Mertens S.D., Del Alamo J.A. // 2001. IPRM. IEEE International Conference On Indium Phosphide and Related Materials. - Nara, 2001. - P. 452-455. ↑

- C2311.** Endoh A. Fabrication technology and device performance of sub-50-nm-gate InP-based HEMTs. / Endoh A., Yamashita Y., Shinohara K., Higashiwaki M., Hikosaka K., Mimura T., Hiyamizu S., Matsui T. // 2001. IPRM. IEEE International Conference On Indium Phosphide and Related Materials. - Nara, 2001. - P. 448-451. ↑
- C2312.** Boos J.B. AlSb/InAs HEMTs with a TiW/Au gate metalization. / Boos J.B., Bennett B.R., Kruppa W., Park D., Mittereder J., Turner N.H. // 2001. IPRM. IEEE International Conference On Indium Phosphide and Related Materials. - Nara, 2001. - P. 460-463. ↑
- C2313.** Takahashi T. Stable and uniform InAlAs/InGaAs HEMT ICs for 40-Gbit/s optical communication systems. / Takahashi T., Nihei M., Makiyama K., Nishi M., Suzuki T., Hara N. // 2001. IPRM. IEEE International Conference On Indium Phosphide and Related Materials. - Nara, 2001. - P. 614-617. ↑
- C2314.** Murata K. High speed optical fiber communication ICs based on InP HEMT. / Murata K., Enoki T., Yamane Y., Sano E. // 2001. IPRM. IEEE International Conference On Indium Phosphide and Related Materials. - Nara, 2001. - P. 610-613. ↑
- C2315.** Yoon S.F. A comparison of deep level effects on the DC characteristics of In<sub>x</sub>Ga<sub>1-x</sub>P/In<sub>0.20</sub>Ga<sub>0.80</sub>As/GaAs and Al<sub>0.24</sub>Ga<sub>0.76</sub>As/In<sub>0.20</sub>Ga<sub>0.80</sub>As/GaAs high electron mobility transistors grown by solid source MBE. / Yoon S.F., Yip K.H., Zheng H.Q., Gay B.P. // 2001. IPRM. IEEE International Conference On Indium Phosphide and Related Materials. - Nara, 2001. - P. 338-341. ↑
- C2316.** Bollaert S. 0.06 μm gate length metamorphic In<sub>0.52</sub>Al<sub>0.48</sub>As/In<sub>0.53</sub>Ga<sub>0.47</sub>As HEMTs on GaAs with high  $f_T$  and  $f_{MAX}$ . / Bollaert S., Cordier Y., Zaknoute M., Happy H., Lepilliet S., Cappy A. // 2001. IPRM. IEEE International Conference On Indium Phosphide and Related Materials. - Nara, 2001. - P. 192-195. ↑
- C2317.** Grundbacher R. 0.1 μm enhancement-mode pseudomorphic InGaAs/InAlAs/InP HEMT. / Grundbacher R., Lai R., Barskey M., Chen Y.C., Tsai R., Dia R.M., Tran L., Chin T.P., Block T., Oki A. // 2001. IPRM. IEEE International Conference On Indium Phosphide and Related Materials. - Nara, 2001. - P. 180-183. ↑
- C2318.** Boudrissa M. A 60 GHz high power composite channel GaInAs/InP HEMT on InP substrate with LG = 0.15 μm. / Boudrissa M., Delos E., Wallaert X., Theron D., De Jaeger J.C. // 2001. IPRM. IEEE International Conference On Indium Phosphide and Related Materials. - Nara, 2001. - P. 196-199. ↑
- C2319.** Yamamoto K. Effect of phosphine plasma treatment on protection from Si passivation in AlInAs/InGaAs HEMT due to F atoms. / Yamamoto K., Fujita N., Nakajima S., Sugino T. // 2001. IPRM. IEEE International Conference On Indium Phosphide and Related Materials. - Nara, 2001. - P. 248-251. ↑
- C2320.** Kawano Y. High-speed operation of a novel frequency divider using resonant tunneling chaos circuit. / Kawano Y., Ohno Y., Kishimoto S., Maezawa K., Mizutani T. // 2001. IPRM. IEEE International Conference On Indium Phosphide and Related Materials. - Nara, 2001. - P. 236-239. ↑
- C2321.** Lee J.-W. Demonstration of push-pull operation of AlGaIn/GaN HEMTs on SiC. / Lee J.-W., Lee S., Webb K.J. // 2001 Device Research Conference. - Notre Dame, IN, 2001. - P. 203-204. ↑
- C2322.** Yu-Jiu Wang. A V-Band MMIC SPDT passive HEMT switch using impedance transformation networks. / Yu-Jiu Wang, Kun-You Lin, Dow-Chih Niu, Huei Wang. // 2001 IEEE MTT-S International Microwave Symposium Digest. - Phoenix, AZ, 2001. - Vol. 1. - P. 253-256. ↑
- C2323.** Shimura T. High isolation V-band SPDT switch MMIC for high power use [HEMTs application]. / Shimura T., Mimino Y., Nakamura K., Aoki Y., Kuroda S. // 2001 IEEE MTT-S International Microwave Symposium Digest. - Phoenix, AZ, 2001. - Vol. 1. - P. 245-248. ↑
- C2324.** Morkner H. A 1.7 mA low noise amplifier with integrated bypass switch for wireless 0.05-6 GHz portable applications. / Morkner H., Frank M., Yajima S. // 2001 IEEE MTT-S International Microwave Symposium Digest. - Phoenix, AZ, 2001. - Vol. 1. - P. 293-296. ↑
- C2325.** Laloue A. A measurement based distributed low frequency noise HEMT model: application to design of millimeter wave automotive radar chip sets. / Laloue A., Lyoubi A., Camiade M., Nallatamby J.C., Valenza M., Prigent M., Obregon J. // 2001 IEEE MTT-S International Microwave Symposium Digest. - Phoenix, AZ, 2001. - Vol. 1. - P. 423-426. ↑
- C2326.** Angelov I. A simple bias dependant LF FET noise model for CAD. / Angelov I., Kozhuharov R., Zirath

H. // 2001 IEEE MTT-S International Microwave Symposium Digest. - Phoenix, AZ, 2001. - Vol. 1. - P. 407-410.



**C2327.** Zeji Gu. A high-performance GaAs SP3T switch for digital cellular systems. / Zeji Gu, Shuyun Zhang, Johnson D., Belletete S., Ayzvazian M., Fryklund D. // 2001 IEEE MTT-S International Microwave Symposium Digest. - Phoenix, AZ, 2001. - Vol. 1. - P. 241-244.

**C2328.** Werthof A. High gain PHEMT frequency doubler for 76 GHz automotive radar. / Werthof A., Tischer H., Grave T. // 2001 IEEE MTT-S International Microwave Symposium Digest. - Phoenix, AZ, 2001. - Vol. 1. - P. 107-109.

**C2329.** Morgan M. A monolithic HEMT diode balanced mixer for 100-140 GHz. / Morgan M., Weinreb S. // 2001 IEEE MTT-S International Microwave Symposium Digest. - Phoenix, AZ, 2001. - Vol. 1. - P. 99-102.

**C2330.** Kimishima M. A family of Q, V and W-band monolithic resistive mixers. / Kimishima M., Ataka T., Okabe H. // 2001 IEEE MTT-S International Microwave Symposium Digest. - Phoenix, AZ, 2001. - Vol. 1. - P. 115-118.

**C2331.** Miyaguchi K. An ultra broad band reflection type 180° phase shifter with series and parallel LC circuits. / Miyaguchi K., Hieda M., Nakahara K., Kurusu H., Nii M., Kasahara M., Takagi T. // 2001 IEEE MTT-S International Microwave Symposium Digest. - Phoenix, AZ, 2001. - Vol. 1. - P. 237-240.

**C2332.** Piernas B. Improved three-dimensional GaAs inductors. / Piernas B., Nishikawa K., Kamogawa K., Nakagawa T., Araki K. // 2001 IEEE MTT-S International Microwave Symposium Digest. - Phoenix, AZ, 2001. - Vol. 1. - P. 189-192.

**C2333.** David S. Thermal transients in microwave active devices and their influence on intermodulation distortion. / David S., Batty W., Panks A.J., Johnson R.G., Snowden C.M. // 2001 IEEE MTT-S International Microwave Symposium Digest. - Phoenix, AZ, 2001. - Vol. 1. - P. 431-434.

**C2334.** Batty W. Global electrothermal CAD of complex nonlinear 3-D systems based on a fully physical time-dependent compact thermal model. / Batty W., Christoffersen C.E., David S., Panks A.J., Johnson R.G., Snowden C.M., Steer M.B. // 2001 IEEE MTT-S International Microwave Symposium Digest. - Phoenix, AZ, 2001. - Vol. 2. - P. 667-670.

**C2335.** Rogues D. Ku-band Quadri-SSPA for Stentor satellite transmit active antenna. / Rogues D., Chane-Kee-Sheung H., Dubos F., Cogo B., Cazaux J.-L. // 2001 IEEE MTT-S International Microwave Symposium Digest. - Phoenix, AZ, 2001. - Vol. 2. - P. 657-660.

**C2336.** Jong-Wook Lee. Scalable large-signal device model for high power-density AlGaN/GaN HEMTs on SiC. / Jong-Wook Lee, Sungjae Lee, Webb K.J. // 2001 IEEE MTT-S International Microwave Symposium Digest. - Phoenix, AZ, 2001. - Vol. 2. - P. 679-682.

**C2337.** Shuyun Zhang. E-PHEMT, single supply, high efficient power amplifiers for GSM and DCS applications. / Shuyun Zhang, Jiang Cao, Mcmorrow R. // 2001 IEEE MTT-S International Microwave Symposium Digest. - Phoenix, AZ, 2001. - Vol. 2. - P. 927-930.

**C2338.** Abey W. A single supply high performance PA MMIC for GSM handsets using quasi-enhancement mode PHEMT. / Abey W., Moriuchi T., Hajji R., Nakamura T., Nonaka Y., Mitani E., Kennan W., Dang H. // 2001 IEEE MTT-S International Microwave Symposium Digest. - Phoenix, AZ, 2001. - Vol. 2. - P. 923-926.

**C2339.** Miller M. A power PHEMT device technology for broadband wireless access. / Miller M., Peatman B., Hooper R. // 2001 IEEE MTT-S International Microwave Symposium Digest. - Phoenix, AZ, 2001. - Vol. 2. - P. 637-640.

**C2340.** Virdee A.S. A novel high efficiency multioctave amplifier using cascaded reactively terminated single-stage distributed amplifiers for EW system applications. / Virdee A.S., Virdee B.S. // 2001 IEEE MTT-S International Microwave Symposium Digest. - Phoenix, AZ, 2001. - Vol. 1. - P. 519-522.

**C2341.** Rudge P.J. Two-tone intermodulation distortion simulations in the time domain using a quasi-2D physical pHEMT model. / Rudge P.J., Miles R.E., Steer M.B., Snowden C.M. // 2001 IEEE MTT-S International Microwave Symposium Digest. - Phoenix, AZ, 2001. - Vol. 1. - P. 439-442.



- C2342.** Emrick R. Monolithic 6W Ka-band high power amplifier. 2001 IEEE MTT-S International Microwave Symposium Digest. - Phoenix, AZ, 2001. - Vol. 1. - P. 527-529. ↑
- C2343.** Suzuki T. 40-Gbit/s D-type flip-flop and multiplexer circuits using InP HEMT. / Suzuki T., Kano H., Nakasha Y., Takahashi T., Imanishi K., Ohnishi H., Watanabe Y. // 2001 IEEE MTT-S International Microwave Symposium Digest. - Phoenix, AZ, 2001. - Vol. 1. - P. 595-598. ↑
- C2344.** Ahmed A. Temperature dependence of intermodulation and linearity in GaN based devices. / Ahmed A., Islam S.S., Anwar A.F.M. // 2001 IEEE MTT-S International Microwave Symposium Digest. - Phoenix, AZ, 2001. - Vol. 1. - P. 579-582. ↑
- C2345.** Carroll J.M. A 14-Vpp 10 Gbit/s E/O modulator driver IC. / Carroll J.M., Campbell C.F. // 2001. 23rd Annual Technical Digest Gallium Arsenide Integrated Circuit (GaAs IC) Symposium. - Baltimore, MD, 2001. - P. 277-279. ↑
- C2346.** Shih-Cheh Yen. Phase conjugation array using subharmonically injection locked self-oscillating mixers. / Shih-Cheh Yen, Tah-Hsiung Chu. // 2001. IEEE Antennas and Propagation Society International Symposium. - Boston, MA, 2001. - Vol. 3. - P. 692-695. ↑
- C2347.** Hwee Har Lim. Optical control on HEMT devices. / Hwee Har Lim, Alphones A. // 2001. IEEE Antennas and Propagation Society International Symposium. - Boston, MA, 2001. - Vol. 2. - P. 518-520. ↑
- C2348.** Smith P.M. Advances in InP HEMT technology for high frequency applications. / Smith P.M., Nichols K., Kong W., MtPleasant L., Pritchard D., Lender R., Fisher J., Actis R., Dugas D., Meharry D., Swanson A.W. // 2001. 23rd Annual Technical Digest Gallium Arsenide Integrated Circuit (GaAs IC) Symposium. - Baltimore, MD, 2001. - P. 7-10. ↑
- C2349.** Xian-Jie Li. An 850 nm wavelength monolithic integrated photoreceiver with a single-power-supplied transimpedance amplifier based on GaAs PHEMT technology. / Xian-Jie Li, Jin-Ping Ao, Rong Wang, Wei-Ji Liu, Zhi-Gong Wang, Qing-Ming Zeng, Shi-Yong Liu, Chun-Guang Liang. // 2001. 23rd Annual Technical Digest Gallium Arsenide Integrated Circuit (GaAs IC) Symposium. - Baltimore, MD, 2001. - P. 65-69. ↑
- C2350.** Gasmi A. Ultra low noise 2.5 Gbit/s 3.3V transimpedance amplifier with automatic gain control. / Gasmi A., Wroblewski B., Leblanc R., Smith D., Rocchi M. // 2001. 23rd Annual Technical Digest Gallium Arsenide Integrated Circuit (GaAs IC) Symposium. - Baltimore, MD, 2001. - P. 61-64. ↑
- C2351.** Kozhuharov R. A millimeter wave monolithic VCO with an integrated HEMT as a varactor. / Kozhuharov R., Zirath H. // 2001. Proceedings of the 2001 IEEE International Frequency Control Symposium and PDA Exhibition. - Seattle, WA, 2001. - P. 820-823. ↑
- C2352.** Parker A. Dynamics of microwave FET behaviour. / Parker A., Rathmell J. // 2001. Tutorial Guide: ISCAS 2001. The IEEE International Symposium on Circuits and Systems. - Sydney, NSW, 2001. - P. 2.6.1-2.6.10. ↑
- C2353.** Lambert B. Influence of impact ionization stresses on AlGaAs-InGaAs HEMT performances. / Lambert B., Malbert N., Labat, Touboul A., Huguet P. // 2001. IPFA 2001. Proceedings of the 2001 8th International Symposium on the Physical and Failure Analysis of Integrated Circuits. 2001. - P. 238-242. ↑
- C2354.** Nguyen T. A compact K-band transceiver module for broadband wireless and LMDS applications. / Nguyen T., Novak J., Gawron J., Dietz G., Sahm P., Ferek A., Bourgeois B., Haubenstricker R., Bogus E., Peterson K., Becker R., Consolazio S., Van Der Star J. // 2001. RAWCON 2001. IEEE Radio and Wireless Conference. - Waltham, MA, 2001. - P. 49-52. ↑
- C2355.** Markovic V. Neural models of microwave transistor noise parameters based on bias conditions and S-parameters. / Markovic V., Marinkovic Z. // 2001. TELSIS 2001. 5th International Conference on Telecommunications in Modern Satellite, Cable and Broadcasting Service. - Nis, 2001. - Vol. 2. - P. 683-686. ↑
- C2356.** Roberts M. Highly linear low voltage GaAs pHEMT MMIC switches for multimode wireless handset applications. / Roberts M., Albasha L., Bosch W., Gotch D., Mayock J., Sandhiya P., Bisby A. // 2001. RAWCON 2001. IEEE Radio and Wireless Conference. - Waltham, MA, 2001. - P. 61-64. ↑
- C2357.** Lai R. Extremely high P1dB MMIC amplifiers for Ka-band applications. / Lai R., Grundbacher R.,

Barsky M., Oki A., Siddiqui M., Pitman B., Katz R., Tran P., Callejo L., Streit D. // 2001. 23rd Annual Technical Digest Gallium Arsenide Integrated Circuit (GaAs IC) Symposium. - Baltimore, MD, 2001. - P. 115-117. ↑

C2358. Hsu S.S.H. Low noise AlGaIn/GaN MODFETs with high breakdown and power characteristics. / Hsu S.S.H., Pavlidis D. // 2001. 23rd Annual Technical Digest Gallium Arsenide Integrated Circuit (GaAs IC) Symposium. - Baltimore, MD, 2001. - P. 229-232. ↑

C2359. Murgadella F. Comparisons of technologies and MMICS results for military needs. / Murgadella F., Coulon P., Moreau C. // 2001. 23rd Annual Technical Digest Gallium Arsenide Integrated Circuit (GaAs IC) Symposium. - Baltimore, MD, 2001. - P. 223-227. ↑

C2360. Huang H.K. Super low noise InGaP gated PHEMT. / Huang H.K., Wang Y.H. // 2001. 23rd Annual Technical Digest Gallium Arsenide Integrated Circuit (GaAs IC) Symposium. - Baltimore, MD, 2001. - P. 237-245. ↑

C2361. Hsien-Chin Chiu. Low-k BCB passivated Al<sub>0.5</sub>Ga<sub>0.5</sub>As/In<sub>0.15</sub>Ga<sub>0.85</sub>As enhancement-mode pHEMTs. / Hsien-Chin Chiu, Shih-Cheng Yang, Yi-Jen Chan. // 2001. 23rd Annual Technical Digest Gallium Arsenide Integrated Circuit (GaAs IC) Symposium. - Baltimore, MD, 2001. - P. 269-272. ↑

C2362. Streit D. InP and GaAs components for 40 Gbps applications. / Streit D., Lai R., Gutierrez-Aitken A., Siddiqui M., Allen B., Chau A., Beale W., Oki A. // 2001. 23rd Annual Technical Digest Gallium Arsenide Integrated Circuit (GaAs IC) Symposium. - Baltimore, MD, 2001. - P. 247-250. ↑

C2363. Tayrani R. A monolithic X-band class-E power amplifier. 2001. 23rd Annual Technical Digest Gallium Arsenide Integrated Circuit (GaAs IC) Symposium. - Baltimore, MD, 2001. - P. 205-208. ↑

C2364. Shigematsu H. 45 GHz distributed amplifier with a linear 6-V<sub>p-p</sub> output for a 40 Gb/s LiNbO<sub>3</sub> modulator driver circuit. / Shigematsu H., Yoshida N., Sato M., Hara N., Hirose T., Watanabe Y. // 2001. 23rd Annual Technical Digest Gallium Arsenide Integrated Circuit (GaAs IC) Symposium. - Baltimore, MD, 2001. - P. 137-140. ↑

C2365. Leoni R.E. III. A DC-45 GHz metamorphic HEMT traveling wave amplifier. / Leoni R.E. III, Lichwala S.J., Hunt J.G., Whelan C.S., Marsh P.F., Hoke W.E., Kazior T.E. // 2001. 23rd Annual Technical Digest Gallium Arsenide Integrated Circuit (GaAs IC) Symposium. - Baltimore, MD, 2001. - P. 133-136. ↑

C2366. Welch R. Low noise hybrid amplifier using AlGaIn/GaN power HEMT devices. / Welch R., Jenkins T., Neidhard B., Kehias L., Quach T., Watson P., Worley R., Barsky M., Sandhu R., Wojtowicz M. // 2001. 23rd Annual Technical Digest Gallium Arsenide Integrated Circuit (GaAs IC) Symposium. - Baltimore, MD, 2001. - P. 153-155. ↑

C2367. Chou Y.C. High reliability of 0.1 μm InGaAs/InAlAs/InP HEMT MMICs on 3-inch InP production process. / Chou Y.C., Leung D., Lai R., Scarpulla J., Barsky M., Grundbacher R., Eng D., Liu P.H., Oki A., Streit D.C. // 2001. 23rd Annual Technical Digest Gallium Arsenide Integrated Circuit (GaAs IC) Symposium. - Baltimore, MD, 2001. - P. 174-179. ↑

C2368. Chou Y.C. High reliability non-hermetic 0.1 μm GaAs pseudomorphic HEMT MMIC amplifiers. / Chou Y.C., Leung D., Lai R., Scarpulla J., Biedenbender M., Grundbacher R., Eng D., Liu P.H., Oki A., Streit D.C. // 2001. 23rd Annual Technical Digest Gallium Arsenide Integrated Circuit (GaAs IC) Symposium. - Baltimore, MD, 2001. - P. 170-173. ↑

C2369. Poti B. High-quality MOCVD AlGaIn/GaN structure for HEMT applications. / Poti B., Passaseo A., De Vittorio M., Peroni M., Cetronio A., Romanini P. // Ph. D. Research in Microelectronics and Electronics 2006. - Otranto, {no data available}. - P. 425-428. ↑